ISSN 2071-4726
2071-0305

Инженерно-строительный журнал

НАУЧНОЕ ИЗДАНИЕ

№4(80) 2018

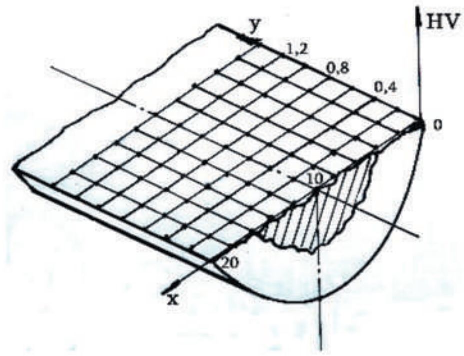

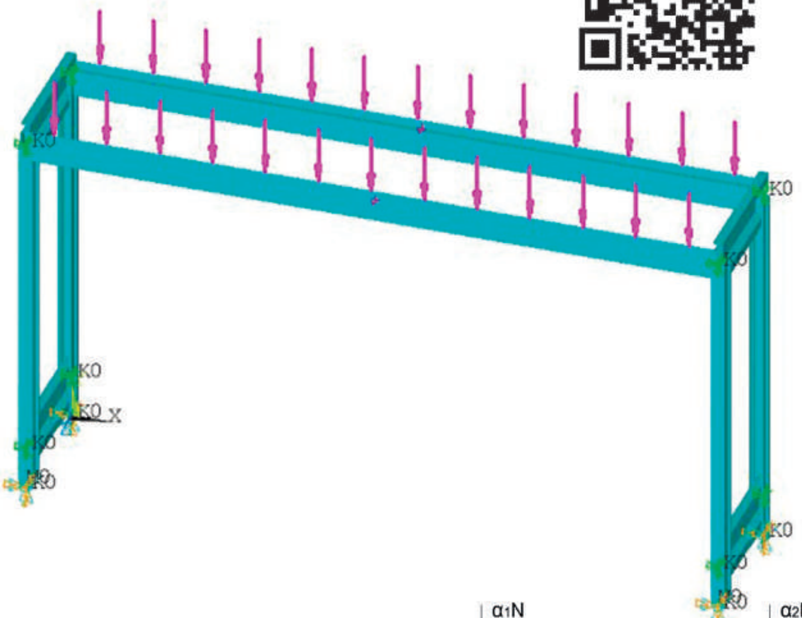

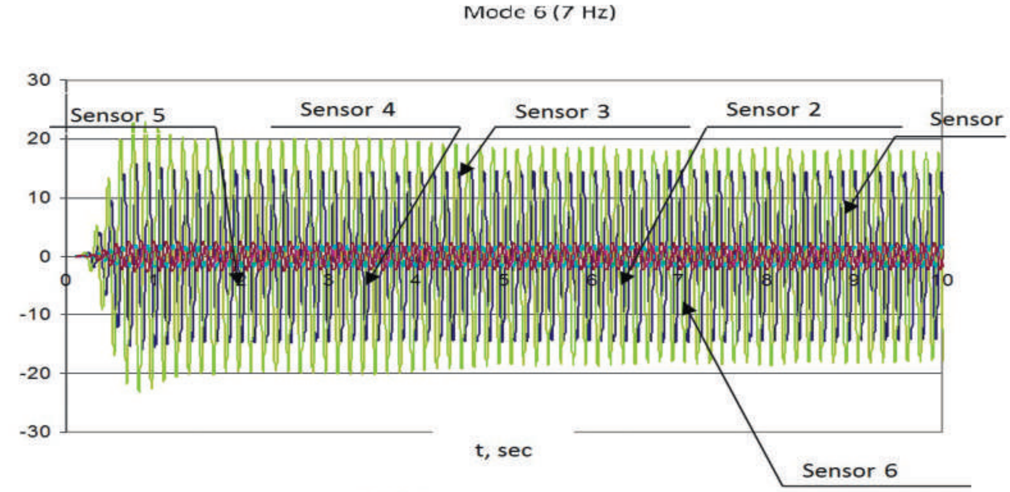

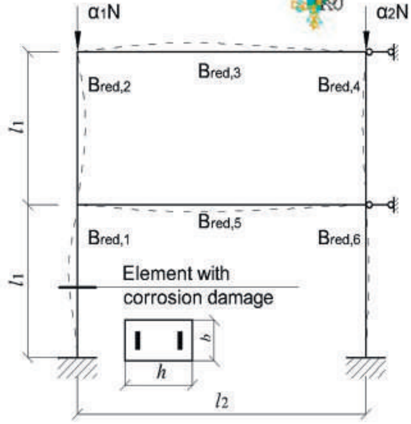

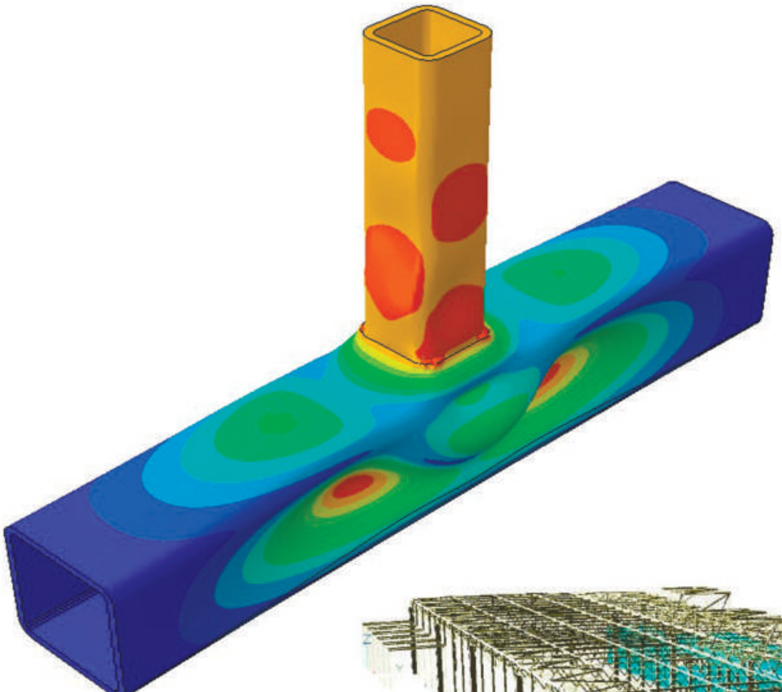

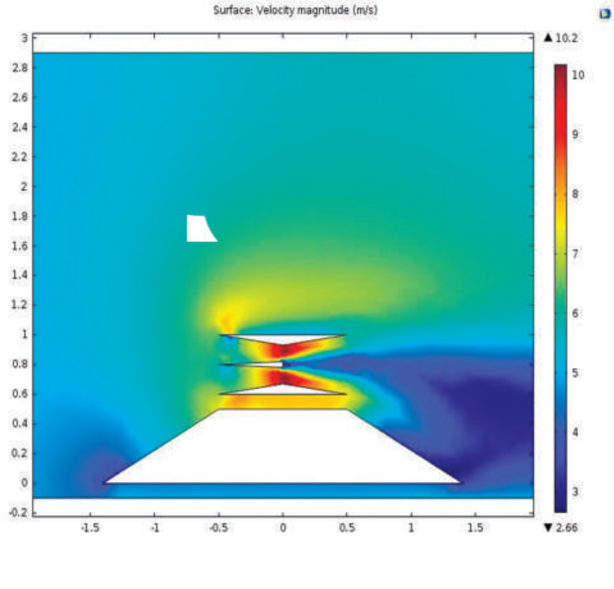

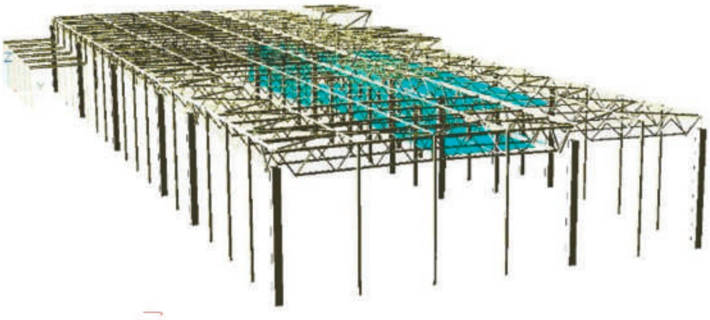

**Федеральное государственное автономное образовательное учреждение высшего образования
Санкт-Петербургский политехнический университет Петра Великого**

ПОЛИТЕХ
Санкт-Петербургский политехнический университет Петра Великого

**Инженерно-строительный институт
Центр дополнительных профессиональных программ**

*195251, г. Санкт-Петербург, Политехническая ул., 29,
тел/факс: 552-94-60, www.stroikursi.spbstu.ru,
stroikursi@mail.ru*

**Приглашает специалистов организаций, вступающих в СРО,
на курсы повышения квалификации (72 часа)**

Код	Наименование программы	Виды работ*
	Курсы по строительству	
БС-01-04	«Безопасность и качество выполнения общестроительных работ»	**п.1,2, 3, 5, 6, 7, 9, 10, 11, 12, 13, 14**
БС-01	«Безопасность и качество выполнения геодезических, подготовительных и земляных работ, устройства оснований и фундаментов»	**1,2,3,5**
БС-02	«Безопасность и качество возведения бетонных и железобетонных конструкций»	**6,7**
БС-03	«Безопасность и качество возведения металлических, каменных и деревянных конструкций»	**9,10,11**
БС-04	«Безопасность и качество выполнения фасадных работ, устройства кровель, защиты строительных конструкций, трубопроводов и оборудования»	**12,13,14**
БС-05	«Безопасность и качество устройства инженерных сетей и систем»	**15,16,17,18,19**
БС-06	«Безопасность и качество устройства электрических сетей и линий связи»	**20,21**
БС-08	«Безопасность и качество выполнения монтажных и пусконаладочных работ»	**23,24**
БС-12	«Безопасность и качество устройства мостов, эстакад и путепроводов»	**29**
БС-13	«Безопасность и качество выполнения гидротехнических, водолазных работ»	**30**
БС-14	«Безопасность и качество устройства промышленных печей и дымовых труб»	**31**
БС-15	«Осуществление строительного контроля»	**32**
БС-16	«Организация строительства, реконструкции и капитального ремонта. Выполнение функций технического заказчика и генерального подрядчика»	**33**
	Курсы по проектированию	
БП-01	«Разработка схемы планировочной организации земельного участка, архитектурных решений, мероприятий по обеспечению доступа маломобильных групп населения»	**1,2,11**
БП-02	«Разработка конструктивных и объемно-планировочных решений зданий и сооружений»	**3**
БП-03	«Проектирование внутренних сетей инженерно-технического обеспечения»	**4**
БП-04	«Проектирование наружных сетей инженерно-технического обеспечения»	**5**
БП-05	«Разработка технологических решений при проектировании зданий и сооружений»	**6**
БП-06	«Разработка специальных разделов проектной документации»	**7**
БП-07	«Разработка проектов организации строительства»	**8**
БП-08	«Проектные решения по охране окружающей среды»	**9**
БП-09	«Проектные решения по обеспечению пожарной безопасности»	**10**
БП-10	«Обследование строительных конструкций и грунтов основания зданий и сооружений»	**12**
БП-11	«Организация проектных работ. Выполнение функций генерального проектировщика»	**13**
Э-01	«Проведение энергетических обследований с целью повышения энергетической эффективности и энергосбережения»	
	Курсы по инженерным изысканиям	
И-01	«Инженерно-геодезические изыскания в строительстве»	**1**
И-02	«Инженерно-геологические изыскания в строительстве»	**2,5**
И-03	«Инженерно-гидрометеорологические изыскания в строительстве»	**3**
И-04	«Инженерно-экологические изыскания в строительстве»	**4**
И-05	«Организация работ по инженерным изысканиям»	**7**

***(согласно приказам Минрегионразвития РФ N 624 от 30 декабря 2009 г.)**

По окончании курса слушателю выдается удостоверение о краткосрочном повышении квалификации установленного образца (72 ак. часа)

Для регистрации на курс необходимо выслать заявку на участие, и копию диплома об образовании по телефону/факсу: 8(812) 552-94-60, 535-79-92, , e-mail: stroikursi@mail.ru.

Инженерно-строительный журнал
НАУЧНОЕ ИЗДАНИЕ

ISSN 2071-4726, 2071-0305

Свидетельство о государственной регистрации: ПИ №ФС77-38070, выдано Роскомнадзором

Специализированный научный журнал. Выходит с 09.2008.

Включен в Перечень ведущих периодических изданий ВАК РФ

Периодичность: 8 раз в год

Учредитель и издатель:

Санкт-Петербургский политехнический университет Петра Великого

Адрес редакции:

195251, СПб, ул. Политехническая, д. 29, Гидрокорпус-2, ауд. 227А

Дата выхода: 10.08.2018

Содержание

На обложке: иллюстрации авторов к статьям номера

Контакты:
Тел. +7(812)535-52-47 E-mail: mce@spbstu.ru
Web: http://www.engstroy.spbstu.ru

Magazine of Civil Engineering
SCHOLAR JOURNAL

ISSN 2071-4726, 2071-0305
Peer-reviewed scientific journal
Start date: 2008/09
8 issues per year

Publisher:
Peter the Great St. Petersburg Polytechnic University

Indexing:
Scopus, Russian Science Citation Index (WoS), Compendex, DOAJ, EBSCO, Google Academia, Index Copernicus, ProQuest, Ulrich's Serials Analysis System

Corresponding address:
227a Hydro Building, 29 Polytechnicheskaya st., Saint-Petersburg, 195251, Russia

Date o0f issue: 10.08.2018

Contents

On the cover: authors' illustrations

+7(812) 535-52-47
E-mail: mce@spbstu.ru
Web: http://www.engstroy.spbstu.ru/eng/index.html

doi: 10.18720/MCE.80.1

The improving of the concrete quality in a monolithic clip

Повышение качества бетона в монолитной обойме

A.M. Sychova*,
Military Space Academy named after A.F. Mozhaysky, St. Petersburg, Russia,
L.B. Svatovskaya,
Emperor Alexander I St. Petersburg State Transport University, St. Petersburg, Russia,
D.S. Starchukov,
Military Space Academy named after A.F. Mozhaysky, St. Petersburg, Russia,
V.Y. Soloviova,
Emperor Alexander I St. Petersburg State Transport University, St. Petersburg, Russia,
M.V. Gravit,
Peter the Great St. Petersburg Polytechnic University, St. Petersburg, Russia

Д-р техн. наук, профессор А.М. Сычева*,
Военно-космическая академия имени А.Ф. Можайского, Санкт-Петербург, Россия,
д-р техн. наук, профессор Л.Б. Сватовская,
Петербургский государственный университет путей сообщения Императора Александра I, Санкт-Петербург, Россия,
канд. техн. наук, доцент Д.С. Старчуков,
Военно-космическая академия имени А.Ф. Можайского, Санкт-Петербург, Россия,
д-р техн. наук, профессор В.Я. Соловьева,
Петербургский государственный университет путей сообщения Императора Александра I, Санкт-Петербург, Россия,
канд. техн. наук, доцент М.В. Гравит,
Санкт-Петербургский политехнический университет Петра Великого, Санкт-Петербург, Россия

Key words: clip; silica Sol; heavy concrete; Gibbs free energy; surface energy; surface hardness; corrosion resistance

Ключевые слова: обойма; кремнезоль; тяжелый бетон; энергия Гиббса; поверхностная энергия; твердость поверхности; коррозионная устойчивость

Abstract. The article deals with the possibility of increasing strength, hardness, frost resistance, water and corrosion resistance of concrete. The reduction of its abrasion resistance and water absorption by creating a layer of nonorganic monolithic high-strength clip on its surface is also considered. The possibility of synthesis of such clip by impregnating the concrete surface with a Sol of SiO2 is shown and thermodynamically substantiated. The mathematical dependence reflecting the strength of concrete in such a clip is developed. The distribution of efforts between the clip and not strengthened kernel in the case of load action is shown. The methods of X-ray, differential thermal analysis, electron microscopy and analysis of pore size were used for researching the phase composition and structure of the clip, as well as its porous structure. It was established experimentally the improvement of the various performance properties of concrete due to the presence of inorganic monolithic clip up to 200 %. Corrosion resistance of concrete in various aggressive environments is demonstrated and the concrete corrosion depth under the age of 50 years is calculated.

Аннотация. В статье показана возможность повышения прочности, твердости, морозостойкости, водонепроницаемости, коррозионной устойчивости, а также снижения истираемости и водопоглощения бетона за счет создания на его поверхности слоя неорганической монолитной высокопрочной обоймы. Показана и термодинамически обоснована возможность синтеза такой обоймы путем пропитки поверхности бетона золем SiO2. Разработана математическая зависимость, отражающая прочность бетона в такой обойме. Показано распределение усилий между обоймой и не упрочненным ядром в случае действия нагрузки. Рентгенографическим, дериватографическим методом, а также методом электронной микроскопии и порометрии исследован фазовый состав и структура новообразований обоймы, а также ее пористая структура. Экспериментально установлено улучшение до 200 % различных эксплуатационных свойств бетона за счет присутствия неорганической монолитной обоймы. Показано коррозионная устойчивость бетона в различных агрессивных средах и рассчитана глубина коррозии бетона в возрасте до 50 лет.

Сычева А.М., Сватовская Л.Б., Старчуков Д.С., Соловьева В.Я., Гравит М.В. Повышение качества бетона в монолитной обойме // Инженерно-строительный журнал. 2018. № 4(80). С. 3–14.

1. Introduction

It is known that there are various ways to increase concrete strength, for example, by the mechanical activation of the concrete mix [1–3]. In addition, methods of physical-chemical and mechanical activation of cement are widely used in practice [4–7]. But it is well known that the introduction of modifying additives in the concrete mixture [8–11] cannot implement the provision of cement completely, and it continues to harden with time.

The use of nanoparticles of different nature to improve the various properties of the concrete follows from the literature review.

TiO_2 nanoparticles effects on physical, thermal and mechanical properties of self-compacting concrete with ground granulated blast furnace slag as binder is shown in [12].

The effect of limewater on strength and percentage of water absorption of Al_2O_3 nanoparticles blended concrete has been investigated was studied. Portland cement was partially replaced by Al_2O_3 nanoparticles with the average particle size of 15 nm. Utilizing up to 2.0 wt. % Al_2O_3 nanoparticles could produce concrete with improved strength and water permeability [13].

Splitting tensile strength of concrete using ground granulated blast furnace slag and SiO_2 nanoparticles as binder was studied in [14].

Abrasion resistance and compressive strength of concrete specimens containing SiO_2 and Al_2O_3 nanoparticles which are cured in different curing media have been investigated was studied [15]. Portland cement was partially replaced by up to 2.0 wt. % SiO_2 and Al_2O_3 nanoparticles and mechanical properties of the produced specimens were measured. Increasing the nanoparticles content has found to increase the abrasion resistance.

The effect of curing medium on microstructure together with physical, mechanical and thermal properties of concrete containing ZnO_2 nanoparticles have been investigated was present in the work [16]. Portland cement was partially replaced by ZnO_2 nanoparticles with the average particle size of 15 nm and the specimens were cured in water and saturated limewater for specific ages. The results indicate that the ZnO_2 nanoparticle up to maximum of 2.0 % produces concrete with improved compressive strength.

The use of nanoparticles in SiO_2 Sol to harden the surface of concrete has not been investigated to date, follows from the review of scientific articles.

Nanocoatings are regarded as the most promising high-performance materials for construction applications [17, 18]. Due to their self-assembly effect, they represent remarkable characteristics against environmental agents compared to conventional coating materials in construction industry. They also show high performance in contradiction of energy efficiency, CO_2 emission, and the air quality improvement.

Active pozzolacic admixtures, such as silica fume (SF) and metakaolin, are used in modern concrete technology to obtain high performance properties [19]. Nano-scale pozzolans helps to achieve more dense microstructural packing and more impermeable cement matrix.

From a review of existing methods of construction hardening it follows that there are many scenarios of their strengthening, including through the implementation of the clip effect [20]. Nowadays there are different variants of clips such as metal and concrete which are used as the individual reinforcing layers [21]. But modification options for creating of a monolithic nonorganic clip in the surface layer of the concrete at the expense of its impregnation with the solution based on nanoparticles (a colloidal solution) are not discussed. In addition, from the literature review it follows that the mechanical hardening of the concrete core due to the creation of such a monolithic durable clip in its surface layer has not been investigated yet.

The purpose of the research. The development of a method to improve the quality of heavy concrete by impregnating it with a colloidal solution.

The object of the research. The concrete quality indicators in a monolithic inorganic clip obtained in the surface layer of concrete due to its impregnation with a colloidal solution.

The subject of the research. Physical and chemical hardening processes occurring in the surface layer of concrete impregnated with a colloidal solution.

The research problems.

1. Research of physico-chemical and thermodynamic processes of hardening the concrete surface when it is impregnated with a colloid solution.
2. Research of the value of mechanical hardening of the concrete core due to the effect of the resulting monolithic clip and the factors affecting it.
3. The evaluation of the concrete quality obtained.

2. Methods

We have investigated and scientifically grounded the following idea: when creating high-performance concrete it is possible to strengthen not the whole volume of concrete but only its surface layer. It can be done by means of its impregnation with sol solution with particle sizes of 1...100 nm. This process is called Sol-impregnate [22].

In this case two mechanisms will operate, the enabling to improve the concrete strength and other physico-mechanical characteristics of concrete. The first mechanism is the physical-chemical hardening of the concrete surface layer, resulting in the creation of a monolithic inorganic ultra strong clips. The second one is connected with the fact that in the case of the load action the synthesized monolithic clip will mechanically strengthen the concrete core. In addition to hardening synthesized clip can give concrete the new operational properties, such as hardness, abrasion resistance, etc.

Figure 1 shows a concrete cube under the action of load *P*, which consists of a hardened part – inorganic monolithic ultra-strong clips and nonhardened part – concrete core.

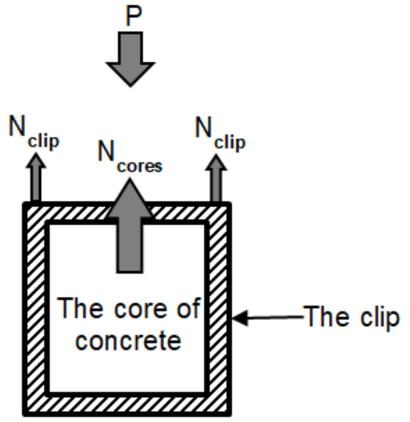

Figure 1. The concrete cube in the monolithic ultra-strong clip

In the first stage, the calculation of load redistribution R between the synthesized clip and concrete core for the sample of 100 x 100 x 100 mm has been done. The calculation has shown that when the layer thickness of the synthesized clips is up to 10 mm and in the case of exceeding its strength in relation to the concrete core 1.5 times there will be 0.65 *R* on a concrete core and 0.35 *P* on a monolithic inorganic clips.

Then, we have developed a mathematical dependence (1). It takes into account the influence of the following factors on the compressive strength of the sample *R* which is located in the clip: the load redistribution between the clip and the concrete core; the number of Sol-impregnate faces; cross-sectional form of the sample and the distance between the upper and lower Sol-impregnate faces.

$$R_{str}=((0.35R)_{\mathrm{clips}}+(0.65R)_{\mathrm{core}})\cdot K_f\cdot n\cdot 1.7(h/a)^{-0.4} \tag{1}$$

where K_f – is the coefficient taking into account the cross-sectional form of the sample:
if a cube with sides of 100 mm, then $K_f = 1$
if the cylinder, then $K_f = 1.15$;
n – is the number of Sol-impregnate faces:
if there are 6 faces, then $n = 1.7$,
if there are 4 faces (lateral), then $n = 1.5$
if there are 2 faces (top and bottom), then $n = 1.3$;
h/a – is the ratio of sample's height to its width.

The developed formula allows for the first time to calculate and predict the compressive strength of concrete located in the inorganic monolithic clip.

Then the theoretical principles are given. Their implementation will allow to realize physico-chemical synthesis of ultra-strong monolithic clips and to obtain concretes with high performance properties.

1. One of the thermodynamic parameters for solid phases of concrete, in accordance with the third law of thermodynamics is the Gibbs free energy, ΔG^0_{298}, kJ/mol. The Gibbs free energy reflects the part of the energy directed into the system from outside (for example, surface energy) which can be converted into the useful work. The lower the value of the Gibbs free energy of solid phases of concrete, the more

work is performed by the system in the process of hardening. Figures 2 and 3 show that lower values of the Gibbs energy and such high physical and mechanical characteristics as compressive strength and hardness [23, 24] correspond to the low-basic hydrosilicates (CaO/SiO_2 ratio < 1.2).

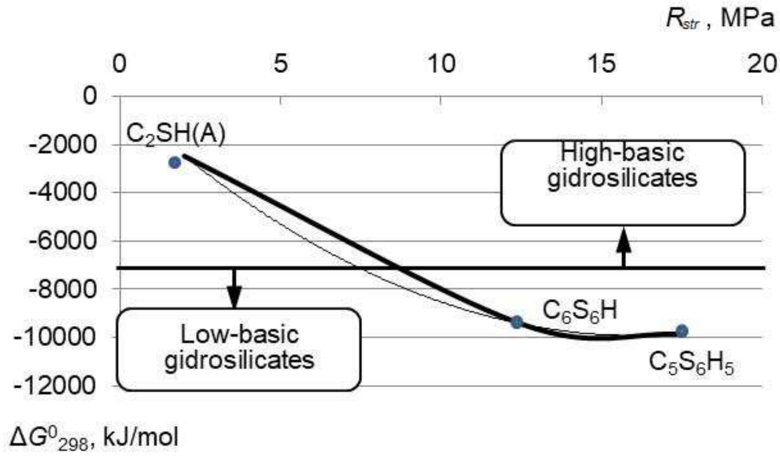

Figure 2. The interrelation of the Gibbs energy with compressive strength of hydrosilicates

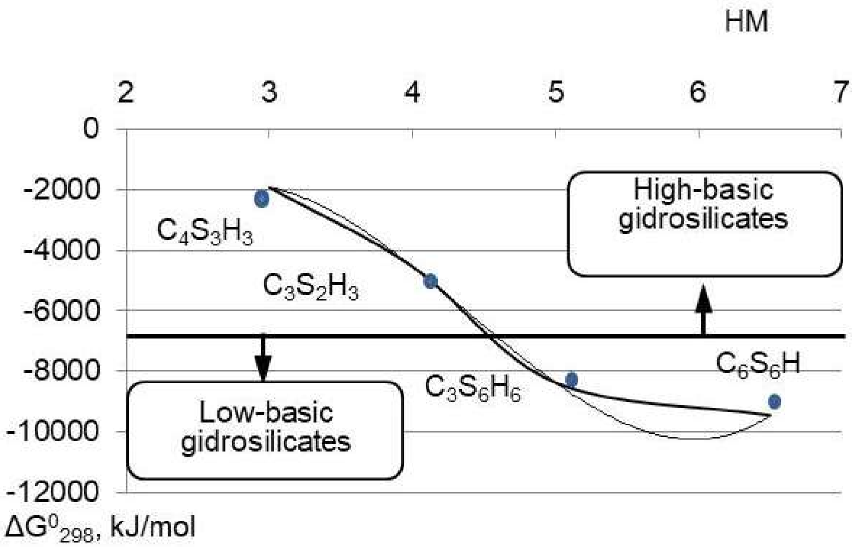

Figure 3. The interrelation of the Gibbs energy with the hardness of hydrosilicates

We are to specify the synthesis of the high strength clip so that the cement system would make the maximum useful work, i.e. low-basic hydrosilicates with low values of the Gibbs energy possessing high strength and high hardness would originate on its basis.

2. As well known, nanoparticles have a huge surplus surface energy. In the impregnation with the sol solution containing nanoparticles in the concrete surface will occur spontaneous reset of this energy (ΔG^0_{298} process < 0). Then, in accordance with the third law of thermodynamics, it will be additional useful work, which is expressed in the formation of low-basic hydrosilicates and improving physical and mechanical properties of high strength concrete Figure 4.

3. The use of the ability of high-strength concrete to the spontaneous capillary liquid absorption (ΔG^0_{298} physical process < 0) will allow to achieve ultra-high concentration of sol additives in the surface layer of the concrete at its impregnation. This, in its turn, will increase the intensity of spontaneous hardening process and speed up their flow, Table 1.

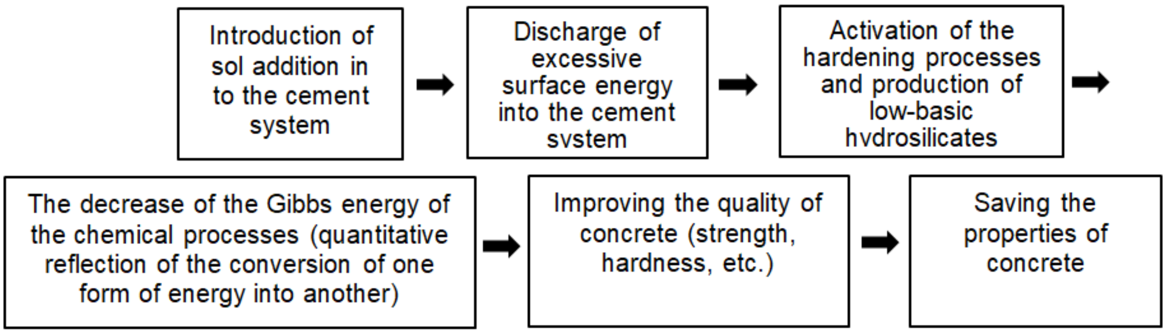

Figure 4. The scheme of realization of the law of energy conservation while obtaining a high-strength clip by impregnating the concrete surface with sol solution

Table 1. Spontaneous processes occurring during impregnation of concrete surface with the sols

The type of process	ΔG^0_{298}, kJ/mol
Capillary ascent	$\Delta G^0_{298}<0$
Discharge of the excessive surface energy of sol nanoparticles	$\Delta G^0_{298}<0$
The process of hardening of concrete with the formation of low-basic hydrosilicates	$\Delta G^0_{298}<0$
Corking of pores with particles of SiO_2 gel and new low-basic hydrosilicates	$\Delta G^0_{298}<0$

4. Extraction of the additional cement reserves at the expense of the energy nanoparticles of the injected sols will allow to obtain high-strength monolithic clip by spontaneous physico-chemical processes (ΔG^0_{298} process<0):

- binding of $Ca(OH)_2$ resulting from the basic reactions of hardening, in additional low-basic hydrosilicates, table 2;
- the increase of the number of the cement having reacted and the decrease of basicity of hydrosilicates;
- the acceleration of the hardening process in time.

Table 2. The results of thermodynamic calculation of the Gibbs energy, ΔG^0_{298}, kJ/mol of the possible solid phases formed in the surface layer of concrete

The chemical reaction of hardening	**The estimated ΔG^0_{298}, kJ/mol**
The main reaction of cement hardening	
$3CaO{\cdot}SiO_2+3H_2O \rightarrow 2CaO{\cdot}SiO_2{\cdot}2H_2O+Ca(OH)_2$	–356
$2(2CaO{\cdot}SiO_2)+3H_2O \rightarrow 3.3CaO{\cdot}2SiO_2{\cdot}2.3H_2O+0.7Ca(OH)_2$	–218
Additional reactions of cement hardening for the technology of Sol-impregnate	
$Ca(OH)_2+SiO_2{\cdot}H_2O \rightarrow 2CaO{\cdot}SiO_2{\cdot}1.17H_2O+1.83H_2O$	–95
$2CaO{\cdot}SiO_2{\cdot}1.17H_2O + 2(SiO_2{\cdot}H_2O) \rightarrow 2CaO{\cdot}3SiO_2{\cdot}2.5H_2O\ (C_2S_3H_{2.5})$ + + $0.67H_2O$	–180
$Ca(OH)_2+2(SiO_2{\cdot}H_2O) \rightarrow CaO{\cdot}2SiO_2{\cdot}2H_2O+H_2O$	–169
$6Ca(OH)_2+6(SiO_2{\cdot}H_2O) \rightarrow 6CaO{\cdot}6SiO_2{\cdot}H_2O\ (C_6S_6H)+11H_2O$	–117.0
$5Ca(OH)_2+6(SiO_2{\cdot}H_2O) \rightarrow 5CaO{\cdot}6SiO_2{\cdot}5.5H_2O\ (C_5S_6H_5)+5.5H_2O$	–585

The implementation of the sum of these theoretical positions will allow to create energy-saving technology of Sol-impregnate (surface hardening) of concrete without using additional energy from outside. The use of such technology will allow to obtain an inorganic mineral super strong clip and the bulk of fundamentally important performance characteristics of concrete such as strength, hardness, abrasion resistance, frost resistance, water absorption and integrity of the protective properties of concrete over time (corrosion resistance).

In the next part of the work the synthesis of monolithic high -strength clips was carried out. According to the previous calculation the task of the synthesis was to obtain the strength characteristics of monolithic inorganic clip 1.5 times higher than of not hardened concrete core.

In accordance with the earlier developed method silica Sol (SiO_2) was chosen for the impregnation, because previous studies showed its activating effect on the concrete.

At the beginning the most rational conditions of hardening necessary for obtaining a high strength of the concrete surface layer due to its impregnation with a Sol of SiO_2 were stated. For this purpose, samples of heavy concrete class B30 with the size 100 x 100 x 100 mm have been produced. In the process of their production Portland cement CEM 42.5, granite crushed stone of 5–10 mm and pit sand with a fineness modulus of *Mr* = 2.26 were used. The composition of concrete are shown in table 3.

Table 3. The consumption of the components per 1 m3 of concrete mix, kg

Cement	Sand	Crushed stone	Water
370	802	1063	155

In order to achieve a well-developed pore structure, providing spontaneous capillary inflow of the sol into concrete surface, the time of concrete hardening was investigated under normal conditions before the impregnation. The time period was twenty four hours because the mass of the absorbed silica sol in this case was maximum.

Then the assessment of the rational time of impregnation of concrete samples in the SiO_2 Sol solution with their subsequent hardening under normal conditions (temperature = 20 ± 2 ºC and humidity = 95 %) for 28 days was made. The impregnation time was 3 days. For impregnation of concrete surfaces the industrial silica Sol SITEK of 3 % concentration was used.

3. Results and Discussion

The quality indexes developed by the concrete which has been obtained by the technology of Sol-impregnation are given in the Table 4. The table shows that in comparison with the control samples hardness increases by 30 %, the compressive strength of concrete increases by 78 %, tensile strength in bending of 76 %, the water resistance increases by 75 %, frost resistance increases by 200 %, the water absorption decreases by 60 %.

Table 4. Quality indexes of the concrete developed on the basis of surface strengthening by Sol-impregnation

The name of index	**Control sample**	**Strengthen of the sol SiO_2 sample**	**Increase of quality, %**
Hardness number by Moos	4	6	75
Compressive strength	39.3 MPa	69.9 MPa	78
Tensile strength in bending	5.2 MPa	9.2 MPa	76
Index of crack resistance	0.132	0.153	16
Abrasion resistance	0.89 g/cm^2	0.67 g/cm^2	25
Water resistance	0.8 MPa	1.4 MPa	75
Frost resistance, cycles	200	600	200
Water absorption	4.7 %	1.9 %	60
Elastic strength, MPa·10^{-3}	32.5	44.5	37

Further work was connected with physico-chemical investigation of sol strengthen concrete layer.

In accordance with the carried out X-ray investigations, and differential thermal analysis, Figures 5, 6, Table 5, it was revealed [25] that the increase of the mechanical properties is connected with the formation of the concrete low-basic hydrosilicates of type C_6S_6H, CSH(I), $C_2S_3H_{2.5}$, $C_3S_2H_3$ with low values of the Gibbs energy in the surface sol strengthen concrete layer, table.2. Besides that, $Ca(OH)_2$ and C_3S are absent in the samples, which confirmed the previous assumption that with the injection of sol SiO_2, calcium hydroxide is bound in the additional low-basic hydrosilicates and the main cement reserve is exhausted.

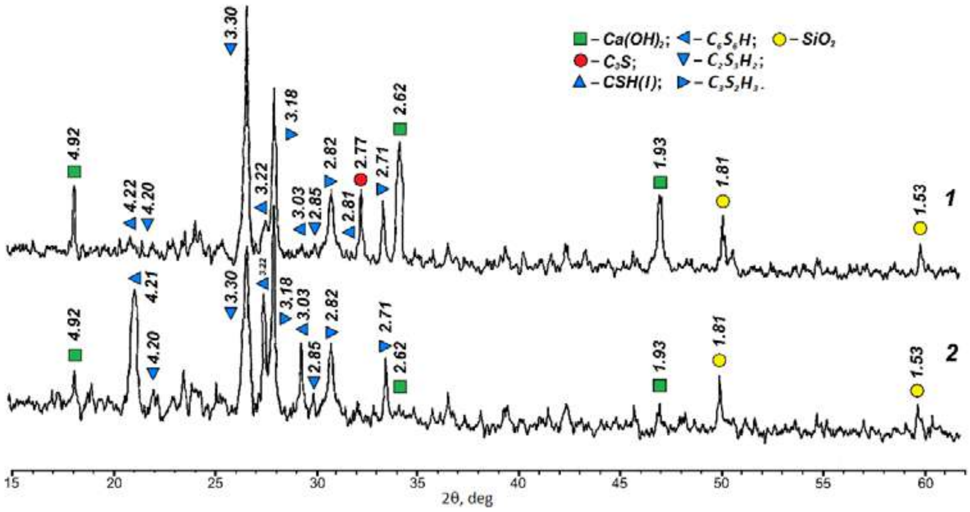

Figure 5. X-ray analyses of samples of cement stone:
1 – control sample; 2 –sample impregnated with silica Sol

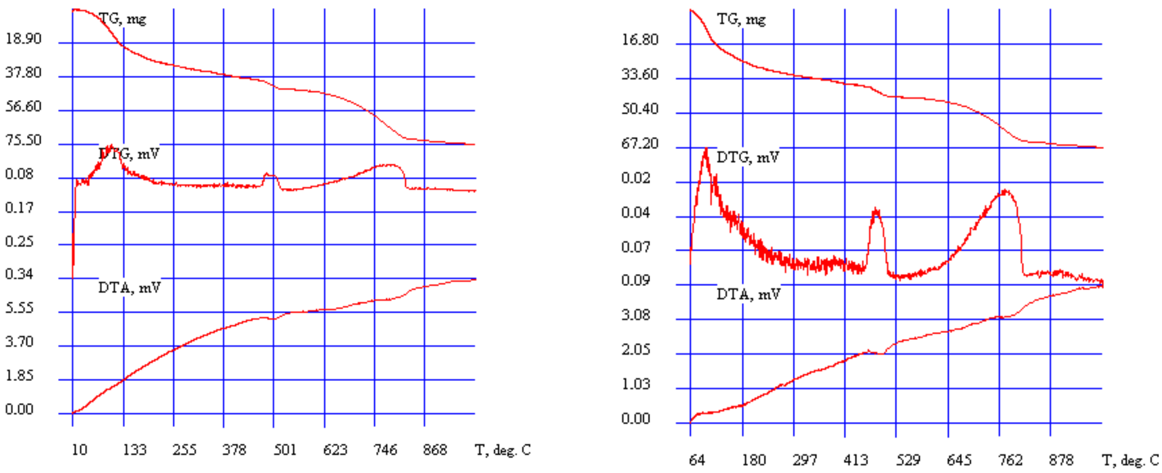

a

b

Figure 6. Diversional thermal analysis of the cement stone samples: a – control sample, b – sample, impregnated with silica Sol

Table 5. Results of calculation differential thermal analysis of the cement stone samples

The composition of the impregnate	**Endothermic effect T, ºC**			**Total mass loss on the effects, mg**	**Loss of water in the gel phase, mg**
	Loss of water, mg				
	(30-170)	(470-530)	(680-820)		
–	15.00	7.60	15.20	37.80	37.70
Sol SiO_2	31.70	5.30	24.60	61.60	8.70

The data shown in the Table 5 confirm the data of X-ray studies. Endothermic effects in the region of 30 to 170 °C, 470–530 ºC, 680–820 ºC correspond to dehydration of $C_2S_3H_{2.5}$, endothermic effect in the field of 680-820ºC also corresponds to the dehydration of C_6S_6H and endothermal effect in the field 400^{0}C corresponds to the dehydration of $C_3S_2H_3$ [25]. The total mass loss on the effects increases 1.6 times, indicating a deeper degree of cement hydration in the presence of silica sol. The loss of water in the gel phase of the Sol sample decreases 4 times, which confirms that the redistribution of water in the direction of its increase in the crystalline phase takes place.

By means of the electron microscopy it was revealed that the new phases of hydrosilicates are concentrated in the surface layer of 1 sm depth and in the pores, causing their blockage, Figure 7. The largest concentration takes place in the layer the thickness of which is up to 7 mm.

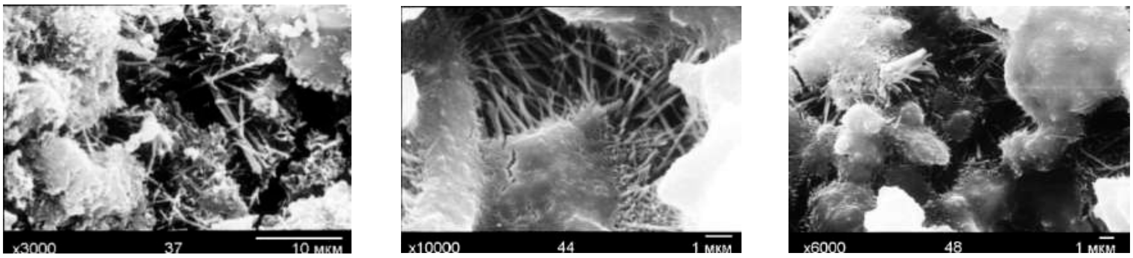

1 2 3

Figure 7. Photographs of the slice of the sample impregnated with silica Sol, in secondary electrons at different magnification: the 1 – low-basic hydrosilicates at the depth of h=1 mm; the 2 – low-basic hydrosilicates at the depth h=2 mm; the 3 – low-basic hydrosilicates at the depth h=3 mm

New phases form the "bridges" that binds the grains of the cement stone. At the depth of 1 cm the composition of the sol strengthen concrete is equal to the composition of the control sample.

Then, the authors investigated the porous structure of concrete samples of the class B30. Studies have shown, table 6, that in the samples impregnated with SiO_2 Sol the specific surface area of the pores decreases 2.14 times, the volume of sorbenting pores with a radius ≤ 50 nm reduces 1.3 times, the volume of macropores with a radius of ≥ 50 nm decreases 1.28 times. These results confirm the data of microscopic researches and shows that new phases fill the pores of the cement stone, which makes the structure more dense and also contributes to the increase of the strength, hardness, frost resistance, water resistance, corrosion resistance and durability of concrete.

Table 6. The results of determining the pores structure of the concrete samples

The name of the sample	The specific surface of pores, S_{sp}, m^2/g	The volume of sorbent pores, V_s, cm^3/g	The volume of macropores, V_m, cm^3/g	The total volume of the pores, V_Σ, cm^3/g
Control	3.0	0.04	0.09	0.13
Strengthened with the sol SiO_2	1.4	0.03	0.07	0.10

Thus, it was proved experimentally and based scientifically that the technology of surface hardening of concrete with a Sol of SiO_2 leads to production of inorganic high-strength clip. The effect of its action allows to increase the strengthen of the concrete core mechanically and to get the bulk of fundamentally important performance properties.

Then the degree of the preservation in time of the achieved level of the concrete properties was evaluated.

The assessment includes two stages. The first stage estimates the corrosion resistance of concrete after surface hardening, because physico-chemical studies have shown that the technology of surface hardening of concrete $Ca(OH)_2$ transforms into the new phases concentrated in the pores of the surface layer and increasing its strength and density. Thus, the created inorganic high-strength clip acts as a protective corrosion barrier. It eliminates two main causes of the corrosion: chemical – due to the reaction $Ca(OH)_2$ with the reagents of the environment [26], and physical – due to the formation slightly soluble salts in the pores and capillaries of the concrete, causing considerable stress and , contributing to the destruction of the concrete structure [27, 28].

The evaluation of corrosion resistance was made in three types of aggressive environments causing the cement stone corrosion: 1 medium-5% solution of $MgCl_2$-causes the magnesia corrosion, 2 medium-5 % H_2SO_4 solution-causes the acid corrosion, 3 medium-5% Na_2CO_3 solution - causes the alkaline corrosion, table 7. As a result the coefficient of corrosion resistance (2) in different physical environments k_i was calculated.

$$k_i=R_1/R_2 \tag{2}$$

where R_1 – tensile strength in bending of surface-hardened sample in the aggressive environment;

R_2 – tensile strength in bending of the control sample at the age of 28 days under the condition of normal hardening.

Analysis of the data achieved shows that according to the normative classification for chemical resistance of concrete in aggressive environments the concrete sample after surface hardening with a Sol of SiO_2 can be attributed to chemically resistant concrete, because its corrosion resistance coefficient is above 0.8. So the developed anti-corrosion barrier can significantly increase the coefficient of corrosion resistance of concrete at the age of 12 months. It increases up to 27 %.

Table 7. The coefficient of corrosion protection of concrete in various aggressive environments

The kind of simple	The coefficient of corrosion resistance of concrete in various aggressive environments								
	Magnesia corrosion, $MgCl_2$			The acid corrosion, H_2SO_4			The alkaline corrosion, Na_2CO_3		
	The time of the samples using in an aggressive environment, months								
	1	6	12	1	6	12	1	6	12
Control	0.84	0.78	**0.72**	0.78	0.73	**0.68**	0.85	0.80	**0.74**
Impregnated with the sol SiO_2	0.97	0.95	**0.92**	0.95	0.90	**0.87**	0.98	0.97	**0.94**

At the second stage, the time of preservation of the achieved level of physical and mechanical properties of high strength concrete is estimated. For this purpose the calculations of the destruction depth of the synthesized concrete in the time *h*, in accordance with the existing formula (3) was made. The calculation showed that at the age of 50 years, the corrosion depth does not exceed 0.74 cm, which is 8 times lower than the allowable corrosion depth of concrete at the age of 50 years in accordance with the building codes. This ensures the preservation of the achieved level of operational properties of concrete in time, Table 8.

$$h=(k \cdot t^{0.5}-\alpha)/(S \cdot P^1_{CaO}) \qquad (3)$$

where k – the experimental coefficient, determined by preliminary tests;

t – the time for which the depth of destruction (days) is forecasted;

α – the correction factor taking into account that the initial period of corrosion passes through a diffusion-kinetic mechanism;

S – the consumption of cement in concrete, kg/m^3;

P^1_{CaO} – the content of CaO in cement, %.

Table 8 The results of the calculation of the corrosion depth of concrete after surface hardening with the Sol of SiO_2

Age of concrete, years	Corrosion depth of concrete impregnated with Sol, cm
10	0.3
20	0.45
30	0.57
40	0.67
50	0.74

On the basis of obtained results it can be concluded that the forecast expressed previously have been confirmed, and the developed technology allows to obtain such solid phases in the strengthened surface layer of concrete, which have lower values of the Gibbs energy. These phases have increased strength and hardness and lead to the formation of inorganic high-strength clip. It improves the physico-mechanical characteristics of concrete up to 200 %, and allows to preserve them in time.

The proposed technology of concrete surface hardening allows to obtain high-strength concrete. In comparison with other methods of hardening, for example, the use of pozzolanic additives or changes in concrete hardening conditions [29, 30], the efficiency is much higher (the compressive strength increases by 78 %). But other high-strength concrete, do not have high hardness, corrosion resistance, etc.

4. Conclusions

1. This paper proposes the method to improve the quality of concrete at the expense of its surface hardening by impregnating with an inorganic Sol of SiO_2 with the creation of a monolithic inorganic high-strength clips.

2. It is shown that under the action of load P the redistribution of the gains in the sol strengthen sample between the clip and the hardened core takes place: $N_{cl} = 0.35\ R$, $N_{core} = 0.65\ R$; the presence of the clip provides an increase in strength of the entire sample up to 50 %.

3. For the first time we have developed a mathematical dependence, allowing to calculate the strength of the concrete sample in the monolithic inorganic clip depending on the cross-sectional form of the sample, the number of Sol-impregnate faces and the ratio of the height of the sample to its width.

4. It is determined that the surface strengthening of concrete with a Sol of SiO_2 results in the creation of a high strength layer. The basis of the layer consists of the low-basic hydrosilicates with lower values of the Gibbs energy, ΔG^0_{298}, kJ/mol and with high values of strength and hardness.

5. It is stated that the surface strengthening technology allows to improve the physical-mechanical properties of concrete such as compressive strength, and tensile strength in bending, frost resistance, hardness, abrasion resistance, water absorption, water resistance up to 200 %.

6. It is shown that the technology of surface hardening of concrete leads to the formation of corrosion-protective barrier, which greatly increases the resistance of concrete to various aggressive environments, the corrosion depth of concrete not exceeding 0.74 cm for 50 years.

References

1. Ibragimov R.A., Pimenov S.I. Influence of mechanochemical activation on the features in the of hydration of cement. *Magazine of Civil Engineering*. 2016. No. 2. Pp. 3–12. doi: 10.5862/MCE.62.1 (rus)
2. Hameed A.H. Effect of superplasticizer dosage on workability of self-compact concrete. *Diyala Journal of Engineering Sciences.* 2012. Vol. 05. No. 02. Pp. 66–81.
3. Naydenov Yu.A., Veprinyak I.A. Innovatsionnaya tekhnologiya aktivirovaniya betonov, osnovannaya na yavlenii kavitatsii [Innovative technology of concrete activation, based on the phenomenon of cavitation]. *Nauka XXI veka.* 2013. No. 4. Pp. 12–15. (rus)
4. Bids V.A., Sir E.A., Kutugin V.A. Physical and chemical processes in the activation of cement-sand mixture in a centrifugal mixer. *Proceedings of the universities. Physics.* 2011. No. 11/3. Pp. 346–349.
5. Bogdanov R.R., Ibragimov R.A. Process of hydration and structure formation of the modified self-compacting concrete. *Magazine of Civil Engineering.* 2017. No. 5. Pp. 14–24. doi: 10.18720/MCE.73.2.
6. Gayfullin A.R., Rakhimov R.Z., Rakhimova N.R. Vliyaniye dobavok glinitov v portlandtsement na prochnost pri szhatii tsementnogo kamnya [The effect of clay additives in Portland cement on the compressive strength of cement stone]. *Magazine of Civil Engineering.* 2015. No. 7(59). Pp. 66–73.(rus)
7. Sychova A.M., Svatovskaya L.B., Mjakin S.V., Vasiljeva I.V. Modification of fillers for cements. *Book Chapter Electron Beam Modification of Solids: Mechanisms, Common Features and Promising Applications*. 2009. Pp. 35–37.
8. Vatin N.I., Barabanshikov Yu.G., Komarinsky M.V., Smirnov S.I. Modifikatsiya litoy betonnoy smesi vozdukhovovlekayushchey dobavkoy [Modification of cast concrete mix by air-entraining admixture]. *Magazine of Civil Engineering.* 2015. No. 04(56). Pp. 3–10.(rus)
9. Taheri Fard A.R., Soheili H., Ramzani Movafagh S., Farnood Ahmadi P. Combined Effect of Glass Fiber and Polypropylene Fiber On Mechanical Properties of Self-

Литература

1. Ибрагимов Р.А., Пименов С.И. Влияние механохимической активации на особенности процессов гидратации цемента // Инженерно-строительный журнал. 2016. № 2(62). С. 3–12.
2. Hameed A.H. Effect of superplasticizer dosage on workability of self-compact concrete // Diyala Journal of Engineering Sciences. 2012. Vol. 05. No. 02. Pp. 66–81.
3. Найденов Ю.А., Веприняк И.А. Инновационная технология активирования бетонов, основанная на явлении кавитации // Наука XXI века. 2013. № 4. С. 12–15.
4. Bids V.A., Sir E.A., Kutugin V.A. Physical and chemical processes in the activation of cement-sand mixture in a centrifugal mixer // Proceedings of the universities. Physics. 2011. No. 11/3. Pp. 346–349.
5. Богданов Р.Р., Ибрагимов Р.А. Процессы гидратации и структурообразования модифицированного самоуплотняющегося бетона // Инженерно-строительный журнал. 2017. № 5(73). С. 14–24.
6. Гайфуллин А.Р., Рахимов Р.З., Рахимова Н.Р. Влияние добавок глинитов в портландцемент на прочность при сжатии цементного камня// Инженерно-строительный журнал. 2015. № 7(59). С. 66–73.
7. Sychova A.M., Svatovskaya L.B., Mjakin S.V., Vasiljeva I.V. Modification of fillers for cements // Book Chapter Electron Beam Modification of Solids: Mechanisms, Common Features and Promising Applications. 2009. Pp. 35–37.
8. Ватин Н.И., Барабанщиков Ю.Г., Смирнов С.И. Модификация литой бетонной смеси воздухововлекающей добавкой//Инженерно-строительный журнал. 2015. № 04(56). С. 3–10.
9. Тахери Фард А.Р., Сохели Х., Рамзани Мовафах С., Фарнуд Ахмади П. Совместное действие стеклянной и полипропиленовой фибры на механические свойства самоуплотняющихся бетонов // Инженерно-строительный журнал. 2016. № 2(62). С. 26–31
10. Низина Т.А., Балыков А.С., Володин В.В., Коровкин Д.И. Дисперсно-армированные мелкозернистые

Compacting Concrete. *Magazine of Civil Engineering*. 2016. No. 2. Pp. 26–31. doi: 10.5862/MCE.62.3

10. Nizina T.A., Balykov A.S., Volodin V.V., Korovkin D.I. Disperse-reinforced fine-grained concrete with a polyfunctional modifying additives. *Magazine of Civil Engineering.* 2017. No. 4(72). Pp. 73–83.(rus)
11. Boikova T., Solovyov D., Solovyova V. Concrete For Road Pavements. *Procedia Engineering.* 2017. Vol. 189. Pp. 800–804.
12. Nazari A., Riahi S. TiO2 nanoparticles effects on physical, thermal and mechanical properties of self compacting concrete with ground granulated blast furnace slag as binder. *Energy and Buildings.* 2011. Vol. 43. Pp. 995–1002.
13. Nazari A., Riahi S. Al2O3 nanoparticles in concrete and different curing media. *Energy and Buildings.* 2011. Vol. 43. Pp. 1480–1488.
14. Nazari A., Riahi S. Splitting tensile strength of concrete using ground granulated blast furnace slag and SiO2 nanoparticles as binder. *Energy and Buildings.* 2011. Vol. 43. Pp. 864–872.
15. Nazari A., Riahi S. Abrasion resistance of concrete containing SiO2 and Al2O3 nanoparticles in different curing media. *Energy and Buildings.* 2011. Vol. 43. Pp. 2939–2946.
16. Riahi S., Nazari A. Physical, mechanical and thermal properties of concrete in different curing media containing ZnO2 nanoparticles. *Energy and Buildings*. 2011. Vol. 43, Pp. 1977–1984.
17. Boostani H., Modirrousta S. Review of Nanocoatings for Building Application. *Procedia Engineering.* 2016. Vol. 145, Pp. 1541–1548.
18. Zhu W., Bartos P.J.M., Porro A. Application of nanotechnology in construction. *Materials and Structures.* 2004. No. 37(9), Pp. 649–658.
19. Shakhmenko G., Juhnevica I., Korjakins A. Influence of Sol-Gel Nanosilica on Hardening Processes and Physically-Mechanical Properties of Cement Paste. *Procedia Engineering.* 2013. Vol. 57. Pp. 1013–1021.
20. Teryanik V.V., Biryukov A.Yu., Borisov A.O., Shipanov R.V. Novyye konstruktivnyye resheniya usileniya szhatykh elementov oboymami [New design solutions for strengthening compressed elements with clips]. *The housing construction.* 2009. No. 7. Pp. 8–9. (rus)
21. Podnebesov P.G., Teryanik V.V. Vnetsentrenno szhatyye kolonny, usilennyye oboymami iz samouplotnyayushchegosya stalefibrobetona [Extra-compressed columns reinforced with clips of self-compacting steel-fiber concrete]. *The Concrete and reinforced concrete.* 2015. No. 3. Pp. 7–10. (rus)
22. Svatovskaya L., Sychova A., Sychov M., Okrepilov V. Quality Improvement of Concrete Articles. *MATEC Web of Conferences* 2016. 53.01024. DOI: 10/1051/matecconf/20165301024.
23. Babushkin V.I., Matveyev G.M., Mchedlov-Petrosyan O.P. *Termodinamika silikatov* [Thermodynamics of silicates] Moscow: Stroyizdat, 1986. 408 p. (rus)
24. Svatovskaya L.B., Solovyeva V.Ya. i dr. *Termodinamicheskiye i elektronnyye aspekty svoystv kompozitsionnykh materialov dlya stroitelstva i ekozashchity* [Thermodynamic and electronic aspects of the properties of composite materials for construction and environmental protection] Saint-Petersburg.: Stroyizdat, 2004. 174 p. (rus)
25. Gorshkov V.S., Timashev V.V., Savelyev V.G. *Metody fiziko-khimicheskogo analiza vyazhushchikh veshchestv* [Methods of physical and chemical analysis of binders]. Moscow: The higher school, 1981. 336 p. (rus)
26. Klueva N, Emelyanov S, Kolchunov V, Maria Gubanova. Criterion of Crack Resistance of Corrosion Damaged

бетоны с полифункциональными модифицирующими добавками // Инженерно-строительный журнал. 2017. № 4(72). С. 73–83.

11. Boikova T., Solovyova D., Solovyova V. Concrete For Road Pavements // Procedia Engineering. 2017. Vol. 189. Pp. 800–804.
12. Nazari A., Riahi S. TiO2 nanoparticles effects on physical, thermal and mechanical properties of self compacting concrete with ground granulated blast furnace slag as binder // Energy and Buildings. 2011. Vol. 43. Pp. 995–1002.
13. Nazari A., Riahi S. Al2O3 nanoparticles in concrete and different curing media // Energy and Buildings. 2011. Vol. 43. Pp. 1480–1488.
14. Nazari A., Riahi S. Splitting tensile strength of concrete using ground granulated blast furnace slag and SiO2 nanoparticles as binder // Energy and Buildings. 2011. Vol. 43. Pp. 864–872.
15. Nazari A., Riahi S. Abrasion resistance of concrete containing SiO2 and Al2O3 nanoparticles in different curing media // Energy and Buildings. 2011. Vol. 43. Pp. 2939–2946.
16. Riahi S., Nazari A. Physical, mechanical and thermal properties of concrete in different curing media containing ZnO2 nanoparticles // Energy and Buildings. 2011. Vol. 43. Pp. 1977–1984.
17. Boostani H., Modirrousta S. Review of Nanocoatings for Building Application // Procedia Engineering. 2016. Vol. 145. Pp. 1541–1548.
18. Zhu W., Bartos P.J.M., Porro A., Application of nanotechnology in construction // Materials and Structures. 2004. No. 37(9). Pp. 649–658.
19. Shakhmenko G., Juhnevica I., Korjakins A. Influence of Sol-Gel Nanosilica on Hardening Processes and Physically-Mechanical Properties of Cement Paste // Procedia Engineering. 2013. Vol. 57. Pp. 1013–1021.
20. Теряник В.В., Бирюков А.Ю., Борисов А.О., Щипанов Р.В. Новые конструктивные решения усиления сжатых элементов обоймами // Жилищное строительство. 2009. № 7. С. 8–9.
21. Поднебесов П.Г., Теряник В.В. Внецентренно сжатые колонны, усиленные обоймами из самоуплотняющегося сталефибробетона // Бетон и железобетон. 2015. № 3. С. 7–10.
22. Svatovskaya L., Sychova A., Sychov M., Okrepilov V. Quality Improvement of Concrete Articles // MATEC Web of Conferences 53.01024. 2016. DOI: 10/1051/matecconf/20165301024.
23. Бабушкин В.И., Матвеев Г.М., Мчедлов-Петросян О.П. Термодинамика силикатов. М.: Стройиздат, 1986. 408 с.
24. Сватовская Л.Б., Соловьева В.Я. и др. Термодинамические и электронные аспекты свойств композиционных материалов для строительства и экозащиты. СПб.: Стройиздат, 2004. 174 с.
25. Горшков В.С., Тимашев В.В., Савельев В.Г. Методы физико-химического анализа вяжущих веществ. М.: Высшая школа, 1981. 336 с.
26. Klueva N, Emelyanov S, Kolchunov V, Maria Gubanova. Criterion of Crack Resistance of Corrosion Damaged Concrete in Plane Stress State // Procedia Engineering. 2015. Vol. 117. Pp. 179–185.
27. Eskandari H., Mozafari Nic A., Ghanei A. Effect of Air Entraining Admixture on Corrosion of Reinforced Concrete // Procedia Engineering. 2016. Vol. 150. Pp. 2178–2184.
28. Sulikowskia J., Kozubal J. The Durability of a Concrete Sewer Pipeline Under Deterioration by Sulphate and Chloride Corrosion // Procedia Engineering. 2016. Vol. 153. Pp. 698–705.

Concrete in Plane Stress State. *Procedia Engineering*. 2015. Vol. 117. Pp. 179–185.

27. Eskandaria H., Mozafari Nicb A., Ghaneia A. Effect of Air Entraining Admixture on Corrosion of Reinforced Concrete. *Procedia Engineering.* 2016. Vol. 150. Pp. 2178–2184.
28. Sulikowskia J., Kozubal J. The Durability of a Concrete Sewer Pipeline Under Deterioration by Sulphate and Chloride Corrosion. *Procedia Engineering.* 2016. Vol. 153. Pp. 698–705.
29. Sumrerng R., Prinya C. Use of ternary blend of Portland cement and two pozzolans to improve durability of high-strength concrete. *KSCE Journal of Civil Engineering.* 2014. Vol. 18. Pp. 1745–1752.
30. Fanghui H., Zengqi Z. Hydration, mechanical properties and durability of high-strength concrete under different curing conditions. *Journal of Thermal Analysis and Calorimetry.* 2018. Vol. 132. Pp. 823–834.

29. Sumrerng R., Prinya C. Use of ternary blend of Portland cement and two pozzolans to improve durability of high-strength concrete // KSCE Journal of Civil Engineering. 2014. Vol. 18. Pp.1745–1752.
30. Fanghui H., Zengqi Z. Hydration, mechanical properties and durability of high-strength concrete under different curing conditions // Journal of Thermal Analysis and Calorimetry. 2018. Vol. 132. Pp. 823–834.

Anastasia Sychova,
+7(921)857-22-17; amsychova@yandex.ru

Larisa Svatovskaya,
+7(911)919-54-84; lbsvatovskaya@yandex.ru

Dmitriy Starchukov,
+7(904)519-85-43; starchukov@mail.ru

Valentina Soloviova,
+7(921)353-05-07; 9046185117@mail.ru

Marina Gravit,
+7(912)912-64-07; marina.gravit@mail.ru

Анастасия Максимовна Сычева,
+7(921)857-22-17;
эл.почта: amsychova@yandex.ru

Лариса Борисовна Сватовская,
+7(911)919-54-84;
эл. почта: lbsvatovskaya@yandex.ru

Дмитрий Сергеевич Старчуков,
+7(904)519-85-43; эл. почта:
starchukov@mail.ru

Валентина Яковлевна Соловьева,
+7(921)353-05-07;
эл. почта: 9046185117@mail.ru

Марина Викторовна Гравит,
+7(912)912-64-07;
эл. почта: marina.gravit@mail.ru

doi: 10.18720/MCE.80.2

Mechanical properties of synthetic fibers applied to concrete reinforcement

Механические свойства синтетических волокон для армирования бетона

A.I. Kirsanov*,
O.N. Stolyarov,
Peter the Great St. Petersburg Polytechnic University, St. Petersburg, Russia.

Студент А.И. Кирсанов*,
канд. техн. наук, доцент О.Н. Столяров,
Санкт-Петербургский политехнический университет Петра Великого, Санкт-Петербург, Россия

Key words: fiber reinforcement; polymeric fiber; creep; uni-axial strength; mechanical properties

Ключевые слова: армирование волокнами; полимерное волокно; ползучесть; прочность; механические свойства

Abstract. Short synthetic fibers are increasingly used for reinforcing of cement-based composites along with metallic and inorganic fibers. In this work, the mechanical properties of short polypropylene fibers with different structures were investigated. The main characteristics, including tensile strength, Young's modulus, strain at maximum load, and work of rupture were determined. In addition, fiber samples were examined for creep at various loading levels up to 50 % of the tensile strength. Relationship between the creep strain rate and applied stress for the fiber samples was determined. The results obtained can be used for selection the synthetic fibers for the reinforcement of cement-based composites.

Аннотация. Короткие синтетические волокна приобретают всё большое распространение для армирования бетона наряду с металлическими и неорганическими волокнами. В данной работе исследованы механические свойства коротких полипропиленовых волокон различного строения. Определены основные характеристики, включая прочность при растяжении, удлинение при максимальной нагрузке, работа разрыва и модуль упругости. Кроме того, образцы волокон исследованы на ползучесть при различных уровнях нагружения до 50 % от прочности при растяжении. Для образцов волокна была выведена зависимость между скоростью ползучести и приложенной нагрузкой. Полученные результаты могут быть использованы при выборе армирующих волокон для бетона.

1. Introduction

The development of structural cement composites reinforced with short fibers has been the focus of many studies in the last three decades [1–9]. This is mainly due to a significant improvement in the mechanical properties of concrete composites. The combination of short fiber reinforcement and the concrete matrix has led to the formation of fiber-reinforced concrete (FRC). FRC finds different applications in civil engineering, ranging from architectural elements to precast structural elements. Synthetic fibers may replace the conventional steel bar reinforcement, or along with it. The main advantage of FRC is the control of concrete cracking, the weight reduction of the building structure and the consumption of conventional steel reinforcement. It also significantly minimized the need for concrete, improves ductility, impact resistance, and increases the durability, which helps to reduce the amount of harmful emissions during its manufacture.

Various short fibers made of different raw materials have been employed for concrete composites. These short fibers include metal fibers, glass fiber, natural fibers and synthetic fibers [10]. Metal fibers are usually made of steel [11]. Their main undoubted advantage is the high Young's modulus of around 210 GPa. The main disadvantage is their low corrosion resistance, as well as for traditional steel reinforcement. Inorganic fibers mainly include glass and basalt fibers containing in their structure special additives (for example, zirconium dioxide ZrO_2), which leads to a significant increase in resistance to aggressive environment [12]. In practice, some manufacturers produce special types of alkali-resistant fibers (AR glass fibers), designed specially for reinforcing concrete. Natural fibers include sisal, jute, hemp, etc. [13]. Their main advantage is low cost. However, the main drawback is high water absorption and low biological stability. Another type of fiber used in reinforcing concrete is synthetic fibers. The variety of properties of the synthetic polymers makes it possible to obtain fibers with different properties. Many types of synthetic fibers, such as polypropylene (PP), polyethylene (PE), polyvinylalcohol (PVA), etc., are used to reinforce concrete. The mechanical properties of fibers depend on the material, density, length, length-to-diameter ratio, fiber shape, etc.

The reinforcing mechanism of a fiber in a concrete matrix is very different from a polymer matrix because of the brittleness of the concrete. In polymer composites, the matrix is usually more ductile than fiber. Therefore, in concrete composites, the matrix is destroyed before the strength properties of the fiber can be realized. Thus, fiber reinforcement becomes effective mainly after the crack of the matrix. The main characteristics influenced by the addition of short fibers to concrete are impact strength, fracture toughness, fatigue strength, dynamic strength, tensile strength [14–16]. In addition, short fibers are used as a supplement to conventional steel reinforcement to prevent cracking and improve resistance to degradation of properties resulting from fatigue, impact, shrinkage and thermal stress [17, 18]. To increase the work of rupture or toughness of concrete structures, metal fibers are used, while synthetic fibers are more often used to reduce crack opening during shrinkage [3, 19]. However, the equal amount of steel and synthetic fibers did not lead to the same results in toughness. In [3], the influence of steel and synthetic fibres on the flexural and compressive performance of FRC was investigated. It was found that that the steel fibres reinforcement increased the compressive strength by about 4 and 5 MPa while the synthetic fibres increased it only by 2–3 MPa. According to other studies, the effect of synthetic fibers on the toughness is comparable to steel fibers [4]. Cifuentes et al found that synthetic PP fibers in FRC slightly increased the mechanical properties, but greatly increased its fracture behaviour and ductility [20]. Freitas et al found that the presence of a short randomly oriented polypropylene fiber (1.7 % by volume) leads to a decrease in compressive strength and modulus of elasticity by 20 % and 15 %, respectively [21]. In [22], fiber-reinforced concrete samples with addition of steel, polypropylene, polyolefin fibers were investigated. The addition of fibers had no any considerable effect on compressive strength of the FRC. However, the properties of fibers affected on reducing the cracking width. The steel fibers showed the best performance due to their hook-shaped tail compared to PP fibers.

Considering the properties of fibers, one should especially highlight their viscoelastic behavior, which is common for polymer materials [23–25]. Since synthetic fibers are a polymer material, creep deformation is observed when constant load is applied to the samples. This phenomenon has been extensively studied in fiber-reinforced concrete samples by many authors [26–31]. The viscoelastic properties of the fibers and their effect on structural properties of FRC have been only investigated in a small number of works [32–35]. However, the viscoelastic properties of the fibers used for reinforcing concrete can have a significant effect on the mechanical performance of FRC. Vrijdaghs et al [32] evaluated the creep of two types of PP fibers with a length of 45 mm and diameter of 0.90 and 0.95 mm. To determine the Young's modulus and the maximum tensile load, tensile tests were carried out. In creep test, the load levels of 22, 36, 43, 53, 63 % of the maximum tensile strength were applied to the samples. It was shown that the load level influences the time to failure. They also concluded that creep deformation can play an important role in the total crack width growth in FRC elements. In [33], viscoelastic properties of concrete reinforced with synthetic PP macrofiber were considered. The individual fiber was tested for creep. For a four-day period, a constant load of 30 % of the average tensile strength of fibers was applied to the sample. It was found that synthetic fibres showed significant tensile creep at the load level of 30% and higher. The crack widening in FRC under loading has two mechanisms: time-dependent fibre pull-out and time-dependent fibre creep. Zhao et al [36] studied the effect of the fiber type (Steel, PP, PVA, basalt) on the creep of FRC. It was concluded that the Young's modulus of the added fiber exerts the greatest influence on the creep of the samples: if it is higher than the Young's modulus of the concrete, then creep resistance decreases, if lower then increases.

This work aims to study the mechanical and creep properties of macro PP fibers applied to concrete reinforcement. The objective of this work included:

1. evaluate mechanical properties of PP synthetic fibers with different configurations;
2. study the creep of PP fibers at different load levels;
3. establish the relationship between the fiber configuration and their mechanical properties.

2. Methods and materials

2.1. Materials

In this work, macro PP fibers with different configuration (fiber geometries) were studied. Generally, two types of fiber configurations including crimped (wave shaped) and surface intended geometries were selected for this study. This modification along the fiber length significantly improves the bond characteristics. Synthetic fibers for concrete reinforcement is shown in Figure 1a. Close view with magnification of 45× of two different types of synthetic fibers with different configurations is shown in Figure 1b. The upper picture denotes the fiber with surface intended geometry and the lower picture denotes the fiber with crimped geometry. Both considered fiber types had elliptical cross-sectional geometry. The characteristic of the investigated PP fiber samples are listed in Table 1. These two types of PP fibers are dominated in the market of FRC.

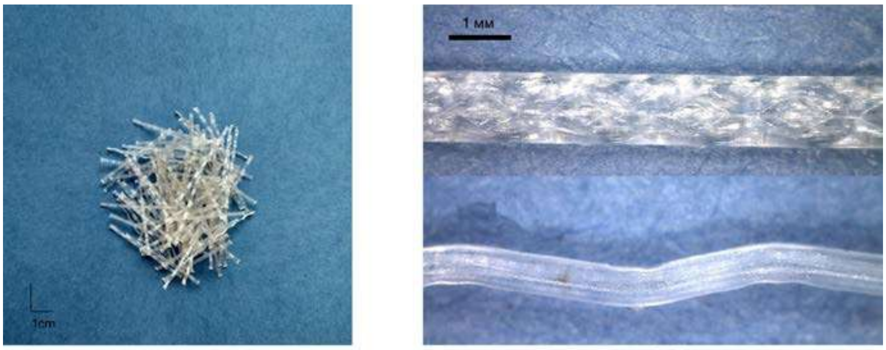

(a) (b)

Figure 1. Synthetic fibers for concrete reinforcement (a) and view with magnification of 45× (b)

Table 1. Properties of PP fibres

Sample designation	Fibres Length, mm	Cross-sectional area, mm2	Linear density, tex	Fiber configuration
#1	53	0.8	610	surface intended
#2	37	0.72	590	crimped
#3	46	0.54	510	surface intended
#4	37	0.66	600	crimped

2.2. Methods

2.2.1. Tensile test

Computer controlled electronic universal testing machine Instron 5965 was used in this work. This machine enables for conducting tension, bending, and compression testing of various materials. The short PP fibers were tested in uniaxial tensile test. Samples of short fibers for tensile testing were prepared according to following method. The free ends of the fiber specimen were clamped to a special paper frame as shown in Figure 2. The fixing of the fiber end was ensured by applying glue. Then, specimens were left until tensile testing. Five specimens were tested for each type of PP fiber. The fiber specimens were tested with a test speed of 10 mm/min and a gauge length of 20 mm. The tensile strength (σ_{max}), strain at maximum load, Young's modulus and work of rupture (also called *toughness)* were determined from the stress-strain curves.

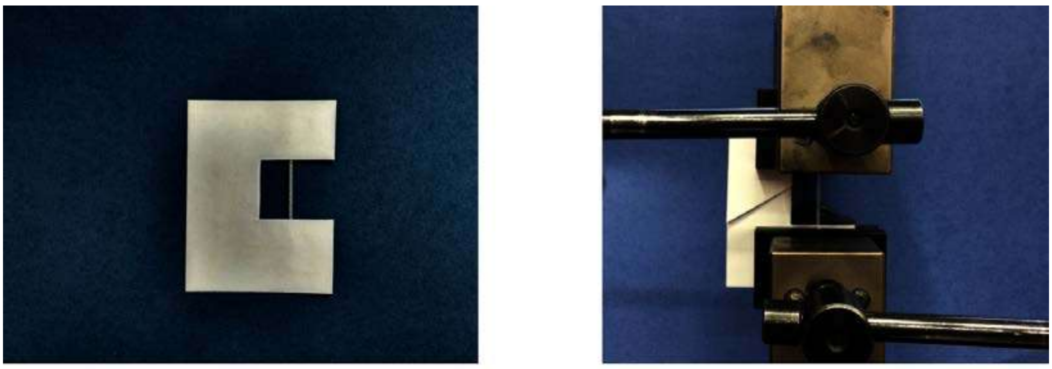

(a) (b)

Figure 2. Fiber in a paper frame for tensile testing (a) and uni-axial tensile test (b)

2.2.2. Creep test

The creep test was performed on an Instron 5965 tensile machine. The creep behaviour of fibre samples was performed at different levels of loading up to 50 % of the tensile strength with the step of 10 %. Preparation of specimens for creep test was done similar as for tensile tests described above.

3. Results and Discussion

3.1. Tensile properties of the fiber samples

The stress-strain curves obtained from all the studied fiber samples are shown in Figure 3. As can be seen from these curves, the fiber samples have a different curve type. Mechanical behavior differs significantly for different fiber types. The tensile characteristics of fiber samples were determined from the stress-strain curves. These characteristics were plotted as histograms and are shown in Figure 4.

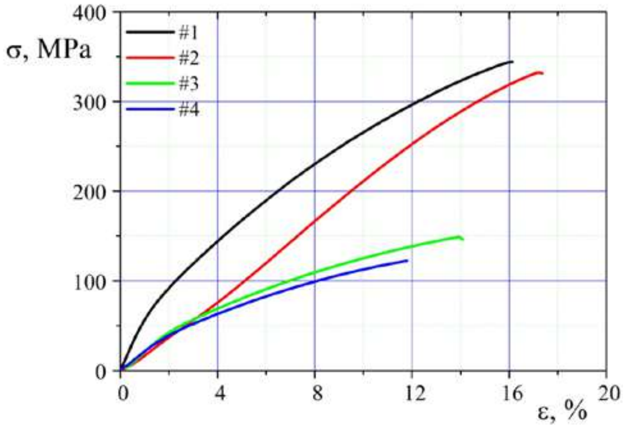

Figure 3. Stress-strain curves of PP fiber samples

The tensile strength of fibers differs more than twice and does not depend on the fiber type. The fiber samples of the first group, both with an intended surface (#1) and crimped surface (#2), showed a maximum tensile strength of about 350 MPa. However, the Young's modulus for these two fiber samples varies substantially, i.e. it differs by a factor of ~ 3. This is clearly demonstrated by the slope of the initial part of the stress-strain curve. The lower values of the Young's modulus of fiber sample #2 are affected by the structure of the fiber geometry. The fiber with crimped geometry shows a lower value of the Young's modulus; since to remove the crimp some additional work is necessary. The fibers of the second group #3 and #4 have a lower strength compared to values of fiber samples #1 and #2. In this case, the tensile strength and Young's modulus values were similar for both fiber samples.

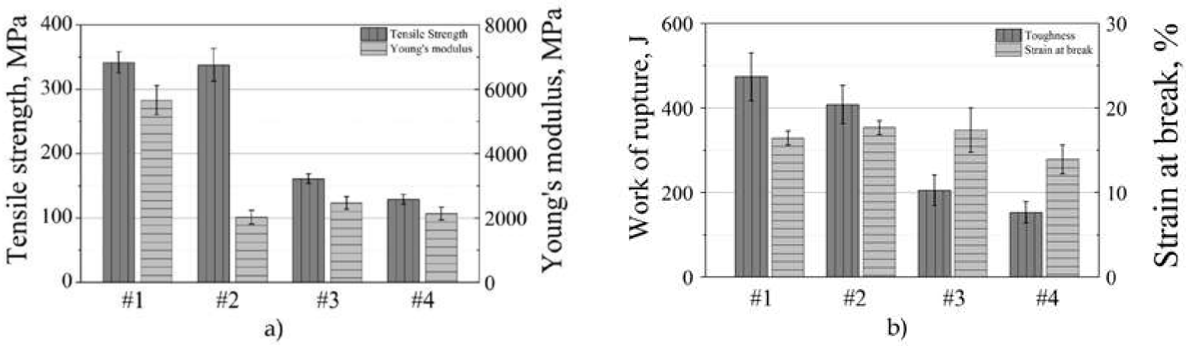

Figure 4. Tensile properties of PP fiber sample, including 95% confidence interval

Analyzing the obtained data on mechanical characteristics, it should be noted that the characteristics of the fibers are in similar ranges obtained by other authors. According to [37], tensile strength of the PP fiber varies from 310 to 760 MPa and Young's modulus – from 3.5 to 4.9 GPa. In [20], studied PP fibers with different properties have the tensile strength in the range from 288 to 450 MPa. In work [4] tensile strength and Young's modulus values of selected PP fibers were 640 MPa and 10 GPa, respectively. Another important mechanical characteristic of fibers for reinforcing concrete is plastic deformation and work of rupture. These characteristics determine the ability of the PP fibers and, consequently, of concrete to resist prolonged plastic deformation. This also provides a large residual load-bearing capacity of the concrete elements. Analyzing the data presented in Figure 4b, we can conclude that the obtained values of the characteristics of plasticity strongly depend on the work factor of the tensile diagram and values of the tensile strength. For the first group of fibers #1 and #2 with higher characteristics, the plasticity are higher in comparison to that of the samples #3 and #4. This fact will ensure a longer work of the fiber in concrete and, as a consequence, its plasticity. The magnitude of the work of rupture decreases proportionally with decreasing their tensile strength.

To conclude, the mechanical characteristics of synthetic fibers used for concrete reinforcement differ significantly. The fibers studied in this paper represent the optimal sample for a range of properties in terms of tensile strength, Young's modulus, strain at break and work of rupture among all typical reinforcing short fibers for concrete.

3.2. Creep behaviour of the fiber samples

When performing creep tests, the loading levels of the PP fibers are of particular interest. Creep tests are generally performed at the load levels up to 50% of the maximum tensile strength. If we compare loading levels with other researchers, then we can note that they lie approximately in the same range. Only the load step is varied. For example, in [32] the load levels were chosen at 22, 36, 43, 53 and 63 % of σ_{max}, then in [35] these steps were equal to 25, 40, 50, 60 and 75% of σ_{max}. The load levels, which are more than half of the tensile strength, lead to a sharp increase in the creep rate, which does not quite objectively reflect the real properties of the synthetic fibers for creep. Load levels from 60 to 90% are usually used in creep rupture test. Therefore, when planning the experiment, loads of up to 50% of the maximum load were applied with the step of 10 %. This approach makes it possible to perform comparative analysis for different fibers at the same relative loading levels.

The creep curves obtained for PP fiber samples #1, #2, #3, #4 are shown in Figure 5a, b, c, d, respectively. As can be seen from the presented curves, all the samples have exceptional viscoelastic properties, which manifest themselves in a significant increase in the creep strain with an increase in the level of the applied load. This behavior is typical for all synthetic fibers, including PP fibers for reinforcing concrete [32, 35]. The slope of the creep curve determines the creep rate. As can be seen for all the curves, the creep strain rate starts to grow already at a level of 20–30 % of σ_{max}. At a load level of 50 % of σ_{max}, the creep rate increases significantly. In practice, this means that the fiber does not exist for an arbitrarily long time to sustain such deformation. In order to compare the different fiber samples, the values of strain rate were plotted against the applied load as shown in Figure 6. These curves show a change in the creep rate with increasing applied load. A greater slope of the curve indicates a worse creep resistance of the PP fiber.

Relationship between the creep strain rate and applied stress for the fiber samples #1 #4 are given in equations 1-4 respectively.

$$\dot{\varepsilon} = \left(-42.59 + 7.23\sigma_{\max}^{\%}\right)\cdot 10^{-8} \quad (1)$$

$$\dot{\varepsilon} = \left(28.20 + 5.75\sigma_{\max}^{\%}\right)\cdot 10^{-8} \quad (2)$$

$$\dot{\varepsilon} = \left(-116.16 + 13.03\sigma_{\max}^{\%}\right)\cdot 10^{-8} \quad (3)$$

$$\dot{\varepsilon} = \left(-91.50 + 8.59\sigma_{\max}^{\%}\right)\cdot 10^{-8} \quad (4)$$

As can be seen from Figure 6, the curves of fiber samples #1 and #2 have the smallest slope as expected. However, fiber sample #2 demonstrates less stability in creep rate than sample #1. Although the slope of its curve is the lowest, the initial creep at a level of 10 of σ_{max} here is much higher than for the other three samples. Thus, the positive effect of a smaller angle of slope here is not determined by greater initial creep. At the structural level, this can be explained by crimp removal behavior of the fiber.

The practical application of the equations has two aspects. First, the comparative analysis of short reinforcing fibers of different structures can be made from the obtained coefficient. The selected fiber type based on this comparison will show a more stable behavior to load resistance already directly in the fiber reinforced concrete. This is very important, for example, with the ability of the stretched fiber to maintain the concrete when broken. Secondly, these equations allow us to determine the allowable stresses applied to the PP fiber.

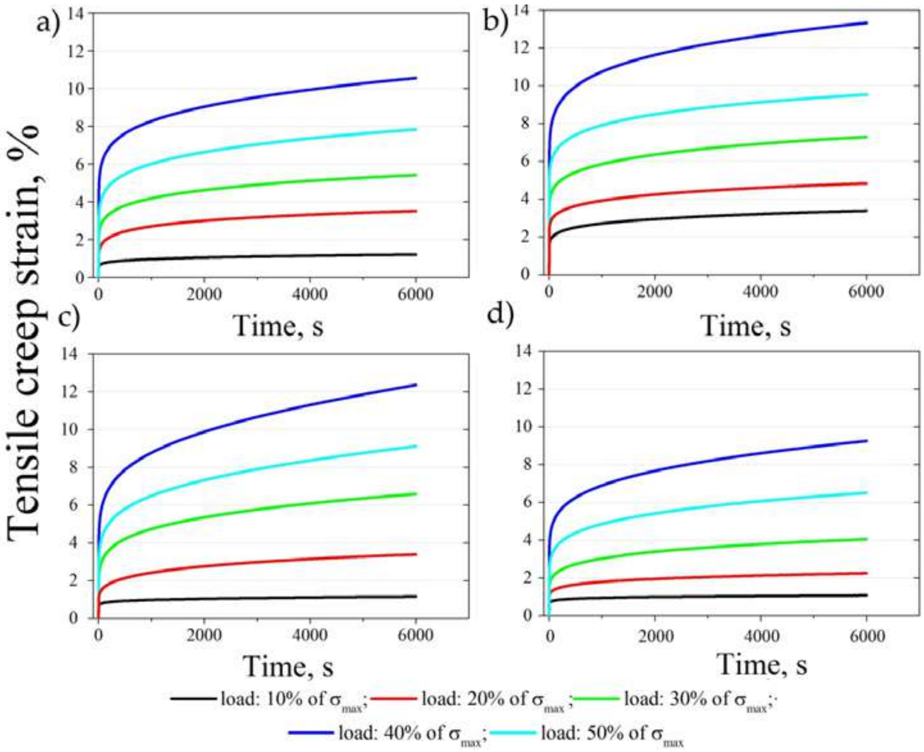

Figure 5. Creep curves of PP fiber samples at the temperature 20 ºC and the indicated assigned loads

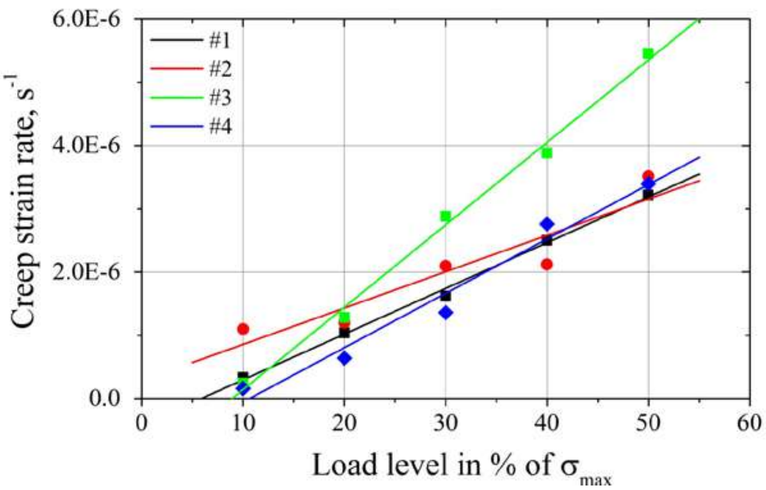

Figure 6. Creep strain rate vs. load level of PP fiber samples

4. Conclusions

In this paper, four different types of PP short fibers having different configurations and mechanical characteristics were investigated. The mechanical characteristics including tensile strength, Young's modulus, strain at maximum load and rupture work were determined. The results showed that the mechanical characteristics of the reinforcing PP fibers are dependent on their structure and the fiber geometry. According to the results obtained, the fiber samples can be divided into two groups, including PP fibers with a minimum tensile strength range (~150 MPa) and an average tensile strength range (~350–400 MPa). Moreover, it was shown that configuration of the fiber is not a key factor in determining the tensile strength parameters of the fiber. The characteristics of the fibers in the creep tests were also examined at different load levels up to 50 % of σ_{max}. It was shown that the creep rate increases substantially with increasing level of the applied load. For fibers with higher strength, the creep rate is not as high as for fibers with lower strength. Summarizing the results, the relationship between configuration of the fibers and their mechanical properties was established.

5. Acknowledgment

The work was funded by RFBR according to the research project no.16-08-00845.

References

1. Yoo D.-Y., Yoon Y.-S. A review on structural behavior, design, and application of ultra-high-performance fiber-reinforced concrete. *International Journal of Concrete Structures and Materials.* 2016. No. 10(2). Pp. 125–142.
2. Cascardi A., Longo F., Micelli F., Aiello M.A. Compressive strength of confined column with Fiber Reinforced Mortar (FRM): New design-oriented-models. *Construction and Building Materials*. 2017. No. 156. Pp. 387–401.
3. Soutsos M.N., Le T.T., Lampropoulos A.P. Flexural performance of fibre reinforced concrete made with steel and synthetic fibres. *Construction and Building Materials*. 2012. No. 36. Pp. 704–710.
4. Alani A.M., Beckett D. Mechanical properties of a large scale synthetic fibre reinforced concrete ground slab. *Construction and Building Materials*. 2013. No. 41. Pp. 335–344.
5. Morozov V.I., Pukharenko Yu.V. Effektivnost primeneniya fibrobetona v konstruktsiyakh pri dinamicheskikh vozdeystviyakh [Efficiency of using fiber-reinforced concrete in structures under dynamic loads]. *Vestnik MGSU*. 2014. No. 3. Pp. 189–196. (rus)
6. Pukharenko Yu.V. Restavratsiya i stroitelstvo: potentsial fibroarmirovannykh materialov i izdeliy [Restoration and constructing: the potential of fiber-reinforced materials and products]. *Sovremennyye problemy nauki i obrazovaniya*. 2012. No. 4. Pp. 359. (rus)
7. Golovanov V.I., Novikov N.S., Pavlov V.V., Antonov S.P. Prochnostnyye kharakteristiki fibrobetona dlya tonnelnykh sooruzheniy v usloviyakh vysokikh temperatur [Strength properties of fiber-reinforced concrete applied to tunnel constructions in high-temperature conditions]. *Pozhary i chrezvychaynyye situatsii: predotvrashcheniye, likvidatsiya.* 2017. No. 2. Pp. 63–67. (rus)
8. Klyuyev S.V. Vysokoprochnyy fibrobeton dlya promyshlennogo i grazhdanskogo stroitelstva [High-strength fiber-reinforced concrete for industrial and civil engineering]. *Magazine of Civil Engineering*. 2012. No. 8 (34). Pp. 61–66. (rus)
9. Klyuyev S.V., Klyuyev A.V., Sopin D.M., Netrebenko A.V., Kazlitin S.A. Tyazhelonagruzhennyye poly na osnove melkozernistykh fibrobetonov [Heavy loaded floors based on fine-grained fiber-reinforced concrete]. *Magazine of Civil Engineering*. 2013. No. 3 (38). Pp. 7–14. (rus)
10. Zollo R.F. Fiber-reinforced concrete: An overview after 30 years of development. *Cement and Concrete Composites*. 1997. No. 19(2). Pp. 107–122.
11. Brandt A.M. Fibre reinforced cement-based (FRC) composites after over 40 years of development in building and civil engineering. *Composite Structures*. 2008. No. 86(1-3). Pp. 3–9.
12. Sim J., Park C., Moon D.Y. Characteristics of basalt fiber as a strengthening material for concrete structures. *Composites Part B: Engineering.* 2005. No. 36(6-7). Pp. 504–512.
13. Aziz M.A., Paramasivam P., Lee S.L. Prospects for natural fibre reinforced concretes in construction. International *Journal of Cement Composites and Lightweight Concrete*. 1981. No. 3(2). Pp. 123–132.
14. Nizina T.A., Balykov A.S. Experimental-statistical models of the properties of modified dispersed-reinforced fine-grained concrete. *Magazine of Civil Engineering*. 2016. No. 2(62). Pp. 13–26. (rus)
15. Nikolenko S.D., Sushko E.A., Sazonova S.A., Odnolko A.A., Manokhin V.Ya. Behaviour of concrete with a

Литература

1. Yoo D.-Y., Yoon Y.-S. A review on structural behavior, design, and application of ultra-high-performance fiber-reinforced concrete // International Journal of Concrete Structures and Materials. 2016. № 10(2). Pp. 125–142.
2. Cascardi A., Longo F., Micelli F., Aiello M.A. Compressive strength of confined column with Fiber Reinforced Mortar (FRM): New design-oriented-models // Construction and Building Materials. 2017. № 156. Pp. 387–401.
3. Soutsos M.N., Le T.T., Lampropoulos A.P. Flexural performance of fibre reinforced concrete made with steel and synthetic fibres // Construction and Building Materials. 2012. № 36. Pp. 704–710.
4. Alani A.M., Beckett D. Mechanical properties of a large scale synthetic fibre reinforced concrete ground slab // Construction and Building Materials. 2013. № 41. Pp. 335–344.
5. Морозов В.И., Пухаренко Ю.В. Эффективность применения фибробетона в конструкциях при динамических воздействиях // Вестник МГСУ. 2014. № 3. С. 189–196.
6. Пухаренко Ю.В. Реставрация и строительство: потенциал фиброармированных материалов и изделий // Современные проблемы науки и образования. 2012. № 4. С. 359.
7. Голованов В.И., Новиков Н.С., Павлов В.В., Антонов С.П. Прочностные характеристики фибробетона для тоннельных сооружений в условиях высоких температур // Пожары и чрезвычайные ситуации: предотвращение, ликвидация. 2017. № 2. С. 63–67.
8. Клюев С.В. Высокопрочный фибробетон для промышленного и гражданского строительства // Инженерно-строительный журнал. 2012. № 8(34). С. 61–66.
9. Клюев С.В., Клюев А.В., Сопин Д.М., Нетребенко А.В., Казлитин С.А. Тяжелонагруженные полы на основе мелкозернистых фибробетонов // Инженерно-строительный журнал. 2013. № 3(38). С. 7–14.
10. Zollo R.F. Fiber-reinforced concrete: An overview after 30 2018s of development // Cement and Concrete Composites. 1997. № 19(2). Pp. 107–122.
11. Brandt A.M. Fibre reinforced cement-based (FRC) composites after over 40 2018s of development in building and civil engineering // Composite Structures. 2008. № 86(1-3). Pp. 3–9.
12. Sim J., Park C., Moon D.Y. Characteristics of basalt fiber as a strengthening material for concrete structures // Composites Part B: Engineering. 2005. № 36 (6-7). Pp. 504–512.
13. Aziz M.A., Paramasivam P., Lee S.L. Prospects for natural fibre reinforced concretes in construction // International Journal of Cement Composites and Lightweight Concrete. 1981. № 3(2). Pp. 123–132.
14. Низина Т.А., Балыков А.С. Экспериментально-статистические модели свойств модифицированных дисперсно-армированных мелкозернистых бетонов // Инженерно-строительный журнал. 2016. № 2(62). С. 13–26.
15. Николенко С.Д., Сушко Е.А., Сазонова С.А., Однолько А.А., Манохин В.Я. Поведение бетона с дисперсным армированием при динамических воздействиях // Инженерно-строительный журнал. 2017. № 7(75). С. 3–14.
16. Taheri Fard A.R., Soheili H., Ramzani Movafagh S., Farnood Ahmadi P. Combined effect of glass fiber and

disperse reinforcement under dynamic loads. *Magazine of Civil Engineering.* 2017. No. 7. Pp. 3–14.

16. Taheri Fard A.R., Soheili H., Ramzani Movafagh S., Farnood Ahmadi P. Combined effect of glass fiber and polypropylene fiber on mechanical properties of self-compacting concrete. *Construction and Building Materials*. 2016. No. 2. Pp. 26–31.
17. Korsun V., Vatin N., Franchi A., Korsun A., Crespi P., Mashtaler S. The strength and strain of high-strength concrete elements with confinement and steel fiber reinforcement including the conditions of the effect of elevated temperatures. *Procedia Engineering*. 2015. No. 117(1). Pp. 975–984.
18. Travush V.I., Konin D.V., Krylov A.S. Strength of reinforced concrete beams of high-performance concrete and fiber reinforced concrete. *Magazine of Civil Engineering.* 2018. No. 1. Pp. 90–100.
19. Buratti N., Mazzotti C., Savoia M. Post-cracking behaviour of steel and macro-synthetic fibre-reinforced concretes. *Construction and Building Materials.* 2011. No. 25. Pp. 2713–2722.
20. Cifuentes H., García F., Maeso O., Medina F. Influence of the properties of polypropylene fibres on the fracture behaviour of low-, normal- and high-strength FRC. *Construction and Building Materials.* 2013. No. 45. Pp. 130–137.
21. De Freitas I., Darwish F., Pereira M.V., Allende K. Fracture behavior of polymeric fiber reinforced lightweight structural concrete. *Materials Research*. 2014. No. 17(6). Pp. 1588–1593.
22. Yousefieh N., Joshaghani A., Hajibandeh E., Shekarchi M. Influence of fibers on drying shrinkage in restrained concrete. *Construction and Building Materials.* 2017. No. 148. Pp. 833–845.
23. Nikolayeva I.P., Ogorodov L.I., Krasikov S.V. Polzuchest polietilena vysokoy prochnosti pri razlichnykh rezhimakh nagruzheniya [The creep of high density polyethylene at various loading conditions]. *Construction of Unique Buildings and Structures.* 2014. No. 12(27). Pp. 49–63. (rus)
24. Nikolayeva I.P., Ogorodov L.I., Yakovleva Ye.L. Creep polytetrafluoroethylene modifications under various loading conditions. *Construction of Unique Buildings and Structures.* 2017. No. 3(54). Pp. 7–17. (rus)
25. Alekseyev N.N., Kovalenko I.A., Stolyarov O.N., Melnikov B.Ye. [Viscoelastic properties of geosynthetic materials. *Construction of Unique Buildings and Structures*. 2017. No. 5(56). Pp. 17–32. (rus)
26. Zhao G., di Prisco M., Vandewalle L. Experimental investigation on uniaxial tensile creep behavior of cracked steel fiber reinforced concrete. *Materials and Structures.* 2015. No. 48(10). Pp. 3173–3185.
27. Gettu R., Zerbino R., Jose S. Factors influencing creep of cracked fibre reinforced concrete: What we think we know and what we do not know. *RILEM Bookseries*. 2017. No. 14. Pp. 3–12.
28. García-Taengua E., Arango S., Martí-Vargas J.R., Serna P. Flexural creep of steel fiber reinforced concrete in the cracked state. *Construction and Building Materials*. 2014. No. 65. Pp. 321–329.
29. Blyszko J. Comparative analysis of creep in standard and fibre reinforced concretes under different load conditions. *Procedia Engineering*. 2017. No. 193. Pp. 478–485.
30. Bywalski C., Kamiński M., Maszczak M., Balbus L. Influence of steel fibres addition on mechanical and selected rheological properties of steel fibre high-strength reinforced concrete. *Archives of Civil and Mechanical Engineering*. 2015. No. 15. Pp. 742–750.
31. Pujadas P., Blanco A., Cavalaro S., de la Fuente A., Aguado A. The need to consider flexural post-cracking creep behavior of macro-synthetic fiber reinforced

polypropylene fiber on mechanical properties of self-compacting concrete // Construction and Building Materials. 2016. № 2. Pp. 26–31.

17. Korsun V., Vatin N., Franchi A., Korsun A., Crespi P., Mashtaler S. The strength and strain of high-strength concrete elements with confinement and steel fiber reinforcement including the conditions of the effect of elevated temperatures // Procedia Engineering. 2015. № 117(1). Pp. 975–984.
18. Травуш В.И., Конин Д.В., Крылов А.С. Прочность железобетонных балок из высокопрочных бетонов и фибробетонов // Инженерно-строительный журнал. 2018. № 1(77). С. 90–100.
19. Buratti N., Mazzotti C., Savoia M. Post-cracking behaviour of steel and macro-synthetic fibre-reinforced concretes // Construction and Building Materials. 2011. № 25. Pp. 2713–2722.
20. Cifuentes H., García F., Maeso O., Medina F. Influence of the properties of polypropylene fibres on the fracture behaviour of low-, normal- and high-strength FRC // Construction and Building Materials. 2013. № 45. Pp. 130–137.
21. De Freitas I., Darwish F., Pereira M.V., Allende K. Fracture behavior of polymeric fiber reinforced lightweight structural concrete // Materials Research. 2014. № 17(6). Pp. 1588–1593.
22. Yousefieh N., Joshaghani A., Hajibandeh E., Shekarchi M. Influence of fibers on drying shrinkage in restrained concrete // Construction and Building Materials. 2017. № 148. Pp. 833–845.
23. Николаева И.П., Огородов Л.И., Красиков С.В. Ползучесть полиэтилена высокой прочности при различных режимах нагружения // Строительство уникальных зданий и сооружений. 2014. № 12(27). С. 49–63.
24. Николаева И.П., Огородов Л.И., Яковлева Е.Л. Ползучесть модификаций политетрафторэтилена при различных режимах нагружения // Строительство уникальных зданий и сооружений. 2017. № 3(54). С. 7–17.
25. Алексеев Н.Н., Коваленко И.А., Столяров О.Н., Мельников Б.Е. Вязкоупругие свойства геосинтетических материалов // Строительство уникальных зданий и сооружений. 2017. № 5(56). С. 17–32.
26. Zhao G., di Prisco M., Vandewalle L. Experimental investigation on uniaxial tensile creep behavior of cracked steel fiber reinforced concrete // Materials and Structures. 2015. № 48(10). Pp. 3173–3185.
27. Gettu R., Zerbino R., Jose S. Factors influencing creep of cracked fibre reinforced concrete: What we think we know and what we do not know // RILEM Bookseries. 2017. № 14. Pp. 3–12.
28. García-Taengua E., Arango S., Martí-Vargas J.R., Serna P. Flexural creep of steel fiber reinforced concrete in the cracked state // Construction and Building Materials. 2014. № 65. Pp. 321–329.
29. Blyszko J. Comparative analysis of creep in standard and fibre reinforced concretes under different load conditions // Procedia Engineering. 2017. № 193. Pp. 478–485.
30. Bywalski C., Kamiński M., Maszczak M., Balbus L. Influence of steel fibres addition on mechanical and selected rheological properties of steel fibre high-strength reinforced concrete // Archives of Civil and Mechanical Engineering. 2015. № 15. Pp. 742–750.
31. Pujadas P., Blanco A., Cavalaro S., de la Fuente A., Aguado A. The need to consider flexural post-cracking creep behavior of macro-synthetic fiber reinforced concrete // Construction and Building Materials. 2017. № 149. Pp. 790–800.
32. Vrijdaghs R., di Prisco M., Vandewalle L. Creep

concrete. *Construction and Building Materials*. 2017. No. 149. Pp. 790–800.
32. Vrijdaghs R., di Prisco M., Vandewalle L. Creep deformations of structural polymeric macrofibers. *RILEM Bookseries*. 2017. No. 14. Pp. 53–61.
33. Babafemi A.J., Boshoff W.P. Tensile creep of macro-synthetic fibre reinforced concrete (MSFRC) under uni-axial tensile loading. *Cement and Concrete Composites*. 2015. No. 55. Pp. 62–69.
34. Nieuwoudt P.D., Boshoff W.P. Time-dependent pull-out behaviour of hooked-end steel fibres in concrete. *Cement and Concrete Composites.* 2017. No. 79. Pp. 133–147.
35. Vrijdaghs R., di Prisco M., Vandewalle L. Short-term and creep pull-out behavior of polypropylene macrofibers at varying embedded lengths and angles from a concrete matrix*. Construction and Building Materials.* 2017. No. 147. Pp. 858–864.
36. Zhao Q., Yu J., Geng G., Jiang J., Liu X. Effect of fiber types on creep behavior of concrete. *Construction and Building Materials.* 2016. No. 105. Pp. 416–422.
37. Löfgren I. *Fibre-reinforced concrete for industrial construction. Department of Civil and Environmental Engineering, Structural engineering.* Chalmers University of Technology. Göteborg, Sweden. 2005. 276 p.

deformations of structural polymeric macrofibers // RILEM Bookseries. 2017. № 14. Pp. 53–61.
33. Babafemi A.J., Boshoff W.P. Tensile creep of macro-synthetic fibre reinforced concrete (MSFRC) under uni-axial tensile loading // Cement and Concrete Composites. 2015. № 55. Pp. 62–69.
34. Nieuwoudt P.D., Boshoff W.P. Time-dependent pull-out behaviour of hooked-end steel fibres in concrete // Cement and Concrete Composites. 2017. № 79. Pp. 133–147.
35. Vrijdaghs R., di Prisco M., Vandewalle L. Short-term and creep pull-out behavior of polypropylene macrofibers at varying embedded lengths and angles from a concrete matrix // Construction and Building Materials. 2017. № 147. Pp. 858–864.
36. Zhao Q., Yu J., Geng G., Jiang J., Liu X. Effect of fiber types on creep behavior of concrete // Construction and Building Materials. 2016. № 105. Pp. 416–422.
37. Löfgren I. Fibre-reinforced concrete for industrial construction. Department of Civil and Environmental Engineering, Structural engineering. Chalmers University of Technology. Göteborg, Sweden. 2005. 276 p.

Andrey Kirsanov,*
+7(921)323-66-43; kirsanov.ai@edu.spbstu.ru

Oleg Stolyarov,
+7(812)552-63-03; oleg.stolyarov@rambler.ru

Андрей Игоревич Кирсанов,*
+7(921)323-66-43;
эл. почта: kirsanov.ai@edu.spbstu.ru

Олег Николаевич Столяров,
+7(812)552-63-03;
эл. почта: oleg.stolyarov@rambler.ru

doi: 10.18720/MCE.80.3

Influence of the compensating device parameters on the underwater pipeline stability

Влияние параметров компенсирующего устройства на устойчивость подводного трубопровода

K.V. Kozhaeva,
Ufa State Petroleum Technological University, Ufa, Russia

Канд. техн. наук, старший преподаватель К.В. Кожаева,
Уфимский государственный нефтяной технический университет, Уфа, Россия

Key words: experiment; compensating device; rational parameters; correction coefficient of the compensator form; ensuring the pipeline stability

Ключевые слова: эксперимент; компенсирующее устройство; рациональные параметры; коэффициент уточнения формы компенсатора; обеспечение устойчивости трубопровода

Abstract. The definition of rational parameters of the developed compensating device of a triangular shape by calculation and experimental investigation methods is considered in the article. The proposed compensating device with the bent taps use has a more rigid design than the compensating device in the form of a broken bolt. Consequently, the correction coefficient of the compensator form, structurally executed with the use of bent taps is received by calculation and experimental methods for decreasing the longitudinal compressive force arising from the temperature drop to the ensuring level of the overall pipeline stability in the longitudinal direction, which allows to determine its rational parameters and is taken to be k = 0.85. The condition is obtained for determining the rational parameters of the proposed compensating device for underwater pipeline transitions in order to increase the overall stability in the longitudinal direction. In addition, the patented technology of laying the proposed compensating device is shown.

Аннотация. В статье рассматривается определение рациональных параметров разработанного компенсирующего устройства треугольной формы с помощью расчетно-экспериментальных методов исследования. Предлагаемое компенсирующее устройство с применением гнутых отводов обладает более жесткой конструкцией, чем компенсирующее устройство в виде ломаного ригеля. Поэтому расчетно-экспериментальным методом получен коэффициент уточнения формы компенсатора, конструктивно выполненного с применением гнутых отводов, для снижения продольного сжимающего усилия, возникающего от температурного перепада, до уровня обеспечения общей устойчивости трубопровода в продольном направлении, который позволяет определить его рациональные параметры, и принимается равным k = 0,85. Получено условие для определения рациональных параметров предлагаемого компенсирующего устройства для подводных переходов трубопроводов с целью повышения общей устойчивости в продольном направлении. Также приведена запатентованная технология укладки предлагаемого компенсирующего устройства.

1. Introduction

The stabilization loss of the underwater pipelines sections position leads to emergencies and the removal of the pipeline from service. In most cases, the stabilization loss of the pipeline (including arched emissions) occurs due to the action of compressive longitudinal forces, which must be prevented or reduced [1–7].

The analysis of foreign works devoted to ensuring the stability and reliability of pipelines, including submarine ones, prove the relevance of the solved problems not only in Russia [8–21].

In the Russian regulatory documents, the calculation of the underwater pipeline for longitudinal stability is not carried out, albeit these calculations are needed abroad. This fact is confirmed also by the authors of the works [22, 23]. Indeed, at present time, most underwater pipelines operate at significant positive temperature changes, which causes large compressive longitudinal forces that can lead to the pipeline from a stable state. In the work [23], the authors focus on the calculation of the operational reliability

Кожаева К.В. Влияние параметров компенсирующего устройства на устойчивость подводного трубопровода // Инженерно-строительный журнал. 2018. № 4(80). С. 24–36.

of a gas underwater pipeline in which a loss of longitudinal stability occurred. This is very important, since the pipeline, which lost its longitudinal stability, is primarily susceptible to destruction. The following issues are considered in detail in the article:

– who dealt with the issues of ensuring the longitudinal stability of pipelines;
– what methods determine the critical longitudinal force and possible loss forms of the pipeline stability;
– a comprehensive assessment of the technical condition of the gas pipeline sections based on numerical methods;
– reliability analysis of underwater pipelines based on traditional methods of structural mechanics, as well as the finite element method;
– assessment of the pipeline reliability with arched ejection under the random weight load influence from the backfill ground, as well as random operational loads, using the probabilistic estimation method.

The methods of ensuring the spatial gas pipeline stability on the watered sections of the route were considered in detail in [24, 25], taking into account the influence of variable ground conditions (water saturation, ultimate shear resistance and cohesion). The authors considered the gas pipeline section on which the design position loss of the pipeline in the arch form due to high water and also the temperature increase of the transported product - gas. According to the approach proposed by the authors, the main provisions of the methodology and the procedure for calculating additional ballasting of the adjacent areas were developed. As a result, there is a reduction in possible displacements in the central region. The proposed methodology is applicable both in the operation period and in major overhaul of pipelines and for newly laid gas pipelines. Calculation of this method on real objects showed the decrease in the final longitudinal force at the beginning of the adjoined section with additional ballasting in 2,625 times (from 0.42 MN to 0.16 MN). Thereby ballasting of adjoined section reduces the ultimate longitudinal force effect due to the temperature expansion of the pipeline material in the central region and therefore ensures the design position stability of this main gas pipeline section.

However, such pipelines ballasting can lead to additional large costs. Therefore, there is a need to look for an alternative way with minimum costs and maximum reliability. Consider the same adjoined area, but instead of ballasting, it will be equipped with a compensator. There are divergent views and evidence in that regard. In the article [26], the authors considered the stress-strain state modeling of the underground pipelines sections, which consist of a concave or convex insert curve with a curved hollow rod in an elastic medium. The calculations made by the authors confirm the conclusions of the accidents acts that the insert curves are stress concentrators in the gas pipeline. Calculations also allow identifying the physical picture of the insert curve deformation at the stresses concentration in it and highlighting its main parameters, by increasing the insertion curve length and reducing its curvature, the insert will be experienced excessively large bending deformations in the restrained part.

In the articles [27, 28], it was considered how the moist ground degree of adjoined underground areas will affect the underwater gas pipelines stress-strain state. The authors made the following conclusions: when calculating underwater sections of a gas pipeline and also strength and stability evaluating, it is necessary to take into account the internal working pressure effect, the temperature stresses on the pipeline bend and the grounds condition, which adjoin the regions with their properties changes within one year. When constructing subsea gas pipelines, it is necessary to provide for the compensator installation at one end of the underwater transition in the soil of the adjoined regions. In order to reduce the resistance of the pipe movement principle, it is necessary to fill the underground compensators with a soft loosened soil during their laying in mineral grounds. Since the defective properties of the moist ground covers are high, in the flood period the compensator stabilizes the pipeline location and ensures its durability, stability and reliability in operation.

Thereby, it is possible to provide a general stability in the longitudinal direction of the underwater pipeline transition with the compensator installed on an adjoined area to the underwater transition region. As such a design, there is a compensating device for a pipeline, which the calculations and experimental studies are given below [29, 30].

2. Methods

2.1. The experiment planning and modeling

To increase the overall the pipeline stability in the longitudinal direction, it is proposed to reduce the equivalent axial compressive force by installation a compensating device on the adjoined section of the underwater pipeline.

The solution of the problem is to determine the rational compensator parameters with reduction the longitudinal compressive force to a safe level at a specified N_{cr}, an internal pressure p and temperature difference Δt.

The most appropriate for the underwater main pipeline section is the triangular shape of the compensating device, where the straight parts connection of the compensator are carried out by cold bending diversions ensuring the transition of inside pipe devices and instruments.

The trench for laying the compensator should be prepared taking into account the free compensator movement and then backfilling features, thereby reducing the longitudinal force (Figure 1).

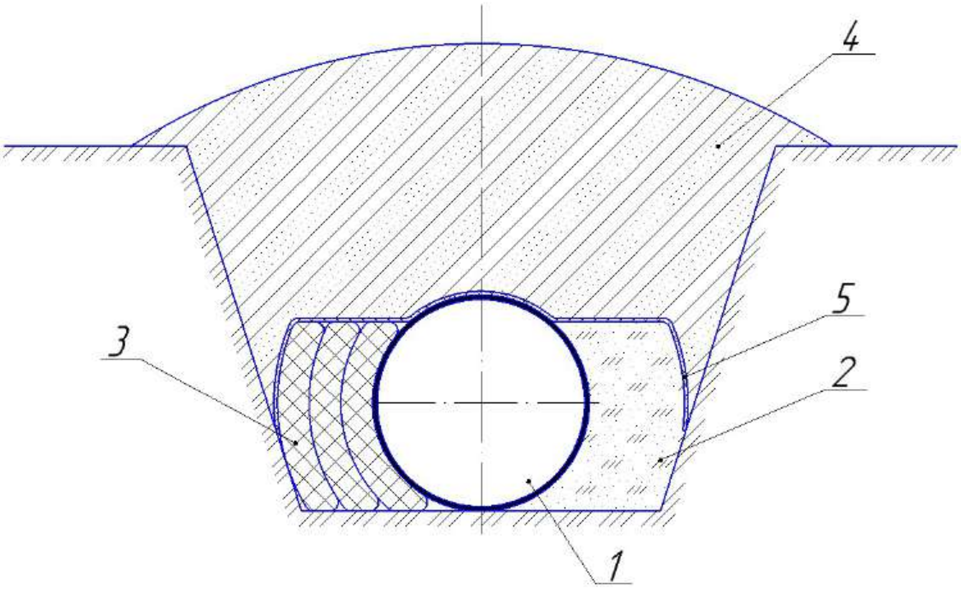

Figure 1. Preparation features and trenches backfilling with the compensator: 1 – compensator; 2 – elastic strain ground; 3 – elastic strain parts; 4 – mineral ground back-filling; 5 – cushioning material

The free pipeline movement into the trench and the natural longitudinal movement compensation of the compensator 1 occur after elastic strain ground 2 back-filling or elastic strain parts 3 installation. It is also necessary to lay the cushioning material 5 along the entire length of the compensator 1 to prevent the mineral ground back-filling 4 between the elastic strain parts 3 or mixing the mineral ground back-filling 4 and the elastic strain ground 2. The cushioning material 5 is a polymeric tape (for example, rubber, polyethylene, polypropylene, polyvinyl chloride), recycled metal cord conveyor belt. The remaining trench volume covers by the mineral ground back-filling 4.

The elastic strain parts 3 are bags or containers of various geometric shapes and sizes depending on the pipeline diameter and the construction area filled with chips of non-pressed fiberglass materials or foam propylene, foam and other elastic strain materials that withstand up to 2 t/m^2 of ground with deformation up to 5–10% from the maximum deformation potential. A peat can be used as an elastic strain ground.

According to the Figure 2, longitudinal compressive force quantity S in the underwater transition will depend on the compensator parameters: length l и deflection f.

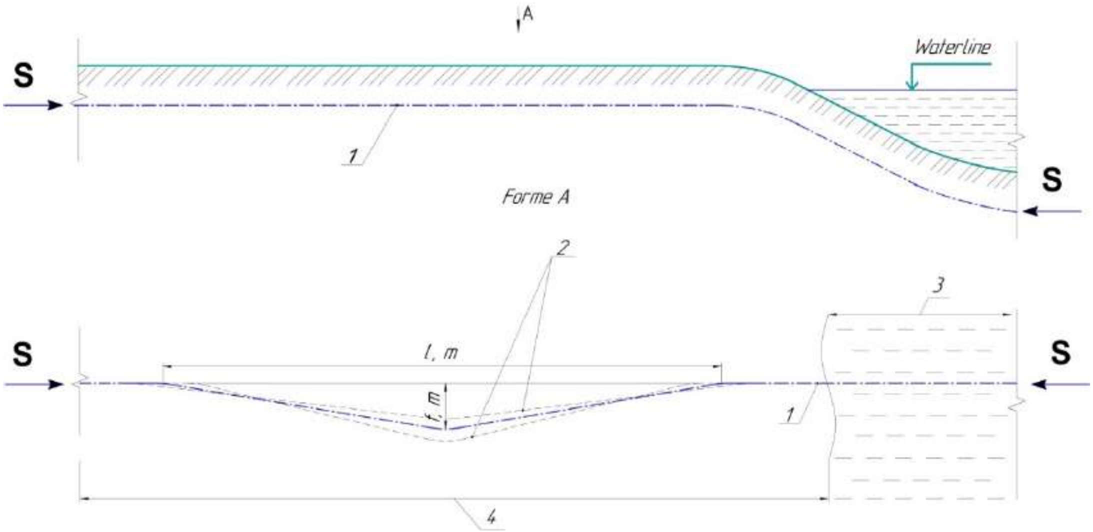

Figure 2. Underwater pipeline transition with a compensating device on an adjoined area: 1 – pipeline axis; 2 – possible compensator axis movements; 3 – underwater area; 4 – the adjoined compensator area of a triangular shape

The selection of the compensator parameters in the form of "snake" (Figure 3) and their calculation are considered in detail in [31]. The value of the equivalent longitudinal axial force S taking into account the longitudinal displacements compensation caused by the temperature change the pipe walls and internal pressure is determined by the formula (1):

$$S = \frac{3 \cdot cos\varphi \cdot I \cdot (\alpha \cdot E \cdot \Delta t + 0{,}2 \cdot \sigma_{an})}{f^2}, \quad (1)$$

where φ– the angle taken from the condition of the cleaning device pass, deg.;

I – inertia moment of the pipe cross-section, m^4;

α – temperature coefficient of linear expansion of the pipe metal, 1/°C;

E – modulus of elasticity of the pipeline metal, Pa;

Δt –positive temperature difference, °C;

σ_{an} – annular stresses in the pipe wall from the calculated internal pressure, Pa;

f – compensator deflection, m.

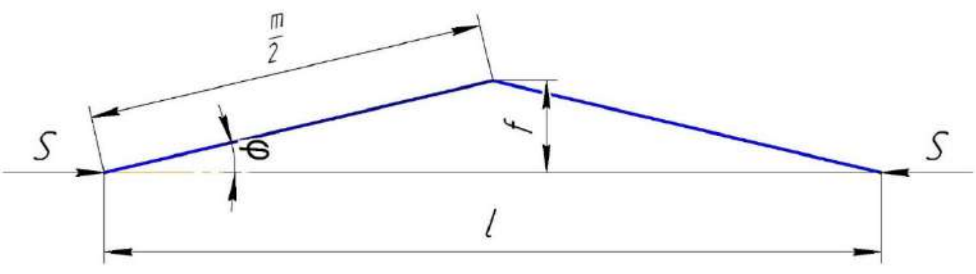

Figure 3 - Calculation scheme of the half-wave length «snake»: l –compensator length; f – compensator deflection; m – length of the compensator's arm

The described investigations in [31] and analysis of the expression (1) demonstrate that for the small deflection values f longitudinal force S reaches significant quantity. Thus, for small values of f compensating ability of the compensator (i.e., the ability to reduce the longitudinal force) is insignificant. The increase f leads to a monotone decrease S and the compensating ability growth.

In order to ensure the overall longitudinal stability of the underwater pipeline with the compensator application, the condition should be observed (2).

$$S \leq N_{cr}, \tag{2}$$

where N_{cr}– critical longitudinal compressive force, N.

Using the relation of $cos\varphi = \frac{l}{m}$, the condition (2) will have the form (3).

$$\left(\frac{l}{f}\right)^2 \cdot \frac{3 \cdot I}{m \cdot l} \leq \frac{N_{cr}}{\alpha \cdot E \cdot \Delta t + 0{,}2 \cdot \sigma_{an}}. \tag{3}$$

The condition (3) allows to take the geometric parameters of the compensator, based on the value of the critical force N_{cr}, temperature difference and operating pressure.

The analysis of the calculation procedure of the researched design according to [31] (Figure 3) demonstrates that the pipes connection at the top of the rotation angle, where the maximum deflection f, is made without the bends use. On the compensator boundaries, the pipelines are connected rectilinearly without the rotation angle. The proposed compensator construction at the top of the rotation angle and at the ends has a welded pipes connection with bends use. These design differences introduce some variation in the quantity of longitudinal force S. To determine the amount changes, the studies have been undertaken.

Therefore, the experiment purpose is the determination the amount changes in the longitudinal force of the compensating device according to the invention with bends use from a previously known compensating device structurally designed as a broken bolt.

When testing theoretical dependencies and the general revealing of the system's operation nature under load, there is not necessary to address the issue of the transition conditions from model to nature. In these cases, it is recommended to calculate the actual model and then compare the theoretical results with the appropriate experimental data.

When choosing the parameters of the physical model, it is necessary to take into account the condition (4):

$$\begin{gathered} \frac{3 \cdot E \cdot I \cdot \alpha \cdot \Delta t \cdot cos\varphi}{f^2} < N_0, \\ \frac{3 \cdot I \cdot cos\varphi}{f^2} < F, \end{gathered} \tag{4}$$

where N_0 – longitudinal force from the temperature difference for the straight pipeline sections, N; $N_0 = \alpha \cdot E \cdot \Delta t \cdot F.$

The basis on recommendations [31], conditions (4), and also taking into account the clearance conditions and diagnostics (radius bends is not less than $5 \cdot D_{out}$, where D_{out} – the outside pipeline diameter), the following parameters of the physical model of the compensating device have been taken: pipe diameter – 25 mm, wall thickness – 2 mm, and a length of 2.05 m will be consistent with deflections from 0.02 to 0.08 m. Maximum temperature difference $\Delta t = 50℃$ is chosen, based on actual and often encountered operating conditions.

The measured longitudinal force from the pipeline elongation caused by the change in the pipe walls temperature must be compared with the design force determined by formula (5):

$$S_d = \frac{3 \cdot E \cdot I \cdot \alpha \cdot \Delta t \cdot cos\varphi}{f^2}. \tag{5}$$

2.2. Description of the experimental setup

On a metal sheet – foundation 1 lenght 2.5 m and width 0.5 m support elements 2 are placed on which the compensator 3 is installed (Figure 4).

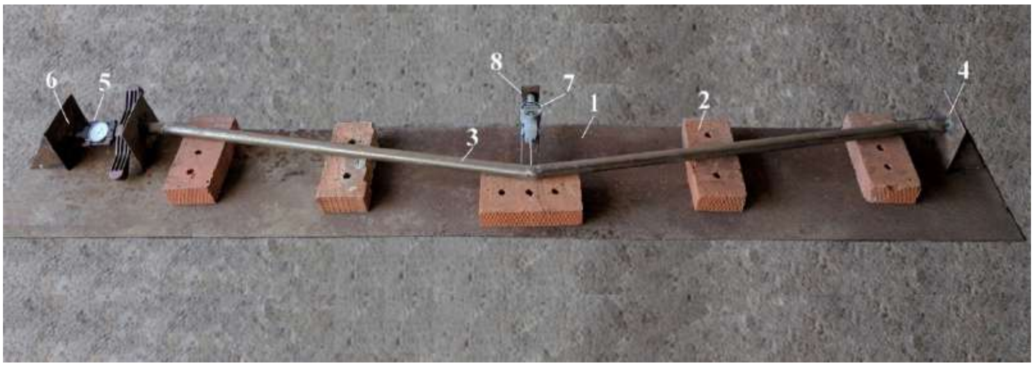

Figure 4. Elements of the experimental setup:

1 – metal foundation; 2 – support elements; 3 – compensator; 4 – displacement tether; 5 – compression dynamometer; 6 – dynamometer fastening system; 7 – displacement indicator; 8 – fastening system of displacement indicator

This is done that the pipe is prevented from making contact with the metal base during the study, since when the pipe is heated, the sheet may become deformed due to heating, which will give an error in the measurements.

Also, in order to rigidly fix the pipe during the experiment, it is necessary to provide displacement tether 4 which are also made of metal plates and welded to the base 1.

To fix the dynamometer 5 reliably during the experiment, we make a special fastening system 6, which consists of a nut and threaded stud. In the displacement tether, a hole is made, where a nut is then fastened.

The displacement indicator 7 is fixed by a clamp on a welded structure (the fastening system of displacement indicator 8) and is in contact with the compensator so that during the pipe heating the displacement measurement occurs.

The experimental setup scheme is shown in Figure 5.

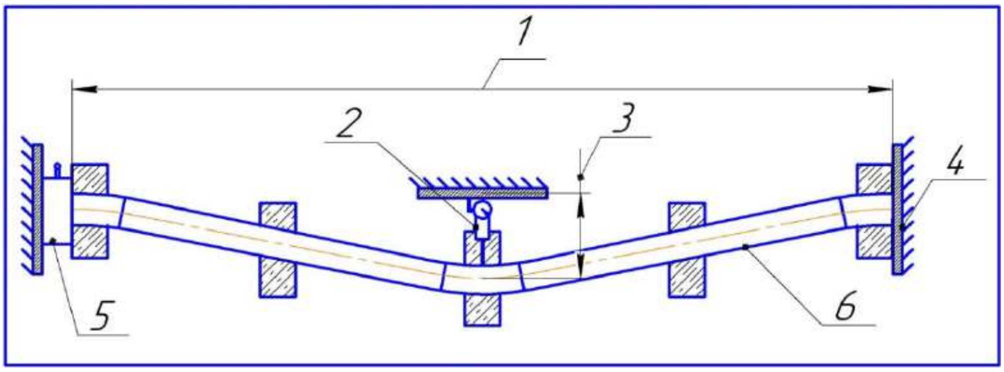

Figure 5. Diagram of the experimental setup:
1 – compensator length; 2 – displacement indicator; 3 – compensator deflection; 4 – stop; 5 – compression dynamometer; 6 – compensator

2.3. Experiment procedure

Experimental technique:

– measurement of temperature (contact thermometer) along the entire length of the pipe before the study;
– verification of the dynamometer reading (initial value must be set);
– uniform heating with gas burners use;
– measurement of force (dynamometer readings) and temperature measurement (contact thermometer readings), which occur during the temperature increases;
– control temperature measurement (indication of the contact thermometer) along the entire length of the pipe after the end of heating and fixing the indication of the dynamometer;
– analysis of the results.

Heating of the experimental the pipe pieces conducted simultaneously by several gas burners with the maximum possible uniform heating (+0 °C to +50 °C). The control measurements of temperature along the pipe length showed a temperature difference ± 3 °C.

During the experiment, as it was supposed, during heating of the pipe longitudinal force was recorded according to the indications of the dynamometer. This experiment was carried out for all physical models with the geometric characteristics given above.

During the study, we used the contact thermometer TK-5.01, the compression dynamometers DOSM-3-1U, DOSM-3-2U, DOSM-3-10U.

The error in the indicator readings of the IC-50 exceeded the permissible limits because of a violation of the device operating temperature, so further consideration of them is not advisable.

According to the theory of mathematical statistics, to reduce the random measurement errors to a confidence interval with a given reliability, the required measurements number was determined.

It was decided to conduct 8 measurements with confidence $\alpha = 0.9$.

3. Results and Discussion

Graphs of changes in the experimental and calculated values of the longitudinal force S from temperature difference Δt compensating device are demonstrated in Figures 6–9.

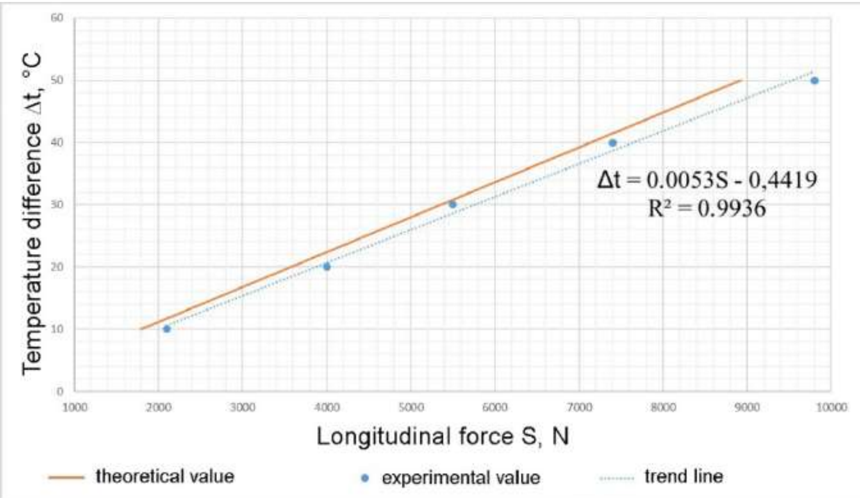

Figure 6. Graph of longitudinal force changing S from temperature difference Δt compensating device with deflection $f = 0.02$ m

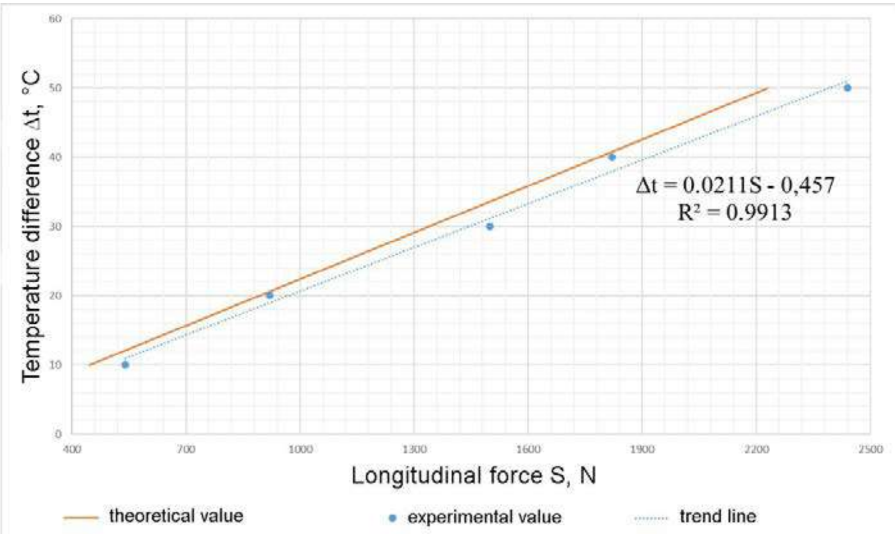

Figure 7. Graph of longitudinal force changing S from temperature difference Δt compensating device with deflection $f = 0.04$ m

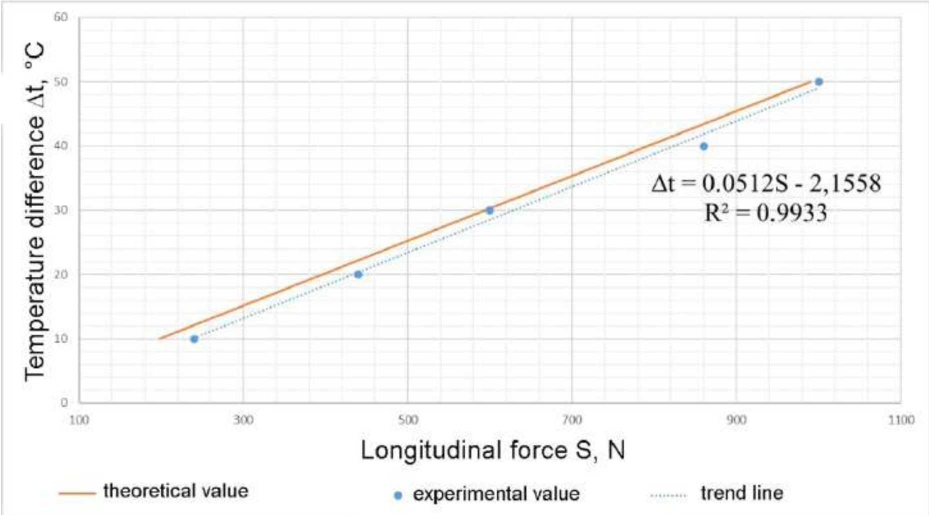

Figure 8. Graph of longitudinal force changing S from temperature difference Δt compensating device with deflection $f = 0.06$ m

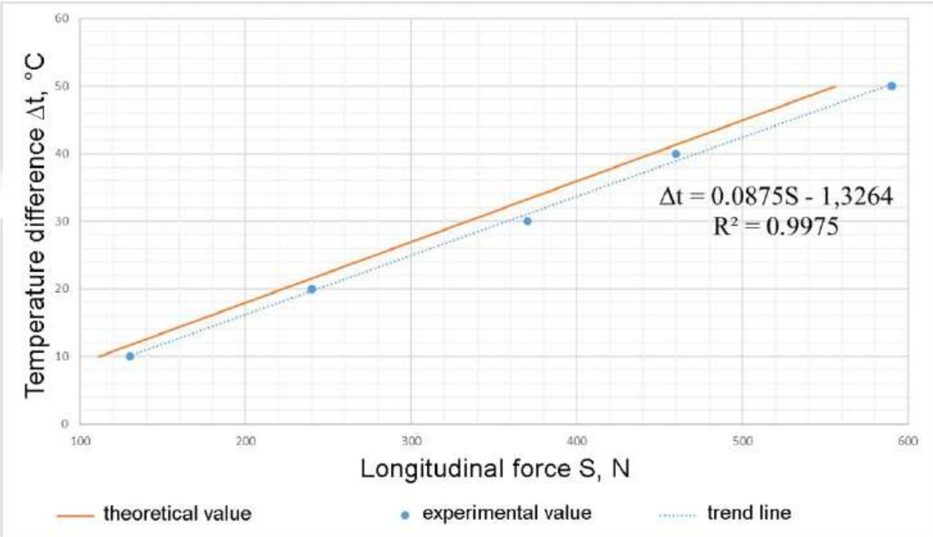

Figure 9. Graph of longitudinal force changing S from temperature difference Δt compensating device with deflection $f = 0.08$ m

As a result of the correlation analysis of the experimental data, the following is established:

– the correlation field showed a positive correlation between the value of the temperature difference and the longitudinal force obtained experimentally, that is, during an increase in one value, the other increases on average;

– for the analysis, an approximating curve was chosen in the form of a linear function;

– the selective correlation coefficient varies $r_{xy} = 0.93 \ldots 0.96$, which indicates that a strong connection between the value of the temperature difference and the experimentally obtained longitudinal force.

As a result of the regression analysis, the following is established:

– using the least squares method the parameters of linear regression equations are obtained;

– estimate of the quality of the regression equations demonstrated an average relative error of approximation not exceeding $\overline{A} = 1.18\%$, which indicates a good selection of regression equations to the original data.

As a result of checking the adequacy of the mathematical model, the following is established:

– since the experimental Fisher test is larger than the tabulated values for all experimental curves, the determination coefficient is statistically significant, and the regression equation adequately describes the experimental data;

– verification of the coefficients significance of the regression equations in the Student's t-test shows that the statistical the coefficients significance is confirmed.

The graphs (Figures 6–9) show a systematic deviation of the measured value of the longitudinal force S_{ex} depend on the estimated S_d. Taking into account all the errors in the experimental measurements, it can be established that the design of the compensating device proposed by us changes the magnitude of the longitudinal force S_d by formula (5) for the broken bolt construction by a specific value, which varies from 0.851 to 0.902.

The value of the longitudinal force for the proposed design of the compensating device (6):

$$S_d = k \cdot S_{ex} \quad (6)$$

where k – refinement coefficient obtained as a result of experimental measurements.

This fact is explained that the proposed compensating device with the bends use has a more rigid design than the compensating device in the form of a broken bolt. Identifying the obtained value of the deviation for the refinement coefficient of the compensator form, it will take equal to $\mathrm{k} = 0.85$, taking into account in the calculations the most unfavorable loading case.

Consequently, the rational parameters of the proposed compensating device for underwater pipeline transitions in order to increase the overall stability in the longitudinal direction must be determined by the condition (7):

$$\left(\frac{l}{f}\right)^2 \cdot \frac{3 \cdot I}{m \cdot l} \leq \frac{k \cdot N_{cr}}{\alpha \cdot E \cdot \Delta t + 0{,}2 \cdot \sigma_{an}}. \quad (7)$$

As an example, an underwater gas pipeline of diameters $D = 530\ mm$, a wall thickness $\delta = 25\ mm$ for the case of the ground erosion over the pipeline on the entire length of the curved section equal to $l = 85\ m$. The lower critical force is equal to $N_{cr} = 8.4\ MN$, which does not provide the conditions for the overall pipeline stability in the longitudinal direction. Consequently, according to the formula (7), the rational parameters of the proposed compensating device are determined, for which the length is equal to $l = 50\ m$ and deflection $f = 2\ m$.

The authors of the work [31] considered the change in the longitudinal force from the compensating device parameters of a triangular shape, and also assumed that the cold bends change the parameter of the longitudinal force. But there were no specific recommendations, studies, analyzes in their work. They relied on the fact that the parameter of the change in longitudinal force would not be significant. However, as our studies have shown, the parameter of the longitudinal force varies by 15 %, which is quite significant in determining the stability of the pipeline.

An analysis was conducted of the stress-strain state of the proposed compensating device with the use of bent taps in comparison with the previously known compensating device, structurally made in the form of a broken bolt, by the finite element method in the software complex Ansys. The description of the numerical experiment is given in Table 1.

Table 1. Description of the numerical experiment

Name	Description
Geometry	Calculation is made using thick-walled cylindrical shells; the parameters of the models are assumed to be analogous to the laboratory experiment
Material	Steel grade K60 is specified with the following strength characteristics: tensile strength 590 MPa and yield strength 460 MPa.
Border conditions	The boundary conditions included the tasks of rigidly fixing the pipe ends with the help of the command Fixed Support
Loads and effects	In the section Loads thermal loads are specified with stepwise loading of 10 ° C to a maximum value of 50°C.

The results of calculations for compensators with a maximum deflection *f* = 0.08 m and a maximum temperature difference *Δt* = 50 ℃ are shown in Figures 10–11 in the form of stress fields and displacements from the graphic window of the software complex Ansys.

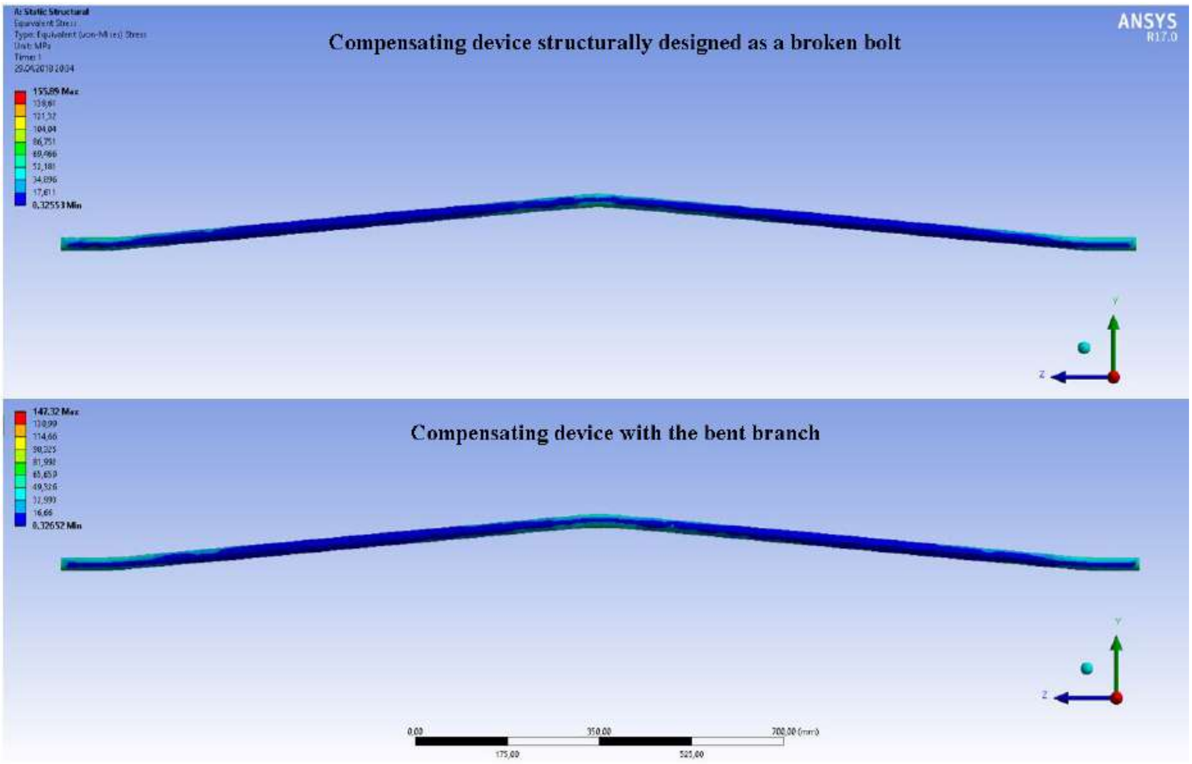

Figure 10. The stress field of the compensators

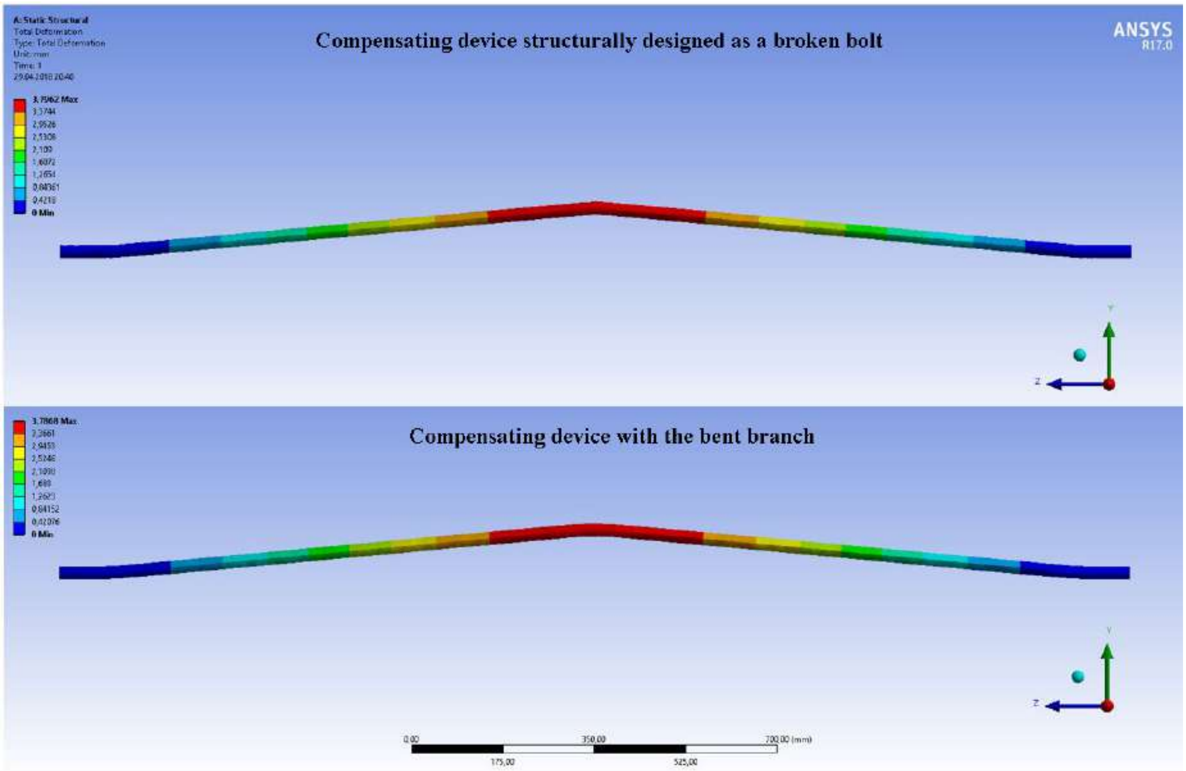

Figure 11. The field of displacement of the compensators

The values of movements do not practically change, however, the voltage in the proposed form of the compensator is less by 5.5%. In pipeline construction, this is the percentage reduction in the stress state in the pipeline is very significant. Consequently, the proposed form of the compensator, in addition to increasing the equivalent longitudinal force S by 15 %, also reduces the stress-strain state of the pipeline.

4. Conclusions

1. It has been determined that ballasting of adjoined areas allows to reduce the effect of the ultimate longitudinal force due to the temperature expansion of the pipeline material in the central part, and also during constructing underwater gas pipelines it is necessary to provide for the compensator facility at one of the ends of the underwater transition in the ground of adjoined areas to ensure the underwater transitions stability of gas and oil pipelines.

2. The refinement coefficient of the compensator shape, constructively obtained with the bends use, to reduce the longitudinal compressive force emerging from the temperature difference to the level of ensuring the overall pipeline stability in the longitudinal direction, which makes it possible to determine its rational parameters and is assumed to be equal $k = 0.85$.

3. For underwater pipeline transitions, taking into account the actual conditions of the laying according to the proposed technology, using elastically deformable materials or grounds for the free compensator displacement, the correction coefficient of the compensator form must not exceed $\mathrm{k} \leq 0.85$.

4. The proposed form of the compensator, in addition to increasing the equivalent longitudinal force S by 15%, also reduces the stress-strain state of the pipeline by 5.5%.

References

1. Kozhaeva K.V., Mustafin F.M., Yakupova D.Ye. Metody rascheta prodolnoy ustoychivosti truboprovoda i mery po yeye obespecheniyu na uchastke podvodnogo perekhoda [Methods of calculation of longitudinal stability of the pipeline and measure for her providing on the site of underwater transition]. *Neftyanoye khozyaystvo*. 2016. No. 2. Pp. 102–104. (rus)
2. Mustafin F.M., Abzalov A.K., Kozhaeva K.V. (Kutsenko K.V.), Mamliyev E.V. Diagnostika i raschet ustoychivosti truboprovoda na uchastke podvodnogo perekhoda [Diagnostics and calculation of stability of the pipeline on the site of underwater transition]. *Gazovaya promyshlennost*. 2013. No. 700. Pp. 41–43. (rus)
3. *Svidetelstvo o gosudarstvennoy registratsii programmy dlya EVM No. 2013615632.* Mustafin F.M., Kozhaeva K.V. (Kutsenko K.V.), Mamliyev E.V., Absalyamov E.R. Raschet ustoychivosti truboprovoda protiv vozdeystviya prodolnykh sil na uchastke podvodnogo perekhoda [Calculation of stability of the pipeline against influence of longitudinal forces on the site of underwater transition]. Zaregistrirovano v Reyestre programm dlya EVM 17.06.2013 g. Opublikovano 20.09.2013. (rus)
4. Filatov A.A. *Raschetno-eksperimentalnyye issledovaniya napryazhenno-deformirovannogo sostoyaniya podvodnykh perekhodov magistralnykh gazoprovodov*: dissertatsiya ... kandidata tekhnicheskikh nauk: 25.00.19 [Calculation-experimental studies of the stress-strain state of underwater transitions of main gas pipelines]. Institut problem transporta energoresursov. Moscow, 2013. 115 p. (rus)
5. Dudnikov Yu.V. *Nauchnyye osnovy proyektirovaniya i obespecheniya bezopasnosti slozhnykh uchastkov lineynoy chasti magistralnykh nefteprovodov*: dissertatsiya ... doktora tekhnicheskikh nauk: 25.00.19, 05.26.03 [Scientific fundamentals of designing and securing the complex parts of the linear part of the main oil pipelines]. Institut problem transporta energoresursov. Ufa, 2012. 366 p. (rus)
6. Filatov A.A. Mekhanicheskiye napryazheniya i peremeshcheniya truboprovoda na uchastkakh rechnykh podvodnykh perekhodov MG [Mechanical stresses and pipeline movements on sections of river underwater transitions of MG]. *Territoriya Neftegaz*. 2011. No. 9. Pp. 56–60. (rus)
7. Vagner V.V., Kushnir S.Ya., Pulnikov S.A. Raspredeleniye strely progiba arochnogo vybrosa po dline podzemnogo gazoprovoda [Arc arch deflection distribution along the

Литература

1. Кожаева К.В., Мустафин Ф.М., Якупова Д.Е. Методы расчета продольной устойчивости трубопровода и меры по ее обеспечению на участке подводного перехода // Нефтяное хозяйство. 2016. № 2. С. 102–104.
2. Мустафин Ф.М., Абзалов А.К., Кожаева К.В. (Куценко К.В.), Мамлиев Э.В. Диагностика и расчет устойчивости трубопровода на участке подводного перехода // Газовая промышленность. 2013. № 700. С. 41–43.
3. Свидетельство о государственной регистрации программы для ЭВМ №2013615632. Мустафин Ф.М., Кожаева К.В. (Куценко К.В.), Мамлиев Э.В., Абсалямов Э.Р. Расчет устойчивости трубопровода против воздействия продольных сил на участке подводного перехода // Зарегистрировано в Реестре программ для ЭВМ 17.06.2013 г. Опубликовано 20.09.2013.
4. Филатов А.А. Расчётно-экспериментальные исследования напряжённо-деформированного состояния подводных переходов магистральных газопроводов: диссертация ... кандидата технических наук: 25.00.19. Институт проблем транспорта энергоресурсов. Москва, 2013. 115 с.
5. Дудников Ю.В. Научные основы проектирования и обеспечения безопасности сложных участков линейной части магистральных нефтепроводов: диссертация ... доктора технических наук: 25.00.19, 05.26.03. Институт проблем транспорта энергоресурсов. Уфа, 2012. 366 с.
6. Филатов А.А. Механические напряжения и перемещения трубопровода на участках речных подводных переходов МГ // Территория Нефтегаз. 2011. № 9. С. 56–60.
7. Вагнер В.В., Кушнир С.Я., Пульников С.А. Распределение стрелы прогиба арочного выброса по длине подземного газопровода // Известия вузов «Нефть и газ». 2008. № 4. С. 101–104.
8. Rashidov T.R., An E.V. Geometrically nonlinear buckling stability analysis of axially loaded underground pipelines // Soil mechanics and foundation engineering. 2017. Vol. 54. № 2. Pp. 76–80.
9. Bai Y., Xu W.P., Ruan W.D., Tang J.W. On-bottom stability of subsea lightweight pipeline (LWP) on sand soil surface // Ships and offshore structures. 2017. Vol. 2. № 7. Pp. 954–962.
10. Carkovs J., Matvejevs A., Pavlenko O. Stochastic stability of a pipeline affected by pulsate fluid flow // ICTE

length of the underground gas pipeline]. *Izvestiya vuzov «Neft i gaz»*. 2008. No. 4. Pp. 101–104. (rus)

8. Rashidov T. R., An E. V. Geometrically nonlinear buckling stability analysis of axially loaded underground pipelines. *Soil mechanics and foundation engineering*. 2017. Vol. 54. No. 2. Pp. 76–80.
9. Bai Y., Xu W.P., Ruan W.D., Tang J.W. On-bottom stability of subsea lightweight pipeline (LWP) on sand soil surface. *Ships and offshore structures*. 2017. Vol. 12. No. 7. Pp. 954–962.
10. Carkovs J., Matvejevs A., Pavlenko O. Stochastic stability of a pipeline affected by pulsate fluid flow. *ICTE Conference.* Riga Tech. Univ., Riga, LATVIA, 2017. Vol. 104. Pp. 12–19.
11. Draper S., An H., Cheng L. Stability of subsea pipelines during large storms. *Philosophical transactions of the royal society a-mathematical physical and engineering sciences*. 2015. Vol. 373. No. 2033. Pp. 1–22.
12. Jha P. C., Balasubramaniam V. R., Sandeep N. Application of GPR in assessing the stability of oil pipeline. *15th International Conference on Ground Penetrating Radar (GPR).* Brussels, BELGIUM, 2014. Pp. 441–446.
13. Yu S. Y., Choi H. S., Lee S. K. An optimum design of on-bottom stability of offshore pipelines on soft clay. *International journal of naval architecture and ocean engineering.* 2013. Vol. 5. No. 4. Pp. 598–613.
14. Youssef B. S., Cassidy M. J., Tian Y. Application of statistical analysis techniques to pipeline on-bottom stability analysis. Journal of offshore mechanics and arctic engineering-transactions of the asme. 2013. Vol. 135. No. 3. Pp. 598–613.
15. Yang H., Wang A. Dynamic stability analysis of pipeline based on reliability using surrogate model. *Journal of marine engineering and technology*. 2013. Vol. 12. No. 2. Pp. 75–84.
16. Gaeta M. G., Lamberti A., Ricchieri F. Articulated concrete mattress for submarine pipeline protection: evaluation of the wave-induced forces and stability analysis. *6th International Conference on Coastal Structures*. Yokohama, JAPAN: 2013. Vol. 1-2. Pp. 1116–1125.
17. Azevedo-Perdicoulis T.P., Jank G., dos Santos P.L. Modelling a gas pipeline as a repetitive process: controllability, observability and stability. *Multidimensional systems and signal processing.* 2015. Vol. 26. No. 4. Pp. 967–984.
18. McMaster S.Y., O'Brien D., Scholtz D.E., Ryan J.R. On-bottom stability analysis for a pipeline on a mobile seabed. *31st ASME International Conference on Ocean, Offshore and Arctic Engineering.* Rio de Janeiro, Brazil: 2012. Vol. 3. Pp. 225–233.
19. Tian Y.H., Cassidy M.J., Chang C.K. Assessment of offshore pipelines using dynamic lateral stability analysis. *Applied ocean research.* 2015. Vol. 50. Pp. 47–57.
20. Meshkov Y.Y., Shyyan A.V., Zvirko O.I. Evaluation of the in-service degradation of steels of gas pipelines according to the criterion of mechanical stability. *Materials science*. 2015. Vol. 50. No. 6. Pp. 830–835.
21. Ji G.M., Li L.J., Ong M.C. A comparison of simplified engineering and fem methods for on-bottom stability analysis of subsea pipelines. *35th ASME International Conference on Ocean, Offshore and Arctic Engineering*. Busan, SOUTH KOREA: 2016. Vol. 1.
22. Kozhaeva K.V. *Obespecheniye stabilizatsii proyektnogo polozheniya podvodnykh perekhodov gazonefteprovodov*: dissertatsiya ... kandidata tekhnicheskikh nauk: 25.00.19 [Ensuring stabilization of design provision of underwater transitions of gas and oil pipelines]. FGBOU VO Ufimskiy gosudarstvennyy neftyanoy tekhnicheskiy universitet. Ufa, 2017. 139 p. (rus)
23. Muravyeva L., Vatin N. Elaboration of the method for safety assessment of subsea pipeline with longitudinal

Conference. Riga Tech. Univ., Riga, LATVIA, 2017. Vol. 104. Pp. 12–19.

11. Draper S., An H., Cheng L. Stability of subsea pipelines during large storms // Philosophical transactions of the royal society a-mathematical physical and engineering sciences. 2015. Vol. 373. № 2033. Pp. 1–22.
12. Jha P.C., Balasubramaniam V. R., Sandeep N. Application of GPR in assessing the stability of oil pipeline // 15th International Conference on Ground Penetrating Radar (GPR). Brussels, BELGIUM, 2014. Pp. 441–446.
13. Yu S.Y., Choi H.S., Lee S.K. An optimum design of on-bottom stability of offshore pipelines on soft clay // International journal of naval architecture and ocean engineering. 2013. Vol. 5. No. 4. Pp. 598–613.
14. Youssef B.S., Cassidy M. J., Tian Y. Application of statistical analysis techniques to pipeline on-bottom stability analysis // Journal of offshore mechanics and arctic engineering-transactions of the asme. 2013. Vol. 135. No. 3. Pp. 598–613.
15. Yang H., Wang A. Dynamic stability analysis of pipeline based on reliability using surrogate model. Journal of marine engineering and technology. 2013. Vol. 12. No. 2. Pp. 75–84.
16. Gaeta M.G., Lamberti A., Ricchieri F. Articulated concrete mattress for submarine pipeline protection: evaluation of the wave-induced forces and stability analysis // 6th International Conference on Coastal Structures. Yokohama, JAPAN: 2013. Vol. 1-2. Pp. 1116–1125.
17. Azevedo-Perdicoulis T.P., Jank G., dos Santos P.L. Modelling a gas pipeline as a repetitive process: controllability, observability and stability // Multidimensional systems and signal processing. 2015. Vol. 26. No. 4. Pp. 967–984.
18. McMaster S.Y., O'Brien D., Scholtz D.E., Ryan J.R. On-bottom stability analysis for a pipeline on a mobile seabed // 31st ASME International Conference on Ocean, Offshore and Arctic Engineering. Rio de Janeiro, Brazil: 2012. Vol. 3. Pp. 225–233.
19. Tian Y.H., Cassidy M.J., Chang C.K. Assessment of offshore pipelines using dynamic lateral stability analysis // Applied ocean research. 2015. Vol. 50. Pp. 47–57.
20. Meshkov Y.Y., Shyyan A.V., Zvirko O.I. Evaluation of the in-service degradation of steels of gas pipelines according to the criterion of mechanical stability // Materials science. 2015. Vol. 50. No. 6. Pp. 830–835.
21. Ji G.M., Li L.J., Ong M.C. A comparison of simplified engineering and fem methods for on-bottom stability analysis of subsea pipelines // 35th ASME International Conference on Ocean, Offshore and Arctic Engineering. Busan, SOUTH KOREA: 2016. Vol. 1.
22. Кожаева К.В. Обеспечение стабилизации проектного положения подводных переходов газонефтепроводов: диссертация ... кандидата технических наук: ФГБОУ ВО Уфимский государственный нефтяной технический университет. Уфа, 2017. 139 с.
23. Muravyeva L., Vatin N. Elaboration of the method for safety assessment of subsea pipeline with longitudinal buckling. Advances in Civil Engineering. 2016. Vol. 2016. 7581360
24. Сысоев Ю.С. Устойчивость подземного магистрального газопровода на обводненных участках трассы: диссертация ... кандидата технических наук: 25.00.19. Место защиты: Институт проблем транспорта энергоресурсов. Тюмень, 2012. 168 с.
25. Сысоев Ю.С., Кушнир С.Я., Пульников С.А. Пространственная устойчивость подземного магистрального газопровода на обводненных участках трассы // Известия вузов «Нефть и газ». 2012. № 1. С. 72–76.
26. Бахтизин Р.Н., Масалимов Р.Б., Зарипов Р.М., Шварева Е.Н. Моделирование напряженно-

buckling. *Advances in Civil Engineering*. 2016. Vol. 2016. 7581360.

24. Sysoyev Yu.S. *Ustoychivost podzemnogo magistralnogo gazoprovoda na obvodnennykh uchastkakh trassy*: dissertatsiya ... kandidata tekhnicheskikh nauk: 25.00.19 [Stability of the underground main gas pipeline on watered sections of the route]. Institut problem transporta energoresursov. Tyumen, 2012. 168 p. (rus)
25. Sysoyev Yu.S., Kushnir S.Ya., Pulnikov S.A. Prostranstvennaya ustoychivost podzemnogo magistralnogo gazoprovoda na obvodnennykh uchastkakh trassy [The spatial stability of underground main gas pipeline on the flooded sections of the route]. *Izvestiya vuzov «Neft i gaz»*. 2012. No. 1. Pp. 72-76. (rus)
26. Bakhtizin R.N., Masalimov R.B., Zaripov R.M., Shvareva Ye.N. Modelirovaniye napryazhenno-deformirovannogo sostoyaniya podzemnogo uchastka truboprovoda, sostavlennogo iz krivoy vognutoy ili vypukloy vstavki krivolineynym polym sterzhnem v uprugoy srede [Modeling of the stress-deformed state of the underground portion of pipe composed of convex or concave curve insert curved hollow shaft in an elastic medium]. *Neftegazovoye delo*. 2012. No. 6. [online]. URL: http://ogbus.ru/authors/Bakhtizin/Bakhtizin_5.pdf (date of reference: 10.09.2016). (rus)
27. Islamgaleyeva L.F., Zaripov R.M. Vliyaniye stepeni obvodneniya grunta prilegayushchikh podzemnykh uchastkov na napryazhenno-deformirovannoye sostoyaniye podvodnogo gazoprovoda [Influence of the degree of watering of the soil of adjacent underground sections on the stress-strain state of the underwater gas pipeline*]. Neftegazovoye delo*. 2011. No. 6. [online]. URL: http://ogbus.ru/authors/Islamgaleeva/Islamgaleeva _1.pdf (date of reference: 08.10.2016). (rus)
28. Islamgaleyeva L.F. *Napryazhenno-deformirovannoye sostoyaniye podvodnykh perekhodov magistralnykh gazoprovodov s uchetom izmeneniya stepeni vodonasyshchennosti grunta na prilegayushchikh podzemnykh uchastkakh*: dissertatsiya ... kandidata tekhnicheskikh nauk: 25.00.19 [Stress-strain state of underwater transitions of main gas pipelines taking into account changes in the degree of water saturation of the ground in adjacent underground areas]. Islamgaleyeva Liliya Faritovna; [Mesto zashchity: Ufimskiy gosudarstvennyy neftyanoy tekhnicheskiy universitet]. – Ufa, 2013. 179 p. (rus)
29. *Patent RF № 141422, 10.06.2014*. Mustafin F.M., Shammazov A.M., Kozhaeva K.V. (Kutsenko K.V.), Abzalov A.K., Absalyamov E.R., Mamliyev E.V., Mashin A.Yu. Dugoobraznyy kompensator dlya truboprovoda [An arc-shaped compensator for the pipeline]. Bulletin "Inventions. Utility Models". 2014, No. 16. (rus)
30. Mustafin F.M., Kozhaeva K.V. Eksperimentalnyye issledovaniya po umensheniyu prodolnykh usiliy ot temperaturnykh vozdeystviy na podvodnykh uchastkakh truboprovodov [Experimental studies on the reduction of longitudinal forces from temperature effects on underwater sections of pipelines]. *Truboprovodnyy transport: teoriya i praktika*. 2014. No. 5-6 (45-46). Pp .59–65. (rus)
31. Borodavkin P.P., Taran V.D. *Truboprovody v slozhnykh usloviyakh* [Pipelines in difficult conditions]. M.: Nedra, 1968. 304 p. (rus)

деформированного состояния подземного участка трубопровода, составленного из кривой вогнутой или выпуклой вставки криволинейным полым стержнем в упругой среде // Нефтегазовое дело. 2012. № 6. [Электронный ресурс]. URL: http://ogbus.ru/authors/Bakhtizin/Bakhtizin_5.pdf (дата обращения: 10.09.2016).

27. Исламгалеева Л.Ф., Зарипов Р.М. Влияние степени обводнения грунта прилегающих подземных участков на напряженно-деформированное состояние подводного газопровода // Нефтегазовое дело. 2011. №6. [Электронный ресурс]. URL: http://ogbus.ru/authors/Islamgaleeva/Islamgaleeva_ 1.pdf (дата обращения: 08.10.2016).
28. Исламгалеева Л.Ф. Напряженно-деформированное состояние подводных переходов магистральных газопроводов с учетом изменения степени водонасыщенности грунта на прилегающих подземных участках: диссертация ... кандидата технических наук: 25.00.19. Уфимский государственный нефтяной технический университет. Уфа, 2013. 179 с.
29. Патент РФ № 141422, 10.06.2014. Мустафин Ф.М., Шаммазов А.М., Кожаева К.В. (Куценко К.В.), Абзалов А.К., Абсалямов Э.Р., Мамлиев Э.В., Машин А.Ю. Дугообразный компенсатор для трубопровода // Официальный бюллетень Федеральной службы интеллектуальной собственности «Изобретение. Полезные модели». 2014, № 16.
30. Мустафин Ф.М., Кожаева К.В. Экспериментальные исследования по уменьшению продольных усилий от температурных воздействий на подводных участках трубопроводов // Трубопроводный транспорт: теория и практика. 2014. № 5-6 (45-46). С. 59–65.
31. Бородавкин П.П., Таран В.Д. Трубопроводы в сложных условиях. М.: Недра, 1968. 304 с.

Ksenia Kozhaeva,
+7(917)4702615; st_kafedra@bk.ru

Ксения Валерьевна Кожаева,
+7(917)4702615; эл. почта: st_kafedra@bk.ru

Кожаева К.В. Влияние параметров компенсирующего устройства на устойчивость подводного трубопровода // Инженерно-строительный журнал. 2018. № 4(80). С. 24–36.

doi: 10.18720/MCE.80.4

Min-cut algorithm for network schedule by merging the vertices

Алгоритм поиска минимального разреза сетевой модели слиянием вершин

Yu.B. Kalugin*,
Military Institute of rail transport troops and military communications, Saint-Petersburg, Russia
A. Kaklauskas,
Vilnius Gediminas Technical University, Vilnius, Lithuania
Yu.N. Kazakov,
St. Petersburg State University of Architecture and Civil Engineering, Saint-Petersburg, Russia

Д-р техн. наук, профессор Ю.Б. Калугин*,
Военный институт железнодорожных войск и военных сообщений, г. Санкт-Петербург, Россия
д-р техн. наук, декан А. Каклаускас,
Вильнюсский технический университет им. Гедиминаса, г. Вильнюс, Литва
д-р техн. наук, профессор Ю.Н. Казаков,
Санкт-Петербургский государственный архитектурно-строительный университет, г. Санкт-Петербург, Россия

Key words: civil engineering; construction management; project scheduling; critical path method; crashing; minimum cut problem

Ключевые слова: календарное планирование и управление проектом; метод критического пути; оптимизация календарных графиков по срокам; минимальный разрез критической сети

Abstract. The task of reducing the total duration of the project ("compression", "crashing") occurs when developing and adjusting schedules. The activities requiring crashing are determined by the minimum of added resources at the unit reduction of the schedule. The minimum cut in a critical network determines such activities. The essence of searching the minimum cut by merging vertices (edge tightening) of the critical network is presented. The procedure of selecting vertices consists of the following. Possible merge options (tentative steps) are evaluated by equivalent cuts. The minimum cut will define priority vertex of a critical network. After this merging algorithm re-examines all the possible options of joining of adjacent vertices (on next step). The general applicability of the algorithm is demonstrated. Conditions of effective application of a method of the merge of vertexes are established. Search results of the minimum cuts of the critical network by means of this method are presented. Calculations have shown that in 14 of 15 examples the algorithm has established the global minimum cuts. Implementation of the proposed approaches will allow determining the activities to be optimized, calculate the size of reduction and the number of resources involved. The suggested methodology can be recommended for use by construction project managers.

Аннотация. Задача сокращения общей продолжительности проекта («сжатие») возникает при разработке и корректировке календарных графиков. Работы, требующие «сжатия», определяются минимумом дополнительно привлекаемых ресурсов при их единичном сокращении. Минимальный разрез критической сети определяет такие работы. Представлена сущность поиска минимального разреза путем слияния вершин (стягивания ребер) критической сети. Порядок выбора вершин состоит в следующем. Возможные варианты слияния (предварительные шаги) оцениваются эквивалентными разрезами. Минимальный разрез определяет приоритетную для слияния вершину критической сети. После этого алгоритм повторно исследует все возможные варианты присоединения смежных вершин (на следующем шаге). Показана общая применимость алгоритма. Установлены условия эффективного применения метода слияния вершин. Представлены результаты поиска минимальных разрезов критической сети с помощью данного метода. Расчеты показали, что в 14 из 15 примеров алгоритм установил глобальные минимальные разрезы. Реализация предложенных подходов позволит определить работы графика, подлежащие оптимизации, рассчитать размер сокращения и количество привлекаемых ресурсов. Предложенная методика может быть рекомендована для использования руководителями строительных проектов.

1. Introduction

A construction project is a complex process, which includes a large number of different tasks performed by different crews and displayed by calendar charts. When forming the schedules in case of

Калугин Ю.Б., Каклаускас А., Казаков Ю.Н. Алгоритм поиска минимального разреза сетевой модели слиянием вершин // Инженерно-строительный журнал. 2018. № 4(80). С. 37–47.

exceeding the planned duration over deadlines requires a reduction in the total duration. In addition, with the operational management of the progress of work, it is also necessary to periodically adjust the schedule by dates.

Reduces the planned time schedule and decision-making (compression) involves primarily the intensification of activities critical path. It is obvious that critical activity that requires a minimum number of attracted resources for such compression must be reduced in the first place [1–6].

After the compression of the critical path by the minimum value of the total float [6], the schedule is recalculated with the repeated determination of all critical activities. It is obvious that in this case the chain of operations of the only critical path is transformed into a critical network, for optimization (compression) which can be used appropriate approaches and methods [1, 3, 6, 7].

The Ford-Fulkerson algorithm for maximum flow (minimum cut) and its variety [8, 9] is most often used to find such critical actions of the network model. The use of flow algorithms implies integer values of flows and multistage iterative procedures [10–19].

A simple and quite effective method of finding the minimum cut in critical networks is the methods based on the use of dual graph [20–23] and the method of branch-and-bound [24–26].

The dual graph is constructed as follows: on each face of the primary graph (a network model consisting of critical activities the vertex of the dual is placed. The vertices of the dual graph lying on the neighboring faces of the primary are connected so that each arc of the primary graph corresponds to one arc of the dual graph. The shortest path on the network of the dual graph defines the minimum cut of the primary graph (critical network) [23].

This approach is applicable only to planar networks. Although the vast majority of network schedules are planar, there are cases when network schedules that is not planar.

An interesting way to find the minimum cut in an undirected graph is the Stoer-Wagner algorithm and related approaches [27, 28].

The idea of the method is as follows. The most "connected" vertices are added sequentially to the randomly selected vertex of the graph, forming the first set. Then the local minimum cut separates either the last two vertices, or these vertices are in the second set, and the cut separates the two sets. After merging the last two vertices, the loop repeats until there are two vertices. The minimum among all the local sections and will be the desired global minimum cut.

It seems appropriate to consider the possibility of using a similar approach to find the minimum cut in a network model, which is a directed graph with one start and one end vertices.

The aim of the present paper is to substantiate the algorithm for finding the minimum cut in a directed graph by merging vertices.

Objectives of the study are:

1. Justification of general approach;
2. Substantiate the procedure for selection of vertices;
3. Determining the scope of effective application of the vertex merge method.

2. Methods

2.1. General approach

The general approach to finding the minimum cut of the network model by merging vertices (edge tightening) is quite simple [29]. Consider a critical network (a fragment of the network schedule in which all activities are critical) (Figure 1). Over arcs are represented the values of the resources involved to reduce the activity per unit time.

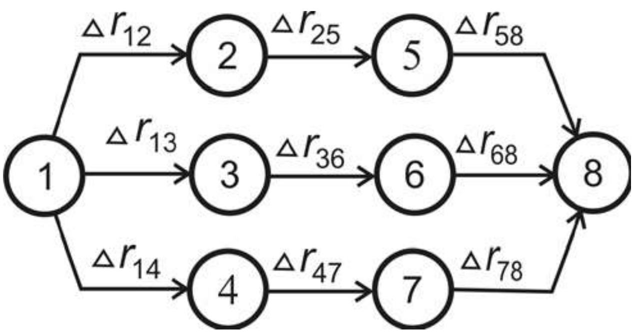

Figure 1. Fragment of a critical network

It is obvious that for any cut, the start and end vertices must be in different sets. First, a cut is defined between vertex 1 and adjacent vertices 2, 3, 4 (Figure 2), (1).

$$S_0 = \sum \Delta r_{1j}. \tag{1}$$

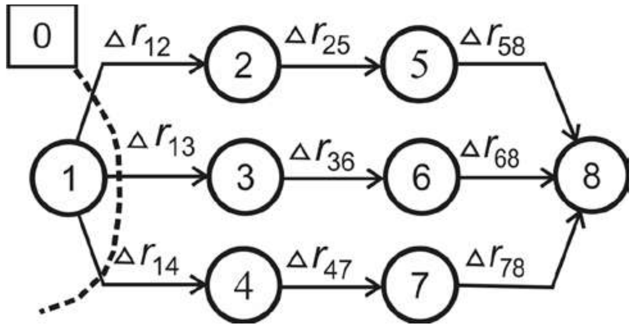

Figure 2. Initial cut

Then there is a sequential merge (Union) of vertex 1 with these neighboring vertices. The first step merges vertices 1 and 2 (Figure 3).

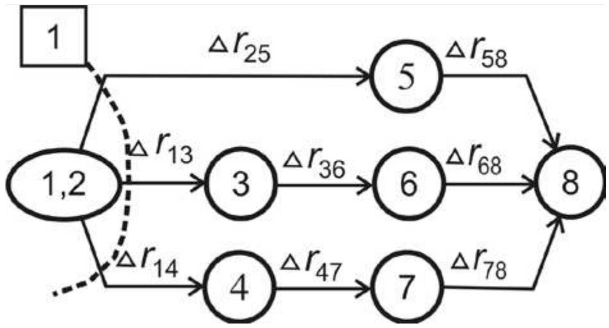

Figure 3. First step of the merger

In the second step, vertex 3 is added to the combined vertices 1 and 2 (combined vertex 1, 2), (Figure 4).

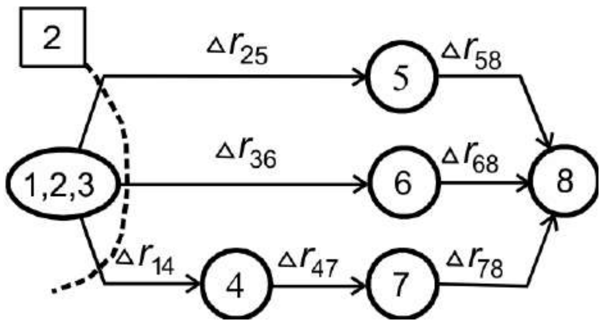

Figure 4. Second step of the merger

At each m-th step is determined by the value of the corresponding cut (2).

$$S_m = \sum \Delta r_{ij}, \tag{2}$$

i – is the number of the event entering the merged vertex;

j – is the number of the event adjacent to the merged vertex.

In the third step, vertex 4 is added to the combined vertices 1, 2 and 3 (combined vertex 1, 2, 3), (Figure 5).

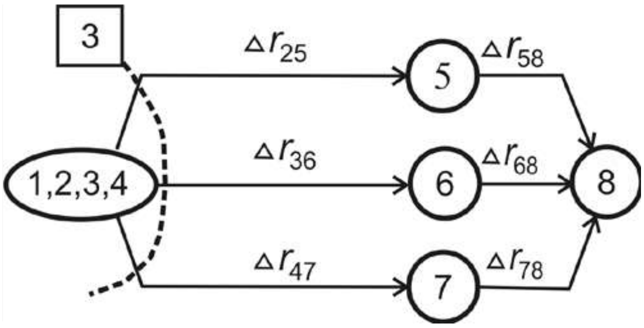

Figure 5. Third step of the merger

After a number of similar procedures, the network acquires the following form at step 6 (Figure 6).

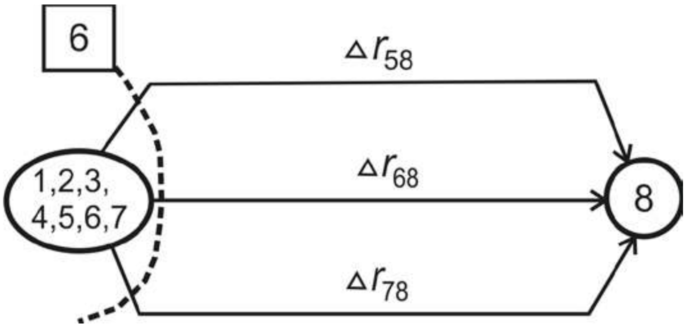

Figure 6. Sixth step of the merger

The minimum of all cuts at each step determines the desired activities for "compression".

$$S = \min S_m. \tag{3}$$

The calculations [29] showed that the correctness of determining the global minimum cut significantly depends on the selected sequence of merging vertices. Under these conditions, it is necessary to justify the order of selection of vertices to merge, allowing you to determine the global (or close to it local) minimum cut.

2.2. Procedure of selecting vertices

The procedure for selecting promising to join (merge) neighboring vertices of the network at each step is as follows. The author examines the possible merging of the vertices (tentative steps).

For each variant (tentative step), the corresponding cuts separating the combined vertex from the rest of the network are calculated. The minimum value of the corresponding cut determines the priority for merging vertex at this step.

After this merge (definite step) again considers all possible options of merging the neighboring vertices (the next step).

As an illustration of this procedure, the first step considers the following possible options for merging vertices (tentative steps) – (1,2); (1,3); (1,4), (Figures 7, 8, 9).

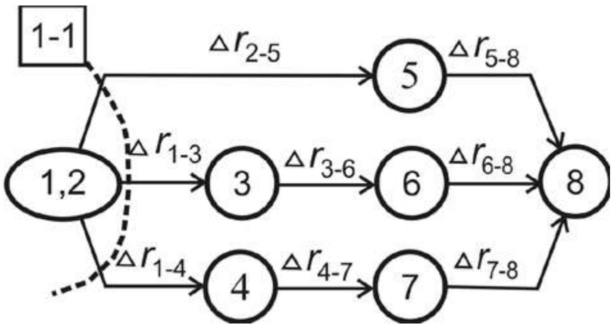

Figure 7. The variant of merging vertices 1 and 2 (step 1)

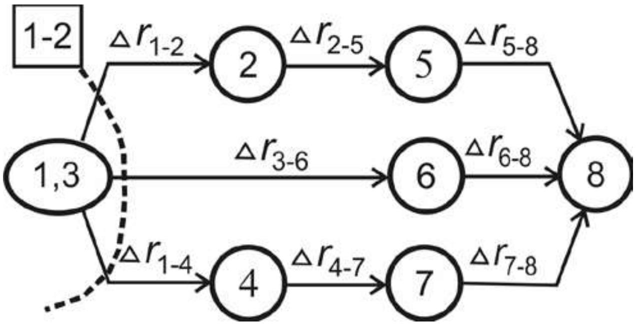

Figure 8. The variant of merging vertices 1 and 3 (step 1)

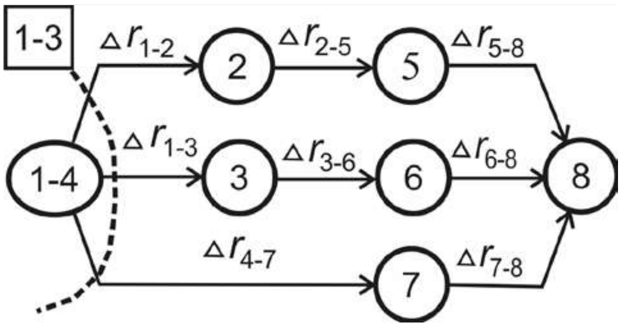

Figure 9. The variant of merging vertices 1 and 4 (step 1)

Let the minimum cut in the first step corresponding to the combined vertex (1,4), (Figure 9). This variant is a priority definite step. The value of the corresponding cut is remembered.

The second step sequentially considers the variants of merging the merged vertex (1-4) and of vertices 2, 3, 7.

The process repeats as long as is not merged by all the vertices except the end vertex (Figure 10).

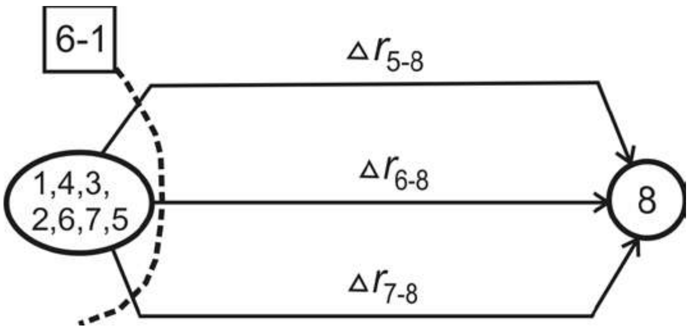

Figure 10. The variant of merging the vertices 1,4,3,2,6,7,5 (step 6)

Therefore, each step defined a local minimum cut. In total, taking into account the initial cut (at near the vertex 1), eight local minimum cuts were established (with the total number of considered cuts – 15). The minimum value of these local cuts will determine the required global minimum cut.

Table 1 presents the results of the implementation of the algorithm for finding minimal network sections (Figure 1) according to [29]. The parameters of the activities (the resource values involved to reduce activity by one unit time) are random numbers from 1 to 9.

Table 1. Results of determination cuts of the network when using a rule of the choice preferable neighbor vertex (the minimum cut of tentative step)

##	The parameters of the activities									Local minimum cuts	Global minimum
	Δr_{12}	Δr_{13}	Δr_{14}	Δr_{25}	Δr_{36}	Δr_{47}	Δr_{58}	Δr_{68}	Δr_{78}		
1	2	6	1	3	4	9	4	5	8	12-36-14 S=7	12-36-14 S=7
2	5	8	9	1	9	4	9	3	6	25-68-47 S=8	25-68-47 S=8
3	4	3	8	6	4	7	5	5	9	12-13-47 S=14	12-13-47 S=14
4	2	1	9	6	2	3	3	9	7	12-13-47 S=6	12-13-47 S=6
5	9	1	1	8	4	3	7	6	6	58-13-14 S=9	58-13-14 S=9
6	2	6	9	5	5	1	3	3	4	12-68-47 S=6	12-68-47 S=6
7	9	9	2	4	4	3	2	1	4	58-68-14 S=5	58-68-14 S=5
8	3	8	4	5	4	3	6	5	1	12-36-78 S=8	12-36-78 S=8
9	5	1	5	6	8	2	2	6	4	58-13-47 S=5	58-13-47 S=5
10	6	4	1	7	2	3	5	8	4	58-36-14 S=8	58-36-14 S=8
11	1	8	9	9	4	2	8	1	5	12-68-47 S=4	12-68-47 S=4
12	9	1	3	1	8	4	6	7	9	25-13-14 S=5	25-13-14 S=5
13	7	5	4	3	7	3	2	3	5	58-68-47 S=8	58-68-47 S=8
14	4	9	2	1	6	3	3	8	7	25-36-14 S=9	25-36-14 S=9
15	7	7	1	9	5	8	4	6	3	58-68-14 S=11	58-36-14 S=10

An analysis of the data presented in table 2 shows that, in 14 of 15 cases, global lows have been identified. In the last example, the algorithm set only the local minimum.

The presented example does not guarantee that the stated algorithm determines the global minimum cut. In this regard, it is necessary to justify the conditions for the effective application of the method of merging vertices (conditions under which the minimum cut is found to be global).

2.3. The scopes of effective application of the vertex merge method

All activities of any critical network can be divided as follows.

Activities of stage 1, for which the merged vertex is the initial event: 1-2; 1-3; 1-4 (A_1, B_1, C_1), (Figure 11).

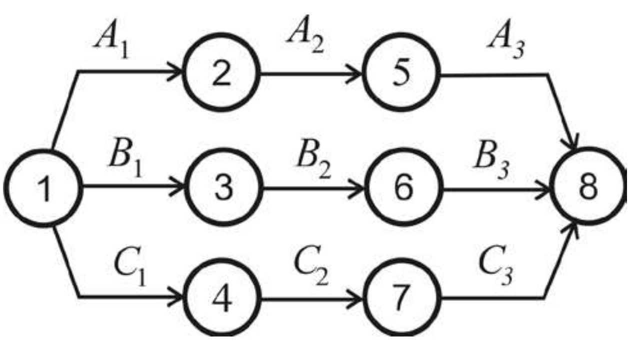

Figure 11. Fragment of a critical network

Activities of the 2 stage-initial events are the final events of the first stage: 2-5; 3-6; 4-7 (A_2, B_2, C_2).

Activities of the 3 stage-initial events are the final events of the second stage: 5-8; 6-8; 7-8 (A_3, B_3, C_3).

Activities of the i-th stage, for which the initial events are the final work events (i – 1) of the stage.

The proposed algorithm is guaranteed to determine the global minimum cut, passing through the activities of one or two adjacent stages.

If the global minimum cut passes through three stages of a critical network, the following variants are possible (Figure 12).

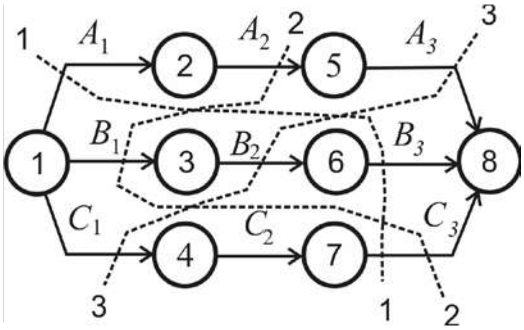

Figure 12. Variants of cuts through the activities of three stages

When two-way merging vertices (left and right), the algorithm detects all global minimum cuts of type 1-1, most of the cuts of type 2-2 and 3-3.

Studies have shown that the probability of finding a global minimum cut in the presented critical network (Fig. 11) is greater than 0.95. This is consistent with the data of table 1.

The practice of optimization of schedules shows that the compressible activities is not substantially spaced in time and are typically located in the progress line area. Therefore, the presented algorithm, which determines the global minimum cut, passing through 1-2-3 adjacent stages, is quite effective.

3. Results and Discussion

The method presented was used to optimize the network graph (Figure 13), [12, 23].

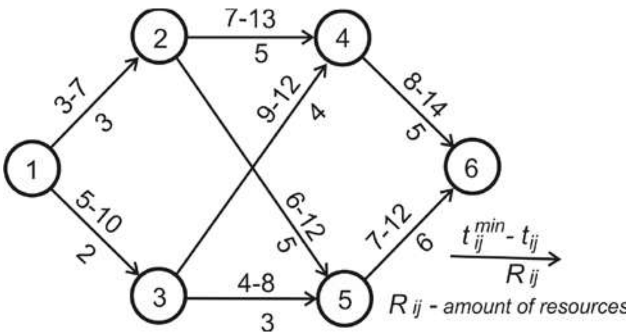

Figure 13. The Initial network schedule

Compression of the critical path from 36 to 22 days was carried out for 14 iterations.

After 13 iterations, the network graph was as follows (Figure 14). The total duration was 23 days. All paths of this graph are critical. Activities 3-4 and 4-6 are reduced to a minimum. Further, their compression is impossible.

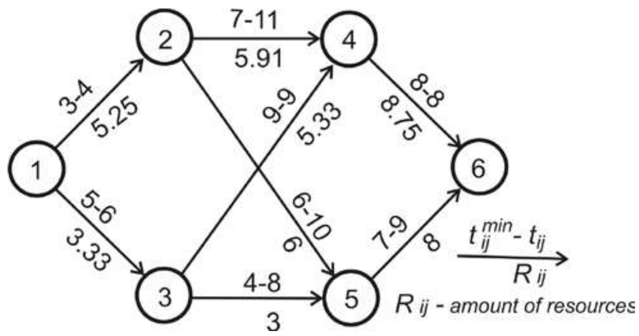

Figure 14. The network schedule after 13th iteration

The next iteration defines the activities that allow you to compress the schedule for another day with a minimum increase in resources (find the minimum cut off the critical network).

The critical network on 14th iteration looked as follows (Figure 15). The values of increase of resources for reduction of the corresponding work for one day are presented over the activities of the critical network.

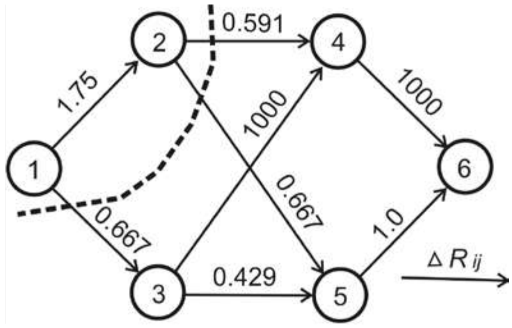

Figure 15. The critical network on the 14th iteration

After compression of activities 2-4, 2-5, 1-3 on the unit (one day) the optimum schedule was received (Figure 16).

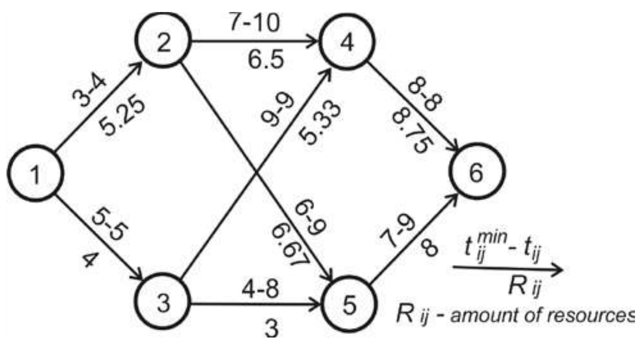

Figure 16. The optimal network schedule

The schedule provides a required duration (22 days). At the same time, the number of additional attracted resources is minimal (14.5).

The method presented in this study used Microsoft Excel [30].

4. Conclusions

1. When forming the schedules in case of exceeding the planned duration over deadlines requires a reduction in the total duration. Reduces the planned time schedule and decision-making (compression) involves primarily the intensification of activities critical path (critical network). Critical activities that require a minimum number of attracted resources for such compression must be reduced in the first place. These critical network operations are determined by the minimum cut.

There are a number of methods for finding the minimum cut in the network.

2. The essence of searching the minimum cut by merging vertices (edge tightening) of the critical network is presented.

The procedure of selecting vertices consists in the following. Possible merge options (tentative steps) are evaluated by equivalent cuts. The minimum cut will define priority vertex of a critical network. After this merge (definite step) again considers all possible options of merging the neighboring vertices (the next step).

Results of determination minimum cuts of the 15 networks when using a rule of the choice preferable neighbor vertex (the minimum cut of tentative step) are presented. They show that, in 14 of 15 cases, global lows have been identified.

3. Conditions of effective application of a method of the merge of vertexes are established. In networks activities of 1, 2, 3 stage is revealed. The proposed algorithm is guaranteed to determine the global minimum cut, passing through the activities of one or two adjacent stages. The probability of finding a global minimum cut in any critical networks is very high.

4. The method presented was used to optimize the network schedule. Compression of the critical path from 36 to 22 days was carried out for 14 iterations. As a result, the optimal schedule was obtained. At the same time, the number of additional attracted resources is minimal.

The method presented in this study used Microsoft Excel.

The suggested method can be recommended for use by construction project managers in order to prevent a potential failure of project completion deadlines.

References

1. Avdeev Yu.A. *Vyrabotka i analiz planovykh resheniy v slozhnykh proyektakh* [Development and the analysis of planned decisions in complex projects]. Moscow: Economy. 1971. 96 p. (rus)
2. Afanasyev V.A. *Potochnaya organizatsiya rabot v stroitelstve* [Flowing organization works in construction]. Leningrad, 1990. 169 p. (rus)
3. Barkalov P.S., Burkova I.V., Glagolev A.V., Kolpachev V.N. Zadachi raspredeleniya resursov v upravleniya proyektami [Problems of distribution of resources in project management]. Moscow: IPU RAN. 2002. 65 p. (rus)
4. Kaklauskas A. Kelpsiene L. Zavadskas E.K., (…) Urbonas M., Sorakas V. Crisis management in construction and real estate: Conceptual modeling at the micro-, meso- and macro-levels. *Land Use Policy.* 2011. No. 28(1). Pp. 280–293.
5. Kaklauskas A. Zavadskas E.K., Banaitis A. Banaitiene N. Kanapeckiene L. Knowledge management in construction project management. *Book Chapter. Knowledge Management: Technology, Applications and Impact. Vilnius Gediminas Technical University.* 2013. Pp. 91–188.
6. Kalugin Yu.B., Tupitsyn R.Yu. Optimizatsiya kalendarnykh planov po srokam (szhatiye) [Optimizing time schedules (compression)]. Computer program № 2017618044. 21.07.17.
7. Kalugin Yu. B., Tupitsyn R.Y. 2017. Vybor rabot dlya «szhatiya» kriticheskogo puti kalendarnogo grafika [Choice of activities for crashing the critical path of the network schedule]. *News of Higher Educational Institutions. Construction.* 2017. No. 2. Pp. 29–38. (rus)
8. Ford L.R., Fulkerson D.R. Maximal flow through a network. *Canadian Journal on Mathematics.* 1956. No. 8. Pp. 394–404.
9. Mubarak S. *Construction Project Scheduling and Control Second Edition*. John Wiley & Sons, Inc. 2010. 437 p.
10. Elmabrouk O.M. Scheduling Project Crashing Time using Linear Programming Technique. *Proceedings of the 2012 International Conference on Industrial Engineering and Operations Management.* Istanbul, Turkey, July 3–6, 2012.
11. Haga W.A., O'keefe T. Crashing PERT networks: a simulation approach. *Paper presented at the 4th International conference of the Academy of Business and Administrative Sciences Conference.* Quebec City, Canada July 12-14, 2001.
12. Kolish R., Hartmann S. Heuristic algorithms for the resource-constrained project scheduling problem: classification and computational analysis. *Project Scheduling—Recent*

Литература

1. Авдеев Ю.А. Выработка и анализ плановых решений в сложных проектах. М.: Экономика, 1971. 96 с.
2. Афанасьев В.А. Поточная организация строительства. Л.:Стройиздат, 1990. 303 с.
3. Баркалов П.С., Буркова И.В., Глаголев А.В., Колпачев В.Н. Задачи распределения ресурсов в управления проектами. М.: ИПУ РАН, 2002. 65 с.
4. Kaklauskas A. Kelpsiene L. Zavadskas E.K., (…) Urbonas M., Sorakas V. Crisis management in construction and real estate: Conceptual modeling at the micro-, meso- and macro-levels // Land Use Policy. 2011. № 28(1). Pp. 280–293.
5. Kaklauskas A. Zavadskas E.K., Banaitis A. Banaitiene N. Kanapeckiene L. Knowledge management in construction project management // Book Chapter. Knowledge Management: Technology, Applications and Impact. Vilnius Gediminas Technical University 2013. Pp. 91–188.
6. Калугин Ю.Б., Тупицын Р.Ю. Оптимизация календарных планов по срокам (сжатие). Программа для ЭВМ. № 2017618044. 21.07.17.
7. Калугин Ю.Б. , Тупицын Р.Ю. Выбор работ для «сжатия» критического пути календарного графика // Известия вузов. Строительство. Новосибирск. 2017. № 2. С. 29–38.
8. Ford L.R., Fulkerson D.R. Maximal flow through a network // Canadian Journal on Mathematics. 1956. № 8. Pp. 394–404.
9. Mubarak S. Construction Project Scheduling and Control Second Edition. John Wiley & Sons, Inc. 2010. 437 p.
10. Elmabrouk O.M. Scheduling Project Crashing Time using Linear Programming Technique // Proceedings of the 2012 International Conference on Industrial Engineering and Operations Management. Istanbul, Turkey, July 3 – 6, 2012.
11. Haga W.A., O'keefe T. Crashing PERT networks: a simulation approach // Paper presented at the 4th International conference of the Academy of Business and Administrative Sciences Conference Quebec City, Canada July 12-14, 2001.
12. Kolish R., Hartmann S. Heuristic algorithms for the resource-constrained project scheduling problem: classification and computational analysis // Project Scheduling—Recent Models, Algorithms and Applications. Boston: Kluwer Academic Publishers. 1999. Pp. 147–178.

Models, Algorithms and Applications. Boston: Kluwer Academic Publishers. 1999. Pp. 147–178.

13. Najib G., Nabil S., Rizk J. Crash: an automated tool for schedule crashing. *International Journal of Science and Technology*. 2014. Vol. 3. No. 2. Pp. 374–394.
14. Perera S. Linear Programming Solution to Network Compression. *Journal of the Construction Division. Proceedings of the ASCE*. 1980. Vol. 106. No. 3. Pp. 315–316.
15. Sahu K., Sahu M. Cost & Time and Also Minimum Project Duration Using Alternative Method. *International Review of Applied Engineering Research.* 2014. Vol. 4. No. 5. Pp. 403–412.
16. Chassiakos A.P., Sakellaropoulos S.P., Time–cost optimization of construction projects with generalized activity constraints. *J. Constr. Eng. Manag., ASCE.* 2005. Vol. 131(10). Pp. 1115–1124.
17. Jiang A., Issa R.R.A., Malek M. Construction project cash flow planning using the Pareto optimality efficiency network model. *Journal of Civil Engineering and Management.* 2011. Vol. 17(4). Pp. 510–519.
18. Liu S.-S., Wang C.-J. Optimizing project selection and scheduling problems with time-dependent resource constraints. Automation in Construction. 2011. Vol. 20. No. 8. Pp. 1110–1119.
19. Chiu H.N., Tsai D.M. An efficient search procedure for the resource-constrained multi-project scheduling problem with discounted cash flows. *Construction Management and Economics*. 2002. Vol. 20(1). Pp. 55–66.
20. Demeneva E.A. 2012. Optimizatsija raspisanij stroitelstva transportnyh vodopropusknyh sooruzhenij po vremeni i resursam. [Optimization of schedules of construction of transport water throughput constructions on time and resources]. *Transport construction.* No. 5. Pp. 20–21. (rus)
21. Klykov M.S., Demeneva E.A. 2012. Vybor variantov intensifitsirovaniya stroitelstva malykh vodopropusknykh sooruzheniy zheleznoy dorogi [Choice of options of an intensification of construction of small artificial constructions of the railroad]. *Architecture and construction of Russia.* No. 3. Pp. 2–12. (rus)
22. Malyshev B.S. Dvoystvennyy setevoy grafik [Dual network schedule]. *Problems of development and deployment of ACS at machine-building enterprises.* Novosibirsk. 1972. 164 p. (rus)
23. Kalugin Yu.B., Klykov M.S., Tupitsyn R.Yu. 2017. Osobennosti primenenija dvojstvennogo grafa dlja opredelenija minimalnogo razreza setevoj modeli.[Features use the dual graph to determine the minimum cut of the network schedule]. *News of Higher Educational Institutions. Construction.* 2017. No. 6. Pp. 94–100. (rus)
24. Rogalska M., Bojeiko W., Hejducki Z. Time/cost optimization using hybrid evolutionary algorithm in construction project scheduling. *Automation in Construction.* 2008. Vol. 18. Pp. 24-31.
25. Adeli H., Karim A. Scheduling/cost optimization and neural dynamics model for construction. *J. Constr. Engrg. and Mgmt., ASCE.* 1997. Vol. 123. Pp. 450–458.
26. Barkalov S.A., Vorotilina M.A., Kurochka P.N., Potapenko A.M. Raspredelenie resursov po minimal'noj prodolzhitel'nosti rabot.[Distribution of resources on the minimum duration of works]. *Control systems and information technologies.* 2005. No. 2(19). Pp. 64–67. (rus)
27. Stoer M., Wagner F. (1997). A simple min-cut algorithm. *Journal of the ACM*. 1997. Vol. 44(4). Pp. 585–591.
28. Nagamochi H., Ibaraki T. Computing edge-connectivity in multiple and capacitated graphs. *SIAM Journal on Discrete Mathematics*. 1992. No. 5. Pp. 54–66.
29. Kalugin Yu.B. Poisk minimalnogo razreza setevoy modeli sliyaniem vershin pri optimizatsii kalendarnykh planov po srokam.[Search of a minimum cut of the network schedule

13. Najib G., Nabil S., Rizk J. Crash: an automated tool for schedule crashing // International Journal of Science and Technology. 2014. Vol. 3. № 2. Pp. 374–394.
14. Perera S. Linear Programming Solution to Network Compression // Journal of the Construction Division. Proceedings of the ASCE. 1980. Vol. 106. № 3. Pp. 315–316.
15. Sahu K., Sahu M. Cost & Time and Also Minimum Project Duration Using Alternative Method // International Review of Applied Engineering Research. 2014. Vol. 4. № 5. Pp. 403–412.
16. Chassiakos A.P., Sakellaropoulos S.P., Time–cost optimization of construction projects with generalized activity constraints // J. Constr. Eng. Manag., ASCE. 2005. Vol. 131(10). Pp. 1115–1124
17. Jiang A., Issa R.R.A., Malek M. Construction project cash flow planning using the Pareto optimality efficiency network model // Journal of Civil Engineering and Management. 2011. Vol. 17(4). Pp. 510–519.
18. Liu S.-S., Wang C.-J. Optimizing project selection and scheduling problems with time-dependent resource constraints. Automation in Construction. 2011. Vol. 20. № 8. Pp. 1110–1119.
19. Chiu H. N., Tsai D. M. An efficient search procedure for the resource-constrained multi-project scheduling problem with discounted cash flows // Construction Management and Economics. 2002. Vol. 20(1). Pp. 55–66.
20. Деменева Е.А. Оптимизация расписаний строительства транспортных водопропускных сооружений по времени и ресурсам // Транспортное строительство. 2010. № 5. С. 20–21.
21. Клыков М.С., Деменева Е.А. Выбор вариантов интенсифицирования строительства малых водопропускных сооружений железной дороги // Архитектура и строительство России. 2012. №3. С. 2–12.
22. Малышев Б.С. Двойственный сетевой график // В сб. Проблемы разработки и внедрения АСУ на машиностроительных предприятиях. Новосибирск, 1972. 164 с.
23. Калугин Ю.Б., Клыков М.С., Тупицын Р.Ю. Особенности применения двойственного графа для определения минимального разреза сетевой модели// Известия вузов. Строительство. Новосибирск. 2017. № 6. С. 94–100.
24. Rogalska M., Bojeiko W., Hejducki Z. Time/cost optimization using hybrid evolutionary algorithm in construction project scheduling // Automation in Construction. 2008. Vol. 18. Pp. 24–31.
25. Adeli H., Karim A. Scheduling/cost optimization and neural dynamics model for construction // J. Constr. Engrg. and Mgmt., ASCE. 1997. Vol. 123. Pp. 450–458.
26. Баркалов С.А., Воротилина М.А., Курочка П.Н., Потапенко А.М. Распределение ресурсов по минимальной продолжительности работ // Системы управления и информационные технологии. 2005. № 2(19). С. 64–67.
27. Stoer M., Wagner F. A simple min-cut algorithm // Journal of the ACM. 1997. Vol. 44(4). Pp. 585–591.
28. Nagamochi H., Ibaraki T. Computing edge-connectivity in multiple and capacitated graphs // SIAM Journal on Discrete Mathematics. 1992. № 5. Pp. 54–66.
29. Калугин Ю.Б. Поиск минимального разреза сетевой модели слиянием вершин при оптимизации календарных планов по срокам // Известия вузов. Строительство. Новосибирск, 2018. № 1. С. 104–112.
30. Калугин Ю.Б. Поиск минимального сечения в критической сети методом слияния вершин. Программа для ЭВМ, № 2018613988, 27.03.18.

by merging vertices]. *News of Higher Educational Institutions. Construction.* 2018. No. 1. Pp. 104–112. (rus)

30. Kalugin Yu. B. Poisk minimalnogo secheniya v kriticheskoy seti metodom sliyaniya vershin. Programma dlya EVM [Search of a minimum cut of the network schedule by merging vertices. Computer program]. № 2018613988, 27.03.18.(rus).

Yurii Kalugin,*
+7(905)216-28-25; yuri_kalugin@inbox.ru

Arturas Kaklauskas,
+3705-274-52-34; arturas.kaklauskas@vgtu.lt

Yurii Kazakov,
+7(981)757-57-77; kazakov@spbgasu.ru

Юрий Борисович Калугин,*
+7(905)216-28-25;
эл. почта: yuri_kalugin@inbox.ru

Артурас Каклаускас
+3705-274-52-34;
эл. почта: arturas.kaklauskas@vgtu.lt

Юрий Николаевич Казаков,
+7(981)757-57-77;
эл. почта: kazakov@spbgasu.ru

doi: 10.18720/MCE.80.5

Influence of stiffness of node on stability and strength of thin-walled structure

Влияние жесткости узловых соединений на устойчивость и прочность тонкостенных конструкций

I.V. Atavin,
B.E. Melnikov,
Peter the Great St. Petersburg Polytechnic University, St. Petersburg, Russia
A.S. Semenov,
Dresden University of Technology, Dresden, Germany
N.V. Chernysheva*,
E.L. Yakovleva,
Peter the Great St. Petersburg Polytechnic University, St. Petersburg, Russia

Студент И.В. Атавин,
д-р техн. наук, профессор Б.Е. Мельников,
Санкт-Петербургский политехнический университет Петра Великого, г. Санкт-Петербург, Россия
канд. физ.-мат. наук, ведущий научный сотрудник А.С. Семенов,
Дрезденский технический университет, г. Дрезден, Германия
канд. техн. наук, доцент Н.В. Чернышева*,
канд. техн. наук, доцент Е.Л. Яковлева,
Санкт-Петербургский политехнический университет Петра Великого, г. Санкт-Петербург, Россия

Key words: light steel thin-walled structure; torsional stiffness; finite element method (FEM); girder rack; beam; pillar; tier; buckling; critical load

Ключевые слова: легкая стальная тонкостенная конструкция; крутильная жесткость; метод конечных элементов (МКЭ); стеллаж; балка; стойка; ярус; потеря устойчивости; критическая сила

Abstract. The article is devoted to the evaluation of the torsional stiffness of the beam-pillar nodal connection of thin-walled rack structures. Results of in-place testing of several girder rack models are described, beam model and combined one are considered. Computational finite element (FE) models of these racks are designed to develop a FE analysis by software complex ANSYS. Assessment of the torsional stiffness of the beam-pillar nodal connection in these structures is obtained by comparison of results of computation and experimental ones. Critical buckling load for the first buckling mode is determined both experimentally and computationally. Buckling modes of “out of the face plate” and “in the face plate” are considered. The influence of the torsional stiffness of the beam-pillar nodal connection on bearing capacity and buckling stability of thin-walled rack structure is investigated. Correspondence of these characteristics and number of tiers is revealed.

Аннотация. Выполнена оценка крутильной жесткости узлового соединения балка-стойка в тонкостенной конструкции стеллажа. Проведены натурные испытаний различных моделей стеллажей, рассматриваются конструкции балочного и комбинированного типов. Построены расчетные схемы этих конструкций, произведены расчеты методом конечных элементов (МКЭ) в программном комплексе ANSYS. Из сравнения экспериментальных данных и результатов расчета на устойчивость получены оценки значения жесткости на кручение для соединения балка-стойка в этих конструкциях. Экспериментально и численно определены значения критической силы, соответствующей первой форме потери устойчивости. При этом рассматривались формы потери устойчивости во фронтальной плоскости конструкции и с выходом из плоскости. Проанализировано влияние крутильной жесткости соединения балка-стенка на несущую способность и устойчивость конструкции тонкостенного стеллажа. Отмечена зависимость этих характеристик от количества этажей в модели стеллажа.

Атавин И.В., Мельников Б.Е., Семенов А.С., Чернышева Н.В., Яковлева Е.Л. Влияние жесткости узловых соединений на устойчивость и прочность тонкостенных конструкций // Инженерно-строительный журнал. 2018. № 4(80). С. 48–61.

1. Introduction

Wide use of metalwork in industrial and civil engineering is one of the modern development trends in construction industry. Metalwork attractiveness is connected to development and deployment of new production technologies.

Use of construction designed of light steel cold-formed thin-walled cross-section (LSTC) is a new and fast-progressing trend. The low metal consumption, optimum parameters of cross-section, simplicity of transportation and installation are the general advantages of LSTC.

Estimation of strength and operational characteristics of new types of sections and connections is made gradually. The first stage is a test of real construction, and the second stage is a numerical analysis of construction by specialized program complexes. The standard estimate norms are used to interpret data obtained. Other important factors that influence on operational characteristics of LSTC can be defined experimentally. In particular, the longevity of connections which considerably influences on endurance of LSTC can be defined.

Eurocode-3 and AISI are the relevant standards and regulations to be in use now for analysis of LSTC.

The first who have investigated deformation of thin-walled constructions was S.P. Timoshenko [1, 2]. Torsion stiffness of thin-walled bar of open cross-section is estimated experimentally. Also the behavior of thin-walled bars of different cross-section is investigated.

The principles of buckling analysis of thin-walled bar of open cross-section in view of application of force out of cross-section core as well as of torsion and bending analysis are worked out by V.Z. Vlasov in [3–5]. Another way to analyze bending with constrained torsion of thin-walled bar is proposed by A.A. Umanskyi in [6].

D.V. Bychkov and A.K. Mrozchinskyi [7–9] perform a significant contribution to the theory of calculation of thin-walled constructions. They worked out an algorithm of analysis of torsion beam forces depend upon number of beam spans and way of end fastening. This algorithm employed as force or deflection method allows to analyze restrained torsion of frames and other thin-walled constructions.

The FE analysis is applied to torsion and bending of thin-walled constructions in paper by A.R. Tusnin [10]. This approach appreciates influence of type of connections, centre-of-gravity position, beam deflection and amount of eccentricity.

Improved algorithm of LSTC analysis is elaborated and fail-safety and endurance of constructions and way to increase them are examined by V.A. Rybakov [11, 12]. Also Russian regulations imperfections are pointed out and ways of correction them are proposed.

Reviewing in paper [13] provides insight into production engineering, features of setting-up and operation of LSTC.

A method of thin-walled constructions with built-up section analysis is developed in paper [14]. This approach consists in general buckling analysis in terms of limit state of stress in view of form of section.

Composite materials technologies of production reinforced concrete construction are considered in [15, 16]. In this context, quality control, materials specification, setting-up and operating regulations, structural reinforcement are also discussed.

Deformations and damage accumulation take their cue for the approaches of thin-walled constructions analysis developed in [17–19].

General rules, definition, typical thin-walled member specification, reference models and design techniques are presented in [20–22].

The effect of temperature (from low to high, including fire conditions) on the strength and operating characteristics of thin-walled structures is discussed in [23, 24].

In-place testing results and results of simulation experiments by means of specialized software complexes are compared in [25, 26].

Post-buckling behavior columns and rods with open and semi-open thin-walled cross-section are considered in [27, 28]. The effect of eccentric applying of axial load on the deformation and deflections of frames and beams in this connection is discussed in [29, 30].

A review of Russian and foreign references is made in [35–38]. General attention is paid to the studies of buckling of cold-formed thin-walled beams. The experimental data are compared with values obtained by using both beam and shell finite elements in a computer simulation. In this context, arising problems are formulated and ways to solve them are proposed.

The analytic model of the long span footway bridge is studied and tested in [39, 40]. The effect of the types of thin-walled cold-formed profile members on the operating characteristics of the bridge construction is tested by numerical simulation.

The new specialized software complex "Stalkon" is presented in [41–43]. This software is meant to be used for design and static analysis of thin-walled member construction (three-dimensional one includes) according to modern rules and regulations. An example of pin-ended column's analysis is presented. The possibility of restrained torsion analysis of thin-walled structures by software complexes ANSYS and NASTRAN is discussed.

The purpose of works [44–46] is to develop a numerical method of thin-walled bar systems design by using semi-sheared and non-sheared theories. Matrixes of the inflexibility of thin-walled finite elements of four various types are created. Some test torsion problems of the thin-walled beam having various supporting are solved by the FEM.

Reduction of thin-walled member's cross-section is asserted in [47–49] by investigating of load carrying capacity. Optimal cross-section area is calculated on the base of buckling analysis. A problem of analysis of thin-walled member of double-corrugated profile is solved by linear and non-linear approaches. The results are compared with in-place testing results. Also results of in-place test for real thin-walled cold-formed member truss with span of 18 m are considered.

Fatigue analysis of LSTC in terms of nonlinear damage accumulation and fatigue rupture is considered in [50–53]. The energy approach is used in [54–58] to estimate the low-cycle fatigue of thin-walled member structures. A kinetic algorithm of damage analysis of LSTC is developed and experimentally verified. The problem of mechanochemical corrosion of a thin-walled pillar under its own weight is considered in [59].

The objective of this work is to evaluate the stiffness of the beam-pillar connection of thin-walled members of a three-dimensional structure. Stages of implementation of handling the problem are:

- to construct an experimental set-up for testing of thin-walled structures;
- to develop an analytical finite element model of structures by the ANSYS software complex, to verify results of numerical solution experimentally;
- to define stiffness properties of the connection computationally and experimentally.

2. Methods

2.1. Stiffness of connections of horizontal, diagonal and vertical LSTC members

Accounting of a torsional stiffness of connections in a beam rack is important for assessment of girder rack critical buckling load by a stability criterion. The study request provided only the computational and experimental evaluation of a beam rack connection stiffness.

A new approach in girder racks design includes only horizontal braces unlike diagonal bracing of pallet racks that provides the lack of buckling with escaping of the face plane. So in new modification of a girder rack such buckling mode could appear, and corresponding critical buckling load generally depends on torsion stiffness of brace-pillar connection. Therefore the need of accounting of brace-pillar connection stiffness was revealed in the course of the researches. A test trial of indirect observation of the stiffness not the bound to direct measurements is made. To receive precise assessment extension studies are recommended.

A complex study both experimental and computational is pursued to determine torsion stiffness of beam-pillar connection, included in-place testing of girder rack simplified model and the FE analysis.

Beam and pillar members of the model rack are made of BT-PN-1.5 steel band conforming to Russian State Standard GOST 19904–90. The thickness of the steel band is 1.5 mm. The yield stress for steel 20 is 230 MPa, allowable stress used in computations is 160 MPa. Bearing horizontal beam members have closed box-shaped cross-section of 70x30 mm in Figure 1. Bearing vertical members have opened profile cross-section of 90x30 mm in Figure 2.

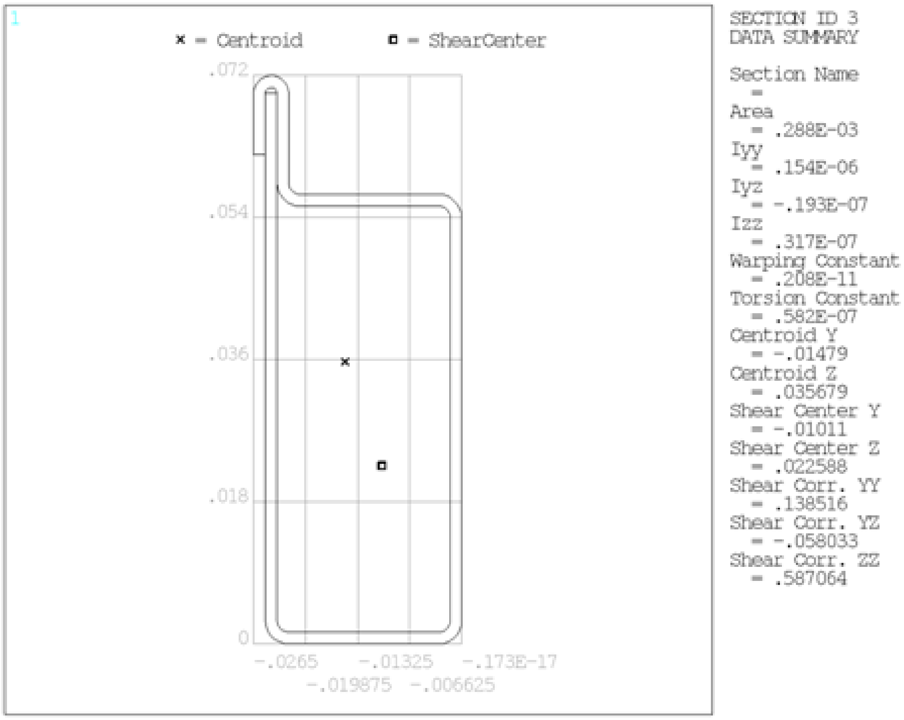

Figure 1. The cross-section of bearing horizontal beams

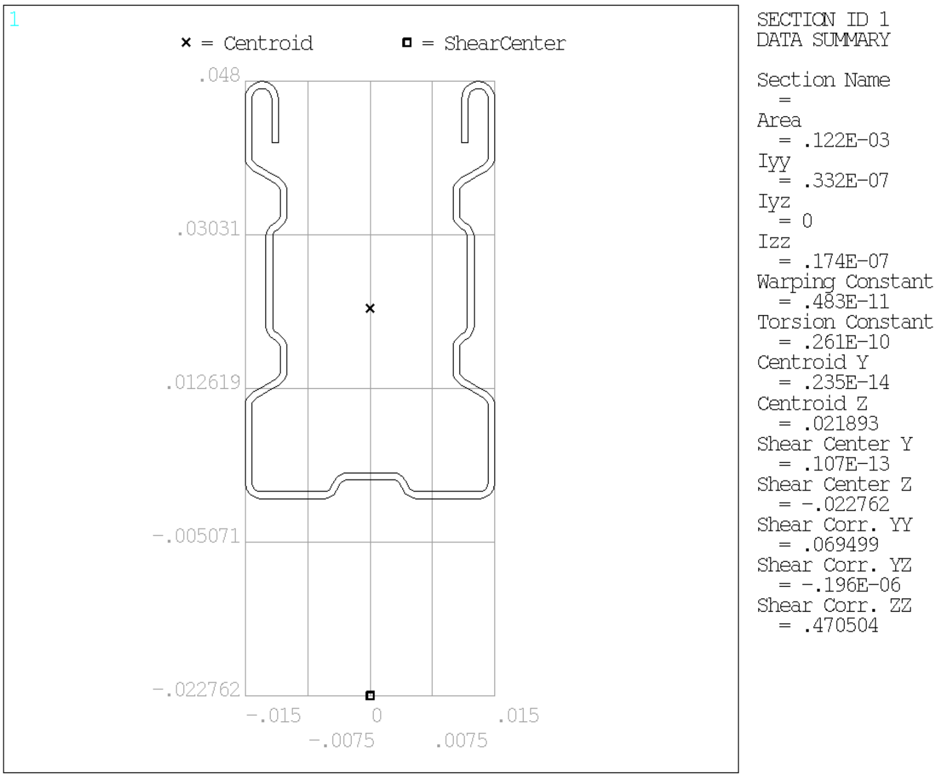

Figure 2. The cross-section of bearing vertical pillars

The model rack studied consists of two horizontal 1500 mm long beams (see Figure 3), the height of the vertical pillars is 1000 mm, each beam is connected with two pillars apart 135 mm from their upper edge and with two pillars apart 110 mm from their lower edge and then the frames obtained are connected with two 300 mm long braces. The distance between the pillars is 1500 mm in face plane direction and 300 mm in crosswise direction. Despite the absence of rack baseplate's horizontal and vertical restraint no displacements of baseplates are obtained during tests.

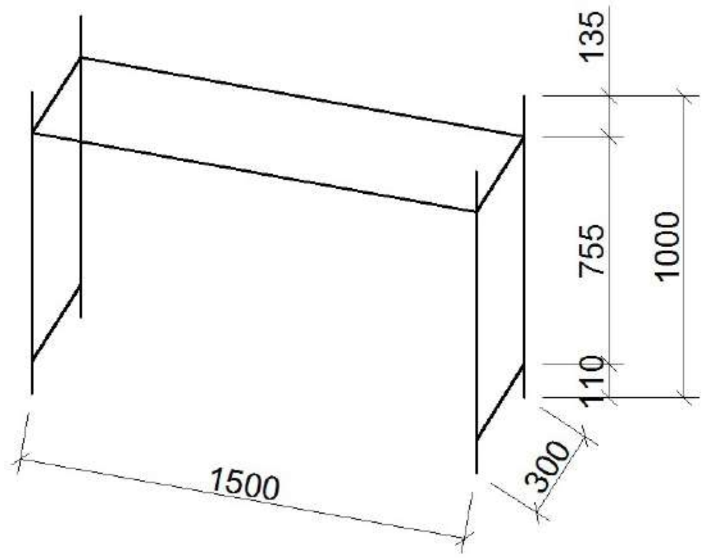

Figure 3. The geometrical parameters of the model rack

The model is loaded by “Armsler” testing machine through auxiliary device intended to simulate a uniformly distributed load. The load was converted from concentrated to distributed using an auxiliary structure. The system was made from channels 16P. The lower part consisted of 4 beams 350 mm long, located transversely with the investigated. The next tier was made of two beams 50 cm long. The final tier had a length of 100 cm. The additive weight load from the auxiliary structure is 0.5 kN, which was taken into account during the tests.

Beams are connected by wire in horizontal direction to prevent a horizontal bending and therefore keep safety arrangements. Central nodes of beams in computational model have rigid connection in z-direction to consider this construction feature. Displacements of pillars are measured by dial indicators.

In an experiment the following results are obtained. Under total load of 11.2 kN the model gets a stability mode without inelastic deformation. This load can be considered as a first buckling mode critical load for the model. The load of 11.2 kN was determined from the indications of a dynamometer attached to the moving part of the "Armsler" power machine.

The numerical simulations were performed by the FE tool ANSYS. The model consists of beam finite elements. This FE model is represented in Fig. 4. Beam-pillar connection torsional stiffness with regard to the turn about Z-axis (plane deformation in face plane) can be calculated by computational analysis of the model.

In computations, the dead load of the beams was not taken into account, since it is negligibly small in comparison with the permissible load of the structure.

Supporting nodes of pillars are connected with rigid base (displacements U_x, U_y and U_z are zeros), angular rotation R_y is also zero, non-zero angular rotations R_x, R_z are defined automatically in the FE computations by means of account of elastic torsional stiffness of supports.

Transfer of loads from beams to pillars is simulated by elastic z-axis turn-elements.

Arrangement of nodes allows to consider effect of non-centering load applying correctly by simulation of interaction between pillars and beams through spiked hooks (the beam loads the pillar along rigid wall).

Required value of beam-pillar connection torsional stiffness is approximately defined by the iterative method with considering experimental data. Convergence condition of the iterative process is agreement of the first buckling mode and corresponding critical load obtained numerically and experimentally.

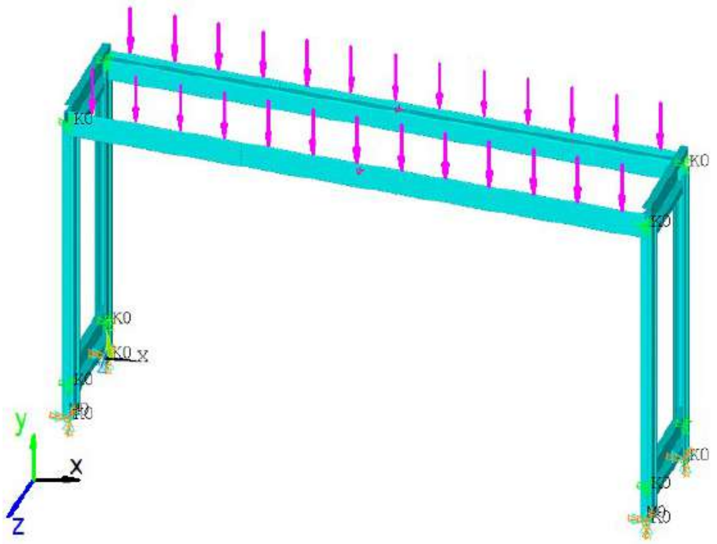

Figure 4. Computational model of rack for evaluation of beam-pillar connection torsional stiffness

In computation the following results are received. Torsional rigidity of beam-pillar connection with regard to the rotation about z-axis for simplified single-span girder rack model is 2820 N•m/rad. Corresponding buckling mode is represented in Fig. 5. Further tests are needed to reveal dependence torsional stiffness of beam-pillar connection and critical tier load from number of tiers. The “Eigen Buckling” type of analysis based on block Lanczos method was used in FE computations.

Figure 5. The first buckling mode (plane deformation in face plate). Critical load is 11.2 kN (experimental value). Torsional stiffness of beam-pillar connection with regard to the rotation about z-axis is 2820 N·m/rad

2.2. Experimental invesrigation of the connection stiffness

In order to confirm the reliability of the obtained results of the buckling critical load, in-place tests of real girder racks were carried out and additional analysis of elaborated rack models was done to imitate real structures as close as possible. Two versions of the rack design were tested: beam and combined (plate-beam) versions. The cross-sections and characteristics of the beams and pillars correspond to those used in the experiment with the simplified model. Geometric parameters of both versions are (see Figures 6a and b): single-section or three-section rack, height $H = 2500$ mm, length of span $L = 1500$ mm, height of the first loaded level $h = 135$ mm, width of the rack $b = 600$ mm.

Structure was loaded by a uniformly distributed load through the shelves made of the same rolled steel as the beams (see Figure 6c). Loads for all tiers were equal. Boxes filled with metal blanks of 1 kg weigh were used to simulate load on the shelves.

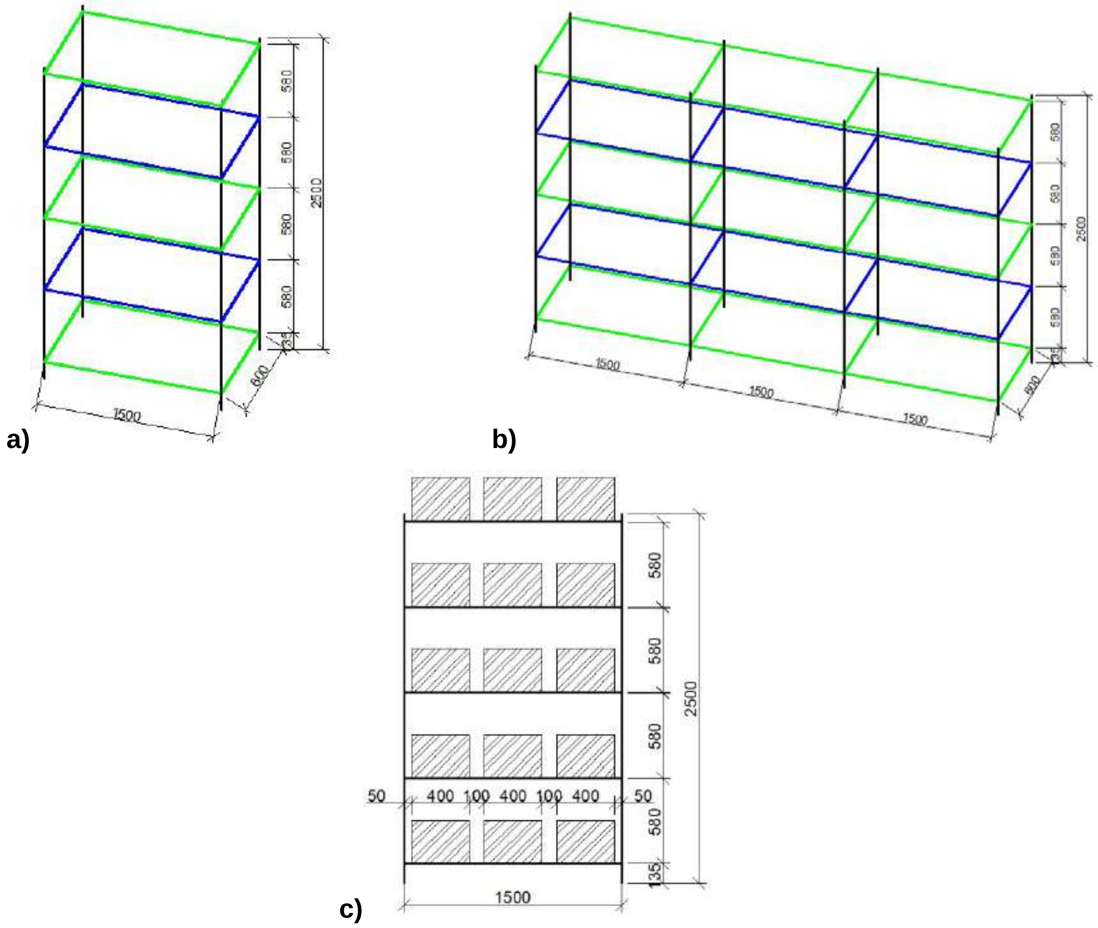

Figure 6. Geometry of a) one-section and b) three-section racks;
c) quasi-uniformly distributed loading

Measurements of the displacements of the investigated thin-walled structure were made by several dial indicators. Dial indicators have an operating range from 0 to 80 mm, the measurement accuracy is 0.01 mm. In the case of a single-section rack, the indicators for a single-section girder rack are installed to determine the displacements of one of the pillars along the X and Z axes in its upper part. On the other hand, the indicators determine displacements of one of the two most stressed internal pillars when a three-section girder rack is tested.

Beam finite elements are used to make a FE model of the racks. This approach allows to take into account the shape of the beam cross-section profile in the most correct way. The horizontal beams of all tiers are loaded with equal uniformly distributed load.

Boundary conditions are the conditions of the elastic rotation connections (an elastic flap hinge) of the pillar's supporting nodes with the rigid base. The displacements U_x, U_y, U_z, and also the angular rotation R_y are fixed, the angular rotations R_x and R_z are defined by the elastic flap hinge stiffness.

The main difference between the beam and combined FE models is except that in the combined one the upper and lower tiers also consist of beam element (with a certain value of torsional stiffness of the beam-pillar connection), the other tiers are replaced by shelves (with zero value of the torsional stiffness of the beam-pillar connection).

3. Results and Discussion

The results of calculations of the critical buckling load according to the approach developed above for the considered versions of girder rack's design are presented in Table 1. In the same table, the results of computations for a three-section girder rack are given for comparison (Figure 7).

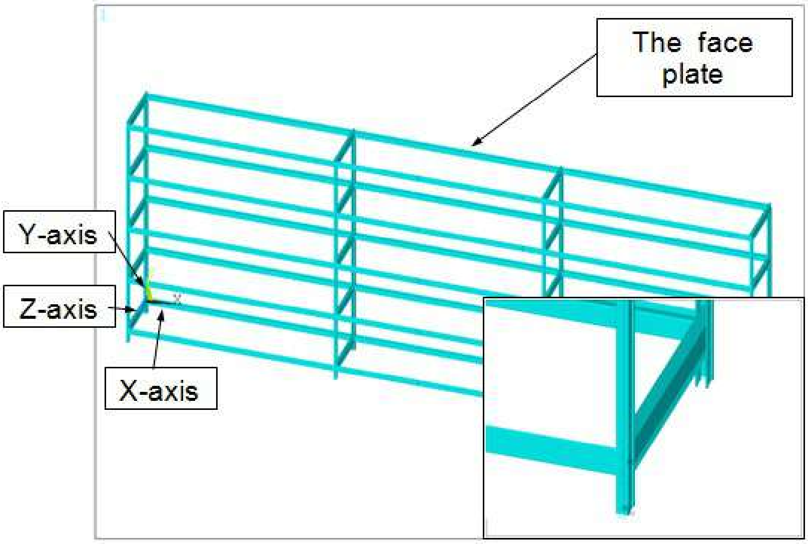

Figure 7. The FEM model of the three-section girder rack

Table 1. Estimated critical buckling load on the level (in kN)(H = 2500 mm, L = 1500 mm, h = 135 mm, b = 600 mm, 5 tiers)

	Beam model		**Combined model**	
	1 section	3 sections	1 section	3 sections
"Out of the face plane"	***3.36***	2.35	***3.49***	2.44
"In the face plane"	**6.29**	5.87	**2.46**	2.17

According to the results represented in Table.1 a single-section rack is more stable than a three-section one. This effect can be explained by the fact that the most stressed pillar's load of the three-section rack is 2 times greater than in the one-section. So if the beam-pillar node connection would be hinged, the critical load for "in the face-plane" buckling of the single-section rack would be 2 times greater than the critical load for the three-section one. But since this node has definite stiffness, the difference in values of critical loads is smaller than 2. Moreover, a certain ratio of the stiffness of the beam-pillar connection and the stiffness of the pillar itself allows the critical load for a three-section rack to be greater than one for the one-section rack. This situation is typical for pallet girder racks, where the stiffness of both the pillar itself and the beam-pillar connection are large enough.

Table 2. Experimental critical buckling load for combined girder rack (in kN)

	1 section			**3 sections**		
	1	2	3	1	2	3
"Out of the face plane"	2.49	2.49	2.48	1.74	1.74	1.75
"In the face plane"	1.75	1.77	1.76	1.56	1.54	1.57

As a result of the experiments, the following data were obtained. In the course of the experiment, three girder racks of each type were tested. The test results are shown in Table 2. The average critical load on the combined girder rack was 1.76 kN. It corresponds to the initial stage of buckling "in the face plane". The structure got an adjacent deflected equilibrium state. The rack did not fracture. The maximum load reached during the test was 2.49 kN. the test was stopped due to the fact that the load exceeded the expected calculated value of 2.46 kN. The rack under this load had stability mode deflected from the vertical one, the deviation was 60 mm. The ratio of the experimental and calculated critical load values is 1.76 / 2.46 = 0.717.

Table 3. Experimental critical buckling load for beam girder rack (in kN)

	1 section			**3 sections**		
	1	2	3	1	2	3
"Out of the face plane"	-	-	-	-	-	-
"In the face plane"	3.34	3.36	3.33	3.12	3.10	3.13

Testing beam girder racks had the same amount of sections that combined one. The average value of the critical load for the beam rack was 3.34 kN. This value corresponds to the initial stage of buckling “in the face plane”. The rack got a adjacent deflected equilibrium state and did not fracture. The maximum load reached during the test was 3.76 kN. The rack under this load had stability mode deflected from the vertical one, the deviation was 15 mm. A tendency to "out of the face plane" buckling isn’t observed. The value of the expected calculated critical "in the face plane" buckling load of 6.29 kN was not achieved. The ratio of the experimental and calculated critical load values is 3.34 / 6.29 = 0.532.

The difference between experimental and estimated critical buckling loads for the beam and combined racks is given in Table 4 and 5.

Table 4. Comparison of experimental and estimated critical buckling loads for beam girder rack

	1 section			**3 sections**		
	Estimated, N	Experimental, N	Difference, %	Estimated, N	Experimental, N	Difference, %
"Out of the face plane"	3.36	-	-	2.35	-	-
"In the face plane"	6.29	3.34	53.2	5.87	3.12	53.15

Table 5. Comparison of experimental and estimated critical buckling loads for combined girder rack

	1 section			**3 sections**		
	Estimated, N	Experimental ,N	Difference, %	Estimated, N	Experimental , N	Difference, %
"Out of the face plane"	3.49	2.49	71.3	2.44	1.74	71.3
"In the face plane"	2.46	1.76	71.7	2.17	1.56	71.9

Reduction of the experimental values of the calculated critical "in the face plane" buckling load in comparison with the calculated ones has two main causes.

The first reason is that the calculation of this work is based on value of the stiffness of the beam-pillar connection equal to 2820 N·m/rad. This value obtained in part 2.1 due to experimental data of the simplified model and corresponds to a load of 11.2 kN. In this assumption the calculation model (the simplified model in the beginning of the paper) has a deflected (not vertical) stability mode. Thus, the calculation is based on an overestimated value of this rigidity. The actual value of the equivalent stiffness of the beam-pillar connection is in the range 1330–2030 N·m/rad.

The second reason is more complicated. Increasing of the number of tiers of the rack without change of its height results in non-uniform distribution of the stiffness of the middle tiers located in the zone of kink of buckling pillars decreases. Thus equivalent stiffness of the middle tiers located in the zone of kink of buckling pillars decreases. An analysis of causes of this non-uniform distribution of the level of stiffness decrease and of the way to consider influence of these factors on calculating of the rack critical buckling loads would be the topic of future studies.

4. Conclusions

The results of the computational and experimental work can be formulated as follows:

1. The torsional stiffness of the beam-pillar connection for turning around the Z-axis is 1330-2030 N·m / rad.
2. The values of the critical buckling loads of the beam and combined models of girder racks (on the level) are determined by the stability condition. The values are given in tables 2-3.

To verify the results we recommend that:

1. The combined computational and experimental determination of the stiffness of the beam-pillar connection. For the most accurate results it is recommended to take into account the connecting plates in the joints, bolts, and contact between the elements on the surface.
2. The combined computational and experimental correction of the stiffness of the brace-pillar connection.
3. To evaluate the influence of the height of the first loaded level on the critical buckling loads for beam and combined girder racks of different types.

4. To investigate the causes of the non-uniform distribution of the stiffness of the beam-pillar connection. To consider influence of these factors on calculating of the rack critical buckling loads.

5. Acknowledgement

The reported study was funded by RFBR according to the research project 16-29-15128.

References

1. Timoshenko S.P. Ob ustoychivosti ploskoy formy izgiba dvutavrovoy balki [About stability of a bending in-plane mode of a double-tee beam]. *Izvestiya SPb Politekhnicheskogo instituta*. Vol. IV—V. Pp. 1905–1906.(rus)
2. Timoshenko S.P. *Istoriya nauki o soprotivlenii materialov: S kratkimi svedeniyami iz istorii teorii uprugosti i teorii sooruzheniy* [History of strength of materials with quick info on history of theory of elasticity and civil engineering]. Pod red. A.N. Mitinskogo. Izd. 2-ye, stereotipnoye. Moscow: KomKniga, 2006. 536 p.(rus)
3. Vlasov V.Z. *Tonkostennyye uprugiye sterzhni: Prochnost, ustoychivost, kolebaniya* [Thin-walled elastic bars: Strength, stability, oscillations]. Moscow, Leningrad : Gosudarstvennoye izdatelstvo stroitelnoy literatury, 1940. 276 p. (rus)
4. Vlasov V.Z. Krucheniye i ustoychivost tonkostennykh otkrytykh profiley [Torsion and stability of thin-walled opened profile cross-section]. *Stroitelnaya promyshlennost.* 1938. No. 6. Pp. 49–53; No. 7. Pp. 55–60. (rus)
5. Vlasov V.Z. *Obshchaya teoriya obolochek i yeye prilozheniya v tekhnike* [General theory and engineering applications of theory of shells]. Moscow: Gostekhizdat, 1949. 784 p. (rus)
6. Umanskiy A.A. *Krucheniye i izgib tonkostennykh aviakonstruktsiy* [Torsion and bending of thin-walled aviation-related structures]. Moscow: Oborongiz, 1939. 112 p. (rus)
7. Bychkov D.V. *Stroitelnaya mekhanika sterzhnevykh tonkostennykh konstruktsiy* [Structural mechanics of thin-walled bar systems]. Moscow: Gosstroyizdat, 1962. 476 p.(rus)
8. Bychkov D.V. *Raschet balochnykh i ramnykh sterzhnevykh sistem iz tonkostennykh elementov* [Analysis of thin-walled beam and frame structures]. Moscow, 1948. 208 p.(rus)
9. Bychkov D.V. *Mroshchinskiy A.K. Krucheniye metallicheskikh balok* [Torsion of steel beams]. Moscow, 1944. 260 p.(rus)
10. Tusnin A.R. *Raschet i proyektirovaniye konstruktsiy iz tonko- stennykh sterzhney otkrytogo profilya* [Analysis and design of thin-walled opened profile bar structures]: Avtoref. dis. na soisk. uchen. step. d.t.n.[PHD thesis]: Spec. 05.23.01 /A.R. Tusnin. M. 2004. 37 p.(rus)
11. Rybakov V.A. Sovremennyye metody rascheta metallokonstruktsiy iz tonkostennykh profiley [Modern computational methods of thin-walled metalwork analysis]. *Stroymetall.* 2007. No. 2(2). Pp. 36–38. (rus)
12. Rybakov V.A. Nadezhnost metallokonstruktsiy iz tonkostennykh profiley [Thin-walled metalwork reliability]. *Nauchno-tekhnicheskiye problemy prognozirovaniya nadezhnosti i dolgovechnosti konstruktsiy i metody ikh resheniya: Trudy Mezhdunar. Konf.* Saint-Petersburg, 2008. Pp. 292–295. (rus)
13. Alkhimenko A.I., Vatin N.I., Rybakov V.A. *Tekhnologiya legkikh stalnykh tonkostennykh konstruktsiy* [Production technologies of light steel thin-walled cross-section]. Saint-Petersburg: Izd-vo SPbGPU, 2008. 27 p.(rus)
14. Belyy G.I. K raschetu na ustoychivost sterzhnevykh

Литература

1. Тимошенко С.П. Об устойчивости плоской формы изгиба двутавровой балки // Известия СПб Политехнического института. Т. IV—V. С. 1905–1906
2. Тимошенко С.П. История науки о сопротивлении материалов: С краткими сведениями из истории теории упругости и теории сооружений: пер. с англ. Под ред. А.Н. Митинского. Изд. 2-е, стереотипное. М.: КомКнига, 2006. 536 с.
3. Власов В.З.Тонкостенные упругие стержни: Прочность, устойчивость, колебания. Москва, Ленинград: Государственное издательство строительной литературы, 1940. 276 с
4. Власов В.З. Кручение и устойчивость тонкостенных открытых профилей // Строительная промышленность. 1938. № 6. С. 49–53; № 7. С. 55–60.
5. Власов В.З. Общая теория оболочек и ее приложения в технике. М.: Гостехиздат, 1949. 784 с.
6. Уманский А.А. Кручение и изгиб тонкостенных авиаконструкций. М.: Оборонгиз, 1939. 112 с.
7. Бычков Д.В. Строительная механика стержневых тонкостенных конструкций. М.: Госстройиздат, 1962. 476 с.
8. Бычков Д.В. Расчет балочных и рамных стержневых систем из тонкостенных элементов. М. 1948. 208 с.
9. Бычков Д.В., Мрощинский А.К. Кручение металлических балок. М., 1944. 260 с.
10. Туснин А.Р. Расчет и проектирование конструкций из тонко- стенных стержней открытого профиля: Автореф. дис. на соиск. учен. степ. д.т.н.: Спец. 05.23.01 / А.Р. Туснин. М. 2004. 37 с.
11. Рыбаков, В.А. Современные методы расчета металлоконструкций из тонкостенных профилей // Стройметалл. 2007. № 2(2). С. 36–38.
12. Рыбаков В.А. Надежность металлоконструкций из тонкостенных профилей // Научно-технические проблемы прогнозирования надежности и долговечности конструкций и методы их решения: Труды Междунар. Конф. СПб., 2008. С. 292–295.
13. Альхименко А.И., Ватин Н.И., Рыбаков В.А. Технология легких стальных тонкостенных конструкций. СПб: Изд-во СПбГПУ, 2008. 27 с.
14. Белый Г.И. К расчету на устойчивость стержневых элементов конструкций из тонкостенных холодногнутых профилей // Вестник гражданских инженеров. 2016. № 3(56). С. 46–51.
15. Волкова А.А., Пайков А.В., Столяров О.Н., Семенов С.Г., Мельников Б.Е. Структура и свойства текстильно-армированного бетона // Инженерно-строительный журнал. 2015. №7(59).
16. Шилин А.А., Пшеничный В.А, Картузов Д.В. Внешнее армирование железобетонных конструкций композиционными материалами. М: Изд-во Стройиздат. 2007. 184 с.
17. Бондарь В.С., Даншин В.В., Семенов П.В. Численное моделирование нелинейных процессов накопления повреждений при циклическом нагружении // Вычислительная механика сплошных сред. 2013. Т. 6, № 3. С. 286–291.
18. Шульженко Н.Г., Гонтаровский П.П., Гармаш Н.Г.,

elementov konstruktsiy iz tonkostennykh kholodnognutykh profiley [Buckling analysis of light steel cold-formed thin-walled cross-section members]. *Vestnik grazhdanskikh inzhenerov.* 2016. No. 3(56). Pp. 46–51. (rus)

15. Volkova A.A., Paykov A.V., Stolyarov O.N., Semenov S.G., Melnikov B.E. Struktura i svoystva tekstil'no-armirovannogo betona [Structure and properties of textile reinforced concrete]. *Magazine of Civil Engineering.* 2015. No. 7(59). Pp. 50–56. (rus)
16. Shilin A.A., Pshenichnyy V.A, Kartuzov D.V. *Vneshneye armirovaniye zhelezobetonnykh konstruktsiy kompozitsionnymi materialami* [Outer composite reinforcing of concrete structures]. Moscow: Izd-vo Stroyizdat. 2007. 184 p.(rus)
17. Bondar V.S., Danshin V.V., Semenov P.V. Chislennoye modelirovaniye nelineynykh protsessov nakopleniya povrezhdeniy pri tsiklicheskom nagruzhenii [Computational simulation of non-linear cyclic stressing damage accumulation]. *Vychislitelnaya mekhanika sploshnykh sred.* 2013. Vol. 6. No. 3. Pp. 286–291. (rus)
18. Shulzhenko N.G., Gontarovskiy P.P., Garmash N.G., Melezhik I.I. Otsenka razvitiya treshchin pri mnogorezhimnom tsiklicheskom nagruzhenii na osnove analiza rasseyannykh povrezhdeniy materiala. Dinamika i prochnost mashin [Crack propagation under multicycle stressing analysis in terms of interspersed damage]. *Dinamika i prochnost' mashin.* 2015. Vol. 18. No. 4/2. Pp. 53–58. (rus)
19. Bondar V.S., Danshin V.V., Makarov D.A. Matematicheskoye modelirovaniye protsessov deformirovaniya i nakopleniya povrezhdeniy pri tsiklicheskikh nagruzheniyakh [Mathematical simulation of cyclic stressing deformation and damage accumulation]. *Vestnik Permskogo natsionalnogo issledovatelskogo politekhnicheskogo universiteta.* 2014. Vol. 8. No. 2. Pp. 125–144. (rus)
20. *Eurocode 3: Design of steel structures. EN 1993-1-3: 2004 Part 1-3: General rules.* Supplementary rules for cold-formed members and sheeting. CEN. European Committee for Standardisation. 2004.
21. Louise C.N., Md Othuman A.M., Ramli M. Performance of lightweight thin-walled steel sections: theoretical and mathematical considerations. *Applied Science Research*. 2012. No. 3(5). Pp. 2847–2859.
22. Tenek L. A Beam Finite Element Based on the Explicit Finite Element Method. *International Review of Civil Engineering (IRECE).* 2015. No. 6(5). Pp. 124–132.
23. Keerthan P., Mahendran M. Thermal performance of load bearing cold-formed steel walls under fire conditions using Numerical studies. *Journal of Constructional Steel Research*. 2013. No. 80. Pp. 412–428.
24. Sarawit A.T., Kim Y., Bakker M.M., Pekoz T. The finite element method for thin-walled members-applications. *Proceedings of the 3rd ICTWS.* 2001. Pp. 437–448.
25. Soegihardjo O., Suhardjono S., Pramujati B., Pramono A.S. Parametric beam modeling to predict the first natural bending frequency of thin wall box-shaped structures verified using experimental modal analysis. *International Review of Mechanical Engineering.* 2017. Vol. 11. No. 1. Pp. 77–86.
26. Sanyal G., Samal K. A geometry-dependent generalized shape function for calculation of stress intensity factor for axially cracked thin-walled tubes. *International Journal of Advanced Structural Engineering (IJASE).* 2014. Vol. 6. No. 2.
27. Teter A., Kolakowski Zb. Coupled dynamic buckling of thin-walled composite columns with open cross-sections. *Composite Structures.* 2013. Vol. 95. Pp. 28–34.
28. Kobelev V. Thin-Walled Rods With Semiopened Profiles.

Мележик И.И. Оценка развития трещин при многорежимном циклическом нагружении на основе анализа рассеянных повреждений материала // Динамика и прочность машин. 2015. Т. 18. № 4/2. С. 53–58.

19. Бондарь В.С., Даншин В.В., Макаров Д.А. Математическое моделирование процессов деформирования и накопления повреждений при циклических нагружениях // Вестник Пермского национального исследовательского политехнического университета. 2014. Т. 8. № 2. С. 125–144.
20. Eurocode 3: Design of steel structures. EN 1993-1-3: 2004 Part 1-3: General rules. Supplementary rules for cold-formed members and sheeting. CEN. European Committee for Standardisation. 2004.
21. Louise C.N., Md Othuman A.M., Ramli M. Performance of lightweight thin-walled steel sections: theoretical and mathematical considerations // Applied Science Research. 2012. № 3(5). Pp. 2847–2859.
22. Tenek L. A Beam Finite Element Based on the Explicit Finite Element Method // International Review of Civil Engineering (IRECE). 2015. Vol. 6(5). Pp. 124–132.
23. Keerthan P., Mahendran M. Thermal performance of load bearing cold-formed steel walls under fire conditions using Numerical studies // Journal of Constructional Steel Research. 2013. № 80. Pp. 412–428.
24. Sarawit A.T., Kim Y., Bakker M.M., Pekoz T. The finite element method for thin-walled members-applications // Proceedings of the 3rd ICTWS. 2001. Pp. 437–448.
25. Soegihardjo O., Suhardjono S., Pramujati B., Pramono A.S. Parametric Beam Modeling to Predict the First Natural Bending Frequency of Thin Wall Box-Shaped Structures Verified Using Experimental Modal Analysis // International Review of Mechanical Engineering. 2017. Vol. 11. №1. Pp. 77–86.
26. Sanyal G., Samal K. A geometry-dependent generalized shape function for calculation of stress intensity factor for axially cracked thin-walled tubes // International Journal of Advanced Structural Engineering (IJASE). 2014. Vol. 6. № 2.
27. Teter A., Kolakowski Zb. Coupled dynamic buckling of thin-walled composite columns with open cross-sections // Composite Structures. 2013. Vol. 95. Pp. 28–34.
28. Kobelev V. Thin-Walled Rods With Semiopened Profiles // Journal of Applied Mechanics. 2013. Vol. 80. № 1. Pp. 100–111.
29. Rizzi N.L., Varano V., Gabriele St. Initial post buckling behavior of thin-walled frames under mode interaction // Thin-Walled Structures. 2013. Vol. 68. Pp. 124–134.
30. Janevski G., Kozić P., Pavlović R. Moment lyapunov exponents and stochastic stability of a thin-walled beam subjected to eccentric axial loads // Journal of Theoretical and Applied Mechanics.2012. Vol. 50. № 1. Pp. 61–83.
31. Левандовский А.Н., Мельников Б.Е., Шамкин А.А. Моделирование разрушения пористого материала // Инженерно-строительный журнал. 2017. № 1(69). С. 3–22.
32. Бенин А.В., Семенов А.С., Семенов С.Г., Мельников Б.Е. Математическое моделирование процесса разрушения сцепления арматуры с бетоном Часть 1. Модели с учетом несплошности соединения // Инженерно-строительный журнал. 2013. № 5(40). С. 86–99.
33. Бенин А.В., Семенов А.С., Семенов С.Г., Мельников Б.Е. Математическое моделирование процесса разрушения сцепления арматуры с бетоном. Часть 2. Модели без учета несплошности соединения. // Инженерно-строительный журнал. 2014. № 1(45). С. 23–40.

Journal of Applied Mechanics. 2013. Vol. 80. No. 1. Pp. 100–111.

29. Rizzi N.L., Varano V., Gabriele St. Initial post buckling behavior of thin-walled frames under mode interaction, *Thin-Walled Structures.* 2013. Vol. 68. Pp. 124–134.
30. Janevski G., Kozić P., Pavlović R. Moment lyapunov exponents and stochastic stability of a thin-walled beam subjected to eccentric axial loads. *Journal of Theoretical and Applied Mechanics.* 2012. Vol. 50. No. 1. Pp. 61–83.
31. Levandovskiy A.N., Melnikov B.E., Shamkin A.A. Modeling of porous material fracture. *Magazine of Civil Engineering.* 2017. No. 1. Pp. 3–22. (rus)
32. Benin A.V., Semenov A.S., Semenov S.G., Melnikov B.E. Matematicheskoye modelirovaniye protsessa razrusheniya stsepleniya armatury s betonom. Chast 1. Modeli s uchetom nesploshnosti soyedineniya[Simulation of degradation of bond between reinforcing bar and concrete. Part 1. Models with account of the discontinuity]. *Magazine of Civil Engineering.* 2013. No. 5(40). Pp. 86–99. (rus)
33. Benin A.V., Semenov A.S., Semenov S.G., Melnikov B.E. Matematicheskoye modelirovaniye protsessa razrusheniya stsepleniya armatury s betonom. Chast 2. Modeli bez ucheta nesploshnosti soyedineniya [The simulation of bond fracture between reinforcing bars and concrete. Part 2. Models without taking the bond discontinuity into account]. *Magazine of Civil Engineering.* 2014. No.1(45). Pp. 23–40. (rus)
34. Nazmeeva T.V. Nesushchaya sposobnost szhatykh stalnykh tonkostennykh elementov sploshnogo i perforirovannogo secheniya iz kholodnognutogo S-profilya [Bearing capacity of compressed continuous and perforated thin-walled steel members of C-shaped cold-formed profiles]. *Magazine of Civil Engineering.* 2013. No. 5(40). Pp. 44–51. (rus)
35. Vatin N.I., Nazmeeva T., Guslinscky R. Problems of Cold-Bent Notched C-Shaped Profile Members. *Advanced Materials Research.* 2014. Vol. 941-944. Pp. 1871–1875.
36. Nazmeyeva T.V. Buckling analysis of thin-walled cold-formed beams –short reviewings. *Construction of Unique Buildings and Structures*. 2014. No. 6(21). Pp. 32–57. (rus)
37. Garifullin M., Vatin N., Jokinen T., Heinisuo M. Numerical solution for rotational stiffness of RHS tubular joints. *Advances and Trends in Engineering Sciences and Technologies II - Proceedings of the 2nd International Conference on Engineering Sciences and Technologies.* 2016. Pp. 81–86.
38. Garifullin M.R., Vatin N.I. Buckling analysis of thin-walled cold-formed beams. *Construction of Unique Buildings and Structures.* 2014. No. 6(21). Pp. 32–57.
39. Vatin N.I., Sinelnikov A.S. Footway bridges: cold formed steel cross-section. *Construction of Unique Buildings and Structures.* 2012. No. 3. Pp. 39–51.
40. Vatin N. I., Sinelnikov A. S. Long span footway bridges: coldformed steel cross-section. *Construction of Unique Buildings and Structures.* 2012. No. 1. Pp. 47-53. (rus)
41. Tusnin A.R., Tusnina O.A. Vychislitelnaya sistema «Stalkon» dlya rascheta i proyektirovaniya sterzhnevykh konstruktsiy iz tonkostennykh sterzhney otkrytogo profilya [Software complex “Stalkon” for analysis and design of thin-walled opened cross-section bar structures]. *Promyshlennoye i grazhdanskoye stroitelstvo.* 2012. No. 8. Pp. 62–64. (rus)
42. Tusnin A.R. Osobennosti chislennogo rascheta konstruktsiy iz tonkostennykh sterzhney otkrytogo profilya [Special aspects of computational analysis of thin-walled opened cross-section bar structures]. *Promyshlennoye i grazhdanskoye stroitelstvo.* 2010. No. 11. Pp. 60–62. (rus)

34. Неклюдова Е.А., Семенов А.С., Мельников Б.Е., Семенов С.Г. Экспериментальное исследование и конечно-элементный анализ упругих и прочностных свойств стекловолоконного композиционного материала (англ.) // Инженерно-строительный журнал. 2014. № 3(47). С. 25–39
35. Vatin N.I., Nazmeeva T., Guslinscky R. Problems of Cold-Bent Notched C-Shaped Profile Members // Advanced Materials Research. 2014. Vol. 941–944. С. 1871–1875.
36. Назмеева Т.В. Несущая способность сжатых стальных тонкостенных элементов сплошного и перфорированного сечения из холодногнутого С-профиля // Инженерно-строительный журнал. 2013. № 5(40). С. 44–51.
37. Garifullin M., Vatin N., Jokinen T., Heinisuo M. Numerical solution for rotational stiffness of RHS tubular joints // Advances and Trends in Engineering Sciences and Technologies II - Proceedings of the 2nd International Conference on Engineering Sciences and Technologies. 2016. Pp. 81–86.
38. Гарифуллин М.Р., Ватин Н.И. Устойчивость тонкостенного холодногнутого профиля при изгибе – краткий обзор публикаций // Строительство уникальных зданий и сооружений. 2014. № 6(21). С. 32–57.
39. Ватин Н.И., Синельников А.С. Холодногнутый стальной профиль в малых мостовых конструкциях // Строительство уникальных зданий и сооружений 2012. № 3. С. 39–51.
40. Ватин Н.И., Синельников А.С. Большепролетные надземные пешеходные переходы из легкого холодногнутого стального профиля // Строительство уникальных зданий и сооружений. 2012. № 1. С. 47–53.
41. Туснин А.Р., Туснина О.А. Вычислительная система «Сталькон» для расчета и проектирования стержневых конструкций из тонкостенных стержней открытого профиля // Промышленное и гражданское строительство. 2012. № 8. С. 62–64.
42. Туснин А.Р. Особенности численного расчета конструкций из тонкостенных стержней открытого профиля // Промышленное и гражданское строительство. 2010. № 11. С. 60–62.
43. Туснин А.Р. Некоторые вопросы расчета тонкостенных стальных конструкций // Научное обозрение. 2015. № 11. С. 79–82.
44. Дьяков С.Ф., Лалин В.В. Построение и анализ конечных элементов стержня открытого профиля с учетом деформаций сдвига и кручения // Вестник Пермского государственного технического университета. Охрана окружающей среды, транспорт, безопасность жизнедеятельности. 2011. № 2. С. 130–140.
45. Лалин В.В., Рыбаков В.А. Конечные элементы для расчета ограждающих конструкций из тонкостенных профилей // Инженерно-строительный журнал. 2011. № 8. С. 69–80.
46. Лалин В.В., Рыбаков В.А., Морозов С.А. Исследование конечных элементов для расчета тонкостенных стержневых систем // Инженерно-строительный журнал. 2012. № 1. С. 53–73.
47. Подзоров А.В., Зверев В.В., Тезиков Н.Ю., Карманов И.В., Жидков К.Е. Имитационное моделирование напряженно-деформированного состояния тонколистового профилированного элемента с двойным гофрированием // Наука и бизнес: пути развития. 2015. № 5. С. 103–105.
48. Подзоров А.В., Зверев В.В., Тезиков Н.Ю., Жидков К.Е., Карманов И.В. Редуцирование площади поперечного сечения стального профиля при центральном сжатии.// Строительная механика и

43. Tusnin A.R. Nekotoryye voprosy rascheta tonkostennykh stalnykh konstruktsiy [Some approaches of thin-walled steel structure's analysis]. *Nauchnoye obozreniye.* 2015. No. 11. Pp. 79–82. (rus)

44. Dyakov S.F., Lalin V.V. Postroyeniye i analiz konechnykh elementov sterzhnya otkrytogo profilya s uchetom deformatsiy sdviga i krucheniya [Construction and investigation of opened cross-section bar finite element with account of shear and torsion]. *Vestnik Permskogo gosudarstvennogo tekhnicheskogo universiteta. Okhrana okruzhayushchey sredy, transport, bezopasnost zhiznedeyatelnosti.* 2011. No. 2. Pp. 130–140. (rus)

45. Lalin V.V., Rybakov V.A. The finite elements for design of building walling made of thin-walled beams. *Magazine of Civil Engineering.* 2011. No. 8(26). Pp. 69–80. (rus)

46. Lalin V.V., Rybakov V.A., Morozov S.A. Issledovaniye konechnykh elementov dlya rascheta tonkostennykh sterzhnevykh sistem [The finite elements research for calculation of thin-walled bar systems]. *Magazine of Civil Engineering.* 2012.No. 1(27). Pp. 53–73. (rus)

47. Podzorov A.V., Zverev V.V., Tezikov N.Yu., Karmanov I.V., Zhidkov K.Ye. Imitatsionnoye modelirovaniye napryazhenno-deformirovannogo sostoyaniya tonkolistovogo profilirovannogo elementa s dvoynym gofrirovaniyem [Simulation of stress-strain state of thin-walled double corrugated sheeting member]. *Nauka i biznes: puti razvitiya.* 2015. No. 5. Pp. 103–105. (rus)

48. Podzorov A.V., Zverev V.V., Tezikov N.Yu., Zhidkov K.Ye., Karmanov I.V. Redutsirovaniye ploshchadi poperechnogo secheniya stalnogo profilya pri tsentralnom szhatii.[Reduction of cross-section area of steel axial compressed member]. *Structural Mechanics and Analysis of Constructions.* 2015. No. 6(263). Pp. 24–28. (rus)

49. Zverev V.V., Semenov A.S. Vliyaniye podatlivosti boltovykh soyedineniy na deformativnost fermy iz tonkostennykh profiley The influence of bolted-on connection flexibility on the thin-walled profile framework deformability]. *Russian Journal of Building Construction and Architecture.* 2008. No. 2. Pp. 9–17. (rus)

50. Adegova L.A., Rudzey G.F. Prognozirovaniye raschetnoy ustalosti dolgovechnosti elementov konstruktsiy s primeneniyem modifitsirovannykh krivykh ustalosti [Prediction of expected fatigue endurance of structural member by use of modified stress-cycle diagram]. *Izvestiya Transsiba* 2014. No. 2. Pp. 86–94. (rus)

51. Bondar V.S., Danshin V.V., Semenov P.V. Nelineynyye protsessy nakopleniya povrezhdeniy pri tsiklicheskikh nagruzheniyakh [Non-linear damage accumulation process in cyclic stressing]. *Natsionalnyy issledovatelskiy Nizhegorodskiy gosudarstvennyy universitet im. N.I. Lobachevskogo.* 2013. No. 2. Pp. 96–114. (rus)

52. Adegova L.A. Primeneniye modifitsirovannykh krivykh ustalosti dlya raschetnoy otsenki dolgovechnosti tonkostennykh elementov konstruktsiy [A modified stress-cycle diagram approach of numerical estimate of fatigue endurance of thin-walled structural member]. *Izvestiya vysshikh uchebnykh zavedeniy.* 2015. No. 2. Pp. 92–98. (rus)

53. Arutyunyan R.A. Problemy ustalosti i veroyatnostnyye metody yeye resheniya [Probabilistic fatigue problem-solving approaches]. *Vestnik Rossiyskogo Fonda Fundamentalnykh Issledovaniy.* 2006. No. 2. Pp. 47–60. (rus)

54. Melnikov B.Ye., Semenov A.S. Energeticheskaya model nakopleniya povrezhdeniy pri malotsiklovoy ustalosti [An energy model of damage accumulation for low-cycle-fatigue failure]. *Peterburgskiye chteniya po problemam prochnosti. K 100-letiyu so dnya rozhdeniya L.M. Kachanova i Yu.N. Rabotnova.* 2014. Pp. 59–61. (rus)

55. Melnikov B.Ye., Kuznetsov N.P., Mityukov A.G., Semenov A.S., Semenov S.G. Primeneniye energeticheskoy modeli

расчет сооружений. 2015. № 6(263). С. 24–28.

49. Зверев В.В., Семенов А.С. Влияние податливости болтовых соединений на деформативность фермы из тонкостенных профилей // Научный журнал строительства и архитектуры. 2008. № 2. С. 9–17.

50. Адегова Л.А., Рудзей Г.Ф. Прогнозирование расчетной усталости долговечности элементов конструкций с применением модифицированных кривых усталости // Известия Транссиба. 2014. № 2. С. 86–94.

51. Бондарь В.С., Даншин В.В., Семенов П.В., Нелинейные процессы накопления повреждений при циклических нагружениях // Национальный исследовательский Нижегородский государственный университет им. Н.И. Лобачевского. 2013. № 2. С. 96–114.

52. Адегова Л.А., Применение модифицированных кривых усталости для расчетной оценки долговечности тонкостенных элементов конструкций // Известия высших учебных заведений. 2015. № 2. С. 92–98.

53. Арутюнян Р.А., Проблемы усталости и вероятностные методы ее решения // Вестник Российского Фонда Фундаментальных Исследований. 2006. № 2. С. 47–60.

54. Мельников Б.Е., Семенов А.С., Энергетическая модель накопления повреждений при малоцикловой усталости // Петербургские чтения по проблемам прочности. К 100-летию со дня рождения Л.М. Качанова и Ю.Н. Работнова. 2014. С. 59–61.

55. Мельников Б.Е., Кузнецов Н.П., Митюков А.Г., Семенов А.С., Семенов С.Г., Применение энергетической модели оценки прочности при нескольких циклах нагружения в случае сложного неоднородного напряженного состояния // Современные проблемы ресурса материалов и конструкций. 2009. С. 140–147.

56. Павлов П.А. Основы инженерных расчетов элементов машин на усталость и длительную прочность. Ленинград, изд. Машиностроение. 1988. С. 247.

57. Sorochan E.N., Artiukh V.G., Melnikov B.E., Raimberdiyev T.P. Mathematical model of plates and strips rolling for calculation of energy power parameters and dynamic loads // MATEC Web of Conferences. 2016. Vol. 73. no. 04009. DOI: http://dx.doi.org/10.1051/matecconf/20167304009

58. Artiukh V.G., Raimberdiyev T.P., Mazur V. O. Use of CAE-Systems at Evaluation of Shock Absorbers for Metallurgical Equipment // MATEC Web of Conferences. 2016. Vol. 53. no. 01039. DOI: http://dx.doi.org/10.1051/matecconf/20165301039

59. Stareva I.A., Pronina Y.G., The influence of the initial thickness deviation of a steel tube subjected to general corrosion under its own weight on its durability // AIP Conference Proceedings. 2018. Vol. 1959. № 1. no. 070034. doi:10.1063/1.5034709.

otsenki prochnosti pri neskolkikh tsiklakh nagruzheniya v sluchaye slozhnogo neodnorodnogo napryazhennogo sostoyaniya [Application of energy approach of strength assessment for low-cycle loading in non-uniform complex stress state]. *Sovremennyye problemy resursa materialov i konstruktsiy.* 2009. Pp. 140–147. (rus)

56. Pavlov P.A. *Osnovy inzhenernykh raschetov elementov mashin na ustalost i dlitelnuyu prochnost* [Principle of engineering calculation of fatigue endurance of machine elements]. Leningrad, izd. Mashinostroyeniye. 1988. 247 p. (rus)
57. Sorochan E.N., Artiukh V.G., Melnikov B.E., Raimberdiyev T.P. Mathematical Model of Plates and Strips Rolling for Calculation of Energy Power Parameters and Dynamic Loads. *MATEC Web of Conferences.* 2016. Vol.73. 04009. DOI: http://dx.doi.org/10.1051/matecconf/20167304009
58. Artiukh V.G., Raimberdiyev T.P., Mazur V. O. Use of CAE-Systems at Evaluation of Shock Absorbers for Metallurgical Equipment. *MATEC Web of Conferences*. 2016. Vol. 53. 01039. DOI: http://dx.doi.org/10.1051/matecconf/20165301039
59. Stareva I.A., Pronina Y.G., The influence of the initial thickness deviation of a steel tube subjected to general corrosion under its own weight on its durability. *AIP Conference Proceedings.* 2018, Vol. 1959. No. 1. 070034. doi:10.1063/1.5034709

Ilya Atavin,
+7(999)284-84-63; ilya_region51@mail.ru

Boris Melnikov,
+7(812)5526303; kafedra@ksm.spbstu.ru

Artem Semenov,
+7(905)2721188;Semenov.Artem@googlemail.com

Natalia Chernysheva,*
+7(981)7713236; chernat0000@mail.ru

Elena Yakovleva,
+7(812)552-63-03; helena47@mail.ru

Илья Вадимович Атавин,
+7(999)284-84-63;
эл. почта: ilya_region51@mail.ru

Борис Евгеньевич Мельников,
+7(812)552-63-03;
эл. почта: kafedra@ksm.spbstu.ru

Артем Семенович Семенов,
+7(905)272-11-88;
эл. почта: Semenov.Artem@googlemail.com

Наталия Вячеславовна Чернышева,*
+7(981)771-32-36;
эл. почта: chernat0000@mail.ru

Елена Леонидовна Яковлева,
+7(812)552-63-03;
эл. почта: helena47@mail.ru

doi: 10.18720/MCE.80.6

The seismic stability of facade system with facing by composite panels

Сейсмостойкость фасадной системы с облицовкой композитными панелями

V.M. Tusnina*,
National Research Moscow State Civil Engineering University, Moscow, Russia
D.A. Emelianov,
Center of Engineering Services and Technical Expertise, Moscow, Russia

Канд. техн. наук, доцент В.М. Тусина*,
Национальный исследовательский Московский государственный строительный университет, Москва, Россия
канд. техн. наук, ведущий инженер Д.А. Емельянов,
Центр инжиниринговых услуг и технической экспертизы, Москва, Россия

Key words: suspended facade system; composite cladding panels; notched hub mounting; seismic resistance; dynamic load; vibration platform; acceleration

Ключевые слова: навесная фасадная система; облицовка из композитных панелей; зубчатое узловое крепление; сейсмостойкость; динамическая нагрузка; виброплатформа; ускорение

Abstract. The hinged ventilated facades installing is a perspective technology of buildings decoration. Suspended facade systems are widely used for construction and reconstruction of residential, administrative, public and industrial buildings. Using suspended facade systems for decorating exterior walls is helping designers to solve the problems of thermal protection and architectural and artistic expressiveness of buildings by using modern heat-insulating and decoration materials. The finishing of facades with composite panels is especially effective for buildings erected in areas with seismic activity because the using of lightweight cladding leads to a significant reduction in the mass of external walls and to the reduction of seismic loads. In this article we present the results of the experimental study of bearing capacity and operational reliability under dynamic loads of hinged facade system with toothed nodal fastening of aluminum composite panels, which was developed in the Moscow State Construction University. The tests were conducted on a vibrating platform of a pendulum type by a vibrational (resonant) method, which allows to determine the power load simulating seismic actions in a wide range of frequencies, in the Central Research Institute of Building Constructions named after V.A. Kucherenko (CRIBC). The results of experimental studies clearly demonstrated the increased seismic stability of the structure with toothed nodal fastening of composite panels in comparison with facade systems having a similar type of cladding. We found out that the developed design is able to dissipate the energy from the dynamic load due to the presence of additional connections in the structural solution of the tooth assemblies and allow to quench the energy of the oscillation of the system under seismic influences.

Аннотация. В настоящее время перспективной технологией отделки зданий является устройство навесных вентилируемых фасадов. Навесные фасадные системы широко используются для строительства и реконструкции жилых, административных, общественных и промышленных зданий. Применение систем навесных фасадов для отделки наружных стен позволяет проектировщикам эффективно решать задачи тепловой защиты и архитектурно-художественной выразительности зданий, используя современные теплоизоляционные и отделочные материалы. Отделка фасадов панелями из композитных материалов особенно эффективна для зданий, возводимых в районах с сейсмической активностью, поскольку применение лёгкой облицовки приводит к существенному снижению массы наружных стен и, следовательно, к снижению сейсмических нагрузок. В настоящей статье приводятся результаты экспериментального исследования несущей способности и эксплуатационной надежности в условиях динамических нагрузок, разработанной в Московском государственном строительном университете, навесной фасадной системы с зубчатым узловым креплением облицовки из алюминиевых композитных панелей. Испытания проводились в ЦНИИСК им. В.А. Кучеренко на виброплатформе маятникового типа вибрационным (резонансным) методом, позволяющим определять силовую нагрузку, имитирующую сейсмические воздействия в широком диапазоне

Туснина В.М., Емельянов Д.А., Сейсмостойкость фасадной системы с облицовкой композитными панелями // Инженерно-строительный журнал. 2018. № 4(80). С. 62–72.

частот. Результаты экспериментальных исследований наглядно продемонстрировали повышенную сейсмостойкость конструкции с узловым зубчатым креплением композитных панелей в сравнении с фасадными системами, имеющими аналогичный тип облицовки. Установлено, что за счет наличия дополнительных связей в конструктивном решении зубчатых узлов, разработанная конструкция способна хорошо рассеивать энергию от динамической нагрузки, что позволяет гасить энергию колебания системы, имеющей место при сейсмических воздействиях.

1. Introduction

Various in design and finishing hinged facade systems (HFS) are widely used in building and reconstruction of buildings [1–6]. HFS allows to effectively solve energy conservation problems [7–9] and to give the building the necessary architectural look in the high tech style.

Thermotechnical and economic calculations [10–15] and studies on the operational reliability of ventilated facades [16–19] clearly demonstrate the effectiveness of HFS.

Facade systems with aluminum composite panels finishing (ACP) amount a great part in the total volume of applied facade systems in construction. The using facades with composite panels is especially effective for buildings erected in areas with seismic activity because the using of lightweight cladding leads to a significant reduction in the mass of outer walls and to the reduction of seismic loads [20–22].

There are some constructive solutions for fastening linings from aluminum composite material which meet the safety requirements under the action of dynamic loads. But these systems are characterized by increased material consumption and, correspondingly, low economic indicators. Some systems do not allow creating the required architectural appearance of the facade. This applies to systems in which the cladding is fixed with the help of visible rivets on the façade. Also designs fastening lining in such systems do not take into account the deformation elements from temperature effects [23-26].

The design of a hinged facade system with toothed lining fasteners made of aluminum composite panels was developed and researched in the Moscow State University of Civil Engineering. The fastening cladding elements in the design is carried out by the toothed connection hook with carriage bracket. The design of gear units is capable of receiving all horizontal and vertical loads while earthquakes due the L-shaped hooks, which are arranged specularly to each other. There is no need for temperature-strain joints due the absence of vertical and horizontal guides in the structure. There are special ventilated channels, arranged with cutouts in the lower sides of the cassettes made for airflow in the structure. The structural elements of the system are made of aluminum alloy. Finishing cassettes are inserted into the gear connection, but mounted on vertical guides, which reduces the complexity of installing such structures.

A detailed description of the constructive solution of the HFS is presented in the works [27–31].

The purpose of this article is to study the bearing capacity and operational reliability of the developed vented HFS with toothed lining fasteners made of ACP under dynamic loads, simulating the 7-9 point seismic and wind pulsation effects.

The HFS tests on a vibrating platform allowed to solve the following problems:

- to set dynamic indicators, physico-mechanical and operational characteristics of HFS with toothed lining fasteners made of ACP;
- to determine the scope of possible use of the developed HFS design, taking into account all requirements required for constructions erected in areas with seismicity of 7-9 points on the MSK-64 scale [32];
- to reveal the increased seismic resistance of the developed design in comparison with existing facade systems with a similar material consumption.

2. Methods

Experimental studies on dynamic loads simulating 7-9 point seismic and wind pulsation (at a height of 75 m from ground level) were carried out to assess the operational reliability of the HFS with toothed lining fasteners made of ACP (Figure 1). The tests were conducted on a vibrating platform of a pendulum type by a vibrational (resonant) method, which allows to determine the power load simulating seismic actions in a wide range of frequencies in the Research Institute of Building Constructions (TSNIISK) named after V.A. Koucherenko.

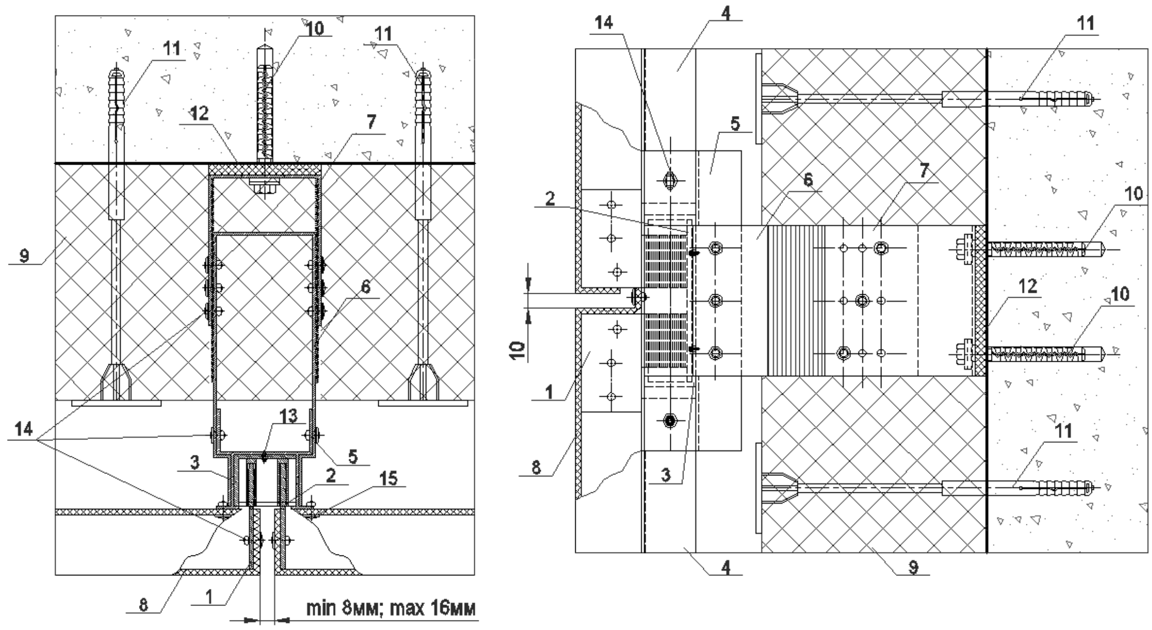

Figure 1. The HFS fastening unit: a – vertical joint; b - horizontal joint; 1 – the gear hook (iklya); 2 – the carriage gear bracket; 3 – the carriage; 4 – the drainage profile; 5 – the extension reverse part; 6 – the extension; 7 – the bracket; 8 – the HFS; 9 – the mineral wool insulation; 10 – the anchor dowel; 11 – the bowl dowel; 12 – the paronit cushion; 13 – the self-tapping screw; 14 – the exhaust rivet Ø 5 × 12 mm; 15 – the exhaust rivet Ø 3.2×10 mm

The study of the actual work of the developed design was carried out on two experimental models: “angular” – made from one HFS formed the facade angle and “fragmentary” – made from several HFS’s bilateral facade of the experimental stand (Figure 2).

We used brackets with emission set at 100 mm, which were mounted on a stand with a vertical and horizontal step equal to 1200 mm for experimental models. The total overhang was 200 mm. To excite dynamic effects on the system under test, we used a pendulum-type vibration platform with a VID-12M vibrator (Figure 3). To control the given loads, the accelerometers were mounted on a vibration platform near the oscillation excitation source. The displacement and acceleration from the given loads were measured by six sensors mounted on the model (sensors 1-4) and on the platform (sensors 5,6) (Figure 4). Measuring, recording, processing and transmission of information from sensors were carried out using a specialized measuring and computing complex MIC-036. Automation of processing of strain-gauge records was carried out with the help of WinPOS software.

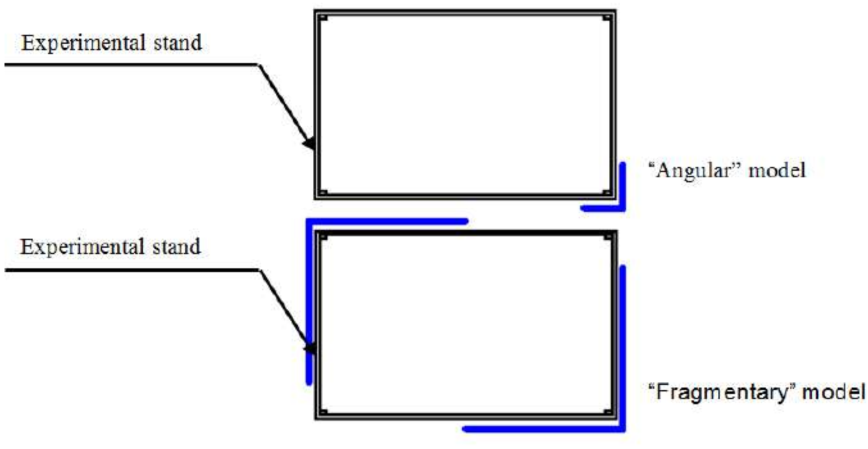

Figure 2. The scheme of the experimental stand

The HFS estimation of the limiting state was carried out on the basis of a comparative analysis of the test results with the data of the instrumental part of the macroseismic scale MSK-64 according to [15].

Figure 3. General view of the experimental equipment

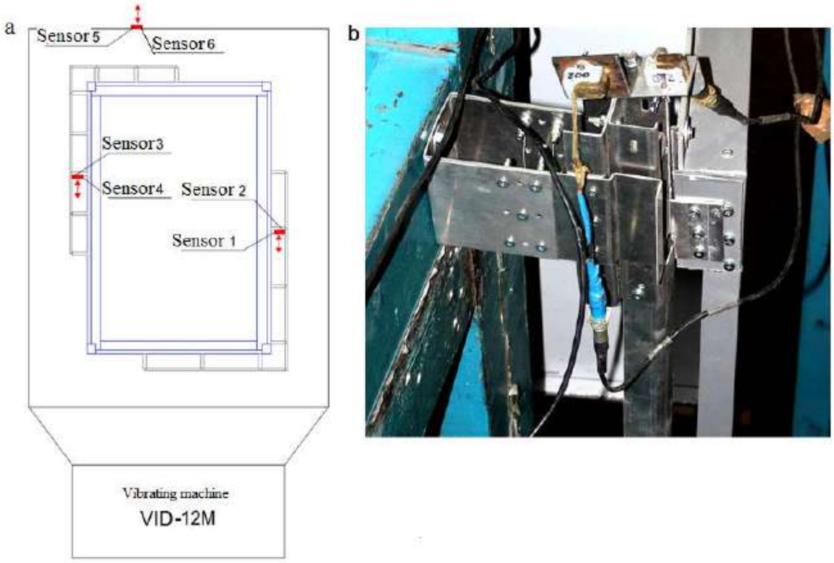

Figure 4. Experimental equipment: a – arrangement of sensors; b – system node with measuring equipment

Tests were carried out in several stages. The frequency spectrum varied from 0 to 10 Hz at the initial stage, with the amplitude of the movements of the vibrating platform unchanged. Then the amplitude value varied with the frequency assignment in the same spectrum. The duration of each stage of the dynamic loading of the system fragment was from 20 to 25 seconds. Acceleration levels of the vibratory platform corresponding to 7 ÷ 9 points on the MSK-64 scale and the levels of impacts corresponding to the resonance oscillations of the system were established based on the results of the first stage of the tests. Then repeated tests of the system were performed with combinations of the amplitude-frequency parameters of the vibratory platform corresponding to resonant oscillations of the system at 7 ÷ 9 points. The test duration was 40 ÷ 50 sec.

3. Results and Discussion

In the course of the test, the acceleration of the vibrating platform varied in the range from 0.4 to 5.05 m/s^2 according to the accelerometers. The oscillation frequencies of the system varied in the range from 1.6 to 7.8 Hz, the vibration amplitude of the vibratory platform – from 0.6 to 3.8 mm. The acceleration in different system points varied in the range from 0.01 to 30.82 m/s^2.

Accelerograms recorded from the sensors installed on the system fragment (sensors 1-4) and on the platform (sensors 5, 6) are shown in Figure 5.

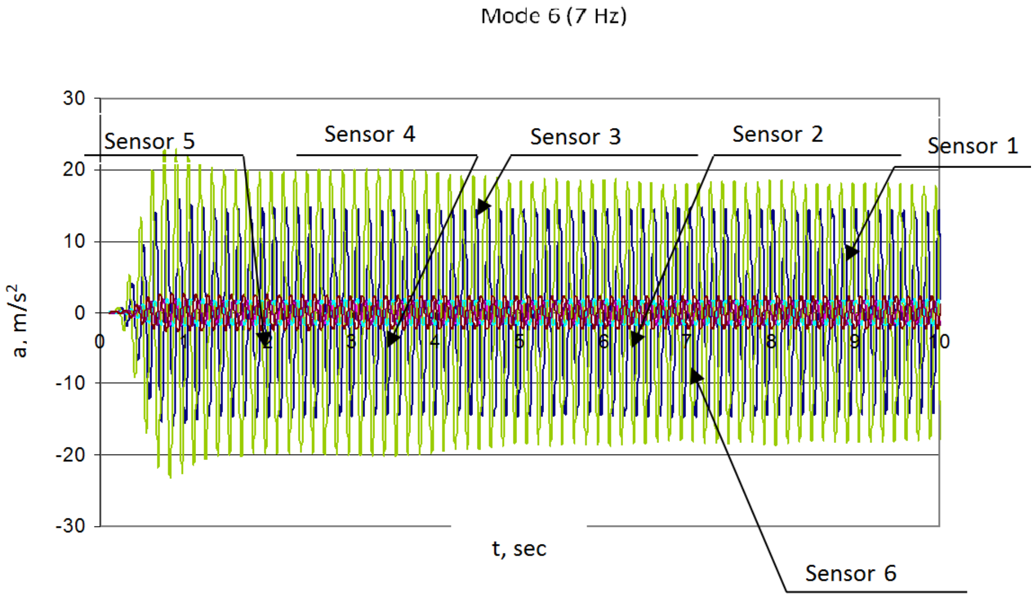

Figure 5. Accelerograms recorded from the sensors 1-6 (mm)

Centering and filtering of the accelerograms were made for a fragment of the developed system. Spectra of peak values of accelerations for sensors at various stages of loading are obtained using a fast Fourier transform. Spectra of peak values of accelerations for one of the stages of loading are shown in

The peak values of the oscillation frequencies were determined from the spectra. The values of displacements at various stages of loading were obtained by double integration of the accelerogram function.

Graphs of the dependence of accelerations and displacements on the frequency of system oscillations are obtained from the results of tests (Figures 7–14).

As can be seen from Figure 7, the maximum peak acceleration value with horizontal oscillations of the system of 36.0 m/s^2 at a frequency of 5.9 Hz was recorded by the sensor 3 installed at the top of the structure at an altitude of 3000 mm from the platform level. The peak acceleration value for the platform is equal to 5.1 m/s^2 is observed at frequencies of 3.3 Hz ÷ 4.0 Hz.

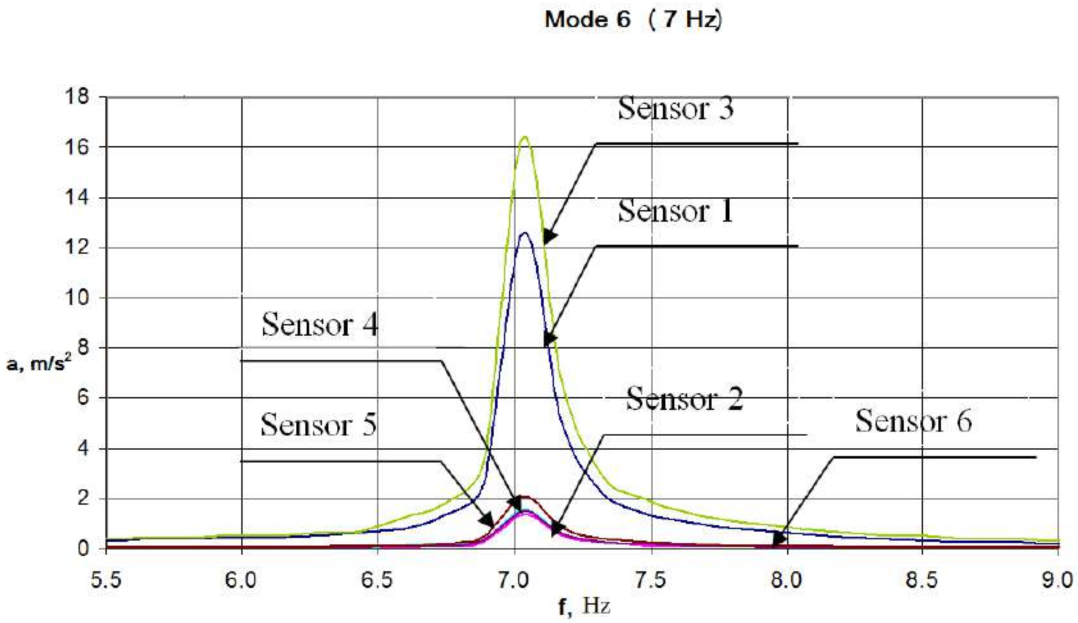

Figure 6. Spectra of peak values of accelerations for sensors 1-6

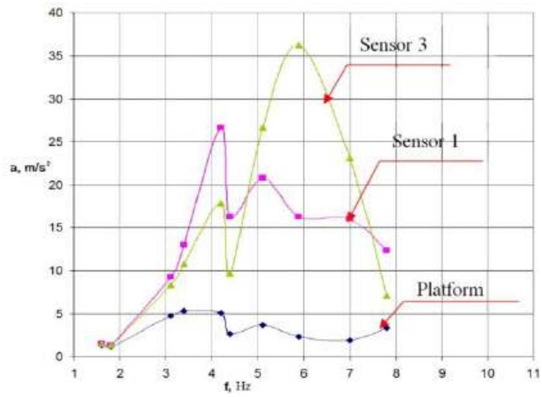

Figure 7. Graphs of the dependence of acceleration on the frequency of system horizontal vibrations

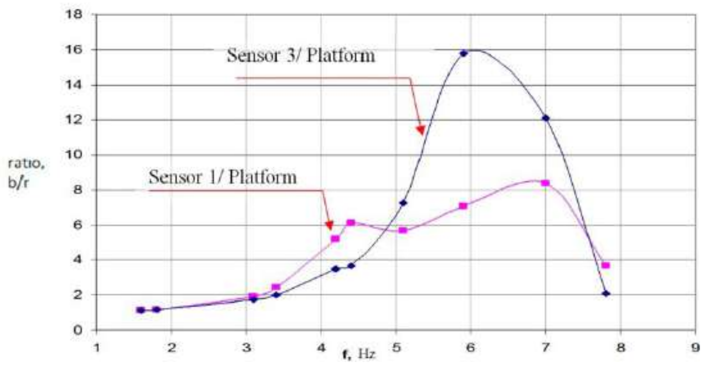

Figure 8. Graphs of the dependence of the relative acceleration σp "system-platform" on the frequency of horizontal oscillations

As can be seen from the graph in Figure 8, the acceleration value of the system upper part (sensor 3) considerably exceeds the acceleration of the lower part of the structure with the same frequency of horizontal oscillations (where σ_p is a dimensionless quantity equal to the ratio of the accelerations of the system and the platform).

The peak value of the system acceleration equal to 7.1 m/s^2 was recorded at a frequency of 5.9 Hz with vertical oscillations. The peak acceleration value of the platform, equal to 5.0 m/s^2, was observed at a frequency of 7.8 Hz. The maximum system acceleration at the same frequency of vertical oscillations is noted in the upper part of the structure, at the location of the sensor 4 (Figure 9).

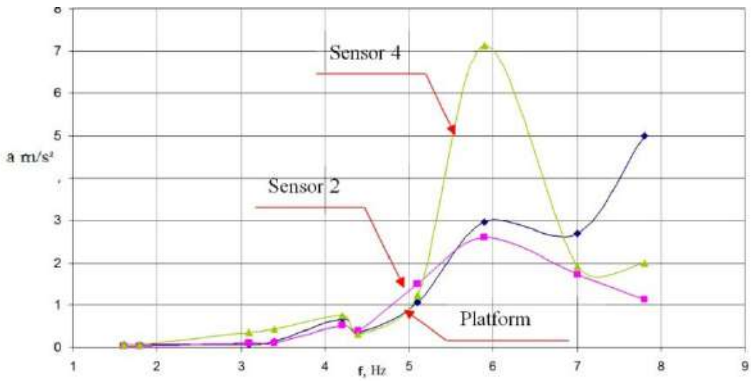

Figure 9. Graphs of the dependence of acceleration on the frequency of vertical oscillations of the system

Graphs of the dependence of the relative acceleration σ_p "system-platform" on the frequency of vertical oscillations are shown in Figure 10. It is noted that the acceleration in the system upper part (sensor 4) exceeds the accelerations in the lower part of the structure (sensor 2) at the same frequency of vertical oscillations.

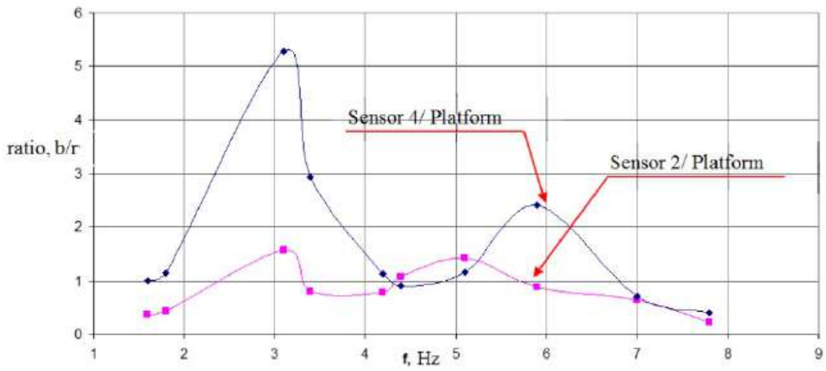

Figure 10. Graphs of the dependence of the relative acceleration σp "system-platform" on the frequency of vertical oscillations

As can be seen in Figure 11, the maximum value of the system displacement at the frequency of horizontal oscillations of the structure was 37 mm at a frequency of 4.3 Hz (sensor 1). The maximum value of the horizontal platform displacement, equal to 15.1 mm, was observed at a system oscillation frequency of 1.7 Hz.

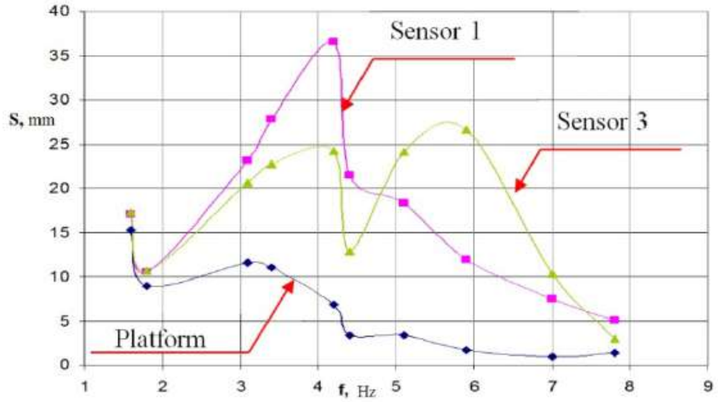

Figure 11. Graphs of the dependence of displacements on the frequency of horizontal system oscillations

The graphs of the dependence of the relative displacement (σ_p) "system-platform" on the horizontal frequency are shown in Figure 12. The maximum movement of the tested structure is marked in its upper part (sensor 3).

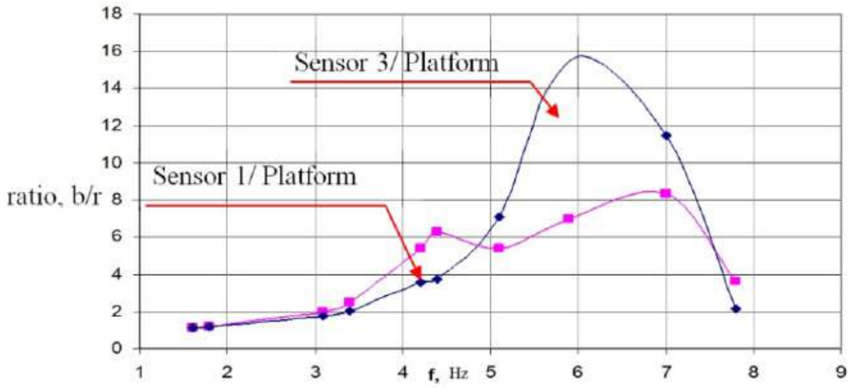

Figure 12. Graphs of the dependence of the relative displacement (σ_p) "system-platform" on the horizontal frequency

The maximum value of moving the system equal to 5.2 mm was fixed by the sensor at a frequency of vertical oscillations corresponding to 5.9 Hz. The maximum displacement value of the platform was 3.0 mm at an oscillation frequency of 5.0 Hz. Maximum movements with vertical oscillations of the structure occur in its upper part (sensor 4) (Figure 13).

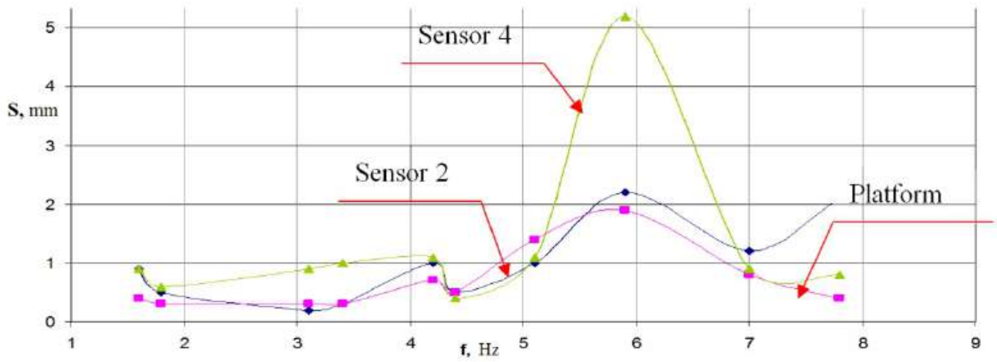

Figure 13. Graphs of the dependence of displacements on the frequency of vertical system oscillations

Graphs of the dependence of the relative displacement (σ_p) "system-platform" on the frequency of vertical oscillations are shown in Figure 14. The maximum displacement of the structure with vertical, as in the case of horizontal oscillations (Figure 12), is marked in its upper part (sensor 4).

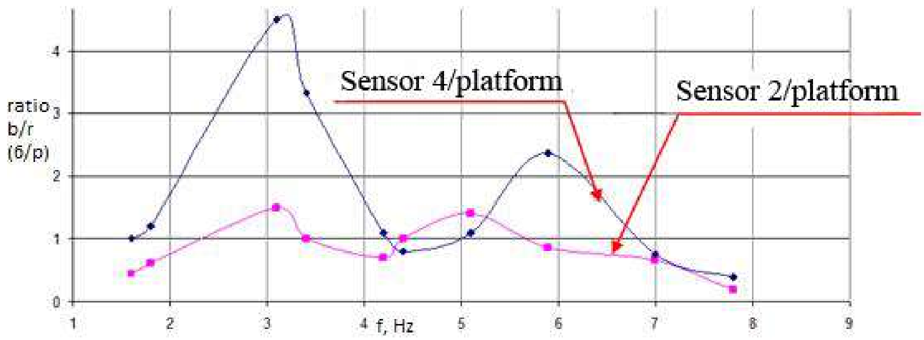

Figure 14. Graphs of the dependence of the relative displacement (σp) "system-platform" on the vertical frequency

At the moment when the natural frequencies of the system oscillations coincided with the forced oscillation frequencies of the vibrating platform, a phenomenon of resonance was observed. The phenomenon of resonance was observed at different stages of loading at a frequency of f = 6.4 ÷ 6.6 Hz. The operational reliability of the system was not affected by resonance.

It should be noted that the developed facade system dampens the vibrations from the dynamic loads effectively due to the features of the structural solution of the toothed junction of the facing with the substructure.

An estimation of HFS with a toothed fastening of the cladding seismic resistance was made on the basis of a comparative analysis of the results of an experimental study of the operation of a structure under dynamic loads with data from similar tests of a traditional system with fastening of facing plates to the guides [22–25, 33].

The generalized test results of the developed and traditional HFS designs are given in Table 1.

Table 1. Test results of the developed and traditional HFS designs

HFS designs	HFS's natural vibration frequency, Hz		HFS's maximum acceleration, m/s²		HFS's maximum displacement, mm	
	horizontal oscillations	vertical oscillations	horizontal oscillations	vertical oscillations	horizontal oscillations	vertical oscillations
Developed HFS (with toothed fastening of the lining) No damage detected	3÷4	6	37	7	37	5
Traditional HFS (with fastening of facing to guides) Damage detected [24]	5÷6	6	19	7.8	55	5.7

4. Conclusions

It is possible to conclude from the results of an experimental study of the load-bearing capacity of the HFS structure with toothed fastening of the lining of ACP under conditions of dynamic loads:

1. The developed system with toothed units for fastening facing plates is characterized by increased seismic resistance with less material capacity, operational reliability of which has not been disturbed at all stages of dynamic loading in comparison with existing facade systems.

2. As a result of testing, visible defects and damages in the elements of the developed HFS design were not detected in contrast to traditional systems.

3. It is established that the developed HFS well dampens the oscillations from the effect of dynamic loads due to the features of the node-toothed clamping of the cladding, which confirms the possibility of its effective use in areas with seismicity of 7-9 points on the MSK-64 scale.

Taking into account the above mentioned, it can be concluded that the HFS design with the clamping of the lining of ACP has a high load-bearing capacity under conditions of high wind and seismic loads and can be recommended for use in high-rise buildings for all Russian climatic regions. This will expand the area of effective use of hinged facade systems with aluminum composite panels.

References

1. Ventiliruemye fasady. Mify i realnost [Ventilated facades. Myths and Reality]. *Tehnologii stroitel'stva.* 2004. No. 5. Pp. 4-11. (rus).
2. Vatin N.I., Gorshkov A.S., Rymkevich P.P. Methodology for calculating the recoupment of investments for renovating the facades of existing buildings. *Construction of Unique Buildings and Structures.* 2014. No. 2(17). Pp. 82–106. (rus).
3. Glikin S.M., Kodysh EH.N. Navesnye fasadnye sistemy s ehffektivnoj teploizolyaciej i ventiliruemym vozdushnym zazorom [Hinged facade systems with effective thermal insulation and ventilated air gap]. *Promyshlennoe i grazhdanskoe stroitel'stvo*. 2008. No. 9. Pp. 36–37. (rus).
4. Nemova D.V. Navesnyye ventiliruyemyye fasady: obzor osnovnykh problem [Hinged ventilated facades: an overview of the main problems]. *Magazine of Civil Engineering*. 2010. No. 5. Pp. 7–11. (rus).
5. *Fasadnyye teploizolyatsionnyye sistemy s vozdushnym zazorom. Rekomendatsii po sostavu i soderzhaniyu dokumentov i materialov, pred"yavlyayemykh dlya tekhnicheskoy otsenki prigodnosti produktsii* [Facade thermal insulation systems with air gap. Recommendations on the composition and content of documents and materials required for technical evaluation of the suitability of products]. Moscow. 2004. 59 p. (rus).
6. *Rekomendatsii po proyektirovaniyu navesnykh fasadnykh sistem s ventiliruyemym vozdushnym zazorom dlya novogo stroitel'stva i rekonstruktsii zdaniy* [Recommendations for the design of hinged facade systems with ventilated air gap for new construction and reconstruction of buildings]. M.: Moskomarkhitektura. 2002. 98 p. (rus).
7. Vatin N.I., Gorshkov A.S., Nemova D.V. Energy efficiency of enclosing structures during major overhaul. *Construction of Unique Buildings and Structures.* 2013. No. 3(8). Pp. 1–11. (rus).
8. Gamayunova O., Vatin N. The role of the state and citizens to improve energy efficiency. *Applied Mechanics and Materials.* 2015. Vols. 725–726. Pp. 1493–1498.
9. Perlova E., Karpova S., Rakova X.M., Bondarenko E., Platonova M., Gorshkov A. The architectural concept of the building with low energy consumption. *Applied Mechanics and Materials*. 2015. Vols. 725–726. Pp. 1580–1588.
10. Dagnall M., Window A., Leung A., Thompson D. Analytical assessment of thermal performance of a ventilated glazed facade system. *Proceedings of Building Simulation: 12th Conference of International Building Performance Simulation Association*. Sydney, 2011. Pp. 808–815.
11. Vatin N.I., Gorshkov A.S., Nemova D.V., Staritcyna A.A., Tarasova D.S. The energy-efficient heat insulation thickness for systems of hinged ventilation facades. *Advanced Materials Research*. 2014. No. 941–944. Pp. 905–920.
12. Vatin N., Gorshkov A., Rymkevich P., Nemova D., Tarasova D. Nonstationary thermal conduction through the building envelope. *Applied Mechanics and Materials*. 2014. No. 670–671. Pp. 365–369.
13. Patania F., Gagliano A., Nocera F., Ferlito A., Galesi A. Thermofluid-dynamic analysis of ventilated facades. *Energy and Buildings*. 2010. Vol. 42. Pp. 1148–1155.
14. Suarez C., Joubert P., Molina J.L., Sánchez F.J. Heat transfer and mass flow correlations for ventilated facades. *Energy and Buildings*. 2011. Vol. 43. Pp. 3696–3703.
15. Nizovtsev M.I., Belyi V.T., Sterlygov A.N. The facade system with ventilated channels for thermal insulation of newly constructed and renovated buildings. *Energy and Buildings*. 2014. Vol. 75. Pp. 60–69.
16. Šagát E., Matějka L. Experimental assessment of the

Литература

1. Вентилируемые фасады. Мифы и реальность // Технологии строительства. 2004. № 5. С. 4–11.
2. Ватин Н.И., Горшков А.С., Рымкевич П.П. Методика расчета окупаемости инвестиций по реновации фасадов существующих зданий // Строительство уникальных зданий и сооружений. 2014. № 2(17). С. 82–106.
3. Гликин С.М., Кодыш Э.Н. Навесные фасадные системы с эффективной теплоизоляцией и вентилируемым воздушным зазором // Промышленное и гражданское строительство. 2008. № 9. С. 36–37.
4. Немова Д.В. Навесные вентилируемые фасады: обзор основных проблем // Инженерно-строительный журнал. 2010. № 5. С. 7–11.
5. Фасадные теплоизоляционные системы с воздушным зазором. Рекомендации по составу и содержанию документов и материалов, предъявляемых для технической оценки пригодности продукции. Москва. 2004. 59 с.
6. Рекомендации по проектированию навесных фасадных систем с вентилируемым воздушным зазором для нового строительства и реконструкции зданий. М.: Москомархитектура, 2002. 98 с.
7. Ватин Н.И., Горшков А.С., Немова Д.В. Энергоэффективность ограждающих конструкций при капитальном ремонте // Строительство уникальных зданий и сооружений. 2013. № 3(8). С. 1–11.
8. Gamayunova O., Vatin N. The role of the state and citizens to improve energy efficiency // Applied Mechanics and Materials. 2015. Vols. 725–726. Pp. 1493–1498.
9. Perlova E., Karpova S., Rakova X.M., Bondarenko E., Platonova M., Gorshkov A. The architectural concept of the building with low energy consumption // Applied Mechanics and Materials. 2015. Vols. 725–726. Pp. 1580–1588.
10. Dagnall M., Window A., Leung A., Thompson D. Analytical assessment of thermal performance of a ventilated glazed facade system // Proceedings of Building Simulation: 12th Conference of International Building Performance Simulation Association. Sydney, 2011. Pp. 808–815.
11. Vatin N.I., Gorshkov A.S., Nemova D.V., Staritcyna A.A., Tarasova D.S. The energy-efficient heat insulation thickness for systems of hinged ventilation facades // Advanced Materials Research. 2014. № 941–944. Pp. 905–920.
12. Vatin N., Gorshkov A., Rymkevich P., Nemova D., Tarasova D. Nonstationary thermal conduction through the building envelope // Applied Mechanics and Materials. 2014. № 670–671. Pp. 365–369.
13. Patania F., Gagliano A., Nocera F., Ferlito A., Galesi A. Thermofluid-dynamic analysis of ventilated facades // Energy and Buildings. 2010. Vol. 42. Pp. 1148–1155.
14. Suareza C., Joubertb P., Molinaa J.L., Sánchez F.J. Heat transfer and mass flow correlations for ventilated facades // Energy and Buildings. 2011. Vol. 43. Pp. 3696–3703.
15. Nizovtsev M.I., Belyi V.T., Sterlygov A.N. The facade system with ventilated channels for thermal insulation of newly constructed and renovated buildings // Energy and Buildings. 2014. Vol. 75. Pp. 60–69.
16. Šagát E., Matějka L. Experimental assessment of the influence of wind speed on the airflow and temperatures in the open joint ventilated façade cavity // Applied Mechanics and Materials. 2016. Vol. 835. Pp. 444–449.
17. Šagát E., Matějka L., Pěnčík J. Experimental assessment of the influence of outlet geometry on the airflow and temperatures in the ventilated façade cavity // Applied Mechanics and Materials. 2016. Vol. 824. Pp. 641–648.

influence of wind speed on the airflow and temperatures in the open joint ventilated façade cavity. *Applied Mechanics and Materials*. 2016. Vol. 835. Pp. 444–449.

17. Šagát E., Matějka L., Pěnčík J. Experimental assessment of the influence of outlet geometry on the airflow and temperatures in the ventilated façade cavity. *Applied Mechanics and Materials.* 2016. Vol. 824. Pp. 641–648.
18. Ryabukhina S., Simankina T., Koshkarova M., Sokolovskii N., Ryzhkov O. Combined thermal insulating module of mounted vented facades. *MATEC Web of Conferences.* 2016. Vol. 73. 02005.
19. Peci López F., Jensen R.L., Heiselberg P., Ruiz de Adana Santiago M. Experimental analysis and model validation of an opaque ventilated facade. *Building and Environment*. 2012. Vol. 56. Pp. 265–275.
20. *SP 14.13330.2014. SNiP II-7-81* Stroitelstvo v seysmicheskikh rayonakh* [Russian Set of Rules SP 14.13330.2014. SNiP II-7-81* Construction in seismic regions]. TsNIISK im. V.A. Kucherenko, OAO «NITs «Stroitelstvo». M.: OAO «TsPP», 2014. 126 p.
21. Ajzenberg Ja.M., Akbiev R.T., Smirnov V.I., Chubakov M.Zh. Dinamicheskie ispytanija i sejsmostojkost' navesnyh fasadnyh system [Dynamic testing and seismic stability of hinged facade systems]. *Sejsmostojkoe stroitel'stvo. Bezopasnost' sooruzhenij*. 2008. No. 1. Pp. 13–15. (rus).
22. Granovskij A.V., Haktaev S.S. K voprosu o primenenii fasadnyh teploizoljacionnyh kompozitnyh sistem dlja sten zdanij, vozvodimyh v obychnyh i sejsmoopasnyh regionah Rossii [To the problem of the application of facade heat-insulating composite systems for walls of buildings erected in conventional and seismic regions of Russia]. *Promyshlennoe i grazhdanskoe stroitel'stvo.* 2015. No. 4. Pp. 96–100. (rus).
23. Granovskiy A.V., Kiselev D.A. Eksperimental'nyye issledovaniya raboty ankernogo krepezha pri dinamicheskikh vozdeystviyakh [Experimental studies of the work of anchoring fasteners under dynamic actions]. *Seysmicheskoye stroitel'stvo. Bezopasnost' sooruzheniy.* 2012. No. 1. Pp. 43-45. (rus).
24. *Tekhnicheskiy otchet po rezul'tatam eksperimental'nykh issledovaniy seysmostoykosti konstruktsiy navesnykh ventiliruyemykh fasadnykh sistem «AL-SITI» tipov «AL-SITI» K i «AL-SITI» A.* [Technical report on the results of experimental seismic resistance studies of ventilated facade systems "AL-CITY" types "AL-CITY" K and "AL-CITY" A]. M.: TSNIISK im. V.A. Kucherenko. 2007. 30 p. (rus).
25. Granovskij A.V., Dottuev Z.I., Hasanov T.M. K voprosu o metodike ispytanij i ocenke sejsmostojkosti navesnyx fasadnyx sistem [To the problem of the method of testing and evaluation of seismic resistance of hinged facade systems]. *Promyshlennoe i grazhdanskoe stroitel'stvo*. 2009. No. 10. Pp. 15–17. (rus).
26. Wen Y.K., Kang Y.J. Minimum building life-cycle cost design criteria. II. Applications. *Journal of Structural Engineering New York*. 2001. No. 127(3). Pp. 338–346.
27. Tusnina V.M, Emel'janov A.A., Granovskij A.V. Puti povyshenija sejsmostojkosti ventiliruemyh fasadnyh system [Ways to increase seismic resistance of ventilated facade systems]. *Promyshlennoe i grazhdanskoe stroitel'stvo*. 2014. No. 11. Pp. 63–65. (rus).
28. Tusnina V.M., Emel'janov D.A. Uzlovye soedineniya elementov v nesushhix sistemax navesnyx ventiliruemyx fasadov [Nodal connections of elements in load-bearing systems of hinged ventilated facades]. *Promyshlennoe i grazhdanskoe stroitel'stvo*. 2013. No. 9. Pp. 11–13. (rus).
29. Tusnina V.M., Yemel'yanov D.A. Eksperimental'noye issledovaniye uzlov krepleniya otdelochnykh kasset dlya sistem navesnykh ventiliruyemykh fasadov [Experimental research of the attachment points of finishing cassettes for systems of hinged ventilated facades]. *Promyshlennoye i grazhdanskoye stroitel'stvo*. 2015. No. 3. Pp. 11–13. (rus).

18. Ryabukhina S., Simankina T., Koshkarova M., Sokolovskii N., Ryzhkov O. Combined thermal insulating module of mounted vented facades // MATEC Web of Conferences. 2016. Vol. 73. 02005.
19. Peci López F., Jensen R.L., Heiselberg P., Ruiz de Adana Santiago M. Experimental analysis and model validation of an opaque ventilated facade // Building and Environment. 2012. Vol. 56. Pp. 265–275.
20. СП 14.13330.2014. СНиП II-7-81* Строительство в сейсмических районах / ЦНИИСК им. В.А. Кучеренко, ОАО «НИЦ «Строительство». М.: ОАО «ЦПП», 2014. 126 с.
21. Айзенберг Я.М., Акбиев Р.Т., Смирнов В.И., Чубаков М.Ж. Динамические испытания и сейсмостойкость навесных фасадных систем // Сейсмостойкое строительство. Безопасность сооружений. 2008. № 1. С. 13-15.
22. Грановский А.В., Хактаев С.С. К вопросу о применении фасадных теплоизоляционных композитных систем для стен зданий, возводимых в обычных и сейсмоопасных регионах России // Промышленное и гражданское строительство. 2015. № 4. С. 96–100.
23. Грановский А.В., Киселев Д.А. Экспериментальные исследования работы анкерного крепежа при динамических воздействиях // Сейсмическое строительство. Безопасность сооружений. 2012. № 1. С. 43-45.
24. Технический отчет по результатам экспериментальных исследований сейсмостойкости конструкций навесных вентилируемых фасадных систем «AL-СИТИ» типов «AL-СИТИ» К и «AL-СИТИ» А. М: ЦНИИСК им. В.А. Кучеренко. 2007. 30 с.
25. Грановский А.В., Доттуев З.И., Хасанов Т.М. К вопросу о методике испытаний и оценке сейсмостойкости навесных фасадных систем // Промышленное и гражданское строительство. 2009. № 10. С. 15–17.
26. Wen Y.K., Kang Y.J. Minimum building life-cycle cost design criteria. II. Applications // Journal of Structural Engineering New York. 2001. № 127(3). Pp. 338–346.
27. Туснина В.М, Емельянов А.А., Грановский А.В. Пути повышения сейсмостойкости вентилируемых фасадных систем // Промышленное и гражданское строительство. 2014. № 11. С. 63–65.
28. Туснина В.М., Емельянов Д.А. Узловые соединения элементов в несущих системах навесных вентилируемых фасадов // Промышленное и гражданское строительство. 2013. № 9. С. 11–13.
29. Туснина В. М., Емельянов Д.А. Экспериментальное исследование узлов крепления отделочных кассет для систем навесных вентилируемых фасадов // Промышленное и гражданское строительство. 2015. № 3. С. 46–49.
30. Tusnina V.M., Emelyanov D.A., Tusnina O.A. Design of a Suspended Ventilated Fasade with composite Fasing // Applied Mechanics and Materials. 2014. Vols. 578-579. Pp. 226–229.
31. Туснина В.М., Емельянов Д.А. К вопросу расчёта и проектирования навесных вентилируемых фасадных систем // Промышленное и гражданское строительство. 2016. № 3. С. 38–42.
32. MSK-64. Шкала сейсмической интенсивности MSK. 1964.
33. СТО 44416204-012-2013. Элементы облицовочные навесных фасадных систем с воздушным зазором и детали их крепления. Метод определения несущей способности по результатам лабораторных испытаний. Москва. ФАУ «ФЦС». ЦНИИПСК им. Н.П. Мельникова. 2013. 30 с.

30. Tusnina V.M., Emelyanov D.A., Tusnina O.A.. Design of a Suspended Ventilated Fasade with composite Fasing. *Applied Mechanics and Materials*. 2014. Vols. 578-579. Pp. 226–229.
31. Tusnina V.M., Yemel'yanov D.A. K voprosu raschota i proyektirovaniya navesnykh ventiliruyemykh fasadnykh system [To the question of calculation and design of hinged ventilated facade systems]. *Promyshlennoye i grazhdanskoye stroitel'stvo*. 2016. No. 3. Pp. 38–42. (rus).
32. *MSK-64.* Shkala seysmicheskoy intensivnosti MSK [MSK-64. Scale of seismic intensity MSK].1964.
33. *STO 44416204-012-2013.* Elementy oblitsovochnyye navesnykh fasadnykh sistem s vozdushnym zazorom i detali ikh krepleniya. Metod opredeleniya nesushchey sposobnosti po rezul'tatam laboratornykh ispytaniy [Russian technical standard of the organization STO 44416204-012-2013. Elements facing facade systems with an air gap and details of their fastening. The method of determining the load-bearing capacity by the results of laboratory tests]. Moscow. FAI "FCS". TsNIIPSK them. N.P. Melnikov. 2013. 30 p. (rus).

Valentina Tusnina,*
+7(916)510-72-24; valmalaz@mail.ru

Denis Emelianov,
+7(903)751-75-29; snegiri_emelianov@mail.ru

Валентина Матвеевна Туснина,*
+7(916)510-72-24; эл. почта: valmalaz@mail.ru

Денис Андреевич Емельянов,
+7(903)751-75-29;
эл. почта: snegiri_emelianov@mail.ru

doi: 10.18720/MCE.80.7

Survivability criteria for reinforced concrete frame at loss of stability

Критерии живучести железобетонной рамы при потере устойчивости

V.I. Kolchunov,
S.Yu. Savin*,
Southwest State University, Kursk, Russia

Д-р техн. наук, заведующий кафедрой В.И. Колчунов,
канд. техн. наук, доцент С.Ю. Савин*,
Юго-Западный государственный университет, г. Курск, Россия

Key words: survivability; stability; multi-storey frame; reinforced concrete; corrosion damage

Ключевые слова: живучесть; устойчивость; многоэтажная рама; железобетон; коррозионные повреждения

Abstract. Analysis of scientific publications on the assessment of resistance of structures to progressive collapse, as well as existing and projects of design codes of different countries, in particular the project of Design Code "Protection of buildings and structures against progressive collapse. The design requirements. General conclusions", shows, that the main evaluating criteria are strength parameters. At the same time, structures, which are made of high– strength materials and have small sizes of cross-sections, as well as structures operating in aggressive conditions, when the cross-section decrease or the computational length suddenly increase, should be checked to the loss of stability of the bearing elements. The purpose of this study is to obtain the evaluating criteria of the survivability and residual life of reinforced concrete (RC) structural systems at sudden loss of stability of the element, caused by the evolutionary accumulation of a critical level of corrosion damage. The article presents analytical dependences to determine the critical value of the cross-section stiffness of the corrosively damaged element and the critical time, after which the structural system lose stability in conditions of simultaneous action of forces and aggressive environmental influences. Proposals are given to assign the survivability parameters of reinforced concrete structural systems, operating under exceeding limit states, that caused by the sudden loss of stability of the carrier element at the accumulation of critical value of corrosion damages.

Аннотация. Анализ научных публикаций, посвященных оценке сопротивляемости конструктивных систем зданий и сооружений прогрессирующему обрушению, а также существующих и разрабатываемых нормативных документов разных стран, в частности проекта СП «Защита зданий и сооружений от прогрессирующего обрушения. Правила проектирования. Основные положения», показывает, что в качестве критериев такой оценки, как правило, выступают прочностные показатели. В то же время для конструктивных систем из высокопрочных материалов при малых размерах поперечных сечений их элементов, а также для конструктивных систем, работающих в условиях воздействия агрессивных сред, когда уменьшается поперечное сечение или расчетной длины – в качестве критерия оценки сопротивляемости прогрессирующему обрушению необходимо рассматривать и потерю устойчивости несущего элемента конструктивной системы. Целью настоящего исследования являлось построение критериев для оценки живучести и остаточного ресурса конструктивных систем из железобетона при внезапной потере устойчивости одного из элементов, вызванной эволюционным накоплением критического уровня коррозионных повреждений. В статье приведены аналитические зависимости для определения критического значения жесткости поперечного сечения коррозионно повреждаемого элемента и критического времени, при котором конструктивная система потеряет устойчивость в условиях одновременного проявления силовых и средовых воздействий. Даны предложения по нормированию параметров живучести железобетонных конструктивных систем при запредельных состояниях, вызванных внезапной потерей устойчивости несущего элемента от накопления коррозионных повреждений.

Колчунов В.И., Савин С.Ю., Критерии живучести железобетонной рамы при потере устойчивости // Инженерно-строительный журнал. 2018. № 4(80). С. 73–80.

1. Introduction

A series of accidents and destruction of buildings and structures that occurred in the XX – early XXI century, such as the destruction of the WTC towers in New York, destructions of panel high-rise buildings caused by natural gas explosions, etc., gave a powerful impetus to the development of a new direction in building science – the calculation of buildings and structures against progressive collapse. The current regulatory documents of a number of countries, in particular the USA, Great Britain, EU, Ukraine, Russia [1–5] contain the basic provisions, allowing to carry out an assessment of risk of progressive collapse of buildings and structures. However, the number of new scientific publications on this subject suggests that there are many aspects, which still require further study. A significant number of recent publications are devoted to the study of the progressive collapse caused by explosive loads [6-11]. However, the start of avalanche destruction of the structural system may be caused by the accumulation of a critical level of damage of another nature [12–14], in particular of a corrosive damage [15–18]. At the same time, the loss of strength of bearing elements of the system is considered as a main criterion of such a process in an overwhelming number of scientific publications, devoted to the assessment of resistance of building and structures against progressive collapse. In our opinion it is expedient to consider the loss of stability of bearing elements as an additional criterion of resistance of designed and operating frameworks against progressive destruction. However, currently there are only a few papers in this direction [19–23], mainly presented in foreign publishing, the main number of which cover the assessment of resistance against progressive collapse of steel frames [20–26]. A number of authors in their publications combine the terms of stability and resistance against progressive collapse, implying in this case destruction due to the loss of strength of structural elements [27–28].

In this way, the purpose of the paper is to obtain criteria for evaluate state of structures over the limit state, caused by loss of stability of a bearing reinforced concrete element at corrosion damage accumulation. The following tasks are solved to achieve this purpose: obtain analytical model to evaluate bending stiffness of reinforced concrete element cross section, destructured by corrosion; derive relationship to determine critical time tcr, when structural element loss stability because of corrosion damages.

2. Methods

This article explores the issues of survivability of reinforced concrete structural system at sudden buckling of the bearing structural element due to the accumulation of a critical level of corrosion damage. Stability problem are solved analytically by Euler's statement using deformation method. The phenomenological model proposed by V.M. Bondarenko [15] is used in this paper to account for long-term processes of corrosion damage of structural elements, contacting with aggressive environment.

According to this model the depth of corrosion damage of reinforced concrete structure $\delta(t,t_0)$ at colmatation can be described by the following mathematical relationship as it is shown in Figure 1 (a).

$$\delta(t,t_0)=\delta_{cr}\left\{1-\left[\alpha(m-1)(t-t_0)+\left(1-\frac{\delta(t_0,t_0)}{\delta_{cr}}\right)^{1-m}\right]^{\frac{1}{1-m}}\right\} \quad (1)$$

where δ_{cr} is ultimate depth of corrosion damage at colmatation; α and m are parameters, which characterize penetration speed of the corrosion damage front; t and t_0 are current time and initial time of observation the damaged structural element. It should be noted that $m < 0$ corresponds to the area of avalanche penetration of corrosion front in time; $m > 0$ corresponds to the area of colmatation (penetration of corrosion front damped in time); $m = 0$ corresponds to the boundary line of the filtration development of the damage process. The parameters δ_{cr}, α and m can be approximated by polynomials [16], as it is shown in Figure 1 (b):

$$\delta_{cr}=\sum_{i=0}^{3}q_{\delta_i}\cdot(\sigma/R_b)^i,$$

$$\alpha=\sum_{i=0}^{3}q_{\alpha_i}\cdot(\sigma/R_b)^i,$$

$$m = \sum_{i=0}^{3} q_{m_i} \cdot (\sigma / R_b)^i ,$$

where q_δ, q_α, q_m are parameters, which should be determined empirically for defined aggressive environment and initial mechanical characteristics of concrete.

Also it should be noted, that the function of corrosion damage depth $\delta(t, t_0)$ can take the trajectory of avalanche (1) or fading (2) development once more after an additional dynamic impact on the reinforced concrete element with depth of corrosion damage about δ_{cr} at time t_1 , as it is shown in Figure 1 (a).

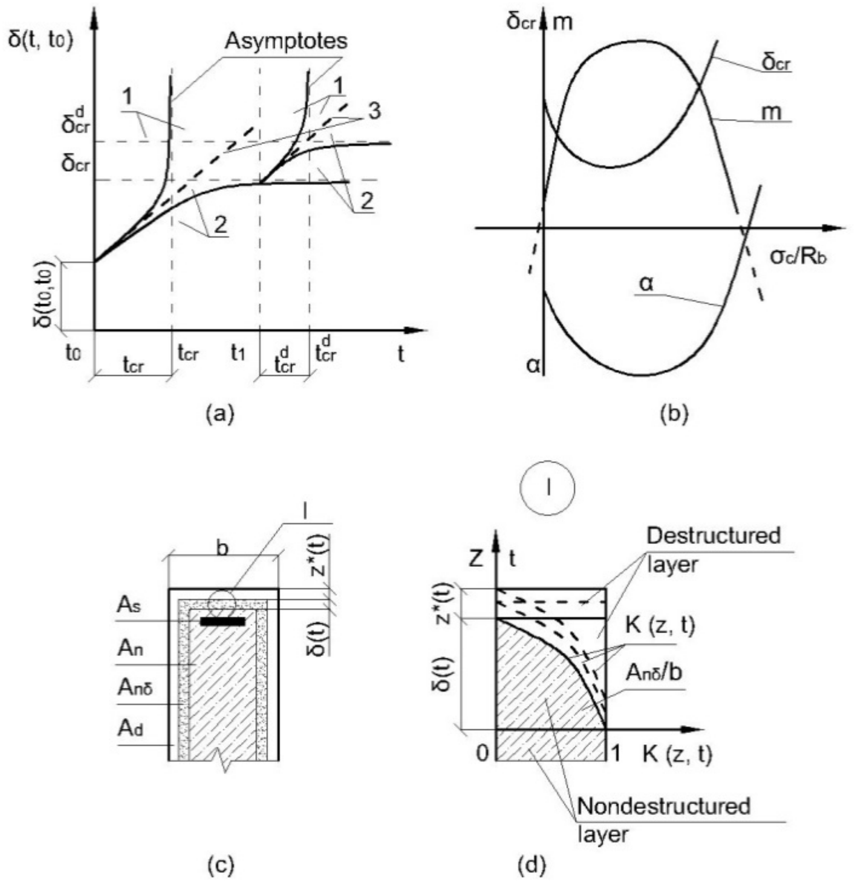

Figure 1. Scheme of the corrosion damage kinetics of compressed concrete
(a): scheme to determine parameters δcr, α, m;
(b): cross-section of the corrosion-damaged reinforced concrete element;
(c): general view of the corrosion damage function K(z, t);
(d): 1 corresponds to the area of avalanche corrosion penetration (m < 0);
2 corresponds to the area of colmatation (m > 0);
3 is the boundary line (m = 0)

3. Results and Discussion

In the present article we consider only colmatational process of corrosion damage development in accordance to which the stiffness of the cross section of corrosion damaged element can be determined from the following expression:

$$B_{red}(\delta(t)) = E_t \cdot I_{red}(\delta(t)) \tag{2}$$

where E_t is variable strain modulus of concrete, which depends on deformation, caused by loading and creep [21];

I_{red} *(δ(t))* is the reduced inertia moment of cross section, which can be calculated by the formula:

$$I_{red}\left(\delta(t)\right)=A_n r_{cn}^2+\sum_{i=1}^{l}A_{n\delta,i}r_{cn\delta,i}^2+I_n+\sum_{i=1}^{l}I_{n\delta,i}+\frac{\omega_s}{\psi_s}\cdot\alpha\cdot A_s\cdot r_{cs}^2 \tag{3}$$

where A_n is area of part of section without corrosion damage; $A_{n\delta,i}$ is area of i-th part of section exposed to corrosion, which is determined in accordance to function of corrosion damage *K(z, t)* as it is shown in Figure 1 (c); A_s is area of reinforcement cross section; r_{cn}, $r_{cn\delta,i}$ are distance from center of mass of not damaged section to center of mass of whole section and distance from center of mass of i-th part of section damaged by corrosion to center of mass of whole section, which is determined in accordance to function of corrosion damage *K(z, t)*, respectively; r_{cs} is distance from center of mass of reinforcement cross section to center of mass of whole section; In is inertia moment of not damaged section with respect to own center of mass; $I_{n\delta,i}$ is inertia moment of i-th part of damaged section with respect to own center of mass; ω_s is coefficient of corrosion damage of reinforcement; ψ is coefficient of influence of tensiled concrete; $\alpha = E_s / E_t$ is coefficient of reduction of reinforcement to concrete.

Assuming that the corrosion damage of the section can be modeled by the function *K (z, t),* as it is shown in Figure 1 (d), taking into account the scheme shown in figure 1 (c), we obtain:

$$\begin{aligned}I_{red}(t)=&\left(b-2z^*(t)\right)\frac{4\delta(t)}{3}\left(\frac{h}{2}-z^*(t)-\frac{3}{5}\delta(t)\right)^2+\frac{\left(b-2z^*(t)\right)}{6}\left(\frac{2\delta(t)}{3}\right)^3+\\&+\left[h-2z^*(t)-2\delta(t)\right]^3\frac{\delta(t)}{9}+\frac{1}{12}\left[b-2z^*(t)-2\delta(t)\right]\cdot\left[h-2z^*(t)-2\delta(t)\right]^3+\\&+\frac{\omega_s}{\psi}\cdot\alpha\cdot A_s\cdot(h-2a)^2\end{aligned} \tag{4}$$

where h and b are the height and width of the intact section respectively; a is the distance from the center of gravity of the reinforcement to the face of the reinforced concrete element as it is shown in Figure 1 (c); $\delta(t)$ is the thickness of the layer, is partially damaged by corrosion which can be determined from the expression

$$\delta(t)=\delta(t,t_0)-z^*(t) \tag{5}$$

In which $\delta(t,t_0)$ can be obtained by the formula (1); $z^*(t)=t\dfrac{d}{dt}\left(z^*\right)$ is the approximate relationships for the depth of the entirely destructured concrete; approximate model of corrosion destruction ω_s of steel reinforcement can be calculated from the equations:

$$\begin{cases}\omega_s=1 \quad at \quad \delta(t,t_0)<a-d/2;\\ \omega_s=\dfrac{\pi}{4A_s}\left[d-\dfrac{t-t_s}{8760}\dfrac{d}{dt}(\omega_s)\right]^2 \quad at \quad \delta(t,t_0)>a-d/2;\\ \omega_s=0 \quad at \quad z^*(t)\geq a-d/2.\end{cases} \tag{6}$$

Let us consider a fragment of a multi-storey frame (Figure 2) to develop an algorithm for analytical stability analysis of corrosion-damaged concrete structural system of the building. For this construction, we define the value of the parameter k_{cr} of special functions of the method of displacement, which characterize critical force and can be determined from the expression:

$$k_{cr}^2=\frac{P_{cr}l^2}{B_{red}} \tag{7}$$

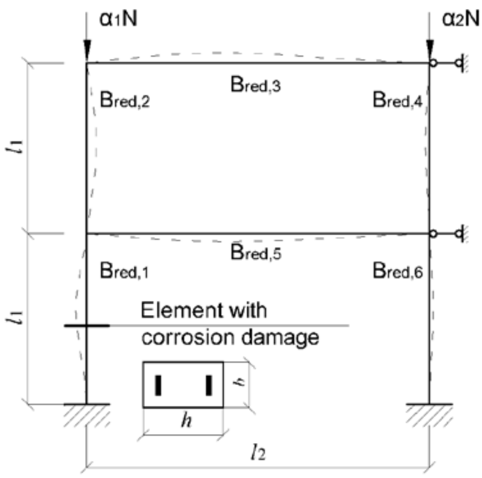

Figure 2. Computational model of the fragment of a multi-storey reinforced concrete frame

Let us assume that the elements of the structural system are compressed by longitudinal forces $N_i = \xi_i \cdot P_{cr}$, where ξ_i is the safety factor of stability of the i-th element of the system at the most unfavorable calculated combination of forces, P_{cr} – Euler's critical force for the structural system.

Taking into account that the k_{cr} parameter depends only on the boundary conditions at the end sections of the frame structural element, we carried out an expression for the critical value of the bending stiffness of the corrosion-damaged element, at which it will lose the stability:

$$B_{red,cr} = \frac{\xi_i P_{cr} l^2}{k_{cr}^2} \tag{8}$$

Equating expressions (8) and (2) and taking into account expressions (1), (5), (6), we obtain an equation, in which all parameters can be expressed through a critical time t_{cr}, corresponding to the moment of loss of the stability due to reaching a critical level of corrosion damage:

$$\begin{aligned} \frac{\xi_i P_{cr} E_t l^2}{k_{cr}^2} &= \left(b - 2z^*(t_{cr})\right)\frac{4\delta(t_{cr})}{3}\left(\frac{h}{2} - z^*(t_{cr}) - \frac{3}{5}\delta(t_{cr})\right)^2 + \frac{\left(b - 2z^*(t_{cr})\right)}{6}\left(\frac{2\delta(t_{cr})}{3}\right)^3 + \\ &+ \left[h - 2z^*(t_{cr}) - 2\delta(t_{cr})\right]^3 \frac{\delta(t_{cr})}{9} + \frac{1}{12}\left[b - 2z^*(t_{cr}) - 2\delta(t_{cr})\right]\cdot\left[h - 2z^*(t_{cr}) - 2\delta(t_{cr})\right]^3 + \\ &+ \frac{\omega_s}{\psi}\cdot \alpha \cdot A_s \cdot (h - 2a)^2 \end{aligned} \tag{9}$$

Let us analyze the stability of a fragment of a reinforced concrete frame (figure 2), one of the bearing elements of which (the lower left rack) is subject to the action of an aggressive environment. Initial parameters of the frame: l_1 = 3 m, l_2 = 6 m, initial section width b = 0.2 m, initial section height h = 0.35 m, the distance from the most compressed face to the center of gravity of the reinforcement a = 40 mm as it is shown in Figure 1 (a). Concrete B25 class, reinforcement $A_s = A'_s$ – 4 rod A400 class with a diameter of 16 mm. The level of aggressiveness of the environment is medium ($z'(t)$ = 1 mm/year). Values of parameters δ_{cr}, α, m are taken by paper V.M. Bondarenko [15]. At the moment t_0 = 0 the safety factor of the stability of the corrosion-damaged rack ξ_i = 0.8, and the value of the critical force P_{cr} = 2860 kN, the ratio of the load parameters $\alpha_2 / \alpha_1 = 4$.

Solving equation (9) in accordance with expressions (1), (5), (6), we obtain the graph B_{red} - t, which is shown in Figure 3 (b). The intersection point of this graph with the line of the ultimate value of stiffness $B_{red,cr}$ corresponds to the value of the critical time of the aggressive environment impact on the loaded structure t_{cr}, after which the frame will lose the stability.

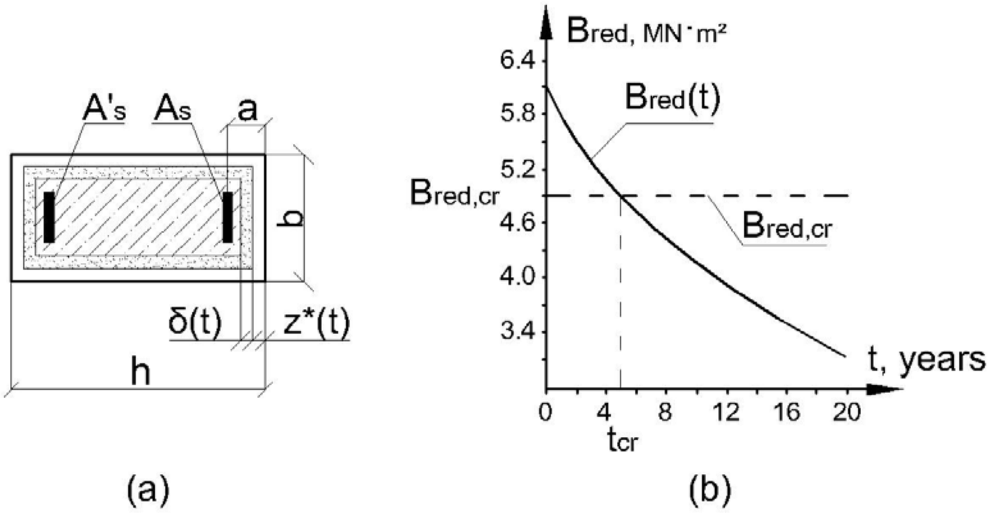

Figure 3. Scheme of the rack cross section (a) and graph B_{red} – t (b) for corrosion-damaged structural element

The ultimate value of the cross-section stiffness of the damaged structural element $B_{red,cr}$ or critical time t_{cr}, after which the structural system will lose stability, can be used as criteria to assess the survivability of reinforced concrete structural system at exceeding of the limit states, caused by a sudden loss of stability of the bearing element at acting of the loading and corrosion.

4. Conclusions

1. Analytical relationships for the critical stiffness value of the cross-section $B_{red,cr}$ of the corrosion-damaged element of the reinforced concrete frame are obtained.
2. "Exposure time of survivability" (by the terminology of V.M. Bondarenko, V.I. Kolchunov [29]) t_{cr} is determined on the basis of the stability criteria of a structural system, subjected acting of load and aggressive environment impact.
3. It is proposed criteria to assess the survivability of reinforced concrete structural system at exceeding of the limit states, caused by a sudden loss of stability of the bearing element at acting of the loading and corrosion.

References

1. *UFC 4-023-03 (Including Change 3, 2016) Unified facilities criteria.* Design of buildings to resist progressive collapse. Department of Defense. 2016.
2. *BS 8110-1:1997 Structural use of concrete.* London. 1998.
3. *EN 1992-1-1-2009 Eurocode 2: Design of concrete structures. European committee for standardization.* 2009.
4. *EN 1991-1-7-2009 General Actions – Accidental Actions. European committee for standardization.* 2009.
5. *State Building Standard of Ukraine DBN V.1.2-14-2009.* Obshchiye printsipy obespecheniya nadezhnosti i konstruktivnoy bezopasnosti zdaniy, sooruzheniy stroitelnykh konstruktsiy i osnovaniy [State Building Code B.1.2-14-2009 General principles of ensuring the reliability and constructive safety of buildings, structures and bases]. Kiev, 2009. (rus)
6. Pham A.T., Tana K.H., Yu J. Numerical investigations on static and dynamic responses of reinforced concrete sub-assemblages under progressive collapse. *Engineering Structures.* 2017. Vol. 149. Pp. 2–20. Doi: 10.1016/j.engstruct.2016.07.042.
7. Al-Salloum Y. A., Abbas H., Almusallam T. H., Ngo T., Mendis P. Progressive collapse analysis of a typical RC high-rise tower. *Journal of King Saud University – Engineering Sciences.* 2017. Vol. 29. Pp. 313–320. Doi: 10.1016/j.jksues.2017.06.005.
8. Dinua F., Marginean I., Dubina D., Kovacs A., Ghicioi E. Experimental testing and numerical modeling of steel frames under close-in detonations. *Procedia Engineering.*

Литература

1. UFC 4-023-03 (Including Change 3, 2016) Unified facilities criteria. Design of buildings to resist progressive collapse. Department of Defense. 2016.
2. BS 8110-1:1997 Structural use of concrete. London. 1998.
3. EN 1992-1-1-2009 Eurocode 2: Design of concrete structures. European committee for standardization. 2009.
4. EN 1991-1-7-2009 General Actions – Accidental Actions. European committee for standardization. 2009.
5. ДБН В.1.2-14-2009 Общие принципы обеспечения надежности и конструктивной безопасности зданий, сооружений строительных конструкций и оснований. Кіев, 2009.
6. Pham A.T., Tana K.H., Yu J. Numerical investigations on static and dynamic responses of reinforced concrete sub-assemblages under progressive collapse // Engineering Structures. 2017. Vol. 149. Pp. 2–20. doi: 10.1016/j.engstruct.2016.07.042.
7. Al-Salloum Y. A., Abbas H., Almusallam T. H., Ngo T., Mendis P. Progressive collapse analysis of a typical RC high-rise tower // Journal of King Saud University - Engineering Sciences. 2017. Vol. 29. Pp. 313–320. doi: 10.1016/j.jksues.2017.06.005.
8. Dinua F., Marginean I., Dubina D., Kovacs A., Ghicioi E. Experimental testing and numerical modeling of steel frames under close-in detonations // Procedia Engineering. 2017. Vol. 210. Pp. 377–385. Doi: 10.1016/j.proeng.2017.11.091.

2017. Vol. 210. Pp. 377–385. Doi: 10.1016/j.proeng.2017.11.091.

9. Goel M.D., Agrawal D., Choubey A. Collapse Behavior of RCC Building under Blast Load. *Procedia Engineering.* 2017. Vol. 173. Pp. 1943–1950. Doi: 10.1016/j.proeng.2016.12.256.
10. Elsanadedy H.M., Almusallam T.H., Alharbi Y.R., Al-Salloum Y.A., Abbas H. Progressive collapse potential of a typical steel building due to blast attacks. *Journal of Constructional Steel Research.* 2014. Vol. 101. Pp. 143–157. Doi: 10.1016/j.jcsr.2014.05.005
11. Weng J., Lee C.K., Tan K.H., Lim N.S. Damage assessment for reinforced concrete frames subject to progressive collapse. *Engineering Structures.* 2017. Vol. 149. Pp. 147–160. Doi: 10.1016/j.engstruct.2016.07.038.
12. Shapiro G.I., Obukhova L.V., Eysman Yu.A., Sirotina Ye.V. Zashchita ot progressiruyushchego obrusheniya zhilykh domov pervogo perioda industrialnogo domostroyeniya seriy 1-510, 1-511, 1-515 [Protection against the progressive collapse of residential buildings of the first period of industrial construction series 1-510, 1-511, 1-515]. *Promyshlennoye i grazhdanskoye stroitelstvo.* 2006. No. 4. Pp. 32–35. (rus)
13. Kolchunov V.I., Savin S.Y. Dynamic effects in a composite two-component rods which appear when local fracture of the matrix is occurred. *Journal of Applied Engineering Science.* 2017. Vol. 15. No. 3. Pp: 325–331. Doi:10.5937/jaes15-14602.
14. Benin A.V., Semenov A.S., Semenov S.G., Melnikov B.E. Konechno-elementnoye modelirovaniye protsessov razrusheniya i otsenka resursa elementov avtodorozhnogo mosta s uchotom korrozionnykh povrezhdeniy [Finite element modeling of fracture processes and estimation of durability of the road bridge with account of corrosion damages]. *Magazine of Civil Engineering.* 2012. No. 7. Pp. 32–42. (rus)
15. Bondarenko V.M., Klyuyeva N.V. K raschetu sooruzheniy, menyayushchikh raschetnuyu skhemu vsledstviye korrozionnogo povrezhdeniya [Calculation of structures that change the design scheme due to corrosion damage]. *Izvestiya vuzov. Stroitelstvo.* 2008. No. 1. Pp. 4–12. (rus)
16. Bondarenko V.M., Kolchunov V.I. Ekspozitsiya zhivuchesti zhelezobetona [Exposure of the survivability of reinforced concrete]. *Izvestiya vysshikh uchebnykh zavedeniy. Stroitelstvo.* 2007. No. 5. Pp. 4–8. (rus)
17. Selyayev V.P., Selyayev P.V., Alimov M. F., Sorokin Ye. V. Otsenka ostatochnogo resursa zhelezobetonnykh izgibayemykh elementov, podverzhennykh deystviyu khloridnoy korrozii [Evaluation of Residual Resource of Reinforced Concrete Elements Subject to Chloride Corrosion]. *Stroitelstvo i rekonstruktsiya.* 2017. No. 6. Pp. 49–58. (rus)
18. Selyaev V.P., Neverov V.A., Selyaev P.V., Sorokin E.V., Yudina O.A. Prognozirovaniye dolgovechnosti zhelezobetonnykh konstruktsiy s uchetom sul'fatnoy korrozii betona [Predicting the durability of concrete structures, including sulfate corrosion of concrete]. *Magazine of Civil Engineering.* 2014. No. 1. Pp. 41–52. Doi: 10.5862/MCE.45.5. (rus)
19. Schafer B.W., Bajpai P. Stability degradation and redundancy in damaged structures. *Engineering Structures.* 2005. Vol. 27. Pp. 1642–1651. Doi: 10.1016/j.engstruct.2005.05.012.
20. Mc Connell J.R., Brown H. Evaluation of progressive collapse alternate load path analyses in designing for blast resistance of steel columns. *Engineering Structures.* 2011. Vol. 33. Pp. 2899–2909. Doi: 10.1016/j.engstruct.2011.06.014.
21. Szyniszewski S., Krauthammer T. Energy flow in progressive collapse of steel framed buildings. *Engineering Structures.* 2012. Vol. 42. Pp. 142–153.

9. Goel M.D., Agrawal D., Choubey A. Collapse Behavior of RCC Building under Blast Load // Procedia Engineering. 2017. Vol. 173. Pp. 1943–1950. Doi: 10.1016/j.proeng.2016.12.256.
10. Elsanadedy H.M., Almusallam T.H., Alharbi Y.R., Al-Salloum Y.A., Abbas H. Progressive collapse potential of a typical steel building due to blast attacks // Journal of Constructional Steel Research. 2014. Vol. 101. Pp. 143–157. Doi: 10.1016/j.jcsr.2014.05.005.
11. Weng J., Lee C.K., Tan K.H., Lim N.S. Damage assessment for reinforced concrete frames subject to progressive collapse // Engineering Structures. 2017. Vol. 149. Pp. 147–160. Doi: 10.1016/j.engstruct.2016.07.038.
12. Шапиро Г.И., Обухова Л.В., Эйсман Ю.А., Сиротина Е.В. Защита от прогрессирующего обрушения жилых домов первого периода индустриального домостроения серий 1-510, 1-511, 1-515 // Промышленное и гражданское строительство. 2006. № 4. С. 32–35.
13. Kolchunov V.I., Savin S.Y. Dynamic effects in a composite two-component rods which appear when local fracture of the matrix is occurred // Journal of Applied Engineering Science. 2017. Vol. 15. № 3. Pp: 325–331. doi: 10.5937/jaes15-14602.
14. Бенин А.В., Сменов А.С., Семенов С.Г., Мельников Б.Е. Конечно-элементное моделирование процессов разрушения и оценка ресурса элементов автодорожного моста с учётом коррозионных повреждений // Инженерно-строительный журнал. 2012. № 7(33). С. 32–42.
15. Бондаренко В.М., Клюева Н.В. К расчету сооружений, меняющих расчетную схему вследствие коррозионного повреждения // Известия вузов. Строительство. 2008. № 1. С. 4–12.
16. Бондаренко В.М., Колчунов В.И. Экспозиция живучести железобетона // Известия высших учебных заведений. Строительство. 2007. № 5. С. 4–8.
17. Селяев В.П., Селяев П.В., Алимов М.Ф., Сорокин Е.В. Оценка остаточного ресурса железобетонных изгибаемых элементов, подверженных действию хлоридной коррозии // Строительство и реконструкция. 2017. № 6. С. 49–58.
18. Селяев В.П., Неверов В.А., Селяев П.В., Сорокин Е.В., Юдина О.А. Прогнозирование долговечности железобетонных конструкций с учетом сульфатной коррозии бетона // Инженерно-строительный журнал. 2014. № 1(45). С. 41–52. doi: 10.5862/MCE.45.5.
19. Schafer B.W., Bajpai P. Stability degradation and redundancy in damaged structures // Engineering Structures. 2005. Vol. 27. Pp. 1642–1651. doi: 10.1016/j.engstruct.2005.05.012.
20. Mc Connell J.R., Brown H. Evaluation of progressive collapse alternate load path analyses in designing for blast resistance of steel columns // Engineering Structures. 2011. Vol. 33. Pp. 2899–2909. doi: 10.1016/j.engstruct.2011.06.014.
21. Szyniszewski S., Krauthammer T. Energy flow in progressive collapse of steel framed buildings // Engineering Structures. 2012. Vol. 42. Pp. 142–153. doi: 10.1016/j.engstruct.2012.04.014.
22. Gerasimidis S., Sideri J. A new partial-distributed damage method for progressive collapse analysis of steel frames // Journal of Constructional Steel Research. 2016. Vol. 119. Pp. 233–245. doi: 10.1016/j.jcsr.2015.12.012.
23. Gerasimidis S., Khorasani N. E., Garlock M., Pantidis P., Glassman J. Resilience of tall steel moment resisting frame buildings with multi-hazard post-event fire // Journal of Constructional Steel Research. 2017. Vol. 139. Pp. 202–219. doi: 10.1016/j.jcsr.2017.09.026.
24. Li L.-L., Li G.-Q., Jiang B., Lu Y. Analysis of robustness of steel frames against progressive collapse // Journal of

Doi: 10.1016/j.engstruct.2012.04.014.

22. Gerasimidis S., Sideri J. A new partial-distributed damage method for progressive collapse analysis of steel frames. *Journal of Constructional Steel Research.* 2016. Vol. 119. Pp. 233–245. Doi: 10.1016/j.jcsr.2015.12.012.
23. Gerasimidis S., Khorasani N.E., Garlock M., Pantidis P., Glassman J. Resilience of tall steel moment resisting frame buildings with multi-hazard post-event fire. *Journal of Constructional Steel Research.* 2017. Vol. 139. Pp. 202–219. Doi: 10.1016/j.jcsr.2017.09.026.
24. Li L.-L., Li G.-Q., Jiang B., Lu Y. Analysis of robustness of steel frames against progressive collapse. *Journal of Constructional Steel Research.* 2018. Vol. 143. Pp. 264–278. Doi: 10.1016/j.jcsr.2018.01.010.
25. Song B.I., Giriunas K.A., Sezen H. Progressive collapse testing and analysis of a steel frame building. *Journal of Constructional Steel Research.* 2014. Vol. 94. Pp. 76–83. Doi: 10.1016/j.jcsr.2013.11.002.
26. Indeykin I.A., Chizhov S.V., Shestakova E.B., Antonyuk A.A., Evtukov E.S., Kulagin K.N., Karpov V.V., Golitsynsky G.D. Dynamic stability of the lattice truss of the bridge taking into account local oscillations. *Magazine of Civil Engineering.* 2017. No. 8. Pp. 266–278. Doi: 10.18720/MCE.76.23.
27. Liu X., Tang Y., Lu Z., Huang H., Tong X., Ma J. ESMD-based stability analysis in the progressive collapse of a building model: A case study of a reinforced concrete frame-shear wall model. *Measurement.* 2018. Vol. 120. Pp. 34–42. Doi: 10.1016/j.measurement.2018.01.038.
28. Semenov A.A., Porivaev I.A., Kuznetcov D.V., Nguen T.H., Saitgalina A.S., Tregubova E.S. Stress-strain state of high-rise building under wind load and progressive collapse. *Construction of Unique Buildings and Structures.* 2017. No. 8(59). Pp. 7–26. Doi:10.18720/CUBS.59.1. (rus).
29. Bondarenko V.M., Kolchunov V.I. Kontseptsiya i napravleniya razvitiya teorii konstruktivnoy bezopasnosti zdaniy i sooruzheniy pri silovykh i sredovykh vozdeystviyakh [Concept and directions of development of the theory of structural safety of buildings and constructions at power and environmental influences]. *Promyshlennoye i grazhdanskoye stroitelstvo.* 2013. No. 2. Pp. 28–31 (rus).

Constructional Steel Research. 2018. Vol. 143. Pp. 264–278. doi: 10.1016/j.jcsr.2018.01.010.

25. Song B.I., Giriunas K.A., Sezen H. Progressive collapse testing and analysis of a steel frame building // Journal of Constructional Steel Research. 2014. Vol. 94. Pp. 76–83. doi: 10.1016/j.jcsr.2013.11.002.
26. Индейкин А.В., Чижов С.В., Шестакова Е.Б., Антонюк А.А., Евтюков С.А., Кулагин Н.И., Карпов В.В., Голицынский Д.М. Динамическая устойчивость решетчатой фермы моста с учетом местных колебаний // Инженерно-строительный журнал. 2017. № 8(76). С. 266–278. doi: 10.18720/MCE.76.23.
27. Liu X., Tang Y., Lu Z., Huang H., Tong X., Ma J. ESMD-based stability analysis in the progressive collapse of a building model: A case study of a reinforced concrete frame-shear wall model // Measurement. 2018. Vol. 120. Pp. 34–42. Doi: 10.1016/j.measurement.2018.01.038
28. Семенов А.А., Порываев И.А., Кузнецов Д.В., Нгуен Т.Х., Саитгалина А.С., Трегубова Е.С., Напряженно-деформированное состояние высотного здания при ветровом воздействии и прогрессирующем обрушении // Строительство уникальных зданий и сооружений. 2017. № 8(59). С. 7–26. Doi:10.18720/CUBS.59.1.
29. Бондаренко В.М., Колчунов В.И. Концепция и направления развития теории конструктивной безопасности зданий и сооружений при силовых и средовых воздействиях // Промышленное и гражданское строительство. 2013. № 2. С. 28–31.

Vitaly Kolchunov,
+7(4712)22-24-61; asiorel@mail.ru

Sergey Savin,*
+7(920)812-59-09; suwin@yandex.ru

Виталий Иванович Колчунов,
+7(4712)22-24-61; эл. почта: asiorel@mail.ru

Сергей Юрьевич Савин,*
+7(920)812-59-09; эл. почта: suwin@yandex.ru

doi: 10.18720/MCE.80.8

Cold-formed RHS T joints with initial geometrical imperfections

Сварные узлы холодногнутых труб прямоугольного сечения с начальными несовершенствами

M. Garifullin*,
Tampere University of Technology, Tampere, Finland
M.K. Bronzova,
Peter the Great St. Petersburg Polytechnic University, St. Petersburg, Russia
M. Heinisuo,
K. Mela,
S. Pajunen,
Tampere University of Technology, Tampere, Finland

Аспирант М.Р. Гарифуллин*,
Технологический университет Тампере, Тампере, Финляндия
студент М.К. Бронзова,
Санкт-Петербургский политехнический университет Петра Великого, г. Санкт-Петербург, Россия
д-р техн. наук, профессор М. Хейнисуо,
канд. техн. наук, старший научный сотрудник К. Мэла,
канд. техн. наук, доцент С. Паюнен,
Технологический университет Тампере, Тампере, Финляндия

Key words: hollow section joint; resistance; initial stiffness; finite element analysis; imperfection

Ключевые слова: трубный узел; прочность; начальная жесткость; метод конечных элементов; несовершенства

Abstract. Generally, numerical simulations of structures are carried out in such a way as to most accurately repeat their real behavior. The current rules for finite element modeling of tubular joints oblige scientists and engineers to construct their numerical models considering initial imperfections. However, not all joints are sensitive to initial imperfections. Often consideration of initial imperfections brings no reasonable improvements in the accuracy of results, but severely complicates numerical simulations. In such cases, the effect of geometrical imperfections can be effectively replaced by a simple theoretical equation or neglected entirely. This paper evaluates the effect of initial geometrical imperfections on the structural behavior of cold-formed rectangular hollow section T joints. Imperfections are simulated using the conventional approach for thin-walled structures, applying corresponding buckling modes to the perfect geometry. The paper analyzes several buckling modes and their combinations to identify the most rational technique for simulation of imperfections under in-plane bending and axial loading. Based on the obtained results, parametric studies are conducted to investigate the effect of initial imperfections on joints with various geometry and material properties. The results demonstrate that initial imperfections reduce the resistance and initial stiffness of joints. However, the observed effect has been found sufficiently small to be safely ignored in computational analyses.

Аннотация. Как правило, конечно-элементный анализ строительных конструкций проводится таким образом, чтобы максимально точно повторить их реальную работу. Современные требования к конечно-элементному анализу трубных узлов обязывают ученых и инженеров учитывать влияние начальных несовершенств. Однако, как показывает практика, не все узлы чувствительны к начальным несовершенствам. Часто учет несовершенств не позволяет получить более точные результаты, однако серьезно усложняет расчет конструкций. В таких случаях влияние несовершенств может быть учтено простой аналитической формулой или не учитываться вообще. Данная статья исследует влияние начальных геометрических несовершенств на несущую способность Т-образных узлов из труб прямоугольного сечения. Несовершенства моделируются при помощи традиционного для тонкостенных конструкций метода, когда соответствующая форма потери устойчивости узла прикладывается к его идеальной геометрии. Чтобы определить наиболее целесообразный подход к моделированию несовершенств для изгиба в плоскости узла и продольного сжатия, статья анализирует несколько форм потери устойчивости, а также их возможные комбинации. На основании полученных данных статья проводит параметрические исследования, чтобы определить влияние несовершенств на работу узлов с различной геометрией и свойствами стали. Результаты показали, что начальные несовершенства уменьшают несущую способность трубных узлов. Однако наблюдаемый

Гарифуллин М.Р., Бронзова М.К., Хейнисуо М., Мэла К., Паюнен С. Сварные узлы холодногнутых труб прямоугольного сечения с начальными несовершенствами // Инженерно-строительный журнал. 2018. № 4(80). С. 81–94.

негативный эффект достаточно мал и позволяет проводить расчет конструкций без учета влияния геометрических несовершенств.

1. Introduction

To provide most reliable results, numerical simulations are carried out in such a way as to most accurately repeat the real behavior of structures. Generally, the finite element analysis of tubular joints incorporates nonlinear large deflection theory for displacements, a nonlinear elastic-plastic material law as well as initial imperfections [1]. Initial imperfections include the deviations of geometry, imperfections in boundary conditions and residual stresses. Cold-formed tubular welded joints are generally influenced by initial geometrical imperfections, welding residual stresses and the residual stresses that occur from the cold-forming process.

The influence of welding residual stresses on structural behavior of rectangular hollow section joints was investigated in [2, 3] and was found negligible. Residual stresses in tubular joints obtained from cold-forming process were studied in [4–6]. However, very limited research is dedicated to studying initial geometrical imperfections in tubular joints. Most of the current papers conduct finite element analyses ignoring deviations in geometry of tubular members [7–10]. Although such an approach can be fully justified for members with very thick walls, it is not clear, whether or not the same can be assumed for tubes with relatively thin walls. These joints may behave similarly to thin-walled structures, which demonstrate considerable reduction of resistance due to imperfections in geometry [11, 12]. Moreover, the effect of initial imperfections might differ for the joints made of high strength steels, which are known to be particularly sensitive to any uncertainties. If the influence of initial imperfections is considerable, ignoring them in the design of tubular joints can lead to the overestimation of their load-bearing capacity, leading thus to unsafe results.

This paper investigates numerically the effect of initial geometrical imperfections on the resistance and initial stiffness of rectangular hollow section (RHS) T joints. A T joint represents the simplest joint configuration, when a brace is welded to a chord at an angle of 90°, as shown in Figure 1a. Section 2 develops the finite element (FE) model for RHS T joints and briefly describes its structural behavior under in-plane bending M_{ip} and axial brace loading N. The loading cases are demonstrated in Figure 1b. Initial imperfections are modelled by applying the scaled buckling modes to perfect geometry. Section 3.1 considers various buckling modes and their combinations by comparing the structural behavior of perfect and imperfect FE models. Finally, Section 3.2 provides parametric studies of RHS T joints with varying geometry and steel grades. The paper investigates only butt-welded joints, with no welding imperfections considered.

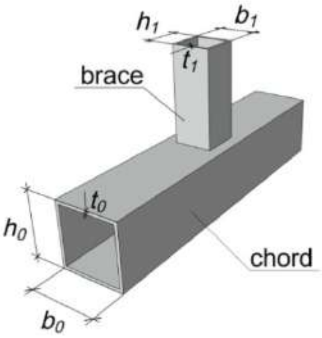

a)

b_0	Chord width
h_0	Chord height
t_0	Chord wall thickness
f_{y0}	Chord yield strength
b_1	Brace width
h_1	Brace height
t_1	Brace wall thickness
β	b_1/b_0 ratio
η	h_1/b_0 ratio
γ	$b_0/2t_0$ ratio

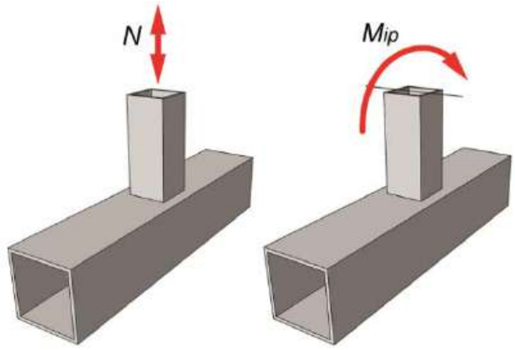

b)

Figure 1. RHS T joint: a) notations; b) loading cases

2. Methods

2.1. Development of FE model

The FE model for RHS T joints under in-plane bending was developed in [13]. This paper conducts numerical analyses employing the FE package Abaqus/Standard [14]. Cold-formed sections were modeled with round corners, according to EN 10219-2:2006 [15]. Residual stresses due to cold-forming were not considered. To exclude the possible effects of chord boundary conditions, its length was selected as $6b_0$, as recommended in [16], while the brace length was chosen as $4b_1$, as shown in Figure 2a. The wall thickness of the brace t_1 was chosen so that it did not exceed the thickness of the chord t_0. Following the recommendations of [17], the sections were modelled using solid quadratic finite elements with reduced integration (C3D20R), with two elements in the thickness direction. To capture large stress gradients, the mesh was refined near the connection area.

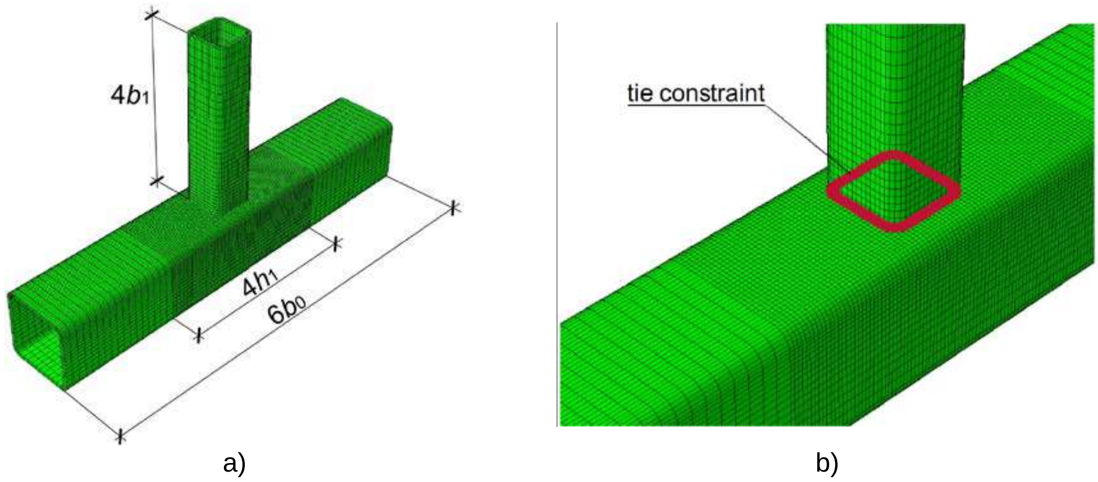

Figure 2. FE model: a) meshing; b) welds modeling

The joints were modelled with butt welds, considering them as the continuation of the brace parent material. The connection was simulated using the tie constraint [14], which ties two separate surfaces together with no relative motion between, as shown in Figure 2b. This approach allows using individual meshes for the connected members with no direct matching of their nodes [18]. All calculations employed the elastic-plastic material model with linear strain hardening according to EN 1993-1-5:2006 [19], with the Young's modulus of E = 210 GPa and the Poisson's ratio of v = 0.3, as shown in Figure 3a.

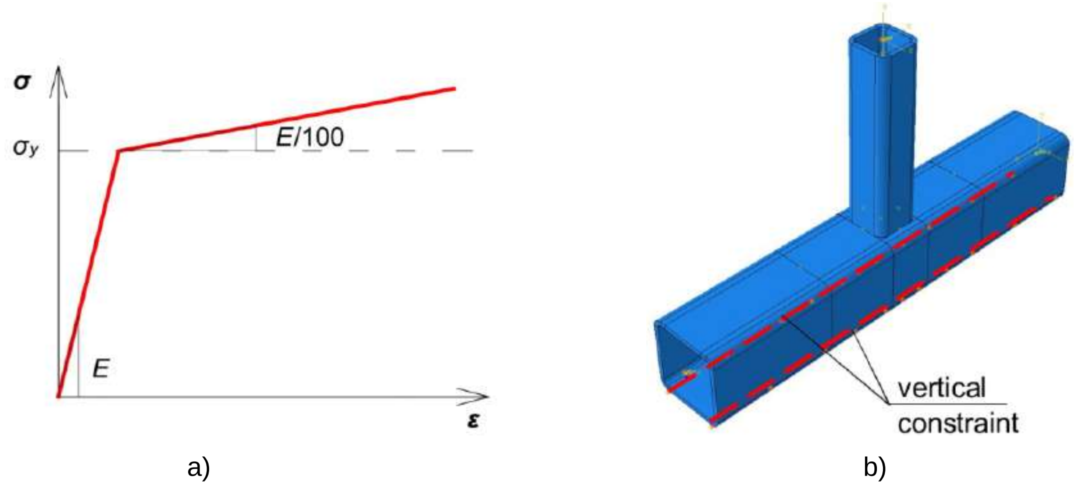

Figure 3. a) Material model; b) boundary conditions to prevent bending of the chord

Loading was performed using a force-controlled nonlinear static analysis. The load was applied to the end of the brace by a concentrated in-plane moment M or an axial force N. In case of axial brace loading, the axial force N causes in-plane bending of the chord, producing additional normal stresses on its faces. These stresses affect the structural behavior of tubular joints, reducing their resistance and initial stiffness [20]. To eliminate this effect, the bottom flange of the chord was restrained along the whole length against vertical displacements, as shown in Figure 3b.

2.2. Modeling imperfections

Currently, there are two main approaches for the implementation of geometrical imperfections to the perfect model. The first method represents measuring the real imperfections of members using non-contact 3D deformation scanners [21, 22]. The measured imperfections are then added to the FE model. Such a method provides a very realistic distribution of imperfections along the surface of members but is very time-consuming and is not widely used due to the high price of the measuring equipment.

The second approach is described in Appendix C.5 of EN 1993-1-5:2006 [19] and it represents the simulation of equivalent imperfections. On the first step, a linear buckling analysis is performed. The obtained buckling modes are then scaled and implemented to a model with perfect geometry. The direction of the applied imperfections should be such that the lowest resistance is obtained. Although the resulting distribution of imperfections in this case represents a rather simplified pattern, this straightforward method is widely used, particularly for thin-walled structures [23, 24]. This approach is employed in the present study in all FE analyses. According to EN 1993-1-8:2005 [25], the most typical failure modes for RHS T joints are chord face bending for $\beta \leq 0.85$ and chord side walls failure for $0.85 < \beta \leq 1.0$. This means that local deformations in RHS T joints are generally located in the chord. Therefore, this paper considers geometrical imperfections only in relation to the chord member.

When imperfections are applied based on a linear buckling analysis, attention should be paid on two issues. The first one concerns the shape and the amplitude of imperfections. To apply imperfections in the most unfavorable way, their shape should possibly repeat the deformation pattern of the joint under the corresponding load. Figure 4a shows the typical deformation pattern of the RHS T joint under an axial brace loading. In this case, imperfections can be applied as the concavity of the chord top face x_1 and the convexity of its web x_2. The deformation of the RHS T joint under in-plane bending can be considered as a combination of a compressed and a tensile part. In this case, geometrical imperfections can be applied similarly using the corresponding buckling modes.

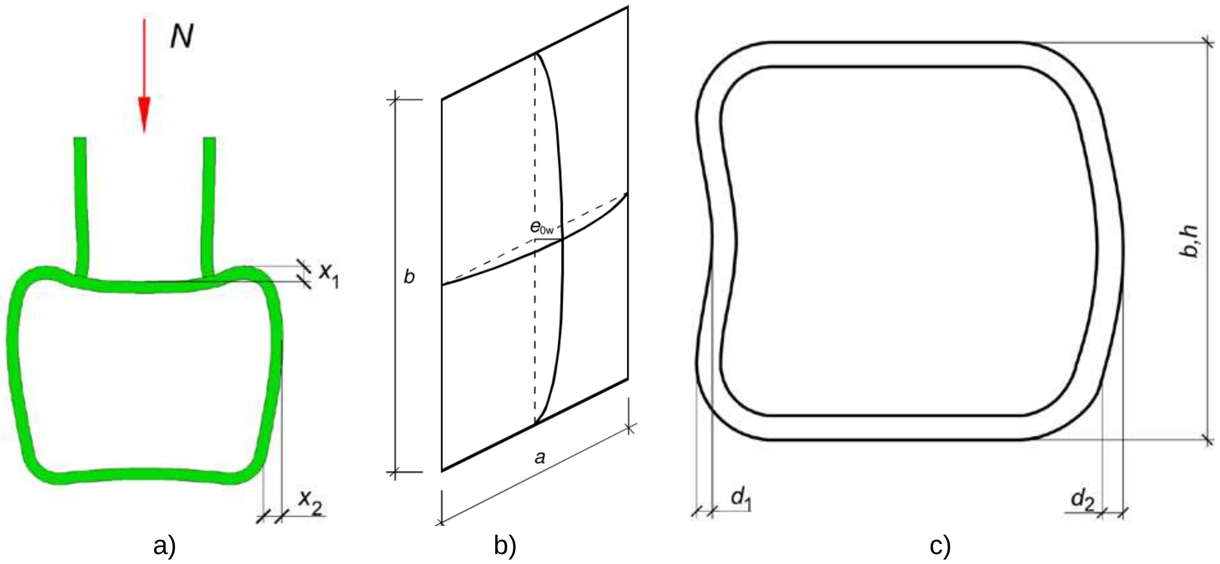

Figure 4. a) Deformation shape of RHS T joint under axial brace loading; b) limitations provided in EN 1993-1-5:2006 [19]; c) limitations provided in EN 10219-2:2006

According to [4], maximum measured imperfections can be conservatively used to predict lower bound strength in the FE analysis. The required magnitudes of imperfections can be found in Eurocode. Appendix C.5 of EN 1993-1-5:2006 [19] specifies local imperfections equal to $e_w = a/200$ or $b/200$, as shown in Figure 4b. In relation to a RHS chord, these values respectively correspond to $b_0/200$ and $h_0/200$. The same amplitudes are used in many publications [26, 27]. Another value can be found in EN 10219-2:2006 [15], which limits the concavity and convexity of cold-formed RHS tubes by 0.8 % with a minimum of 0.5 mm, see d_1 and d_2 in Figure 4c. This corresponds to the values of $b_0/125$ and $h_0/125$. The same limit can be found in [28]. Experimental measurements of the imperfections on hollow sections [5, 29, 30] demonstrate that real imperfections generally do not exceed these amplitudes. This paper employs the values of $b_0/125$ and $h_0/125$, as the most conservative limitations.

The second issue of this approach relates to the combination rules for buckling modes, i.e. the number of buckling modes to be applied and their corresponding scaling factors. Generally, the deformation pattern of the joint is governed by the first buckling mode [4]. However, if the difference between the first and subsequent eigenvalues is small, some subsequent buckling modes can also contribute to the overall deformation. To take into account several buckling modes, a combination rule for their imperfections should be considered. Appendix C of EN 1993-1-5:2006 [19] states that any buckling mode can be taken as the leading imperfection, and the accompanying modes may have their values reduced to 70 %. This leads to the following combination rule:

$$e_0 = e_1 + 0.7\left(e_2 + e_3 + \ldots + e_n\right), \tag{1}$$

where e_0 is the total amplitude, e_n is the amplitude from buckling mode n, n is the amount of considered buckling modes. It should be noted that the summation should be conducted very thoroughly, paying attention to the shape of buckling modes. Eq. (1) considers the amplitudes at some particular point of interest. This paper considers the imperfections of the chord; therefore, Eq. (1) regulates the convexity of the chord side walls, denoted as x_2 in Figure 4a. Therefore, it should include only those modes that have the maximum (or at least considerable) deformation in the chord side walls. The direction of imperfections is also important: if negative buckling modes are included Eq. (1), they have to be multiplied by negative scaling factors to be applied in the proper direction.

2.3. Structural behavior of RHS T joints

The local beam model for semi-rigid tubular T joints has been developed in [31]. The models under in-plane bending moment and axial brace loading are depicted in Figure 5, where $S_{j,ini}$ and $C_{j,ini}$ denote initial rotational and axial stiffnesses, which are modelled by rotational and linear springs, respectively. It should be noted that the springs are located at the upper flange of the chord and they are connected to the chord axis by a rigid beam.

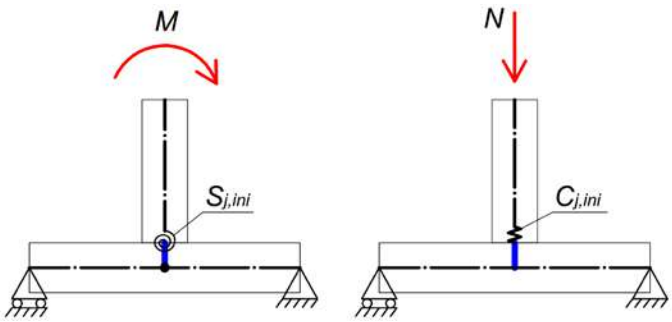

Figure 5. Design local models for RHS T joint: a) in-plane bending; b) axial brace loading

Generally, displacements and rotations measured in a FE analysis reflect the global behavior of the joint, including deformations of the chord and the brace, as well as the local deformations of the joint. The latter represents the deformations at the connection area, where the brace and the chord meet. In particular, to obtain the local rotation of the joint φ in case of in-plane bending, the rotation of the brace φ_{br} and the rotation of the chord φ_{ch} are subtracted from the measured rotation in the end of the brace φ_{tot} (Figure 6):

$$\varphi = \varphi_{tot} - \varphi_{br} - \varphi_{ch} \tag{2}$$

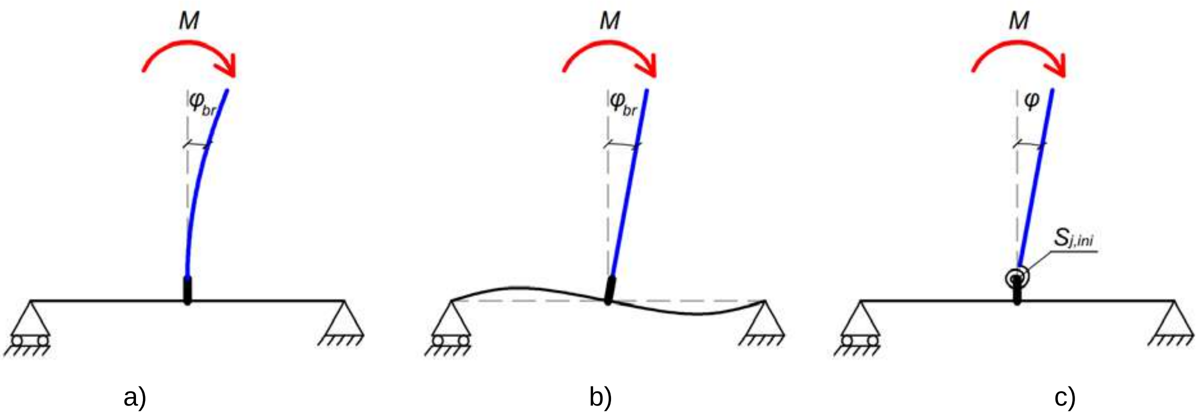

Figure 6. Behavior under in-plane bending: a) elastic rotation of the brace; b) elastic rotation of the chord; c) local rotation of the joint

To obtain local displacements in case of axial loading, the displacement in the end of the brace δ_{tot} is reduced by the brace shortening δ_{sh}:

$$\delta = \delta_{tot} - \delta_{sh} . \quad (3)$$

The motions of the members are supposed to be elastic (assuming that plastic deformations occur only in the connection area); therefore, the values φ_{br}, φ_{ch}, and δ_{sh} are calculated manually using the well-known beam equations from strength of materials:

$$\varphi_{br} = \frac{Ml_1}{EI_1}; \quad \varphi_{ch} = \frac{Ml_0}{12EI_0}; \quad \delta_{sh} = \frac{Nl_1}{EA_1} \quad (4)$$

where l_0 and l_1 are respectively the lengths of the chord and the brace, I_0 and I_1 are respectively the second moments of area of the chord and the brace, A_1 is the cross-sectional area of the brace, E is the Young's modulus.

The structural behavior of tubular joints demonstrates certain similarities in case of in-plane bending and axial brace loading and it is best described by corresponding load-deformation curves. The initial stiffness and resistance of joints are found graphically, using a manual curve-fitting approach. To evaluate the deformation capacity of joints, the 3%b_0 deformation limit is calculated in accordance with [32]. Following this rule, for a joint loaded by an axial brace force, the deformation limit δ_{lim} is found as

$$\delta_{\lim} = 0.03b_0 \quad (5)$$

Similarly, for a joint loaded by an in-plane moment the deformation limit $\varphi_{\lim}$ is

$$\varphi_{\lim} = \frac{0.03b_0}{h_1/2} = \frac{0.06}{\eta} \quad (6)$$

Initial stiffness $S_{j,ini}$ ($C_{j,ini}$) is found as the tangent line in the elastic phase of the curve, as shown in Figure 7. The resistance of joints is determined depending on their brace-to-chord width ratio β [33]. For the joints with $\beta \le 0.85$, bending of the chord top face governs the deformation of the whole joint, and the load-deformation curve has a clearly observed hardening phase, as shown in Figure 7. In this case, plastic resistance M_{pl} (N_{pl}) is determined as the intersection of two tangent lines corresponding to initial stiffness $S_{j,ini}$ ($C_{j,ini}$) and hardening stiffness $S_{j,h}$ ($C_{j,h}$), as demonstrated in [34]. Ultimate resistance M_u (N_u) in this case usually corresponds to very large deformations, considerably exceeding the deformation limit; therefore, it is not considered in this paper.

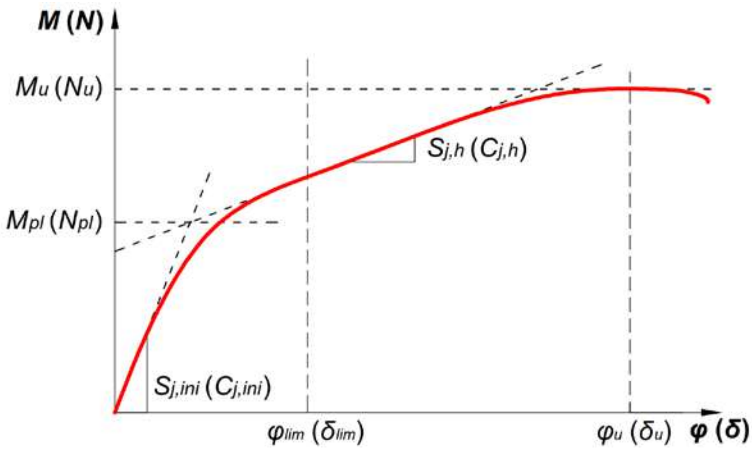

Figure 7. Load-deformation curve for T joint with $\beta \le 0.85$

The behavior of joints with $0.85 < \beta \le 1.0$ is generally governed by chord side walls buckling. Instead of a well-developed hardening phase, the action-deformation curves of such joints have a clear peak load M_{max} (N_{max}). The resistance of such joints depends on the correlation between this peak load and the 3%b_0 deformation limit [35]. If a joint has a peak load M_{max} (N_{max}) at a deformation smaller than φ_{lim} (δ_{lim}), the peak load is considered to be the resistance of the joint, as shown in Figure 8a. If a joint has a peak load M_{max} (N_{max}) at a deformation larger than φ_{lim} (δ_{lim}), resistance is determined as equal to the load at the deformation limit, as shown in Figure 8b.

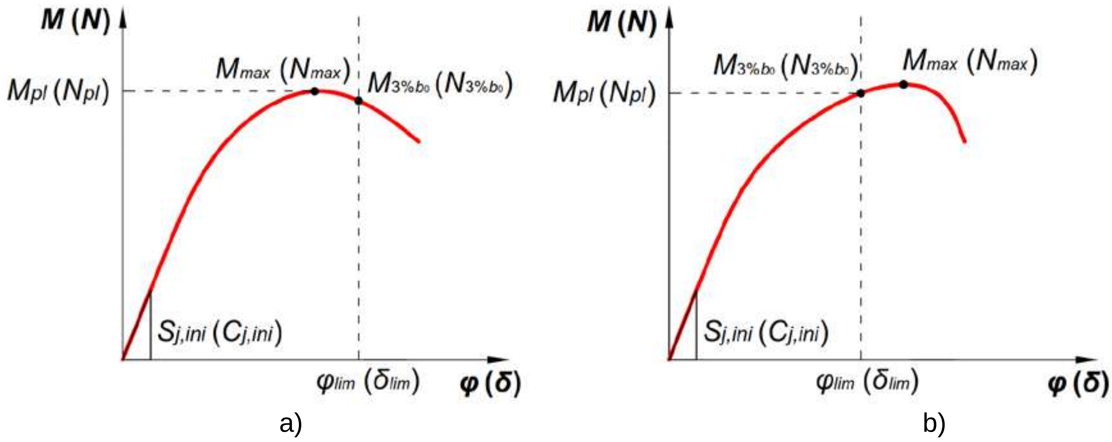

Figure 8. Load-deformation curves for T joint with 0.85 < β ≤ 1.0

3. Results and Discussion

3.1. Influence of initial imperfections on structural behavior of joints

This section investigates the effect of initial geometric imperfections on the structural behavior of RHS T joints under two loading cases: an axial load and an in-plane bending moment. Attention is paid particularly on the buckling modes and their possible combinations that can be used to the proper modeling of imperfections. All analyses were conducted on a single joint with a 100 x 100 x 6 mm chord and a 60 x 60 x 6 mm brace (β = 0.6), made of S355 steel grade.

On the first step, a linear buckling analysis was conducted for the case of in-plane bending and axial brace loading to obtain desired buckling modes. Figure 9 presents the first 10 buckling modes for the case of in-plane bending. As can be seen, Modes 3–10 represent local buckling of the brace and they cannot be applied to simulate chord imperfections. Modes 1 and 2 most closely correspond to the deformation pattern under the moment loading; however, major displacements are observed in the end of the brace, but not in the chord web. For this reason, buckling modes obtained from in-plane bending were found inapplicable for the simulation of imperfections for the considered joint.

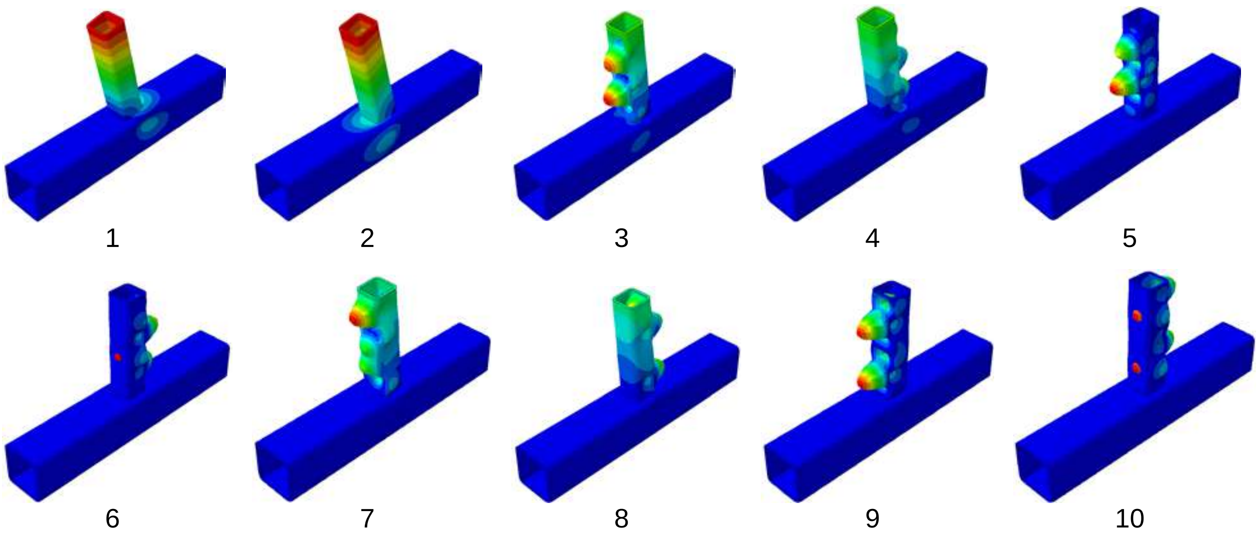

Figure 9. Buckling modes, in-plane bending

The buckling modes for axial loading are provided in Figure 10. A negative Mode 1 represents a buckling mode closest to the real deformation pattern of the joint under an axial load (compare with Figure 4a). Modes 4 and 9 correspond to the lateral buckling of the chord and cannot be used to simulate local imperfections of the cross-section. Modes 5 and 10 are located in the brace. Modes 7 and 8 are similar to Modes 1 and 6, respectively. Mode 3 represents the buckling of the chord side walls in opposite direction, i.e. inwards the tube. Based on these observations, Modes 1, 2 and 6 were selected as the most reliable for the simulation of imperfections, both in the case of in-plane bending and axial loading.

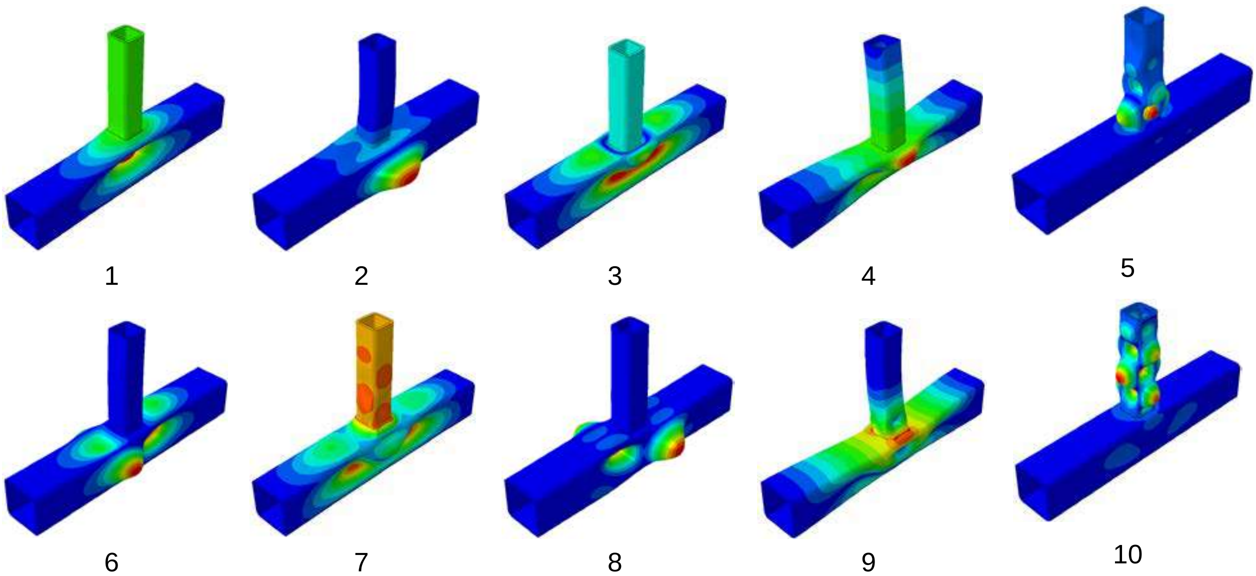

Figure 10. Buckling modes, axial loading

On the second step, a nonlinear static analysis was conducted for the joint separately under in-plane bending and axial loading. The analyses were conducted with and without imperfections. Imperfections were simulated using Modes 1, 2 and 6 for both loading cases. Each buckling mode was first applied independently and then in a combination with others. The combination was introduced according to Eq. (1), employing the following equation:

$$e_0 = e_1 + 0.7e_2 + 0.7e_6 \tag{7}$$

The scaling factors for the buckling modes were selected such that the total convexity on the web e_0 was equal to the assumed limitation of $h_0/125$ = 0.8 mm. Being negative, Mode 1 was applied in the opposite direction. The outcome of the numerical analyses included the plastic resistance and initial stiffness of the analyzed joints. The results are presented in Table 1, where “Imperfect-N” relates to the model with imperfections obtained from a buckling mode *N*. “Imperfect-C” corresponds to the model with imperfections obtained from the combination of buckling modes, Eq. (7). The results are presented in absolute values and in relation to “Perfect” model.

Table 1. Structural behavior of joints with various imperfections

	M_{pl} [kNm]		$S_{j,ini}$ [kNm/rad]		N_{pl} [kN]		$C_{j,ini}$ [kN/mm]	
Perfect	3.15	1	262.0	1	121.9	1	219.9	1
Imperfect-1	3.12	0.99	256.9	0.98	120.1	0.98	210.4	0.96
Imperfect-2	3.15	1.00	262.0	1.00	121.9	1.00	220.0	1.00
Imperfect-6	3.15	1.00	262.1	1.00	122.9	1.01	220.0	1.00
Imperfect-C	3.13	1.00	259.0	0.99	120.8	0.99	214.3	0.97

As can be seen, the influence of initial geometric imperfections on the structural behavior is negligibly small. The reduction of resistance does not exceed 1 % for moment load and 2 % for axial load. For initial stiffness, the values account for 2 % and 4 % respectively. For both loading cases, the most conservative results are observed employing buckling Mode 1, i.e. the mode that as close as possible corresponds to the deformation pattern of the joint under an axial brace loading. This buckling mode can be considered further as the bounding buckling mode. Although in this section it corresponded to the first computed buckling mode, its number can be different for other joints.

3.2. Parametric studies for joints with various geometry and steel grades

This section evaluates the effect of geometric imperfections on the structural behavior of RHS T joints with varying geometries and steel grades. The variations of geometry are considered in relation to chord wall thickness and the width of the brace. As in Section 3.1, firstly a linear buckling analysis was conducted for every joint, followed by a nonlinear static analysis. Initial imperfections were simulated using the bounding buckling mode that maximally repeats the deformation of the joint under an axial load. The results are evaluated in relation to resistance and initial stiffness, separately under moment and axial loading.

3.2.1. Joints with various steel grade

Consider firstly the effect of steel grade on the behavior of the joint. The analyses were conducted on the same joint as was used in Section 3.1. In addition to S355, the study considered steel grades S500 and S700, employing similar bi-linear material models. The results are presented in Figure 11 and Table 2, where indices *p* and *i* relate to perfect and imperfect models, respectively. As can be seen, the small influence of initial imperfections remains also for higher steel grades. Similarly, imperfections reduce plastic moment and axial resistance by 1 % and 2 % respectively. Initial rotational and axial stiffness is reduced by 2 % and 4 % respectively.

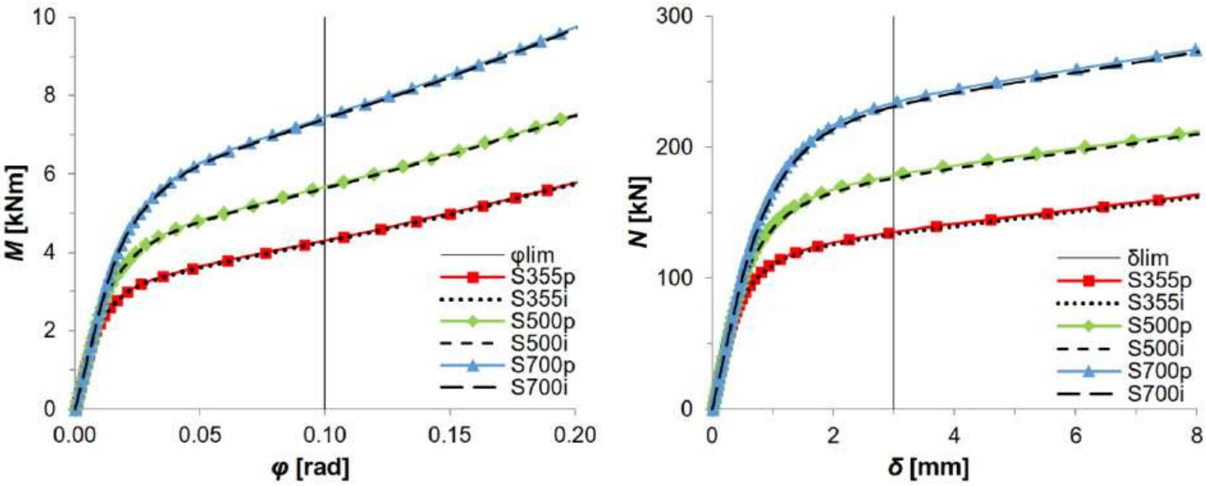

Figure 11. Influence of initial imperfections on joints with various steel grades

Table 2. Influence of initial imperfections for joints with various steel grades

Steel grade	S355p	S355i	S355i/ S355p	S500p	S500i	S500i/ S500p	S700p	S700i	S700i/ S700p
M_{pl} [kNm]	3.15	3.12	0.99	4.26	4.23	0.99	5.73	5.69	0.99
$S_{j,ini}$ [kNm/rad]	262.0	256.9	0.98	262.0	256.9	0.98	262.0	256.9	0.98
N_{pl} [kN]	121.9	120.1	0.98	165.4	162.6	0.98	221.7	218.2	0.98
$C_{j,ini}$ [kN/mm]	219.9	210.4	0.96	219.9	210.4	0.96	219.9	210.4	0.96

3.2.2. Joints with various chord wall thickness

The next parametric study investigates the effect of initial geometric imperfections on the behavior of joints with varying chord wall thickness. Generally, this thickness is characterized by the chord width-to-thickness ratio $\gamma = b_0/2t_0$, which for simplicity is often considered as $2\gamma = b_0/t_0$. Chapter 7 of EN 1993-1-8:2005 [25] limits 2γ in the range of $10 \leq 2\gamma \leq 35$. Initial geometrical imperfections are known to considerably reduce the resistance of thin-walled members [4]. For this reason, a more pronounced effect can be expected for the joints with 2γ close to its upper limit.

Section 3.1 evaluated the joint with $2\gamma = 100/6 = 16.6$, which is close to the lower bound of γ. In the following, two additional chord thicknesses are considered: $2\gamma = 25.0$ ($t_0 = 4$ mm) and $2\gamma = 33.3$ ($t_0 = 3$ mm). The thickness of the brace was selected as equal to the thickness of the chord. The results are presented graphically in Figure 12 and collected in Table 3, where indices *p* and *i* relate to perfect and imperfect models, respectively. As can be seen, the effect of initial imperfections is more pronounced for joints with thinner walls, reducing their moment and axial resistance by 3 % for $2\gamma = 33.3$. A more pronounced infunence is observed for initial stiffness: rotational stiffness is reduced by 4 %, while axial stiffness is reduced by 6 %.

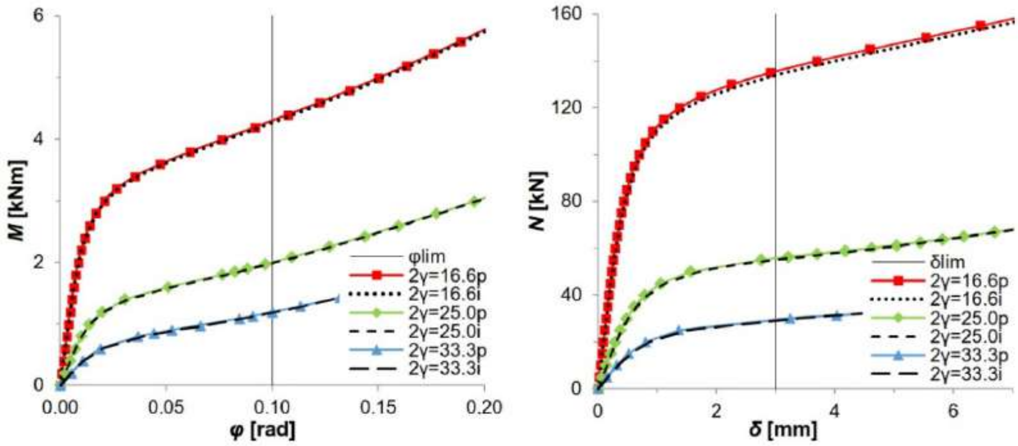

Figure 12. Influence of initial imperfections on joints with various chord wall thickness

Table 3. Influence of initial imperfections for joints with various chord wall thickness

2γ	16.6p	16.6i	16.6i/ 16.6p	25.0p	25.0i	25.0i/ 25.0p	33.3p	33.3i	33.3i/ 33.3p
M_{pl} [kNm]	3.15	3.12	0.99	1.29	1.27	0.98	0.67	0.65	0.97
$S_{j,ini}$ [kNm/rad]	262.0	256.9	0.98	86.4	84.1	0.97	39.6	38.1	0.96
N_{pl} [kN]	121.9	120.1	0.98	48.8	47.9	0.98	25.0	24.3	0.97
$C_{j,ini}$ [kN/mm]	219.9	210.4	0.96	70.9	67.6	0.95	31.9	30.1	0.94

3.3. Joints with various brace width

The third and the last parametric study evaluates the influence of initial imperfections of joints with different brace widths. Generally, the brace width is represented by the brace-to-chord width ratio β. EN 1993-1-8:2005 [25] limits β for RHS T joints in the range of $0.25 \le \beta \le 1.0$. All previous analyses considered the joints with $\beta = 0.6$ and demonstrated a negligibly small effect of initial imperfections. Although this finding can be justified for the joints that fail from chord face bending, the results can differ for the joints with other failure modes, e.g. chord side walls buckling, which is critical when $0.85 < \beta \le 1.0$.

Consider the structural behavior of equal-width joints ($\beta = 1.0$). The analyses were conducted for a joint with a 100x100 chord and a 100x100 brace, made of S355, with three chord wall thicknesses: $2\gamma = 16.6$ ($t_0 = 6$ mm), $2\gamma = 25.0$ ($t_0 = 4$ mm) and $2\gamma = 33.3$ ($t_0 = 3$ mm). The wall thickness of the brace was selected as equal to the wall thickness of the chord. The resistance of the joints was determined according to Figure 8. The structural behavior of the joints is illustrated in Figure 13 and summarized in Table 4, where indices *p* and *i* relate to perfect and imperfect models, respectively. As can be seen, the negative influence of initial imperfections observed for joints with $\beta = 0.6$ remains also for equal-width joints. Similarly, the effect is more pronounced for the joints with thinner walls, reducing their moment and axial resistance by 2% and 5% respectively for $2\gamma = 33.3$. In relation to initial stiffness, the reducing effect does not exceed 7%. It should be noted that the effect is more pronounced for axial loading than for in-plane bending.

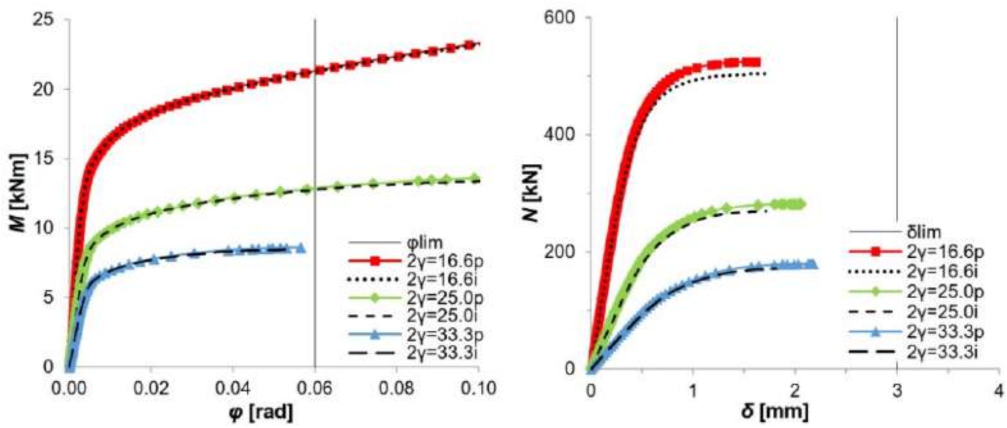

Figure 13. Influence of initial imperfections on joints with β = 1.0

Table 4. Influence of initial imperfections on joints with β = 1.0

2γ	16.6p	16.6i	16.6i/ 16.6p	25.0p	25.0i	25.0i/ 25.0p	33.3p	33.3i	33.3i/ 33.3p
M_{pl} [kNm]	21.34	21.29	1.00	12.85	12.77	0.99	8.61	8.44	0.98
$S_{j,ini}$ [kNm/rad]	4281	4237	0.99	2332	2295	0.98	1578	1538	0.97
N_{pl} [kN]	525.3	503.7	0.96	282.0	269.3	0.95	179.9	171.2	0.95
$C_{j,ini}$ [kN/mm]	1181	1102	0.93	429	403	0.94	213	201	0.94

3.4. Discussion

In this paper, geometrical imperfections were modelled applying scaled buckling modes to the perfect geometry. Buckling modes were obtained from linear buckling analyses for the corresponding loading type. The comparative buckling analyses under axial loading have showed that the first buckling mode most closely corresponds to the deformation pattern of T joints, being thus the most desirable for the simulation of initial imperfections. The consideration of higher buckling modes as well as their possible combinations brought no noticeable changes in further results and therefore was found unnecessary. At the same time, all buckling modes resulted from in-plane bending loading were located in the brace and therefore could not be employed to simulate local deformations of the chord walls. For this reason, imperfections for both loading cases were modelled using the first buckling mode obtained from axial loading. This resulted to the fact that the observed influence of imperfections was less pronounced for in-plane bending than for axial loading. In all cases studied in this paper, the first buckling mode was negative and was multiplied by a negative scaling factor to be applied in the proper direction.

The conducted parametric studies have demonstrated a small negative influence of initial imperfections on both design resistance and initial stiffness of the investigated joints. The effect was observed for the joints governed by chord face bending ($\beta \leq 0.85$) as well as the joints with chord side walls buckling as the dominating failure mode ($\beta > 0.85$). The structural properties were found to decrease for the joints with thinner walls, particularly those with 2γ ratio close to its upper limit specified by the Eurocode ($2\gamma = 35$). For the joints beyond this limit ($2\gamma > 35$), the effect is expected to be more pronounced, making these joints behave similar to thin-walled sections. At the same time, the negative effect of imperfections showed no correlation with steel grade in the considered range from S355 to S700.

The maximum observed reduction of resistance accounted 3 % and 5 % for in-plane bending moment and axial loading respectively. In practice, these reductions are taken into account by partial safety factors and thus do not have to be considered in theoretical calculations. At the same time, initial imperfections reduce initial rotational stiffness by 4 % and initial axial stiffness by 7 %. Since the accuracy requirements for initial stiffness are not as strict as for resistance, these small reductions of stiffness are acceptable and can be ignored in the design. It should be noted that in this paper imperfections were modelled rather conservatively, using the maximum allowed value of $h_0/125$. The experimental measurements of on RHS tubes [5, 29, 30] demonstrate that real imperfections are generally smaller than this amplitude. Moreover, imperfections were applied in the most unfavorable way, i.e. providing the most unsafe behavior. In real members, the distribution of imperfections is more random. These findings allow to conclude that initial geometrical imperfections do not seriously affect the structural behavior of RHS T joints in the range defined by the regulations of the Eurocode.

4. Conclusions

This paper analyzed the effect of initial geometric imperfections on the structural behavior of tubular joints. In this study, initial geometrical imperfections were simulated using the conventional approach for thin-walled sections, applying corresponding buckling modes scaled in accordance with allowable fabrication tolerances. The comparative FE analyses for RHS joints with perfect and imperfect geometry have showed that the effect of initial geometric imperfections on the strength of joints is smaller than that observed for thin-walled cold-formed structures. For this reason, geometrical imperfections can be neglected in the design of RHS T joints with no serious consequences on their design results.

The presented results can serve as a starting point for studying the issue of initial imperfections in relation to welded tubular joints. This paper considered the joints that follow the requirements of Eurocode, i.e. $0.25 \leq \beta \leq 1.0$, $10 \leq 2\gamma \leq 35$, steel grades from S355 to S700, under in-plane bending and axial loading. For joints with $\beta \leq 0.85$, chord face bending governs the deformation of the joint under all loading cases; therefore, the obtained conclusions can be extended also for the case of out-of-plane bending. Some comparative numerical analyses can be conducted to eliminate a possible scaling effect, considering joints with different sections of the chord. Moreover, some calculations can be useful to extend the conclusions for other welded connections, including K and X joints, as well as circular hollow section joints. In addition, particularly important results can be obtained considering geometrical imperfections in welds, i.e., the deviations of fillet welds from their nominal dimensions.

References

1. *European Committee for Standardization (CEN). Eurocode 3.* Design of steel structures. Part 1-6: Strength and Stability of Shell Structures (EN 1993-1-6:2007). Brussels, 2007.
2. Brar G.S., Singh C.S. FEA of residual stress in cruciform welded joint of hollow sectional tubes. *Journal of Constructional Steel Research.* 2014. Vol. 102. Pp. 44–58.
3. Moradi Eshkafti M. *Influence of various welding sequence schemes on the load bearing capacity of square hollow section T-joint.* PhD thesis. Cottbus: Brandenburg University of Technology, 2017.
4. Dubina D., Ungureanu V., Landolfo R. *Design of Cold-formed Steel Structures: Eurocode 3: Design of Steel Structures, Part 1-3: Design of Cold-formed Steel Structures* . ECCS, 2012.
5. Jiao H., Zhao X.-L. Imperfection, residual stress and yield slenderness limit of very high strength (VHS) circular steel tubes. *Journal of Constructional Steel Research.* 2003. Vol. 59. No. 2. Pp. 233–249.
6. Feldmann M., Schillo N., Schaffrath S., Virdi K., Björk T., Tuominen N., Veljkovic M., Pavlovic M., Manoleas P., Heinisuo M., Mela K., Ongelin P., Valkonen I., Minkkinen J., Erkkilä J., Pétursson E., Clarin M., Seyr A., Horváth L., Kövesdi B., Turán P., Somodi B. *Rules on high strength steel.* Luxembourg: Publications Office of the European Union, 2016.
7. Pavlenko A.D., Rybakov V.A., Pikht A.V., Mikhailov E.S. Non-uniform torsion of thin-walled open-section multi-span beams. *Magazine of Civil Engineering.* 2016. Vol. 67, No. 7. Pp. 55–69.
8. de Matos R.M.M.P., Costa-Neves L.F., de Lima L.R.O., Vellasco P.C.G.S., da Silva J.G.S. Resistance and elastic stiffness of RHS “T” joints: Part I - Axial brace loading. *Latin American Journal of Solids and Structures.* 2015. Vol. 12. No. 11. Pp. 2159–2179.
9. Christitsas A.D., Pachoumis D.T., Kalfas C.N., Galoussis E.G. FEM analysis of conventional and square bird-beak SHS joint subject to in-plane bending moment — experimental study. *Journal of Constructional Steel Research.* 2007. Vol. 63. No. 10. Pp. 1361–1372.
10. Tusnina O.A., Danilov A.I. The stiffness of rigid joints of beam with hollow section column. *Magazine of Civil Engineering.* 2016. Vol. 64. No. 4. Pp. 40–51.
11. Nazmeeva T.V., Vatin N.I. Numerical investigations of notched C-profile compressed members with initial imperfections. Magazine of Civil Engineering. 2016. Vol. 62. No. 2. Pp. 92–101.
12. Zeinoddini V., Schafer B.W. Global Imperfections And Dimensional Variations In Cold-Formed Steel Members. *International Journal of Structural Stability and Dynamics*. 2011. Vol. 11. No. 5. Pp. 829–854.
13. Garifullin M., Pajunen S., Mela K., Heinisuo M., Havula J. Initial in-plane rotational stiffness of welded RHS T joints with axial force in main member. *Journal of Constructional Steel Research.* 2017. Vol. 139. Pp. 353–362.
14. *Abaqus 6.12.* Getting Started with Abaqus: Interactive Edition . Dassault Systèmes, 695 p., 2012.
15. *European Committee for Standardization (CEN). Cold formed welded structural hollow sections of non-alloy and fine grain steels.* Part 2: Tolerances, dimensions and sectional properties (EN 10219-2:2006). Brussels, 2006.
16. van der Vegte G.J., Makino Y. Further research on chord length and boundary conditions of CHS T- and X-joints. *Advanced Steel Construction.* 2010. Vol. 6. No. 3.

Литература

1. European Committee for Standardization (CEN). Eurocode 3. Design of steel structures. Part 1-6: Strength and Stability of Shell Structures (EN 1993-1-6:2007). Brussels, 2007.
2. Brar G.S., Singh C.S. FEA of residual stress in cruciform welded joint of hollow sectional tubes // Journal of Constructional Steel Research. 2014. Vol. 102. Pp. 44–58.
3. Moradi Eshkafti M. Influence of various welding sequence schemes on the load bearing capacity of square hollow section T-joint. PhD thesis . Cottbus: Brandenburg University of Technology, 2017.
4. Dubina D., Ungureanu V., Landolfo R. Design of Cold-formed Steel Structures: Eurocode 3: Design of Steel Structures, Part 1-3: Design of Cold-formed Steel Structures . ECCS, 2012.
5. Jiao H., Zhao X.-L. Imperfection, residual stress and yield slenderness limit of very high strength (VHS) circular steel tubes // Journal of Constructional Steel Research. 2003. Vol. 59. № 2. Pp. 233–249.
6. Feldmann M., Schillo N., Schaffrath S., Virdi K., Björk T., Tuominen N., Veljkovic M., Pavlovic M., Manoleas P., Heinisuo M., Mela K., Ongelin P., Valkonen I., Minkkinen J., Erkkilä J., Pétursson E., Clarin M., Seyr A., Horváth L., Kövesdi B., Turán P., Somodi B. Rules on high strength steel. Luxembourg: Publications Office of the European Union, 2016.
7. Павленко А.Д., Рыбаков В.А., Пихт А.В., Михайлов Е.С. Стесненное кручение многопролетных тонкостенных балок открытого профиля // Инженерно-строительный журнал. 2016. № 7(67). С. 55–69
8. de Matos R.M.M.P., Costa-Neves L.F., de Lima L.R.O., Vellasco P.C.G.S., da Silva J.G.S. Resistance and elastic stiffness of RHS “T” joints: Part I - Axial brace loading // Latin American Journal of Solids and Structures. 2015. Vol. 12. № 11. Pp. 2159–2179.
9. Christitsas A.D., Pachoumis D.T., Kalfas C.N., Galoussis E.G. FEM analysis of conventional and square bird-beak SHS joint subject to in-plane bending moment — experimental study // Journal of Constructional Steel Research. 2007. Vol. 63. № 10. Pp. 1361–1372.
10. Туснина О.А., Данилов А.И. Жесткость рамных узлов сопряжения ригеля с колонной коробчатого сечения // Инженерно-строительный журнал. 2016. № 4(64). С. 40–51.
11. Назмеева Т.В., Ватин Н.И. Численные исследования сжатых элементов из холодногнутого просечного С-профиля с учетом начальных несовершенств // Инженерно-строительный журнал. 2016. № 2(62). С. 92–101.
12. Zeinoddini V., Schafer B.W. Global Imperfections And Dimensional Variations In Cold-Formed Steel Members // International Journal of Structural Stability and Dynamics. 2011. Vol. 11. № 5. Pp. 829–854.
13. Garifullin M., Pajunen S., Mela K., Heinisuo M., Havula J. Initial in-plane rotational stiffness of welded RHS T joints with axial force in main member // Journal of Constructional Steel Research. 2017. Vol. 139. Pp. 353–362.
14. Abaqus 6.12. Getting Started with Abaqus: Interactive Edition . Dassault Systèmes, 695 p., 2012.
15. European Committee for Standardization (CEN). Cold formed welded structural hollow sections of non-alloy and fine grain steels. Part 2: Tolerances, dimensions and sectional properties (EN 10219-2:2006) . Brussels, 2006.
16. van der Vegte G.J., Makino Y. Further research on chord

Pp. 879–890.

17. van der Vegte G.J., Wardenier J., Puthli R.S. FE analysis for welded hollow-section joints and bolted joints. *Proceedings of the Institution of Civil Engineers — Structures and Buildings.* 2010. Vol. 163. No. SB6. Pp. 427–437.
18. AlHendi H., Celikag M. Behavior of reverse-channel and double-reverse-channel connections to tubular columns with HSS. *Journal of Constructional Steel Research*. 2015. Vol. 112. Pp. 271–281.
19. *European Committee for Standardization (CEN). Eurocode 3.* Design of steel structures. Part 1-5: Plated structural elements (EN 1993-1-5:2006). Brussels, 2006.
20. Packer J., Puthli R., van der Vegte G.J., Wardenier J. Discussion on the paper "Experimental and numerical assessment of RHS T-joints subjected to brace and chord axial forces", by Nizer et al., Steel Construction 9 (2016), No. 4, pages 315–322. *Steel Construction.* 2017. Vol. 10. No. 1. Pp. 89–90.
21. Tran A.T., Veljkovic M., Rebelo C., da Silva L.S. Resistance of cold-formed high strength steel circular and polygonal sections - Part 2: Numerical investigations. *Journal of Constructional Steel Research.* 2016. Vol. 125. Pp. 227–238.
22. Zhao X., Tootkaboni M., Schafer B.W. Laser-based cross-section measurement of cold-formed steel members: Model reconstruction and application. *Thin-Walled Structures.* 2017. Vol. 120. Pp. 70–80.
23. Schafer B.W., Peköz T. Computational modeling of cold-formed steel: characterizing geometric imperfections and residual stresses. *Journal of Constructional Steel Research.* 1998. Vol. 47. Pp. 193–210.
24. Rybakov V.A., Al Ali M., Panteleev A.P., Fedotova K.A., Smirnov A. V. Bearing capacity of rafter systems made of steel thin-walled structures in attic roofs. Magazine of Civil Engineering. 2017. Vol. 76. No. 8. Pp. 28–39.
25. *European Committee for Standardization (CEN). Eurocode 3.* Design of steel structures, Part 1–8: Design of joints (EN 1993-1-8:2005). Brussels, 2005.
26. Hoang V.L., Demonceau J.-F., Jaspart J.-P. Resistance of through-plate component in beam-to-column joints with circular hollow columns. *Journal of Constructional Steel Research.* 2014. Vol. 92. Pp. 79–89.
27. Pavlovčič L., Detzel A., Kuhlmann U., Beg D. Shear resistance of longitudinally stiffened panels-Part 1: Tests and numerical analysis of imperfections. *Journal of Constructional Steel Research.* 2007. Vol. 63. Pp. 337–350.
28. Ongelin P., Valkonen I. *SSAB Domex Tube. Structural hollow sections.* EN 1993 - Handbook 2016. SSAB Europe Oy, 2016.
29. Hayeck M., Nseir J., Saloumi E., Boissonnade N. Experimental characterization of steel tubular beam-columns resistance by means of the Overall Interaction Concept. *Thin-Walled Structures*. 2017. Vol. In press.
30. Ellobody E., Young B. Structural performance of cold-formed high strength stainless steel columns. *Journal of Constructional Steel Research.* 2005. Vol. 61. No. 12. Pp. 1631–1649.
31. Garifullin M., Pajunen S., Mela K., Heinisuo M. 3D component method for welded tubular T joints. *Tubular Structures XVI – Proceedings of the 16th International Symposium on Tubular Structures (ISTS 2017).* Melbourne, Australia, 2017 / ed. Heidarpour A., Zhao X.-L. London: Taylor & Francis Group, 2018. Pp. 165–173.
32. Lu L.H., de Winkel G.D., Yu Y., Wardenier J. Deformation limit for the ultimate strength of hollow section joints. *Tubular Structures VI. 6th International Symposium on Tubular Structures.* Melbourne, Australia / ed. Grundy P.,

length and boundary conditions of CHS T- and X-joints // Advanced Steel Construction. 2010. Vol. 6, No. 3. Pp. 879–890.

17. van der Vegte G.J., Wardenier J., Puthli R.S. FE analysis for welded hollow-section joints and bolted joints. Proceedings of the Institution of Civil Engineers — Structures and Buildings. 2010. Vol. 163, No. SB6. Pp. 427–437.
18. AlHendi H., Celikag M. Behavior of reverse-channel and double-reverse-channel connections to tubular columns with HSS. Journal of Constructional Steel Research. 2015. Vol. 112. Pp. 271–281.
19. European Committee for Standardization (CEN). Eurocode 3. Design of steel structures. Part 1-5: Plated structural elements (EN 1993-1-5:2006) . Brussels, 2006.
20. Packer J., Puthli R., van der Vegte G.J., Wardenier J. Discussion on the paper "Experimental and numerical assessment of RHS T-joints subjected to brace and chord axial forces", by Nizer et al. Steel Construction 9 (2016), No. 4, pages 315–322 // Steel Construction. 2017. Vol. 10, № 1. Pp. 89–90.
21. Tran A.T., Veljkovic M., Rebelo C., da Silva L.S. Resistance of cold-formed high strength steel circular and polygonal sections - Part 2: Numerical investigations // Journal of Constructional Steel Research. 2016. Vol. 125. Pp. 227–238.
22. Zhao X., Tootkaboni M., Schafer B.W. Laser-based cross-section measurement of cold-formed steel members: Model reconstruction and application // Thin-Walled Structures. 2017. Vol. 120. Pp. 70–80.
23. Schafer B.W., Peköz T. Computational modeling of cold-formed steel: characterizing geometric imperfections and residual stresses // Journal of Constructional Steel Research. 1998. Vol. 47. Pp. 193–210.
24. Рыбаков В.А., Ал Али М., Пантелеев А.П., Федотова К.А., Смирнов А.В. Несущая способность стропильных систем из стальных тонкостенных конструкций в чердачных крышах // Инженерно-строительный журнал. 2018. № 8(76). С. 28–39.
25. European Committee for Standardization (CEN). Eurocode 3. Design of steel structures, Part 1–8: Design of joints (EN 1993-1-8:2005) . Brussels, 2005.
26. Hoang V.L., Demonceau J.-F., Jaspart J.-P. Resistance of through-plate component in beam-to-column joints with circular hollow columns // Journal of Constructional Steel Research. 2014. Vol. 92. Pp. 79–89.
27. Pavlovčič L., Detzel A., Kuhlmann U., Beg D. Shear resistance of longitudinally stiffened panels-Part 1: Tests and numerical analysis of imperfections // Journal of Constructional Steel Research. 2007. Vol. 63. Pp. 337–350.
28. Ongelin P., Valkonen I. SSAB Domex Tube. Structural hollow sections. EN 1993 - Handbook 2016 . SSAB Europe Oy, 2016.
29. Hayeck M., Nseir J., Saloumi E., Boissonnade N. Experimental characterization of steel tubular beam-columns resistance by means of the Overall Interaction Concept // Thin-Walled Structures. 2017. Vol. In press.
30. Ellobody E., Young B. Structural performance of cold-formed high strength stainless steel columns // Journal of Constructional Steel Research. 2005. Vol. 61. № 12. Pp. 1631–1649.
31. Garifullin M., Pajunen S., Mela K., Heinisuo M. 3D component method for welded tubular T joints // Tubular Structures XVI – Proceedings of the 16th International Symposium on Tubular Structures (ISTS 2017). Melbourne, Australia, 2017 / ed. Heidarpour A., Zhao X.-L. London: Taylor & Francis Group, 2018. Pp. 165–173.
32. Lu L.H., de Winkel G.D., Yu Y., Wardenier J. Deformation

Holgate A., Wong B. Rotterdam: Balkema, 1994. Pp. 341–347.

33. Zhao X.-L., Hancock G.J. T-joints in rectangular hollow sections subject to combined actions. *Journal of Structural Engineering.* 1991. Vol. 117. No. 8. Pp. 2258–2277.
34. Grotmann D., Sedlacek G. *Rotational stiffness of welded RHS beam-to-column joints.* Cidect 5BB-8/98 . Aachen: RWTH-Aachen, 1998.
35. Zhao X.-L. Deformation limit and ultimate strength of welded T-joints in cold-formed RHS sections. *Journal of Constructional Steel Research.* 2000. Vol. 53. No. 2. Pp. 149–165.

limit for the ultimate strength of hollow section joints // Tubular Structures VI. 6th International Symposium on Tubular Structures. Melbourne, Australia / ed. Grundy P., Holgate A., Wong B. Rotterdam: Balkema, 1994. Pp. 341–347.

33. Zhao X.-L., Hancock G.J. T-joints in rectangular hollow sections subject to combined actions // Journal of Structural Engineering. 1991. Vol. 117. № 8. Pp. 2258–2277.
34. Grotmann D., Sedlacek G. Rotational stiffness of welded RHS beam-to-column joints. Cidect 5BB-8/98 . Aachen: RWTH-Aachen, 1998.
35. Zhao X.-L. Deformation limit and ultimate strength of welded T-joints in cold-formed RHS sections // Journal of Constructional Steel Research. 2000. Vol. 53. № 2. Pp. 149–165.

Marsel Garifullin,*
+7(999)034-60-70; marsel.garifullin@tut.fi

Maria Bronzova,
+7(921)330-25-29; bronzochka@mail.ru

Markku Heinisuo,
+358(40)596-58-26; markku.heinisuo@tut.fi

Kristo Mela,
+358(40)849-05-63; kristo.mela@tut.fi

Sami Pajunen,
+358(40)849-05-71; sami.pajunen@tut.fi

Марсель Ринатович Гарифуллин,*
+7(999)034-60-70;
эл. почта: marsel.garifullin@tut.fi

Мария Константиновна Бронзова,
+7(921)330-25-29;
эл. почта: bronzochka@mail.ru

Маркку Хейнисуо,
+358(40)596-58-26;
эл. почта: markku.heinisuo@tut.fi

Кристо Мэла,
+358(40)849-05-63; эл. почта: kristo.mela@tut.fi

Сами Паюнен,
+358(40)849-05-71;
эл. почта: sami.pajunen@tut.fi

doi: 10.18720/MCE.80.9

Seismic stability of a tsunami-resistant residential buildings

Сейсмостойкость цунамистойких жилых зданий

T.A. Belash*,
A.D. Yakovlev,
Petersburg State Transport University,
St. Petersburg, Russia

д.т.н., проф. Т.А. Белаш*,
аспирант А.Д. Яковлев,
Петербургский государственный университет путей сообщения Императора Александра I, Санкт-Петербург, Россия

Key words: tsunami; tsunami resistance; tsunami protection; seismic stability; build

Ключевые слова: цунами; цунамистойкость; цунамизащита; сейсмостойкость; здания

Abstract. We have analyzed data on the mechanism of tsunami waves formation and destruction caused by thereby, and also have summarized recommendations on tsunami-resistant construction. For reduction of damage and loss from strong earthquakes and high tsunami waves, hereon the solution for tsunami protection of the construction area is proposed in which small typical residential buildings are located in the upper part of the motor road trestle. At such solution, residential buildings are “torn off” from the earth surface on considerable height, and, as result, are not exposed to tsunami wave impact. By using the computerized complex SCAD 21.1, four options of the proposed tsunami-protection solutions have been analyzed. In the course of such analysis, the optimal option – from the point of view of seismic stability – has been selected. For this option, we have checked sections of elements for arising forces, and also made necessary corrections in structures. Final proposed option of the structure provides high seismic and tsunami safety.

Аннотация. Проанализированы данные по механизму образования волн цунами и разрушения от них, а также обобщены рекомендации по цунамистойкому строительству. Для уменьшения ущерба от сильных землетрясений и высоких волн цунами предлагается решение, в котором небольшие типовые жилые здания располагаются в верхней части автомобильной эстакады. При таком решении жилые здания «оторваны» от поверхности земли на значительную высоту и, как результат, не подвергаются удару волны цунами. С помощью вычислительного комплекса SCAD 21.1 проведено исследование четырех вариантов предложенного решения по цунамизащите. В ходе исследования выбран наиболее оптимальный вариант с точки зрения сейсмостойкости. Для данного варианта произведена проверка сечений элементов на возникающие усилия, а также выполнена необходимая корректировка конструкций. Предложенный конечный вариант конструкции имеет высокую сейсмо- и цунамибезопасность.

1. Introduction

Tsunami is a natural disaster referring to most destructive natural phenomena. These are huge waves which are capable to wipe off whole cities. Most frequently, (in about 90 %) tsunami occurs because of strong earthquakes occurring under the sea or ocean bottom. Thus, any tsunami protection should have sufficient seismic stability. Based on the foregoing, the object of this article is the seismic resistance of the proposed tsunami protection device.

Tsunami waves are dangerous not only because of damages which they are can cause to coastal objects, but also because it is impossible to detect tsunami waves in the deep-water area of water spaces with the naked eye, though studies [1, 2] show that many animals can feel seismic shocks which lead to tsunami formations. Tsunami waves at the time of their formation in the open ocean have height of about 0.6 m as compared to the height of wind waves up to 5–7 meters. With their small height, tsunami waves have speed in the open ocean of about 800–1000 km/h, and therefore they can quickly cover essential distances [3–7].

However, as reduction of depth the speed of such waves decreases, but their height increases many-fold. These changes of tsunami begin from the depth of 200 meters, and occur most intensively on depths of 10 to 15 meters [7–11].

Most of destructions caused by tsunamis occur as a result of wave impacts. Then, because of land flooding, washout of buildings foundations, bridges and roads occurs. As a result of tsunami transporting effect, tsunami wave contains fragments of boats, coastal structures, cars which forcefully strike against buildings, thus inflicting additional loss [5].

For a better understanding of tsunami waves formation process, change of tsunami waves characteristics and effects, the world scientific community has come a long way in their studying, description and simulation [12, 13].

Furthermore, at present new early tsunami waves detection systems are developed which are able to detect a tsunami wave in the open ocean, send a signal about the tsunami hazard to the coast, and thus avoid human victims [10, 14–18].

To avoid material losses, tsunami protection activities should be carried out as described below.

As follows from the sad experience of the emergency at Fukushima-1 NPP [19–21], the first thing to do is to define correctly the tsunami-hazard construction area. Also, among simple coastline protection activities many researchers [22, 23] recommend planting of trees along the coast, construction of earthen embankments and special cost-protection structures such as walls, bulwarks, piers, and dams.

Beside coast-protection structures, for safety of residents living in tsunami-hazard regions of our planet, it is proposed to build tsunami-resistant buildings. So, scientists [5, 24–26] in their works give some recommendations concerning construction of buildings in tsunami-hazard regions. First, the building should be strong, capable to withstand high shock loads. Second, it is recommended to arrange the building with its long side length wise to the direction of tsunami wave movement. At such arrangement, the smaller part of the building will be subject to shock, thus providing its higher strength. Third, the foundations should be built so that they should not be subject to soil erosion effects and undercutting as a result of currents. Fourthly, the ground floor should be made as “open” as possible. It allows the wave to pass easily through the building without making a strong impact on it. As the experiments have shown [27], load on bearing elements of the building decreases by 25–50 %, if the building has any through apertures. It is desirable to make the ground floor non-residential. Fifth, key elements of the building infrastructure (emergency generators, lift motor compartments, etc.) should be located on non-flooded floors.

From the foregoing, it follows that in the practice of designing tsunami-resistant buildings, a lot of experience has accumulated, but the consequences of strong destructive tsunami that has passed in different countries of the world, for an example, in Japan in 2011, indicate the need to continue researching for new approaches to designing tsunami protection of buildings that provide reliability and safety of people living in them. This article is devoted to the study of these questions.

Thus, the purpose of the article is studying the seismic resistance of the proposed tsunami protection. To achieve this goal, a number of tasks are set forth that need to be addressed in this study:

1. Development of proposals for tsunami protection of buildings;
2. Conducting theoretical studies.

As a tsunami-dangerous region, the Kuril Islands region was chosen.

2. Methods

Proceeding from recommendations on tsunami-resistant construction, for the maximum load reduction from moving tsunami wave, it was decided to “lift” the building over the ground surface to the height of 18 meters (the maximum tsunami wave height on the Kuriles during the last for 100 years). To increase economic benefit from such solution, it was decided to locate the buildings on the automobile trestle. Thus, in case of tsunami wave attack on the building, it will pass under the residential sections, and the load from the wave will be applied only to trestle supports. Besides, the matter of seismic stability of bridges is studied well enough [28]. Schematic cross-section (a) and ground floor plan (b) are given in Figure 1.

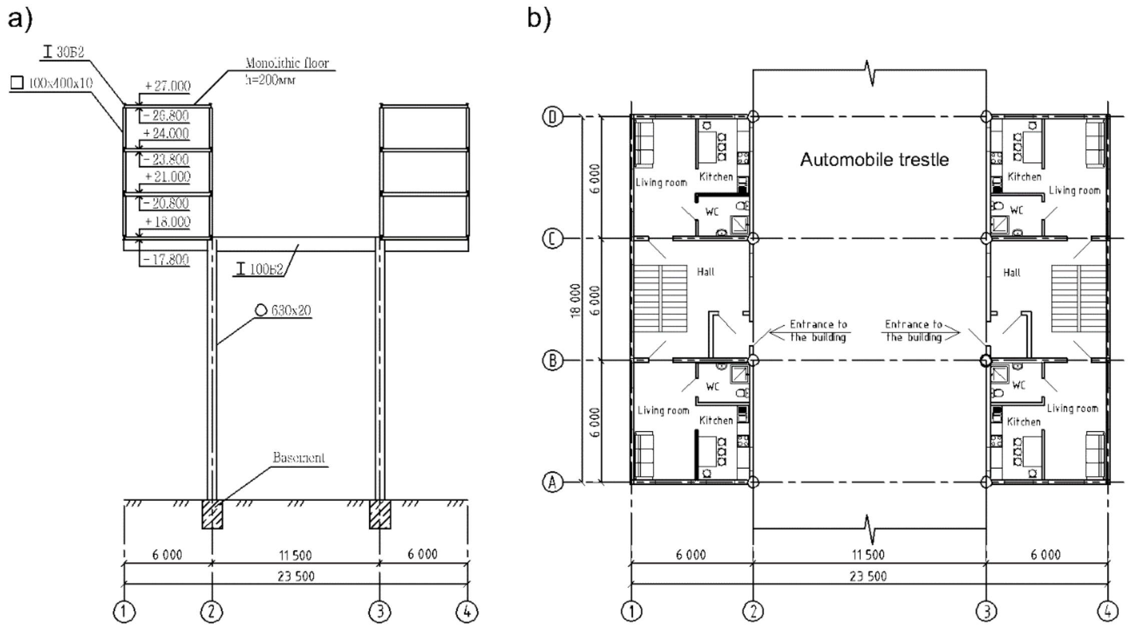

Figure 1. Schematic cross-section (a) and ground floor plan (b)

As it is evident from figure 1, the residential building consists of two symmetrical three-storey interconnected blocks with dimensions within gridlines 6 x 18 meters. It has a rigid frame-type structure. Such system is adopted according to recommendations for seismic- and tsunami-resistant construction.

The building and a part of the trestle have common supports – metal pipes 630x20 in accordance with Russian State Standard GOST R 54157-2010 [29]. Trestle rigidity is achieved by using I-beams erected in accordance with Russian State Standard GOST 26020-83 [30], No. 100B2 arranged in the direction normal to the trestle axis, and No. 60B2 – located along the trestle axis. Rigidity of the building is achieved by use of square pipes 400x10, erected in accordance with Russian State Standard GOST R 54157-2010 [29] as columns, and cast-in-situ reinforced-concrete lift slabs 200 mm high.

For defining loads, movements and vibration periods as a result of seismic forces effect, spectral method described in Russian Set of Rule SP 14.13330.2014 "Construction in seismic areas" [31] has been used. Calculations have been carried out using SCAD 21.1 computer system.

3. Results and Discussion

In Figure 2, schematic cross-section (a), simulation model (b) and the deformed state diagram from seismic load effect (c) are given for the first option.

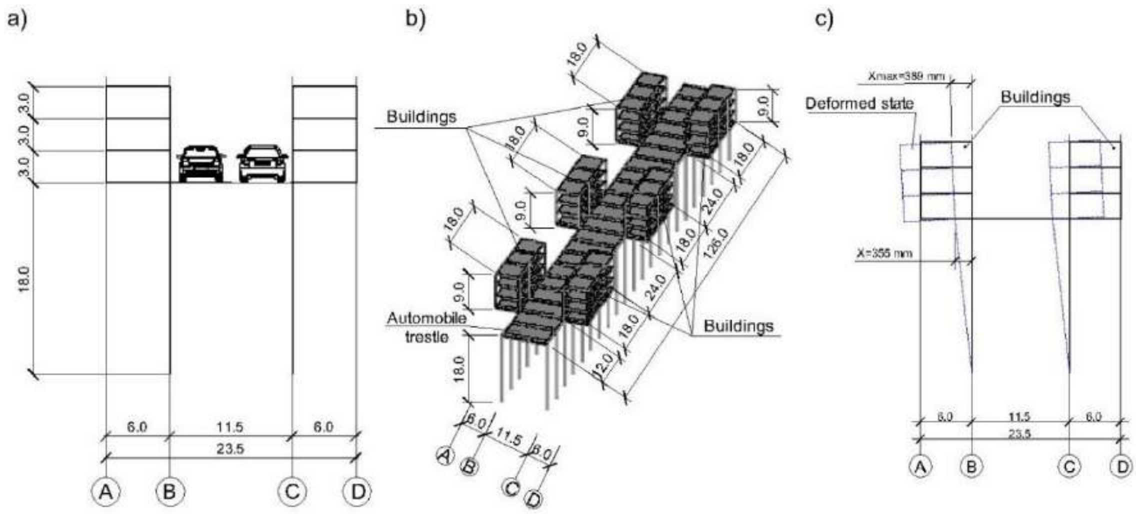

Figure 2. Schematic cross-section (a), simulation model (b), and the deformed state diagram from seismic load effect (c) for the first option

Analysis of calculation results for this model has shown that the maximum movements of 389 mm are reached in the top point of the building. Vibration period of the building is 3.2 seconds.

In order to find the optimal from the point of view of seismic stability solution, three more simulation models have been created. In figure 3, schematic cross-section (a), simulation model (b) and the deformed state diagram from seismic load effect (c) are given for the second option.

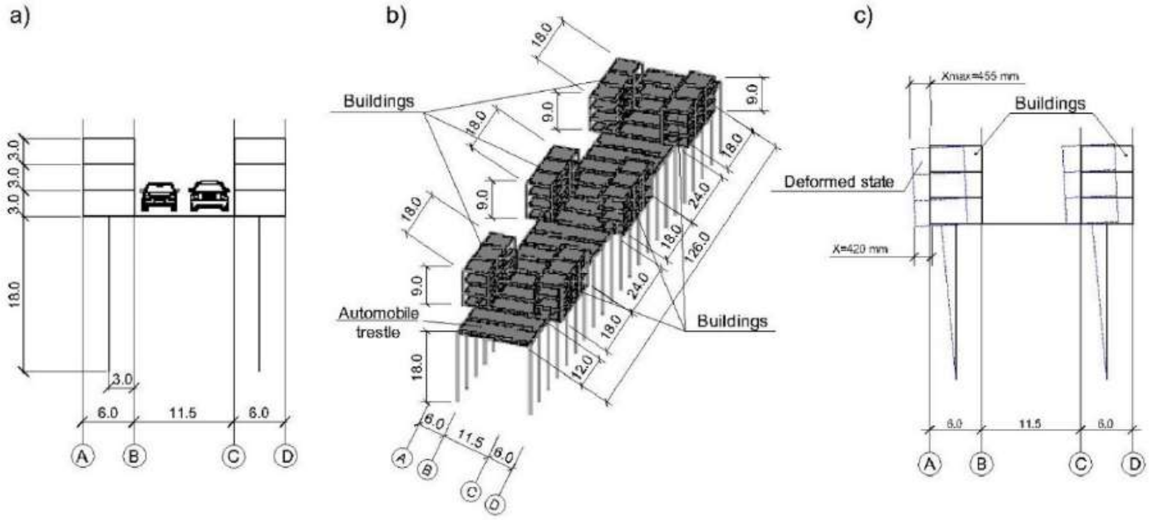

Figure 3. Schematic cross-section (a), simulation model (b), and the deformed state diagram from seismic load effect (c) for the second option

As it can be seen from Figure 3a, the second option differs from the first one by wider spacing between automobile trestle supports. Thus, residential buildings are supported by the trestle at their central axis, and are not using the console scheme as in the first option.

Analysis of calculation results for this model has shown that the maximum movements of 455 mm are reached in the top point of the building. Vibration period of the building is 3.6 seconds. Wider arrangement of trestle supports and, hence, the changed building support scheme on trestle structures have increased building movements by 66 mm and vibration periods – by 0.4 seconds.

In the third option considered, buildings are located over the automobile trestle. In Figure 4, schematic cross-section (a), simulation model (b) and the deformed state diagram from seismic load effect (c) are given for the third option.

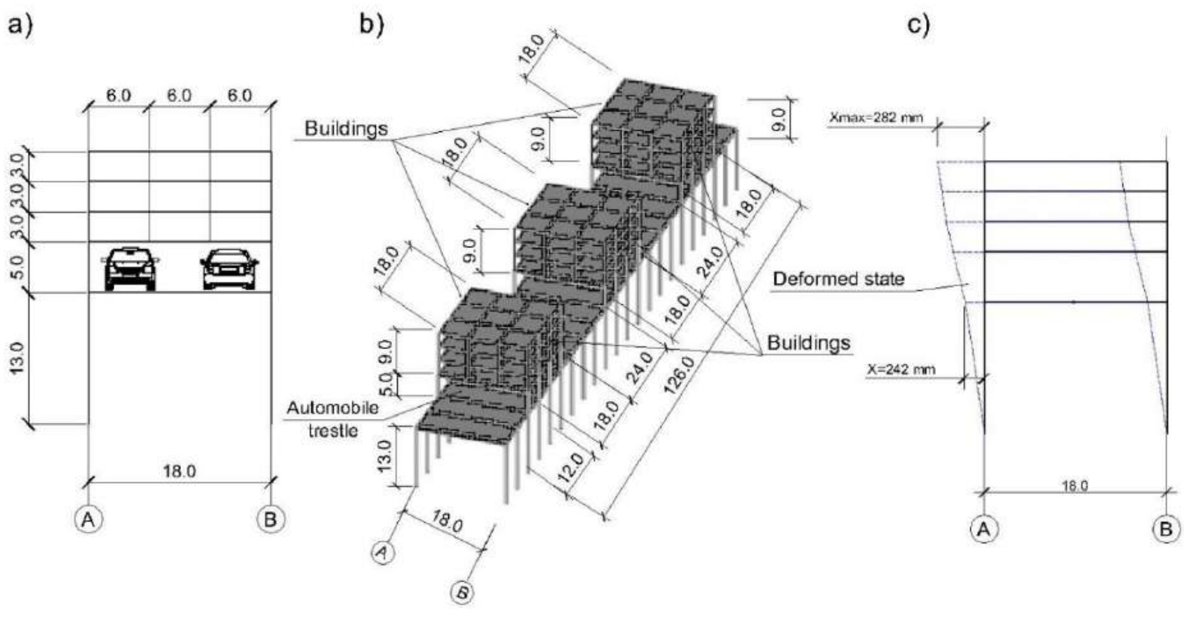

Figure 4. Schematic cross-section (a), simulation model (b), and the deformed state diagram from seismic load effect (c) for the third option

Analysis of calculation results for the last model has shown that the maximum movements of 282 mm, and as well as in previous schemes, are reached in the top point of the building. Vibration period of the building is 2.5 seconds. Due to lower arrangement of automobile roadbed and changes in the scheme of buildings arrangement on the trestle, it became possible to decrease maximum movements by 107 mm as compared to the first scheme.

Finally, the fourth option was considered. Schematic cross-section (a), simulation model (b), and the deformed state are given on Figure 5.

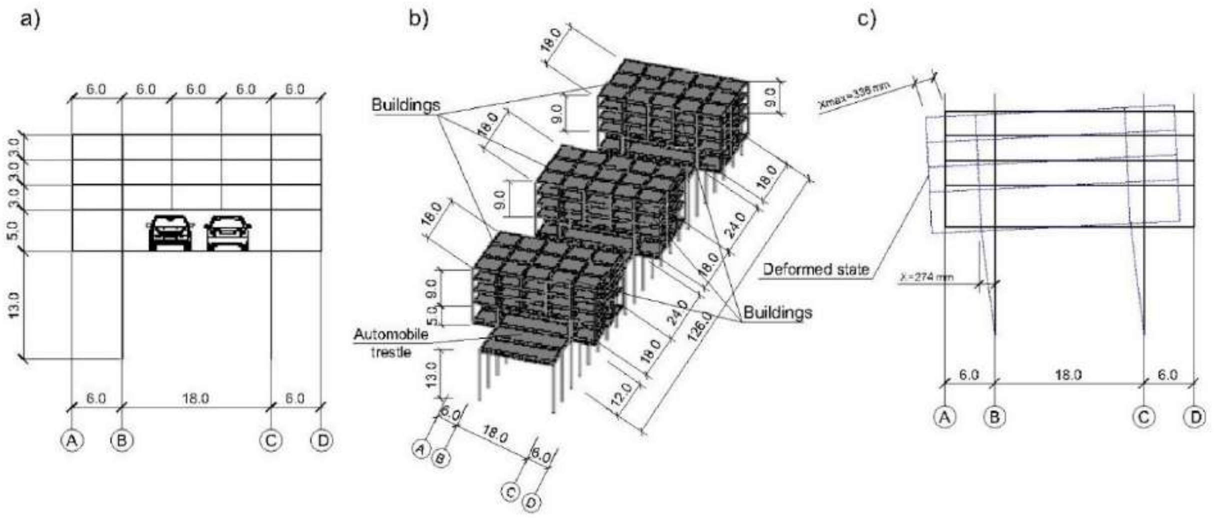

Figure 5. Schematic cross-section (a), simulation model (b), and the deformed state diagram from seismic load effect (c) for the fourth option

Assessment of the deformed state from seismic loading has shown, that movements have values equal to 336 mm and are reached in the top part of a building. Vibration period is 2.8 seconds.

As a result of this study, it has been found out that the third scheme of tsunami-resistant buildings is most aseismic from among the considered options.

Also, in the course of the study it has been revealed that most dangerous elements of the building are trestle struts as maximum forces occur there. For checking parameters of these struts, Crystal software has been used in the scope of SCAD computer system.

As a result of calculation of trestle struts section, the material operations factor was obtained as equal to 1.982 which is inadmissible according to Russian Set of Rule SP 16.13330.2011, since in case of 9 points design earthquake, there can occur the structure collapse situation.

The material operations factor can be decreased by several ways: by increasing the number of struts, by reducing spacing between them, and by increasing their section or reducing their height. Doubling the number of struts (so that spacing between them decreased from 6 to 3 meters) has led to decreasing of the operations factor: it has decreased from 1.982 to 1.584, but still remained higher than 1. Thus, this method won't let to use this structure in 9-points earthquake conditions. Besides, the increase in the struts number will lead to essential increase in the cost of the whole structure. Increase of struts section also insignificantly affects the material operations factor as the maximum size of sections in accordance with Russian State Standard GOST R 54157-2010 is 630 x 22 mm, which is not enough for using such struts in areas with high seismic activity.

To define the maximum struts height, the additional study was performed. As a result of this study, it has been found out that trestle struts of 6 meters high at the given space-planning solution of the building are capable to withstand seismic loads from 9-point earthquakes.

Schematic section (a), simulation model (b), deformed status (c), and panorama (d) of the final adopted option are given in Figure 6.

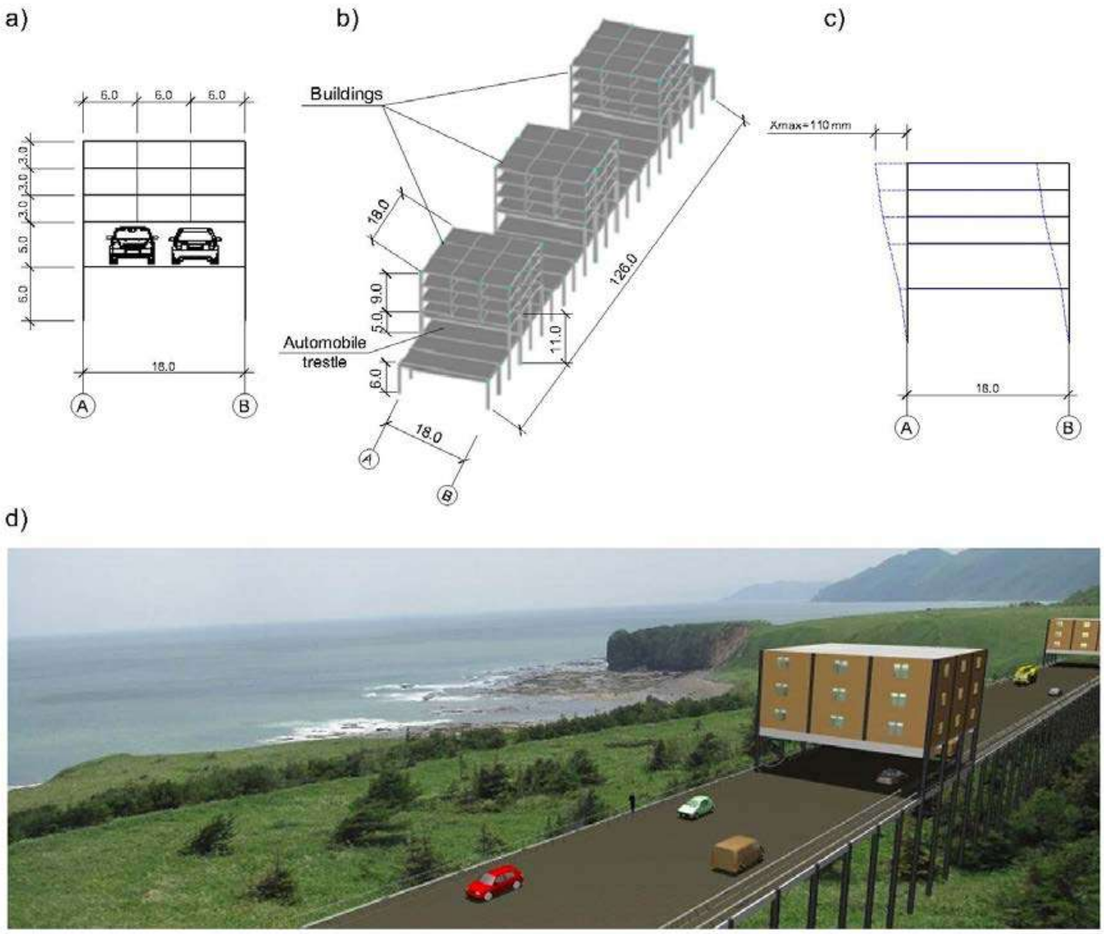

Figure 6. Schematic section (a), simulation model (b), deformed status (c), and panorama (d) of the final adopted option

Analysis of seismic load calculation results for this model has shown that the maximum movements of 110 mm are reached in the top point of the building. Vibration period changes within 1 second.

Software complex SCAD 21.1 has been also used for defining tsunami impact on the building. The amount of load from tsunami waves was defined according to Russian guidance document RD 31.33.07-86 Guide to Calculation of Impact of Tsunami Waves on Port Structures, Water Bodies, and Territories. Recommended Practice for Design [32], however at present extra studies are carried out for simulation of tsunami waves surge on various geometry objects for detailing formulas for calculation of loads from tsunami waves [33–36]. In this study, loads calculation has been performed for two tsunami options: design tsunami equal to 4.3 meters and the maximum and safe for the building tsunami of 11 meters height.

As a result of calculation of this scheme for the design tsunami, it has been found out that in trestle elements only minor forces occur, and that the operations factor of trestle struts at wave impact 4.3 meters is 0.077, which is less than 1.

At estimation of the 11-meter tsunami wave height, forces occurring in trestle elements do not exceed maximum admissible values, and in this case the material operations factor was 0.986.

4. Conclusions

Based on the results of the research conducted the following conclusions were drawn:

1. Studies have confirmed that the use of free space under the building is an effective means of tsunami protection.

2. Creation of free space by erection of low-rise buildings on automobile overpasses provides their uninterrupted operation at 9-point earthquakes and 11-meter tsunami waves.

References

1. Meenakshi A.N., Juvanna B.I. Tsunami detection system using unusual animal behavior-A specified approach. *Earth Sciences*. 2013. Vol. 2. No. 1. Pp. 9–13.
2. Stepanyuk I.A., Frolova N.S. Vozmozhnosti ispolzovaniya ryb v prognosticheskikh tselyakh dlya predskazaniya opasnykh protsessov v prirode [The possibility of using fish in prognostic purposes for predicting hazardous natural processes]. *Society. Environment. Development.* 2011. No. 3. Pp. 218–222. (rus)
3. Dotsenko S.F., Bazykina A.Yu., Ingerov A.V. Osobennosti rasprostraneniya voln tipa tsunami v pribrezhnoy zone Chernogo morya [Peculiarities of tsunami wave propagation in the black sea coastal zone]. *Ekologicheskaya bezopasnost pribrezhnoy i shelfovoy zon moray*. 2017. No. 2. Pp. 10–19. (rus)
4. Dimova Ye.V. Priroda, geografiya voln tsunami i opasnost ikh proyavleniya dlya naseleniya Dalnego Vostoka [Nature, geography of tsunami waves and their danger to the population of the Far East]. Life safety. 2013. No. 4. Pp. 31–35. (rus)
5. Vorobyev Yu.L., Akimov V.A., Sokolov Yu.I. *Tsunami: preduprezhdeniye i zashchita* [Tsunami: prevention and protection]. Moscow: MChS Rossii, 2006. 264 p. (rus)
6. Syvorotkin V.L. Tsunami. *Space and time*. 2011. No. 3. Pp. 144–153. (rus)
7. Levin B.V., Nosov M.A. *Fizika tsunami i rodstvennykh yavleniy v okeane*. [Physics of tsunami and related phenomena in the ocean]. Moscow: Izd-vo Yanus-K, 2005. 360 p. (rus)
8. Satake K., Rabinovich A., Lu U.K.N., Tinti S. Introduction to ‘‘Tsunamis in the World Ocean: Past, Present, and Future. Volume I’’. *Pure and Applied Geophysics*. 2011. Vol. 168. No. 6-7. Pp. 963–968.
9. Constantin A., Henry D. Solitons and Tsunamis. *A Journal of Physical Sciences*. 2009. Vol. 64. No. 1-2. Pp. 65–68.
10. Bethany D., Hinga R. *Ring of fire: an encyclopedia of the Pacific Rim’s earthquakes, tsunamis, and volcanoes.* ABC-CLIO, California. 2015. 403 p.
11. Helal M.A., Mehanna M.S. Tsunamis from nature to physics. *Chaos, Solitons and Fractals*. 2008. Vol. 36. No. 4. Pp. 787–796.
12. Yim S.C., Cox D.T., Park M.M. Experimental and computational activities at the Oregon State university NEES tsunami research facility. *Science of tsunami hazards*. 2009. Vol. 28. No. 1. Pp. 1–14.
13. Synolakis C.E., Bernard E.N. Tsunami science before and beyond boxing day 2004. *Philosophical Transactions: Mathematical, Physical and Engineering Sciences (Series A)*. 2006. Vol. 364. No. 1845. Pp. 2231–2265.
14. Kurkin A.A., Pelinovskiy Ye.N., Belyakov V.V., Makarov V.S., Zezyulin D.V. Novyye tendentsii v obsledovanii tsunami [New trends in tsunami survey]. *Engineering physics*. 2016. No. 5. Pp. 96–106. (rus)
15. Pudov V.D. Tsunami. *Issues of risk analysis.* 2007. Vol. 4. No. 2. Pp. 165–173. (rus)
16. Beyzel S.A., Gusyakov V.K., Rychkov A.D., Chubarov L.B. Vychislitelnyye tekhnologii opredeleniya zapleskov voln tsunami na otdelnyye uchastki dalnevostochnogo poberezhya Rossii [Computational technologies for determining tsunami wave patches on parts of the far East coast of Russia]. Trudy konfererencii “*Problemy kompleksnogo geofizicheskogo monitoringa Dalnego Vostoka Rossii”* [Proceedings. Problems of complex geophysical monitoring of the Russian Far East]. 2013. Pp. 241–245. (rus)
17. Vinokurov L.V. Avtomatizirovannaya sistema opredeleniya tsunami [Automated tsunami detection system]. *Tekhnologii grazhdanskoy bezopasnosti*. 2011. Vol. 8. No. 2. Pp. 14–19. (rus)

Литература

1. Meenakshi A.N., Juvanna B.I. Tsunami detection system using unusual animal behavior-A specified approach // Earth Sciences. 2013. Vol. 2. № 1. Pp. 9–13.
2. Степанюк И.А., Фролова Н.С. Возможности использования рыб в прогностических целях для предсказания опасных процессов в природе // Общество. Среда. Развитие. 2011. № 3. С. 218–222.
3. Доценко С.Ф., Базыкина А.Ю., Ингеров А.В. Особенности распространения волн типа цунами в прибрежной зоне Черного моря // Экологическая безопасность прибрежной и шельфовой зон моря. 2017. № 2. С. 10–19.
4. Димова Е.В. Природа, география волн цунами и опасность их проявления для населения Дальнего Востока // Безопасность жизнедеятельности. 2013. № 4. С. 31–35.
5. Воробьев Ю.Л., Акимов В.А., Соколов Ю.И. Цунами: предупреждение и защита. М.: МЧС России, 2006. 264 с.
6. Сывороткин В.Л. Цунами // Пространство и время. 2011. № 3. С. 144–153.
7. Левин Б.В., Носов М.А. Физика цунами и родственных явлений в океане. М.: Изд-во Янус-К, 2005. 360 с.
8. Satake K., Rabinovich A., Lu U.K.N., Tinti S. Introduction to ‘‘Tsunamis in the World Ocean: Past, Present, and Future. Volume I’’ // Pure and Applied Geophysics. 2011. Vol. 168. № 6-7. Pp. 963–968.
9. Constantin A., Henry D. Solitons and Tsunamis // A Journal of Physical Sciences. 2009. Vol. 64. № 1-2. Pp. 65–68.
10. Hinga B.D.R. Ring of fire: an encyclopedia of the Pacific Rim’s earthquakes, tsunamis, and volcanoes. ABC-CLIO, California. 2015. 403 p.
11. Helal M.A., Mehanna M.S. Tsunamis from nature to physics // Chaos, Solitons and Fractals. 2008. Vol. 36. № 4. Pp. 787–796.
12. Yim S.C., Cox D.T., Park M.M. Experimental and computational activities at the Oregon State university NEES tsunami research facility // Science of tsunami hazards. 2009. Vol. 28. № 1. Pp. 1–14.
13. Synolakis C.E., Bernard E.N. Tsunami science before and beyond boxing day 2004. // Philosophical Transactions: Mathematical, Physical and Engineering Sciences (Series A). 2006. Vol. 364. № 1845. Pp. 2231–2265.
14. Куркин А.А., Пелиновский Е.Н., Беляков В.В., Макаров В.С., Зезюлин Д.В. Новые тенденции в обследовании цунами // Инженерная физика. 2016. № 5. С. 96–106.
15. Пудов В.Д. Цунами // Проблемы анализа риска. 2007. Т. 4. № 2. С. 165–173.
16. Бейзель С.А., Гусяков В.К., Рычков А.Д., Чубаров Л.Б. Вычислительные технологии определения заплесков волн цунами на отдельные участки дальневосточного побережья России // Проблемы комплексного геофизического мониторинга Дальнего Востока России. 2013. С. 241–245.
17. Винокуров Л.В. Автоматизированная система определения цунами // Технологии гражданской безопасности. 2011. Т. 8. № 2. С. 14–19.
18. Куликов Е.А., Ивельская Т.Н. Современные методы оперативного прогноза цунами // Труды государственного океанографического института. 2014. № 215. С. 126–135.
19. Белов Д.А., Шарапов Р.В. Авария на "Фукусима-1" // Международный журнал прикладных и фундаментальных исследований. 2012. № 1. С. 109.
20. Королев Ю. П., Шевченко Г. В. Оперативный прогноз цунами // История науки и техники. 2016. № 6. С. 28–41.

18. Kulikov Ye.A., Ivelskaya T.N. Sovremennyye metody operativnogo prognoza tsunami [Modern methods of operational tsunami forecast]. *Trudy gosudarstvennogo okeanograficheskogo instituta* [Proceedings of the state Oceanographic Institute]. 2014. No. 215. Pp.126–135. (rus)
19. Belov D.A., Sharapov R.V. Avariya na "Fukusima-1" [Accident at "Fukushima-1"]. *Mezhdunarodnyy zhurnal prikladnykh i fundamentalnykh issledovaniy*. 2012. No. 1. Pp. 109. (rus)
20. Korolev Yu. P., Shevchenko G. V. Operativnyy prognoz tsunami [Operational forecast tsunami]. *History of Science and Engineering*. 2016. No. 6. Pp. 28–41. (rus)
21. Additional Report of the Japanese Government to the IAEA. *The Accident at TEPCO's Fukushima Nuclear Power Stations. Nuclear Emergency Response Headquarters. Government of Japan September 2011.*
22. Tikhonov M.N. Antologiya katastrofy na yaponskoy atomnoy stantsii "Fukusima-1" [Anthology of the disaster at the Japanese nuclear power plant "Fukushima-1"]. *Health risk analysis.* 2015. No. 1. Pp. 82–102. (rus)
23. *Informatsiya tsentra tsunami* [Tsunami center information] [electronic resource]. URL: http://kammeteo.ru/gms_interest3.html. (Date of access: 28.05.2017)
24. Shulchin V.N. Inzhenernaya zashchita naseleniya i territorii v chrezvychaynykh situatsiyakh mirnogo i voyennogo vremeni. Kniga 1. Osnovy inzhenernoy zashchity naseleniya i territorii v chrezvychaynykh situatsiyakh [Engineering protection of population and territory in emergency situations of peace and war. Book 1. Fundamentals of engineering protection of population and territory in emergency situations.] Moscow: Izd-vo Akademicheskiy Proyekt, 2010. 688 p. (rus)
25. Klyachko M.A. O normakh proyektirovaniya zdaniy i sooruzheniy v tsunamiopasnykh rayonakh [On the design standards of buildings and structures in tsunami-prone areas]. *Fundamental and Applied Hydrophysics.* 2017. Vol. 10. No. 3. Pp. 5–25. (rus)
26. Zlobin T.K., Polets A.Yu. Penkovaya O.V. Glubinnoye stroyeniye litosfery pod deystvuyushchimi vulkanami kurilskikh ostrovov i ochagi zemletryaseniy [Deep structure of the lithosphere beneath the active volcanoes of the Kuril Islands and earthquake]. *Space and Time.* 2014. No. 3. Pp. 220–230. (rus)
27. Lukkunaprasit P., Ruangrassamee A., Thanasisathit N. Tsunami loading on buildings with openings. *Science of tsunami hazards*. 2009. Vol. 28. No. 5. Pp. 303–310.
28. Noori H.Z., Amiri G.G., Nekooei M., Zakeri B. Seismic Fragility Assessment of Skewed MSSS-I Girder Concrete Bridges with Unequal Height Columns. *Journal of Earthquake and Tsunami*. 2016. Vol. 10. No. 1. 16 p.
29. *Russian State Standard GOST R 54157-2010*: Shaped steel tubes for steel structures. Technical conditions. (rus)
30. *Russian State Standard GOST 26020-83*: Steel hot-rolled I-beams with parallel sides of shelves. Assortment. (rus)
31. *SP 14.13330.2014. Stroitelstvo v seysmicheskikh rayonakh* [Russian Set of Rules Construction in seismic areas] (aktualizirovannaya redaktsiya SNiP). Moscow: Minstroy Rossii, 2014. 126 p. (rus)
32. *RD 31.33.07-86 Rukovodstvo po raschetu vozdeystviya voln tsunami na portovyye sooruzheniya, akvatorii i territorii. Rekomendatsii dlya proyektirovaniya* [Russian guidance document Guidelines for calculating the impact of tsunami waves on port facilities, water areas and territories. Recommendations for design]. Moscow: SOYuZMORNIIPROEKT, 1986. 53 p. (rus)
33. Kuswandi. K, Triatmadja R., Istiarto I. Simulation of scouring around a vertical cylinder due to tsunami. *Science of tsunami hazards*. 2017. Vol. 36. No. 2. Pp. 59–69.
34. Fostera A.S.J., Rossettoa T., Allsopb W. An experimentally validated approach for evaluating tsunami inundation forces

21. Additional Report of the Japanese Government to the IAEA. The Accident at TEPCO's Fukushima Nuclear Power Stations. Nuclear Emergency Response Headquarters. Government of Japan September 2011.
22. Тихонов М.Н. Антология катастрофы на японской атомной станции "Фукусима-1" // Анализ риска здоровью. 2015. № 1. С. 82–102.
23. Информация центра цунами [электронный ресурс]. URL: http://kammeteo.ru/gms_interest3.html. (дата обращения: 28.05.2017)
24. Шульчин В.Н. Инженерная защита населения и территории в чрезвычайных ситуациях мирного и военного времени. Книга 1. Основы инженерной защиты населения и территории в чрезвычайных ситуациях. М.: Изд-во Академический Проект, 2010. 688 с.
25. Клячко М.А. О нормах проектирования зданий и сооружений в цунамиопасных районах // Фундаментальная и прикладная гидрофизика. 2017. Т. 10. № 3. С. 5–25.
26. Злобин Т.К., Полец А.Ю. Пенькова О.В. Глубинное строение литосферы под действующими вулканами курильских островов и очаги землетрясений // Пространство и время. 2014. № 3. С. 220–230.
27. Lukkunaprasit P., Ruangrassamee A., Thanasisathit N. Tsunami loading on buildings with openings // Science of tsunami hazards. 2009. Vol. 28. № 5. Pp. 303–310.
28. Noori H.Z., Amiri G.G., Nekooei M., Zakeri B. Seismic Fragility Assessment of Skewed MSSS-I Girder Concrete Bridges with Unequal Height Columns // Journal of Earthquake and Tsunami 2016. Vol. 10. № 1. P. 16.
29. ГОСТ Р 54157-2010 Трубы стальные профильные для металлоконструкций. Технические условия.
30. ГОСТ 26020-83. Двутавры стальные горячекатаные с параллельными гранями полок. Сортамент.
31. СП 14.13330.2014. Строительство в сейсмических районах (актуализированная редакция СНиП II-7-81*). М.: Минстрой России, 2014. 126с.
32. РД 31.33.07-86 Руководство по расчету воздействия волн цунами на портовые сооружения, акватории и территории. Рекомендации для проектирования. М.: СОЮЗМОРНИИПРОЕКТ, 1986. 53с.
33. Kuswandi. K, Triatmadja R., Istiarto I. Simulation of scouring around a vertical cylinder due to tsunami // Science of tsunami hazards. 2017. Vol. 36. № 2. Pp. 59–69.
34. Fostera A.S.J., Rossettoa T., Allsopb W. An experimentally validated approach for evaluating tsunami inundation forces on rectangular buildings // Coastal Engineering. 2017. Vol. 128. Pp. 44–57.
35. Zhangping W., Robert A.D. Numerical study on mitigating tsunami force on bridges by an SPH model // Journal of Ocean Engineering and Marine Energy. 2016. Vol. 2. № 3. Pp. 365–380.
36. Дорфман А.А., Печенин С.А., Семенов К.К., Нуднер И.С., Максимов В.В. Воздействие волны цунами на морские гидротехнические сооружения и береговые объекты // Фундаментальная и прикладная гидрофизика. 2017. Т. 10. № 4 С. 16–30.

on rectangular buildings. *Coastal Engineering*. 2017. Vol. 128. Pp. 44–57.

35. Zhangping W., Robert A.D. Numerical study on mitigating tsunami force on bridges by an SPH model. *Journal of Ocean Engineering and Marine Energy*. 2016. Vol. 2. No. 3. Pp. 365–380.
36. Dorfman A.A., Pechenin S.A., Semenov K.K., Nudner I.S., Maksimov V.V. Vozdeystviye volny tsunami na morskiye gidrotekhnicheskiye sooruzheniya i beregovyye obyekty [The impact of the tsunami wave on marine hydraulic structures and coastal facilities]. *Fundamental and Applied Hydrophysics.* 2017. Vol. 10. No. 4. Pp. 16–30. (rus)

Tatiana Belash,*
+7(921)991-01-15; belashta@mail.ru

Anton Yakovlev,
+7(931)966-19-76; anton.yakovlev.94@mail.ru

Татьяна Александровна Белаш,*
+7(921)991-01-15; эл. почта: belashta@mail.ru

Антон Яковлев,
+7(931)966-19-76;
эл. почта: anton.yakovlev.94@mail.ru

doi: 10.18720/MCE.80.10

Engineering solutions for the social housing, integrated into urban environment

Инженерные решения устройства социального жилья, интегрируемого в городскую среду

D.D. Zaborova*,
K.I. Strelets,
J. Bonivento Bruges,
M.I. Asylgaraeva,
Peter the Great St. Petersburg Polytechnic University, St. Petersburg, Russia
M. de Andrade Romero,
University of Sao Paolo, Sao Paolo, Brazil
C. Steffan,
Berlin Institute of Technology, Berlin, Germany

Аспирант Д.Д. Заборова*,
к.т.н., зам.директора ИСИ по доп. проф. образованию К.И. Стрелец,
магистрант Х. Бонивенто Брюгес,
магистрант М.И. Асылгараева,
Санкт-Петербургский политехнический университет Петра Великого, Санкт-Петербург, Россия
д.арх., проф. М. Дэ Андраде Ромеро,
Университет Сан-Паулу, Сан Пауло, Бразилия
д.арх., проф. К. Стефан,
Берлинский Технический Университет, Берлин, Германия

Key words: civil engineering; sustainable development; infrastructure; energy-efficiency; favela; environment; USP

Ключевые слова: гражданское строительство; устойчивое развитие; инфраструктура; энергоэффективность; фавела; окружающая среда

Abstract. Deprived areas integrated into actively developing environment of the modern cities is a burning issue which is being studied in megalopolises of Latin America, Africa and Asia. Diverse controversial issues emerge in the interaction between the city community and inhabitants of the favela. The article deals with the solution for this issue based on the example of interaction between Brazilian favela “Sao Remo” and the University campus of Sao Paulo. Nowadays, this University conducts constant social research to find a suitable integration between both sides of the wall. One of this initiatives was raised in the symposium WC2-2017 which purpose was to elaborate the solution for a social infrastructure to be designed to improve links. Moreover, this infrastructure is sustainable in order to mitigate social, environmental and economic impacts. After an analysis of diverse design strategies, the outcomes were obtained in regard to some technical alternatives which implementation depends on stakeholders’ wiliness to collaborate and understanding to what extent they are ready for compromise.

Аннотация. Неблагополучные районы, интегрированные в активно развивающуюся среду современных городов, являются актуальной проблемой, особенно для мегаполисов Латинской Америки, Африки и Азии. Различные спорные социальные вопросы возникают между городскими общинами и жителями фавелы. В статье рассматривается решение одной из социальных проблем на примере взаимодействия бразильской фавелы "Sao Remo" и университетского городка Сан-Паулу. В настоящее время этот Университет проводит постоянные социальные исследования, чтобы найти подходящую интеграцию между обеими сторонами. Одна из таких инициатив была выдвинута на симпозиуме WC2-2017, целью которого была разработка проекта социальной библиотеки, предназначенной для улучшения связей между университетом и граничащей фавелой. После анализа различных стратегий проектирования было установлено, что наилучшим строительным материалом для данного региона является железобетон, а расположение самой библиотеки должно быть на границе двух взаимодействующих территорий. Реализация данного проекта напрямую зависит от желания заинтересованных сторон сотрудничать и понимания того, в какой степени они готовы к компромиссу.

Заборова Д.Д., Стрелец К.И., Бонивенто Брюгес Х., Асылгараева М.И., Дэ Андраде Ромеро М., Стефан К. Инженерные решения устройства социального жилья, интегрируемого в городскую среду // Инженерно-строительный журнал. 2018. № 4(80). С. 104–118.

1. Introduction

High concentration of poverty and rapid growth of the population within the territory trigger social problems having impact on urban planning of a city. An important example is the “favelas” – Brazilian word to describe a concentration of poor people who live in low quality housing with lack of property rights and primary urban services located in areas geologically inadequate or environmentally sensible [1] – it reflects the extremely unequal economic and social structure of representative cities in Brazil [2]. Most of the citizens who live in favelas are people of lower middle class who cannot afford solutions which housing market offers. From the beginning of 1980 policies of land regulations of the favelas emerged with the focus on urbanizing these areas by using social programs, main public services and relocation from high geological risk [3]. However, due to its rapid proliferation around Brazil and fragmentation of the territory which produces disintegration social [4], nowadays these places have become in spots of lack of participation of the public power and high crime rate, impacting negatively on the people who live there and the surrounding areas. Thus, the urbanization of these places is conceived as a complex integration of the social, environmental and urban spheres [5].

The author [6], through a historical analysis, concluded that the exclusion is main consequence and cause of the expansion of favelas. Moreover, [7–8] affirmed that more than a problem of housing infrastructure, this is a social problem and it should be tackled with integrated programs and promotion of urban planning and inclusive urban management [9]. According to the Secretary of Strategic Affairs of Brasilia DF [10], the lack of integration of these areas with the city deals with two types of consequences: immediate and long-term. The former is the allowance of conditions of illegal activities, segregation, limited presence of the state and guarantee of civil rights and informality, while the latter consequence is opportunities and vision for the future differentiated for the youth and controversial mechanisms for conflict resolution. The secretary recognizes six dimensions to have an effective and sustainable integration: capacity to identify local needs and community action, ability to resolve conflicts, access to public services, economic, physical and symbolic integration and re-signification of the today’s concept of youth conceived in favelas [11].

Different studies have aimed at an inclusive urban management for these sites. Manzione and Antonucci [12] argue that the integration must consider the inclusion of favelas in the mapping of the city and physical and land integration into the formal city. They include also the integration of its inhabitants in the existing social programs and in the discussions on the development ways of the city [13], and of the instruments of planning of the City Statute. Additionally, [5] proposed a model of 5 strategies for the urban requalification of a specific favela in Sao Paulo through the appropriation of interstices and urban interfaces as effective environmental, urban and social infrastructures.

A specific case is the city Sao Paulo, which accounts for the biggest number of favela with more than 15 % (IBGE, 2010) of the population of the city. There is a settled “Jardim São Remo” settlement, with 15 thousand inhabitants, which is a controversial favela because of its contiguous location with the University of Sao Paulo (USP), largest Brazilian public university. However, the land where this favela is situated belongs to the university, but it was historically populated by the inhabitants from Sao Remo. Consequently, as part of this campus, USP is often involved in discussions about the fate of the community [14]. One of the most emblematic and controversial issue which affected the relationship between the community of the campus and the favela was between 1995 and 1997, when the USP built a solid wall with regulated entrance to separate both spaces targeting the preservation of the institute.

Nowadays, sustainability design is one of the main task issues around the world. Each country has its own goals and objectives for the development and preservation of the environment [15–17]. Therefore, the University of Sao Paulo has been working in a sustainable mitigation of the social impacts mentioned. One of its initiatives is the WC2 (World Cities, World Class) Summer Symposium, which took place in 2017 with the focus on integration of the campus community with the people who live in the favela Sao Remo through an infrastructure project. The authors of this paper were involved in the design of efficient and sustainable alternatives of infrastructure throughout the University, which is fenced with the aforementioned wall.

Therefore, the main purpose of this paper is to define the most suitable strategy for the project, which can effectively promote the integration of the USP and the community of the contiguous favela. To archive this goal, the following tasks were solved:

- To consider the main environmental and social factors of the city;
- In the context of detailed consideration of the executed projects to formulate the key factors and main categories for selecting the best solution;

- To choose the most appropriate project, which corresponds to three main categories: location, sustainability, architectures.

2. Methods

The development of this research is based on three different strategies, which are divided in three spheres: location, sustainability and architecture. Those strategies follow common parameters and needs described in the Table 1 and Figure 1, which were consented in the WC2-2017 symposium, hosted by the University of Sao Paulo.

- Localization: this criteria is analysed taking into account the potential social and social impact triggered by setting the construction in the purposed area.
- Sustainability: in this area was technically analysed the materials considered in the architectonic design from the three strategies. Emphasizing the thermal resistance of roof, windows and walls, which are calculated in steady conduction through a constant area plane wall by the Fourier Law. The parameters for resistance for convection indoor and outdoor were taken from the standard IRAM 11601.
- Architectonic: it includes the design and distribution of spaces of each strategy, minding the parameters consented. Autodesk Revit Software and SketchUp program were used to make 3d modeling of the building and topography of the existing area.

Table 1. Parameters of space to be considered

Site area _ around 8.000m²	Sports court (indoors/outdoors) _ 1 or 2
Library _ 1.000m²	Gym (indoors/outdoors) _ 300m²
Multipurpose rooms _ 500m²	Health care facilities _ 500m²
Workshops _ 600m²	Community restaurant _ 300m²
Auditorium _ 500m²	General facilities _400m²
Outdoor arena _ 600m²	Open spaces

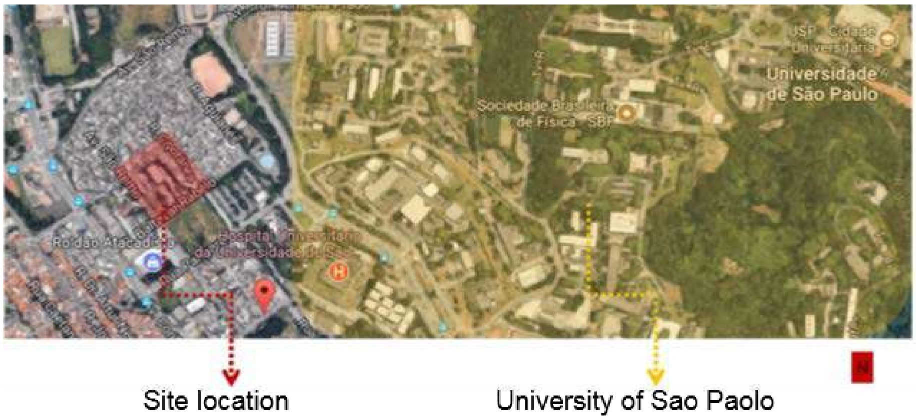

Figure 1. General localization of the project

2.1. First strategy

2.1.1. Location

The localization of the infrastructure to be designed remains unchangeable. However, there are some controversial issues which would come out due to the social factor. A demolition of the wall makes it possible to use an informal construction of housing by the population from the favela. Therefore, in order to keep at the same time both a physical border and accessibility, the wall has an open design as described in Figure 3. The access is shown in red arrows with the ease of access for both communities. Moreover, the design takes into consideration the sun going through the wall to the favela.

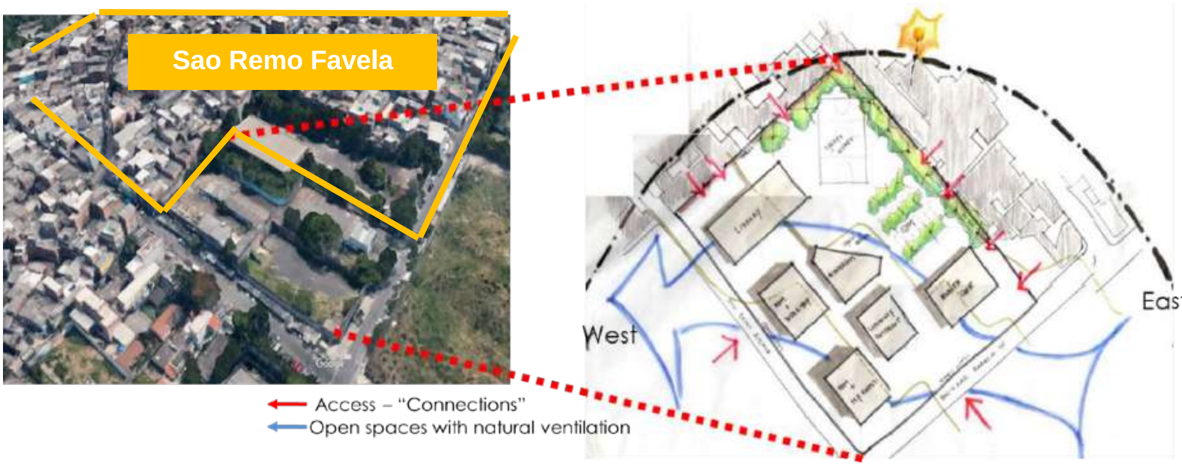

Figure 2. Localization of the infrastructure for integration of the USP community and Favela Sao Remo

2.1.2. Sustainability

The sustainability of this infrastructure is described in the following aspects: Energy Efficient, Social, Technology and Architecture.

Figure 3. Wall design purposed

The buildings are proposed to be with passive cooling and illumination systems, for that, it is divided in 6 units, which orientation and distribution can guarantee wind flow, sun path and shadows. Additionally, the edifications are suspended from the floor to allow a natural passive ventilation, likewise vertical shading in the façade northwest is meant to allow natural illumination.

The main materials used in this strategy is following described:

- Roof: Green Roof (700 m^2) and Solar Panels (1135 m^2). The former aims an insulation for the ceiling and an open area for pedestrian. The latter aims a solar passive electricity generation, with capacity of 455 solar panels of 1.6mx1m of dimension, producing 200 MWh/year and payback period of 8 years.
- Windows: as the temperature in Sao Paulo is about 28 and 14 °C, a single glass, with blackout curtains systems and brise solei facing in the north is considered in the design.
- Walls: in order to promote a social, environment and energetic integration, the walls are designed with two wood panels with an insulation cavity of cellulose fiber (recycled paper). It is important to notice that the high density of people in favelas carries a high demand of waste to be managed, P. Jacobi [18]. This alternative of recycling can generate opportunities of temporary employment to the surrounding community, which can collect the paper and sell them to the recycling company in charge of the fabrication of this insulation. In fact, as the process of fabrication is not complex and does not require specialized equipment, it can be analyzed the alternative of fabrication inside the campus.

The Figure 4 shows the structure of the purposed and a thermal resistance of 3.10 W/mK is calculated as a thermal parameter in the Table 2. According to this table, the dew point is located in the insulation, which is not a technical problem for its suitable operation.

The social factor as a sustainable factor includes primary services, strategies of promoting inter-community cross-culture interaction. The first mentioned are: water, comfortable indoor temperature, gym and an experimental kitchen, where part of the vegetables harvested in the green roof. The strategies of interaction are trough recreational spaces (Figure 5), balconies, interconnection between buildings and a mobile application to keep up to date to the user.

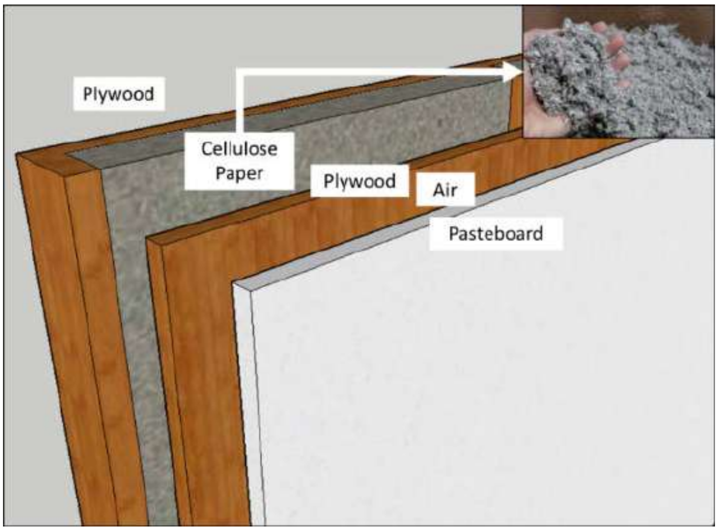

Figure 4. Wall structure for Strategy 1

Table 2. Thermal and Mechanical properties of Wall Strategy 1

Layer	Layer material	Layer thickness [m]	Thermal conductivity [W/m·K]	Specific heat capacity [J/kg/K]	Density [kg/m³]
Indoor					
1	Plywood	0.013	0.130	1600	500
2	**Recycled Cellulose Paper**	0.100	0.040	2020	50
3	Plywood	0.013	0.130	1600	500
4	Air	0.050	0.026	1005	1.25
5	Plasterboard	0.013	0.170	1090	664
Outdoor					

2.1.3. Architecture

Even though the Brazilian law No16.050 of July 2014 (PDE-SP, 2014 [20]) allows as follows: construction of buildings until 8 meters high for this zone, the design ensures the architecture of favelas to remain the same look, so the inhabitants of the surrounding can feel that this infrastructure belongs to this zone. The architecture purposed has no more than 4 floors and is made of brick façade as the surrounding. The library has its own building and it is interconnected with the building for workshops, designed to have a common space for meetings and/or classes lead by volunteers from the University. All buildings are interconnected by bridges as a symbol of integrity and for easy exploring of the facilities. It has an auditorium which north façade works as an outside screen for projection of movies (Figure 4).

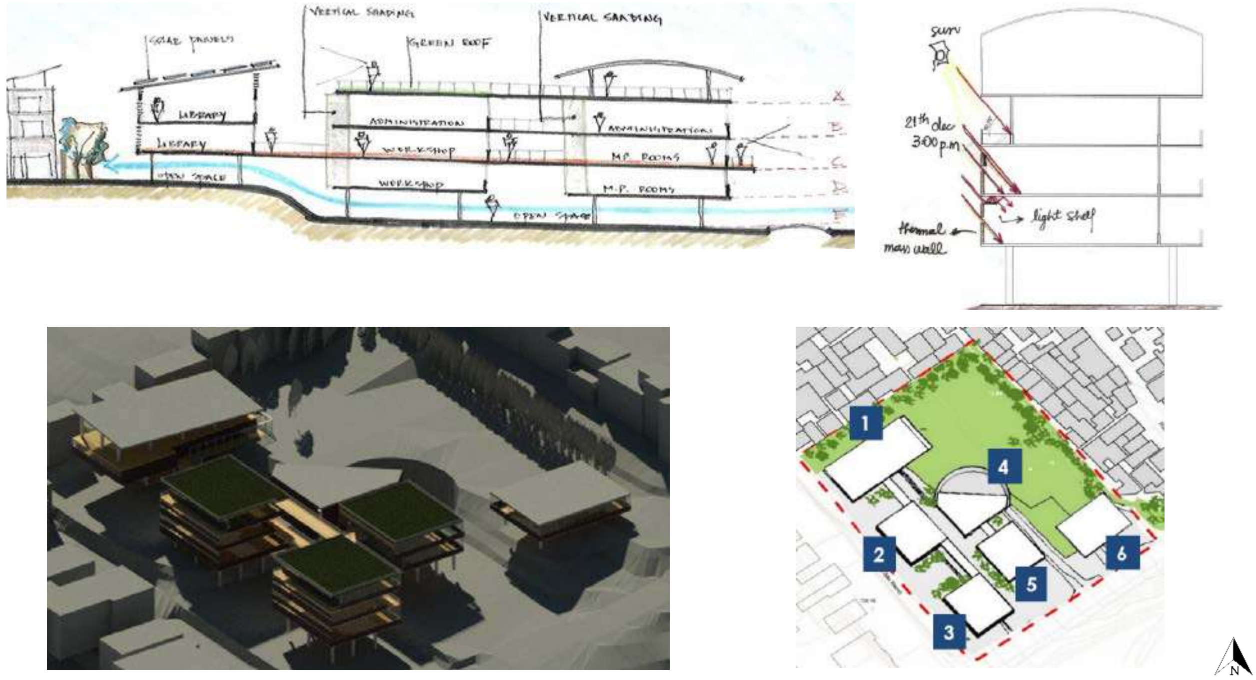

Figure 5. View A-A of buildings and distribution of areas. 1) Library, 2) Workshop + Administration, 3) Multipurpose rooms + Administration, 4) Auditorium + Outdoor arena (cinema), 5) Community Experimental Restaurant and 6) Health Care + Outdoor Gym

2.2. Second strategy

2.2.1. Location

The idea of the second variant is to move the location of future project from the centre of favela to the border (figure 5). This wall separates University of Sao Paulo from the favela. It can be seen in the figure 7 that building has two entrances from the university side and residential district. Therefore, the project brings two different social groups together and every group can feel safely because this territory does not belong to a particular area of USP or favela. The main entrance with the front stair is located in the North-Eastern part of the building.

The building is situated near the soccer field and the volleyball court. Pitches are located in the South-West direction.

Figure 6. Location of the building

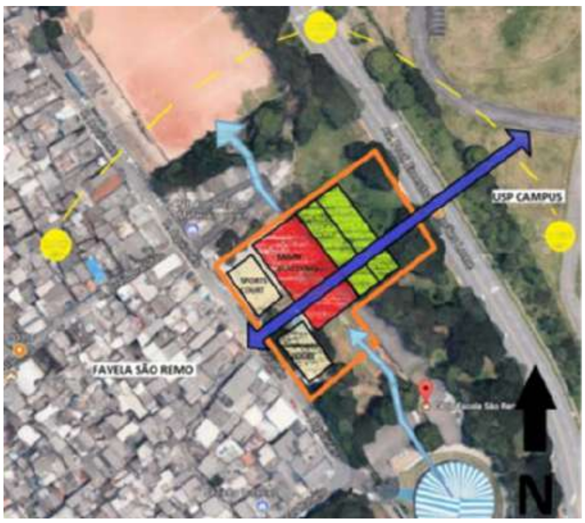

Figure 7. Site plan

2.2.2. Sustainability

In this strategy, the selected materials are conventional and commonly used in this region.

In this strategy is highlighted the structures build with concrete due to its high thermal mass. The main construction materials used in this strategy is following described:

Roof: Building has a flat roof with from concrete with a green roof system, which prolongs the service life of HVAC systems through decreased use.

Windows: The use of artificial light is minimized by the opening space on the first floor. The main façade has the single glazing with shading system. Rainwater storage is also located on the top.

Walls: Materials choice for the project is quite simple. Building frame is made of reinforced concrete; northeast side is covered by wooden hinged facade. The south-eastern side of the building is designed into the form of green wall. Plywood is cheap and simple choice for the façade. Reinforced concrete, as the main structure, accumulate cold air during the night and release it throughout the day. Due to this, a comfortable temperature is maintained indoors. The wall structure is presented in the Table 4.

Slabs: Adiabatic cooling integrated into each floor.

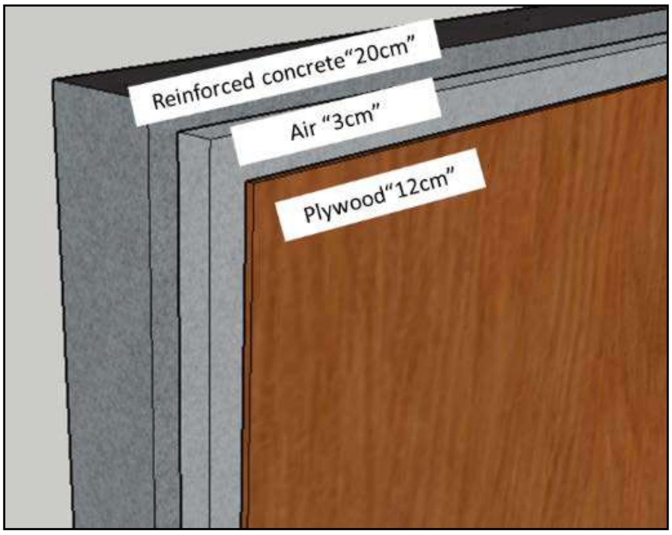

Figure 8. Wall structure for Strategy 2

Table 3. Thermal and Mechanical properties of Wall Strategy 2

Layer	Layer material	Layer thickness [m]	Thermal conductivity [W/m·K]	Specific heat capacity [J/kg/K]	Density [kg/m³]
Indoor					
1	Reinforced concrete	0.200	1.7	800	2500
2	Air	0.030	0.026	1005	1.18
3	Wood panel	0.012	0.130	1600	500
Outdoor					

2.2.3. Architecture

The main idea of the architectural treatment of the building is to connect the University and the favela. Every person, standing from the university side of the building can look through the building and see the favela. And there is the same situation from the other side (Figure 7).

Ground floor is supposed to be an opening space with educational auditorium and restrooms. Two underground levels have a technical room, gym facility, workshop rooms.

First and second floors are supposed to have a library with bookshops and healthcare facilities.

Third floor (last floor) has a community restaurant. It is an open terrace with glass curtain wall and green garden.

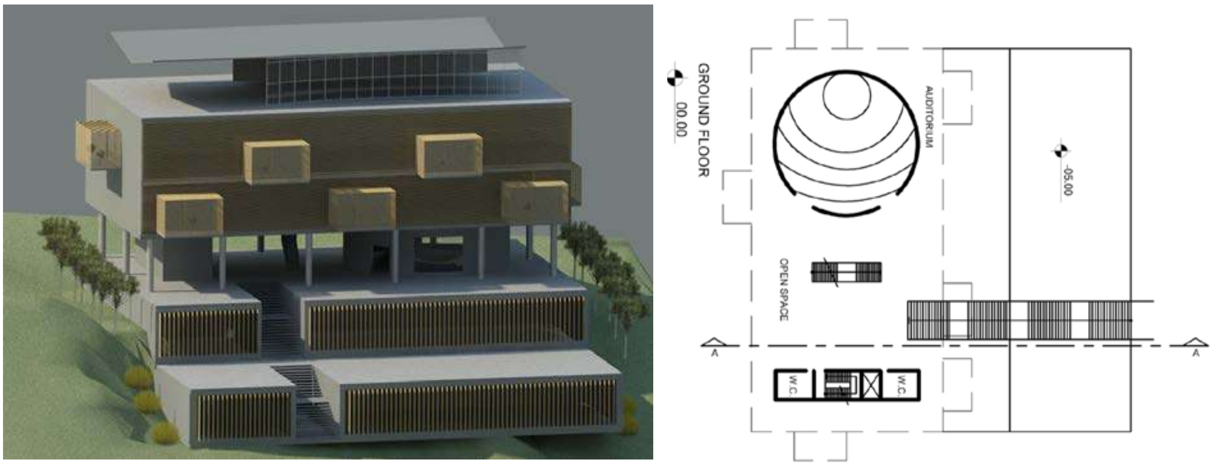

Figure 9. 3D view and Ground floor

2.3. Third strategy

2.3.1. Location

Initially it was suggested for the future building, to locate it within the favela borders which opposed to the main principle of the project to unite the divided parts by destroying the wall. Therefore, it was changed for the place with a more difficult topography but existing as a connecting point for two environments with a city road going along the wall, the university and a public bus stop. New location also gave a possibility to create an interaction between the building project and existing two sport fields found on the other side of the wall (Figure 8).

Figure 10. Initial and changed locations

2.3.2. Architecture

As mentioned, the slope taken into account since changing the location of the project has to be managed in a way to fill the social gaps existing in the society. Thus, the idea of comparing the site to one of the most important philosophical issues – the Maslow's hierarchy of needs – has occurred, and such connection between pyramid has had a response in the process of architectural design (Figures 12). The stories of the center were located in a way that topography allowed to design each section as of approximately 3 m high to form a comfortable space. The ground level (749 m) contains community restaurant separately located on the left side of the plan and an entrance into the community center. There are such rooms as workshop, multipurpose rooms and auditorium included general facilities located respectively are arranged above at the level of 752.5, 755.5, and 758.5 m. The aim of providing places for sport is solved by adding the existing court in favela to the territory of the center uniting these sites. At the top (762.0 m) the library is situated. Open spaces are represented in Figure 11 as terraces on roofs of the building parts, except for the library.

As a result, the concept of the pyramid can be followed. For instance, a community restaurant and a community garden satisfy both psychological part of the basic needs level and psychological needs level itself. On the other hand, Maslow's theory states that motivation to achieve the needs exists but the needs should be particularly ordered - the library, workshop, and auditorium help the favela residents reach the self-actualization level that is on the top of the pyramid.

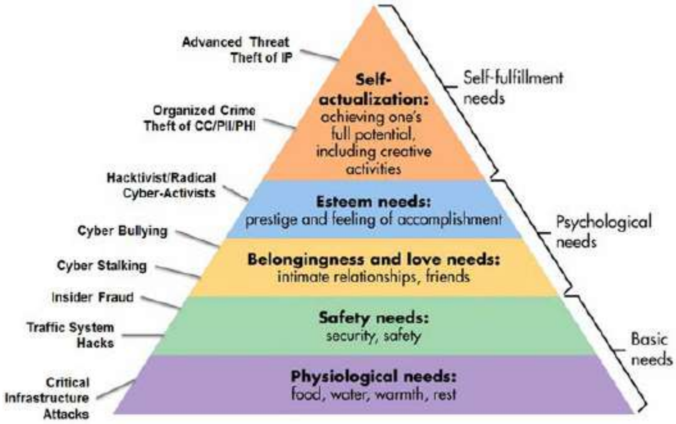

Figure 11. Maslow's hierarchy of needs [19]

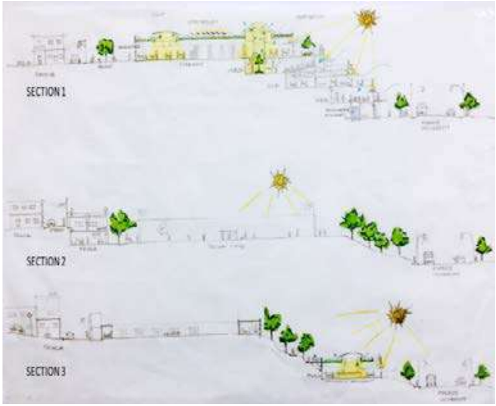

Figure 12. Sections

Figure 13. Sketch of alternative of design No. 3

2.3.3. Sustainability

Due to topography with elevations of about 13 m such sustainable solutions were used:

- Ramps are used to exclude the presence of mechanical and electrical lifts on the territory to reduce electricity consumption;
- Windows: natural light is provided at all levels due to skylights and an abundant glazing and open parts located towards the sun movement (Figure 11); rainwater storage is located on the first level;
- Roof: green roof with installed solar panels and chimney effect is considered as a natural ventilation solution;
- Wall composition: cavity brick wall. Such structure has high thermal mass, keeps comfortable temperature in any season, especially maintains cool temperature in summer. The idea was taken from an Australian research and applied due to the similar climate conditions [20]. The research states that in such structure a large portion of heat can be reflected and radiated back by the exterior surface, so it does not penetrate the internal space (Figure 13). It also was chosen due to its durability, structural capability, fire-resistant and good sound insulation properties, minimal transporting costs.

Table 4. Thermal and Mechanical properties of Wall Strategy 3

Layer	Layer material	Layer thickness [m]	Thermal conductivity [W/m·K]	Specific heat capacity [J/kgK]	Density [kg/m³]
Indoor					
1	Clay Brick	0.250	0.640	880	1600
2	Air	0.100	0.026	1005	1.25
3	Clay Brick	0.060	0.640	880	1600
Outdoor					

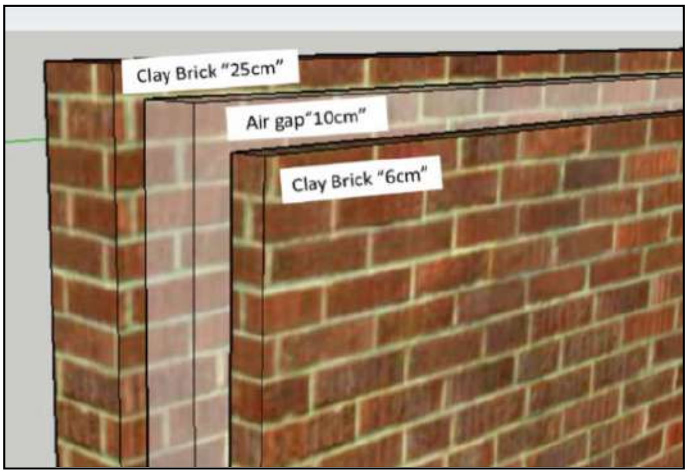

Figure 14. Cavity brick wall purposed for strategy 3

3. Results and Discussion

Based on the projects developed the following results were obtained:

3.1. Location

The best location for the project is between the university and the favela on the border of two territories. (Figure 15). Figure 15 shows the annual wind rose. According to this Frequency Distribution the strongest wind is from Northeast direction. Taking into account this data it is recommended to change the orientation of the main entrance to the Northwest.

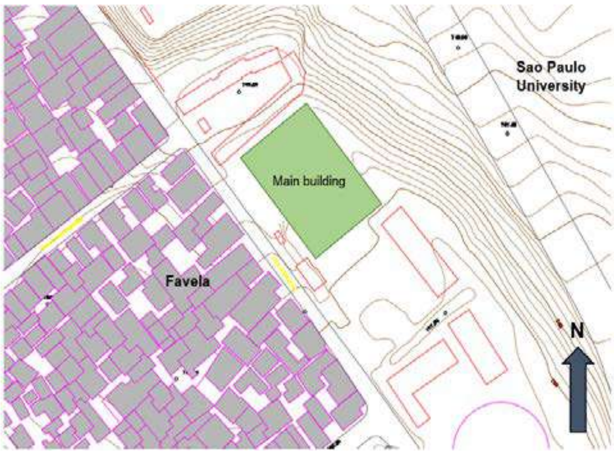

Figure 15. Site view

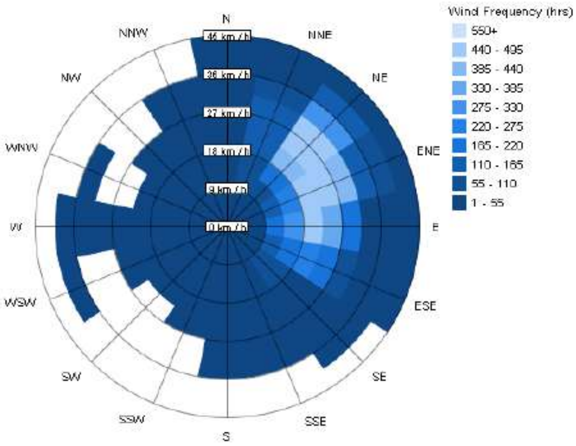

Figure 16. Annual wind rose

3.2 Sustainability

Since the problem in the area is not insulation but the cool temperature inside the building, the assumption is based on average summer temperature. An approximate check of such wall structure was conducted considering the climate of Sao Paulo [23–24] with such initial parameters to provide acceptable thermal comfort conditions indoors:

Humidity: inside – 40 %, outside – 80 %; Temperature: inside – 22 °C; outside – 14 °C.

Table 6. Thermal absorption and thermal resistance of wall strategy 1

Layer	Layer material	Layer thickness [m]	Thermal Absorption β [25] [J/√s·m·K]	Thermal resistance R [m²·K/W]	Temperature °C
Indoor					14.00
Resistance Convection Indoor (IRAM 11601)				0.04	14.07
1	Plywood	0.013	4.19	0.098	14.23
2	Recycled Cellulose Paper	0.100	6.36	2.500	18.34
3	Plywood	0.013	4.19	0.100	18.50
4	Air	0.050	0.29	1.923	21.67
5	Plasterboard	0.013	4.56	0.074	21.79
Resistance Convection Outdoor (IRAM 11601)				0.13	22.00
Outdoor					22.00
Total:			**19.582**	**4.86**	
Internal T °C		22	**External T °C**	14	

Table 7. Thermal absorption and thermal resistance of wall strategy 2

Layer	Layer material	Layer thickness [m]	Thermal Absorption β [25] [J/√s·m·K]	Thermal resistance R [m²·K/W]	Temperature °C
Indoor					14.00
Resistance Convection Indoor (IRAM 11601)				0.04	14.21
1	Reinforced concrete	0.200	368.78	0.118	14.82
2	Air	0.030	0.17	1.154	20.84
3	Plywood	0.012	3.87	0.092	21.32
Resistance Convection Outdoor (IRAM 11601)				0.13	22.00
Outdoor					22.00
Total:			**372.82**	**1.534**	
Internal T °C		22	**External T °C**	14	

Table 8. Thermal absorption and thermal resistance of wall strategy 3

Layer	Layer material	Layer thickness [m]	Thermal Absorption β [25] [J/√s·m·K]	Thermal resistance R [m^2·K/W]	Temperature °C
Indoor					14.00
Resistance Convection Indoor (IRAM 11601)				0.04	14.07
1	Clay Brick	0.250	237.32	0.391	14.77
2	Air	0.100	0.57	3.846	21.60
3	Clay Brick	0.060	56.96	0.094	21.77
Resistance Convection Outdoor (IRAM 11601)				0.13	22.00
Outdoor					22.00
Total :			**294.85**	**4.50**	
Internal T °C		22	**External T °C**	14	

According to the results, the wall No. 1 has the smallest thermal resistance (1.53 m^2·K/W), but the biggest coefficient of thermal absorption (372.82 J/√s·m·K). Whereas air temperature in Sao Paulo never goes below 10 °C. The most important thermal characteristic of the wall is accumulative capacity [26, 27].

Total cost of the wall including material cost and work labor is showed in the Table 9, where the most expensive enclosing structure is structure made of brick.

Table 9. Cost comparison of enclosing structures

Wall type	Strategy 1	Strategy 2	Strategy 3
Cost per m^2	67.87 €	71.98 €	86.45 €

Taking into account the costs and quality of the wall strategies, the most optimal wall for this project will be number two

3.3 Architecture

The best architecture solution is to apply the Maslow's hierarchy of needs. According to this theory, community restaurant and rest rooms have to be in the base of the pyramid, as physiological needs. The library, as a main component should be located on the top of pyramid as well as workshops and auditorium.

All strategies described include sustainable solutions for the project. The first alternative considered passive systems for cooling, heating and illumination, however, as the main variable to be taken into consideration is the social aspect. Its location, almost inside the favela and an open wall can difficult significantly, the security of user from the campus and favela and it is likely to become a spot for illegal actions and vandalism. Furthermore, the use of several time of glazing increases the cost of heating in cold seasons.

With the new location of the second strategy, the aforementioned issue is mitigated, nevertheless, the limited space there, restrict the construction of one unit of building but an integration with both communities is not noticeable due to the wall that it included. Additionally, the material used as a façade, wood, is not recommended because of the high presence of precipitation. The third strategy, which keeps the location of the second, does not considerate a wall fence as a limit. Evidently, this can contribute to informal and illegal construction by the inhabitants of favelas.

4. Conclusions

According to the results of the discussion. the main recommendations were formulated make an optimal design solution in line with three categories:

1. Location: It is important to preserve a physical barrier between the University and favela providing the sufficient system of integration. The best location for the project is between the university and the favela on the border of two territories.
2. Sustainability: The most optimal choice is correctly selected external walls, such as reinforce concrete wall with coefficient of absorption $\beta = 372.82$ J/√s·m·K and cost per $m^2 = 71.98$ €.
3. Architecture: The most correct space zoning based on the Maslow's hierarchy of needs.

Each of the strategies above has strong advantages which combination results in the most suitable option. Location as stipulated in strategy 2 and 3, pointing out that according to historical backgrounds of this area. It is necessary the keep a physical barrier (fence), however, it should also promote the integration between both communities, as the one designed in the strategy 1. Double façade wall with a cavity in-between to tackle the condensation in the conditions in Sao Paulo is suggested as construction materials with high thermal mass in the strategy 3. Finally, the architecture which must take into account the most important factor – the social one – in order to ensure optimal distribution of spaces according to Maslow's hierarchy.

It is important to remark that the viability and sustainability of this research depend on a pre-social work with the potential users and the responsibility of all stakeholders: Government of Sao Paulo, police, community from the campus and from the influence area of the favela Sao Remo.

5. Acknowledgement

Thanks to the work and support of all participants, organizers and mentors of the group 'Eco campus' at the Symposium WC2 held in 2017, which was hosted by the University of Sao Paulo, Brazil.

References

1. Magalhães A. *O direito das favelas.* Letra Capital Editora LTDA. 2014. 494 p. (Bp)
2. Magalhães F., Villarosa F. *Urbanización de Favelas: Lecciones Aprendidas en Brasil.* Banco Interamericano de Desarrollo. 2012. 184 p. (Sp)
3. Soares R. Repensar a regularização fundiária como política de integração socioespacial. *Estudos Avançados.* 2009. Vol.23. No. 66. Pp. 237–250. (Bp)
4. Maricato E. Metrópole, legislação e desigualdade. *Estudos Avançados.* 2003. Vol. 17. No. 48. (Bp)
5. Pimentel E. *Interticios e Interfaces Urbanos como Oportunidades Latentes.* Master Thesis in Architecture and Urbanism. 2014. Sao Paulo University. 188 p. (Bp)
6. Muxica L. La favela como espacio de exclusión social en la ciudad de Rio de Janeiro. *EURE (Santiago).* 2011. Vol. 37. No. 110. Pp. 117–132. (Sp)
7. Ferreira A. *Uma estratégia de relacionamento da favela com a cidade para a integração Uma estratégia de relacionamento da favela com a cidade para a integração social, física e simbólica.* Master Thesis. 2015. State Paulista University. (Bp)
8. Freire P. *Pedagogía de la esperanza: un reencuentro con la pedagogía del oprimido.* Siglo Veintiuno Editores. 1993. 226 p. (Sp)
9. Denaldi R. *Políticas de Urbanização de Favelas: evolução e impasses.* PhD Thesis. 2013. Sao Paulo University. 242 p. (Bp)
10. Barros R., Grosner D., Mascarenhas A., Nimis A. *Integração entre favela e Integração entre favela e cidade.* Secretary of Strategic Affairs of Brasilia D.F. 2012. 18 p. (Bp)
11. Radovic, G., Murgul, V., Vatin, N. Development of the capital Cetinje surrounded by of centuries-old coastal towns of the southern Adriatic sea. *Applied Mechanics and Materials. 2014.* Vol. 641–642. Pp. 634-638.
12. Manzione V., Antonucci D. Urbanização e Integração das Favelas a Cidade: Um Desafio em São Paulo. *Seminary URBFAVELAS.* 2016. Pp. 29. (Bp)

Литература

1. Magalhães A. O direito das favelas. Letra Capital Editora LTDA. 2014. 494 p.
2. Magalhães F., Villarosa, F. Urbanización de Favelas: Lecciones Aprendidas en Brasil. Banco Interamericano de Desarrollo. 2012. 184p.
3. Soares R. Repensar a regularização fundiária como política de integração socioespacial // Estudos Avançados. 2009. Vol.23. No. 66 São Paulo. Pp. 237–250.
4. Maricato E. Metrópole, legislação e desigualdade // Estudos Avançados. 2003. Vol.17 no. 48 São Paulo.
5. Pimentel E. Interticios e Interfaces Urbanos como Oportunidades Latentes. Master Thesis in Architecture and Urbanism. 2014. Sao Paulo University. 188 p.
6. Muxica L. La favela como espacio de exclusión social en la ciudad de Rio de Janeiro // EURE (Santiago). 2011. Vol. 37. No. 110 Santiago. Pp. 117–132.
7. Ferreira A. Uma estratégia de relacionamento da favela com a cidade para a integração Uma estratégia de relacionamento da favela com a cidade para a integração social, física e simbólica. Master Thesis. 2015. State Paulista University.
8. Freire P. Pedagogía de la esperanza: un reencuentro con la pedagogía del oprimido. Siglo Veintiuno Editores. 1993. 226p.
9. Denaldi R. Políticas de Urbanização de Favelas: evolução e impasses. PhD Thesis. 2013. Sao Paulo University. 242 p.
10. Barros R., Grosner D., Mascarenhas A., Nimis A. Integração entre favela e Integração entre favela e cidade. Secretary of Strategic Affairs of Brasilia D.F. 2012. 18 p.
11. Radovic, G., Murgul, V., Vatin, N. Development of the capital Cetinje surrounded by of centuries-old coastal towns of the southern Adriatic sea // Applied Mechanics and Materials. 2014. Vol. 641-642. Pp. 634–638.
12. Manzione V., Antonucci D. Urbanização e Integração das Favelas a Cidade: Um Desafio em São Paulo // Seminary URBFAVELAS. 2016. Pp. 29. (Bp)

Заборова Д.Д., Стрелец К.И., Бонивенто Брюгес Х., Асылгараева М.И., Дэ Андраде Ромеро М., Стефан К. Инженерные решения устройства социального жилья, интегрируемого в городскую среду // Инженерно-строительный журнал. 2018. № 4(80). С. 104–118.

13. Ćetković, J., Rutešić, S., Zarković, M., Knežević, M., Vatin, N. Primary directions and advancements in competitiveness of montenegrin construction sector. *Procedia Engineering*. 2015. Vol. 117(1). Pp. 780–790.
14. Cabette C. How is the relationship between the University City and the São Remo community? *Nexo Jornal Ltda.* 2016. [Electronic resource]. https://www.nexojornal.com.br/expresso/2016/09/06/Como-%C3%A9-a-rela%C3%A7%C3%A3o-entre-a-Cidade-Universit%C3%A1ria-e-a-comunidade-S%C3%A3o-Remo (Accessed: 08.01.2018).
15. De Souza Pirró, L.F., De Andrade Roméro, M. Office buildings façades: The relationship between costs and performance. *PLEA 2006. 23rd International Conference on Passive and Low Energy Architecture. Conference Proceedings.* 2006. Pp. II269-II272.
16. Petrichenko M., Rakova X., Vyatkin M., Musorina T., Kuznetsova D. Architectural renovation of quarter in Mannheim, Germany. *Applied Mechanics and Materials.* 2015. Vol. 725-726. Pp. 1101–1106.
17. Vatin N., Gamayunova O. Energy efficiency and energy audit: the experience of the Russian Federation and the Republic of Belarus. *Advanced Materials Research.* 2015. Vol. 1065-1069. P. 2159.
18. Jacobi, P., Rizpah, G. Solid Waste Management in São Paulo: The challenges of sustainability. *Estudos Avançados.* 2011. Vol. 25. No. 71. Pp. 135–158.
19. Cronemberger J., Caamano E., Vega S. Assessing the solar irradiation potential for solar photovoltaic applications in buildings at low latitudes – Making the case for Brazil. *Energy and Buildings.* 2012. Vol. 55. Pp. 264–272.
20. PDE-SP. Politica de Desenvolvimiento Urbano e o Plano Diretor Estrategico do Municipio de Sao Paulo. *Law No 16.050 of 31 of July. 2014.*
21. McLeod S. A. *Maslow's hierarchy of needs*. 2017. [Electronic resource]. www.simplypsychology.org/maslow.html (Accessed: 03.10.2017).
22. *Energy efficiency and the environment. The case for clay brick*. Think Brick and The University of Newcastle, Australia. 2011. Edition 4. 26 p.
23. Candido C., Lamberts R., Dear R., Vecchi R. *Thermal Comfort. Towards a Brazilian standard on thermal comfort. Research report.* Federal University of Santa Catarina, University of Sydney. 2013. Pp. 17
24. Houska C. *Case study 08, Sao Paulo Building Exterior.* International Molybdenum Association. 2009. 2 p.
25. Antuskov A.L., Ostrovaya A.F., Statsenko Ye.A., Kotov Ye.V., Musorina T.A., Petrichenko M.R. Termoustoychivost ograzhdayushchikh konstruktsiy kak energosberegayushchiy factor [Thermostability of enclosing structures as an energy-saving factor]. *Universitetskiy nauchnyy zhurnal.* 2016. No. 27. Pp. 25–34.
26. Castro J.C.L., Zaborova D.D., Musorina T.A., Arkhipov I.E. Indoor environment of a building under the conditions of tropical climate. *Magazine of Civil Engineering.* 2017. No. 8. Pp. 50–57. doi: 10.18720/MCE.76.5.
27. Tarasova D.S., Petritchenko M.R. Buildings quasi-stationary thermal behavior. *Magazine of Civil Engineering.* 2017. No. 4. Pp. 28–35. doi: 10.18720/MCE.72.4.

13. Ćetković, J., Rutešić, S., Zarković, M., Knežević, M., Vatin, N. Primary directions and advancements in competitiveness of montenegrin construction sector // Procedia Engineering. 2015. Vol. 117(1). Pp. 780–790.
14. Cabette C. How is the relationship between the University City and the São Remo community? Nexo Jornal Ltda. 2016. [Electronic resource]. https://www.nexojornal.com.br/expresso/2016/09/06/Como-%C3%A9-a-rela%C3%A7%C3%A3o-entre-a-Cidade-Universit%C3%A1ria-e-a-comunidade-S%C3%A3o-Remo (Accessed: 08.01.2018).
15. De Souza Pirró L.F., De Andrade Roméro M. Office buildings façades: The relationship between costs and performance // PLEA 2006. 23rd International Conference on Passive and Low Energy Architecture. Conference Proceedings. 2006. Pp. II269-II272.
16. Petrichenko M., Rakova X., Vyatkin M., Musorina T., Kuznetsova D. Architectural renovation of quarter in Mannheim, Germany // Applied Mechanics and Materials. 2015. Vol. 725-726. Pp. 1101–1106.
17. Vatin N., Gamayunova O. Energy efficiency and energy audit: the experience of the Russian Federation and the Republic of Belarus // Advanced Materials Research. 2015. Vol. 1065-1069. P. 2159.
18. Jacobi, P., Rizpah, G. Solid Waste Management in São Paulo: The challenges of sustainability // Estudos Avançados. 2011. Vol. 25. No. 71. Pp. 135–158.
19. Cronemberger J., Caamano E., Vega S. Assessing the solar irradiation potential for solar photovoltaic applications in buildings at low latitudes – Making the case for Brazil // Energy and Buildings. 2012. Vol. 55. Pp. 264–272.
20. PDE-SP. Politica de Desenvolvimiento Urbano e o Plano Diretor Estrategico do Municipio de Sao Paulo. Law No 16.050 of 31 of July. 2014.
21. McLeod S.A. Maslow's hierarchy of needs. 2017. [Electronic resource]. www.simplypsychology.org/maslow.html (Accessed: 03.10.2017).
22. Energy efficiency and the environment. The case for clay brick. Think Brick and The University of Newcastle, Australia. 2011. Edition 4. 26 p.
23. Candido C., Lamberts R., Dear R., Vecchi R. Thermal Comfort. Towards a Brazilian standard on thermal comfort. Research report. Federal University of Santa Catarina, University of Sydney. 2013. Pp. 17
24. Houska C. Case study 08, Sao Paulo Building Exterior. International Molybdenum Association. 2009. 2 p
25. Антуськов А.Л., Островая А.Ф., Стаценко Е.А., Котов Е.В., Мусорина Т.А., Петриченко М.Р. Термоустойчивость ограждающих конструкций как энергосберегающий фактор // Университетский научный журнал. 2016. № 27. С. 25–34.
26. Кастро Х., Заборова Д.Д., Мусорина Т.А., Архипов И.Е. Внутренняя среда жилых помещений в условиях тропического климата // Инженерно-строительный журнал. 2017. № 8(76). С. 50–57.
27. Тарасова Д.С., Петриченко М.Р. Квазистационарные температурные режимы ограждающих конструкций // Инженерно-строительный журнал. 2017. № 4(72). С. 28–35.

Daria Zaborova,*
+7(911)180-60-33; zaborova-dasha@mail.ru

Kseniya Strelets,
+7(812)552-94-60; kstrelets@mail.ru

Jose del Carmen Bonivento Bruges,
+7(931)313-60-98; ing.joseboniventob@gmail.com

Margarita Asylgaraeva,
+7(911)838-96-75;
margarita.asylgaraeva@yandex.ru

Marcelo de Andrade Romero,
+55(11)991-78-23-22; marcelo_romero@icloud.com

Claus Steffan,
+49(30)314-23-301; claus.steffan@tu-berlin.de

Дарья Дмитриевна Заборова,*
+7(911)180-60-33;
эл. почта: zaborova-dasha@mail.ru

Ксения Игоревна Стрелец,
+7(812)552-94-60; эл. почта: kstrelets@mail.ru

Хосе дель Кармен Бонивенто Брюгес,
+7(931)313-60-98;
эл. почта: ing.joseboniventob@gmail.com

Маргарита Искандеровна Асылгараева,
+7(911)838-96-75;
эл. почта: margarita.asylgaraeva@yandex.ru

Марсело Дэ Андраде Ромеро,
+55(11)991-78-23-22;
эл. почта: marcelo_romero@icloud.com

Клаус Стефан,
+49(30)314-23-301;
эл. почта: claus.steffan@tu-berlin.de

doi: 10.18720/MCE.80.11

Temperature and velocity conditions in vertical channel of ventilated facade

Температурный и скоростной режимы в вертикальном канале вентилируемого фасада

E.A. Statsenko*,
A.F. Ostrovaia,
V.Y. Olshevskiy,
M.R. Petrichenko,
Peter the Great St. Petersburg Polytechnic University, St. Petersburg, Russia

Студент Е.А. Стаценко*,
студент А.Ф. Островая,
аспирант В.Я. Ольшевский,
д.т.н., зав. кафедрой М.Р. Петриченко,
Санкт-Петербургский политехнический университет Петра Великого, Санкт-Петербург, Россия

Key words: ventilated facades; convective air flows; grooved lines; air velocity; air temperature; facing layer; air gap

Ключевые слова: вентилируемые фасады; конвективные воздушные потоки; русты; скорость воздуха; температура воздуха; облицовочный слой; воздушный зазор

Abstract. The most economically viable and practicable method of moisture removal from the air gap with the help of free convective air flows are presented in the article. An experiment conducted on a laboratory bench simulating a hinged ventilated facade is described. The parameters and design features of a particular building envelope are determined. Also, the impact of technological gaps – grooved lines is described, which influence the air velocity in the ventilated channel, which in turn affects the temperature and humidity conditions of the building envelope. The experimental evaluation of air velocity and air temperature along the height of ventilated layer is provided in the article. The impact of grooved lines density and the method of hot plane heating on the distribution of air temperature and velocity. Optimal is the construction which is designed with the least number of rusts, from the technological point of view.

Аннотация. Был рассмотрен наиболее экономичный и практичный метод удаления влаги из воздушного зазора навесного вентилируемого фасада – с помощью свободноконвективных потоков воздуха. Описан эксперимент, проведенный на лабораторном стенде, имитирующем собой навесной вентилируемый фасад. Были определены параметры тепломассообмена и конструктивные особенности отдельно взятой ограждающей конструкции. Также было рассмотрено влияние технологических зазоров-рустов, воздействующих на скорость воздуха в вентилируемом канале, которая, в свою очередь, влияет на температурно-влажностный режим ограждающих конструкций. Приведена численная оценка скорости движения и температуры воздуха по высоте вентилируемой прослойки. Установлено влияние рустов и способа обогрева «горячей» стенки на распределение скорости и температуры воздушного потока. Оптимальной является конструкция с наименьшим, с технологической точки зрения, количеством рустов.

1. Introduction

Ventilated facade – is a facade with ventilated air gap aimed at climatic action protection and exterior development.

The system is constructed in the way, where air gap, which is located between insulation and outer cladding, provides free air movement. Free convective air flows occur in air gap because of volume force, which depends on density difference and which is justified by heat energy transfer due to temperature non-uniformity. Besides, there are technological gaps – grooved lines. From a physics perspective, a facade without grooved lines forms an ideal channel.

These constructive features influence air velocity in vertical channel. Air velocity affects temperature and humidity conditions of external envelope.

As can be seen from the above, natural air movement in a gap provides dryness of a wall and prevent condensate formation in insulation layer.

Стаценко Е.А., Островая А.Ф., Ольшевский В.Я., Петриченко М.Р. Температурный и скоростной режимы в вертикальном канале вентилируемого фасада // Инженерно-строительный журнал. 2018. № 4(80). С. 119–127.

At the present times suspended ventilated facades building is relevant to many Russian and foreign scientists. A great contribution to the study of free-convection flow in a vertical ventilated channel was made by Russian and foreign researchers. The article of V.G. Gagarin, V.V. Kozlov, D.V. Nemova, M.V. Petrochenko, E.B. Yevtushenko and many other specialists have been devoted to the determination of the thermophysical properties of ventilated air gaps and their influence on the temperature and humidity conditions of the enclosing structures [1–29].

The paper [1] studies physical processes of free convective current and determines the conditions of cool air filtration in the gap. There are a number of problems associated with the condensation of moisture in the structure in the operation of ventilated facade systems with air gap widely used today in construction [3–7].

The article [8] determines best hydraulic ventilated cavity of a suspended facade. The author of the article [10] estimates the average velocity of free-convective current dependence with different wall temperature.

The author of the article [11] gives the description of air-vent quarter division with different air motion modes. The research [15] determines experimentally and theoretically the average velocity and temperature profiles along the ventilated channel width.

The article [27] provides evaluation methods of thermal insulation with longitudinal air filtration of ventilated facade.

The article describes the impact of arrangement of assembling grooved lines and the heating methods of interior wall plan on air velocity and temperature in vertical ventilated air gap. That is especially important in the conditions of the temperature and climatic zone of St. Petersburg.

Research objective:

- determining the influence of grooved lines density and the method of hot plane heating on the distribution of air temperature and velocity in free convective flow.

Goal Setting:

- determining the average velocity and temperature of free convective flow in air gap in relation to grooved lines pitch with constant geometric parameters of the gap;
- determining of heat and mass transfer parameters for various degrees of hot surface heating.

2. Methods

Imperfection of building constructions leads to excess humidification. That is why it is necessary to focus on water storage capacity of materials. Most methods of insulation layer moisture control aimed at reducing moisture inflow to the air gap.

Moisture removal with the help of free convective air-flows is the most economically viable and practicable method, since the energy source is the heat flow from the hot wall to air. No other external energy sources (ventilators) are needed. Free convection in gravity field is justified by the existence of negative air density gradient, which is associated with temperature gradient. If the surface temperature is higher than the ambient temperature, the air flow in the surface runs hot, becomes lighter and ascends. In this case, less denser air layers replace the ascended layers.

When considering moisture removal, significant attention should be paid to grooved lines, which perform thermal compensator function. Cladding grooved lines provide hydraulic connection with outdoor air. All mentioned factors are prevailing when designing and engineering air cavities. All results of the research were obtained experimentally. Schematic view of a ventilated gap (Fig. 2), which is located between the “hot” plane $y = 0$ (with the temperature $T_h = 67$) and the cold plane $\mathbf{y} = h$ (with the temperature $T_c = 22$). Pressure at level $z = 0$ equals p_0, pressure at level $z = h$ equals p_1, while $p_0 > p_1$. It is required to estimate average velocity and temperature through free-convective flow. To measure the speed are used a thermo-anemometer Testo 435-2, with a resolution of 1 cm/s, it allows to measure the velocity with an error of 0.5 cm/s, air temperature - with an error of 0.1 °C

Required control volume comes over the air-vent and spreads out from zero level to $z = L$ plane, which lays above the outlet air-vent cut in still air. It is taken, that outdoor air penetrates air cavity through lower air holes. Outdoor air ascends along the air-vent and passes through upper air holes [16].

Statsenko E. A., Ostrovaia A. F., Olshevskiy V.Y, Petrichenko M.R. Temperature and velocity conditions in vertical channel of ventilated facade. *Magazine of Civil Engineering*. 2018. No. 4 (80). Pp. 119–127. doi: 10.18720/MCE.80.11

Heating is provided by three vertical fastened thermal elementary units. For equal heat distribution the elementary units are fastened to the tin sheet with high thermal conductivity. Consequently, T_h = const. Model height equals L = 2040 mm, while $L >> h$. When manufacturing the facade model, we should take into consideration the difference in the temperatures of outer and inner layers, which is justified by the heating systems operation. The model considers heating of the wall and heat inflow to the air cavity. For this experiment different combinations of thermal elements are used: lower-middle, lower-upper. Upper-middle combination is not used, since the lower installation section is not heated and there is no air heating in channel inlet. The temperature in this section stays homothermal, consequently, there is no active air movement and the flow is inefficient.

Velocity depends on the air supply method, internal parameters of the gap and the method of hot plane heating. In the experiments the gap width /h/ was set at h = 80 mm = const. In the experiments grooved lines pitch with different fixed activation methods of heating elements was determined. For this purpose, the average velocity and temperature of air in central part of the low were measured.

Figure 1.Thermal anemometer

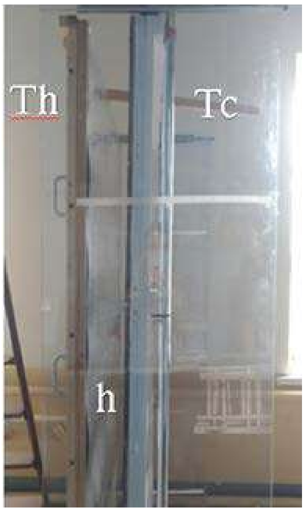

Figures 2,3. Installation scheme

3. Results and Discussion

Within the scope of the given measurements, the following charts were obtained, fig. 4-12. Figures 4-5 show air and velocity dependence on height with different grooved lines pitch and constant heating along the height. Based on the obtained dependencies it was identified that air flow temperature increases when grooved lines pitch increases (with constant heat flow density along the heated channel height). The most significant reason is the decrease of high-density air inflow to the channel. The velocity is maximum in the ideal channel (grooved lines are fully closed).

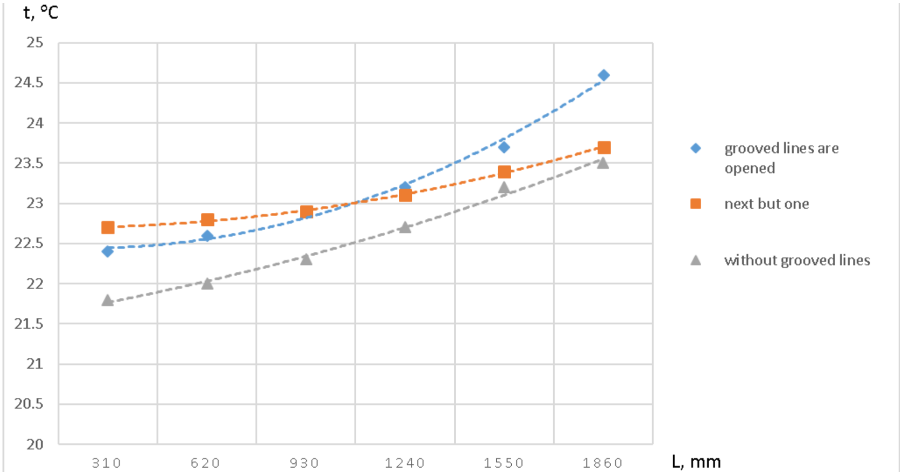

Figure 4. Temperature distribution along the channel height in relation to grooved lines pitch with constant height heating

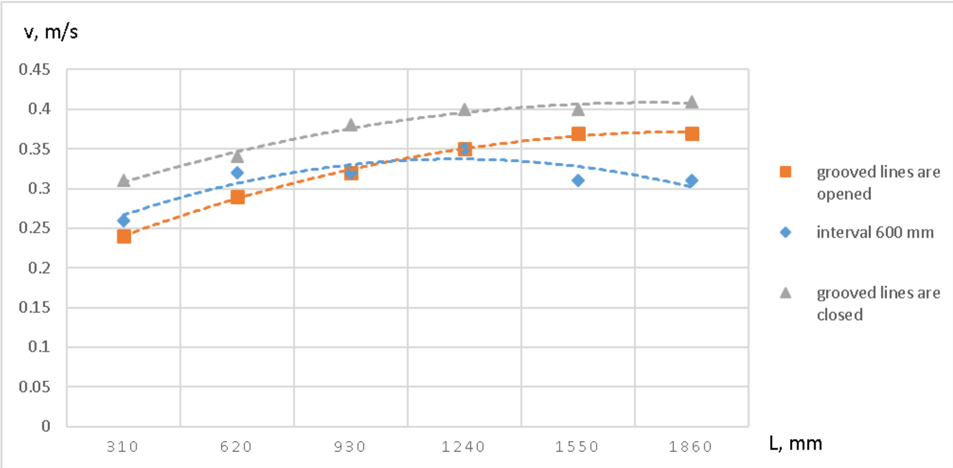

Figure 5. Velocity distribution along the channel height in relation to grooved lines pitch with constant height heating

Figures 6-7 show the velocity-temperature to height relations with different grooved lines pitch and activated central and lower heat sources. While lower and central installation sections heating, the temperature of the top section does not change significantly. As may be supposed, air flow temperature increase occurs due to blowing-out through the upper grooved lines. In the top unheated section of the channel, the velocities converge and have no relations to the grooved lines pitch.

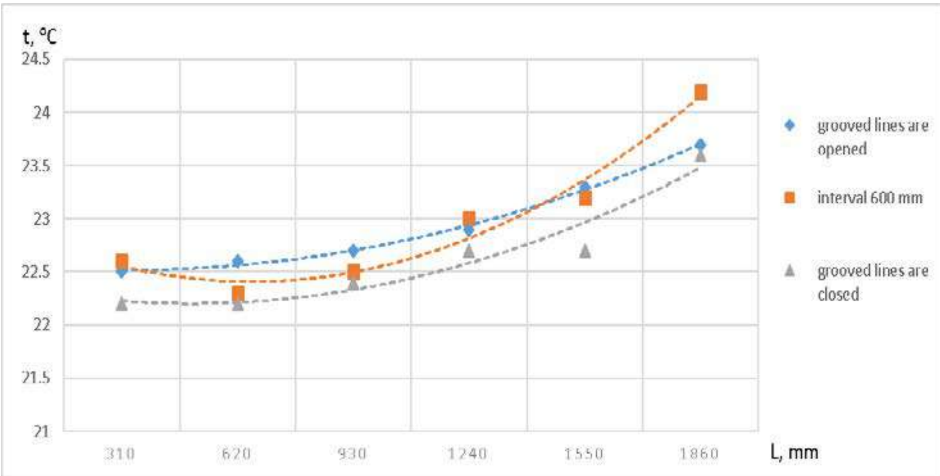

Figure 6. Temperature distribution along the channel height in relation to grooved lines arrangement with activated central and lower heat sources

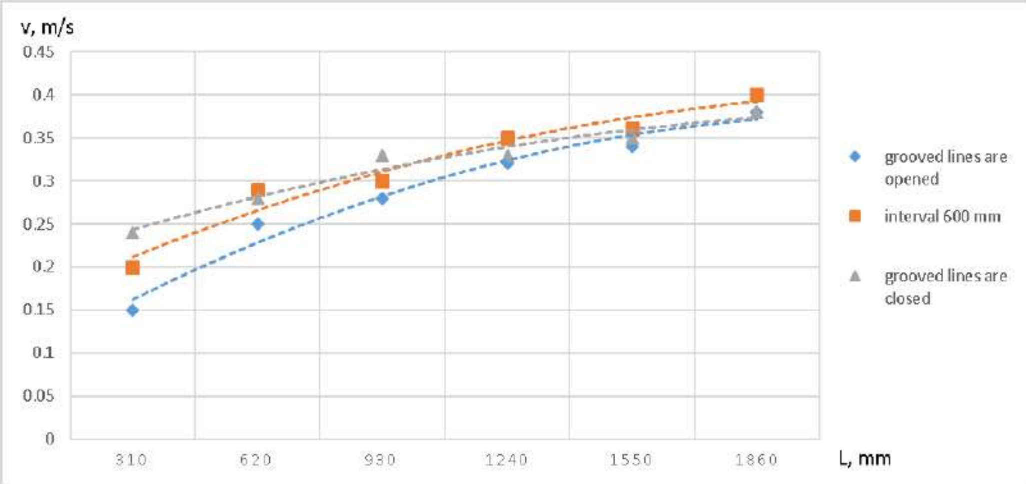

Figure 7. Velocity distribution along the channel height in relation to grooved lines arrangement with activated central and lower heat source

Figures 8-9 show the velocity-temperature to height relations with different grooved lines pitch and activated central and lower heat source. Based on the results it is concluded that temperature and velocity distribution in relation to grooved lines pitch corresponds the above given charts, while heating of channel inlet and outlet, and central section adiabatization. There is minimal fibration of experimental data in central unheated section.

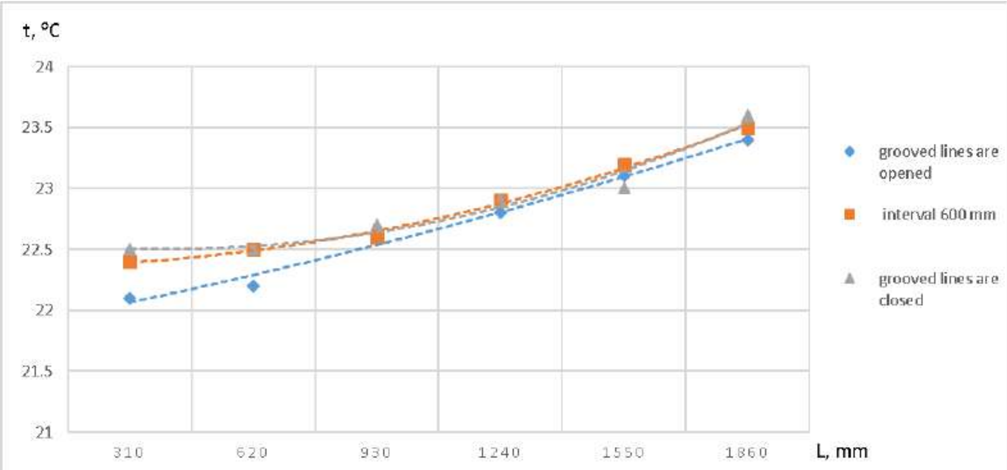

Figure 8. Temperature distribution along the channel height in relation to grooved lines arrangement with activated central and lower heat sources

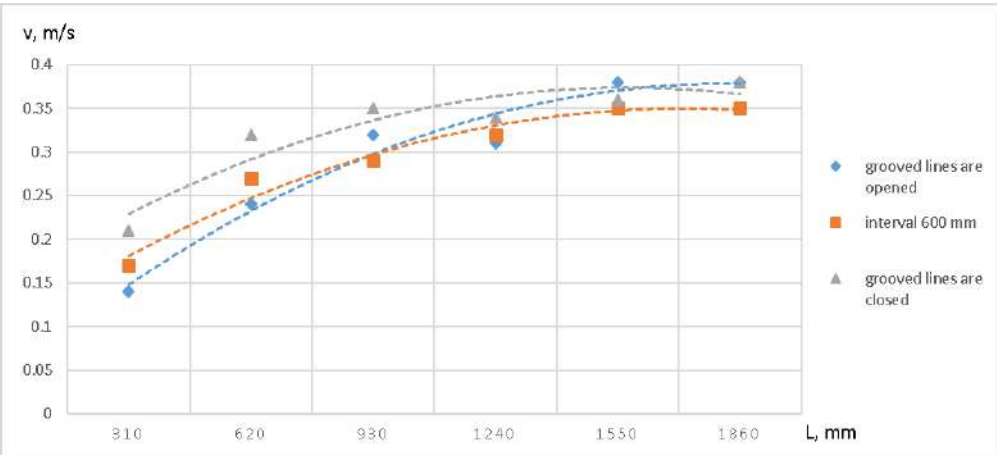

Figure 9. Velocity distribution along the channel height in relation to grooved lines arrangement with activated central and lower heat sources

Figures 10-12 show the velocity to height relation with different variations of heat flow distribution. It was identified that velocity increases in heated areas. From Figures 11, 12 it is observed that the velocity growth rate is maximal in the ideal channel.

This can be explained by inability of high-density air to penetrate the channel, and by change absence of air flow movement with hermetic sealing of grooved lines.

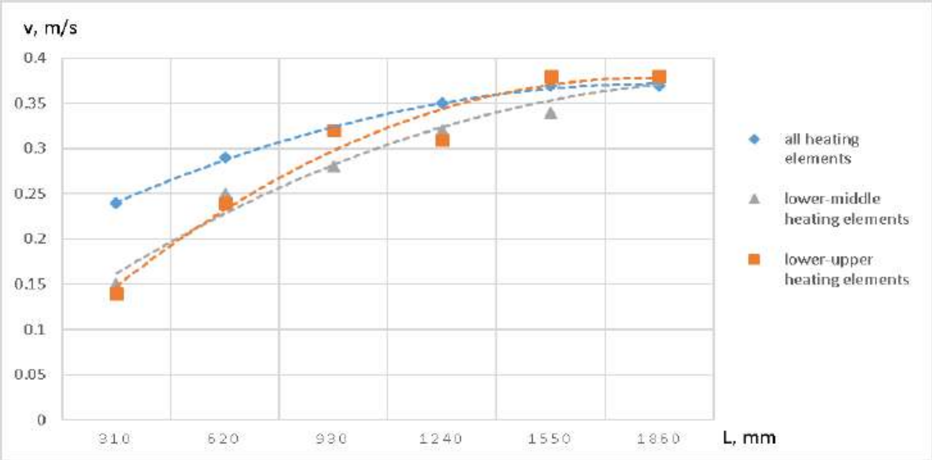

Figure 10. Velocity distribution along the channel height in relation to variations of heat flow with opened grooved lines

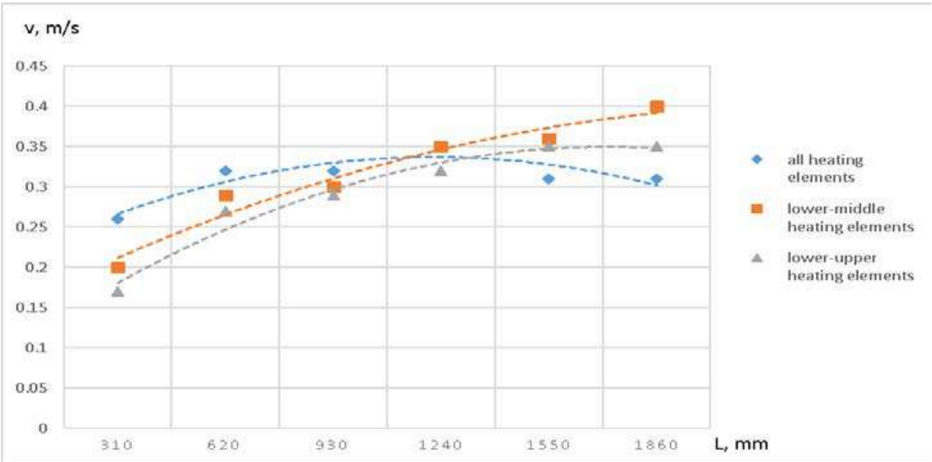

Figure 11. Velocity distribution along the channel height in dependence with heat flow variations with groove line pitch of one meter

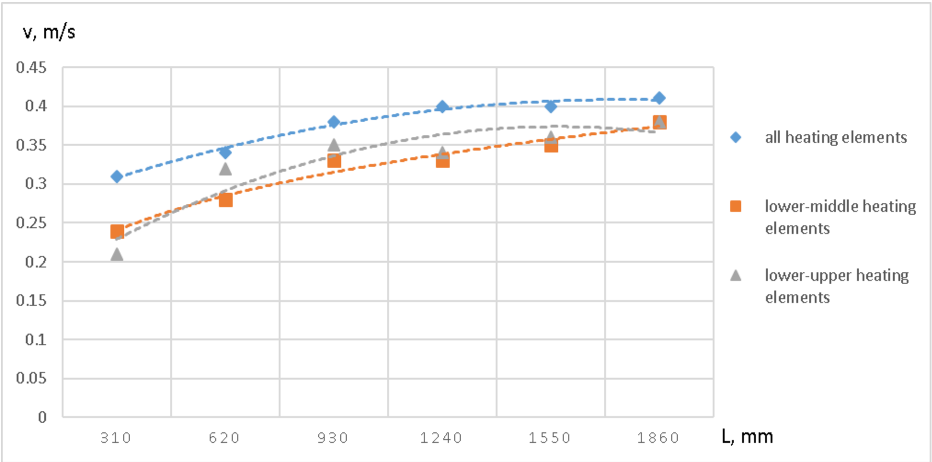

Figure 12. Velocity distribution along the channel height in dependence with heat flow variations in the ideal channel

Statsenko E. A., Ostrovaia A. F., Olshevskiy V.Y, Petrichenko M.R. Temperature and velocity conditions in vertical channel of ventilated facade. *Magazine of Civil Engineering*. 2018. No. 4 (80). Pp. 119–127. doi: 10.18720/MCE.80.11

The main goal of this article is to study the mechanisms of the method of heating the wall on the heat and mass transfer parameters of the facade along its height. The article focuses on the experimental determination of temperature and airflow velocity dependences from combinations of heat sources in the ventilated channel of the facade and the width of the facing layers panels.

In articles by other authors on the same topic are described the heated enclosing structure with a constant temperature and averaged height parameters of the air in the channel [1, 4, 8–9], but the contribution of technological gaps – grooved lines is not taken into account. In this researching examines the influence of the variable position of heat sources and various combinations of grooved lines on the efficiency of the entire system.

4. Conclusions

Based on the results the following conclusions can be summarized:

1. A series of experimental studies was carried out and the result of which it was found that the facade is sensitive to changes in grooved lines number and heating method change.

2. The maximum velocity – around 0.37 m/s – is observed with hermetically-sealed grooved lines (the ideal channel), but at the present time such system is technologically impracticable. Minimum number of grooved lines is optimal (in this case interval is 600 mm).

3. For thermal energy saving purposes, heating of the middle section of the channel can be neglected. When heating of the middle section is neglected, the average velocity undergoes minor changes.

4. Temperature variation rate in different heating areas changes in dependence with grooved lines spacing. The fibration of experimental data in unheated sections is minimal.

Reference

1. Nemova D.V., Olshevskyi V.Ja., Cejtin D.N. Gidrostatika termogravitacionnoj konvekcii v vertikal'nom kanale [Hydrostatics of thermogravitational convection in the vertical channel]. *Nauchno-tehnicheskie vedomosti SPBGPU, Jekonomicheskie nauki.* 2013. Pp. 295–301. (rus)
2. Ostrovaia A.F., Stacenko E.A., Olshevskyi V.Ja., Musorina T.A. Moisture Transfer in Ventilated Facade Structures. *MATEC Web of Conferences*. 2016. Pp. 1-5.
3. Nemova D.V., Emel'janova V.A., Miftahova D.R. Jeksperimental'nye zadachi rascheta svobodnokonvektivnyh dvizhenij v navesnyh ventiliruemyh fasadah [Experimental problems of calculation the free-convection movements in the hinged ventilated facades]. *Magazine of Civil Engineering.* 2010. No. 8. Pp. 46–53. (rus)
4. Emel'janova V.A., Nemova D.V., Miftahova D.R. The optimized design of the hinged ventilated facade. *Magazine of Civil Engineering.* 2014. No. 6. Pp. 67–74. (rus)
5. Petrichenko M.R. Convective heat and mass transfer in combustion chambers of piston engines. Basic results. *Heat transfer. Soviet research.* 1991. Vol. 23(5). Pp. 703–715.
6. Ostrovaia A.F., Petrichenko M.R., Stacenko E.A. The glass ventilated facades. Research of an air gap. *Applied Mechanics and Materials.* 2015. Pp. 725–726.
7. Petrichenko M.R. Rasshcheplyayushchie razlozheniya v predel'nyh zadachah dlya obyknovennyh kvazilinejnyh differencial'nyh [The splitting decomposition in limit tasks for the ordinary quasilinear differential equations]. *Second Edition St. Petersburg State Polytechnical University Journal. Physics and Mathematics.* 2012. Pp. 143–149. (rus)
8. Petrichenko M.R., Petrochenko M.V., Yevtushenko E.B. Hydraulically optimum ventilated gap. *Magazine of Civil Engineering.* 2013. No. 2(37). Pp. 35–40. (rus)

Литература

1. Немова Д.В., Ольшевский В.Я., Цейтин Д.Н. Гидростатика термогравитационной конвекции в вертикальном канале // Научно-технические ведомости СПбПУ, Экономические науки. 2013. С. 295–301.
2. Ostrovaia A.F., Stacenko E.A., Olshevskyi V.Ja., Musorina T.A. Moisture Transfer in Ventilated Facade Structures. MATEC Web of Conferences. 2016. Pp. 1-5.
3. Немова Д.В., Емельянова В.А., Мифтахова Д.Р. Экспериментальные задачи расчета свободноконвективных движений в навесных вентилируемых фасадах // Инженерно-строительный журнал. 2010. № 8. С. 46-53.
4. Емельянова Д.А., Немова Д.В., Мифтахова Д.Р. Оптимизированная конструкция навесного вентилируемого фасада // Инженерно-строительный журнал. 2014. № 6. С. 67–74.
5. Petrichenko M.R. Convective heat and mass transfer in combustion chambers of piston engines. Basic results // Heat transfer. Soviet research. 1991. No. 23(5). Pp. 703–715.
6. Ostrovaia A.F., Petrichenko M.R., Stacenko E.A. The glass ventilated facades. Research of an air gap // Applied Mechanics and Materials. 2015. Pp. 725–726.
7. Петриченко М.Р. Расщепляющие разложения в предельных задачах для обыкновенных квазилинейных дифференциальных уравнений // Научно-технические ведомости Санкт-Петербургского государственного политехнического университета. Физико-математические науки. 2012. С. 143–149.
8. Петриченко М.Р., Петроченко М.В., Явтушенко Е.Б. Гидравлически оптимальная вентилируемая щель // Инженерно-строительный журнал. 2013. № 2(37). С. 35–40.
9. Vatin N.I., Petrichenko M.R., Nemova D.V. Hydraulic methods for calculation of system of rear ventilated facades

9. Vatin N.I., Petrichenko M.R., Nemova D.V. Hydraulic methods for calculation of system of rear ventilated facades. *Applied Mechanics and Materials*. 2014. Vol. 633-634. Pp. 1007–1012.
10. Petrichenko M.R., Petrochenko M.V. Gidravlika svobodnokonvektivnyh techenij v ograzhdayushchih konstrukciyah s vozdushnym zazorom [Hydraulics of free-convective flows in enclosures with an air gap]. *Magazine of Civil Engineering.* 2011. No. 8(26). Pp. 51–56. (rus)
11. Girgidov A.D. Raschety, issledovaniya, ehksperimenty Struktura i teploprovodnost' vozdushnogo potoka v ventiliruemom fasade zdaniya GEHS [Calculations, studies, experiments, Structure and thermal conductivity of the air flow in the ventilated facade of the building HEP]. *Hydraulic engineering*. 2015. No. 6. (rus)
12. Yevtushenko E.B. Fundamentals of hydraulic design for ventilated facades. *Construction of Unique Buildings and Structures.* 2013. No. 2(7). Pp. 55-61. (rus)
13. Gebhart B., Jaluria J., Mahajan R., Sammakia B. *Svobodnokonvektivnye techeniya, teplo - i massoobmen* [Free-convective flow, heat and mass transfer]. MIR. 1991. P. 678. (rus)
14. Lapin V.G., Lapin S.V. Calculation of convective air movement in canadaontario facade in the presence of horizontal cracks between the tiles lining [Calculation of convective air movement in canadaontario facade in the presence of horizontal cracks between the tiles lining]. *Privolzhsky scientific journal.* 2012. No. 2(22). Pp. 85–92. (rus)
15. Petrochenko M.V. *Osnovy gidravlicheskogo rascheta SKT v ograzhdayushchih stroitel'nyh konstrukciyah* [Fundamentals of hydraulic calculation of spiral FCM in the enclosing building structures]. SPbSTU. 2012. P. 20. (rus)
16. Kornienko S.V. Testirovanie metoda rascheta temperaturno-vlazhnostnogo rezhima ograzhdajushhih konstrukcij na rezul'tatah naturnyh izmerenij parametrov mikroklimata pomeshhenij [Testing of a method of calculation of temperature moisture conditions of the protecting designs on results of natural measurements of parameters of a microclimate of rooms]. *Magazine of Civil Engineering.* 2012. No. 2. Pp. 18–23. (rus)
17. Petrichenko M.R., Petrochenko M.V. Dostatochnye uslovija sushhestvovanie svobodno-konvektivnogo techenija v vertikal'nom shhelevom kanale [Sufficient conditions existence of a free and convective current in the vertical slot-hole channel]. *Nauchno-tehnicheskie vedomosti SPBGPU.* 2012. No. 2. Pp. 34–39. (rus)
18. Yevtushenko E.B., Petrochenko M.V. Diffuzornaya konstrukciya navesnogo ventiliruemogo fasada [The diffuser design of ventilated facades]. *Magazine of Civil Engineering.* No. 8. Pp. 38–45. (rus)
19. Nemova D.V., Sistemy ventilyacii v zhilyh zdaniyah kak sredstvo povysheniya ehnergoehffektivnosti [Systems of ventilation in residential buildings as means of increase of energy efficiency]. *Construction of Unique Buildings and Structures.* 2012. Pp. 84–86. (rus)
20. Gagarin V.G., Kozlov V.V. Metodika proverki vypadenija kondensata v vozdushnom zazore ventiliruemogo fasada [Technique of check of loss of condensate in an air gap of the ventilated facade]. *Stroitel'naja fizika v XXI veke.* 2006. Pp. 73–80. (rus)
21. Bukhartsev V.N., Petrichenko M.R. Approximation of the depression curve of the inflow to an ideal trench. *Power Technology and Engineering.* 2011. No. 5. Pp. 374–377.
22. Li J., Chow Y. Heat transfer and air movement behaviour in a double-skin facade. *Centre for Sustainable Energy Technologies (CSET).* 2014. Pp. 198–203.
23. Hana J., Lua L., Penga J., Hongxing Ya. Performance of ventilated double-sided PV facade compared with // Applied Mechanics and Materials. 2014. Vol. 633-634. Pp. 1007–1012.
10. Петриченко М.Р., Петроченко М.В. Гидравлика свободноконвективных течений в ограждающих конструкциях с вентилируемым зазором // Инженерно-строительный журнал. 2011. № 8(26). С. 51–56.
11. Гиргидов А.Д. Расчеты, исследования, эксперименты. Структура и теплопроводность воздушного потока в вентилируемом фасаде здания ГЭС // Гидротехническое строительство. 2015. № 6.
12. Явтушенко Е.Б. Основы гидравлического расчета навесных вентилируемых фасадов // Строительство уникальных зданий и сооружений. 2013. № 2(7). С. 55–61.
13. Гебхарт Б., Джалурия Й., Махаджан Р., Саммакия Б. Свободноконвективные течения, тепло - и массообмен. МИР, 1991. 678 с.
14. Лапин И. Г., Лапин С. В. Расчет конвективного движения воздуха в канале вентилируемого фасада при наличии горизонтальных щелей между плитками облицовки // Приволжский научный журнал. 2012. № 2(22). С. 85–92.
15. Петроченко М.В. Основы гидравлического расчета СКТ в ограждающих строительных конструкциях // Инженерно-строительный журнал. 2012. С. 20–24.
16. Корниенко С.В. Тестирование метода расчета термогравитационного режима ограждающих конструкций на результатах натурных измерений параметров микроклимата помещений // Инженерно-строительный журнал. 2012. № 2. С. 18–23.
17. Петриченко М.Р., Петроченко М.В. Достаточные условия существования свободноконвективного течения в вертикальном щелевом канале // Научно-технические ведомости СПбПУ. 2012. № 32. С. 34–39.
18. Явтушенко Е.Б., Петроченко М.В. Диффузорная конструкция навесного вентилируемого фасада // Инженерно-строительный журнал. № 8. С. 38–45.
19. Немова Д.В. Системы вентиляции в жилых зданиях как средство повышения энергоэффективности // Строительство уникальных зданий и сооружений. 2012. С. 84–86.
20. Гагарин В.Г., Козлов В.В. Методика проверки выпадения конденсата в воздушном зазоре вентилируемого фасада // Строительная физика в XXI веке. 2006. С. 73–80.
21. Bukhartsev V.N., Petrichenko M.R. Approximation of the depression curve of the inflow to an ideal trench // Power Technology and Engineering. 2011. No. 5. Pp. 374–377.
22. Li J., Chow Y. Heat transfer and air movement behaviour in a double-skin facade // Centre for Sustainable Energy Technologies (CSET). 2014. Pp. 198–203.
23. Hana J., Lua L., Penga J., Hongxing Ya. Performance of ventilated double-sided PV facade compared with conventional clear glass façade // Energy and Buildings. 2013. No. 56. Pp. 204–209.
24. Rosca Alin V., Pop Ioan. Flow and heat transfer over a vertical permeable stretching/shrinking sheet with a second order slip // International Journal of Heat and Mass Transfer. 2013. No. 60. Pp. 355–364.
25. Barrios G., Huelsz G., Rechtman R., Rojas J. Wall roof thermal performance differences between air-conditioned and non air-conditioned rooms // Energy and Buildings. 2011. No. 43. Pp. 219–223.
26. Yang H., Feng., Xia G., Wan Q. Experimental study on impact of ventilated double-skin facade on the indoor thermal environment in winter // ISHVAC 2013. 2013. Pp. 384–396.
27. Gaillard L., Giroux-Julien S., Menezo C., Pabiou H. Experimental evaluation of a naturally ventilated PV double-

conventional clear glass façade. *Energy and Buildings.* 2013. Vol. 56. Pp. 204–209.

24. Rosca Alin V., Pop Ioan. Flow and heat transfer over a vertical permeable stretching/shrinking sheet with a second order slip*. International Journal of Heat and Mass Transfer*. 2013. Vol. 60. Pp. 355–364.
25. Barrios G., Huelsz G., Rechtman R., Rojas J. Wall/roof thermal performance differences between air-conditioned and non air-conditioned rooms. *Energy and Buildings*. 2011. Vol. 43. Pp. 219–223.
26. Yang H., Feng., Xia G., Wan Q. Experimental study on impact of ventilated double-skin facade on the indoor thermal environment in winter. *ISHVAC 2013*. 2013. Pp. 384–396.
27. Gaillard L., Giroux-Julien S., Menezo C., Pabiou H. Experimental evaluation of a naturally ventilated PV double-skin building envelope in real operating conditions. *Chair Habitats and Energy Innovations.* 2012. Pp. 54–67.
28. Korniyenko S.V., Vatin N.I., Gorshkov A.S. Thermophysical field testing of residential buildings made of autoclaved aerated concrete blocks. *Magazine of Civil Engineering.* 2016. No. 4(64). Pp. 10–25.
29. Gorshkov A., Vatin N., Nemova D., Shabaldin A., Melnikova L., Kirill P. Using life-cycle analysis to assess energy savings delivered by building insulation. *Procedia Engineering.* 2015. No. 1(117). Pp. 1085–1094.
30. Petritchenko M.R., Subbotina S.A., Khairutdinova F.F., Reich E.V., Nemova D.V., Olshevskiy V.Ya., Sergeev V.V. Effect of rustication joints on air mode in ventilated facade. *Magazine of Civil Engineering.* 2017. No. 5(73). Pp. 40–48.

skin building envelope in real operating conditions // Chair Habitats and Energy Innovations. 2012. Pp. 54–67.

28. Корниенко С.В., Ватин Н.И., Горшков А.С., Натурные теплофизические испытания жилых зданий из газобетонных блоков // Инженерно-строительный журнал. 2016. № 4(64). С. 10–25.
29. Gorshkov A., Vatin N., Nemova D., Shabaldin A., Melnikova L., Kirill P. Using life-cycle analysis to assess energy savings delivered by building insulation // Procedia Engineering. 2015. No. 117(1). Pp. 1085–1094.
30. Петриченко М.Р., Субботина С.А., Хайрутдинова Ф.Ф., Рейх Е.В., Немова Д.В., Ольшевский В.Я., Сергеев В.В. Влияние рустов на воздушный режим в вентилируемом фасаде // Инженерно-строительный журнал. 2017. № 5(73). С. 40–48.

Elena Statsenko,
+7(981)839-85-38; staclena@mail.ru

Anastasiia Ostrovaia,
+7(953)344-90-63; stasya2609@yandex.ru

Vyacheslav Olshevskiy,
+7(911)919-95-26; 79119199526@yandex.ru

Mikhail Petrichenko,
+7(921)330-04-29; fonpetrich@mail.ru

Елена Александровна Стаценко,
+7(981)839-85-38; эл. почта: staclena@mail.ru

Анастасия Федоровна Островая,
+7(953)344-90-63;
эл. почта: stasya2609@yandex.ru

Вячеслав Янушевич Ольшевский,
+7(911)919-95-26;
эл. почта: 79119199526@yandex.ru

Михаил Романович Петриченко,
+7(921)330-04-29; эл. почта: fonpetrich@mail.ru

doi: 10.18720/MCE.80.12

The effect of reinforcement corrosion on the adhesion between reinforcement and concrete

Влияние коррозии арматуры на сцепление между арматурой и бетоном

V.Y. Lushnikova*,
A.G. Tamrazyan,
National Research Moscow State Civil Engineering University, Moscow, Russia

Магистрант В.Ю. Лушникова*,
д.т.н., зав. кафедрой А.Г. Тамразян,
Национальный исследовательский Московский государственный строительный университет, Москва, Россия

Key words: corrosion; mass loss; adhesion strength; anchoring

Ключевые слова: коррозия; потеря массы; прочность сцепления; анкеровка

Abstract. Due to aggressive environmental conditions, the adhesion between reinforcement and concrete deteriorates. This factor has a significant influence on the safety and efficiency of buildings and structures. The strength of adhesion between reinforcement and concrete decreases in the process of corrosion, and therefore requires a longer anchoring length of the reinforcement. The longer the anchoring length, the greater the guarantee that the destruction of the reinforcement in concrete does not occur until the lifetime of the reinforced concrete elements is expired. Various parameters affecting the reinforcement adhesion strength in reinforced concrete elements are considered. The ratio of the thickness of the protective layer and the diameter of the reinforcement (*c/ds*) affects the adhesion strength. With a higher (*c/ds*) ratio the loss of the adhesion strength is less than with a lower (*c/ds*) ratio. The mass loss of the reinforcement is an important parameter, and it can determine the level of corrosion. This value can be used for the development of the correlation between corrosion, cracking, the adhesion and ultimate strength of reinforced concrete elements.

Аннотация. Из-за агрессивных условий окружающей среды происходит ухудшение сцепления между арматурой и бетоном. Это значительно влияет на безопасность и работоспособность зданий и сооружений. Прочность сцепления между арматурой и бетоном уменьшается в процессе коррозии, и поэтому требуется большая длина анкеровки арматуры. Чем больше длина анкеровки, тем больше гарантия, что разрушение арматуры в бетоне не происходит до окончательного срока службы в железобетонных элементах. Рассматриваются различные параметры, влияющие на прочность сцепления арматуры в железобетонных элементах. Соотношение толщины защитного слоя и диаметра арматуры (*c/ds*) влияет на прочность сцепления. С более высоким (*c/ds*) отношением потеря прочности сцепления меньше, чем с более низким (*c/ds*) отношением. Потеря массы арматуры является важным параметром, и она определяет уровень коррозии. Это значение используется для разработки корреляции между коррозией, растрескиванием, прочностью сцепления и предельной прочностью железобетонных элементов.

1. Introduction

The object of the study is the analysis of analytical data of 60x40 cm reinforced concrete beams strengthened with steel bars.

Many scientists were engaged in studying the problems of corrosion of reinforcement in concrete in the field of theoretical and experimental research of reinforced concrete elements. Such names as V.E. Rumyantsev, V.S. Konovalova [1], A.I. Mozhukhina, S.E. Nikin [2, 8], D.S. Popov [3], A.G. Tamrazyan [3–7], L. Amleh [11], W.L. Jin [10, 12], Zhang Ju [15] and many others should be noted.

The relevance of research. Corrosion is a permanent destruction caused by physical and chemical damage of materials under environmental conditions [1]. Metal corrosion is a destructive result of a chemical or electrochemical reaction between a metal and the surrounding environment. It is regulated by energy changes, the release of free energy from the system into the environment. The phenomenon of metal corrosion has attracted much more attention of researchers around the world than any other type of material deterioration. This is because many metals and alloys, including steel, which is an important building material, are corroded and pose a serious challenge for our economy.

Лушникова В.Ю., Тамразян А.Г. Влияние коррозии арматуры на сцепление между арматурой и бетоном // Инженерно-строительный журнал. 2018. № 4(80). С. 128–137.

The behavior of the reinforced concrete element to a certain extent depends on the adhesion between the reinforcement and the surrounding concrete [2]. When the tensile force in the reinforcement can not be transferred to the concrete, or when the adhesion breaks, the resistance of the element will be significantly reduced. The problem of adhesion can be more dangerous than reducing the cross-sectional area of the reinforcement [3–7]. When the reinforcement corrodes due to carbonation or chloride absorption, the amount of corrosion products can increase significantly, thereby producing strong radial pressure inside the concrete on the surface of the reinforcement. Longitudinal and transverse cracking can develop when the radial pressure exceeds the ultimate strength of the concrete. This can worsen the adhesion between the reinforcement and concrete and reduce the bearing capacity of the reinforced concrete element.

The adhesion between the reinforcement and the concrete is due to the engagement of protrusions on the reinforcement surface (mechanical blocking), clutching and friction in the concrete [8].

The mechanical blocking between the reinforcement and the concrete depends on the surface profile of the reinforcement. For the deformed reinforcing steel bars, the geometry of the ribs along the bar length increases the mechanical blocking by the bar and the concrete. At higher load levels, the force is mainly transmitted by mechanical blocking between the ribs and concrete protrusions with adhesion and friction between the concrete and the reinforcement. When the ultimate strength of adhesion is reached, the tensile force in the reinforcement generates considerable crushing around the reinforcement ribs, then the shear cracks begin to form in the concrete protrusions. Two mechanical failures can appear on the edges of the deformed reinforcing steel bars. In one case, the concrete presses locally on the supporting surface of the concrete protrusion (Fig. 1b). Another mechanism is the destruction from shear over the concrete protrusion between the ribs (Fig. 1a). Two mechanisms are shown in the Figure 1.

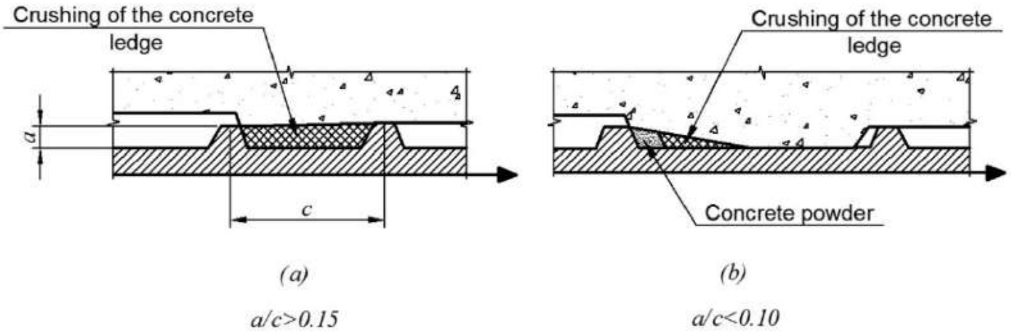

Figure 1. Mechanical failures on the ribs of the deformed reinforcement

Adhesion is a chemical bond on the surface between the reinforcement and the concrete, which plays a significant role in the development of adhesion at relatively low loads. But it is quickly lost as the load increases, so this factor is not reliable. The adhesion strength due to adhesion is generally from 0.48 to 1.03 MPa [9].

Friction: the surface characteristics of the reinforcement influence the frictional adhesion of the reinforcement. Friction engagement serves as a function of adhesion after the loss of chemical adhesion. Friction engagement can provide up to 35 % of the ultimate adhesion strength due to the concrete layer splitting [9].

The aim of the study is to determine the effect of reinforcement corrosion on the adhesion strength between reinforcement and concrete at different levels of corrosion.

Tasks of the study:

- determination of the level of corrosion of the reinforcement from the mass loss of the reinforcement during the process of corrosion;
- influence of various parameters (*W/C*, the ratio of the thickness of the protective layer to the diameter of the reinforcement (c/d_s), the profile of the reinforcement) on the adhesion strength between reinforcement and concrete at different levels of corrosion;
- finding the required length of anchoring in concrete elements.

2. Methods

The adhesion behavior on the reinforcing concrete interface is mainly determined by the surface characteristics of the reinforcing bar, so the transmission of forces at the junction for smooth reinforcing bars and bars of the deformed reinforcement is different [2]. After the reinforcement begins to corrode, corrosion products are formed on its surface, changing the steel bar surface profile. Therefore, the surface characteristics of the reinforcement and the contact conditions between the reinforcement and the concrete vary significantly, which affects the adhesion characteristics between the reinforcement and concrete.

Smooth reinforcing bar: the adhesion strength between the reinforcement and the concrete is mainly determined by chemical adhesion, engagement and friction on the surface of the reinforcement. When the reinforcement begins to corrode, the rust is gradually formed on the surface of the reinforcement, which changes the surface characteristics of the smooth reinforcing bar. Friction between the reinforcement and the concrete is significantly increased, so the adhesion can increase up to 2-3 times after the reinforcement begins to corrode [10]. As the volume of corrosion products increases, the concrete undergoes increased radial pressure, and when the pressure exceeds the adhesion strength cracking occurs. It leads to a rapid reduction of the adhesion strength due to the decrease of concrete protrusions and the peeling layer of corrosion products on the surface of the bar.

Table 1 shows the results of experimental tests of a detailed study of the strength of a smooth reinforcing bar of [10]. The diameter of a smooth reinforcing bar is d_s = 12 mm, the anchoring length l_{an} = 150 mm, the thickness of the concrete protective layer c = 44 mm, w/c = 0.55, R_{sc} = 389 MPa, R_b = 22.1 MPa.

Table 1: Data of the pull-out adhesion strength of a smooth reinforcing bar in concrete samples

Samples	Adhesion strength, (MPa)	Coefficient of adhesion strength (*)	Wight loss Δ_m , (%)	Thickness of corrosion products, (mm)
1	2.65	1.23	0.27	0.0162
2	3.23	1.01	0.29	0.0174
3	5.97	2.27	0.92	0.0549
4	5.84	2.18	1.13	0.0674
5	7.41	2.82	0.78	0.0466
6	8.63	3.28	1.47	0.0876
7	7.3	2.78	1.85	0.1100
8	7.96	3.03	1.50	0.0893
9	9.29	5.53	1.99	0.1182
10	10.26	3.9	1.04	0.1212
11	5.97	2.27	2.75	0.1628
12	4.84	1.84	2.43	0.2024
13	3.75	1.43	4.77	0.2797
14	1.63	0.62	5.01	0.2934

* Coefficient of the adhesion strength is the adhesion strength of a corroded sample / adhesion strength of a non-corroded sample

The results are shown in Figure 2.

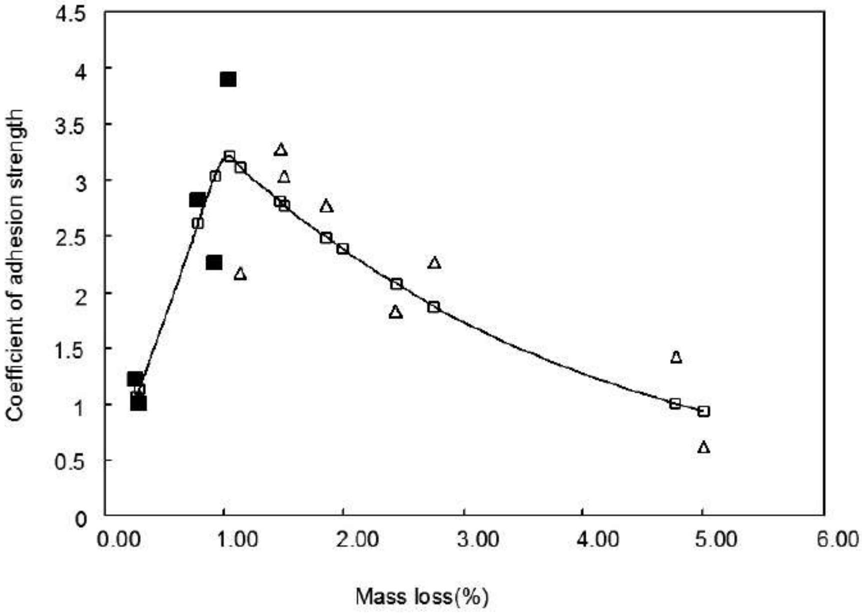

Figure 2. Effect of corrosion on the adhesion of a smooth reinforcement bar in concrete samples [10]

Deformed reinforcement: the adhesion between the deformed reinforcement and the concrete is mainly determined by mechanical blocking between the ribs of the deformed reinforcement and the concrete protrusions and small deposits effected by adhesion and friction [2, 11]. Corrosion affects the connection between the reinforcement and the concrete. Based on the results of pull-out tests (Figure 3 and Table 2) the adhesion strength increases at low corrosion levels (about 1–3 % mass loss) when a thin solid layer of corrosion products forms on the surface of the reinforcement [12]. However, this solid layer of corrosion products is converted into a peeling layer at higher corrosion levels with a corresponding deterioration of both the adhesion strength and sliding characteristics. At higher corrosion levels, the adhesion strength decreases almost linearly with further increase in mass loss. When the mass loss exceeds 20 %, only 15 % of the original adhesion strength remains. A slight improvement in the characteristics of the adhesion strength at low corrosion levels is due to the changes in the characteristics of the deformed reinforcement surface layer. Another crucial factor affecting the change in the adhesion strength between the deformed reinforcement and the concrete at higher corrosion levels is deterioration of the characteristics of the reinforcement protrusions, which significantly reduces the blocking between the reinforcement protrusions and the concrete [13].

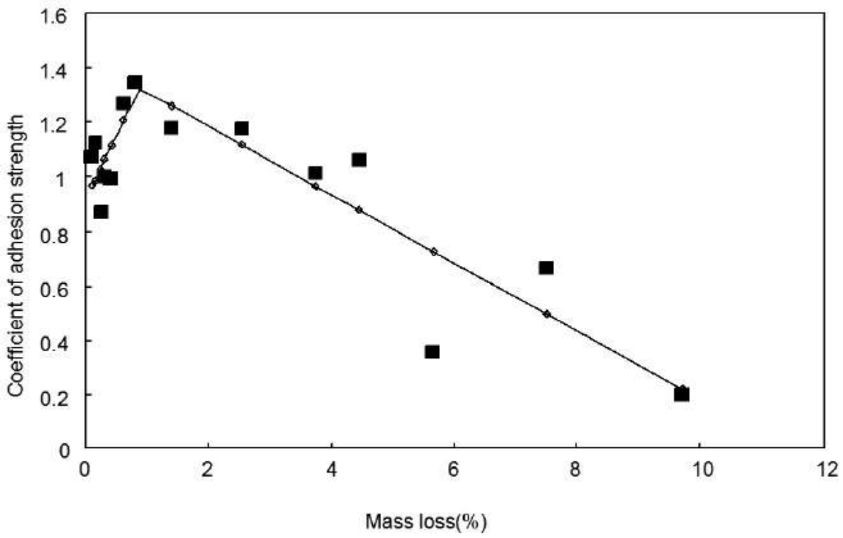

Figure 3. Effect of corrosion on the adhesion for concrete samples with the deformed reinforcement, d_s = 12 mm, the anchoring length is l_{an} = 150 mm, the thickness of the protective layer of concrete c = 44 mm, w/c = 0.55, R_{sc} = 389 MPa, R_b = 22.13 MPa [10]

Table 2. Data of the pull-out adhesion strength of the deformed reinforcement in concrete samples [10]

Samples	Adhesion strength, (MPa)	Coefficient of adhesion strength (*)	Mass loss Δ_m, (%)	Thickness of corrosion products, (mm)
1	8.92	1.07	0.12	0.0072
2	9.49	1.12	0.16	0.0092
3	7.36	0.87	0.24	0.0144
4	8.46	1.00	0.32	0.0192
5	8.39	0.99	0.43	0.0257
6	10.62	1.27	0.62	0.0371
7	11.35	1.34	0.81	0.0484
8	9.99	1.18	1.40	0.0834
9	9.95	1.18	2.54	0.1505
10	8.59	1.02	3.75	0.2209
11	8.70	1.06	4.45	0.2603
12	5.97	0.35	5.68	0.3316
13	4.64	0.67	7.50	0.4343
14	1.66	0.20	9.72	0.5177

Figure 4 shows that the tensile samples show a gradual decrease in the relative adhesion strength with increasing corrosion. It can also be seen from Figure 5 that the adhesion strength of concrete samples *w/c* = 0.32 are close to the samples *w/c* = 0.42.

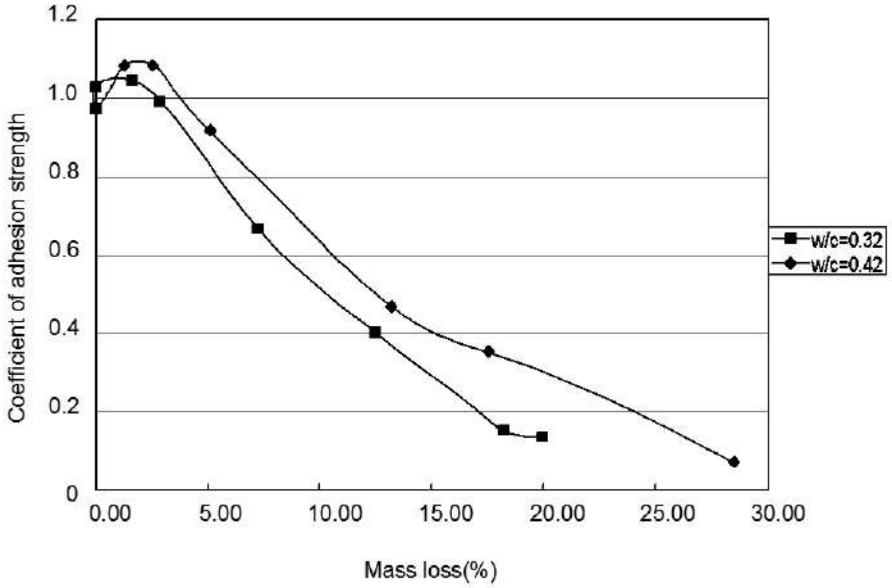

Figure 4. The relationship between the adhesion strength and the reinforcement mass loss [11]

The ratio of the thickness of the protective layer to the reinforcement size (c/d_s) is an equally important variable influencing the concrete resistance to the chloride effect. Figure 5 shows a sharp decrease of the adhesion strength in a sample with a protective layer thickness and bar diameter c/d_s = 1.28, whereas for a sample with a c/d_s ratio of 5.12, a decrease in the adhesion strength is less. It shows that in a sample with a higher (c/d_s) ratio, the loss of bond strength is not as significant as in the case of a lower (c/d_s) ratio. These studies also showed that the ratio of the thickness of the protective layer to the bar diameter is an important indicator of resistance to corrosion of reinforcing bars due to the penetration of chlorides [14–17].

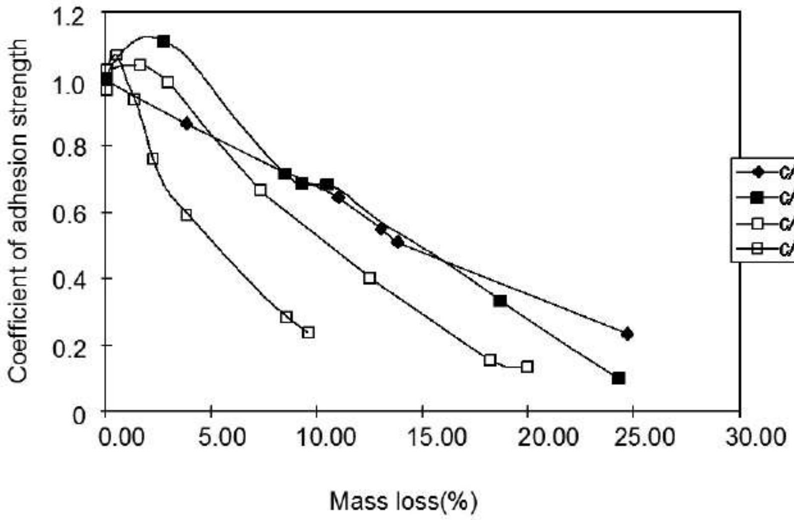

Figure 5. The ratio of the adhesion strength to the corrosion level (ratio of the thickness of the protective layer and the reinforcement diameter (c/d_s)) [11]

Figure 6 shows the mass loss of the reinforcing bar due to chloride corrosion for 70 years for different levels of chloride concentration. This result is applied to a concrete beam in which the reinforcement diameter is d_s = 16 mm, the thickness of the protective layer is c = 40 mm, the compressive strength of concrete, R_b = 30 MPa and the reinforcement strength, R_{sc} = 400 MPa, subjected to different levels of surface chloride varying from 1 to 6 %. In this example, the coefficient of thickness of the protective layer to the reinforcement diameter is c/ds = 2.67. If the structural element is designed for a 70-year lifetime, the mass loss can reach 21% at the end of its lifetime, and loss of the adhesion strength will reach more than 80 % (Figure 5). Therefore, the ratio of the thickness of the concrete protective layer and the size of the reinforcement c/d_s = 2.67 is not sufficient for a lifetime of 70 years. Thus, this design requires a larger ratio of the thickness of the protective layer and the size of the reinforcement (c/d_s).

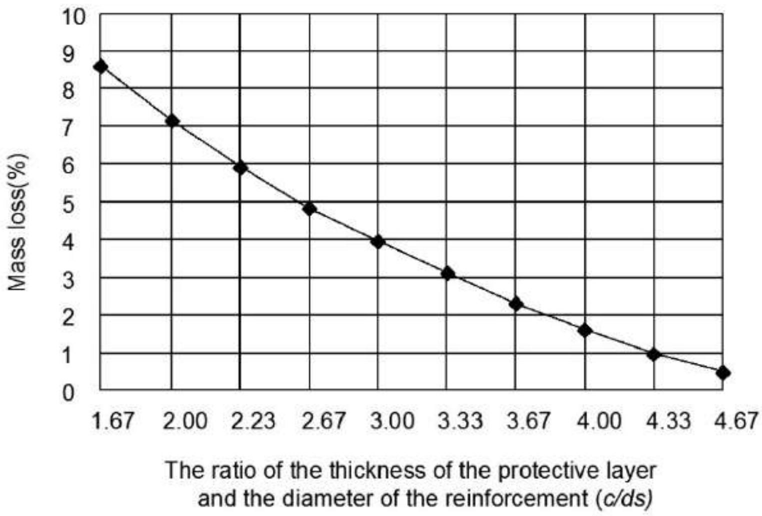

Figure 6. The relationship between the loss of reinforcement mass and the ratio of the thickness of the protective layer and the diameter of the reinforcement (c/d_s) [10]

The examination of the steel bar embedded in the tensile samples showed deep pits on the surface, which showed that the geometric shape and size of the steel bar had a significant effect on the force transfer from steel to concrete due to the mechanical blocking of ribs susceptible to corrosion. Therefore, the adhesion between the deformed reinforcement and the concrete, which mainly depends on the mechanical blocking of the ribs, is weakened by the effect of corrosion.

For durability, you must carefully choose the size and geometry of the reinforcement. Half of the anchoring length remains to ensure safety during the lifetime of the structure in this environment [18–19].

3. Results and Discussion

Based on the pulling-out experimental results [11], formulas for the adhesion strength of the reinforcement depending on the mass loss are presented:

$$\text{at w/c = 0.32, } R_{st} = (0.35 + 0.3\frac{c}{d_s})\sqrt{1.284R_b} - 0.42(\Delta_m \cdot 100\%)$$
$$\text{at w/c = 0.42, } R_{st} = (0.35 + 0.3\frac{c}{d_s})\sqrt{1.425R_b} - 0.34(\Delta_m \cdot 100\%) \quad (1)$$

Let us assume that the reinforcement diameter d_s = 20 mm (the ratio *w/c* = 0.42, R_b = 51 MPa) with a protective layer thick as *c* = 50 mm, has a mass loss Δ_m = 5.1 % for a certain period of the structure. The strength of adhesion between the corroded core and the concrete:

$$R_{st} = \left(0.35 + 0.3\frac{c}{d_s}\right)\sqrt{1.425R_b} - 0.34(\Delta_m * 100\%) = \left(0.35 + 0.3\frac{50}{20}\right)\sqrt{1.425 * 51} - 0.34 * 5.1 = 7.64\ MPa$$

The experimental value of the adhesion strength for the sample (*w/c* = 0.42, Δ_m = 5.1%, thickness of the protective layer *c* = 50 mm, d_s = 20 mm) is R_{st} = 8.14 MPa, which corresponds to the calculated value of R_{st}.

To obtain the estimated strength of adhesion, we take:

$$R_{st.d} = 0.65 \times R_{st} \quad (2)$$

Based on the adhesion strength formulas (1) and (2), the anchoring length l_{an} can be derived. To ensure sufficient adhesion of the reinforcing bar along its length, the anchoring length of the bar l_{an} should be provided. The bar cannot be pulled out if it has sufficient anchoring [20]. When the bar is pulled out, it slides. If at the time of pulling the bar is poorly fixed in the concrete, then it reaches the yield point [21]. The actual adhesion strength will be large near the surface and equal to zero in the anchoring. When the bar slides with a small tensile force, the adhesion strength is higher in the anchoring than in other parts of the bar. With the increase in the applied load, the strength of the adhesion will increase significantly in the anchoring, so the strength of the adhesion along the entire length is not considered. In case of failure, the strength along the bar will be distributed more evenly [22–23]. Therefore, the equilibrium condition between the internal forces of adhesion and the force applied to the anchoring can be:

$$A_s R_{sc} = R_{st} l_{an} \pi d_s \quad (3)$$

where R_{st} – adhesion strength

$A_s = \pi d_s^2 / 4$ – cross-sectional area of the bar

R_{sc} – ultimate tensile strength of reinforcement

l_{an} – length of anchoring of reinforcement in concrete

d_s – bar diameter

Substituting the value of A_s in (3), we obtain:

$$l_{an} = \frac{R_{sc}}{4R_{st}} d_s \quad (4)$$

The structural length of the anchoring of the reinforcement in the concrete can be obtained by increasing the anchoring length l_{an} by 20 % to provide a bearing capacity when the stress in the reinforcement is exceeded, ε_y. Replacing $R_{st,d}$ by R_{st}, to consider the variability of the data:

$$l_{an,d} = 1.2 \times \frac{R_{sc}}{4R_{st.d}} d_s = 1.2 \times \frac{R_{sc}}{4 \times 0.65 R_{st}} d_s = 0.462 \frac{R_{sc}}{R_{st}} d_s \quad (5)$$

Therefore, the minimum anchoring length l_{an} under tension at different corrosion levels can be obtained from equation (1):

$$\text{at w/c = 0.32, } l_{an,d} = 0.462 \times R_{sc} \times d_s / \left[(0.35 + 0.3\frac{c}{d_s})\sqrt{1.284R_b} - 0.42(\Delta_m \cdot 100\%)\right]$$
$$\text{at w/c = 0.42, } l_{an,d} = 0.462 \times R_{sc} \times d_s / \left[(0.35 + 0.3\frac{c}{d_s})\sqrt{1.425R_b} - 0.34(\Delta_m \cdot 100\%)\right] \quad (6)$$

where R_{sc} – ultimate tensile strength of reinforcement

c – thickness of concrete protective layer

Let us assume that the reinforced concrete beam (*w/c* = 0.42) has the lifetime of 70 years, the reinforcement diameter d_s = 16 mm; thickness of the protective layer of concrete *c* = 40 mm; strength of concrete for compression, R_b = 30 MPa; yield strength of steel, R_{sc} = 400 MPa; at a surface chloride concentration of 3 %, the threshold level of corrosion is considered equal to 0.4 % (Cl ') by the cement weight.

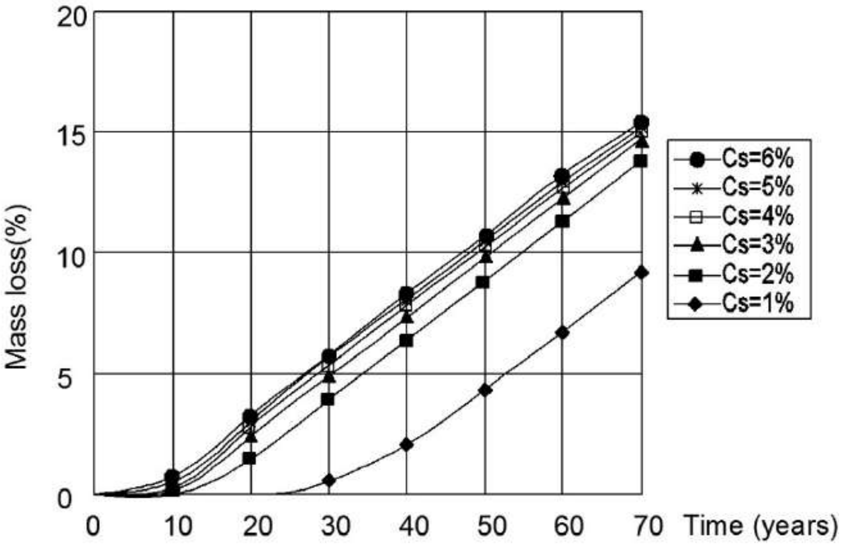

Figure 7. Mass loss of reinforcement due to chloride corrosion over 70 years of lifetime for different concentrations of sodium chloride (Cs))

From Figure 7, the mass loss of the reinforcement in the 70th year is projected at 14.73 %; therefore the estimated length of the anchoring should not be less than:

$$l_{an,d} = 0.462 \times R_{sc} \times d_s / \left[(0.35 + 0.3\frac{c}{d_s})\sqrt{1.425 R_b} - 0.34\left(\Delta_m \cdot 100\%\right) \right] =$$

$$0.462 \times 400 \times 16 / \left[(0.35 + 0.3\frac{40}{16})\sqrt{1.425 \times 30} - 0.34 \times 14.73 \right] = 1350 mm$$

In a corrosion-free environment at Δ_m = 0, the embedment length will be l_{an} = 411 mm.

4. Conclusions

A model for predicting the mass loss of the reinforcement at different levels of corrosion when chloride penetrates concrete is proposed. At the initial stage of reinforcement corrosion due to the peeling layer, the adhesion strength between the reinforcement and concrete is increased to two or three times. The mass loss of the reinforcement is an important parameter; it can determine the level of corrosion and the adhesion strength. The results show that the mass loss of the reinforcing bar in concrete depends on many factors such as chloride concentration on the surface of concrete, the thickness of the protective layer of concrete and permeability of concrete, the size of the reinforcing bar and the ratio of thickness of the protective layer of concrete and the diameter of the steel reinforcement. If the concentration of sodium chloride is more than 2 %, the steel reinforcement in concrete will undergo serious corrosion. An enlarged protective layer of concrete and a lower permeability of concrete can reduce the mass loss of the reinforcement in concrete.

An increase in the ratio (c/d_s) also helps to reduce the mass loss of the reinforcement in concrete, thus prolonging the lifetime of the structural system.

A preliminary design equation for the anchoring length at different corrosion levels is presented. The results show that for an aggressive environment a large anchoring length, approximately 3 times longer than for a non-aggressive environment, for a certain lifetime of the reinforced concrete elements is required. The length of the reinforcement anchoring should not be a "weak link" when chlorides penetrate the concrete.

References

1. Rumyantseva V.E., Konovalova V.S. Korroziya stal'noy armatury v betone: prichiny, posledstviya, sposoby predotvrashcheniya [Corrosion of steel reinforcement in concrete: causes, consequences, methods of prevention]. *Information environment of the university.* 2015. No. 1. Pp. 153–158. (rus)
2. Morzhukhina A.I., Nikitin S.E. Opredeleniye glubiny korrozii armatury v betone pod vozdeystviyem khloridosoderzhashchey sredy [Determination of the depth of corrosion of reinforcement in concrete under the influence of a chloride-containing medium]. *Fundamental and applied scientific research: current issues, achievements and innovations, collection of articles of the IX International Scientific and Practical Conference: in 4 part.* 2018. Pp. 27–29. (rus)
3. Tamrazyan A.G., Popov D.S. K vliyaniyu armirovaniya szhatoy zony izgibayemogo zhelezobetonnogo elementa na kinetiku razvitiya korrozionnykh povrezhdeniy [To the effect of the reinforcement of the compressed zone of a bent ferro-concrete element on the kinetics of the development of corrosion damage]. *Science and Innovations in Construction (to the 45th anniversary of the Department of Construction and Municipal Economy): a collection of reports of the International Scientific and Practical Conference: in 2 tons Belgorod State Technological University V.G. Shukhov*. 2017. Pp. 153–157. (rus)
4. Tamrazyan A.G. Nauchnyye osnovy otsenki riska i obespecheniya bezopasnosti zhelezobetonnykh konstruktsiy, zdaniy i sooruzheniy pri kombinirovannykh osobykh vozdeystviyakh [Scientific basis for risk assessment and safety of reinforced concrete structures, buildings and structures under combined special effects]. *Herald of SIC Construction.* 2018. No. 1(16). Pp. 106–114. (rus)
5. Lublinsky V.A., Tamrazyan A.G. Bezopasnost' nesushchikh sistem mnogoetazhnykh zdaniy pri lokal'nom izmenenii zhestkostnykh kharakteristik nesushchikh elementov [Safety of load-bearing systems in multi-storey buildings with a local change in the stiffness characteristics of load-bearing elements]. *Concrete and reinforced concrete - a look into the future. Scientific works of the III All-Russian (II International) Conference on Concrete and Reinforced Concrete: In seven volumes.* 2014. Pp. 90–99. (rus)
6. Mirsayapov I.T., Tamrazyan A.G. K raschetu zhelezobetonnykh konstruktsiy na vynoslivost' [To the calculation of reinforced concrete structures for endurance]. *Industrial and civil construction.* 2016. No. 11. Pp. 19–23. (rus)
7. Tamrazyan A.G. Beton i zhelezobeton: problemy i perspektivy [Concrete and reinforced concrete: problems and prospects]. *Industrial and civil construction*. 2014. No. 7. Pp. 51–54. (rus)
8. Morzhukhina AI, Nikitin S.E. Korroziya armatury v betone pod vozdeystviyem agressivnoy sredy [Corrosion of reinforcement in concrete under the influence of an aggressive environment]. *INTERNATIONAL INNOVATION RESEARCH the collection of articles of the XII International Scientific and Practical Conference: in 3 parts.* 2018. Pp. 162–165. (rus)
9. Selyaev V.P., Novichkov P.I., Novichkova E.N., Kimyayeva E.V. Napryazhennoye sostoyaniye v betone, svyazannoye s korroziyey armatury [Stress state in concrete associated with corrosion of reinforcement]. *Longevity of building materials, products and structures Materials of the All-Russian scientific and technical conference dedicated to the memory of Honored Scientist of the Russian Federation, Academician of RAASN, Doctor of Technical Sciences, Professor Solomatova Vasily Ilich.* 2016. Pp. 127–135. (rus)
10. Jin W.-l., Yuxi L. Durability of Concrete Structures. Science Publishing Company. Beijing. 2002.

Литература

1. Румянцева В.Е., Коновалова В.С. Коррозия стальной арматуры в бетоне: причины, последствия, способы предотвращения // Информационная среда вуза. 2015. № 1. С. 153–158.
2. Моржухина А.И., Никитин С.Е Определение глубины коррозии арматуры в бетоне под воздействием хлоридосодержащей среды // Сборник: Фундаментальные и прикладные научные исследования: актуальные вопросы, достижения и инновации сборник статей IX Международной научно-практической конференции: в 4 ч. 2018. С. 27–29.
3. Тамразян А.Г., Попов Д.С. К влиянию армирования сжатой зоны изгибаемого железобетонного элемента на кинетику развития коррозионных повреждений // Сборник: Наука и инновации в строительстве (к 45-летию кафедры строительства и городского хозяйства): сборник докладов международной научно-практической конференции: в 2 т. Белгородский государственный технологический университет им. В.Г. Шухова. 2017. С. 153–157.
4. Тамразян А.Г. Научные основы оценки риска и обеспечения безопасности железобетонных конструкций, зданий и сооружений при комбинированных особых воздействиях // Вестник НИЦ Строительство. 2018. № 1(16). С. 106–114.
5. Люблинский В.А., Тамразян А.Г. Безопасность несущих систем многоэтажных зданий при локальном изменении жесткостных характеристик несущих элементов // Сборник: Бетон и железобетон - взгляд в будущее. Научные труды III Всероссийской (II Международной) конференции по бетону и железобетону: В семи томах. 2014. С. 90–99.
6. Мирсаяпов И.Т., Тамразян А.Г. К расчету железобетонных конструкций на выносливость // Промышленное и гражданское строительство. 2016. № 11. С. 19–23.
7. Тамразян А.Г. Бетон и железобетон: проблемы и перспективы // Промышленное и гражданское строительство. 2014. № 7. С. 51–54.
8. Моржухина А.И., Никитин С.Е. Коррозия арматуры в бетоне под воздействием агрессивной среды // Сборник: INTERNATIONAL INNOVATION RESEARCH сборник статей XII Международной научно-практической конференции: в 3 частях. 2018. С. 162–165.
9. Селяев В.П., Новичков П.И., Новичкова Е.Н., Кимяева Е.В. Напряженное состояние в бетоне, связанное с коррозией арматуры // Сборник: Долговечность строительных материалов, изделий и конструкций Материалы Всероссийской научно-технической конференции, посвященной памяти заслуженного деятеля науки Российской Федерации, академика РААСН, доктора технических наук, профессора Соломатова Василия Ильича. 2016. С. 127–135.
10. Jin W.-l., Yuxi L. Durability of Concrete Structures. Science Publishing Company. Beijing. 2002.
11. Amleh L. Bond deterioration of reinforcing steel in concrete due to corrosion. PhD Thesis: Department of Civil Engineering and Applied Mechanics McGill University. 2002.
12. Wong H.S., Karimi A.R., Buenfeld N.R., Zhao Y.X., Jin W.L. On the penetration of corrosion products from reinforcing steel into concrete due to chloride-induced corrosion // Corrosion Science. 2010. Vol. 52. № 7. Pp. 2469–2480.
13. Каблов Е.Н., Старцев О.В., Медведев И.М. Обзор зарубежного опыта исследований коррозии и средств защиты от коррозии // Авиационные материалы и технологии. 2015. № 2(35). С. 76–87.
14. El-Shazly A.H., Wazzan A.A., Radain T.A. Investigation for the possibility of improving the reinforced concrete corrosion resistance using polyaniline coated steel // International

11. Amleh L. *Bond deterioration of reinforcing steel in concrete due to corrosion.* PhD Thesis: Department of Civil Engineering and Applied Mechanics McGill University. 2000.
12. Wong H.S., Karimi A.R., Buenfeld N.R., Zhao Y.X., Jin W.L. On the penetration of corrosion products from reinforcing steel into concrete due to chloride-induced corrosion. *Corrosion Science.* 2010. Vol. 52. No. 7. Pp. 2469–2480.
13. Kablov Ye.N., Startsev O.V., Medvedev I.M. Obzor zarubezhnogo opyta issledovaniy i sredstv zashchity ot korrozii [Overview of foreign experience of corrosion research and protection against corrosion]. *Aviation materials and technologies.* 2015. No. 2(35). Pp. 76-87. (rus)
14. El-Shazly A.H Wazzan A.A., Radain T.A. Investigation for the possibility of improving the reinforced concrete corrosion resistance using polyaniline coated steel. *International Journal of Electrochemical Science*. 2012. Vol. 7. No. 3. Pp. 2416–2429.
15. Shchetkova Ye.A., Kashevarova G.G. Povysheniye prochnosti stsepleniya pri sdvige v zone kontakta «stal'-beton» [Increase of clutch strength at shift in contact "steel-concrete" zone]. *Herald of civil engineers.* 2015. No. 6(53). Pp. 70–75. (rus)
16. Al' Karadi A. Osnovnyye fiziko-mekhanicheskiye svoystva zhelezobetona [Main physico-mechanical properties of reinforced concrete]. *Bulletin of the Belgorod State Technological University. V.G. Shukhov.* 2013. No. 5. Pp. 39–42. (rus)
17. *GBJ10-89.* Structural Concrete Design Code. China. 1989.
18. Zhang Ju., Ling X., Guan Zh. Finite element modeling of concrete cover crack propagation due to non-uniform corrosion of reinforcement. *Construction and Building Materials.* 2017. Vol. 132. Pp. 487–499.
19. Figueira R.B., Pereira E.V., Silva C.J.R. Hybrid sol–gel coatings for corrosion protection of galvanized steel in simulated concrete pore solution. *JCT Research.* 2016. Vol. 13. No. 2. Pp. 355–373.
20. Gedvillo I.A., Zhmakina A.S., Andreev N.N., Vesely S.S. Corrosion and electrochemical behavior of steel in hardening concrete. *International Journal of Corrosion and Scale Inhibition.* 2017. Vol. 6. No. 1. Pp. 82–90.
21. Aguirre-Guerrero A.M., Robayo-Salazar R.A., de Gutiérrez R.M. A novel geopolymer application: coatings to protect reinforced concrete against corrosion. *Applied Clay Science.* 2017. Vol. 135. Pp. 437-446.
22. Song H.-W., Saraswathy V. Corrosion monitoring of reinforced concrete structures - a review. *International Journal of Electrochemical Science.* 2007. Vol. 2. No. 1. Pp. 1–28.
23. Perks R.A. Chloride thresholds for initiation of corrosion of steel reinforcement in concrete. 2001.

Journal of Electrochemical Science. 2012. Vol. 7. № 3. Pp. 2416–2429.

15. Щеткова Е.А., Кашеварова Г.Г. Повышение прочности сцепления при сдвиге в зоне контакта «сталь-бетон» // Вестник гражданских инженеров. 2015. № 6(53). С. 70–75.
16. Аль Каради А. Основные физико-механические свойства железобетона // Вестник Белгородского государственного технологического университета им. В.Г. Шухова. 2013. № 5. С. 39–42.
17. GBJ10-89. Structural Concrete Design Code. China. 1989.
18. Zhang Ju., Ling X., Guan Zh. Finite element modeling of concrete cover crack propagation due to non-uniform corrosion of reinforcement // Construction and Building Materials. 2017. Vol. 132. Pp. 487–499.
19. Figueira R.B., Pereira E.V., Silva C.J.R. Hybrid sol–gel coatings for corrosion protection of galvanized steel in simulated concrete pore solution // JCT Research. 2016. Vol. 13. № 2. Pp. 355–373.
20. Gedvillo I.A., Zhmakina A.S., Andreev N.N., Vesely S.S. Corrosion and electrochemical behavior of steel in hardening concrete // International Journal of Corrosion and Scale Inhibition. 2017. Vol. 6. № 1. Pp. 82–90.
21. Aguirre-Guerrero A.M., Robayo-Salazar R.A., de Gutiérrez R.M. A novel geopolymer application: coatings to protect reinforced concrete against corrosion // Applied Clay Science. 2017. Vol. 135. Pp. 437–446.
22. Song H.-W., Saraswathy V. Corrosion monitoring of reinforced concrete structures - a review // International Journal of Electrochemical Science. 2007. Vol. 2. № 1. Pp. 1–28.
23. Perks R.A. Chloride thresholds for initiation of corrosion of steel reinforcement in concrete. 2001.

Valeria Lushnikova,*
+7(906)074-68-46; N_A_T_E_L_K_A@mail.ru

Ashot Georgiyevich Tamrazyan,
+7(903)7305843; tamrazian@mail.ru

Валерия Юрьевна Лушникова,*
+7(906)074-68-46;
эл. почта: N_A_T_E_L_K_A@mail.ru

Ашот Георгиевич Тамразян,
+7(903)730-58-43; эл. почта: tamrazian@mail.ru

doi: 10.18720/MCE.80.13

Seismic design optimization considering base-isolation system

Оптимизация сейсмостойкого проектирования с учетом применения сейсмоизоляции

A.Y. Ivanov*,
St. Petersburg State University of Architecture and Civil Engineering, St. Petersburg, Russia
S.A. Chernogorskiy,
Peter the Great St. Petersburg Polytechnic University, St. Petersburg, Russia
M.P. Vlasov,
St. Petersburg State University of Architecture and Civil Engineering, St. Petersburg, Russia

Аспирант А.Ю. Иванов*,
Санкт-Петербургский государственный архитектурно-строительный университет, Санкт-Петербург, Россия
к.э.н., доцент С.А. Черногорский,
Санкт-Петербургский политехнический университет Петра Великого, Санкт-Петербург, Россия
д.э.н., проф. М.П. Власов,
Санкт-Петербургский государственный архитектурно-строительный университет, Санкт-Петербург, Россия

Key words: optimization procedure; earthquake engineering; structural damage; seismic base isolation; nonlinear static pushover analysis; averaged response spectrum; capacity curve; economic effect; life-cycle

Ключевые слова: метод оптимизации; сейсмостойкое проектирование; конструктивный ущерб; сейсмоизоляция; нелинейный статический метод расчета; усредненный спектр отклика; кривая несущей способности; экономическая эффективность; жизненный цикл здания

Abstract. Structural seismic design optimization researches reviewing shows that existing economic effect assessment methods take into account only traditional seismic retrofit schemes excluding base-isolation system employment. The purpose of this study is to obtain economic optimization which allows to compare the economic effect *E* of base-isolated structure among with traditional seismic retrofit schemes. Here the approach is proposed of earthquake caused damage state D_{rel} computation in base-isolated structure considering repair works with due regard to its life-cycle *N*. The example of damage state D_{rel} evaluation for base-isolated and traditional retrofitted structures is performed considering different seismic intensities. It is shown how the value of damage state proceeds according to the building life-cycle *N* in each case. The economic effect *E* for these cases is estimated with the aid of proposed optimization algorithm.

Аннотация. Исследования в области оптимизации конструктивных решений сейсмостойкого проектирования показали, что существующие методики оценки экономического эффекта различных проектов не рассматривают применение сейсмоизоляции, принимая во внимание только традиционные варианты сейсмоусиления. Целью работы является получение алгоритма оптимизации конструктивных решений по экономическому критерию, который позволит сравнить экономический эффект *E* от применения сейсмоизоляции наряду с традиционными вариантами сейсмоусиления конструкций. Предложена методика по определению наступившего в результате землетрясения ущерба D_{rel} в сейсмоизолированном здании с учетом возможных ремонтных работ на протяжении жизненного цикла здания *N*. Приведен пример расчета ущерба D_{rel} сейсмоизолированного здания и произведен сравнительный анализ с альтернативными вариантами проектов сейсмоусиления при воздействиях различной интенсивности на протяжении рассматриваемого жизненного цикла здания *N*. Выполнена оценка экономического эффекта этих вариантов *E* по предложенному алгоритму оптимизации.

1. Introduction

The economic optimization problem of buildings structural design is paramount among others and specifically important in earthquake engineering. Therefore, this study proceeds the problem initiated in [1] and associated with economic optimization of seismic structural design considering the base-isolated structures. To provide calculations of economic effect using the method proposed previously in [1], it is necessary to define damage state of base-isolated building caused by earthquakes of different intensities.

Иванов А.Ю., Черногорский С.А., Власов М.П. Оптимизация конструктивных решений сейсмостойкого проектирования по экономическому критерию // Инженерно-строительный журнал. 2018. № 4(80). С. 138–150.

So, the research object in this article is the economic optimization algorithm, which consider the employment of base-isolation system for seismic retrofit of the building.

Economic optimization in earthquake engineering has been developed for the last 15 years [1, 2, 3], and the problem of economic effect assessment in seismic structural design was initiated in [4] at the first time. However, the problem is that the above research works did not propose an algorithm that associates the results of building seismic response computations to economic indicators for characterizing the building damage state. Another problem is that the optimization criteria in these works, except [1], is presented insufficiently specific. In article [1] that the economic effect with consideration of a building life-cycle is assigned as optimization criteria. The cost value of damage state is taken into account with consideration of repair work cost after a certain amount of seismic events. Nevertheless, the main shortage of study [1] is that it was limited by a small range of frame types and seismic retrofit schemes[1] which were engaged for economic analysis. Also the procedure of frames seismic response and damage state evaluation contains many uncertainties and theoretical assumptions. These circumstances led to provide the present study to reduce afore-mentioned drawbacks.

The problem of economic optimization in earthquake engineering was investigated by native and foreign scientists A.M. Yaglom [4], A.M. Uzdin, Yu.L. Rutman [1], M. Papadrakakis, N.D. Lagaros, M. Fragiadakis [2], Y.K. Wen, Y.J. Kang [5, 6] and others.

The big research work for developing of analysis methods and practical employment of seismic base-isolation systems was done by scientists J.M. Kelly [7], R. Scinner, W. Robinson [8, 9], A. Martelli [10], M. Higashino, Sh. Okomoto [11], A. Chopra [12], O.A. Savinov [13], Ya.M. Ayzenberg [14], S.V. Polyakov [15], Yu.L. Rutman [16, 17], A.M. Uzdin [18], Yu.D. Cherepinskiy [19], A.V. Kurzanov were involved in the researching of the seismic behavior of base-isolated structures as well.

The damage state for traditional seismic design schemes was evaluated in [1] with the help of capacity curves. There are also some studies, which consider inelastic seismic response of structures and dynamic properties [20, 21]. These curves were developed using pushover analysis concept. Pushover analysis is the nonlinear static analysis method that allows to evaluate the structural seismic performance of the building under a seismic excitation. This method became popular in foreign code provisions [22, 23, 24, 25] in the last the last 20 years. The basic pushover theoretical foundations were given by H. Krawinkler, G.D.P.K. Seneviranta [26, 27], V. Kilar, P. Fajfar [28], A.K. Chopra, R.K. Goel [29]. Nonlinear static pushover analysis for the last 5 years has also attracted the attention of scientists Yu.I. Nemchinov, N.G. Maryenkov, A.K. Khavkin, K.N. Babik [30], A.V. Sosnin [31, 32], K.T. Chkhikvadze, Ts.G. Tsiskreli, N.Sh. Chlaidze, L.D. Kadzhaya [33]. At the present time this method is not included in Russian seismic code [34] as an acceptable analysis procedure. Nowadays various studies are provided mainly by foreign researchers which investigate the possibility of pushover analysis utilization for different types of structures [35, 36], its compatibility with nonlinear dynamic analysis [37] and its modifications [38]. The big interest for the current research is represented by the study [39], where the application of a N2, extended N2 and modal pushover methods was demonstrated for the base-isolated building frames with lead rubber bearings analysis.

The issue of inelastic behavior of base-isolated buildings, which the present article is deal with, is analyzed in studies [40–42]. As it is seen, the number of studies, which consider the inelastic behavior of base-isolated structures, is small. There is an experimental investigation of inelastic behavior of base-isolated cantilever structure with friction pendulum bearing isolators [40]. The article [39] is aimed to consider the effect of higher modes and to compare different pushover methods for base-isolated frame analysis, but we have to give more clear and understandable procedure for engineering-economical practical purposes of fast cost-effectiveness estimation.

Therefore, the purposes of current research work are:

1. to propose the economic optimization algorithm, which should consider the base-isolated building;
2. to estimate the damage state in base-isolated building;
3. to define the optimal type of seismic retrofit scheme according to proposed criteria.

For achieving these purposes, following problems have to be solved:

1. the objective function and variable parameters of economic optimization algorithm need to be defined;

[1] Seismic retrofit scheme means the term “anti-seismic measures” named in [1].

2. the procedure for damage state evaluation of base-isolated building due the various seismic input need to be developed;

3. the analytical model of the building need to be developed and the proposed optimization algorithm need to be implemented to it.

2. Methods

2.1. Optimization criteria and procedure

Some types of seismic traditional structural retrofit schemes Frame S_{PS} and Frame S_{MS} was considered along with the typical Frame S_{tip} designed without any seismic considerations, and the economic optimization criterion was proposed in [1]. The possible damage was defined as:

$$D(I)=D_{pr}(I)+D_{rel}(I), \tag{1}$$

where D_{pr} defines the prevented damage, D_{rel} defines the real damage and D defines the damage that occurs in Frame S_{tip}, I – earthquake intensity[2]. These economic parameters allow to formulate the optimization criterion as follows:

$$E = -K_{ant} + f(k,N)\sum_{I=I_{min}}^{I=I_{max}} L(I)\cdot D_{pr} \tag{2}$$

where K_{ant} – seismic retrofit cost (otherwise the building may collapse due the seismic ground shaking, and there would not be income profit, or it would be decreased, as the damage would limit the production output); $f(k,N)$ – cost adjustment factor in accordance with recommendations given in [1] under equation $f(k,N)=\left(\frac{1}{k}-1\right)[1-(1-k)^N]$. Here $k=\frac{d+d^*}{1+d}$, where d^* - depreciation rate (the parameter which determines reduction of building value over the time inverse to its maintenance period) d – annual profitability of manufacturing; $L(I)$ – average number of rate I earthquakes on the building site; N – time after the maintenance start (years).

In the Eq. (1) D-D_{pr}=D_{rel} the real damage, as well as the prevented damage, contains the following:

- repair and replacement cost of injured structural elements;
- losses of equipment inside facility;
- losses in profit due to idle period when repairing.

The usage of two types of damage in the optimization criteria provides substantially more universal criteria as it said in [1]. If the typical frame is designed without any seismic considerations, then $K_{ant} = 0$ and $D_{pr}(I) = 0$. Thus, financial losses after earthquakes are defined by the damage $D(I)$, considering a number of certain seismic events with different intensities I, and by the adjustment of repair cost with respect to building life-cycle. If it is applied any type of seismic retrofit scheme like S_{PS}, S_{MS} [1], or if it is a base-isolated Frame S_{SIS}, then real damage $D(I)_{rel}=D(I)-D(I)_{pr}$ is less then $D(I)$, while financial losses increase with the rising of K_{ant}. The optimization objective function E_{eff} is defined by relationship of these parameters.

The prevented damage $D(I)_{pr}$, the real damage $D(I)_{rel}$ and the $D(I)$ damage in Frame S_{tip} can be obtained with the help of capacity spectrum pushover method. For providing computation according this method, firstly, the building capacity (pushover) curve need to be constructed. The capacity curve allows to forecast building damages and the kind of a structural failure corresponding to the roof displacement. The structural damage need to be associated with financial loss given by financial curve, which helps to provide calculations by Eq. (1).

2.2. Damage state and response spectrum developing for SIS buildings

As it was said, the damage state for traditional seismic design schemes is evaluated with the help of capacity curve, and this curve can be plotted using pushover concept. For developing this curve it is necessary to have the acceleration response spectrum which corresponds to the building foundation

[2] The intensities of earthquakes are measured in terms of rate by MSK-64 scale.

Иванов А.Ю., Черногорский С.А., Власов М.П. Оптимизация конструктивных решений сейсмостойкого проектирования по экономическому критерию // Инженерно-строительный журнал. 2018. № 4(80). С. 138–150.

motion. In the case of traditional seismic design[3], it is considered that the motion of the foundation coincides with the ground motion. In this case, the response spectrum is taken from seismic code [34]. Nevertheless, if it is supposed by seismic retrofit scheme the base isolation system (SIS) implementation, the code spectra applying is not justified [25] and this approach is not acceptable. The movement of the superstructure (structure located on SIS) does not coincide with the movement of the substructure (foundation of the structure). Thus, before calculating the economic effect by Eq. (2) the difference between substructure (kinematic foundation) and superstructure (building) motions have to be considered.

The current situation in seismic design practice of base-isolated building usually does not deal with inelastic behavior of superstructure and does not consider its damage caused by earthquake. This is related to the fact that the several code provisions prohibit yielding of base-isolated structures. However, for providing comparable economic analysis of different frame types and solution of structural optimization problem along with varying base-isolator types, it is necessary to consider the possibility of approximate damage, which could be caused to the base-isolated frame by earthquakes of different intensities.

The damage state of base-isolated building can be defined as the result of inelastic structural behavior of the structural elements of the building caused by the earthquake of sufficient intensity. Inelastic structural behavior leads to financial losses in terms of repair cost. So, for economic optimization problem solution the damage state need to be defined as a financial loss for repair works after every earthquake which can occur on the building site. To quantify the value of the damage state it is necessary to associate it with some seismic response parameter of the frame. Here this parameter becomes the frame roof displacement that is why a superstructure (frame) response spectrum have to be developed. This procedure is based on tier-by-tier spectrum approach and implies the following steps:

1. Accelerations of the substructure are obtained through a numerical simulation process involving nonlinear time history analysis of "superstructure - SIS" system response to seismic ground shaking. It is assumed here that the superstructure is extremely rigid. The analysis is performed for representative ground motion ensembles which are grouped by intensities in terms of the rate.

2. When acceleration of substructure for every time history from the ensemble are calculated, it becomes possible to develop the superstructure response spectrum. Therefore, a single degree of freedom system (SDOF) calculation is performed. The oscillator is subjected to total acceleration values from the previous step time history analysis, and the ensemble of response spectrums is obtained. The final superstructure response spectrum for each group of seismic ground shaking intensity can be defined with the help of the statistical analysis as the sum of mathematical expectations assessment and estimation of the standard deviation. Thus, by averaging spectral acceleration values the superstructure response spectrum can be developed

2.3. Economic optimization for SIS buildings

Based on the superstructure response spectrum, the roof displacement, the structural damage of the frame and the corresponding financial loss could be defined with the help of simplified nonlinear static pushover analysis. Then the optimization algorithm described before can be applied. In the case of comparing economic effect from using different types of seismic base isolators, the variable parameters become SIS mechanical characteristics. Therefore, not only the structural repair cost (this kind of loss may not occur) contributes life-cycle investments, but SIS price increase it as well. In the present study it is shown, how the economic effect of base-isolated frame comes out respect to other retrofit schemes proposed in [1].

2.4. Structural model and numerical simulation

2.4.1. Structural frame and SIS characteristics

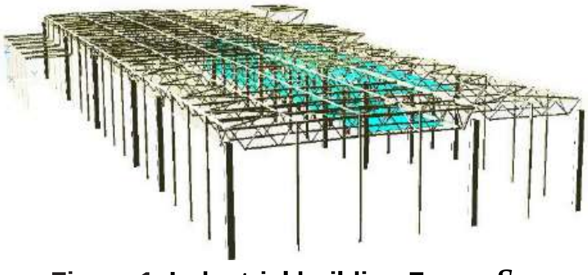

Figure 1. Industrial building Frame S_{tip}

[3] In this study and [1] the traditional seismic design implies strengthening of loadbearing structures by increasing the main reinforcement of the concrete columns and steel structures elements profile sections

The frame which is used for instance of the damage state evaluation process in building with SIS and for representation the economic optimization concept along with other frame types has been already presented in [1]. This is the industrial building frame given in Figure 1, but for the case of SIS applying the foundation framework was designed supported by elastomeric isolators. All strength characteristics of elements sections of Frame SSIS are similar to Frame Stip in study [1]. Total building dead weight plus anticipated live loads is assumed equal to 28000 kN. The construction of SIS building implies to design the foundation framework located on elastomeric isolators. These isolators are presented of two types: with maximum vertical load on one support 1400 kN and with maximum vertical load on one support 600 kN. The combination of these supports with the consideration of relative vertical load distribution composes the layout for the foundation framework (kinematic foundation). The chosen construction parameters of base-isolation supports provide natural frequency of isolation system f = 0.4 Hz.

Ground motions used in this study were generated by PEER ground motion database[4]. Ensembles of ground motions compiled in such manner that the amount of earthquake occurrences of a certain rate does not exceed their average number for considered building life-cycle equal to 50 years. Then, in accordance with the amount of ground motions used in [1], it is necessary to provide numerical simulations for Frame Stip for the number of ground motions shown in the last line of Table 1.

Table 1. Life-cycle earthquake occurrences amount and the number of ground motions in ensembles for numerical simulation

	6 rate	7 rate	8 rate	9 rate
Life-cycle earthquake occurrences amount, N = 50 years	5	4	3	1
Ground motions for numerical simulation	15	12	9	3

2.4.2. Nonlinear time history analysis and mean response spectrum developing

1. The nonlinear time history analysis is provided for every seismic ground motion record from ensembles for the system "superstructure (equivalent SDOF system) - SIS". The calculation is carried out using Nonlin and MathCad programming. In Figure 2, as an example, the seismic ground shaking record of the rate 9 earthquake is shown. After computation, the maximum acceleration 0.46 m/s^2 was obtained (Fig. 3). The same numerical simulations are provided for all time histories divided into 4 groups accordingly to the rate of earthquake.

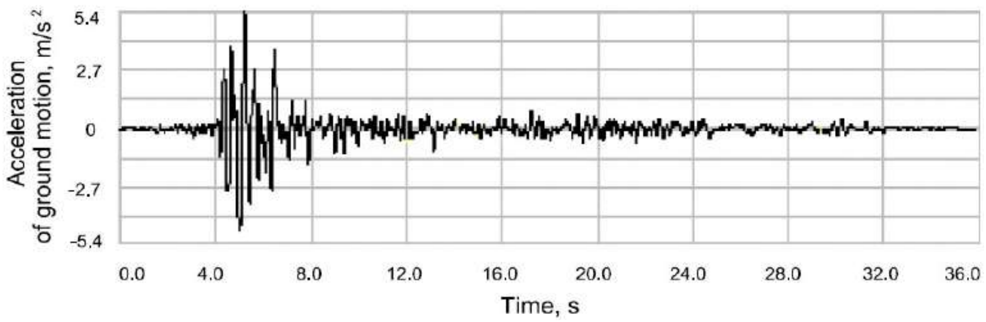

Figure 2. Ground motion record for the rate 9 earthquake

2. The calculation of the single degree of freedom system (SDOF) is provided. The oscillator is subjected to total acceleration values from a previous stage time history analysis (Fig. 3). Thus, the response spectrum is generated in terms "Spectral acceleration – Oscillator frequency" for each kinematic foundation motion, thereat, total acceleration absolute values for discrete oscillator frequencies are fixed. Frequency increments in the peak spectral acceleration range should be small enough not to miss their maxima.

3. The obtained response spectrums are divided into 4 groups depending on the rate of initial seismic ground shaking. Then the statistical processing of response spectrums within each group is performed and oscillator absolute acceleration peak values are derived as well. Consequently, it is possible to determinate the mean response spectrum associated with each group of seismic intensity (Fig. 4).

[4] https://ngawest2.berkeley.edu/

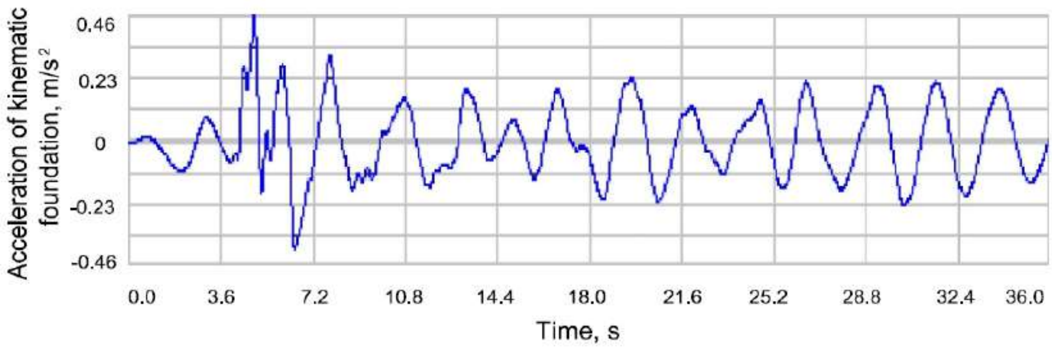

Figure 3. Computed kinematic foundation motion for the rate 9 earthquake

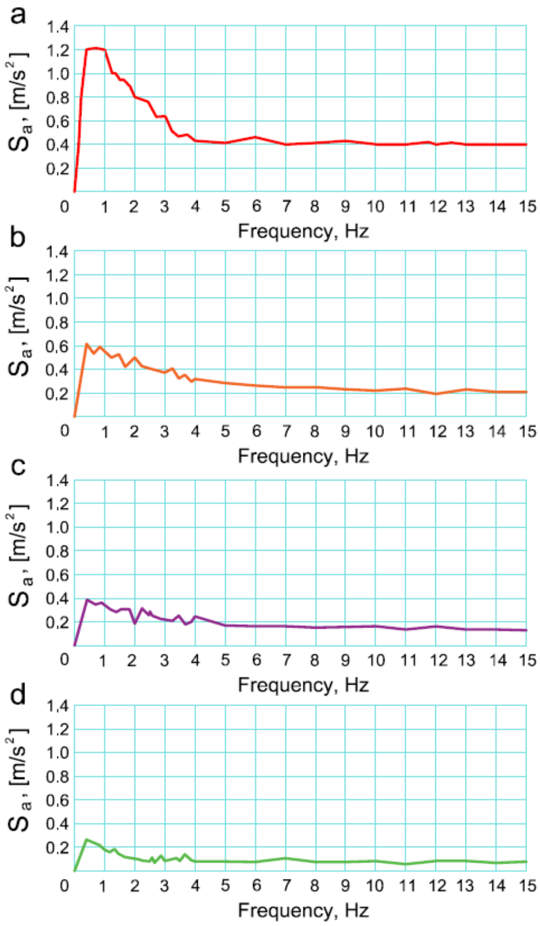

Figure 4. Mean of response spectrums represents time histories ensembles of (a) rate 9 earthquakes (b) rate 8 earthquakes (c) rate 7 earthquakes (d) rate 6 earthquakes

2.4.3. Calculating maximum structural displacement using simplified nonlinear static analysis procedure

Further calculations consist in applying simplified nonlinear static analysis procedure, in particular, the capacity spectrum (pushover) method "A" [20], for calculation the maximum structural displacement. If the maximum structural displacement is computed, then it becomes possible to estimate the structural damage by the displacement demand. The procedure implies the performance of the step-by-step process, the essence of which is as follows:

1. Mean values of response spectrums obtained at stage B are transformed from the Sa vs Frequency format to the Sa vs T format. Then, accordingly to capacity spectrum procedure "A" used for determining system performance point, 5 % elastic response spectrums are constructed from the mean ones. The obtaining results are converted then from the standard Sa vs T representation to Acceleration–Displacement Response Spectra (ADRS) format. Figure 5 shows the mean of 5 % simplified (by enveloping peaks of the initial Sa vs T spectrum) damped elastic response spectrum conversion from the standard simplified Sa vs T format to ADRS format associated with the ensemble of rate 9 ground motions.

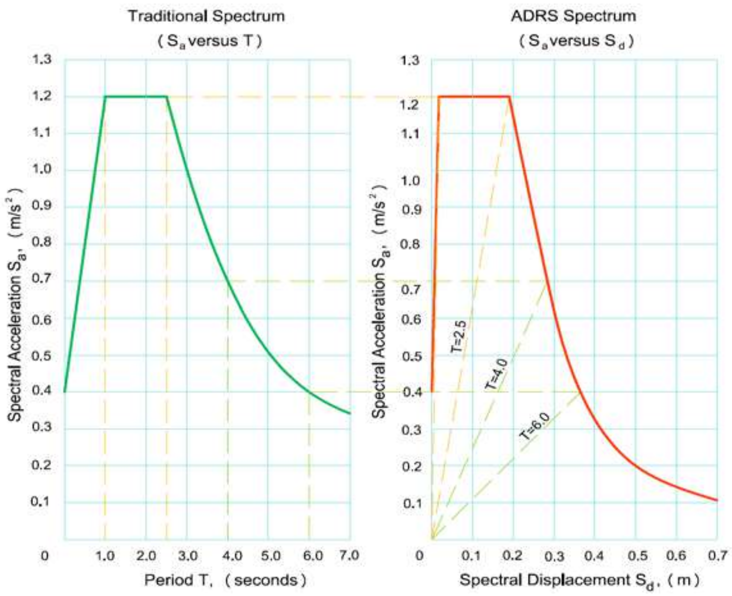

Figure 5. Mean of response spectrums conversion from S_a vs T to ADRS format associated with the ensemble of rate 9 ground motions

2. The obtained in [1] capacity curve for Frame Stip is converted to a capacity spectrum which have to be plotted in ADRS format as well using equations and provisions provided by [24–26]. Computations are performed for 2 points, which was calculated in [1] and used for Frame Stip capacity curve construction. The amount of these points corresponds to the number of selected performance levels. To provide further analysis, the building is substituted with equivalent single-mass system, and modal participation factor PF1, modal mass coefficient α, parameters w and ϕ are computed with consideration of this assumption. Figure 6 depicts the conversion of the capacity (pushover) curve to the capacity spectrum for Frame Stip.

3. A trial performance point is selected. The first choice of the trial performance point could be the displacement obtained using the equal displacement approximation [20]. The construction of this point is given in Figure 7.

4. A bilinear representation of the capacity spectrum is developed emanating from the requirement of the approximate equality of the area designated A1 and the area designated A2. These areas are formed by the rotation of a straight line starting from the trial performance point (Fig. 7).

5. The spectral reduction factors SRA and SRV are calculated as given by equations in [7]. Therefore, the reduced 5 % damped elastic response spectrum, called the demand spectrum, can be developed by the multiplication of the 5 % damped elastic response spectrum points by spectral reduction factors SRA and SRV. The characteristic points of the constant acceleration (horizontal) range of 5 % damped elastic response spectrum are multiplied by the spectral reduction factor SRA and the points of the constant velocity (descending) range are multiplied by the factor SRV. Demand spectrum points are obtained by intersecting horizontal projections of computed spectral acceleration ordinates with lines of constant period radiating from the origin.

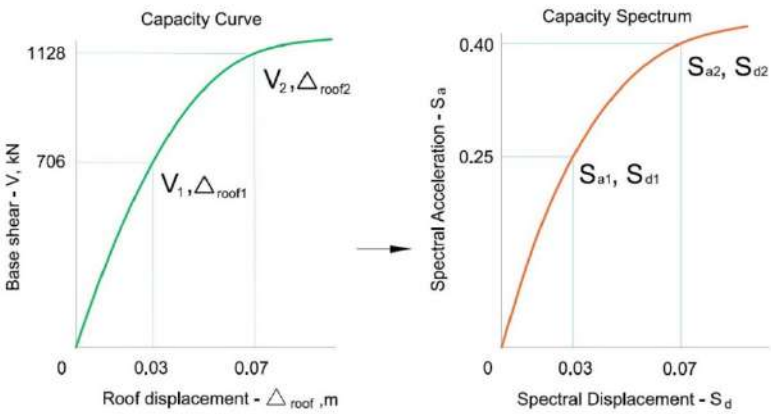

Figure 6. Capacity (pushover) curve to capacity spectrum conversion for Frame S_{tip}

6. Drawing the demand spectrum on the same plot as the capacity spectrum develops the intersection point. This point represents the condition for which the seismic capacity of the structure is equal to the seismic demand imposed on the structure by the specified ground motion [22]. If this point is within acceptable tolerance, then the trial performance point is the performance point and the displacement represents the maximum structural displacement expected for the demand earthquake. If the demand spectrum does not intersect the capacity spectrum within acceptable tolerance, then the obtained intersection point becomes a new trial point and computations are provided again.

In case of this computation, a few iterations have been provided before the demand spectrum intersects the capacity spectrum in the trial performance point obtained on previous step within acceptable tolerance (the first and the last iterations are shown on Figure 7). Thus, the result displacement represents the maximum structural displacement expected for the seismic demand. As the calculation is performed for the multi degree of freedom system, so it is necessary to convert the maximum structural displacement value back into the MDOF format using the equation (14) denoted in [10]. Figure 7 depicts that the considering seismic demand causes the structural displacement which leads the frame to collapse. On the financial curve plotted for the Frame Stip in [1] the obtained performance point is outside the range of displacements limited by performance objectives (Fig. 8a). According to the idea proposed in [1] this fact designates that the considering seismic demand induces the maximum possible damage state equal to 1. In the same way, computations are conducted for ensembles of rate 8, 7 and 6 seismic demands. The corresponding financial curves are plotted in Figure 8b-d. The results of these calculations are summarized in Table 2.

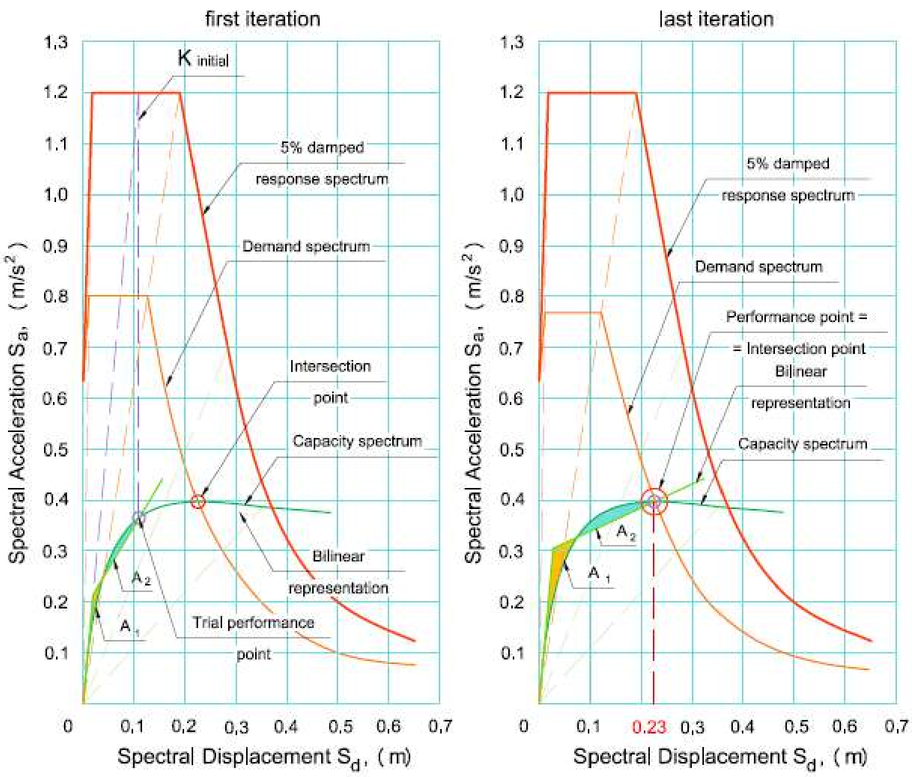

Figure 7. Performance point search using the capacity spectrum method "A" of nonlinear static analysis

Table 2. Nonlinear static analysis results of Frame S_{tip} considering all possible earthquakes of different intensities on the site with due regard to its life-cycle

Ground motion ensembles	Maximum displacement	Damage from caused by a single earthquake D_{rel}	Damage from caused by all earthquakes for considered life-cycle
Rate 6	*0.01*	*0*	*0*
Rate 7	*0.02*	*0*	*0*
Rate 8	*0.06*	*0.011*	*0.033*
Rate 9	*0.23*	*1*	*1*

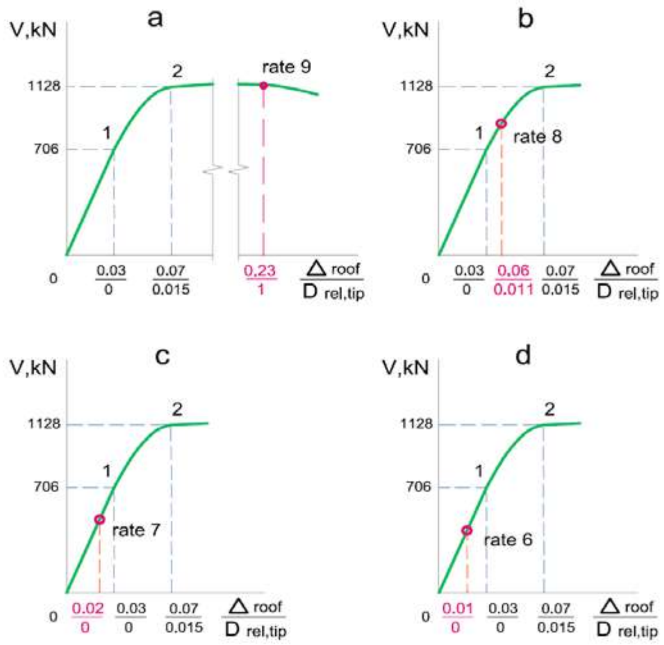

Figure 8. Financial curves with maximum displacements defined by nonlinear static analysis for time histories ensembles of (a) rate 9 earthquakes (b) rate 8 earthquakes (c) rate 7 earthquakes (d) rate 6 earthquakes

2.4.4. Economic effect estimation and seismic retrofit cost

As was quantified in [1], the cost of Frame S_{tip}, including cost of materials and construction works cost, is C_{tip} = 15.9 million rubles. The SIS cost for isolating the entire building is defined as the total cost of considering isolators combination plus seismic foundation framework supported by them. The cost of all supports in accordance with the commercial offer received by the manufacturer plus the seismic foundation framework cost is K_{ant}=0.037 in fractions of the total building cost. Therefore, all necessary data for the economic effect *E* calculation using Eq. (2) are now available.

Values of the economic effect *E* are calculated at seven points that characterize financial loss at a certain moment of building life-cycle. The results are plotted in terms of «economic effect *E* – building life-cycle *N*», each frame corresponds the respective curve. When calculating parameter *f(k,N)* the variable, which characterizes the profitability, is applied equal to *d* = 0.1 and *d** = 0.03, but its value may change depending on the size of income profit

3. Results and Discussion

The diagram in Figure 9 shows that economic effect curves for Frame $S_{\neg PS}$ and Frame $S_{\neg MS}$ are parallel and the curve for Frame SSIS is descending with time. This is associated specifically with the fact that the rate 8 earthquakes drives Frame SSIS into inelastic range and leads to some structural damage and the rate 9 earthquakes causes completely collapse of this frame. Represented at Figure 9 curves were developed by values of total structural damage obtained in Tables 1–3 in study [1] and in Table 2 of this paper. However, as it was previously noted in [1–3, 5, 6], not only structural elements become defected after earthquake, but also non-structural ones (partition walls, false ceiling and etc.) are failed. Furthermore, the utility systems, MEP, technological equipment and site landscaping could be damaged that represents financial losses related with business interruption. Considering this, the approximate assumption that the total damage increases twice in comparison with the structural one (as it was supposed in [1]), is admitted here. Consequently, the economic effect variation is plotted on the graph at Figure 10. Thus, the biggest economic effect E at the end of the building life-cycle can be achieved, as before, applying $S_{\neg PS}$ seismic retrofit scheme. The small economic effect of base-isolated Frame SSIS can be explained by the low initial strength of some elements of the frame itself and small effective SIS construction or mechanical parameters.

In this paper and in the study [1] only 4 types of structural frame is compared: Frame Stip designed without any seismic considerations, partially-reinforced Frame S¬PS, maximum reinforced Frame S¬MS and base-isolated Frame SSIS. However, the greater economic effect at the different life-cycle stages could be achieved considering more options of seismic retrofit schemes, for example:

1. Performing partial reinforcement of the most stressed structural elements in Frame SSIS, for instance, reinforced-concrete columns and braces in truss system. In this case, SIS cost may be decreased;

2. Performing various types of a more effective (in terms of seismic input reduction), but more expensive SIS, and compare economic effects. For instance, the analysis could be provided for some types of rubber elastomeric isolators [7], as it was done in [39], especially high damping soft type isolators. In another case, friction pendulum seismic isolation bearings, discussed in [16], or the similar ones [40] could be considered as well.

3. Involving supplemental damping devices in base isolated frame if it is necessary.

4. As the obtained results have shown, the big problem is still the capacity curve construction and the calculation of points, which could characterize adequately the structural performance of the building.

The optimization algorithm obtained in this study is specific in comparison with optimization algorithms obtained in studies [1–3]. In article [2] optimization algorithm takes into account the life-cycle cost of the building as well. However, the optimization criterion is not represented clearly. The range of frame types is limited with consideration of traditional seismic retrofit schemes. The article is mostly aimed for comparing the different pushover methods. Study [3] is turned to more general economical problem of seismic hazard, it considers the social losses caused by earthquakes, but it does not propose the tool for structural optimization in earthquake engineering. The optimization algorithm proposed in [1] is supplemented by this paper and gives the especial tool for engineering-economical analysis in seismic structural design.

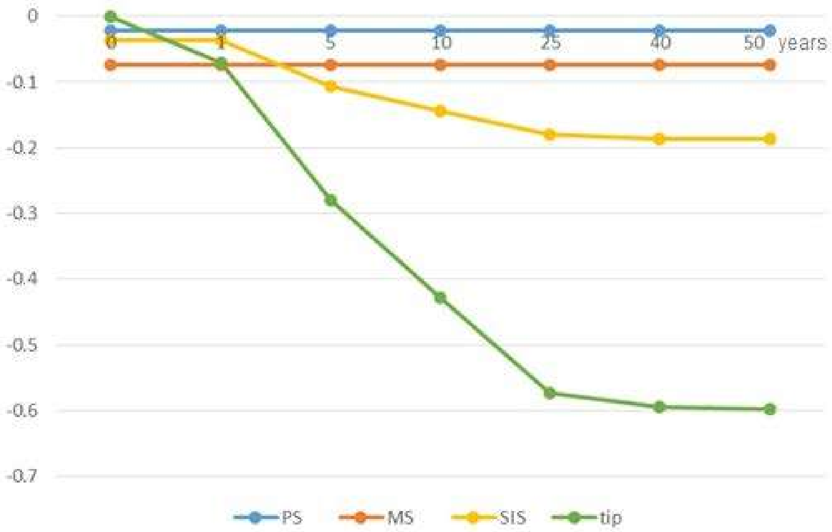

Figure 9. Dependence plot «economic effect *E* – building life-cycle *N*» considering structural damage

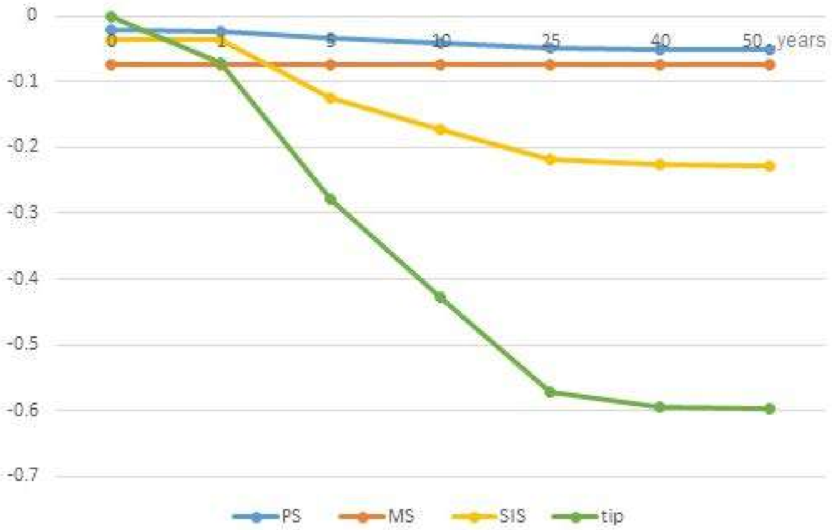

Figure 10. Dependence plot «economic effect *E* – building life-cycle *N*» considering total damage

4. Conclusions

1. In this study the economic optimization algorithm is proposed and it is shown how to use it for the base-isolated frame financial loss estimation along with traditional retrofit schemes. It becomes possible to compare and to find the reasonability of applying any type of mainstream seismic retrofit schemes at the project designing stage.

2. The procedure for estimation the damage state in base-isolated building is proposed by performing the following tasks:

- Consideration of the effect of seismic isolation system implementation with the help of tier-by-tier spectrum approach and time-history analysis of the system "superstructure - SIS";
- Evaluation of the damage state of structural system with a help of nonlinear static pushover analysis capacity spectrum method that allows to take into account the possibility of inelastic behavior in base-isolated frame.

3. The computations were performed and the practical application of proposed economic optimization algorithm and damage state evaluation method was demonstrated by the example of industrial building frame analysis.

References

1. Vatin N.I., Ivanov A.Yu., Rutman Yu.L., Chernogorskiy S.A. Earthquake engineering optimization of structures by economic criterion. *Magazine of Civil Engeneering.* 2017. No. 8(76). Pp. 77–93.
2. Lagaros N.D., Fragiadakis M. Evaluation of ASCE – 41, ATC – 40 and N2 static pushover methods based on optimally designed buildings. *Soil Dynamics and Earthquake Engineering.* 2011. No. 31. Pp. 77–90.
3. Saadat S., Camp C. V., Pezeshk Sh. Seismic performance-based design optimization considering direct economic loss and direct social loss. *Engineering Structures.* 2014. No. 76. Pp. 193–201.
4. Keylis-Borok V.I., Nersesov I.A., Yaglom A.M. *Metody otsenki ekonomicheskogo effekta seysmostoykogo stroitelstva* [Methods of assessment of economic effect in earthquake design]. Moscow: AN SSSR, 1962. 46 p. (rus)
5. Wen Y.K., Kang Y.J. Minimum building life-cycle cost design criteria. I. Methodology. *Journal of Structural Engineering New York.* 2001. No. 127(3). Pp. 330–337.
6. Wen Y.K., Kang Y.J. Minimum building life-cycle cost design criteria. II. Applications. *Journal of Structural Engineering New York.* 2001. № 127(3). Pp. 338–346.
7. Kelly J.M. *Earthquake resistant design with rubber.* London: Springer-Verl., 1997. 243 p.
8. Skinner R.I., Robinson W.H., McVerry G.H. *An introduction to seismic isolation.* New York: Wiley, 2003. 398 p.
9. Skiner R.I. *An introduction to seismic isolation.* New Zeland: John Wiley & Sons, 1993. 353 p.
10. Martelli A., Forny M. Seismic isolation: present application and perspectives. *International Workshop On Base Isolated High-rise Buildings. Yerevan, Armenia*. 2006. Pp. 1–26.
11. Higashino M., Okamoto Sh. *Response Control and Seismic Isolation of Buildings.* New York: Taylor & Francis, 2006. 484 p.
12. Chopra A.K. *Dynamic of structures. Theory and Applications to Earthquake Engineering.* New Jersey: Prentice-Hall, 2006. 794 p.
13. Savinov O.A. Seysmoizolyatsiya sooruzheniy [Seismic insulation of structures]. *Izbrannyye stati i doklady Dinamicheskiye problemy stroitelnoy mekhaniki.* Saint-Petersburg, 1993. Pp. 155–178. (rus)
14. Ayzenberg Ya. M. Seysmoizolyatsiya vysokikh zdaniy [Seismic base isolation of tall buildings]. Seysmostoykoye stroitelstvo. Bezopasnost sooruzheniy. 2004. Vol.1. Pp. 28–32. (rus)

Литература

1. Ватин Н.И., Иванов А.Ю., Рутман Ю.Л., Черногорский С.А. Оптимизация конструкций сейсмостойких сооружений по экономическому критерию // Инженерно-строительный журнал. 2017. № 8(76). С. 77–93.
2. Lagaros N.D., Fragiadakis M. Evaluation of ASCE – 41, ATC – 40 and N2 static pushover methods based on optimally designed buildings // Soil Dynamics and Earthquake Engineering. 2011. No. 31. Pp. 77–90.
3. Saadat S., Camp C.V., Pezeshk Sh. Seismic performance-based design optimization considering direct economic loss and direct social loss // Engineering Structures. 2014. No. 76. Pp. 193–201.
4. Кейлис-Борок В.И., Нерсесов И.А., Яглом А.М. Методы оценки экономического эффекта сейсмостойкого строительства. М.: АН СССР, 1962. 46 с.
5. Wen Y.K., Kang Y.J. Minimum building life-cycle cost design criteria. I. Methodology // Journal of Structural Engineering New York. 2001. No. 127(3). Pp. 330–337.
6. Wen Y.K., Kang Y.J. Minimum building life-cycle cost design criteria. II. Applications // Journal of Structural Engineering New York. 2001. No. 127(3). Pp. 338–346.
7. Kelly J.M. Earthquake resistant design with rubber. London: Springer-Verl., 1997. 243 p.
8. Skinner R.I., Robinson W.H., McVerry G.H. An introduction to seismic isolation. New York: Wiley, 2003. 398 p.
9. Skinner R.I. An introduction to seismic isolation. New Zeland: John Wiley & Sons, 1993. 353 p.
10. Martelli A., Forny M. Seismic isolation: present application and perspectives // International Workshop On Base Isolated High-rise Buildings. Yerevan, Armenia: 2006. Pp. 1–26.
11. Higashino M., Okamoto Sh. Response Control and Seismic Isolation of Buildings. New York: Taylor & Francis, 2006. 484 p.
12. Chopra A.K. Dynamic of structures. Theory and Applications to Earthquake Engineering. New Jersey: Prentice-Hall, 2006. 794 p.
13. Савинов О.А. Сейсмоизоляция сооружений // Избранные статьи и доклады. Динамические проблемы строительной механики. СПб. 1993. С. 155–178.
14. Айзенберг Я.М. Сейсмоизоляция высоких зданий // Сейсмостойкое строительство. Безопасность сооружений. 2004. № 1. С. 28–32.

Иванов А.Ю., Черногорский С.А., Власов М.П. Оптимизация конструктивных решений сейсмостойкого проектирования по экономическому критерию // Инженерно-строительный журнал. 2018. № 4(80). С. 138–150.

15. Polyakov S.V., Kilimnik L.Sh., Soldatova L.A. *Opyt vozvedeniya zdaniy s seysmoizoliruyushchim skolzyashchim poyasom v fundamente* [Experience in the construction of buildings with seismic isolation sliding zone in the basement]. Moscow: Stroyizdat, 1984. 31 p. (rus)
16. Rutman Yu.L. Mayatnikovyye seysmoizoliruyushchiye opory. Konstruktsiya, raschet, eksperiment [Pendulum seismic isolation bearings. Design, analysis, experiment]. *Magazine of Civil Engeneering.* 2012. No. 1. Pp. 31–36.
17. Rutman Yu.L., Chylbak A.A. Otsenka seysmoprochnosti sooruzheniya, raspolozhennogo na sisteme seysmoizolyatsii. [Seismic structural strenght assessment of base-isolated building]. *Vestnik grazhdanskikh inzhenerov.* 2009. No. 1(18). Pp. 30–33.
18. Uzdin A.M., Dolgaya A.A. *Raschet elementov i optimizatsiya parametrov seysmoizoliruyushchikh fundamentov* [Calculation of the elements and optimization of seismic isolation foundation parameters]. Moscow: VNIINTPI, 1997. 76 p. (rus)
19. Cherepinskiy Yu.D., Zhunusov T.Zh., Gorvits I.G. *Aktivnaya zashchita zdaniy i sooruzheniy* [Active protection of buildings and structures]. Alma-Ata: Kaz. NIINTI, 1985. 34 p. (rus)
20. Mrdak I., Rakočević M., Žugić L., Usmanov R., Murgul V., Vatin N. Analysis of the influence of dynamic properties of structures on seismic response according to montenegrin and european regulations. *Applied Mechanics and Materials*. 2014. Vol. 633–634. Pp. 1069–1076.
21. Dražić J., Vatin N. The Influence of Configuration on to the Seismic Resistance of a Building. *Procedia Engineering.* 2016. Vol. 165. Pp. 883–890.
22. *Seismic Evaluation and Retrofit of Concrete Buildings.* Vol. 1: ATC-40 Report. – Applied Technology Council. Redwood City, California. 1996. 334 p.
23. *FEMA 440.* Improvement of nonlinear static seismic analysis procedures. Federal Emergence Managment Agency. Washington, DC. 2005.
24. *ASCE/SEI Standard 41-13.* Seismic Evaluation and of Retrofit of Existing Buildings. Structural Engineering Institute, American society of civil engineers, 2014.
25. *EC8.* Eurocode 8: Design of structures for earthquake resistance. European Committee for Standardisation: Brussels, Belgium, The European Standard EN 1998-1, 2004.
26. Krawinkler H. Pushover analysis: Why, how, when, and when not to use it. *Prosessings 1996 Convention, Structural Engineers Association of California.* Maui, Hawaii, 1996. Pp. 17–36.
27. Krawinkler H., Seneviranta G.D.P.K. Pros and cons of a pushover analysis of seismic performance evaluation. *Engineering Structures.* 1998. No. 20(4). Pp. 452–464.
28. Kilar V., Rilar V., Fajfar P. Simplified pushover analysis of building structures. *11-th World Conference of Earthquake Engineering.* 1996. No. 11. P. 8.
29. Chopra A.K., Goel R.K. A modal pushover analysis procedure for estimating seismic demand of buildings. *Earthquake Engineering and Structural Dynamics.* 2002. No. 31. Pp. 561–582.
30. Nemchinov Yu.I., Maryenkov N.G., Khavkin A.K., Babik K.N. *Proyektirovaniye zdaniy s zadannym urovnem obespecheniya seysmostoykosti (s uchetom rekomendatsiy Yevrokoda 8, mezhdunarodnykh standartov i trebovaniy DBN)* [Performance-based earthquake engineering (taking into account Eurocode 8 recommends and DBN international standarts]. Kiyev: GP GNIISK, 2012. 53 p. (rus).
31. Sosnin A.V. Ob osobennostyah metodologii nelineinogo staticheskogo analiza i ego soglasovannosti s bazovoi normativnoi metodikoi rascheta zdaniy i sooruzheniy na deistvie seismicheskih sil [Nonlinear static analysis procedure details and its assosiating with the code analysis method of buildings and structures]. Vestnik YUrGU. 2017. No. 1(16). Pp. 12–19.

15. Поляков С.В., Килимник Л.Ш., Солдатова Л.А. Опыт возведения зданий с сейсмоизолирующим скользящим поясом в фундаменте. М.: Стройиздат, 1984. 31 с.
16. Рутман Ю.Л. Маятниковые сейсмоизолирующие опоры. Конструкция, расчет, эксперимент // Инженерно-строительный журнал. 2012. № 1. С. 31–36.
17. Рутман Ю.Л., Чылбак А.А. Оценка сейсмопрочности сооружения, расположенного на системе сейсмоизоляции // Вестник гражданских инженеров. 2009. № 1(18). С. 30–33.
18. Уздин А.М., Долгая А.А. Расчет элементов и оптимизация параметров сейсмоизолирующих фундаментов. М.: ВНИИНТПИ, 1997. 76 с.
19. Черепинский Ю.Д., Жунусов Т.Ж., Горвиц И.Г. Активная защита зданий и сооружений. Алма-Ата: Каз. НИИНТИ, 1985. 34 с.
20. Mrdak I., Rakočević M., Žugić L., Usmanov R., Murgul V., Vatin N. Analysis of the influence of dynamic properties of structures on seismic response according to montenegrin and european regulations // Applied Mechanics and Materials. 2014. Vol. 633–634. Pp. 1069–1076.
21. Dražić J., Vatin N. The Influence of Configuration on to the Seismic Resistance of a Building // Procedia Engineering. 2016. Vol. 165. Pp. 883–890.
22. Seismic Evaluation and Retrofit of Concrete Buildings. Vol. 1: ATC-40 Report. – Applied Technology Council. Redwood City, California. 1996. 334 p.
23. FEMA 440. Improvement of nonlinear static seismic analysis procedures. Federal Emergence Managment Agency. Washington, DC. 2005.
24. ASCE/SEI Standard 41-13. Seismic Evaluation and of Retrofit of Existing Buildings. Structural Engineering Institute, American society of civil engineers, 2014.
25. EC8. Eurocode 8: Design of structures for earthquake resistance. European Committee for Standardisation: Brussels, Belgium, The European Standard EN 1998-1, 2004.
26. Krawinkler H. Pushover analysis: Why, how, when, and when not to use it // Prosessings 1996 Convention, Structural Engineers Association of California. Maui, Hawaii, 1996. Pp. 17–36.
27. Krawinkler H., Seneviranta G.D.P.K. Pros and cons of a pushover analysis of seismic performance evaluation // Engineering Structures. 1998. No. 20(4). Pp. 452–464.
28. Kilar V., Rilar V., Fajfar P. Simplified pushover analysis of building structures // 11-th World Conference of Earthquake Engineering. 1996. No. 11. P. 8.
29. Chopra A.K., Goel R.K. A modal pushover analysis procedure for estimating seismic demand of buildings // Earthquake Engineering and Structural Dynamics. 2002. No. 31. Pp. 561–582.
30. Немчинов Ю.И., Марьенков Н.Г., Хавкин А.К., Бабик К.Н. Проектирование зданий с заданным уровнем обеспечения сейсмостойкости (с учётом рекомендаций Еврокода 8, международных стандартов и требований ДБН). Киев: ГП ГНИИСК, 2012. 53 с.
31. Соснин А.В. Об особенностях методологии нелинейного статического анализа и его согласованности с базовой нормативной методикой расчёта зданий и сооружений на действие сейсмических сил // Вестник ЮУрГУ. Серия "Строительство и архитектура". 2016. № 1(16). С. 12–19.
32. Соснин А.В. Особенности оценки дефицита сейсмостойкости железобетонных каркасных зданий методом нелинейного статического анализа в SAP2000 // Техническое регулирование в транспортном строительстве. 2015. № 6(14). С. 97–110.

32. Sosnin A.V. Osobennosti otsenki defitsita seysmostoykosti zhelezobetonnyih karkasnyih zdaniy metodom nelineynogo staticheskogo analiza v SAP2000 [Earthquake resistance shortage estimation features of RC frame buildings using nonlinear static analysis and software SAP2000]. *Tehnicheskoe regulirovanie v transportnom stroitelstve*. 2015. No. 6(14). Pp. 97–110.
33. Chkhikvadze K.T., Tsiskreli Ts.G., Chlaidze N.Sh., Kadzhaya L.D. Priminenie nelineinogo staticheskogo (Pushover) metoda dlya otsenki povedenia konstruktsiy pri seismicheskom vozdeistvii [The application of nonlinear static (Pushover) methods for estimating the behavior of structures under seismic excitation]. *Stroitel'naya mekhanika i raschet sooruzheniy.* 2010. No. 2. Pp. 48–52.
34. *Russian Seismic Code 14.13330.2014.* SNiP II-7-81* Stroitelstvo v seysmicheskikh rayonakh [Construction in seismic regions]. TsNIISK im. V.A. Kucherenko, OAO «NITs «Stroitelstvo». Moscow: OAO «TsPP», 2014. 126 p.
35. Poursha M., Khoshnoudian F., Moghadam A. The extended consecutive modal pushover procedure for estimating the seismic demands of two-way unsymmetric-plan tall buildings under influence of two horizontal components of ground motions. *Soil Dynamics and Earthquake Engineering.* 2014. No. 63. Pp. 162–173.
36. Mohamad A., Poursha M. A non-adaptive displacement-based pushover procedure for the nonlinear static analysis of tall building frames. *Engineering Structures*. 2016. No. 126. Pp. 586–597.
37. Li S., Zuo Zh., Zhai Ch., Xie L. Comparison of static pushover and dynamic analyses using RC building shaking table experiment. *Engineering Structures*. 2017. No. 136. Pp. 430–440.
38. Soleimani S., Aziminejad A., Moghadam A. Approximate two-component incremental dynamic analysis using a bidirectional energy-based pushover procedure. *Engineering Structures.* 2018. No. 157. Pp. 86–95.
39. Faal H.N., Poursha M. Applicability of the N2, extended N2 and modal pushover analysis methods for the seismic evaluation of base-isolated building frames with lead rubber bearings (LRBs). *Soil Dynamics and Earthquake Engineering.* 2017. No. 98. Pp. 84–100.
40. Tsiavos A., Schlatter D., Markic T., Stojadinovic B. Experimental and analytical investigation of the inelastic behavior of structures isolated using friction pendulum bearings. *Procedia Engineering.* 2017. No. 199. Pp. 465–470.
41. Cancellara D., De Angeli F. Assessment and dynamic nonlinear analysis of different base isolation systems for a multi-storey RC building irregular in plan. *Computers & Structures.* 2016.
42. Mazza F. Seismic demand of base-isolated irregular structures subjected to pulse-type earthquakes. *Soil Dynamics and Earthquake Engineering.* 2018. No. 108. Pp. 111–129.

33. Чхиквадзе К.Т., Цискрели Ц.Г., Члаидзе Н.Ш., Каджая Л.Д. Применение нелинейного статического (Pushover) метода для оценки поведения конструкций при сейсмическом воздействии // Строительная механика и расчёт сооружений. 2010. № 2. С. 48–52.
34. СП 14.13330.2014. СНиП II-7-81* Строительство в сейсмических районах / ЦНИИСК им. В.А. Кучеренко, ОАО «НИЦ «Строительство». М.: ОАО «ЦПП», 2014. 126 с.
35. Poursha M., Khoshnoudian F., Moghadam A. The extended consecutive modal pushover procedure for estimating the seismic demands of two-way unsymmetric-plan tall buildings under influence of two horizontal components of ground motions // Soil Dynamics and Earthquake Engineering. 2014. No. 63. Pp. 162–173.
36. Mohamad A., Poursha M. A non-adaptive displacement-based pushover procedure for the nonlinear static analysis of tall building frames // Engineering Structures. 2016. No. 126. Pp. 586–597.
37. Li S., Zuo Zh., Zhai Ch., Xie L. Comparison of static pushover and dynamic analyses using RC building shaking table experiment // Engineering Structures. 2017. No. 136. Pp. 430–440.
38. Soleimani S., Aziminejad A., Moghadam A. Approximate two-component incremental dynamic analysis using a bidirectional energy-based pushover procedure // Engineering Structures. 2018. No. 157. Pp. 86–95.
39. Faal H.N., Poursha M. Applicability of the N2, extended N2 and modal pushover analysis methods for the seismic evaluation of base-isolated building frames with lead rubber bearings (LRBs) // Soil Dynamics and Earthquake Engineering. 2017. No. 98. Pp. 84–100.
40. Tsiavos A., Schlatter D., Markic T., Stojadinovic B. Experimental and analytical investigation of the inelastic behavior of structures isolated using friction pendulum bearings // Procedia Engineering. 2017. No. 199. Pp. 465–470.
41. Cancellara D., De Angeli F. Assessment and dynamic nonlinear analysis of different base isolation systems for a multi-storey RC building irregular in plan // Computers & Structures. 2016.
42. Mazza F. Seismic demand of base-isolated irregular structures subjected to pulse-type earthquakes // Soil Dynamics and Earthquake Engineering. 2018. No. 108. Pp. 111–129.

Andrei Ivanov,*
+(950)031-81-62; andreyivanov4@gmail.com

Sergey Chernogorskiy,
+7(911)917-78-16; chernog_sa@spbstu.ru

Mark Vlasov,
+7(965)061-07-87; markvlasov@mail.ru

Андрей Юрьевич Иванов,*
+(950)031-81-62;
эл. почта: andreyivanov4@gmail.com

Сергей Александрович Черногорский,
+7(911)917-78-16;
эл. почта: chernog_sa@spbstu.ru

Марк Павлович Власов,
+7(965)061-07-87; эл. почта: markvlasov@mail.ru

Иванов А.Ю., Черногорский С.А., Власов М.П. Оптимизация конструктивных решений сейсмостойкого проектирования по экономическому критерию // Инженерно-строительный журнал. 2018. № 4(80). С. 138–150.

doi: 10.18720/MCE.80.14

Analytical determination of thermal expansion of rocks and concrete aggregates

Аналитическое определение термического расширения горных пород и заполнителей бетонов

A.V. Denisov*,
National Research Moscow State Civil Engineering University, Moscow, Russia
A. Sprince,
Riga Technical University, Riga, Latvia

Канд. техн. наук, доцент А.В. Денисов*,
Национальный исследовательский Московский государственный строительный университет, г. Москва, Россия
д-р техн. наук, доцент А. Спринце,
Рижский технический университет, г. Рига, Латвия

Key words: thermal expansion and fracturing; analytical determination; rocks; concrete mineral aggregates

Ключевые слова: термическое расширение и растрескивание; аналитическое определение; горные породы; минеральные заполнители бетонов

Abstract. The article provides selection and approbation of the model and the model-based method for the analytical determination of thermal expansion and rock fracturing (decompression) and concrete mineral aggregates according to the data about thermal deformations of minerals based on information of the mineral composition, the average grain fineness of minerals and the elasticity modulus of rock. To accomplish the research, the author has used two models available in scientific publications: 1. Balashov and Zaraisky Model for calculating the thermal expansion and decompression of rock based on thermal deformations of minerals. The model does not take into account the structure and mechanical properties of rock. 2. The model of Denisov (one of the authors of this work) and Dubrovskiy was developed and evaluated earlier for the analytical determination of radiation expansion and rock fracturing when neutrons are irradiated by nuclear reactors on the basis of radiation deformation of minerals. The model takes into account the grain fineness and elasticity modulus of rock. The model is accepted for research on the basis of the analogy between the processes of thermal and radiation changes of rock at the level of interaction in mineral crystals. The approbation was done on the basis of both the information available in the scientific publications and experimental data obtained in this work which have shown thermal expansion of 22 in magmatic and sedimentary rock in the range from 20 to 700 °C. It has been determined that the model of Denisov and Dubrovskiy especially with correction introduction associated with the increase in the rock plasticity when heated is adequate and better than the Balashov and Zaraisky Model which describes the process of thermal expansion and rock fracturing. This model can be used for the analytical determination of thermal expansion and isotropic rock fracturing and concrete mineral aggregates at temperatures up to 700 °C (the most reliable – up to 500 °C) at normal pressure and humidity with the absence of included minerals that provide water and gases emission when heated.

Аннотация. Выполнен выбор и апробирование модели и основанного на ней метода аналитического определения термического расширения и растрескивания (разуплотнения) горных пород и минеральных заполнителей бетонов по данным о термических деформациях минералов на основании информации о минеральном составе, средней крупности зерен минералов и модуле упругости горных пород. Для исследований выбраны две имеющиеся в литературе модели: 1. Модель Балашова и Зарайского для расчета термического расширения и разуплотнения горных пород на основании термических деформаций минералов, не учитывающую структуру и механические свойства горных пород. 2. Модель Денисова (одного из авторов настоящей работы) и Дубровского, разработанная и апробированная ранее для аналитического определения радиационного расширения и растрескивания горных пород при облучении нейтронами ядерных реакторов на основании радиационных деформаций минералов, учитывающая крупность зерен и модуль упругости горной породы. Модель принята для исследования на основании аналогии между процессами термического и радиационного изменения горных пород на уровне взаимодействия кристаллов минералов. Апробирование выполнено на основании имеющихся в

Денисов А.В., Спринце А. Аналитическое определение термического расширения горных пород и заполнителей бетонов // Инженерно-строительный журнал. 2018. № 4(80). С. 151–170.

литературе и полученных в настоящей работе экспериментальных данных по термическому расширению 22 магматических и осадочных горных пород в интервале от 20 до 700 °С. Установлено, что модель Денисова и Дубровского особенно при введении поправки, связанной с увеличением пластичности горных пород при нагревании, адекватно и лучше, чем модель Балашова и Зарайского, описывает процесс термического расширении и растрескивания горных пород. Эта модель может быть использована для аналитического определения термического расширения и растрескивания изотропных горных пород и минеральных заполнителей бетонов при температурах до 700 °С (наиболее надежно до 500 °С) при нормальном давлении и влажности при отсутствии в их составе минералов, выделяющих при нагревании воду и газы.

1. Introduction

Thermal expansion of rock is very important for their thermal and physical properties Thermal expansion of rock is accompanied not only by the increase in the size and volume of rock massifs and processing of rock. Thermal expansion in rock generates thermomechanical stress at all levels, micro- and macro-cracking (decompression) occured until destruction, as well as a decrease in their physical properties [1–9]. In this regard:

- thermal destruction and rock drilling efficiency [4, 5, 10];

- rock metasomatism [6];

- possibility of using rock massifs to bury radioactive wastes [11–12];

- possibility of using rock massifs to store thermal energy [13, 14];

- thermal deformation and heat resistance of concretes when using crushed stone and sand made from rock as concrete aggregates [15–18].

It is known that thermal expansion and rock fracturing depend on the rock composition and structure and therefore can vary in a relatively wide range even in rock of the same type [1-9, 19-22]. In this regard, when selecting rock for use for various purposes, it is quite relevant to provide the analytical determination of thermal expansion and rock fracturing based on data on their mineral composition, structure and mechanical properties.

A model for describing the process of thermal expansion and rock decompression due to fracturing on the basis of thermal expansion and the content of the constituent mineral composition was developed in the works of Balashov and Zaraiskiy [21, 22]. Along with this one of the works [21] contains the notes about generally good coincidence between the calculated and experimental data, the results of a careful comparison were not shown, though. However, this model does not take into account the influence on the process of thermal expansion, fracturing and mechanical properties of rock.

Denisov A.V. (one of the authors of this work) previously, together with Dubrovskiy V. B. developed and tested a model for the analytical determination of radiation changes in the volume (deformation) of concrete rocks aggregates after irradiation by neutrons of nuclear reactors. This model described in works [23–26] takes into account not only the expansion and content of various minerals in rocks but also a feature of the rock structure such as grain fineness of minerals and also the elasticity modulus of rocks and minerals. Moreover, work [23] has demonstrated the analogies between the mechanisms of radiation and thermal damage of rock – aggregates of concretes at the level of interaction between crystals. The thermal expansion of rock of the work [2] was used in work [23] for preliminary verification of the proposed model. This verification has showed the principal possibility of using the developed model for the analytical determination of thermal changes in the volume of rock. However, the detailed verification of this model for heating process has not been done due to the lack of all necessary data.

The development results of such models have not been found in foreign sources.

The purpose of this work is to select and approbate the model and the model-based method for the analytical determination of thermal expansion and rock fracturing (decompression) according to the data on thermal deformations of minerals on the basis of information on their mineral composition, structure and mechanical properties.

The main objectives of the work were the following:

1. to choose a model or models for the analytical description of the process of thermal expansion and rock fracturing due to the thermal expansion of minerals;

2. to select experimental data available in scientific publications with a full set of information necessary for approbation of selected models;

3. to test scientific publications data on selected models and determine the necessity for additional experimental research;

4. to fulfill additional experimental research and approbate selected models for this data if required.

The article provides substantiation of the use of the evaluated model as the basis for the method of analytical determination of thermal expansion and rock fracturing (decompression) and concrete mineral aggregates for data on thermal deformations of minerals on the basis of information on the mineral composition, structure and mechanical properties of rock.

2. Methods

Both above mentioned models previously proposed for the analytical description of thermal expansion and rock fracturing were accepted for the research in this work.

In the model of Balashov and Zaraiskiy given in works [21, 22] thermal expansion of rock is considered as the sum of the average weighted relative thermal expansion of the minerals (crystal matrix) composing the rock and excessive relative rock expansion due to the formation of micro cavities (micro cracks) between the grains because of anisotropic and thermal expansion in the crystals composed in minerals; thermal expansion can be different in volume as well. In this case the volume of the excessive thermal expansion of rock is taken equal to the average value of all possible absolute values of deformation differences for three principal axes of the adjoining crystals of minerals with their random distribution and orientation. The contribution of each possible difference to their averaged value is taken proportionally to the volume content of minerals, the contiguity; the interaction between them was also being considered.

Thus, the relative linear thermal expansion of rock given in the model of works [21, 22] is determined by the formula:

$$\Delta\ell/\ell = (\Delta\ell/\ell)_{MIN} + (\Delta\ell/\ell)_{EKC} \tag{1}$$

where $\Delta\ell/\ell$ – relative linear thermal change of the rock size (linear thermal expansion of rock);

$(\Delta\ell/\ell)_{MIN}$ – average weighted relative thermal change in size of mineral composition of rock;

$(\Delta\ell/\ell)_{EKC}$ – excessive relative thermal change of rock size due to the formation of micro cavities (micro cracks) between the grains.

Value $(\Delta\ell/\ell)_{MIN}$ is determined by the formula:

$$(\Delta\ell/\ell)_{MIN} = \frac{1}{3}\sum_{k=1}^{n}\left[W_k(\Delta V/V)_k\right] \tag{2}$$

where W_k – the volume ratio of *k* mineral contained in rock with its total number n of unit fraction;

$(\Delta V/V)_k$ – relative thermal change of volume of *k* mineral contained in rocks, %;

3 – a coefficient connecting the change in volume with the change in the material sizes in case of isotropic deformation.

Value $(\Delta\ell/\ell)_{EKC}$ is determined by the formula:

$$(\Delta\ell/\ell)_{EKC} = \frac{1}{9}\sum_{k_1,k_2}W_{k_1}W_{k_2}\sum_{j_1,j_2}^{3}\left|(\Delta\ell/\ell)_{k_1}^{J_1} - (\Delta\ell/\ell)_{k_2}^{J_2}\right| \tag{3}$$

where k_1 = 1,……n and k_2 = 1,……n – numbers of minerals contained in rock with their total number n, the thermal changes in sizes are considered as a pair difference of thermal deformations. In this case k_1 = k_2 when considering the pair difference of deformations between changes in sizes along different axes for crystals of the same mineral;

f_1 = 1, 2, 3 and f_2 = 1, 2, 3 – conditional counting numbers of the principal axes of the crystals; thermal change of sizes of the axes is considered in the pair difference;

$(\Delta\ell/\ell)_{k_1}^{J_1}$ and $(\Delta\ell/\ell)_{k_2}^{J_2}$ – relative thermal changes of sizes of crystals of k_1 mineral along f_1 axis and k_2 crystals of mineral along f_2 axis;

W_{k_1} and W_{k_2} – volume ratio of k_1 and k_2 minerals, the pair difference of deformations of which is considered;

$\left|(\Delta\ell/\ell)_{k_1}^{J_1}-(\Delta\ell/\ell)_{k_2}^{J_2}\right|$ – absolute value of the pair difference of the thermal deformations of k_1 and k_2 minerals by the conditional numbers of the main f_1 and f_2 axes.

$W_{k_1}W_{k_2}/9$ – contribution of each difference of deformations in the excessive thermal expansion of rock.

The thermal expansion in the form of a size change are increased threefold (coefficient of 3 is introduced) to determine the thermal expansion in the form of a volume change (volume thermal expansion).

The advantage of the model in works [21, 22] is its simplicity. However, the approach adopted in this model implies the assumption that the differences in the thermal deformations of crystals of minerals and the related microstructural intensions in this model are fully realized by void with complete relaxation of these intensions, regardless of their values and the strength of rock. The validity of this assumption in describing the process of thermal expansion requires careful verification.

More detailed approach was used when considering the interaction between crystals of minerals in the model of Denisov and Dubrovskiy described in works [23–26]. It was developed for the analytical determination of the radiation expansion of rock aggregates of concretes. This model was obtained on the basis of the following assumptions [23–26]:

1. It was taken into account that the radiation (or thermal) relative increase in the volume of rock aggregate of concretes as polycrystalline polymineral materials mainly consists of the values of the radiation (or thermal) relative change in the volume of crystal of mineral constituents of material and the value of volume change due to the formation of cracks.

2. It was assumed that the crystals composed in the material, which are the most expending during irradiation, are the main source of its radiation (or thermal) expansion and give the main contribution to the magnitude of the microstructural intentions (compression of the most expanding crystals and stretching of the rest ones) aroused in it. These stresses limit the development of radiation (or thermal) deformations of the most expanding crystals, but also cause fracturing of the material and therefore are relaxing. In this case the magnitude of the radiation change in the volume of the material can be determined by the magnitude of the change in the size of the crystals having the greatest free radiation (or thermal) deformations at least along one of the axes reduced to the value of their deformations under the action of the compressive microstructural stresses left after relaxation.

3. We considered crystals with the greatest radiation deformations at least along one of the axes as isotropically expanding, and their stress condition as volume compression. The difference of the considered stress condition and the real condition was taken into account by using their reduced content.

4. It was taken into consideration that the magnitude of microstructural intensions σ_{com} that compress the crystals of the most expanding minerals is related to the magnitude of the microstructural tensile stresses σ_{ctr}. In this case it was taken into account that the actual value σ_{ctr} in the material in the area between the cracks cannot exceed the tensile strength of the material in this area as because of cracking the stresses are relaxing until they reach this value. It was also assumed that while fracturing, when the distance between the cracks decreases to the grain size, the strength of the material in the area between the cracks in accordance with Weibull Strength theory increases until it reaches the tensile strength $R_{ctr.cr}$ of the individual crystals. In this case beginning with some deformation the microstructural intensions cease to grow and are maintained at a constant level determined by the condition $\sigma_{str}=R_{ctr.cr}$.

5. It was believed that the value $R_{ctr.cr}$ is determined by the Griffiths strength theory and the proportionality between the length of the critical crack and the grain size as well as between the surface energy and the elasticity modulus of crystals takes place.

6. The change in the mechanical properties of the crystals composed in minerals was neglected as they are much less than changes in rock.

Based on the realization of the initial assumptions for the analytical determination of the relative radiation (or thermal) change in the volume $\frac{\Delta V}{V}$ of aggregates (rock and ceramics) the expression [23–26] has been obtained:

$$\frac{\Delta V}{V} = \left(\frac{\Delta V}{V}\right)_1 = 3\left(\frac{\Delta \ell}{\ell}\right)_{M.M} - a_M \frac{E_0}{E_{M.M}\sqrt{d_{GR}}} * \frac{1-V_{M.RED}}{V_{M.RED}} \text{ – at } \left(\frac{\Delta V}{V}\right)_1 \geq \left(\frac{\Delta V}{V}\right)_2 \tag{4,a}$$

$$\frac{\Delta V}{V} = \left(\frac{\Delta V}{V}\right)_2 = \left(\frac{\Delta V}{V}\right)_{AD.M} + \frac{3\Delta\varepsilon_{AVE}}{1+2.2a_M/(3\varepsilon_{AVE}\sqrt{d_{GR}})} \text{ - at } \left(\frac{\Delta V}{V}\right)_1 < \left(\frac{\Delta V}{V}\right)_2 \tag{4,b}$$

where $\left(\frac{\Delta \ell}{\ell}\right)_{M.M}$ – maximum of the values of radiation (or thermal) relative changes in size in the most expanding direction of the crystals composed in minerals;

a_M = 3.4 10^{-2} % $cm^{0.5}$ – complex characteristic of the model;

E_0 – elasticity modulus of the material at zero porosity;

d_{GR} – the average size of the crystals composed in the minerals;

$E_{M.M}$ – elasticity modulus of crystals which have an extension $\left(\frac{\Delta \ell}{\ell}\right)_{M.M}$ along the axis where there extension exists $\left(\frac{\Delta \ell}{\ell}\right)_{M.M}$;

$\Delta\varepsilon_{AVE}$ – the average difference of the radiation (or thermal) changes in the crystal size along the various axes composing the material of the minerals;

$V_{M.RED}$ – the introduced relative volume content of crystals of minerals with a change in their sizes $\left(\frac{\Delta \ell}{\ell}\right)_{M.M}$, which takes into account the anisotropy of the radiation (or thermal) deformations and the presence of crystals which have size change $\left(\frac{\Delta \ell}{\ell}\right)_{M.i}$, (different from $\left(\frac{\Delta \ell}{\ell}\right)_{M.M}$ by no more than $a_M/\sqrt{d_{GR}}$);

$\left(\frac{\Delta V}{V}\right)_{AD.M}$ – an increase in the volume of material associated with a free radiation (or thermal) change in the volume of the crystals composed in minerals, and determined by the formula:

$$\left(\frac{\Delta V}{V}\right)_{AD.M} = \sum_{i=1}^{n}\left[\left(\frac{\Delta V}{V}\right)_i V_i\right] \tag{5}$$

where $\left(\dfrac{\Delta V}{V}\right)_i$ and V_i – radiation (or thermal) change in the volume of expansion and volume content of the crystals composed in minerals.

Values $\Delta\varepsilon_{AVE}$ are determined by the formula:

$$\Delta\varepsilon_{AVE} = \sum_{i-1}\sum_{j=1}\left[\left|\left(\frac{\Delta\ell}{\ell}\right)_{ij} - \frac{1}{3}\left(\frac{\Delta V}{V}\right)_{AD.M}\right|\frac{V_i}{3}\right] \tag{6}$$

$$V_{M.RED}\ \frac{n_{m.m}V_{M.M}}{3} + \sum_{i=1}^{n}\left[\frac{n_{m.i}V_{M.i}}{3}\ \frac{\left(\dfrac{\Delta\ell}{\ell}\right)_{M.i}E_{M.i}}{\left(\dfrac{\Delta\ell}{\ell}\right)_{M.M}V_{M.M}}\right] \tag{7}$$

where $\left(\dfrac{\Delta\ell}{\ell}\right)_{ij}$ – an increase in the sizes of the crystals of the i-th mineral along the j-th axis (j = 1 ... 3 along the axes a, b and c) of the crystal;

$n_{m.m}$ and $n_{m.i}$ – number of axes in crystals (1, 2 and 3), along which the extension takes place $\left(\dfrac{\Delta\ell}{\ell}\right)_{M.M}$ and $\left(\dfrac{\Delta\ell}{\ell}\right)_{M.i}$ respectively;

$V_{M.M}$, $V_{M.i}$, $E_{M.M}$, $E_{M.i}$ – relative volume content and modulus of normal elasticity of the crystals of minerals with extension $\left(\dfrac{\Delta\ell}{\ell}\right)_{M.M}$ and $\left(\dfrac{\Delta\ell}{\ell}\right)_{M.i}$.

Radiation and thermal increase in volume of rock due to crack formation $\left(\dfrac{\Delta V}{V}\right)_{CR}$ is determined by the formula:

$$\left(\frac{\Delta V}{V}\right)_{CR.} = \frac{\Delta V}{V} - \left(\frac{\Delta V}{V}\right)_{AD.M} \tag{8}$$

Volume changes are increased threefold (a coefficient of 1/3 is introduced) to determine the radiation and thermal expansion in the form of a change in volume.

The model of Denisov and Dubrovskiy is stricter as it takes into account the influence of the grain size of minerals on the process of radiation and thermal expansion as one of the properties of the structure, as well as the elasticity modulus of rock and composing minerals, as properties characterizing the stiffness and correlating with durability. At the same time under the influence of heating the development of plastic deformations is much more likely than under exposure to radiation as the fragility of materials decreases with heating and increases with irradiation. In this regard the model based on the current research work approved for radiation expansion may require corrections for thermal expansion.

To test the possibility of using the models to describe the thermal expansion of rock, experimental data of works [21, 22] was used as test result of thermal expansion of 11 varieties of magmatic and sedimentary rocks. This data is the most complete information necessary for computational verification. The data on names, mineral composition, average size of mineral grains, the elasticity modulus, density and porosity and rock studied in works [21, 22] accepted in the calculations are given in Table 1. The samples in the form of discs with a diameter of 28 mm and a thickness of 5 mm were mainly used.

Table 1. Name, mineral composition, structure and properties of rock studied in works [21, 22]

No i/o	Rock	Minerals in rock composition and their content by volume	Average size of grains, mm	Elasticity modulus*, 10^4 MPa	Density, kg/m^3	Porosity, %
1	Biotitic granite	Quartz – 31%; Plagioclase No. 26 – 36%; Potassic feldspar – 26%, Biotite – 7%.	0.23	7.4	2650	0.33
2	Granite- aplite	Quartz – 26%; Plagioclase No. 7 – 47%; Potassic feldspar – 25%, Biotite – 2%.	0.27	3.3	2570	1.09
3	Granodiorite	Quartz – 24%; Plagioclase No. 25 – 46%; Potassic feldspar – 15%, Biotite – 10%, Hornblende – 5%.	0.80	3.5	2680	0.74
4	Diorite	Plagioclase No. 12 – 65%; Amphibole – 30%; Magnetite – 5%.	0.1	8.5	2810	2.21
5	Gabbro-dolerite	Plagioclase No. 23 – 55%; Pyroxene – 36%; Amphibole – 6%; Magnetite – 3%.	0.24	12.2	2990	0.86
6	Hornblendite	Amphibole – 77%; Biotite – 23%.	0.1	(10)**	3000	-
7	Andesit-dacitic porphyrite	Quartz – 20%; Plagioclase No. 12 – 30%; Potassic feldspar – 20%, Calcite – 15%, Hematite – 10%, Biotite – 7%.	0.04	5.8	2510	6.7
8	Diabase	Plagioclase №65 – 37%; Pyroxene – 32%; Magnetite – 12%; Glass – 15%.	0.04	(8)**	2870	-
9	Olivinic basalt	Plagioclase №60 – 40%; Pyroxene – 30%; Olivine – 10%; Magnetite – 5%.Glass – 15%.	0.08	2.4	2710	4.5
10	White marble	Calcite – 100%.	0.65	7.0	2700	0.42
11	Dark gray marble	Calcite – 95%; Carbon black – 5%.	0.05	5.5	2730	0.22
12	Magnetite ore	Magnetite – 80%; Chlorite – 20%	0.02	(27)**	4950	-

**Remarks:*

1. All values except elasticity modulus are taken from the data presented in the works [21, 22].

*2. The values of elasticity modulus marked with * were calculated according to the propagation velocities of ultrasound and density given in works [21, 22]. Approximate values accepted in the calculations are given in parentheses and marked ** as there is no data on the speed of propagation of ultrasound.*

The experimental data used to verify the selected models of the works [21, 22] on linear thermal expansion of the rock of Table 1 at different temperatures are shown in Figure 1. Figure 2 shows the relationship between the calculated average weighted thermal changes in the volume of minerals composed in rocks and the calculated thermal changes in the volume of rock according to the experimental data of the works [21, 22]. The difference between the second and the first values characterizes the excess thermal increase in rock volume due to the formation of micro cavities (micro cracks).

Due to the fact that the thermal expansion of basalt (No. 9) is substantially lower than the values of average expansion of the mineral constituents, the data on the thermal expansion of basalt for model verification have not been used. Thermal expansion of basalt as well as of other rock will be either approximately equal (within the error limits) or more (with significant micro cracking) of the average thermal expansion of minerals. And as this is not observed, it is possible that the mineral composition of the studied specific samples of basalt was significantly different from the average mineral rock composition.

In addition, control experimental measurements of thermal deformations of 11 varieties of rock were carried out in this work. At the same time, samples prepared for each rock from a single large monolith were used to exclude the influence of variations of the rock mineral composition during preparation and examination of specimens from various samples for measuring thermal deformations and petrographic studies. Samples in the form of cylinders in diameter 30 mm with a height of 50 to 70 mm were made by the diamond drilling method in the 1980s when performing studies of the radiation changes in rock presented in works [23–26] and stored up to fulfillment of studies in normal conditions. At the same time studies of the mineral composition, structure, and properties of these rocks were carried out and presented in works [23, 26].

The selection of data about the name, mineral composition, structure and properties of rock the thermal expansion of which was investigated is given in Table 2.

The thermal expansion of the samples (2–3 samples of each rock) was investigated in a quartz dilatometer at a heating velocity of 2 °C/min. The deformations were measured with an accuracy of 0.001 mm. The deviations of the values of the relative changes in the sizes of different specimens did not exceed the average values of each rock:

$$\Delta\left(\frac{\Delta\ell}{\ell}\right) = 0.01\% + 0.083\frac{\Delta\ell}{\ell} \tag{9}$$

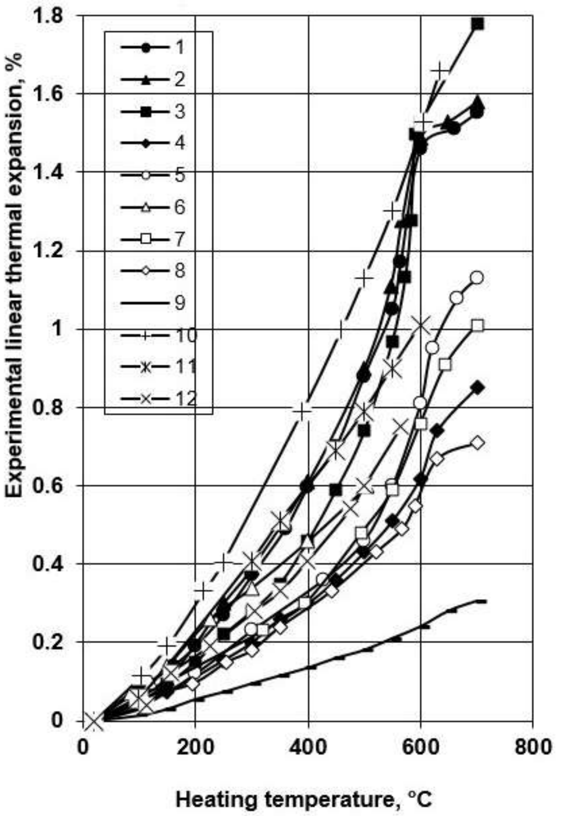

Figure 1. Experimental values of linear thermal expansion of different rocks from Table 1 depending on the heating temperature according to the works [21, 22]

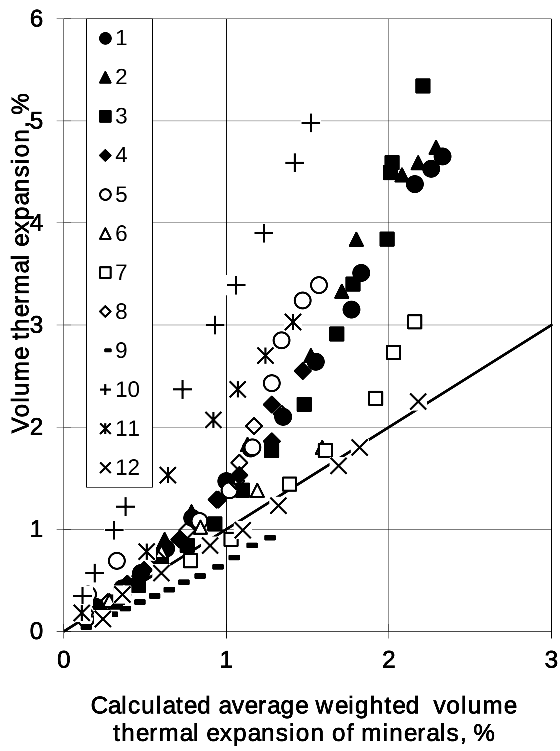

Figure 2. Relation between the calculated averages weighted volume thermal expansion of minerals composed in rock and the thermal volume thermal expansion of rocks from Table 1 calculated from the experimental data of the works [21, 22]

An inclined continuous straight line corresponds to the equality between them.

Table 2. Name, mineral composition, average size of grains and properties of rocks, thermal expansion of which was carried out in the present article based on the works [23, 26]

No. based on [23, 26]	Rock	Minerals in the rock composition and their content by volume	Average size of grains, cm	Elasticity modulus*, 10^4 MPa	Density, kg/m^3	Porosity, %
1	Granite coarse-grained	Quartz – 25%; Microcline – 50%; Oligoclase – 24%, Biotite – 1%.	0.5	1.9	2590	-
3	Granite medium-grained	Quartz – 30%; Microcline – 40%; Oligoclase – 25%, mining - 5%.	0.2	5.89	2620	-
4	Granite-porphyry fine-grained	Quartz – 40%; Microcline – 30%; Oligoclase – 15%, Muscovite -15%.	0.05	3.15	2570	-
5	Granodiorite medium-grained	Quartz – 20%; Microcline – 10%; Oligoclase – 40%, Hornblende - 15%; Biotite - 15%.	0.2	3.4	2680	-
7	Liparite aphanitic	Quartz – 35%; Microcline – 33%; Oligoclase – 32%	0.005	5.77	2640	-
14	Gabbro medium-grained	Labrador - 60%; Diopside – 40%.	0.2	10.7	2970	-
17	Diabase close-grained vesicular	Labrador - 60%; Diopside – 39%, Ore minerals -1%	0.03	3.22	2540	15
19	Diabase close-grained poikilitic	Labrador - 45%; Olivine - 30%; Homblende - 20%; Magnetite – 5%.	0.02	5.89	2760	-
20	Basalt close-grained	Labrador- 50%; Olivine - 30%; mining -10%, glass -10%.	0.01	5.94	2760	-
22	Peridotite medium-grained	Diopside - 15%; Olivine – 80, Ore minerals - 5%.	0.2	15.5	3300	-
29	Sandstone fine-grained	Quartz - 45%, fieldspar –45%, Ore minerals -10%.	0.03	1.98	2540	-

The experimental data used to verify the selected models of the works on the linear thermal expansion of the rock samples from Table 2 at different temperatures are shown in Figure 3. Figure 4 shows the relationship between the calculated average weighted thermal changes in the volume of minerals composed in rocks and the calculated thermal changes in the volume of rock according to the experimental data of the present work. The difference between the second and the first values characterizes the excess thermal increase in rock volume due to the formation of micro cavities (micro cracks).

Verification of the possibility to use the models for the analytical determination of the thermal expansion of rock was carried out by comparing the values calculated for these models and the experimental values of the thermal expansion of rock investigated in works [21, 22] and in this article. For clarity and compactness of such a comparison, the graphs of the relation between the calculated and experimental values of the thermal expansion of rock were constructed in the coordinates: calculated values of the linear thermal expansion $(\Delta\ell/\ell)_{CAL}$ along the horizontal axis X and experimental values of the linear thermal expansion $(\Delta\ell/\ell)_{EXP}$ along the vertical axis Y. Degree of deviation of values from a straight inclined line $(\Delta\ell/\ell)_{EXP} = (\Delta\ell/\ell)_{CAL}$ (match lines) clearly demonstrates the degree of coincidence of calculated and experimental data and makes it possible to easily calculate the necessary statistical characteristics. Data on the thermal deformation of minerals were taken by [1].

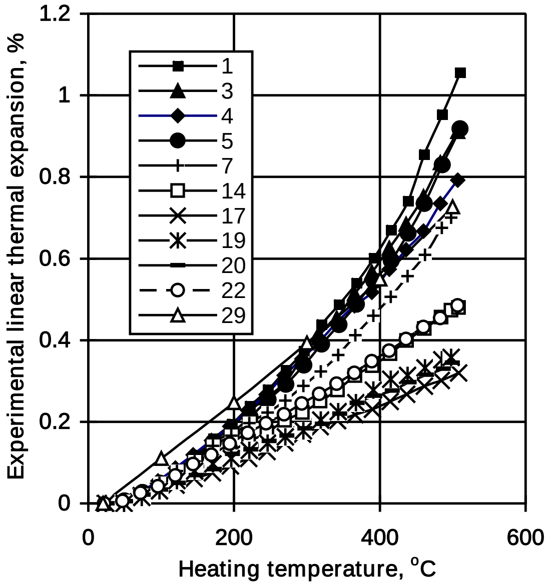

Figure 3. Experimental values of linear thermal expansion of different rocks from Table 2 depending on the heating temperature according to the present work

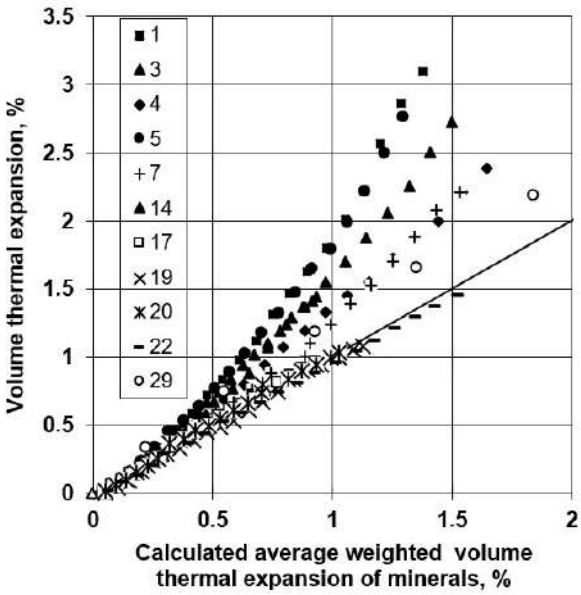

Figure 4. Relation between the calculated averages weighted volume thermal expansion of minerals composed in rock and the thermal volume thermal expansion of rocks from Table 2 calculated from the experimental data of the present work

3. Results and Discussion

The results of verification of the selected models based on the experimental data of works [21, 22] are shown in Figures 5 and 6 in the form of a relation between the values calculated for these models and the experimental data of the thermal change in rock size (linear thermal expansion).

Verifying the model of Balashov and Zaraiskiy [21, 22] we can seen (Figure 5) that the averaged line between the calculated and experimental values (regression line) of the thermal expansion of rock formations is diverted from the line $(\Delta\ell/\ell)_{EXP} = (\Delta\ell/\ell)_{CAL}$ up to 0.1 % and approximated by the expression:

$$(\Delta\ell/\ell)_{EXP} = (\Delta\ell/\ell)_{CAL}^{REF} = 0.9055(\Delta\ell/\ell)_{CAL}^{1.1659} \qquad (10)$$

where $(\Delta\ell/\ell)_{CAL}^{REF}$ - revised estimated change of sizes, %.

In addition, there are quite large deviations in the values of the experimental data from the calculated values of the thermal expansion of rocks. These deviations are up to $\Delta = \pm 0.6$ % from the match line and up to $\Delta = \pm 0.5$ % from the regression line. The reliability magnitude of the approximation is R^2 = 0.9324. The average square deviation of the experimental values from the regression line described by expression (10) and the variance estimate are S_{res} = ±0.19 % and S_{res}^2 = 0.036 %^{2}.

Verification the model of Denisov and Dubrovskiy has shown (Figure 6) that the regression line between the calculated and experimental values of the thermal expansion of rock deviates from the line $(\Delta\ell/\ell)_{EXP} = (\Delta\ell/\ell)_{CAL}$ up to 0.2 % and is approximated by the expression:

$$(\Delta\ell/\ell)_{EXP} = (\Delta\ell/\ell)_{CAL}^{REF} = 0.8992(\Delta\ell/\ell)_{CAL}^{1.0015} \qquad (11)$$

In addition, there are quite large deviations in the values of the experimental data from the calculated values of the thermal expansion of rocks. These deviations are up to $\Delta = \pm 0.6$ % from the match line and up to Δ = ±0.5 % from the regression line. The reliability magnitude of the approximation is R^2 = 0.9341, the average square deviation of the experimental values from the regression line and the variance estimate are S_{res} = ±0.16 % and S_{res}^2 = 0.026 %^{2} respectively.

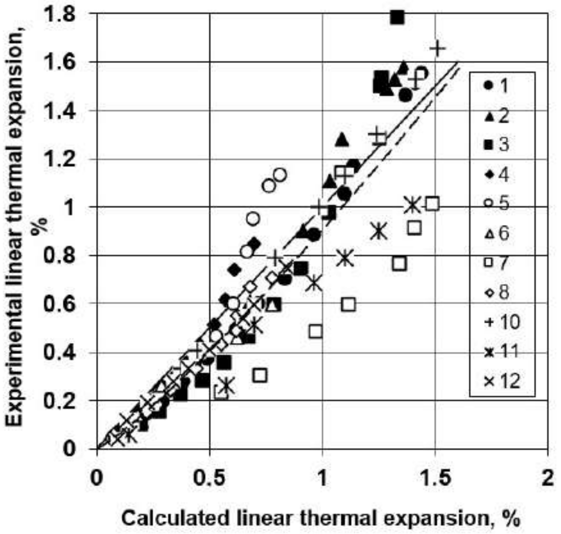

Figure 5. Relation between calculated linear thermal expansions for the model of Balashov and Zaraiskiy [21, 22] and experimental linear thermal expansion of rock dimensions from Table 1 obtained in works [21, 22]

An inclined continuous straight line corresponds to the equality between them. The dotted line shows the regression line. The equation and the value of approximation reliability of the regression line are also given.

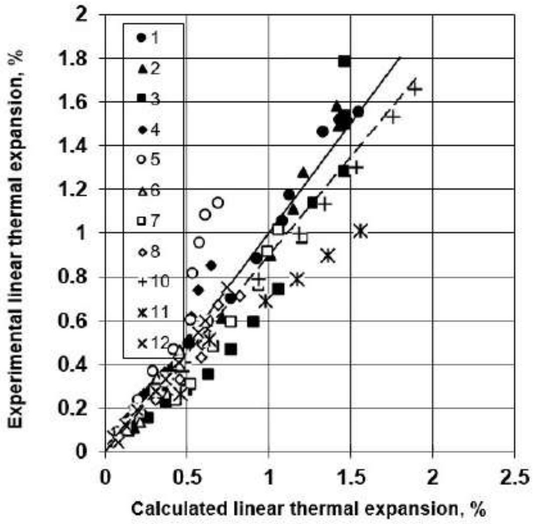

Figure 6. Relation between calculated linear thermal expansions for the model of Denisov and Dubrovskiy [23–26] and experimental linear thermal expansion of rock dimensions from Table 1 obtained in works [21, 22]

An inclined continuous straight line corresponds to the equality between them. The dotted line shows the regression line. The equation and the value of approximation reliability of the regression line are also given.

Thus, when using the experimental data of the works [21, 22] for verification of selected models there are relatively large deviations of the experimental data from the calculated values, which substantially exceed the error of 2 % indicated in these works.

In case of such deviations, it is not possible to establish the most adequate model to describe the process of thermal expansion of rock. Although using the model based on the current research work shows slightly smaller deviations in the values of experimental data from the calculated values of the thermal expansion of rock, which indicates a certain advantage of this model.

The following circumstances can be the causes of significant ranges of differences between the experimental and calculated values of thermal expansion of rocks.

1. Models do not adequately describe the process of thermal expansion.

2. There is influence of additional factors which increase the dispersion of the experimental data.

However, it is unlikely that both very different models are almost not adequate equally. It is possible that large deviations between the calculated and experimental thermal expansion values for the results of works [21, 22] are associated with some differences in the real mineral composition of the investigated rock samples from the average composition of the rock due to variations in the composition of different samples.

The verification results of the selected models based on the experimental data obtained in this article under the conditions of minimizing the possible differences in the indicated and actual characteristics of the mineral composition and the structure of the sample materials are shown in Figures 7–10. The figures show the relation between the models calculated for these models and experimental data of thermal changes in rock size data obtained in this article

During the verification of the model of Balashov and Zaraiskiy [21, 22] we can see (Figure 7) that although the regression line between the calculated and experimental values of the thermal expansion of rock deviates from the line $(\Delta\ell/\ell)_{EXP} = (\Delta\ell/\ell)_{CAL}$ up to 0.2 %, deviations of the values of the experimental data from the calculated values of the thermal expansion of rock is approximately twofold lower than when using data of the works [21, 22].

Deviations of the experimental data for the model of the works [21, 22] are up to Δ = ±0.35 % from the match line and up to Δ = ±0.25 % from the regression line. The average square deviation of the experimental values from the regression line and the variance estimate while using the experimental data amounts to S_{res} = ±0.088 % and S_{res}^2 = 0.0077 %². The reliability magnitude of the approximation is R^2 = 0.9217.

The regression line between the calculated and experimental values of the thermal expansion of rocks is approximated by the expression which describes the correction to be applied to the calculation results by the model as follows:

$$(\Delta\ell/\ell)_{EXP} = (\Delta\ell/\ell)_{CAL}^{REF} = 0.1964(\Delta\ell/\ell)_{CAL}^2 + 0.6802(\Delta\ell/\ell)_{CAL} \quad (12)$$

After recalculating of the calculated values of thermal expansion using formula (12), the relation between the calculated and experimental thermal deformations is shown in Figure 8 and more clearly illustrates the degree of deviation of the experimental data from the calculated ones.

Verification the model of Denisov and Dubrovskiy [23–26] on the experimental results of this work is shown in Figure 9. Figure 9 shows that although the regression line between the calculated and experimental values of the thermal expansion of rock also deviates from the line $(\Delta\ell/\ell)_{EXP} = (\Delta\ell/\ell)_{CAL}$ (in this case up to 0.16 %), the deviation of the values of the experimental data from the calculated values of the thermal expansion of rock is lower than when using data of the works [21, 22].

Moreover when using experimental data of this work to verify this model, the deviation of experimental values from the calculated values of thermal expansion of rock is less than in the model of the works [21, 22] during verification with the same data and is up to Δ = ±0.25 % from the match line and up to Δ = ±0.15 % from the approximation line. The average square deviation of the experimental values from the regression line using the data of this work is also less and amounts to S_{res} = ±0.033 % on S_{res}^2 = 0.0011 %². The reliability magnitude of the approximation is R^2 = 0.9786.

The regression line between the calculated and experimental values of the thermal expansion of rocks is approximated by the expression which describes the correction to be applied to the calculation results by the model as follows:

$$(\Delta\ell/\ell)_{EXP} = (\Delta\ell/\ell)_{CAL}^{REF} = 0.2036(\Delta\ell/\ell)_{CAL}^2 + 0.6331(\Delta\ell/\ell)_{CAL} \quad (13)$$

After recalculating of the calculated values of thermal expansion using formula (13), the relation between the calculated and experimental thermal deformations is shown in Figure 10 and more clearly illustrates the degree of deviation of the experimental data from the calculated ones.

At the same time, Figure 10 demonstrates some asymmetry in dispersion of the experimental data due to an abnormally high deviation of diabase No. 19 and basalt No. 20.

The research has shown that in formula (4a) only the correction factor C = 0.5% can be introduced instead of using a general correction to the calculation results of formula (13).

In this case, formula (4,a) takes the form:

$$\frac{\Delta V}{V} = \left(\frac{\Delta V}{V}\right)_1 = 3\left(\frac{\Delta\ell}{\ell}\right)_{M.M} - a_M \frac{E_0}{E_{M.M}\sqrt{d_{GR}}} * \frac{1-V_{M.RED}}{V_{M.RED}} - C \text{ – at } \left(\frac{\Delta V}{V}\right)_1 \geq \left(\frac{\Delta V}{V}\right)_2 \quad (4,a^I)$$

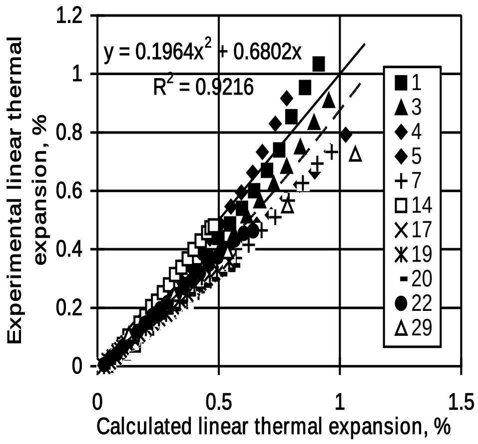

Figure 7. Relation between calculated linear thermal expansions for the model of Balashov and Zaraiskiy [21, 22] and experimental linear thermal expansion of rock dimensions from Table 2 obtained this article

See remarks to Figures 5 and 6 for explanation to the lines.

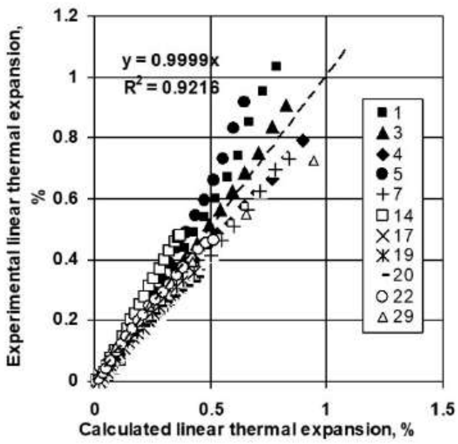

Figure 8. Relation between calculated linear thermal expansions for the model of Balashov and Zaraiskiy [21, 22] with expression correction. (12) and experimental linear thermal expansion of rock dimensions from Table 2 obtained this article

See remarks to Figures 5 and 6 for explanation to the lines.

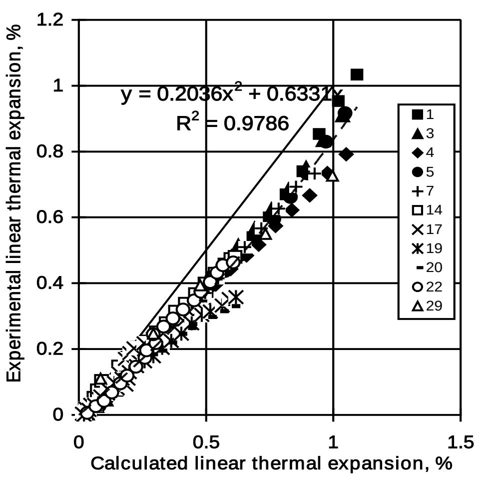

Figure 9. Relation between calculated linear thermal expansions for the model of Denisov and Dubrovskiy [23–26] and experimental linear thermal expansion of rock dimensions from Table 2 obtained in this article

See notes to Figures 5 and 6 for an explanation to the lines.

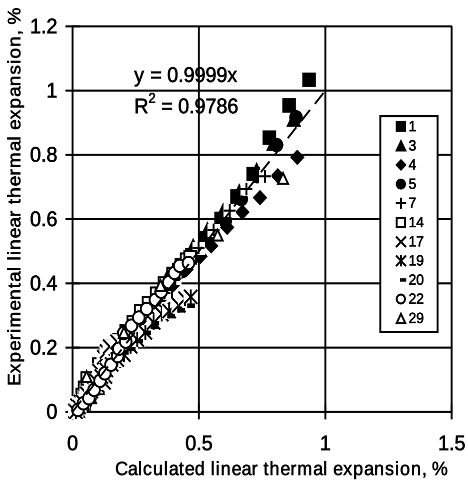

Figure 10. Relation between calculated linear thermal expansions for the model of Denisov and Dubrovskiy [23–26] with the expression correction (13) and experimental linear thermal expansion of rock dimensions from Table 2 obtained in this article

See notes to Figures 5 and 6 for an explanation to the lines.

Taking into account C = -0.5 % (Figure 11) the dispersion of the experimental data becomes more symmetrical, the abnormal deviation of diabase No. 19 and basalt No. 20 disappears, the errors do not change significantly. The maximum and standard square deviation of the experimental values from the regression line $(\Delta\ell/\ell)_{EXP} = (\Delta\ell/\ell)_{CAL}$ as well as the variance estimate are up to $\Delta = \pm 0.13$ %, S_{res} = ±0.038 % and S_{res}^2 = 0.0014 %^{2} respectively. The reliability magnitude of the approximation is R^2 = 0.9745.

Thus, while using the model of Denisov and Dubrovskiy [23–26], there are less deviations between the calculated and experimental values of the thermal expansion of rock than while using the model of Balashov and Zaraiskiy [21, 22] which is clearly shown in Table 3.

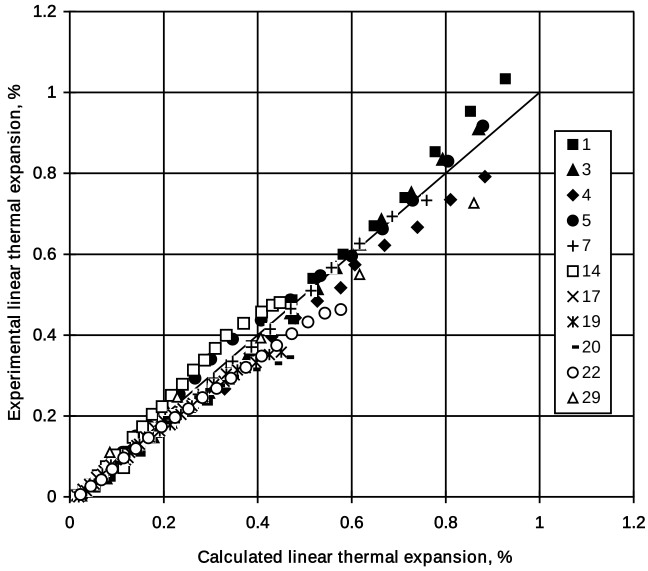

Figure 11. Relation between calculated linear thermal expansions for the model of Denisov and Dubrovskiy [23–26] at C = 0.5 % and experimental linear thermal expansion of rock dimensions from Table 2 obtained in this article.

An inclined continuous straight line corresponds to the equality between them and the regression line.

Table 3. Summarized data about verification results of studied models on the basis of various experimental data

Model	Verification based on works [21, 22]				Verification based on the current research work			
	Deviations of experimental data from regression line	R^2	S_{res}, %	S_{res}^2, %2	Deviations of experimental data from regression line	R^2	S_{res}, %	S_{res}^2, %2
Model of Balashov and Zaraiskiy [21, 22]	up to 0.5 % (Figure 5)	0.9324	0.19	0.036	up to 0.25 % (Figure 8)	0.9217	0.088	0.0077
Model of Denisov and Dubrovskiy [23–26]	up to 0.5 % (Figure 6)	0.9341	0.16	0.026	up to 0.15 % (Figure10)	0.9786	0.033	0.0011
					up to 0.13 % (Figure11)	0.9745	0.038	0.0014

The deviation of the experimental data from the calculated data based on this model is commensurate with the dispersion of the experimental data when measuring the thermal change in the sizes of individual samples of rock which indicates the adequacy of the model to the experimental data without detailed statistical analysis based on the Fisher criterion.

This allows us to recommend the model provided of Denisov and Dubrovskiy with the correction factor C=0.5% for the analytical determination of the thermal expansion of the most part of rocks and concrete mineral aggregates according to the data on thermal deformations of minerals based on information on the mineral composition, the average grain size of the minerals and the elasticity modulus of the rock. The model is applicable in case of heating up to 700 °C under normal pressure and humidity for isotropic rocks with no minerals in them that can decompose at these temperatures with water and gases emission.

The maximum deviations between the calculated and experimental thermal changes in the size based on this model with heating up to 510 ˚C with minimal dispersion of mineral composition, structure and properties amounts are:

$$\Delta\left(\frac{\Delta\ell}{\ell}\right)=\begin{cases}0.02\%+0.2\dfrac{\Delta\ell}{\ell}-at\quad\dfrac{\Delta\ell}{\ell}\leq 0.55\%\\ 0.13\%-at\quad\dfrac{\Delta\ell}{\ell}\geq 0.55\%\end{cases} \tag{14}$$

In the range of 50-700 °C the maximum deviations between the calculated and experimental thermal changes in size are from 0.05 % to 0.5 % when the size is changed from 0 to 1.5–1.7 % respectively.

As this model is used for the analytical determination of the radiation expansion of rock the results of the work confirmed the analogy between the mechanisms of radiation and thermal changes in rock at the level of interaction of the crystals of minerals. However, the necessity to introduce the correction confirms some differences in the mechanisms of thermal and radiation damage of rock associated with the growth of the contribution of plastic deformations to the relaxation of microstructural intensions with increasing temperature.

The correction can be made according to the data of the works [21, 22] in case of high values of pressure and humidity of the environment (in the hydrothermal conditions of the Earth's crust, for example).

The possibility of using the model for anisotropic (stratified, for example) rock, as well as in case of presence of minerals in the rock composition which decompose when heating with water and gases emission, requires additional studies. The thermal expansion of anisotropic rock due to the distribution of minerals in space can vary in different directions. Even if the deformation of the minerals is taken into account, an increase in the expansion of rock can occur due to additional crack opening under the influence of the pressure of gases and water vapor (if water and gases are released).

The possibility of using the model at temperatures over 500 °C and especially more than 700 °C also requires additional studies. The experimental data did not allow reliable verification of the model at temperatures from 500 °C to 700 °C. Although it is possible to use the model for these temperatures taking into account that the inaccuracy can be up to 0.5 %. At the same time as the temperature rises the plasticity of the rock increases, therefore, it may be necessary to use additional corrections at temperatures over 500 °C for more reliable calculations. In addition, some minerals (carbonates, serpentines, chlorites) can partially or completely decompose with water and gases emission at these temperatures which may be the source of the additional expansion mentioned above. In the range of 700–1000 °C, according to the experimental data of the work [27] and the estimated calculations based on formulas (4) experimental thermal changes in the rock size may exceed the calculated values by up to 1 %.

The thermal change in the volume of rock due to the formation of cracks $\left(\frac{\Delta V}{V}\right)_{CR}$ is determined by formula (8) and does not require special verification. The difference in the values of the thermal expansion of different rocks is determined by differences in the degree of their cracking and by differences in the average expansion of the mineral constituents. In this regard, the shown possibility of using the model for the analytical determination of the thermal expansion of rocks shows the possibility of using this model for calculating volume changes due to the formation of cracks.

According to the data of the works [21, 22] and the present work, the residual deformations of rock are observed after heating at temperatures over 200—300 ˚C.

When the temperature is lowered, the formed cracks during heating will be closed. But due to some displacement of the crystals relative to each other only its partial closing occurs which explains the appearance of residual deformations after heating. The values of these deformations increase with increasing heating temperature, the values of thermal expansion, and hence the values of expansion due to the crack formation.

In this regard, it is interesting to consider the dependence of the values of the thermal residual deformations of rock from the values of deformations due to the crack formation. It is obvious that the thermal residual deformations of rock will depend not only on the magnitude of the volume change due to the crack formation but also due to the number of heating cycles, the environmental conditions (humidity, especially). The residual deformations will increase while the number of heating and humidity cycles increases as the degree of crystal displacement rises with the number of cycles and the wedging effect of water increases with increasing humidity. The data of the works [4, 21, 22] have confirmed this.

In this regard, the base deformations will be the thermal residual deformations of rock after the initial heating $\left(\frac{\Delta V}{V}\right)_{RES}$ The influence of the number of cycles and humidity can be estimated from the data of the works [4, 21, 22].

The graphic dependencies $\left(\frac{\Delta V}{V}\right)_{RES}$ from $\left(\frac{\Delta V}{V}\right)_{CR.}$ are shown in Figures 12 and 13 and demonstrate the presence of the dependence of residual deformations of rock after heating from the deformations of rock when heated due to the formation of cracks. As in the case of thermal expansion, fairly large dispersion is observed according to the data of the works [21, 22]. These dispersions are much lower for the data shown in the present article.

The dependencies shown in Figures 12, 13 and their approximation equations at x = $\left(\frac{\Delta V}{V}\right)_{RES}$ and y = $\left(\frac{\Delta V}{V}\right)_{CR}$ can be used for the analytical determination of residual thermal deformations of rock after the first heating and cooling in normal conditions.

Due to residual deformations during rock reheating, as shown in Figures 14 and 15, based on the results of the present work, the change in their sizes relative to the sizes before the first heating, mainly exceeds the size changes during the first heating. However, the temperature is higher so the difference is less. Therefore, at a temperature equal to the maximum temperature of the first heating, the change in size during the second heating is slightly larger than the change in sizes during the first heating. The change in size during cooling after the second heating (including residual deformations) is slightly different from the changes in sizes during the cooling after the first heating.

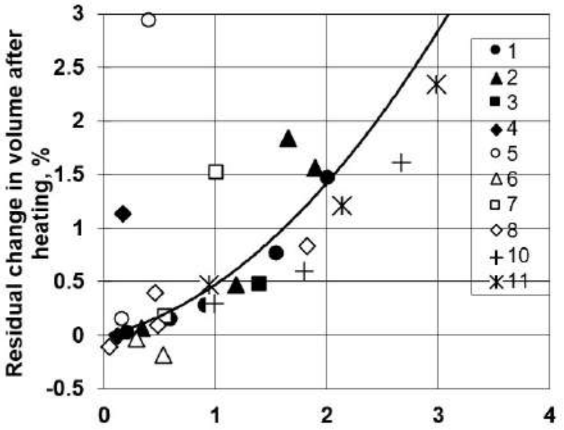

Figure 12. Relation between the calculated increase in volume due to the crack formation of rock from Table 1 when heated and the experimental residual increase in volume after heating to 300–700 °C according to the data of the works [21, 22]

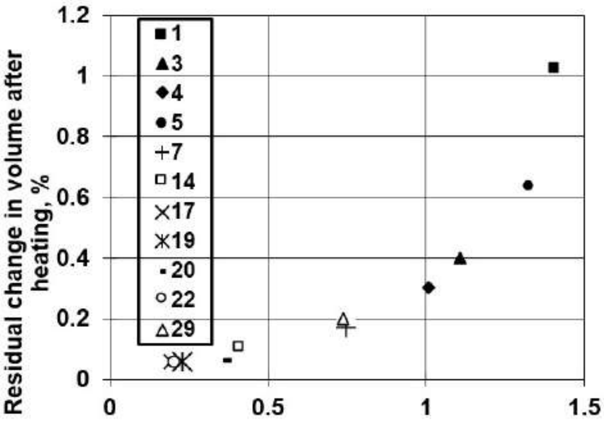

Figure 13. Relation between the calculated volume increase due to the crack formation of rock from Table 2 when heated and the experimental residual volume increase after heating to 490-510 °C according to the data of the current research work

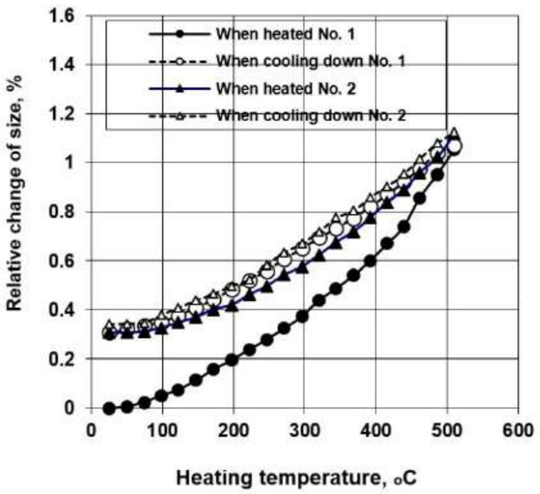

Figure 14. Experimental values of the thermal increase in the size of granite No. 1 according to the Table 2 in case of the first and second heating and cooling

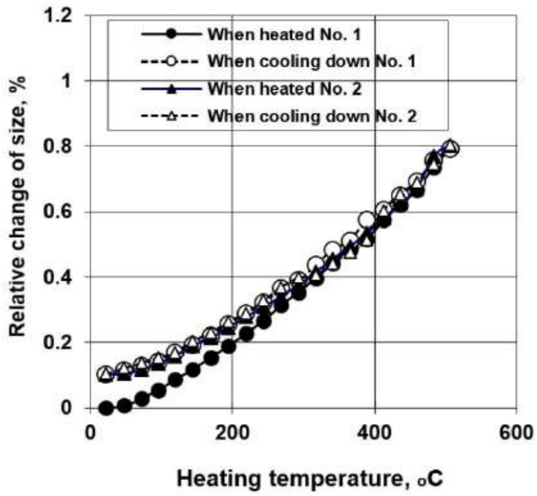

Figure 15. Experimental values of the thermal increase in the size of granite-porphyry No. 4 according to the Table 2 in case of the first and second heating and cooling

In this regard, the thermal expansion, with respect to the sizes before the first heating, is larger and, with respect to the sizes after the first heating, is less than during the first heating when rocks are reheated and can approximately be described by the following expressions:

$$\left(\frac{\Delta\ell}{\ell}\right)_{T2}=\left(\frac{\Delta\ell}{\ell}\right)_{T1}\frac{\left(\frac{\Delta\ell}{\ell}\right)_{TMAX1}-\left(\frac{\Delta\ell}{\ell}\right)_{T1RES}}{\left(\frac{\Delta\ell}{\ell}\right)_{TMAX1}}(1+k_n)+\left(\frac{\Delta\ell}{\ell}\right)_{T1RES} \quad (15)$$

$$\left(\frac{\Delta\ell}{\ell}\right)_{T2RES}=(1+k_n)\left(\frac{\Delta\ell}{\ell}\right)_{T1RES} \quad (16)$$

- in relation to the sizes before the first heating;

$$\left(\frac{\Delta\ell}{\ell}\right)_{T2}=\left(\frac{\Delta\ell}{\ell}\right)_{T1}\frac{\left(\frac{\Delta\ell}{\ell}\right)_{TMAX1}-\left(\frac{\Delta\ell}{\ell}\right)_{T1RES}}{\left(\frac{\Delta\ell}{\ell}\right)_{TMAX1}}(1+k_n) \quad (17)$$

$$\left(\frac{\Delta\ell}{\ell}\right)_{T2RES}=k_n\left(\frac{\Delta\ell}{\ell}\right)_{T1RES} \quad (18)$$

- in relation to the sizes after the first heating (before the second heating),

where $\left(\frac{\Delta\ell}{\ell}\right)_{T1}$ – the relative change in sizes upon the first heating up to temperature T;

$\left(\frac{\Delta\ell}{\ell}\right)_{T2}$ – the relative change in sizes during the second heating up to temperature T in relation to the sizes before the first heating in formula (15) and to the sizes after the first heating in formula (17);

$\left(\frac{\Delta\ell}{\ell}\right)_{TMAX1}$ and $\left(\frac{\Delta\ell}{\ell}\right)_{T1RES}$ – relative change in sizes at the maximum temperature during the first heating and the residual sizes after the first heating, respectively;

$\left(\frac{\Delta\ell}{\ell}\right)_{T2RES}$ – residual changes in sizes after the second heating with respect to the sizes before the first heating in formula (15) and the sizes after the first heating in formula (17);

k_n – coefficient equal to $k_n \approx 0.1$ for the second heating according to the data of the present research work.

In this regard, the model will overestimate thermal deformations of rocks if the rock formation was subjected to high temperature heating before calculating of the thermal expansion and this will not be taken into account by formulas (17) and (18) (if nothing is known about this, for example). Moreover, the temperature of the preceding heating can be restored by the discrepancy between the calculated and experimental thermal deformations of rocks. Prior to the calculations heating of rock and mineral aggregates of concrete in the form of natural gravel and sand must be taken into account if there were no processes of metasomatism and metamorphism after heating. The cracks formed during heating will be filled with new minerals and closed under pressure during metasomatism and metamorphism of the rock formation. The previously fulfilled heating of concrete aggregates made by crushing of rock after their manufacture must be accounted by formulas (15) and (18).

4. Conclusions

1. The article provides selection and approbation of the model and the model-based method for the analytical determination of thermal expansion and rock fracturing (decompression) and concrete mineral aggregates according to the data about thermal deformations of minerals based on information of the mineral composition, the average grain fineness of minerals and the elasticity modulus of rock.

2. To accomplish the research, the author has used two models available in scientific publications:

- Balashov and Zaraiskiy Model for calculating the thermal expansion and decompression of rock based on thermal deformations of minerals. The model does not take into account the structure and mechanical properties of rock.

- The model of Denisov (one of the authors of this work) and Dubrovskiy was developed and evaluated earlier for the analytical determination of radiation expansion and rock fracturing when neutrons are irradiated by nuclear reactors on the basis of radiation deformation of minerals. The model takes into account the grain fineness and elasticity modulus of rock. The model is accepted for research on the basis of the analogy between the processes of thermal and radiation changes of rock at the level of interaction in mineral crystals.

3. To test chosen models, experimental data was selected. It contained all the necessary information on thermal expansion of 11 varieties of magmatic and sedimentary rocks in the range 20 to 700 ˚C. In addition, experimental research of the thermal expansion of 11 varieties of magmatic and sedimentary rocks in the range from 20 to 510 ˚C was carried out to verify the models under the conditions of the minimal influence of the rock dispersion and rock composition by means of a quartz dilatometer. At the same time, there were prepared samples for each rock. Each was taken from a single large monolith to exclude the influence of variations of the rock mineral composition during preparation and examination of various samples taken for measuring thermal deformations and petrographic studies.

4. The model of Denisov and Dubrovskiy describes the process of thermal expansion and rock fracturing. It is more adequate and better than Balashov and Zaraiskiy Model especially when introducing the correction associated with an increase in plasticity of rocks when heated.

This allows us to recommend the model provided of the author of the current research work for the analytical determination of the thermal expansion of the most part of rocks and concrete mineral aggregates according to the data on thermal deformations of minerals based on information on the mineral composition, the average grain size of the minerals and the elasticity modulus of the rock. The model is applicable in case of heating up to 700 °C (is more reliable for 500 °C heating) under normal pressure and humidity for isotropic rocks with no minerals in them that can decompose at these temperatures with water and gases emission.

5. The possibility of using the model for anisotropic rock, in the presence of minerals in the rock composition which decompose when heating with water and gases emission, requires additional studies. The correction can be made according to the scientific literature data in case of high values of pressure and humidity of the environment (in the hydrothermal conditions of the Earth's crust, for ex-ample).

6. There current research established approximate dependence of the residual rock deformations after the first heating from the increase in volume when heated due to the cracks formation. The article also shows the relationship between thermal changes in rock size during the first and second heating and cooling stages.

7. Prior to the calculations heating of rock and mineral aggregates of concrete in the form of natural gravel and sand must be taken into account if there were no processes of metasomatism and metamorphism after heating. The previously fulfilled heating of concrete aggregates made by crushing of rock after their manufacture should be also taken into account.

8. The results of the work can be used to solve the problems of thermal destruction efficiency and rock drilling, rock metasomatism, possibility of using rock massifs to bury radioactive wastes, store thermal energy, predict thermal deformations and heat resistance of concretes with mineral aggregates.

References

1. *Spravochnik fizicheskih konstant gornyh porod* [Handbook of physical constants of rocks]. Pod obshchey redaktsiey S. Klarka ml. Per. s angl. Moscow: Mir. 1969. 544 p. (rus)
2. Dmitriyev A.P., Kuzyayev L.S., Protasov Yu.I., Yumshchikov V.S. *Fizicheskiye svoystva gornyh porod pri vysokih temperaturah* [Physical properties of rocks at high temperatures]. Moscow: Nedra, 1969. 160 p.(rus)
3. Lyubimov N.I., Nosenko L.I. *Spravochnik po fiziko-mekhanicheskim parametram gornyh porod rudnyh rayonov* [Handbook of physical and mechanical parameters of rocks ore areas]. Moscow.: Nedra, 1978. 285 p. (rus)
4. Dmitriyev A.P., Goncharov S.A. *Termicheskoye i kombinirovannoye razrusheniye gornyh porod* [Thermal and combined destruction of rocks]. Moscow: Nedra. 1978. 304 p. (rus)
5. Dmitriyev A.P., Goncharov S.A., Germanovich L.N. *Termicheskoe razrusheniye gornyh porod* [Thermal destruction of rocks]. Moscow: Nedra, 1990. 255 p. (rus)
6. Zarayskiy G.P. *Eksperiment v reshenii problem metasomatizma* [Experiment in solving the problems of metasomatism]. Moscow: GEOS, 2007.136 p. (rus)
7. Sippel J., Siegesmund S., Weiss T., et al. Decay of natural stones caused by fire damage. In:Prikryl R., Smith BJ (eds). *Building Stone Decay: From Diagnosis to Conservation.* Geol Soc Spec Pub, London. 2007. Pp. 139–151.
8. Siegesmund S., Dürrast H. Physical and Mechanical Properties of Rocks. In: Siegesmund S., Snethlage R. (eds). *Stone in Architecture*. Springer, Berlin, Heidelberg. 2011. Pp. 97–225.
9. Goncharov S.A. Mekhanizm termicheskogo rasshireniya gornyh porod [The mechanism of thermal expansion of rocks]. *Gornyy zhurnal.* 2012. No. 9. Pp. 53–55. (rus)
10. Zhang Z.-X. *Rock Fracture and Blasting: Theory and Applications.* Butterworth-Heinemann, 2016. 528 p.
11. Petrov V.A. *Tektonodinamicheskiye usloviya izolyatsii radioaktivnyh othodov v kristallicheskih porodah* [Tectonodynamic conditions of isolation of radioactive waste in crystalline rocks]: Grand PhD dissertation. Moscosw. 2006. 476 p. (rus)
12. *Principles and Standards for the Disposal of Long-lived Radioactive Wastes.* Vol. 3 (Waste Management) Editors: N. Chapman C. McCombie. Hardcover. 2003. 292 p.
13. Tiskatine R., Eddemani A., Gourdo L., Abnay B., Ihlal A., Aharoune A., Bouirden L. Experimental evaluation of thermo-mechanical performances of candidate rocks for use in high temperature thermal storage. *Applied Energy.* 2016. Vol. 171. Pp. 243–255.
14. Tiskatine R., Oaddi R., Ait El Cadi R., Bazgaou A., Bouirden L., Aharoune A., Ihlal A. Suitability and characteristics of rocks for sensible heat storage in CSP plants. *Solar Energy Materials and Solar Cells.* 2017. Vol. 169. Pp. 245–257.
15. Nekrasov K.D., Tarasova A.P. *Zharostoykiy beton na portlandtsemente* [Heat-resistant concrete on Portland

Литература

1. Справочник физических констант горных пород. Под общей редакцией С. Кларка мл. Пер. с англ. М.: Мир, 1969. 544 с.
2. Дмитриев А.П., Кузяев Л.С., Протасов Ю.И., Ямщиков В.С. Физические свойства горных пород при высоких температурах. М.: Недра, 1969. 160 с.
3. Любимов Н.И., Носенко Л. И. Справочник по физико-механическим параметрам горных пород рудных районов. М.: Недра, 1978. 285 с.
4. Дмитриев А.П., Гончаров С.А. Термическое и комбинированное разрушение горных пород. М: Недра, 1978. 304 с.
5. Дмитриев А.П., Гончаров С.А., Германович Л.Н. Термическое разрушение горных пород. М.: Недра, 1990. 255 с.
6. Зарайский Г.П. Эксперимент в решении проблем метасоматизма. М.: ГЕОС, 2007. 136 с.
7. Sippel J., Siegesmund S., Weiss T., et al. Decay of natural stones caused by fire damage. In: Prikryl R., Smith BJ (eds) // Building Stone Decay: From Diagnosis to Conservation. Geol Soc Spec Pub, London. 2007. Pp. 139–151.
8. Siegesmund S., Dürrast H. Physical and Mechanical Properties of Rocks. In: Siegesmund S., Snethlage R. (eds) // Stone in Architecture. 2011. Pp. 97–225.
9. Гончаров С.А. Механизм термического расширения горных пород // Горный журнал. 2012. № 9. С. 53–55.
10. Zhang Z.-X. Rock Fracture and Blasting: Theory and Applications. Butterworth-Heinemann, 2016. 528 p.
11. Петров В.А. Тектонодинамические условия изоляции радиоактивных отходов в кристаллических породах: Дисс. на соиск. д.г-м.н. М., 2006. 476 с.
12. Principles and Standards for the Disposal of Long-lived Radioactive Wastes. Vol. 3 (Waste Management) Editors: N. Chapman C. McCombie. Hardcover. 2003. 292 p.
13. Tiskatine R., Eddemani A., Gourdo L., Abnay B., Ihlal A., Aharoune A., Bouirden L. Experimental evaluation of thermo-mechanical performances of candidate rocks for use in high temperature thermal storage // Applied Energy. 2016. Vol. 171. Pp. 243–255.
14. Tiskatine R., Oaddi R., Ait El Cadi R., Bazgaou A., Bouirden L., Aharoune A., Ihlal A. Suitability and characteristics of rocks for sensible heat storage in CSP plants // Solar Energy Materials and Solar Cells. 2017. Vol. 169. Pp. 245–257.
15. Некрасов К.Д., Тарасова А.П. Жаростойкий бетон на портландцементе. М.: Стройиздат, 1969. 192 с.
16. Невилль А.М. Свойства бетона.. Пер. с англ. М.: Стройиздат,1972. 344 с.
17. Жуков В.В., Цикунов В.С., Хаджишалапов Г.Н., Магомедов А.Д. Жаростойкий бетон и тяжелый бетон для повышенных температур в реакторостроении. Махачкала: Новый день,2002. 151 с.
18. Xing Z, Beaucour A.-L., Hebert R., Noumowe A., Ledesert B. Influence of the nature of aggregates on the

cement]. Moscow: Stroyizdat, 1969. 192 p. (rus)

16. Nevill A.M. *Svoystva betona* [Property of concrete]. Moscow: Stroyizdat,1972. 344 p. (rus)
17. Zhukov V.V., Tsikunov B.C., Hadzhishalapov G.N., Magomedov A.D. *Zharostoykiy beton i tyazhelyy beton dlya povyshennyh temperatur v reaktorostroenii* [Heat-resistant concrete and heavy concrete for elevated temperatures in reactor construction]. Mahachkala: Novyy den. 2002. 151 p. (rus)
18. Xing Z., Beaucour A.-L., Hebert R., Noumowe A., Ledesert B. Influence of the nature of aggregates on the behaviour of concrete subjected to elevated temperature. *Cement and Concrete Research.* 2011. Vol. 41. No. 4. Pp. 392–402.
19. Niry R.R., Beaucour A.-L., Hebert R., Noumowé A., Ledésert B., Bodet R. Thermal stability of different siliceous and calcareous aggregates subjected to high temperature. *MATEC Web of Conferences*. 2013. Vol. 6. 07001.
20. Niry R.R., Beaucour A.-L., Hebert R., Ledesert B., Bodet R., Noumowe A. High temperature behaviour of a wide petrographic range of siliceous and calcareous aggregates for concretes. *Construction and Building Materials.* 2016. Vol. 123. Pp. 261–273.
21. Zarayskiy G.P., Balashov V.N. Teplovoe razuplotneniye gornyh porod kak faktor formirovaniya gidrotermalnyh mestorozhdeniy [Thermal decompaction of rocks as a factor in the formation of hydrothermal deposits]. *Geologiya rudnyh mestorozhdeniy.* 1981. No. 6. Pp. 19–35. (rus).
22. Balashov V.N., Zarayskiy G.P. Eksperimentalnoe i teoreticheskoe issledovanie protsessa razuplotneniya gornyh porod pri nagrevanii [Experimental and theoretical study of the process of disintegration of rocks by heating]. *Ocherki fiziko-himicheskoy petrologii.* 1982. No. 10. Pp. 69–109. (rus).
23. Denisov A.V. *Radiatsionnye izmeneniya zapolniteley tyazhelyh betonov i metod ih analiticheskogo opredeleniya* [Radiation-induced alteration of aggregates of heavy concretes, and method for their analytical determination]. PhD dissertation. Moscow, 1986. 276 p (rus).
24. Denisov A.V. Dubrovskiy V.B. Analiticheskoe opredelenie radiatsionnogo izmeneniya svoystv materialov zapolniteley betonov [Analytical determination of radiation changes in the properties of concrete aggregate materials]. *Voprosy atomnoy nauki i tekhniki. Ser. Proektirovanie i stroitelstvo.* 1984. No. 2(18). Pp. 45–57. (rus)
25. Denisov A.V., Dubrovskiy V.B., Muzalevskiy L.P. Prognozirovanie radiatsionnyh izmeneniy neorganicheskih stroitel'nyh materialov [Prediction of radiation changes in inorganic building materials]. *Voprosy atomnoy nauki i tekhniki. Ser. Proektirovanie i stroitelstvo.* 1990. No. 3. Pp. 98–102. (rus)
26. Denisov A.V., Dubrovskiy V.B., Solovev V.N. *Radiatsionnaya stoykost mineralnyh i polimernyh stroitelnyh materialov* [Radiating stability of mineral and polymeric building materials]. Moscow: Izdatelskiy dom MEI, 2012. 284 p. (rus)
27. Kožušníková A., Konecny P., Plevova E., Králová L. Changes of Physical Properties of Silesian Granite Due to Heat Loading. Symposium of the International Society for Rock Mechanics. *Procedia Engineering.* 2017. Vol. 191. Pp. 426–433.

behaviour of concrete subjected to elevated temperature // Cement and Concrete Research. 2011. Vol. 41. No. 4. Pp. 392–402.

19. Niry R.R., Beaucour A.-L., Hebert R., Noumowé A., Ledésert B., Bodet R. Thermal stability of different siliceous and calcareous aggregates subjected to high temperature // MATEC Web of Conferences. 2013. Vol. 6. 07001.
20. Niry R.R., Beaucour A-L, Hebert R., Ledesert B., Bodet R., Noumowe A. High temperature behaviour of a wide petrographic range of siliceous and calcareous aggregates for concretes // Construction and Building Materials. 2016. Vol. 123. Pp. 261–273.
21. Зарайский Г.П., Балашов В.Н. Тепловое разуплотнение горных пород как фактор формирования гидротермальных месторождений // Геология рудных месторождений. 1981. № 6. С. 19–35.
22. Балашов В.Н., Зарайский Г.П. Экспериментальное и теоретическое исследование процесса разуплотнения горных пород при нагревании // Очерки физико-химической петрологии. М.: Наука, 1982. № 10. С. 69–109.
23. Денисов А.В. Радиационные изменения заполнителей тяжелых бетонов и метод их аналитического определения: Дисс. на соиск. учен. степ. к.т.н. М., 1986. 276 с.
24. Денисов А.В. Дубровский В.Б. Аналитическое определение радиационного изменения свойств материалов заполнителей бетонов // Вопросы атомной науки и техники. Сер. Проектирование и строительство. 1984. № 2(18). С. 45–57.
25. Денисов А.В., Дубровский В.Б., Музалевский Л.П. Прогнозирование радиационных изменений неорганических строительных материалов // Вопросы атомной науки и техники. Сер. Проектирование и строительство.1990. № 3. С. 98–102.
26. Денисов А.В., Дубровский В.Б., Соловьев В.Н. Радиационная стойкость минеральных и полимерных строительных материалов. М.: Издательский дом МЭИ, 2012. 284 с.
27. Kožušníková A., Konecny P., Plevova E., Králová L. Changes of Physical Properties of Silesian Granite Due to Heat Loading. Symposium of the International Society for Rock Mechanics // Procedia Engineering. 2017. Vol. 191. Pp. 426–433.

Aleksandr Denisov,*
+7(499)1832583; den-al-v@inbox.ru

Andina Sprince
andina.sprince@rtu.lv

Александр Викторович Денисов,*
+7(499)1832583; эл. почта: den-al-v@inbox.ru

Андина Спринце
эл. почта: andina.sprince@rtu.lv

Denisov A.V., Sprince A. Analytical determination of thermal expansion of rocks and concrete aggregates. *Magazine of Civil Engineering*. 2018. No. 4. Pp. 151–170. doi: 10.18720/MCE.80.14.

doi: 10.18720/MCE.80.15

Construction of autonomous buildings with wind power plants

Строительство автономных зданий с ветроэнергетическими установками

V.V. Titkov,
Peter the Great St. Petersburg Polytechnic University, St. Petersburg, Russia
A.B. Bekbayev,
T.M. Munsyzbai,
K.B. Shakenov*,
Kazakh National Technical University named after K.I. Satpayev, Almaty, Kazakhstan

Д-р техн. наук, заведующий кафедрой В.В. Титков,
Санкт-Петербургский политехнический университет Петра Великого, г. Санкт-Петербург, Россия
д-р техн. наук, профессор А.Б. Бекбаев, канд. техн. наук, ассоциированный профессор Т.М. Мунсызбай, ассистент К.Б. Шакенов*,
Казахский национальный технический университет имени К.И. Сатпаева, г. Алматы, Казахстан

Key words: wind energy; wind power plants; increase in energy efficiency factor; efficient converters; buildings; structural design; construction; renewable resource; energy efficiency

Ключевые слова: ветроэнергетика; ветроэнергетические установки; увеличение коэффициента использования энергии; эффективные преобразователи; здания; структурное проектирование; строительство; возобновляемый ресурс; энергоэффективность

Abstract. The use of renewable energy converters, including local wind power plants to provide private households and houses with electricity, is gaining popularity, especially in countries where there are appropriate state subsidies. In this paper considered approach to the use of the building roof in the conversion of the kinetic energy of the incoming wind into electrical energy by a closed wind power plant (WPP). The construction of the WPP and the roof are converted into a finite element model for aerodynamic calculations. The model of WPPs and roofs is investigated by changing the angle of attack of the roof, with different roofing applications, and also some other elements of the WPP design in order to find the most optimal conditions for increasing the energy efficiency factor (EEF) of the energy carrier. The described approach with the use of a roof in the conversion of wind energy into electrical energy can be used in the structural design and construction of autonomous houses and buildings.

Аннотация. Использование преобразователей энергии возобновляемых источников, в том числе локальных ветроэнергетических установок для обеспечения частных хозяйств и домов электрической энергией приобретает популярность, особенно в странах, где существуют соответствующие государственные дотации. В настоящей работе рассмотрен подход к применению кровли здании при преобразовании кинетической энергии набегающего ветра в электрическую энергию ветроэнергетической установкой (ВЭУ) закрытого типа. Конструкция ВЭУ и кровля преобразуются в конечно-элементную модель для проведения аэродинамического расчета. Модель ВЭУ и кровли исследуются изменением угла атаки кровли, при различных вариантах применения кровли, а также некоторых других элементов конструкции ВЭУ с целью поиска наиболее оптимальных условий для увеличения коэффициента использования энергии (КИЭ) энергоносителя. Описываемый подход с использованием кровли при преобразовании энергии ветра в электрическую энергию может быть использован при структурном проектировании и строительстве автономных домов и зданий.

1. Introduction

Wind energy in the world is developing in three separate areas:

- wind power complexes of low power of 2–100 kW for feeding autonomous objects that do not require significant capital investment and are easy to operate;

Титков В.В., Бекбаев А.Б., Мунсызбай Т.М., Шакенов К.Б. Строительство автономных зданий с ветроэнергетическими установками // Инженерно-строительный журнал. 2018. № 4(80). С. 171–180.

- energy complexes of average power of 200–800 kW for feeding concentrated load in territories with low population density, which require large capital investments and depreciation charges (renovation costs);

- power complexes of high power of 1000–5000 kW for generating power in centralized power systems that do not pay off and constantly require investment for renovation [1].

Therefore, from the point of view of practicality and efficiency of operation, wind energy needs to be developed for local power supply of autonomous objects [2]. In turn, a local WPP for autonomous power supply can be used in tourist recreation areas, farms, oil pumping stations and other similar organizations located in remote areas from a unified electrical system (UES) [3].

The most common converters of renewable resources are wind and solar energy converters, which are practically present in all parts of the world and apply various conversion methods [4]. In addition, to increase the reliability of power supply used diesel generators, along with renewable resources converters [5]. In order to increase the energy efficiency in the converter, it is necessary to conduct research to find the best construction of the WPP, which allows increasing the air mass flow velocity, since even an insignificant increase in the air mass flow velocity will have a great effect, because the kinetic energy of the stream depends on the velocity in the third degree [6].

The study of the construction of WPPs using the roof of the building was conducted out in the software of engineering analysis COMSOL Multiphysics, which performs calculations using the finite element method. This method is widely used in modeling the processes of diffusion, heat conduction, hydrodynamics, mechanics and expanding its scope with increasing the capacity of computing systems [7].

Usually, the Euler formulation of problems is used to solve the equations of hydrodynamics. The grid applied to the calculated area remains fixed during the entire process of the solution. However, when using this approach, difficulties arise in approximating the convective terms [8].

These difficulties are eliminated by using the Lagrangian description of the field. The essence of this approach is that the grid nodes move with the field, which allows us to consider them as particles of the field; in this case the mesh itself is deformed or rearranged at each step of the solution. One of the methods using the Lagrangian description of the field is the PFEM – method of finite elements with particles [9, 10]. This method is used in software of engineering analysis COMSOL Multiphysics [11].

The finite element method with particles is used to simulate fluid flows in areas of complex shape, fluid flows with a free surface, splash processes, and solutions of the adjoint hydroelasticity problems. To solve these problems Lagrangian methods of various types are used traditionally and very effectively: in conjugate problems of hydroelasticity – the methods of vortex elements [12, 13], in the simulation of flows with a free surface – the method of smoothed particles SPH [14, 15]. Advantages and disadvantages of using grid methods and particle methods for solving various problems are discussed in detail in the paper [16].

To simulate the flow is widely used the Navier-Stokes differential equations system. The main problems in the solution of the Navier-Stokes equation are related to differential equations for the laws of conservation of mass and momentum. To solve these problems are used methods to determine the pressure of the Poisson equation [17], the equations for the corrections [18], the penalty functions [19], the addition of the continuity equation by the no stationary member [20], the regularization of the matrix coefficients for time derivatives [21–26]. In addition, there is the problem of the existence and smoothness of the Navier-Stokes equations for solutions which use different methods [27–34].

The aim of this work is to develop the most efficient converter of wind energy that would optimally convert the kinetic energy of the wind and increase the operating range of its work by lowering its lower threshold. When the WPP construction uses a building roof, where it is located, it additionally enfolds the oncoming wind. In this way, the roof of the building becomes an active element in the transformation of energy.

The task that must be solved: the model of the construction of WPPs and roofs, as well as the flow in simulation of the software of engineering analysis should be sufficiently approximate to the natural model. For this, the model should give the same and convergent results in grids, the grid should be sufficiently shallow on important areas of the construction to avoid errors in hydrodynamic calculations, and the calculation area over the model of the WPP should be high enough to avoid a narrowing of the airflow, which can distort the natural flow conditions.

2. Methods

A three-dimensional model of a closed-type WPP construction and a building roof is shown in Figure 1 and consists of the following elements:

1. the directive cone, located in the middle of the construction on one axis with the WPP housing, directs the air flow to the turbine blades area of the WPP;
2. the housing of the WPP, consisting of a front cavity, made in the form of a truncated cone, and an expanding back cavity, which contribute to the acceleration of the air flow in the area of the turbine blades of the WPP;
3. the ejector which is the outer part of the construction of WPPs, the inner side of which is constant at a small angle relative to the WPP housing, narrows and directs the air flow at the outlet to create a low pressure region behind the turbine by entrainment with a flow of exhaust air molecules. Thus, it additionally contributes to the acceleration of the air flow in the turbine blades area of the WPP.

This design contributes to an increase in the speed of the wind flow due to the use of the confuser and diffuser, which makes it possible to obtain a coefficient of wind energy use from 0.4 to 0.45.

Orientation to wind is carried out due to the shank of the wind turbine located behind the body.

A DC generator is used to convert the rotational mechanical energy into electrical energy and is located behind the guide cone at the border of the confuser and diffuser.

The blades of the proposed low-power WPP are made of light composite materials, so the calculation of the load on them was not considered.

Since a local WPP can be used in tourist recreation areas, farms, etc., where large capacities are not required, it is sufficient to install it on standard buildings without special strengthening of the building elements.

Figure 2 shows a cross-sectional view of a closed-type WPP construction model and a building roof. Since the WPP construction and the roof of the building are rotational bodies, to simplify the calculation, computational operations and analysis of the most effective areas of construction applied cross section model. This model is built in the interface "Geometry" of the software of engineering analysis COMSOL Multiphysics. Further selects the material, depending on the model, in this case air is selected as the flow field and iron is used as a material for the construction of the WPP and the roof of the building. Then the boundary conditions are set: input speed, outlet pressure, symmetrical walls. In this interface, the flow of a fluid with any velocities is modeled on the basis of the solution of the Navier-Stokes equations in various formulations. This interface is intended for modeling the low-velocity streams, creeping (Stokes) flows, laminar and turbulent fluid flows. To describe turbulent flows are used Reynolds-averaged Navier-Stokes equations (RANS), supplemented with the different models of turbulence: standard and low-Reynolds type k-ε models, k-ω and SST (Menter) models and the Spalart-Allmaras model [11]. The Reynolds averaging method for the Navier-Stokes equation consists in replacing the randomly changing flow characteristics (velocity, pressure, density) by the sums of the averaged and pulsating components. The Reynolds equations describe the time-averaged flow of a fluid, their peculiarity (in comparison with the original Navier-Stokes equations) lies in the fact that new unknown functions appear in them that characterize the apparent turbulent stresses.

For calculation is chosen a standard k-ε model to describe the turbulent flow, where the equation of motion is transformed to the form in which the effect of average velocity fluctuations (in the form of turbulent kinetic energy) is added and the process of reducing this fluctuation at the expense of viscosity (dissipation). In this model solved two additional transport equations for the turbulent kinetic energy and turbulent dissipation transport. This model is most often used in solving real engineering problems.

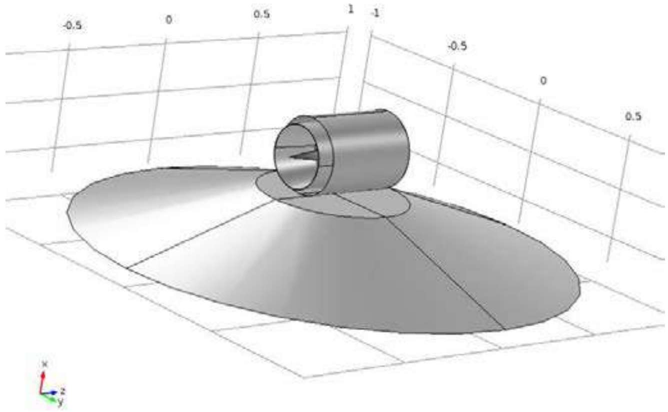

Figure 1. The three-dimensional model of the construction of closed type WPPs and roof of the building

In the grid building interface is selected a method for dividing a model from four types of calibration for each of its sections. There are: “general physics”, “fluid dynamics”, “plasma” and “semiconductor”. Then it specifies a predefined size of the grid. For the flow field area of the model is selected the second type of calibration, namely "fluid dynamics", and for the construction of the WPP and the roof of the building - the first type of calibration, namely "general physics". The constructed grid for one of the variants of the model of closed type WPP construction and the building roof is shown in Figure 3. It can be seen from the figure that the grid near and around the edges of the construction is crushed, which will allow to take into account the changes in the parameters in these important zones for a sufficiently accurate description of the flow processes.

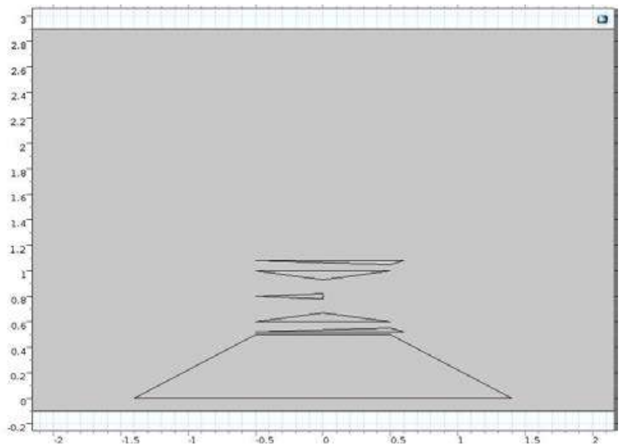

Figure 2. The cross-section of model of the construction of closed type WPPs and roof of the building

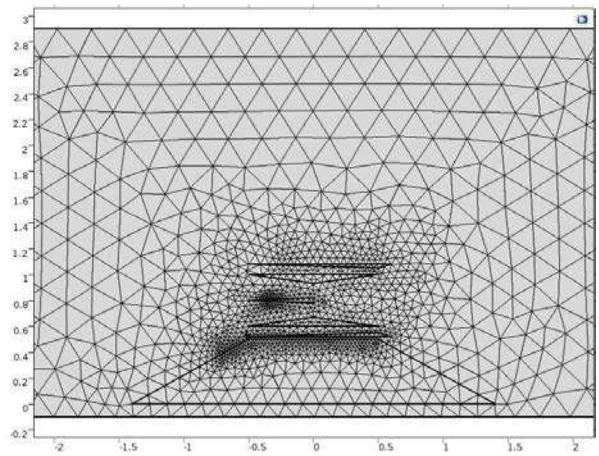

Figure 3. Estimated grid of one of model of the construction of closed type WPPs and roof of the building

3. Results and Discussion

In work [35] the architecture of low-rise buildings with use of wind power installations and principles of form-building in architecture of low-rise buildings is considered. There shaping effect on the increase in the power of wind turbines. The proposed hypotheses on the new formation of residential buildings are not effective enough due to the lack of research on finding the effective angle of the roof of the building. For this, it is necessary to perform calculations under different conditions for each parameter.

The results of the calculations can be obtained in the form of various diagrams and graphs on the necessary parameters for the analysis. Figure 4 shows a diagram of the airflow velocity contours throughout the construction of closed type WPPs and the roof of the building. It shows that in the area of the turbine where the flow is narrowing with the housing and the directive cone of the WPP, the flow velocity reaches a maximum value, behind this zone the flow velocity begins to decrease. A slight decrease in the airflow velocity is observed along the outer edges of the WPP housing, since the ejector creates a low-pressure region in these zones. In this case, the flow velocity reaches 10.2 m/s with its initial value of 5 m/s.

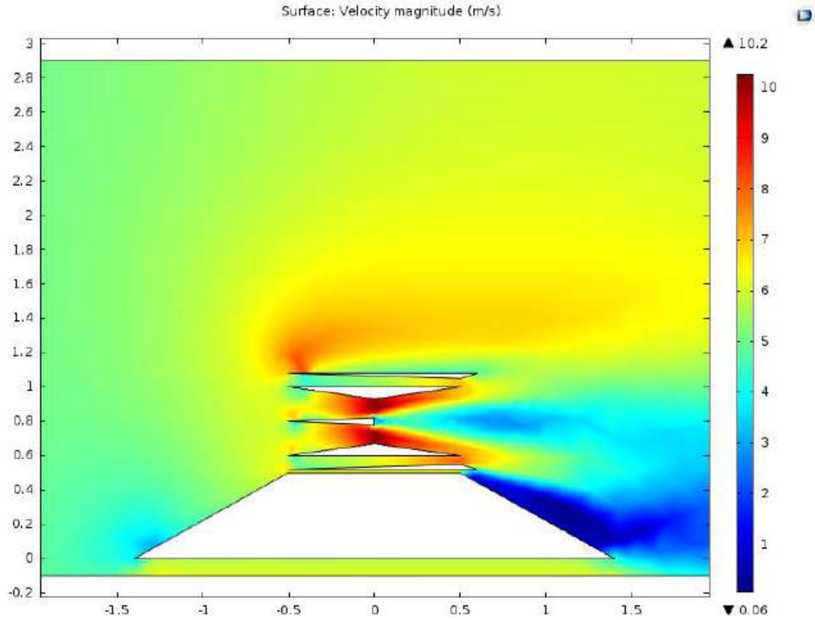

Figure 4. The diagram of the airflow velocity contours throughout the construction of closed type WPPs and roof of the building

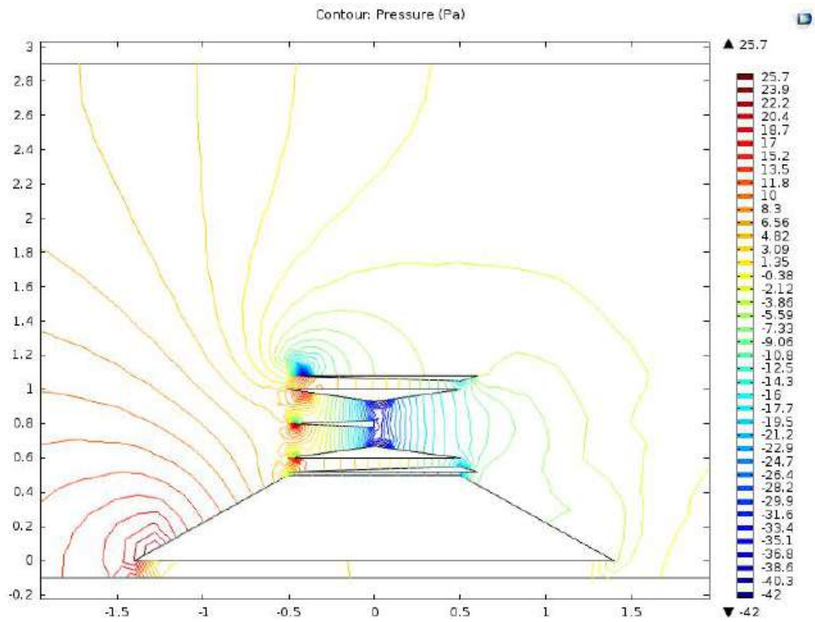

Figure 5. Diagram of airflow pressure contours throughout the construction of closed type WPPs and roof of the building

A diagram of the pressure contours for these conditions is illustrated in Figure 5, where the pressure difference in the construction reaches 67.7 Pa. It can be seen from this figure that the low-pressure zone is behind the turbine of the WPP, especially in the area of the blades of the turbine of the WPP, where achieved the maximum airflow velocity.

To obtain velocity data in the turbine zone (a vertically arranged red line in Figure 6), a graph of the airflow velocity is plotted on the length of this zone, which is shown in Figure 7. The decrease of the velocity of airflow in the middle of the graph shows the shaded area of the closed-type WPP directive cone, where the generator and the turbine housing are located, and also the velocity growth on the both sides – the turbine blade area, where reached the maximum airflow velocity in the construction.

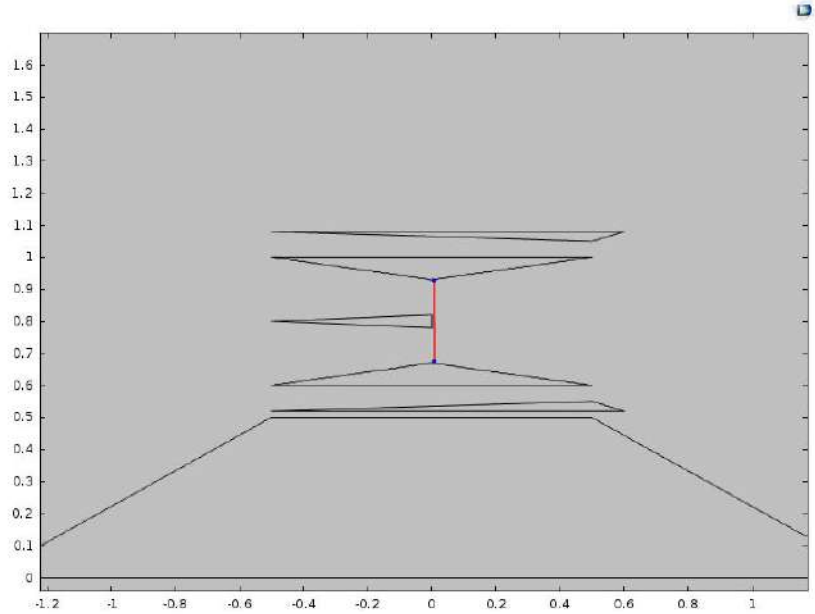

Figure 6. Plot removal area of the airflow velocity

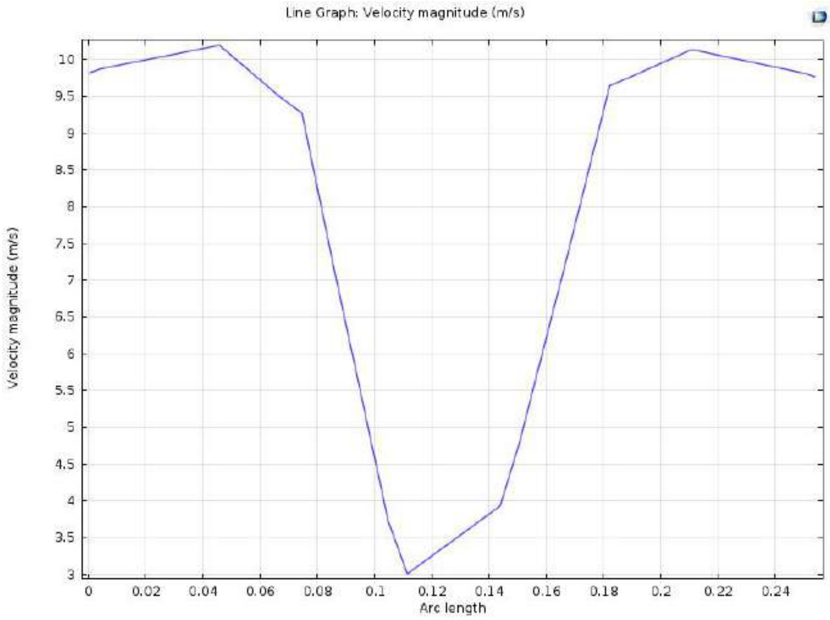

Figure 7. The airflow velocity graph at the location of turbine blades of a closed type WPP

The closed type WPP was also investigated in the absence of an ejector $\vartheta_{w.e.}$ at different angle attack of inclination of the roof of the building α, where the air velocity reaches 10.16 m/s (Figure 8). In addition, her research was conducted in the absence of the roof of the building $\vartheta_{w.r.}$, where a speed of 7.85 m/s is achieved (Figure 9). The results of the calculations performed for different variants with an initial wind velocity of 5 m/s are given in Table 1.

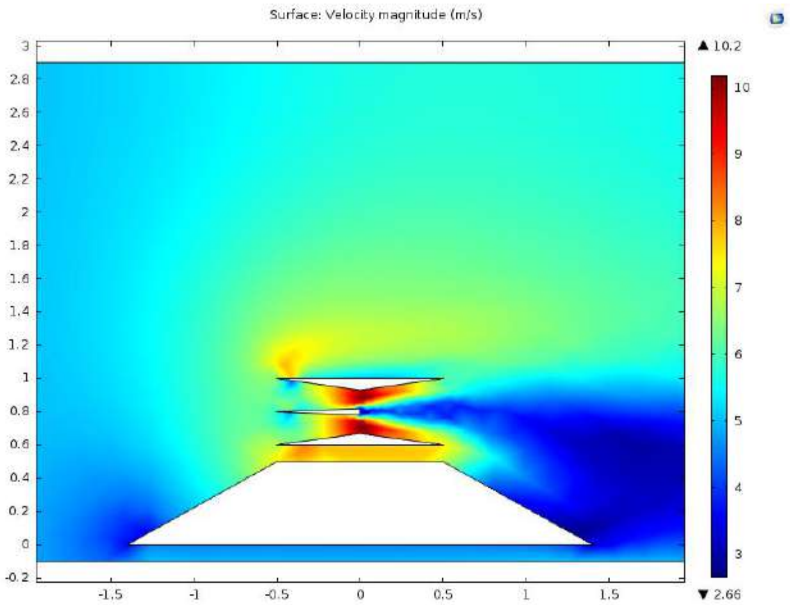

Figure 8. Diagram of airflow velocity contours in the absence of an ejector

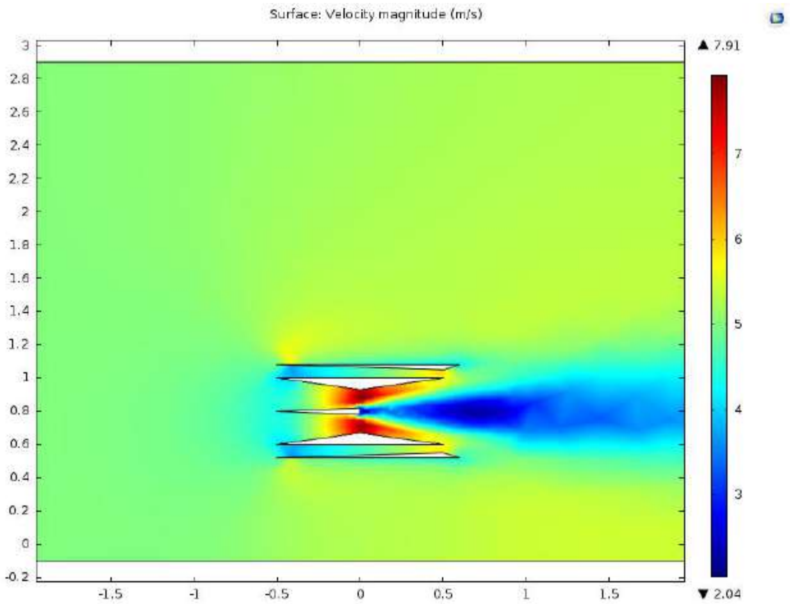

Figure 9. Diagram of airflow velocity contours in the absence of a building roof

Table 1. The results of wind velocity in the zone of the turbine

α, ^{0}	ϑ_{max}, m/s	$\vartheta_{w.e.}$, m/s	$\vartheta_{w.r.}$, m/s
11.31	9.4	9.01	7.85
16.7	9.4	9.01	
26.56	9.5	9.01	
29.1	10.2	10.16	
32	10.14	10.06	
35.5	10.1	9.97	
45	10.01	9.48	

It can be seen from Table 1 that the maximum acceleration of the air flow through the construction in the turbine zone is achieved at an angle of inclination of the roof of the building 29.1^0. Therefore, when designing and building autonomous houses and buildings, it is recommended to take the angle of inclination of the roof in the area 30^0.

4. Conclusions

1. The forms of the WPP construction elements have been developed to effectively increase the velocity of the incoming air flow, such as the directive cone, the installation housing and the ejector.

2. The analysis of the mutual arrangement of the elements of the WPP construction was carried out in the absence of some elements, in the absence of the roof of the building and at various angles of attack of the roof of the building.

3. Based on the results of the analysis an effective version of the construction of the WPP and the roof of the building is identified, where the greatest acceleration of the incoming airflow is achieved.

4. It is recommended to take the angle of inclination of the roof of the building in the area 30^0.

5. Substantiated the construction of a closed type WPP, consisting of a housing of the installation, a directive cone and an ejector, and the roof of a building.

References

1. Bolotov A.V., Bakenov K.A. *Netraditsionnye i vozobnovlyaemye istochniki energii* [Non-traditional and renewable energy sources]. Almaty: AIES, 2007. 40 p. (rus)
2. Titkov V.V., Bekbaev A.B., Munsyzbay T.M., Shakenov K.B. Puti razvitiya elektroenergetiki v kazakhstane [Ways of development of electric power industry in Kazakhstan]. *Trudy Mezhdunarodnogo foruma «Inzhenernoe obrazovanie i nauka v XXI veke: problemy i perspektivy», posvyashchennogo 80-letiyu KazNTU imeni K.I. Satpaeva* [Proceedings of International forum "Engineering education and science in the XXI century: Challenges and perspectives" devoted to the 80th anniversary of Satpaev KazNTU]. Almaty: KazNTU, 2014. Vol. III. Pp. 754-754. (rus)
3. Bekbaev A.B., Munsyzbay T.M., Shakenov K.B., Zhaksylykov K.A. Kompleksnoe ispolzovanie vozobnovlyaemykh energonositeley i poputnykh gazov na nefteperekachivayushchikh nasosnykh agregatakh [Complex use of renewable energy carriers and associated gases at oil pumping units]. *Materialy VI Mezhdunarodnoy nauchno-prakticheskoy konferentsii "Noveyshie tekhnologii osvoeniya mestorozhdeniy uglevodorodnogo syrya i obespechenie bezopasnosti ekosistem Kaspiyskogo shelfa".* Astrakhan: Izd-vo AGTU, 2015. Pp. 204–206. (rus)
4. Bekbaev A.B., Munsyzbay T.M., Shakenov K.B. Kompleksnoe ispolzovanie energii vozobnovlyaemykh istochnikov [Integrated use of renewable energy sources]. *Trudy Mezhdunarodnykh Satpaevskikh chteniy "Rol i mesto molodykh uchenykh v realizatsii novoy ekonomicheskoy politiki Kazakhstana"* [Proceedings of International Satpayev's readings «Role and position of young scientists in implementation Kazakhstan's New Economic Policy»]. Almaty: KazNTU, 2015. Vol. I. Pp. 57–62. (rus)
5. Polina P., Vatin N., Murgul V. The method to determine sites and facilities for wind-diesel power plants construction. *Applied Mechanics and Materials*. 2014. Pp. 510–516. DOI: 10.4028/www.scientific.net/AMM.680.510
6. Munsyzbai T.M. Mathematical model of windmill. *Fifth World Conference on Intelligent Systems for Industrial Automation.* Tashkent. 2008. Pp. 279–284.
7. *Finite element method* [Electronic resource]. URL: https://ru.wikipedia.org/wiki/%D0%9C%D0%B5%D1%82%D0%BE%D0%B4_%D0%BA%D0%BE%D0%BD%D0%B5%D1%87%D0%BD%D1%8B%D1%85_%D1%8D%D0%BB%D0%B5%D0%BC%D0%B5%D0%BD%D1%82%D0%BE%D0%B2 (date: 12.06.2017)
8. Davydova Ye.V., Korchagova V.N., Marchevskiy I.K. Ispolzovanie metoda konechnykh elementovs chastitsami dlya resheniya zadach gidrodinamiki [The use of the finite element method with particles to solve the problems of hydrodynamics]. *Nauka i Obrazovanie*. 2015. No. 6. Pp. 329–345. (rus)
9. Idelsohn S.R., Onate E., Del Pin F. A Lagrangian meshless finite element method applied to fluid-structure interaction

Литература

1. Болотов А.В., Бакенов К.А. Нетрадиционные и возобновляемые источники энергии. Алматы: АИЭС, 2007. 40 с.
2. Титков В.В., Бекбаев А.Б., Мунсызбай Т.М., Шакенов К.Б. Пути развития электроэнергетики в Казахстане // Труды Международного форума «Инженерное образование и наука в XXI веке: проблемы и перспективы», посвященного 80-летию КазНТУ имени К.И. Сатпаева. Алматы: КазНТУ, 2014. Том III. С. 754–754.
3. Бекбаев А.Б., Мунсызбай Т.М., Шакенов К.Б., Жаксылыков К.А. Комплексное использование возобновляемых энергоносителей и попутных газов на нефтеперекачивающих насосных агрегатах // Материалы VI Международной научно-практической конференции "Новейшие технологии освоения месторождений углеводородного сырья и обеспечение безопасности экосистем Каспийского шельфа". Астрахань: Изд-во АГТУ, 2015. С. 204–206.
4. Бекбаев А.Б., Мунсызбай Т.М., Шакенов К.Б. Комплексное использование энергии возобновляемых источников // Труды Международных Сатпаевских чтений "Роль и место молодых ученых в реализации новой экономической политики Казахстана". Алматы: КазНТУ, 2015. Т. I. С. 57–62.
5. Polina P., Vatin N., Murgul V. The method to determine sites and facilities for wind-diesel power plants construction // Applied Mechanics and Materials. 2014. Pp. 510–516. DOI: 10.4028/www.scientific.net/AMM.680.510
6. Munsyzbai T.M. Mathematical model of windmill. Fifth World Conference on Intelligent Systems for Industrial Automation. Tashkent. 2008. Pp. 279–284.
7. Метод конечных элементов [Электронный ресурс]. URL: https://ru.wikipedia.org/wiki/%D0%9C%D0%B5%D1%82%D0%BE%D0%B4_%D0%BA%D0%BE%D0%BD%D0%B5%D1%87%D0%BD%D1%8B%D1%85_%D1%8D%D0%BB%D0%B5%D0%BC%D0%B5%D0%BD%D1%82%D0%BE%D0%B2 (дата обращения: 12.06.2017 г.)
8. Давыдова Е. В., Корчагова В. Н., Марчевский И. К. Использование метода конечных элементовс частицами для решения задач гидродинамики // Наука и Образование. 2015. № 6. С. 329–345.
9. Idelsohn S.R., Onate E., Del Pin F. A Lagrangian meshless finite element method applied to fluid-structure interaction problems // Computer and Structures. 2003. Vol. 81. No. 8(11). Pp. 655–671.
10. Idelsohn S.R., Onate E., Del Pin F. The particle finite element method: a powerful tool to solve incompressible flows with free-surfaces and breaking waves // International Journal for Numerical Methods in Engineering. 2004. Vol. 61. No. 7. Pp. 964–989.
11. Модуль "Вычислительная гидродинамика" CFD [Электронный ресурс]. URL: https://www.comsol.ru/cfd-

problems. *Computer and Structures.* 2003. Vol. 81. No. 8(11). Pp. 655–671.

10. Idelsohn S.R., Onate E., Del Pin F. The particle finite element method: a powerful tool to solve incompressible flows with free-surfaces and breaking waves. *International Journal for Numerical Methods in Engineering.* 2004. Vol. 61. No. 7. Pp. 964–989.
11. *Module "Computational Fluid Dynamics" CFD* [Electronic resource]. URL: https://www.comsol.ru/cfd-module?utm_source=google&utm_medium=cpc&utm_term=%2B%D0%B3%D0%B8%D0%B4%D1%80%D0%BE%D0%B4%D0%B8%D0%BD%D0%B0%D0%BC%D0%B8%D0%BA%D0%B0%20%2Bcomsol&utm_campaign=search&utm_content=.1t1&gclid=CjwKEAjwvYPKBRCYr5GLgNCJ_jsSJABqwfw7oDFap6iGoRBpjWSimbAPYy_JcPojdtTPAM8sdGElChoCiyvw_wcB. (date: 12.06.2017). (rus)
12. Yermakov A.V., Shcheglov G.A. Modelirovanie metodom vikhrevykh elementov dinamiki tsilindricheskoy obolochki v prostranstvennom potoke zhidkosti [Modeling by the method of vortex elements of the dynamics of a cylindrical shell in a spatial fluid flow]. *Izvestiya VUZov.* 2014. No. 3. Pp. 35–41. (rus)
13. Kuzmina K.S., Marchevskiy I.K. Ob uskorenii vychisleniy pri reshenii dvumernykhsopryazhennykh zadach gidrouprugosti vikhrevymi metodami [On the acceleration of calculations in solving two-dimensional conjugate problems of hydroelasticity by vortex methods]. *Vestnik Permskogo natsionalnogo issledovatelskogo politekhnicheskogo universiteta. Ser. Aerokosmicheskaya tekhnika.* 2014. No. 39. Pp. 145–163. (rus)
14. Monaghan J.J. Smoothed Particle Hydrodynamics. *Reports on Progress in Physics.* 2005.Vol. 68. Pp. 1703–1759.
15. Li S., Liu W.K. *Meshfree Particle Methods*. Springer Berlin Heidelberg. 2004. 502 p.
16. Idelsohn S.R., Onate E. To mesh or not to mesh. That is the question. *Computer Methods in Applied Mechanics and Engineering*. 2006. Vol. 195. No. 37-40. Pp. 4681–4696.
17. Belov I.A. *Zadachi i metody resheniya otryvnykh techeniy neszhimaemoy zhidkosti* [Problems and methods for solving separated flow of an incompressible fluid]. Leningrad: Sudostroenie. 1989. 256 p. (rus)
18. Patankar S.V. Chislennye metody resheniya zadach teploobmena i dinamiki zhidkosti [Numerical methods for solving problems of heat transfer and fluid dynamics]. Moscow: Energoatomizdat. 1984. 152 p. (rus)
19. Temam R. *Uravnenie Nave-Stoksa. Teoriya i chislennyy analiz* [The Navier-Stokes equation. Theory and numerical analysis]. Moscow: Mir. 1981. 408 p. (rus)
20. Chorin A.J. A numerical method for solving incompressible viscous flow problems. *Journal of Computation Physics.* 1967. No. 2. Pp. 12–26.
21. Blinova L.A, Shur M.L. Metod “masshtabirovaniya szhimaemosti” dlya rascheta nestatsionarnykh techeniy vyazkogo gaza v shirokom diapazone izmeneniya kharakternykh chisel Makha [The "compressibility scaling" method for calculating unsteady flows of a viscous gas over a wide range of Mach numbers]. *Konstruirovanie algoritmov i reshenie zadach matematicheskoy fiziki.* 1991. Pp. 34–39. (rus)
22. Goncharov V.A., Krivtsov V.M., Charakhchyan A.A. Chislennaya skhema modelirovaniya dozvukovykh techeniy vyazkogo szhimaemogo [A numerical scheme for simulating subsonic viscous compressible flows]. *ZhVM i MF.* 1988. No. 28(12). Pp. 1858–1866. (rus)
23. Lapin Yu.V. Vnutrennie techeniya gazovykh smesey [Internal flows of gas mixtures]. Moscow: Nauka, 1989. 368 p. (rus)
24. Strelets M.Kh., Shur M.L. Metod masshtabirovaniya szhimaemosti dlya rascheta statsionarnykh techeniy vyazkogo gaza pri proizvolnykh chislakh Makha [The method of compressibility scaling for the calculation of stationary viscous gas flows for arbitrary Mach numbers].

module?utm_source=google&utm_medium=cpc&utm_term=%2B%D0%B3%D0%B8%D0%B4%D1%80%D0%BE%D0%B4%D0%B8%D0%BD%D0%B0%D0%BC%D0%B8%D0%BA%D0%B0%20%2Bcomsol&utm_campaign=search&utm_content=.1t1&gclid=CjwKEAjwvYPKBRCYr5GLgNCJ_jsSJABqwfw7oDFap6iGoRBpjWSimbAPYy_JcPojdtTPAM8sdGElChoCiyvw_wcB. (дата обращения: 12.06.2017 г.)

12. Ермаков А.В., Щеглов Г.А. Моделирование методом вихревых элементов динамики цилиндрической оболочки в пространственном потоке жидкости // Известия ВУЗов. 2014. № 3. С. 35–41.
13. Кузьмина К.С., Марчевский И.К. Об ускорении вычислений при решении двумерныхсопряженных задач гидроупругости вихревыми методами // Вестник Пермского национального исследовательского политехнического университета. Сер. Аэрокосмическая техника. 2014. № 39. С. 145–163.
14. Monaghan J.J. Smoothed Particle Hydrodynamics // Reports on Progress in Physics. 2005.Vol. 68. Pp. 1703–1759.
15. Li S., Liu W.K. Meshfree Particle Methods. Springer Berlin Heidelberg. 2004. 502 p.
16. Idelsohn S.R., Onate E. To mesh or not to mesh. That is the question // Computer Methods in Applied Mechanics and Engineering. 2006. Vol. 195. No. 37-40. Pp. 4681–4696.
17. Белов И.А. Задачи и методы решения отрывных течений несжимаемой жидкости. Л.: Судостроение, 1989. 256 с.
18. Патанкар С.В. Численные методы решения задач теплообмена и динамики жидкости. М.: Энергоатомиздат, 1984. 152 с.
19. Темам Р. Уравнение Навье-Стокса. Теория и численный анализ. М.: Мир, 1981. 408 с.
20. Chorin A.J. A numerical method for solving incompressible viscous flow problems // Journal of Computation Physics. 1967. No. 2. Pp. 12–26.
21. Блинова Л.А, Шур М.Л. Метод “масштабирования сжимаемости” для расчета нестационарных течений вязкого газа в широком диапазоне изменения характерных чисел Маха // Конструирование алгоритмов и решение задач математической физики. 1991. С. 34–39.
22. Гончаров В.А., Кривцов В.М., Чарахчьян А.А. Численная схема моделирования дозвуковых течений вязкого сжимаемого // ЖВМ и МФ. 1988. № 28(12). С. 1858–1866.
23. Лапин Ю.В. Внутренние течения газовых смесей. М.: Наука, 1989. 368 с.
24. Стрелец М.Х., Шур М.Л. Метод масштабирования сжимаемости для расчета стационарных течений вязкого газа при произвольных числах Маха // ЖВМ и МФ. 1988. № 28(12). С. 254–266.
25. Briley W.R., McDonald H. Solution of the multidimensional Navier-Stokes equations by a generalized implicit method // Journal of Computation Physics. 1977. No. 24(4). Pp. 372–397.
26. Briley W.R., McDonald H., Shamreth S.J. A low Mach number Euler formulation and application to time-iterative LBI schemes // AIAA Journal. 1983. No. 21(10). Pp. 1464–1469.
27. Durmagambetov A.A., Fazilova L.S. Navier-Stokes Equations—Millennium Prize Problems // Natural Science. 2015. No. 7. Pp. 88–99.
28. Ладыженская О.А. Шестая проблема тысячелетия: уравнения Навье–Стокса, существование и гладкость// Успехи математических наук. 2003. Т. 58. № 2(350). С. 45–78.
29. Cao C., Titi E.S. Regularity criteria for the three-

ZhVM i MF. 1988. No. 28(12). Pp. 254–266. (rus)

25. Briley W.R., McDonald H. Solution of the multidimensional Navier-Stokes equations by a generalized implicit method. *Journal of Computation Physics.* 1977. No. 24(4). Pp. 372–397.
26. Briley W.R., McDonald H., Shamreth S.J. A low Mach number Euler formulation and application to time-iterative LBI schemes. *AIAA Journal.* 1983. No. 21(10). Pp. 1464–1469.
27. Durmagambetov A.A., Fazilova L.S. Navier-Stokes Equations—Millennium Prize Problems. *Natural Science.* 2015. No. 7. Pp. 88–99.
28. Ladyzhenskaya O.A. Shestaya problema tysyacheletiya: uravneniya Nave–Stoksa, sushchestvovanie i gladkost [The Sixth Millennium Challenge: The Navier-Stokes Equation, essence and smoothness]. *Uspekhi matematicheskikh nauk.* 2003. Vol. 58. No. 2(350). Pp. 45–78. (rus)
29. Cao C., Titi E.S. Regularity criteria for the three-dimensional Navier-Stokes equations. *Indiana Univ. Math. J.* 2008. No. 6(57). Pp. 2643–2661.
30. Sheretov Yu.V. O svoystvakh resheniy kvazigidrodinamicheskikh uravneniy v barotropnom priblizhenii [On the properties of solutions of quasi-hydrodynamic equations in the barotropic approximation]. *Vestnik Tverskogo gos. un-ta. Ser.: Prikladnaya matematika*. 2009. No. 14. Pp. 5–19. (rus)
31. Mamontov A. Ye. Globalnaya razreshimost mnogomernykh uravneniy szhimaemoy nenyutonovskoy zhidkosti, transportnoe uravnenie i prostranstva Orlicha [Global solvability of multidimensional equations of compressible non-Newtonian fluid, transport equation and Orlicz spaces]. *Siberian electronic mathematical reports.* 2009. No. 6. Pp. 120–165. (rus)
32. Cao C. Sufficient conditions for the regularity to the 3D Navier-Stokes equations. *Discrete Contin. Dyn. Syst.* 2010. No. 4(26). Pp. 1141–1151.
33. Aristov S.N., Prosviryakov E.Yu. Nonuniform convective Couette flow. *Fluid Dyn.* 2016. No. 5(51). Pp. 581–587.
34. Aristov S.N., Prosviryakov E.Yu. A new class of exact solutions for three-dimensional thermal diffusion equations. *Theor. Found. Chem. Eng.* 2016. No. 3(50) Pp. 286–293.
35. Grunichev I.A. Arkhitektura maloetazhnykh zhilykh zdaniy s ispolzovaniem vetrovykh energoustanovok [Architecture of low-rise residential buildings using wind energy installations]. *Bulletin of Civil Engineers.* 2016. No. 3(56). Pp. 19–28. (rus)

dimensional Navier-Stokes equations // Indiana Univ. Math. J. 2008. No. 6(57). Pp. 2643–2661.

30. Шеретов Ю.В. О свойствах решений квазигидродинамических уравнений в баротропном приближении // Вестн. Тверского гос. ун-та. Сер.: Прикладная математика. 2009. № 14. С. 5–19.
31. Мамонтов А.Е. Глобальная разрешимость многомерных уравнений сжимаемой неньютоновской жидкости, транспортное уравнение и пространства Орлича // Сибирские электронные математические известия 2009. № 6. С. 120–165.
32. Cao C. Sufficient conditions for the regularity to the 3D Navier-Stokes equations // Discrete Contin. Dyn. Syst. 2010. No. 4(26). Pp. 1141–1151.
33. Aristov S.N., Prosviryakov E.Yu. Nonuniform convective Couette flow // Fluid Dyn. 2016. No. 5(51). Pp. 581–587.
34. Aristov S.N., Prosviryakov E.Yu. A new class of exact solutions for three-dimensional thermal diffusion equations // Theor. Found. Chem. Eng. 2016. No. 3(50). Pp. 286–293.
35. Груничев И.А. Архитектура малоэтажных жилых зданий с использованием ветровых энергоустановок // Вестник гражданских инженеров. 2016. № 3(56). С. 19–28.

Vasily Titkov,
+7(812)5554286; titkovprof@yandex.ru

Amangeldi Bekbayev,
+7(707)7610425; bekbaev_a@mail.ru

Toleuhan Munsyzbai,
+7(707)8329373; toleuhan_aidar@mail.ru

Kalizhan Shakenov,*
+7(747)1710691; kalizhan-90@mail.ru

Василий Васильевич Титков,
+7(812)555-42-86;
эл. почта: titkovprof@yandex.ru

Амангельды Бекбаевич Бекбаев,
+7(707)761-04-25; эл. почта: bekbaev_a@mail.ru

Толеухан Мусалимович Мунсызбай,
+7(707)832-93-73;
эл. почта: toleuhan_aidar@mail.ru

Калижан Бахытжанович Шакенов,*
+7(747)171-06-91;
эл. почта: kalizhan-90@mail.ru

doi: 10.18720/MCE.80.16

Fire resistant fibre reinforced vermiculite concrete with volcanic application

Огнезащитные фибровермикулитобетоны с вулканическими добавками

T.A. Hezhev,
A.V. Zhurtov,
A.S. Tsipinov,
Kabardino-Balkar State University named after H.M. Berbekov, Nalchik, Russia
S.V. Klyuev*,
Belgorod State Technological University after V.G.Shukhov, Belgorod, Russia

Д-р техн. наук, заведующий кафедрой, директор института Т.А. Хежев,
старший преподаватель А.В. Журтов,
старший преподаватель А.С. Ципинов,
Кабардино-Балкарский государственный университет им. Х.М. Бербекова, г. Нальчик, Россия
канд. техн. наук, доцент С.В. Клюев*,
Белгородский государственный технологический университет им. В.Г. Шухова, Белгород, Россия

Key words: vermiculite; fly ash; pumice; fibre vermiculite concrete composite; ferrocement; fire-resistance

Ключевые слова: вермикулит; пепел; пемза; фибровермикулитобетонный композит; армоцемент; огнестойкость

Abstract. The results of studies on the development of vermiculite concrete composites with application of volcanic ash and pumice are presented. The composition of cement fibre vermiculite concrete fire resistant composites is offered, which allows reducing the consumption of Portland cement and simultaneously increasing their flame retardant properties. The use of basalt fibers in composites can improve the strength, fracture toughness and fire retardant properties of the coating due to the perception of tensile thermal stresses during the fire. Replacement of cement up to 30 % by weight with volcanic pumice fraction d < 0.16 mm significantly improves heat-resisting properties of cement stone with a simultaneous increase in flexural strength and no significant loss of compressive strength. Experimental and theoretical studies of fire resistance of double-layer ferroconcrete constructions showed high fire resistant properties of the developed cement fibre vermiculite concrete fire resistant composites. The algorithm for calculating the fire resistance of multi-layered building constructions with finite-difference implicit scheme for solving the heat conduction problem and the sweep method, providing reasonable agreement with experimental data is offered.

Аннотация. Представлены результаты исследований по разработке фибровермикулитобетонных композитов с применением вулканического пепла и пемзы. Предложены составы цементных фибровермикулитобетонных огнезащитных композитов, позволяющие существенно сократить расход портландцемента и одновременно повысить их огнезащитные свойства. Применение базальтовых волокон в композитах позволяет повысить прочность, трещиностойкость и огнезащитные свойства покрытия за счет восприятия растягивающих температурных напряжений во время пожара. Замена цемента до 30 % от массы вулканической пемзой фракции d < 0,16 мм существенно повышает жаростойкие свойства цементного камня с одновременным увеличением прочности на изгиб и без заметного снижения прочности на сжатие. Экспериментально-теоретические исследования огнестойкости двухслойных армоцементных конструкций показали высокие огнезащитные свойства разработанных цементных фибровермикулитобетонных огнезащитных композитов. Предложен алгоритм расчета огнестойкости многослойных строительных конструкций с использованием конечноразностной неявной схемы решения задачи теплопроводности и метода прогонки, обеспечивающий приемлемое совпадение с экспериментальными данными.

Хежев Т.А., Журтов А.В., Ципинов А.С., Клюев С.В. Огнезащитные фибровермикулитобетоны с вулканическими добавками // Инженерно-строительный журнал. 2018. № 4(80). С. 181–194.

1. Introduction

The increase in the number of fires in our country and abroad is observed every year. About 10 million fires occur annually, as a result more than 65 thousand people die, and 250 thousand are injured. Material damage from the fires is hundreds of billions of rubles.

The collapse of building constructions is the main cause of loss of life and damage from fires. This is due to the fact that in modern construction in the erection of buildings and structures thin-walled concrete constructions of high-strength concrete are increasingly used. Use of dispersed-reinforced concrete in the construction allows reducing material, labor and energy of ferroconcrete constructions while improving quality. Disperse-reinforced concrete is widely used in the manufacture of thin-walled, including spatial, constructions. It is known that the application of spatial ferro cement constructions in building allows reducing material capacity of constructions by 20–50 %, the complexity of their fabrication and installation – by 10–15 % and cost – up to 20 % with mechanized production [1]. Ferro cement constructions have a number of advantages in comparison with reinforced concrete structures: a lower consumption of concrete (by 30–50 %) and steel (up to 15–20 %); higher fracture toughness, density and water resistance; the use of non-deficient filler [2].

Despite significant progress in the development of spatial constructions, their implementation in the construction practice is still insufficient. One of the reasons restraining the use of thin-walled reinforced concrete structures is their low fire resistance [3–5]. With the increasing span of buildings there is a tendency to reduce the thickness and increase the strength of the material structures that lowers their fire resistance. In addition, financial losses from fire increase sharply with the raising of the span of the building. In recent years, the requirements of possible future use after fire exposure in terms of field of fire are made increasingly to constructions. Abroad there is evidence showing the feasibility and efficiency of reinforced concrete structures with a large limit of fire resistance [6–10].

An effective way to improve the fire resistance of building constructions is the application of thermal barrier coatings with the use of expanded vermiculite and perlite. The effectiveness of their use for fire protection of building constructions is increased by the simultaneous implementation of thermal, acoustic and decorative functions.

The disadvantages of flame retardants are high consumption of Portland cement, the relatively high coefficient of thermal conductivity at high temperature and low temperature resistance.

One material that is effective to replace part of Portland cement and aggregate for flame retardants can be volcanic tuff sawing waste, volcanic ash and pumice. To eliminate the harmful effects of secondary hydration of free calcium oxide on the characteristics of fire-resistant and heat-resistant concrete active mineral additives are used.

Thus, overcoming many of the drawbacks of flame retardants is possible in the creation of fibre reinforced composites using effective fillers.

The aim of this work is to develop an effective fire resistant cement fibre reinforced vermiculite composites with application of volcanic rocks. To achieve this goal compositions of vermiculite concrete and fibre vermiculite concrete flame retardant composites with application of volcanic rocks were developed, the flame retardant properties of the developed composites with experimental and computational methods were investigated.

Over the past decade, there has been growth in the use of dispersed reinforced composites. The fiber-reinforced concrete have higher tensile strength, crack resistance, impact resistance, temperature resistance compared to concrete matrix, which allows extending the scope of their effective application [11–18].

In development of science about the fiber concrete the big contribution was made by scientists of Austria, Australia, Belgium, Germany, Holland, Spain, Canada, China, Poland, the USA, France, the Czech Republic, Switzerland, the Republic of South Africa, Japan, and other countries [19–24].

2. Methods and materials

The Kabardino-Balkar Republic has large reserves of volcanic rocks – tuffs, ashes, pumice, ash pumices. They find their use as filler and active mineral additives in the manufacture of binders, mortars and concretes [4, 5]. However, the scope of volcanic rocks application in construction is insufficient. The use of local raw materials for the manufacture of new efficient building materials and products can significantly reduce the cost of construction.

Research was focused on the development of flame retardant composites with the use of ash and pumice.

In experiments there were used: ash fraction 0–0.16 mm; volcanic pumice of Psykhureysk deposits with a bulk density of 700 kg/m^3; expanded vermiculite fraction of 0.16–5 mm; Belgorod Portland cement PTS500-DO; lime; gypsum brand G–4–II–A; air-entraining additive resin wood saponified (RWS), basalt fiber by JSC "Ivotsteklo" brand of RNB-9-1200-4s.

Granulometric compositions of expanded vermiculite and volcanic pumice are given in Table 1.

Table 1. Granulometric composition of aggregates

Name of the material	**Private residues on the sieves, %**					**Passed through a sieve 0.16**
	2.5	1.25	0.63	0.315	0.16	
Vermiculite	26.7	21.9	31.4	14.7	5.3	–
Volcanic pumice	–	1	11	43.5	35	9.5

Preparation of a mixture was produced in the enforcement action mixer, which in water with RWS dry mixture of Portland cement, gypsum, lime, basalt fibers, volcanic ash (pumice) were consistently loaded, then expanded vermiculite, or a pre-mixed dry mixture of Portland cement, gypsum, lime, basalt fibers, volcanic ash (pumice) and expanded vermiculite. Mixing of all components is continued until a homogeneous fire-resistant fibre vermiculite concrete raw mixture. The duration of mixture stirring was 1.5–2 min.

Samples with sizes 4 x 4 x 16 cm from vermiculite concrete composite was compacted on a standard shaking platform. The mobility of the mixture was 3.5 cm of immersion of the cone StroyTSNIL. Samples were stored in air-dry conditions. Before testing, the beams were dried at t = 105 °C to constant weight in a drying cabinet.

3. *Results and Discussion*

As a result of experiments vermiculite concrete composites with application of volcanic ash were designed (Table 2).

Table 2. The ratio of components in the mixture and physico-mechanical properties of vermiculite concrete composites

No.No. compositions	The ratio of components in the mixture, wt. %					The number of RWS in % by weight of the binder	Average density ρ, kg/m3	The limit of strength, MPa	
	Cement	Vermiculite	Ash	Lime	Gepsum			On compression	On bending
1	2	3	4	5	6	7	8	9	10
1	71.9	29.1	–	–	–	–	750	6.2	2.7
2	50.3	29.1	21.4	–	–	–	762	5.9	2.5
3	22.5	28.3	25.8	22.5	0.9	–	750	6.0	2.4
4	22.5	28.3	25.8	22.5	0.9	0.1	720	6.2	2.6
5	22.5	28.3	25.8	22.5	0.9	0.2	710	6.15	2.5
6	22.5	28.3	25.8	22.5	0.9	0.3	710	6.0	2.4
7	62.1	37.9	–	–	–	–	595	2.9	1.6
8	43.5	37.9	18.4	–	–	–	600	2.7	1.5
9	19.6	38.1	21.9	19.6	0.8	–	590	2.8	1.4
10	19.6	38.1	21.9	19.6	0.8	0.1	570	2.9	1.35
11	19.6	38.1	21.9	19.6	0.8	0.2	560	2.8	1.3
12	19.6	38.1	21.9	19.6	0.8	0.3	540	2.7	1.2
13	56.2	43.8	–	–	–	–	500	1.8	0.65
14	39.3	43.8	16.7	–	–	–	510	1.7	0.6
15	17.9	44.3	19.2	17.9	0.7	–	500	1.7	0.65
16	17.9	44.3	19.2	17.9	0.7	0.1	480	1.8	0.7
17	17.9	44.3	19.2	17.9	0.7	0.2	470	1.7	0.6
18	17.9	44.3	19.2	17.9	0.7	0.3	460	1.6	0.5

The results show that the developed formulations have the same compressive strength and flexural strength compared with the control compositions while reducing the consumption of cement and the density that is provided by the pozzolanic properties of the fly ash and the use of RWS. The use of construction gypsum and lime as the cause of the latent hydraulic activity of volcanic ash significantly reduces the consumption of cement without reducing the strength of fire resistant composite. With the introduction of resin wood saponification of 0.1–0.3 % by weight of the cement the water consumption for mixture is reduced, density of vermiculite concrete composite is decreased by 40–50 kg/m^3.

Developed vermiculite concrete composites have such disadvantages as brittleness, relatively low strength in bending and compression. For obtaining the composites with improved strength and fire resistant characteristics the influence of parameters of the fiber reinforcement by basalt fiber on their properties with the use of rotatable plan of the second order type of a regular hexagon was investigated.

The composition of the original vermiculite concrete matrix and its physico-mechanical properties for reinforcement by the basalt fibers are shown in Table 3.

Table 3. The ratio of components in the mixture and physico-mechanical properties of the vermiculite concrete composite

The ratio of components in the mixture, wt. %					The number of RWS in % by weight of the binder	Average density, ρ, kg/m^3	The limit of strength, MPa	
Cement	Vermic ulite	Ash	Lime	Gypsum			On compression	On bending
1	2	3	4	5	6	7	8	9
19.6	38.1	21.9	19.6	0.8	0.1	570	2.8	1.4

As the investigated factors the main parameters of dispersed reinforcement were adopted: X_1 – the reinforcement ratio by volume μ_v, %; X_2 – the ratio of the length of the fibers to their diameter l/d. As the optimization parameters there were considered: Y_1 – the limit of strength in compression R_b, MPa; Y_2 – tensile strength at bending R_f, MPa.

The matrix of the experiment is as follows (Table 4).

Table 4. The matrix of the experiment

Ordering No.	Natural variables		The matrix of the experiment				
	x_1	x_2	X_1	X_2	X_1^2	X_2^2	X_1X_2
1	0.30	1444	-1	0	+1	0	0
2	0.9	1444	+1	0	-1	0	0
3	0.75	2221	+0.5	+0.87	+0.25	+0.75	+0.43
4	0.75	667	+0.5	-0.87	+0.25	+0.75	-0.43
5	0.45	2221	-0.5	+0.87	+0.25	+0.75	-0.43
6	0.45	667	-0.5	-0.87	+0.25	+0.75	+0.43
7	0.6	1444	0	0	0	0	0

After processing the experimental data the following regression equations in coded form were obtained:

$$Y_1 = 3.6 - 0.2X_1 - 0.3X_1^2 - 0.9X_2^2 + 0.12X_1X_2 \;;$$

$$Y_2 = 2.6 + 0.2X_1 - 0.65X_1^2 - 0.65X_2^2.$$

The regression equations are made on response surface (Fig. 1).

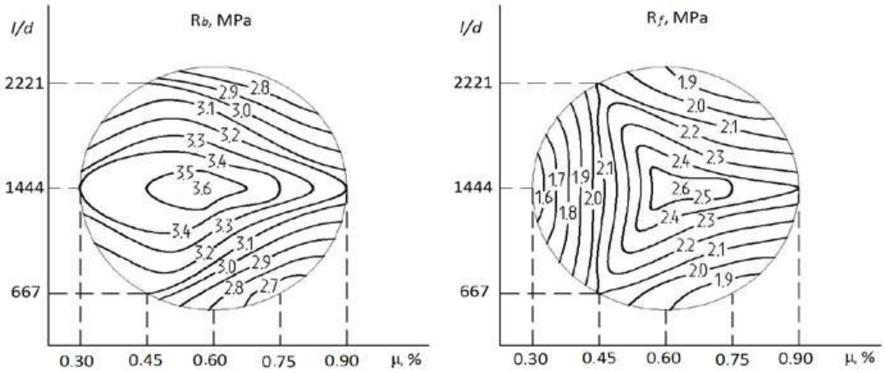

Figure 1. Response surfaces:
R_b – the limit of compressive strength, MPa; R_f – the limit of strength in bending, MPa;
l/d – the ratio of the length of the fibers to their diameter;
μ_v – the percentage of reinforcement by volume

Analysis of the obtained equations and response surfaces showed that the highest values of compressive strength are observed in the plan area with $\mu_v \approx 0.35 - 0.65\%$ and $l/d = 1444$, but flexural strength – $\mu_v \approx 0.6 - 0.85\%$ and $l/d = 1444$. Further increase in reinforcement ratio leads to a decrease in strength, due to violation of the structure of fibre vermiculite concrete composite.

To study the flame retardant properties of the proposed compositions ferro cement slabs with fire-resistant layer with a thickness of 25 mm were made. Studies on the fire resistance were conducted by testing samples with dimensions of 190 × 190 mm in an electric furnace in a horizontal position at temperature mode “standard” fire, regulated by Russian State Standard GOST 30247.1–94. The fire resistance rating for load-bearing capacity (R) of ferro cement slabs was evaluated by heating the woven mesh in the structural layers (on the boundary of layers) to 300 ° C. Humidity of fine-grained concrete ferro cement layer and a flame retardant to the time of testing were respectively 3–4% and 8–10 %. During the fire tests of two-layer elements of violations of their integrity is not detected.

The results of fire tests of ferro cement slabs 20 mm thick with fire resistant layer with a thickness of 25 mm is shown in Figures 2 and 3.

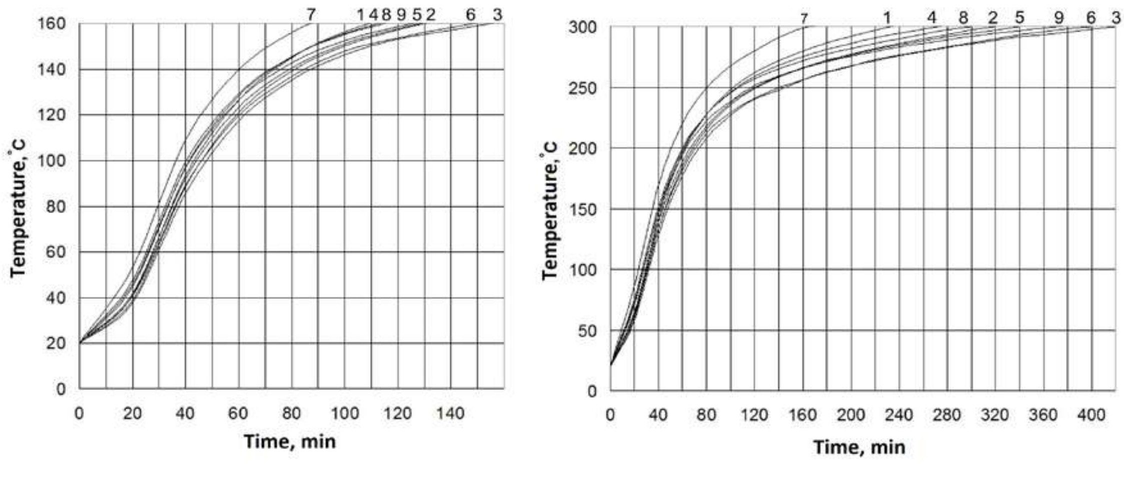

Figure 2. Experimental curves of temperature change on the unheated surface (a) and at the level of the woven mesh (b) double-layer ferro cement samples:
1, 4, 7 – cement vermiculite concrete with average density 500 kg/m^3, 595 kg/m^3 and 740 kg/m^3 respectively;
2, 5, 8 – vermiculite concrete composite with an average density of 480 kg/m^3, 570 kg/m^3 and 730 kg/m^3 respectively;
3, 6, 9 – fibre vermiculite concrete composite with an average density of 470 kg/m^{3,} 560 kg/m^3 and 720 kg/m^3 respectively

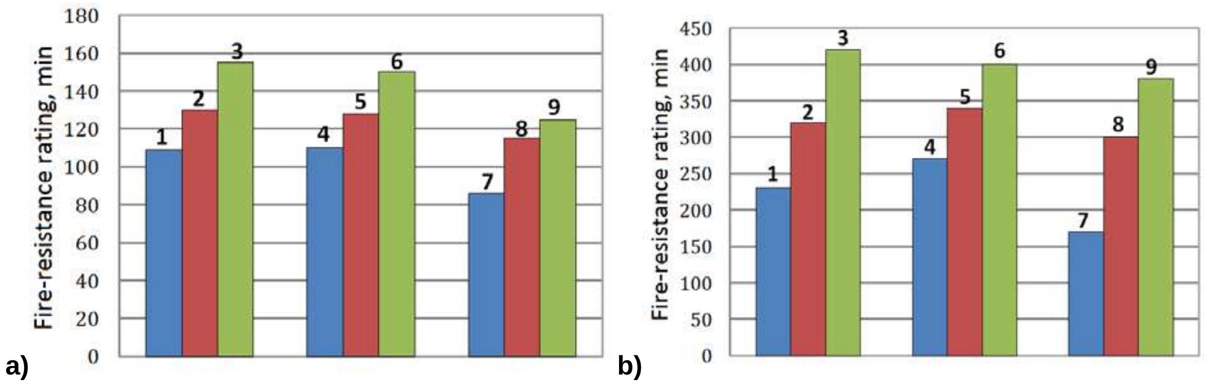

Figures 3. The limit of fire resistance of double-layered ferro cement elements in heat-insulating ability (a) and bearing capacity (b)
Symbols 1-9 look at Figure 2

From Figures 2 and 3 it is followed that the developed fibre vermiculite concrete composites provide higher fire resistance of ferro cement plates in comparison with cement vermiculite concrete. This is due to the better preservation of the flame retardant layer under the influence of high temperatures as a result of dispersal reinforcement with basalt fibers. Furthermore, the addition of RWS additionally forms pores on fibre vermiculite concrete composite, that improving flame retardant properties. The compositions with an average density of 480 kg/m^3 have the highest fire resistant properties.

The study of fire resistance of building constructions with tests for the “standard” temperature is a time-consuming task, which requires expensive equipment. In this regard, the calculation methods determining fire resistance of constructions are of great importance.

For the calculation of fire resistance of building constructions in our country numerical and analytical methods are developed. The greatest preference is for numerical methods because of their simple implementation using modern computer technology.

We developed an algorithm of thermal and technical calculation of the fire resistance of multi-layered building constructions, providing acceptable coincidence of calculated values with experimental data. The algorithm for calculating the fire resistance of building constructions with fire resistant layer is reduced to the solution of the thermal and physical problem. The temperature distribution $t(x, \tau)$ on the thickness of the multilayer structure is described by the Fourier equation

$$\rho(x)\, c(t,x)\frac{\partial t}{\partial \tau} = \frac{\partial}{\partial x}\left(\lambda(t,x)\frac{\partial t}{\partial x}\right)$$
$$(x,\tau) \in Q \equiv \{(x,\tau) : x \in (0,l), \tau \in (0,T)\}, \quad (1)$$

where x, τ – coordinates in space and time; $c(t, x)$, $\lambda(t, x)$, $\rho(x)$ – specific heat, thermal conductivity and material density; l – the thickness of the construction; T – some finite value of time. Not odnoclasnichi design causes a dependence of c and λ on the spatial coordinates x, in addition, they are also functions of time indirectly via t(x, τ). Vermiculations density of the composite is adopted unchanged, as during a fire will not change significantly. Because of the layered design, the density of the material depends on spatial coordinates.

Multi-layer construction determines the dependence of c and λ on the spatial coordinate x; in addition, they are also functions of time indirectly via $t(x, \tau)$. Density of the vermiculite concrete composite is adopted unchanged, as during a fire it will not change significantly. Because of the layered construction, the density of the material depends on spatial coordinates.

To solve the above problem in the work numerical methods were used, found application in various fields of science and technology.

To solve the thermal and physical problem of fire resistance of double-layer building construction from fire resistant and ferro cement layers to the equation (1) the initial and boundary conditions are joined. The initial conditions are set by formula

$$t(x,0) = \varphi(x), \quad x \in [0,l], \quad (2)$$

where $\varphi(x)$ – a function of the temperature distribution along the thickness of the construction. Through the outer surface of the construction there is a heat exchange with the surrounding media, the temperature of which: $T_f(\tau)$ – the temperature of the fire, $T_c(\tau)$ – the outside air temperature, are known. Then the boundary conditions take the form of:

$$\lambda_в(t)\frac{\partial t(0,\tau)}{\partial x}=\alpha_в(t)[t(0,\tau)-T_n(\tau)],\quad \tau>0, \tag{3}$$

$$-\lambda_a(t)\frac{\partial t(l,\tau)}{\partial x}=\alpha_a(t)\,[t(l,\tau)-T_c(\tau)],\quad \tau>0. \tag{4}$$

Here $\lambda_в(t)$ = (t, 0), $\lambda_a(t) = \lambda(t, l)$ – the conductivity coefficients of vermiculite concrete composite and ferrocement, respectively; $\alpha_в$ – the heat transfer coefficient from the heated medium (the firing chamber) to construction surface (vermiculite concrete layer); α_a – the coefficient of heat transfer from the unheated surface (ferro cement layer) to the environment. In this model $T_c(\tau)$ and $\varphi(x)$, as a rule, in practical calculations are constants.

Equation (1), initial and boundary conditions (2) – (4) constitute the problem of the temperature distribution through the thickness of the construction. Coefficients included in the equation and the additional conditions are determined from the known formulas for two-layer construction:

$$\lambda_в(t)=\lambda_1+k_1t,\quad c_в(t)=c_1+k_2t,\quad \lambda_a(t)=\lambda_2+k_3t,\quad c_a(t)=c_2+k_4t,$$

$$\alpha_в(t)=29+\frac{5{,}77\varepsilon_в}{t(0,\tau)-T_n}\left[\left(\frac{T_n+273}{100}\right)^4-\left(\frac{t(0,\tau)+273}{100}\right)^4\right], \tag{5}$$

$$\alpha_a=1{,}5\sqrt{t(l,\tau)-T_c}+\frac{5{,}77\varepsilon_в}{t(l,\tau)-T_c}\left[\left(\frac{t(l,\tau)+273}{100}\right)^4-\left(\frac{T_c+273}{100}\right)^4\right],$$

where λ_1, λ_2, c_1, c_2 – the initial characteristics of the coefficients of thermal conductivity and heat capacity, respectively vermiculite concrete composite and ferrocement; k_1, k_2, k_3, k_4 – coefficients, the numerical values which are determined from the criterion of the satisfactory coincidence of experimental and calculated curves of heating plates; $\varepsilon_в$, ε_a – degree of black vermiculite concrete composite and ferrocement respectively.

Due to the dependence of the specific heat capacities and thermal conductivity coefficients from temperature the equation (1) and boundary conditions (3) – (4) are nonlinear. Therefore, to solve problem (1) – (4) numerical methods are used. In the work [17] the course differential implicit two-layer scheme of calculations combined with the Thomas method and iteration are used. While derivatives included in the heat equation and the boundary conditions are replaced by the known differential relationships.

Then the system of algebraic equations with a tridiagonal coefficient matrix on each upper layer in time is solved. The nonlinearity of the algebraic equations is overcome by using the method of iteration and sweep.

We developed software for thermal and technical calculation of the fire resistance of ferroconcrete construction with fire-resistant layer from vermiculite concrete. With the use of PC calculations with a precision equal to 0.001 were conducted and the coefficients k_1, k_2, k_3, k_4 of formula (5) providing a reasonable correlation between theoretical and experimental curves, in which expressions for the coefficients of thermal conductivity and heat capacity were determined:

ferrocement – $\lambda_a(t)=0.83-0.0004t,\quad c_a(t)=770+0.8t$;

cement vermiculite concrete with density 500 kg/m^3 – $\lambda_o(t)=0.09+0.000093t,\quad c_o(t)=920+0.51t$;

cement vermiculite concrete composite with density of 480 kg/m^3 –

$\lambda_o(t)=0.087+0.00008t,\quad c_o(t)=920+0.51t$;

cement fibre vermiculite concrete composites with density 470 kg/m^3 –

$\lambda_o(t)=0.086+0.00007t,\quad c_o(t)=920+0.51t$;

cement vermiculite concrete with density of 595 kg/m³ – $\lambda_o(t) = 0.11 + 0.000057t, \quad c_o(t) = 920 + 0.51t$;

cement vermiculite concrete composite with density of 570 kg/m³ –

$\lambda_o(t) = 0.1 + 0.00006t, \quad c_o(t) = 920 + 0.51t$;

cement fibre vermiculite concrete composite with density of 560 kg/m³ –

$\lambda_o(t) = 0.099 + 0.00005t, \quad c_o(t) = 920 + 0.51t$;

cement vermiculite concrete with density 740 kg/m³ – $\lambda_o(t) = 0.14 + 0.00004t, \quad c_o(t) = 920 + 0.61t$;

cement vermiculite tuff concrete with density of 730 kg/m³ –

$\lambda_o(t) = 0.125 + 0.00003t, \quad c_o(t) = 920 + 0.61t$;

cement fibre vermiculite concret composite with density of 720 kg/m³

$\lambda_o(t) = 0.120 + 0.00003t, \quad c_o(t) = 920 + 0.61t$;

The dependence of the fire resistance of ferroconcrete constructions on the thickness and composition of the composite obtained by the calculation method is shown in Figure 4.

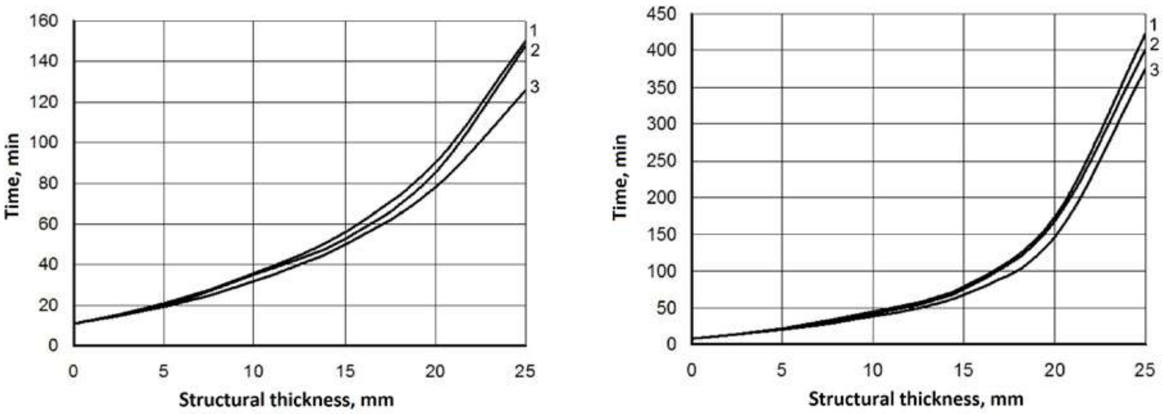

Figure 4. The dependence of the limit of fire resistance of double-layered ferro cement elements on the basis of the loss of insulating ability (a) and the loss of bearing capacity (b) on the thickness and composition of the fire resistant layer:
1, 2, 3 – fibre vermiculite concrete composite with an average density of 470 kg/m³, 560 kg/m³ and 720 kg/m³ respectively

Figure 5 shows the results of calculation of the limit of fire resistance of fibre vermiculite concrete plates on the grounds of loss of insulating ability.

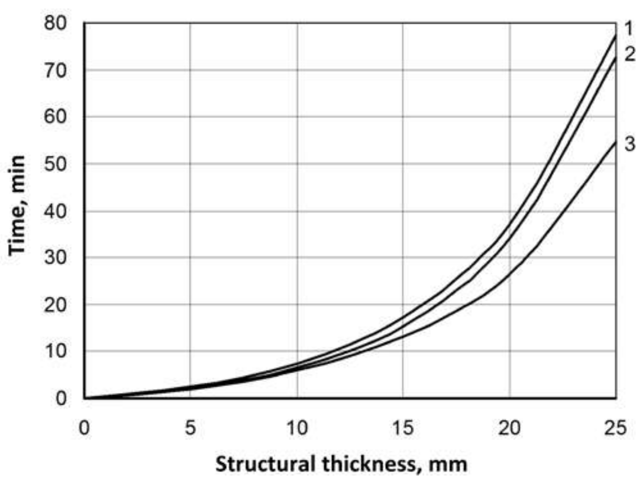

Figure 5. The dependence of the fire resistance of fibre vermiculite concrete plates on the grounds of loss of insulating ability on the thickness and composition of layer:
1, 2, 3 – fibre vermiculite concrete composite with an average density of 470 kg/m³, 560 kg/m³ and 720 kg/m³ respectively

In further experiments to produce flame retardant composites volcanic pumice of Psykhureysk field was used.

The results of studies of the properties of the composites on Portland cement PTS500-DO without additives and with additives of volcanic pumice are given in Table 5.

Table 5. The properties of cement stone and concrete on cement with pumice

The addition of pumice in % by mass of cement	The properties of cement stone (concrete)								
	the average density (kg/m^3), age, days			the limit of flexural strength (MPa) age, days			the limit of compressive strength (MPa) age, days		
	28			28			28		
	heating temperature, °C			heating temperature, °C			heating temperature, °C		
	105	600	800	105	600	800	105	600	800
PTS500-DO, without additives									
0	1788	1769	1760	5.8	5.3	4.4	46.0	26.7	23.2
PTS500-DO, the addition of pumice with a grain size of 0<d<0.16 mm									
30	1609	1538	1528	6.4	6.3	6.3	39.5	25.4	24.2
PTS500-DO, the addition of pumice with a grain size of 0<d<0.31 mm									
20	1764	1746	1717	7.6	7.4	6.2	32.2	31.4	27.6
40	1787	1753	1733	5.4	5.0	3.6	28.5	24.0	23.3
60	1725	1700	1680	4.9	4.6	3.5	16.2	15.5	14.7
PTS500-DO, the addition of pumice with a grain size of 0<d<0.63 mm									
20	1750	1692	1682	7.4	7.0	6.1	35.5	32.8	32.4
40	1656	1623	1606	6.8	6.3	6.2	25.1	23.1	21.7
60	1511	1490	1469	4.6	4.2	3.7	13.7	12.8	12.5
PTS500-DO, the addition of pumice with a grain size of 0<d<1.25 mm									
20	1711	1684	1673	7.1	6.5	5.3	30.7	27.6	22.4
40	1630	1607	1534	7.4	6.6	6.1	20.8	18.9	15.6
60	1423	1392	1385	3.9	3.7	3.3	10.8	8.2	8.0

From Table 5 it follows that the additive of volcanic pumice fraction d < 0.16 mm up to 30 % by weight of cement significantly improves heat-resisting properties of cement stone with a simultaneous increase in flexural strength and no significant loss of compressive strength that is associated with the hydraulic activity of the fraction of pulverized volcanic pumice. The use of pumice with large grain size largely reduces the compressive strength of the composite, but significantly increases heat resistant properties and average density of the composite decreases slightly.

Expanded vermiculite is an expensive material, therefore the possibility of replacing parts of vermiculite fraction of 0.16–5 mm with volcanic pumice was considered.

Further studies were conducted on the development of flame retardant vermiculite concrete with the use of volcanic pumice; the results of the experiments are given in Table 6.

Studies showed that the insertion of up to 30 % pumice fraction 0-0.16 mm by mass of cement strength characteristics of vermiculite concrete decrease slightly, but their heat-resistant properties increase. Replacement of volcanic pumice parts with expanded vermiculite reduces the average density of the vermiculite concrete composite and enhances their heat-resistant properties.

Further research focuses on the study of flame retardant properties of the developed composites with the use of volcanic pumice.

Table 6. Physico-mechanical properties of vermiculite concrete with the use of volcanic pumice

№№ compositions	Features of vermiculite concrete composite								
	average density, kg/m^3			the limit of flexural strength (MPa) at the age of 28 days			the limit of compressive strength (MPa) at the age of 28 days		
	heating temperature, °C			heating temperature, °C			heating temperature, °C		
	105	600	800	105	600	800	105	600	800
1	2	3	4	5	6	7	8	9	10
Cement: vermiculite by volume – 1:3									
1	720	715	710	1.6	1.3	1.0	2.9	2.2	2.1
Cement: vermiculite by volume – 1:3 with the addition of pumice fractions 0-0.16 mm by weight from cement									
2	723	712	707	1.4	1.26	0.9	2.4	1.8	1.7
Cement: pumice (fractions 0-1.25 mm) by volume – 1:3									
3	1461	1436	1426	3.2	2.2	1.9	11.9	7.4	6.7
Cement: pumice (fraction 0.16–0.315 mm)+vermiculite fraction 0.315–5 mm instead of pumice fraction 0.315–1.25 by volume – 1:3									
4	1676	1657	1650	3.6	2.9	1.9	14.0	10.7	8.5
Cement: pumice (fraction 0.16–0.63 mm)+vermiculite fraction of 0.63–5 mm instead of pumice fraction 0.63–1.25 by volume – 1:3									
5	1303	1288	1280	2.1	1.9	1.9	8.8	6.5	6.4

Table 7 presents the results of studies on the fire resistance of ferro cement elements with a thickness of 20 mm, with fire resistant layer with a thickness of 20 mm based on control and proposed compositions of vermiculite concrete composites with volcanic pumice application.

Table 7. The results of studies on the fire resistance of double-layered ferro cement elements

№№ compositions	The composition of the fire resistant layer				Average density, kg/m^3	The limit of fire resistance of slabs, min.	
	Cement: vermiculite by volume	Replacement of vermiculite part with pumice by volume	RWS in % by weight of cement	The reinforcing percentage of fibers by volume		on bearing capacity (*R*)	on the heat-insulating capacity (*E*)
1	2	3	4	5	6	7	8
1	1:2	–	–	–	750	82	57
2	1:3	pumice fraction 0.16–0.315 mm	–	–	847	68	44
3	1:3	pumice fraction 0.16–0.315 mm	0.3	0.6	805	73	48
4	1:4	pumice fraction 0.16–0.63 mm	–	–	855	66	43
5	1:4	pumice fraction 0.16–0.63 mm	0.3	0.6	812	65	46

Developed vermiculite concrete composites using volcanic pumice, air-entraining additives RWS and basalt fibers with higher density in comparison with the reference vermiculite concrete have higher flame retardant properties due to the better preservation of the flame retardant layer as a result of dispersal reinforcement with basalt fiber and additional pore of RWS.

With the use of PC calculations with a precision equal to 0.001 were conducted and the coefficients k_1, k_2, k_3, k_4 of formula (5) providing a reasonable correlation between theoretical and experimental curves, in which expressions for the coefficients of thermal conductivity and heat capacity of developed fibre vermiculite pumice concrete composite with density of 810 kg/m^3 (tab. 7, the composition No. 5) were determined:

$$\lambda_o(t) = 0.180 + 0.00003t, \quad c_o(t) = 920 + 0.63t\,;$$

Figure 6 shows the results of calculating the fire resistance of ferro cement elements, depending on the thickness and composition of fibre vermiculite pumice concrete composite.

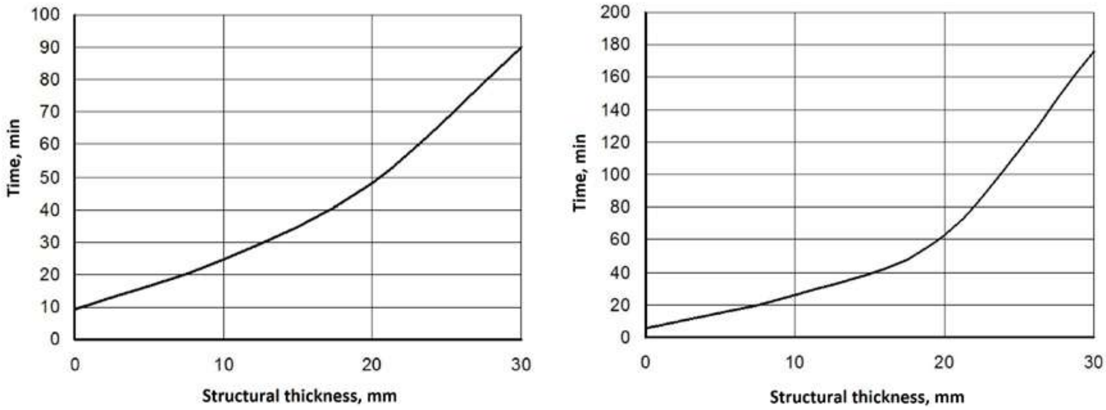

Figure 6. The dependence of the limit of fire resistance of double-layered ferro cement elements on the basis of the loss of insulating ability (a) and the loss of bearing capacity (b) on the thickness of the fibre vermiculite pumice concrete layer

Figure 7 shows the results of calculation of fire resistance of fibre vermiculite pumice concrete plates on the grounds of loss of insulating ability.

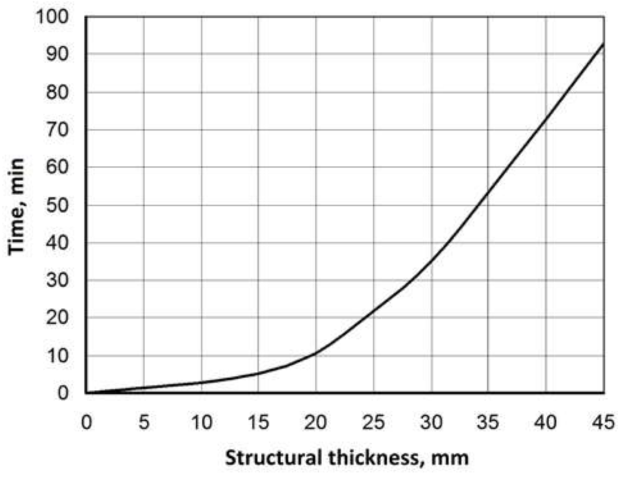

Figure 7. The dependence of the fire resistance of fibre vermiculite pumice concrete plates on the grounds of loss of insulating ability on the layer thickness

Thus, the developed fibre vermiculite concrete and fibre vermiculite pumice concrete composites have high fire retardant properties and improved strength characteristics with less consumption of Portland cement. Using the obtained expressions for the coefficients of thermal conductivity and thermal capacity of flame retardant composites, it is possible to calculate the fire resistance of two-layer structures by numerical methods with application of the developed software.

Thus, the developed fibre vermiculite concrete composites with application of volcanic ash have higher heat resistant properties, thus reducing the consumption of Portland cement without compromising strength characteristics. High flame retardant properties of fibre vermiculite concrete composites are ensured by using RWS, ash and basalt fiber. The use of consrtuction gypsum and lime as the cause of the latent hydraulic activity of volcanic ash reduces significantly the consumption of cement without reducing the strength of fire resistant composite.

Dispersed reinforcement with basalt fiber increases composite fire-resistant and strength characteristics of the original matrix. With the use of rotatable plan of the second order type of a regular hexagon it is found that the highest values of compressive strength are observed in the area plan with $\mu_v \approx 0.35-0.65\%$, and flexural strength – $\mu_v \approx 0.6-0.85\%$ and $l/d = 1444$.

Experimental studies of fire resistance of double-layer ferroconcrete structures showed high fire resistant properties of the developed cement fibre vermiculite concrete fire resistant composites.

The course differencing implicit scheme of solving the problem of thermal conductivity and sweep method in conjunction with the iteration method gives a universal algorithm for determining the temperature across the thickness of the construction, not associated with restrictions on the number of layers on the smallness of the grid and does not require linearization of the basic differential equations of heat conduction and boundary conditions. The proposed algorithm allows selecting and specifying the coefficients and the functional dependencies included in the mathematical model and known a priori only approximately.

Fibre vermiculite concrete composites using volcanic pumice, air-entraining additives RWS and basalt fibres with a higher fire resistant properties in comparison with the reference vermiculite concrete that reduce the consumption of expensive expanded vermiculite were developed.

The expressions of the coefficients of thermal conductivity and heat capacity of fibre vermiculite concrete composites with the use of volcanic pumice and ash for thermal and technical calculation of fire resistance of building constructions by numerical methods were obtained.

The received results are coordinated with the theoretical and pilot studies conducted in the works [6, 10–12].

4. Conclusions

1. Thus, the article considers a number of fundamental issues related to obtaining effective cement fibre vermiculite concrete composites with application of volcanic rocks. It is revealed that the use of volcanic rocks reduces the consumption of Portland cement and improves flame retardant properties of vermiculite concrete composites.

2. Dispersed reinforcement with basalt fiber of source matrix allows improving significantly strength properties while improving the fire retardant properties due to the perception of the tensile forces impacted by fire.

3. The proposed algorithm with the use of finite-difference implicit scheme for solving the heat conduction problem and the sweep method allows selecting and specifying the coefficients and the functional dependencies included in the mathematical model and known a priori only approximately.

4. Using the proposed algorithm the expression for the coefficients of thermal conductivity and heat capacity of fibre vermiculite concrete composites with the use of volcanic pumice and ash for thermal and technical calculation of fire resistance limit of building constructions by numerical methods was obtained. The proposed calculated method of determination of fire resistance limits of constructions provides an acceptable coincidence with the experimental data.

References

1. Morozov A.P. O vedushchey roli Leningradskogo zonalnogo nauchno-issledovatelskogo i proyektnogo instituta tipovogo i eksperimentalnogo proyektirovaniya zhilykh i obshchestvennykh zdaniy v dele vnedreniya prostranstvennykh konstruktsiy v zhilishchno-grazhdanskom stroitelstve [On the leading role of the Leningrad Zonal Research and Design Institute for the typical and experimental design of residential and public buildings in the implementation of spatial structures in housing and civil construction]. *Issledovaniye tonkostennykh prostranstvennykh konstruktsiy i tekhnologiya ikh izgotovleniya.* Leningrad,1980. Pp. 5–10. (rus)

Литература

1. Морозов А.П. О ведущей роли Ленинградского зонального научно-исследовательского и проектного института типового и экспериментального проектирования жилых и общественных зданий в деле внедрения пространственных конструкций в жилищно-гражданском строительстве // Исследование тонкостенных пространственных конструкций и технология их изготовления. Л.,1980. С. 5–10.
2. Митрофанов Е.Н. Армоцемент. Л., 1973. 208 с.
3. Романенков И.Г., Левитес Ф.А. Огнезащита строительных конструкций. М.: Стройиздат, 1991. 320 с.

Hezhev T.A., Zhurtov A.V., Tsipinov A.S., Klyuev S.V. Fire resistant fibre reinforced vermiculite concrete with volcanic application. *Magazine of Civil Engineering*. 2018. No. 4. Pp. 181–194. doi: 10.18720/MCE.80.16.

2. Mitrofanov Ye.N. *Armotsement* [The ferrocement]. Leningrad, 1973. 208 p. (rus)
3. Romanenkov I.G., Levites F.A. Ognezashchita stroitelnykh konstruktsiy [Fire protection of building structures]. Moscow: Stroyizdat, 1991. 320 p. (rus)
4. Kretova V., Hezhev T., Zhukov A., Hezhev K. Fireproofind Cemented Fiber Vermiculite-Conkrete Composites with Application VolkanicAsh. *Applied Mechanics and Materials*. 2015. Pp. 725–726.
5. Khezhev T.A., Pukharenko Yu.V., Khezhev Kh.A., Klyuev S.V. Fiber Gypsum Concrete Composites with Using Volcanic Tuff Sawing Waste*. ARPN Journal of Engineering and Applied Sciences.* 2018. Vol. 13. No. 8. Pp. 2935–2946.
6. Rabinovich F.N. Kompozity na osnove dispersno armirovannykh betonov [Composites based on dispersed reinforced concrete]. *Voprosy teorii i proyektirovaniya, tekhnologiya, konstruktsii: monografiya.* Moscow: ASV, 2004. 560 p. (rus)
7. Klyuev S.V., Klyuev A.V., Abakarov A.D., Shorstova E.S., Gafarova N.G. The effect of particulate reinforcement on strength and deformation characteristics of fine-grained concrete. *Magazine of Civil Engineering.* 2017. No. 7. Pp. 66–75.
8. Lesovik R.V., Klyuyev S.V., Klyuyev A.V., Netrebenko A.V., Yerofeyev V.T., Durachenko A.V. Fine-Grain concrete reinforced by polypropylene fiber. *Research Journal of Applied Sciences.* 2015. No. 10(10). Pp. 624–628.
9. Klyuyev S.V., Guryanov Yu.V. External reinforcing of fiber concrete constructions by carbon fiber tapes. *Magazine of Civil Engineering.* 2013. No. 1. Pp. 21–26.
10. Morozov V.I., Pukharenko Yu.V., Yushin A.V. The numerical investigations of double-span concrete beams strengthened with fiber reinforced plastics across the oblique section. *Materials Physics and Mechanics.* 2017. Vol. 31. No. 1-2. Pp. 40–43.
11. Komarinskiy M.V., Oniskovets R.V., Ostarkova O.A. Strongly reinforced concreting design of cast concrete alloy mixtures. *Construction of Unique Buildings and Structures.* 2017. No. 2(53). Pp. 29–41.
12. Wang W., Liu J., Agostini F., Davy C.A., Skoczylas F., Corvez D. Durability of an Ultra High Performance Fiber Reinforced Concrete under progressive. *Cement and Concrete Research.* 2014. Vol. 55. Pp. 1–13.
13. Albenque M. Hin neues keramisches Material – Schaumton. *Stogel-industrie*. 1972. No. 10. Rp. 452.
14. Harchenko I. Fires and habitability of the person. *Fire Safety Bulletin (Ukr.).* 2000. No. 2(4). Pp. 25–30.
15. Hertz K.D. Reinforcement data for fire safety design. *Magazine of Concrete Research.* 2004. 56. No. 8. Pp. 453–459.
16. Li M., Quan C.X., Sun W. Mechanical properties of high-strength concrete after fire. *Cement and Concrete Research*. 2004. No. 34. Pp. 1001–1005.
17. Krause J.R. *Fibre Cement: Technology and Design*. A Birkhäuser book. 2006. 160 p.
18. Bunsell A.R., Renard J. Fundamentals of Fibre Reinforced Composite Materials (series In Material Science And Engineering). *Institute Of Physics Publishing (gb).* June 2005. 398 p.
19. Yu R., Spiesz P., Brouwers, H.J.H. Development of an ecofriendly Ultra-High Performance Concrete (UHPC) with efficient cement and mineral admixtures uses. *Cement and Concrete Composites.* 2015. Vol. 55. Pp. 383–394.
20. Sivakumar N., Muthukumar S., Sivakumar V., Gowtham D., Muthuraj V. Experimental studies on High Strength Concrete by Using Recycled Coarse aggregate. *Research Inventy: International Journal of Engineering and Science.* 2014. Vol. 4. No. 1. Pp. 27–36.

4. Kretova V., Hezhev T., Zhukov A., Hezhev K. Fireproofind Cemented Fiber Vermiculite-Conkrete Composites with Application VolkanicAsh // Applied Mechanics and Materials. 2015. Pp. 725–726.
5. Khezhev T.A., Pukharenko Yu.V., Khezhev Kh.A., Klyuev S.V. Fiber Gypsum Concrete Composites with Using Volcanic Tuff Sawing Waste // ARPN Journal of Engineering and Applied Sciences. 2018. Vol. 13. № 8. Pp. 2935–2946.
6. Рабинович Ф.Н. Композиты на основе дисперсно армированных бетонов // Вопросы теории и проектирования, технология, конструкции: монография. 3-е изд., перераб. и доп. М.: АСВ, 2004. 560 с.
7. Клюев С.В., Клюев А.В., Абакаров А.Д., Шорстова Е.С., Гафарова Н.Е. Влияние дисперсного армирования на прочностные и деформативные характеристики мелкозернистого бетона // Инженерно-строительный журнал. 2017. № 7(75). С. 66–75.
8. Клюев С.В., Клюев А.В., Сопин Д.М., Нетребенко А.В., Казлитин С.А. Тяжелонагруженные полы на основе мелкозернистых фибробетонов // Инженерно-строительный журнал. 2013. №3(38). С. 7–14**.**
9. Клюев С.В., Гурьянов Ю.В. Внешнее армирование изгибаемых фибробетонных изделий углеволокном // Инженерно-строительный журнал. 2013. №1(36). С. 21–26
10. Morozov V.I., Pukharenko Yu.V., Yushin A.V. The numerical investigations of double-span concrete beams strengthened with fiber reinforced plastics across the oblique section // Materials Physics and Mechanics. 2017. Vol. 31. № 1-2. Pp. 40–43.
11. Комаринский М.В., Онисковец Р.В., Остаркова О.А. Бетонирование густоармированных конструкций литыми смесями // Строительство уникальных зданий и сооружений. 2017. № 2(53). С. 29-41
12. Wang W., Liu J., Agostini F., Davy C.A., Skoczylas F., Corvez D. Durability of an Ultra High Performance Fiber Reinforced Concrete under progressive // Cement and Concrete Research. 2014. Vol. 55. Pp. 1–13.
13. Albenque M. Hin neues keramisches Material – Schaumton // Stogel-industrie. 1972. № 10. Pp. 452.
14. Harchenko I. Fires and habitability of the person // Fire Safety Bulletin (Ukr.). 2000. № 2(4). Pp. 25–30.
15. Hertz K.D. Reinforcement data for fire safety design // Magazine of Concrete Research. 2004. Vol. 56. No. 8. Pp. 453–459.
16. Li M., Quan C.X., Sun W. Mechanical properties of high-strength concrete after fire // Cement and Concrete Research. 2004. № 34. Pp. 1001–1005.
17. Krause J.R. Fibre Cement: Technology and Design. A Birkhäuser book. 2006. 160 p.
18. Bunsell A.R., Renard J. Fundamentals of Fibre Reinforced Composite Materials (series In Material Science And Engineering). Institute Of Physics Publishing (gb). 2005. 398 p.
19. Yu R., Spiesz P., Brouwers, H.J.H. Development of an ecofriendly Ultra-High Performance Concrete (UHPC) with efficient cement and mineral admixtures uses // Cement and Concrete Composites. 2015. Vol. 55. Pp. 383–394.
20. Sivakumar N., Muthukumar S., Sivakumar V., Gowtham D., Muthuraj V. Experimental studies on High Strength Concrete by Using Recycled Coarse aggregate // Research Inventy: International Journal of Engineering and Science. 2014. Vol. 4. № 1. Pp. 27–36.
21. Brouwers H.J.H., Radix H.J. Self-Compacting Concrete: Theoretical and experimental study // Cement and Concrete Research. 2005. Vol. 35. Pp. 2116–2136.
22. Tayeh B.A., Abu Bakar B.H., Megat Johari M.A., Tayeh S.M. Compressive Stress-Strain Behavior of Composite Ordinary

21. Brouwers H.J.H., Radix H.J. Self-Compacting Concrete: Theoretical and experimental study. *Cement and Concrete Research.* 2005. Vol. 35. Pp. 2116–2136.
22. Tayeh B.A., Abu Bakar B.H., Megat Johari M.A., Tayeh S.M. Compressive Stress-Strain Behavior of Composite Ordinary and Reactive Powder Concrete. *Iranica Journal of Energy and Environment.* 2013. Vol. 4. No. 3. Pp. 294–298.
23. Makitani E., Sekiya S., Hagiwara I. A studi on bond strength in steel fibre reinforced concrete. *Rev. 33rd Gren. Meet. Cem. Assoc., Tokyo, 1979.* Sinepses, Tokyo, 1979. Pp. 190–192.
24. Cahn D.S., Phillips J.C. Durability of fiber glass portland cement composites. *J. of the Amerikan Concrete Inst.* 1973. No. 3. Pp. 247.

and Reactive Powder Concrete // Iranica Journal of Energy and Environment. 2013. Vol. 4. № 3. Pp. 294–298.

23. Makitani E., Sekiya S., Hagiwara I. A studi on bond strength in steel fibre reinforced concrete // Rev. 33rd Gren. Meet. Cem. Assoc., Tokyo, 1979. Sinepses, Tokyo, 1979. Pp. 190–192.
24. Cahn D.S., Phillips J.C. Durability of fiber glass portland cement composites // J. of the Amerikan Concrete Inst. 1973. № 3. Pp. 247.

Tolya Hezhev,
+8(928)930-71-85; hejev_tolya@mail.ru

Artur Zhurtov,
+7(967)417-19-76; zhurtovartur@mail.ru

Ayes Tsipinov,
+7(928)700-17-15; czi.ayes69@yandex.ru

Sergey Klyuev,*
+7(951)139-63-27; Klyuyev@yandex.ru

Толя Амирович Хежев,
+8(928)930-71-85;
эл. почта: hejev_tolya@mail.ru

Артур Владимирович Журтов,
+7(967)417-19-76;
эл. почта: zhurtovartur@mail.ru

Ауес Сефович Ципинов,
+7(928)700-17-15;
эл. почта: czi.ayes69@yandex.ru

Сергей Васильевич Клюев,*
+7(951)139-63-27;
эл. почта: Klyuyev@yandex.ru

doi: 10.18720/MCE.80.17

Diagnostics of fatigue fractures of building structures elements

Диагностика усталостных разрушений элементов строительных конструкций

V.K. Sogomonyan,
G.S. Chibukhchyan*,
O.S. Chibukhchyan,
National polytechnic university of Armenia, Yerevan, Republic of Armenia

Аспирант В.К. Согомонян,
магистрант Г.С. Чибухчян*,
магистрант О.С. Чибухчян,
Национальный политехнический университет Армении, Ереван, Армения

Key words: building structures; construction equipment; fatigue fracture; fractography; technical expertise diagnostics

Ключевые слова: строительные конструкции; строительное оборудование; усталостное разрушение; фрактографии; техническая экспертиза диагностики

Аннотация. В статье рассматриваются вопросы повышения усталостной прочности ответственных деталей и узлов строительных машин и оборудования, чаще подверженных усталостному разрушению при воздействии переменного сложного нагружения. Произведена количественная оценка размеров зон усталостного разрушения в деталях и соединениях, установленных в строительных конструкциях и силовых схемах указанных строительных оборудований. Рассмотрена новая методика технической диагностики причин усталостных разрушений узлов строительных машин и конструкций выявлением закономерностей изменения микротвердостей в различных зонах усталостных изломов. Представлены результаты измерений микротвердостей в зонах усталостных изломов получены системы эталонных регрессионных уравнений, позволяющих количественно оценить параметры режима нагружения, приведших разрушению. Создана вычислительная подпрограмма, позволяющая путем обработки данных измерений микротвердостей исследуемого излома получить аналогичные уравнения, и сравнивая их с эталонными уравнениями, дать обоснованное количественное заключения о причинах разрушения.

Abstract. The article deals with the issues of increasing the fatigue strength of critical parts and components of construction machines and equipment, which are more often subjected to fatigue failure under the influence of variable complex loading. A quantitative estimate of the size of the fatigue fracture zones in the parts and joints installed in the building structures and power circuits of this construction equipment has been made. A new technique for technical diagnostics of the causes of fatigue destruction of knots of construction machines and structures is considered, revealing regularities of changes in microhardness in various zones of fatigue fractures. The results of measurements of microhardness in the zones of fatigue fractures are obtained. The systems of standard regression equations are obtained that allow one to quantify the parameters of the loading regime that led to destruction. A computational subroutine has been created that allows us to obtain analogous equations by processing the microhardness measurements of the fracture under study, and comparing them with the reference equations, give a reasonable quantitative conclusion on the causes of failure.

1. Introduction

The increase in the operation speeds, machine capacity, as well as load-carrying capacity of vehicles used for various purposes has led to the growth of production and traffic accidents, which tend to increase. Since the failures of construction elements take place when working with frequent overloads and various applied factors (atmosphere impacts, corrosive environment, heat and frequency fields, etc), they mainly have fatigue behavior (up to 75 %). Therefore, it becomes important to study the problem of the crack resistance of constructions, and give a reliable estimation of the fracture causes. The descriptive cases of failures of constructions are considered. In this field, works on the problems of theoretical and applied mechanics of fracture [1–6] and fractography are known [4] whose results are applied in strength and crack resistance calculations. The working conditions of machines and equipment with the minimal resource of service in the extreme modes and an increased level of failure probability, require in addition to complex measures of constructional, technological, and exploitation-type, a mandatory monitoring of service life and

Согомонян В.К., Чибухчян Г.С., Чибухчян О.С. Диагностика усталостных разрушений элементов строительных конструкций // Инженерно-строительный журнал. 2018. № 4(80). С. 195–203.

regular implementation of technical diagnostics of the construction state which is an actual task of the machines' working capacity assurance.

The most loaded construction elements, the details and joints are selected which work at variable complex loading in the mentioned machines, and they are subjected to fatigue fracture quite often,the types of fatigue fractures of shafts and key joints are presented and their [7–10] fractological analyse with macro and microstructural changes of fracture surface and its layers is given. The fracture samples resulted from fatigue experiments (co-rotating bending and torsion) of flat the details with fillet and surface grooves and prism key joints at different cyclic overloading are selected. Stress conditions in mentioned stress concentrators are studied and the dangerous sections are determined in case of their combined influence. The selected fractures are classified by affecting factors [11–16].

The aim of the work is to study the physico-mechanical condition of the surface layers of the the details fatigue fractures, and the development of the technical diagnostics method for revealing the causes of fracture. To achieve this goal, the following problems are solved:

a) classification of fatigue fractures of the details and joints according to the acting factors;
b) study of the the details variable complex loading impact on the certain zones of the fatigue fracture surface;
c) microhardness measurements of the fracture surface layers in the zones of plastic and brittle fracture, and obtaining strengthening regularities in these zones;
d) database creation of the microhardness measurements and obtaining their functional connections with the parameters of the fracture surface layers;
e) development of the technical diagnostics method for revealing the causes of fractures of the details and joints.

2. Methods

These measurements are processed by the methods of mathematical statistics, and regression functions are derived which are actually 4th degree polynomial equations. The Wolfram Mathematica standard computer software package is used to carry out these calculations and present the functions in 2D and 3D coordinate systems [17–21].

3. Results and Discussion

Typical cases of fatigue fracture of the details and joints, the loading condition – the joint action of bending and torsion with $\tau/\sigma = 0.6$ constant ratio, specific for midshafts of the mentioned units are considered. For the generalization and practical application of the obtained results, specific cases of the machine element constructive forms are selected – smooth the details, with fillet and V-shape surface notch, the details with keyway and transition fit. The distribution diagrams of contour and contact stresses are studied and built for the mentioned cases.

The selection of stress concentrator types and steel sample fractures tested at different levels of cyclic overloading, as well as the microhardness measurement method in different zones of fatigue fracture are introduced in detail in [4]. The expansion of the scope of work and the preferential use of construction and installation equipment with a low service life lead to an increase in the failure of individual elements and units. The case of fatigue failure of the lifting element of the crane for transportation of finished products (plates, elements of the building structure, etc.) in the construction organization is considered. ntensive operation and frequent overloading of the load-gripping device led to the formation, development and ultimate destruction of the most loaded element-the upper clamp of the load-holding device (Figure 1).

Figure 1. Fatigue fracture of the element of the load-lifting device of the construction crane

Structural fibers, fossils, character traits and proportions of dimensions, as well as the breakdown of the structural integrity of the grain, as well as the characteristics of the concentrated hormone concentrates. It was found that the three-dimensional condensation was applied to the three-dimensional concentration of the polymer (bush, slot, passage). It is prescribed that the exterior surfaces of the outer shell are contacted with the workpiece of the workpiece, leading to the primary structural shock [22–26]. Produced by the classification of the entire spectrum of action factors (Figure 2).

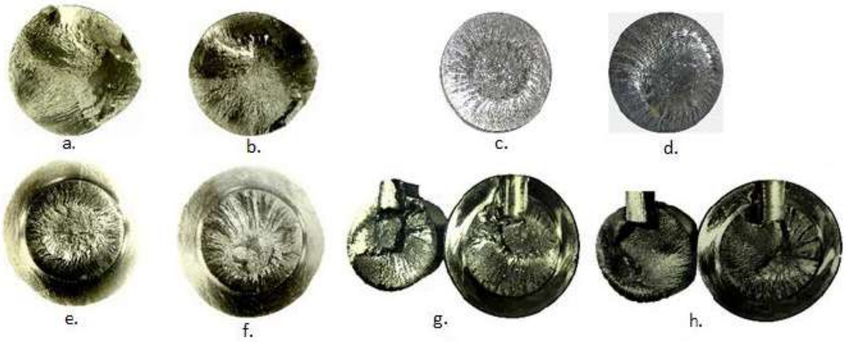

Figure 2. Heat shrinkage shafts and shaft joints (a, e, c, g) and low (b, f, d, h): a, b – glossy; e, f – with a rounding; e, d – with V-shaped knuckles; g and h – shontoons

The fractographic analysis of fatigue fractures at different overvoltage levels is given. Microstructural analysis of the surface layer indicates a change in the forms and quantitative ratio of microstructural components (Figure 3).

Thanks to the microplastic deformations caused by the maximum stresses at the top of the microcracks, as well as the contact closure of their shores, as the annular crack front moves to the center of the fracture, hardening of the surface layers occurs, the depth and degree of which depend on the cyclic loading parameters σ_i, N_i and geometric parameters of concentrators.

Structural features of fracture surfaces, shapes, character of distribution and ratio of sizes of zones of viscous and brittle fractures, as well as the influence of the type of concentrator on these parameters are given.

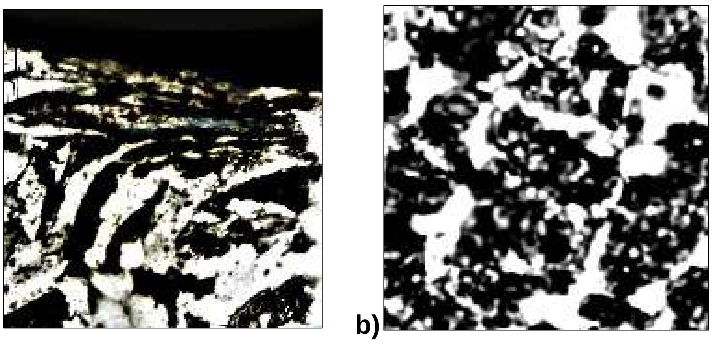

Figure 3. Microstructure of surface fracture layers:
a – at a depth $y = 0.2$ mm, b – the initial state ($y = 1.8$ mm)

The irregular plastic flow of metal in microvolumes of the fracture surface layers forms strengthening processes, and as a result – cyclic failure initiation and propagation. Therefore, for quantitative estimation of variation of the physico-mechanical condition indices of these layers, the measurement method of their HV microhardnesses is used. The changes of $HV = f_1(y)$ and $f_2(x)$ functions are studied, which are mathematical models of the strengthening processes in the fracture surface layers of machine elements. With a glance to these changes, in the layout of HV measurement, the step by y axis is taken $\Delta y = 0.2\ mm$, and by x axis – $\Delta x = 2\ mm$ (Figure 4).

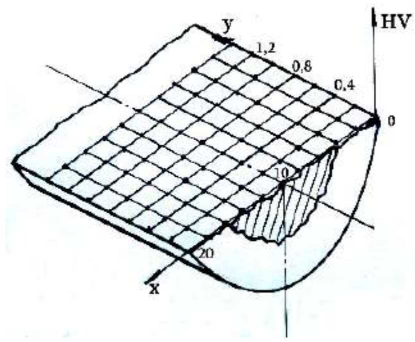

Figure 4. HV measurement layout

For the fractures of the details with fillet at $\sigma_1 = 225\ MPa$ and $\sigma_2 = 177\ MPa$ cyclic overloading, the identical form of the $HV = f_1(y)$ curves is observed, but with different HV_{max} (Figure 5a), and for $HV = f_2(x)$ curves at low σ_2 not only the symmetry is violated because of the variation of mutual arrangement of the plastic and brittle fracture zones, but also the HV_{max} values on the opposite sites of the plastic fracture zone are changed (Figure 5b). The initial state of HV_0 by y and x axes is determined at the depth of $y = 1.2 - 1.4\ mm$, therefore, obtaining the $HV = F(x, y)$ 3D function is reasonable for the complete estimation of the strengthening effect (Figure 6).

For the unification of calculation procedures, the HV measurement results of all types of fatigue fractures are processed by the method of curvilinear regression. The preliminary analysis of the function forms shows the existence of power functional relation in the form of the 4th degree equation

$$\begin{cases} HV = a_1y^4 + b_1y^3 + c_1y^2 + d_1y + e_1, \\ HV = a_2x^4 + b_2x^3 + c_2x^2 + d_2x + e_2, \end{cases} \tag{1}$$

as well as

$$HV = F(x, y) = [f_1(y) + f_2(x)]/2, \tag{2}$$

which are obtained by using the Wolfram Mathematica standard software. The $R^2 = 0.96 \ldots 0.99$ values of the determination coefficient indicate the high level regression relation.

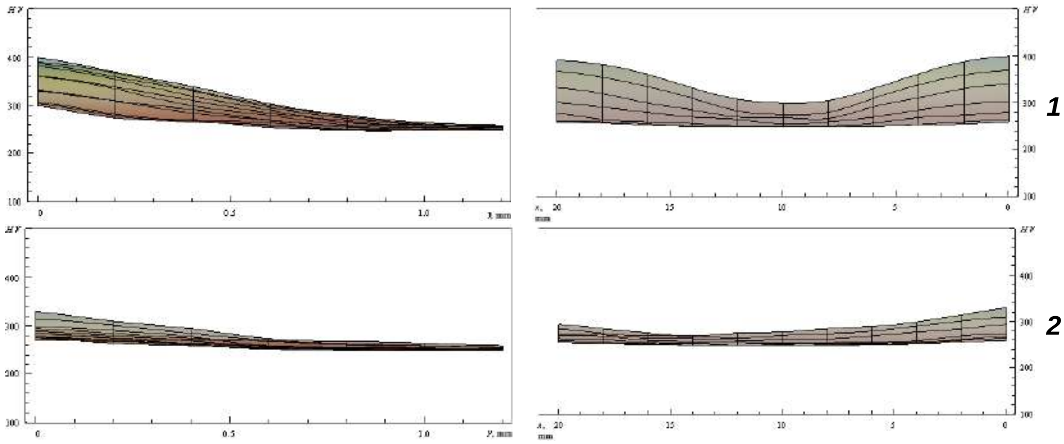

a b

Figure 5. The changes of HV on diametric section of fracture of the details with fillet
a By y axis; b By x axis
graphs 1 refer to $\sigma_1 = 225\ MPa$, and 2 – $\sigma_2 = 177\ MPa$

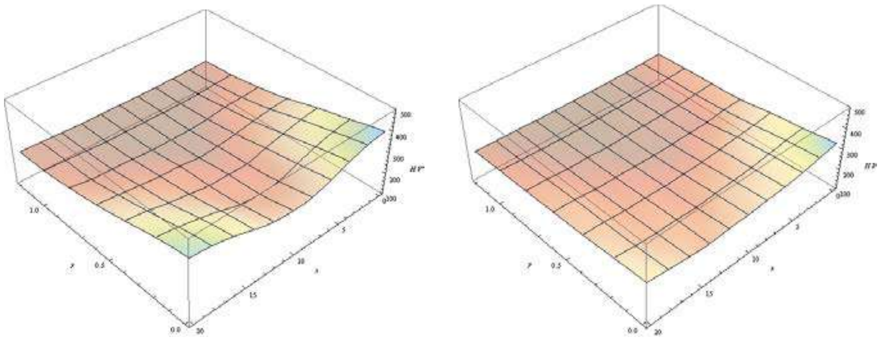

a b

Figure 6. $HV = F(x, y)$ surfaces at $\sigma_1 = 225\ MPa$ (a) and $\sigma_2 = 177\ MPa$ (b)

Similarly, the equation systems (1) are obtained for the remaining types of stress concentrators.

The $HV = f_1(y)$, $f_2(x)$, and $F(x, y)$ functions in the integral form take into account the physical-mechanical processes, flowing in fracture surface layers, and for obtaining a full picture of fatigue fracture based on the classification of fracture types and HV complex measurements, it is possible to create a database of equations (1) for carrying out expert conclusion and technical diagnostics of the fracture causes. In this work, the mentioned database is created for specific loading conditions (joint bending and torsion) and the most frequently occurring cases of stress concentrators in structural elements.

The revealed HV regularities in fatigue fracture surface layers allow to carry out quantitative estimation of fatigue fracture causes in 2 ways: firstly – estimate the loaded condition on the peak of the crack and the level of σ_i cyclic overloading, describing the real loading condition of the the details; and secondly – the strengthening effect from the contact healing of the crack edges in the plastic fracture zone, depending on N_i fatigue life which describes the lifetime of the shaft. Knowing σ_i and N_i, and using the equation of the fatigue curve, it is possible to give a substantial conclusion on the loading condition and lifetime, as well as determine the remaining life of the details.

Taking into account the variety of the acting factors and the significant volume of searching and calculation-graphic procedures, a computer software is necessary for efficient expertize and time reduction. For this, the Wolfram Mathematica standard software is used which includes a subprogram (Microsoft Office Access 2007, 0.8 MB) for carrying out the calculation procedures. The calculation algorithm includes the following blocks:

The database consists of the following sections:

1.1. Join type;

1.2. The details material;
1.3. The details diameter – $d < 20\ mm$, $d = 20 - 60\ mm$, $d > 60\ mm$;
1.4. Stress concentrator type;
1.5. Loading type;
1.6. Stress type;
1.7. Stress level;
1.8. The details fracture type;
1.9. Studied fracture zone – plastic, brittle;
1.10. Mutual arrangement of the fracture zones;
1.11. The systems of the $HV = f_1(y)$ and $HV = f_2(x)$ standard equations are grouped according to the 1.1-1.10 points;

2. Input and processing of HV measurements of the surface layers of the researched the details fracture;

3. Deriving the $HV = f_1(y)$, $HV = f_2(x)$ and $HV = F(x, y)$ functions by providing the $R^2 > 0.9$ condition;

4. The graphical presentation of the functions according to the 3rd point;

5. Compiling and inputting materials science, geometric, loading, and fractographic indices of the researched the details;

6. Comparison of the obtained data with the database according to the 3rd and 5th points, selection of the optimal variant of functions and data group;

7. Conclusion making and quantitative estimation of parameters of the acting factors leading to the fracture.

The scheme of the algorithm of the computational subroutine is given in Figure 7.

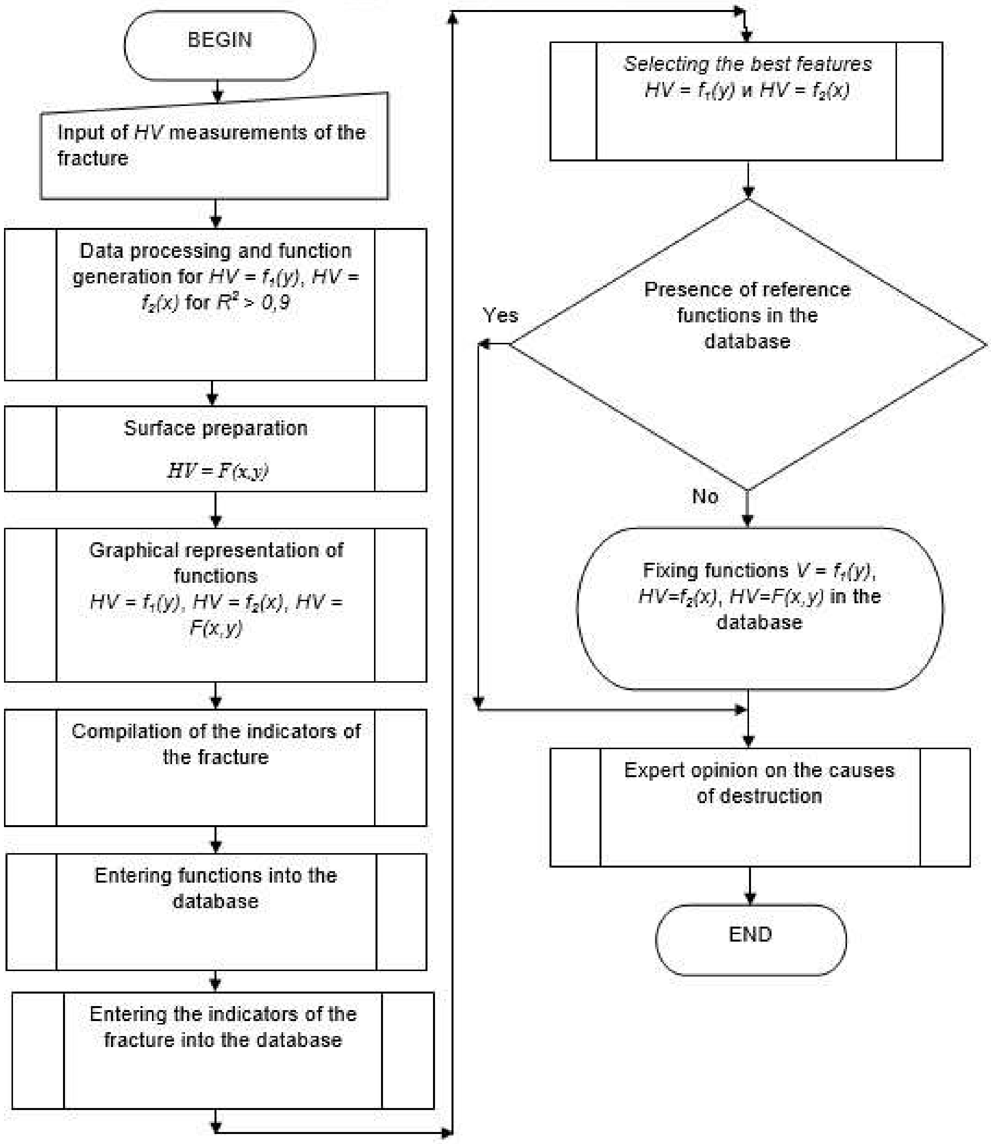

Figure 4. The algorithm of the computational subroutine

4. Conclusion

1. The article has a scientific-practical value since the methods of fractography have been applied for the real elements of construction machines, working at variable complex loading. A database is created based on the obtained systems of $HV = f_1(y)$ and $HV = f_2(x)$ parametric equations and $HV = F(x, y)$ surfaces for identifying the loading conditions and carrying out technical diagnostics of fatigue fracture causes of the details and joints. From this perspective, the systems of microhardness equations are derivatively qualifying the main parameters of fatigue fracture and can be reliable means for recovering fracture prehistory and making quantitative estimations of causes. In addition, the combined influence of joint acting stress concentrators in the fracture processes on the dangerous sections of joints and the dominant meaning of transitional precipitate under loading variability conditions in the joint that results initiation of plastic fracture zone and its propagation from the opposite fragment of key groove are considered. The system of obtained regression equations allows to formulate database for making substantiated and reliable technical diagnostics of fatigue fractures of the details and joints.

2. The results of the work can be used in 2 ways: a) including them into the maintenance processes of technical state mandatory monitoring of overloaded construction elements, and if required, carrying out current repair or replacement of a damaged machine element; b) in case of an occurred fracture,

conducting technical diagnostics of fracture causes and quantitative estimation of the acting factors by using database of the above mentioned regression equations. The second way is of practical interest for the specialists of the structures of emergency situations [26–29].

3. The general condition in many industries, including the construction industry and road and transport communications in the last decade, is characterized by the desire to increase productivity and reduce the start-up time of facilities using a significant number of technological equipment, mainly exhausted the main resource of durability. This is the reason for the sharp increase in cases of failure and destruction of building structures, as well as road accidents. In the created conditions, the primary action is the drawing up of an informed schedule for technical inspection, maintenance and repair of equipment, and in the event of an accident, an accurate assessment and technical diagnosis of the causes of destruction by a relatively accessible measurement method (a well-known PMT-3 device is used to measure microhardness according to Vickers).

4. These measures will make it possible, as far as possible, to reduce the timeframe for the failure of construction equipment and structures, and in the second case, to identify the responsible organization that has allowed the equipment to be unloaded.

References

1. Matvienko, Yu.G. *Modeli i kriterii mekhaniki razrusheniya* [Models and criteria for fracture mechanics]. Moscow: Fizmatlit, 2006. 328 p. (rus)
2. Lassen T., Spagnoli A. Fatigue Crack Paths in Shafts Subjected to Bending and Torsion. *Proc. of Crack Paths.* Parma, Italy, 2006. Pp. 35–42.
3. Stakyan M.G., Soghomonyan V.K. Izucheniye fiziko-mekhanicheskogo sostoyaniya poverkhnostnykh sloyev ustalostnykh izlomov v soyedineniyakh “val-stupitsa” [The Research of Physical-Mechanical Condition of Fatigue Fracture Surface Layers in the “Shaft-Hub”]. *BULLETIN of National University of Architecture and Construction of Armenia*. 2015. No. 3(47). Pp. 53–61.(rus)
4. Soghomonyan, V.K. Diagnostika ustalostnykh povrezhdeniy valov izmereniyami mikrotverdostey poverkhnostnykh sloyev izlomov [Diagnostics of Fatigue Damages of Shafts by Microhardness Measurements of Fracture Surface Layers]. *Mezhdunarodnaya nauchno-teqnicheskaya conferenciya. Sbornik dokladov. Detali mashin I mechanizmov.* [International scientific- technical conference, Section of Machine Elements and Mechanisms]. Moscow: MADI, 2007. Pp. 43–47. (rus)
5. Indeykin A.V., Chizhov S.V., Shestakova E.B., Antonyuk A.A., Kulagin N.I., Smirnov V.N., Karpov V.V., Golitsynsky D.M. Approximated methods of estimation of the reliability of framed railway structures of railway bridges. *Magazine of Civil Engineering.* 2017. No. 7. Pp. 150–160.
6. Priadko I.N., Mushchanov V.P., Bartolo E., Vatin N.I., Rudnieva I.N. Improved numerical methods in reliability analysis of suspension roof joints. *Magazine of Civil Engineering.* 2016. No. 5. Pp. 27–41.
7. Boltin V.V. Treshinostoykost materialov I kontinualnaya mexanika povrejdenii [Crack Resistance of Materials and Continuum Mechanics of Damage]. *DAN.* 2001. Vol. 376. No. 6. Pp. 760–762. (rus)
8. Volkov V.M., Mironov A.A. Obedinenaya model obrazovaniya I rosta ustalostnix treshin v koncentratorax napryajenii [Combined model of formation and growth of fatigue cracks in stress concentrators]. *Problemi prochnosti I plastichnosti.* 2005. Vol. 67. Pp. 20–25. (rus)
9. Bakirov M.B., Gromakovski D.G., Dinnikov A.V. et al. Diagnostika sostoyaniya I ocenka ostatochnogo resursa elementov mashin I konstrukcii [Diagnosis of the state and evaluation of residual life of machine elements and structures]. *Kontrol. Diagnostika.* 2004. No. 1. Pp. 13–16. (rus)
10. Ibatullin I.D. Kinetika ustalostnoi povrejdaemosti i rarusheniya poverxnostnix sloev, deformiruemikh treniem [Kinetics of fatigue damage and destruction of surface layers

Литература

1. Матвиенко Ю.Г. Модели и критерии механики разрушения. М.: Физматлит, 2006. 328 с.
2. Lassen T., Spagnoli A. Fatigue Crack Paths in Shafts Subjected to Bending and Torsion // Proc. of Crack Paths. Parma, Italy, 2006. Pp. 35–42.
3. Стакян М.Г. Согомонян В.К. Изучение физико-механического состояния поверхностных слоев усталостных изломов в соединениях “вал-ступица” // Изв. НУАСА. 2015. № 3(47). С. 53–61.
4. Согомонян В.К. Диагностика усталостных повреждений валов измерениями микротвердостей поверхностных слоев изломов // Международная научно-техническая конференция. Сборник докладов. Московский автомобильно-дорожный государственный технический университет (МАДИ): Детали машин и теория механизмов. Москва: 2015. С. 43–47.
5. Индейкин А.В., Чижов С.В., Шестакова Е.Б., Антонюк А.А., Кулагин Н.И., Смирнов В.Н., Карпов В.В., Голицынский Д.М. Приближенные методы оценки надежности балочных пролетных строений железнодорожных мостов // Инженерно-строительный журнал. 2017. № 7(75). С. 150–160.
6. Прядко Ю.Н., Мущанов В.Ф., Бартоло Х., Ватин Н.И., Руднева И.Н. Усовершенствование численных методов расчета надежности узлов висячих покрытий // Инженерно-строительный журнал. 2016. № 5(65). С. 27–41.
7. Болотин В.В. Трещиностойкость материалов и континуальная механика повреждений // ДАН. 2001. Т. 376. № 6. С. 760–762.
8. Волков В.М., Миронов А.А. Обьединенная модель образования и роста усталостных трещин в концентраторах напряжений // Проблемы прочности и пластичности. 2005. № 67. С. 20–25.
9. Бакиров М.Б., Громаковский Д.Г., Дынников А.В. и др Диагностика состояния и оценка остаточного ресурса элементов машин и конструкций // Контроль. Диагностика. 2004. № 1. С. 13–16.
10. Ибатуллин И.Д. Кинетика усталостной повреждаемости и разрушения поверхностных слоев, деформируемых трением // Вестник СГАУ. Самара, СГАУ. 2006. № 2(10). Ч. 2. С. 204–209.
11. Кольцун Ю.И. Макроструктурный анализ усталостных изломов. Проблемы, достижения и перспективы // Проблемы прочности материалов и сооружений на транспорте: Сборник докладов VII Международной конференции по проблемам прочности материалов и сооружений на транспорте. 2008. Петербургский

deformed by friction]. *Vestnik SGAU.* Samara, SGAU. 2006. No. 2(10). Vol. 2. Pp. 204–209. (rus)

11. Kolcun Yu.I. Makrostruinnii analiz ustalostnix izlomov. Problemi, dostijeniya I perspektivi. Problemi prochnosti materialov I soorujenii na transporte [Macro-structural analysis of fatigue kinks. Problems, achievements and prospects. Problems of Strength of Materials and Structures in Transport]. *VII Mejdunarodnaya konferenciya po problemam prochnosti materialov i soorujenii na transporte. Sbornik dokladov* [International scientific on Strength of Materials and Structures in Transport]. Saint-Petersburg: Gos. un-t put. Soobsh. 2008. Pp. 149–182. (rus)
12. Mikhalkina S.V. *Makroanaliz I defektoskopiya metallov* [Macroanalysis and flaw detection of metals] Vladimir Vladimir State university. 2014. 46 p. (rus)
13. Patron B.Z. *Mekhanika razrusheniya: Ot teorii k praktike* [Mechanics of destruction: From theory to practice]. Moscow: Nauka, 1990. 240 p. (rus)
14. Petukhov A.N. Ob osobennostyakh vozniknoveniya I razvitiya ustalostnikh treshin v detlyakh GTD [On the features of the appearance and development of fatigue cracks in the details of GTE]. *Aviacionno-kosmicheskaya tekhnika I tekhnologiya.* 2005. No. 9. Pp. 56–62. (rus)
15. Sogomonyan V.K. Raschetnaya ocenka treshinostoikosti valov [Estimated assessment of fracture toughness of shafts]. *Mezhdunarodnaya nauchno-prakticheskaya Conferenciya. Logistika, transport, prirodoobustroistvo. Sbornik dokladov* [International scientific-practical conference. Logistics, transport, environmental management]. Yerevan: Armenpak, 2014. Pp. 135–141. (rus)
16. Sogomonyan V.K., Stakyan M.G. Modelirovanie processa ustalostnogo razrusheniya valov pri slojnom nagrujenii [Modeling the process of fatigue failure of shafts under complex loading]. *Proceedings of national Politechnic University of Armenia: Mechanics, Machine science, Machine-Bulding.* 2015. No. 1. Pp. 56–65. (rus)
17. Stepnov M.N., Shavrin A.B. *Statisticheskie metodi obrabotki rezultatov mekhanicheskikh ispitanii: Spravochnik* [Statistical methods for processing the results of mechanical tests: Directory]. Moscow: Mashinostroenie. 2005. 400 p. (rus)
18. Korolev I.K., Petinov S.B., Freydin A.B. Chislennoye modelirovanie nakopleniya povrejdenij I razvitiya ustalostnoi treshin v uprugikh materialakh. *Vichislitelnaya mekhanika sploshnikh sred.* 2009. Vol. 2. No. 3. Pp. 34–43. (rus)
19. Shanyavski A.A. *Modelirovanie ustalostnikh razrushenii metalov. Sinergetika v aviacii.* Ufa: OOO Monografiya, 2007. 500 p. (rus)
20. Ronchei C., Vantadori S. et al. Analysis of cracked and notched round bars under rotary bending. Materials Refformance and Characterization. Special Isssue. 2005. Vol. 4. No. 2. Pp. 131–142.
21. Brigenthi R., Carpinteri A. Surface cracks in fatigued structural components: a review. *Fatigue and Facture of Engineering Materials and Structures.* 2013. Vol. 36. No. 12. Pp. 1209–1222.
22. Carpinteri A., Vantadori S. Sickle-shaped surface crack in a notched round bar under cyclic tension and bending. *Fatigue and fracture of Engineering Materials and Structures.* 2009. Vol.32. No. 3. Pp. 223–232.
23. Brighenti R., Scorza D. et al. Fatigue crack proparation simulating fibre debonding in cyclically loaded composites. *Procedia Materials Science.* 2014. Vol. 3. Pp. 357–362.
24. Spagnoli A., Vantadori S. et al. Influence of the crack morphology on the fatigue crack growth rate: a continuously-kinked crack model based on fractals. Engineering Fracture Mechanics. Special Issue on Crack Paths. 2008. Vol.75. No. 3-4. Pp. 579–589.

Государственный университет путей сообщения. Санкт-Петербург, 2008. С. 149–182.

12. Михалкина С.В. Макроанализ и дефектоскопия металлов. Владимир: Владимирский государственный университет, 2014. 46 с.
13. Патрон В.З. Механика разрушения: От теории к практике. М.: Наука, 1990. 240 с.
14. Петухов А.Н. Об особенностях возникновения и развития усталостных трещин в деталях ГТД // Авиационно-космическая техника и технология. 2005. № 9. С. 56–62.
15. Согомонян В.К. Расчетная оценка трещиностойкости валов // Международный научно-практическая конференция. Логистика, транспорт, природообустройство. 2014, Ереван: Арменпак, 2014. С. 135–141.
16. Согомонян В.К., Стакян М.Г. Моделирование процесса усталостного разрушения валов при сложном нагружении // Вестник НПУА. Механика, машиноведение, машиностроение. 2015. № 1. С .56–65.
17. Степнов М.Н. Шаврин А.В. Статистические методы обработки результатов механических испытаний: Справочник. М.: Машиностроение, 2005. 400 с.
18. Королев И.К., Петинов С.В., Фрейдин А.Б. Численное моделирование накопления повреждений и развития усталостной трещин в упругих материалах / // Вычислительная механика сплошных сред. 2009. Т. 2. № 3. С. 34–43.
19. Шанявский А.А. Моделирование усталостных разрушений металлов. Синергетика в авиации. Уфа: ООО Монография, 2007. 500 с.
20. Ronchei C., Vantadori S. et al. Analysis of cracked and notched round bars under rotary bending // Materials Refformance and Characterization. Special Issue. 2005. Vol. 4. No. 2. Pp. 131–142.
21. Brigenthi R., Carpinteri A. Surface cracks in fatigued structural components: a review // Fatigue and Facture of Engineering Materials and Structures. 2013. Vol. 36. No. 12. Pp. 1209–1222.
22. Carpinteri A., Vantadori S. Sickle-shaped surface crack in a notched round bar under cyclic tension and bending // Fatigue and fracture of Engineering Materials and Structures. 2009. Vol. 32. No. 3. Pp. 223–232.
23. Brighenti R., Scorza D. et al. Fatigue crack proparation simulating fibre debonding in cyclically loaded composites // Procedia Materials Science. 2014. Vol. 3. Pp. 357–362.
24. Spagnoli A., Vantadori S. et al. Influence of the crack morphology on the fatigue crack growth rate: a continuously-kinked crack model based on fractals // Engineering Fracture Mechanics. Special Issue on Crack Paths. 2008. Vol. 75. No. 3-4. Pp. 579–589.
25. Shen H., Guo W. 3D fracture mechanics investigation on surface fatigue crack propagation // Fatigue Fract Enging Mater Struct. 2011. No. 34. Pp. 682–688.
26. Moser B., Schwaiger R., Dao M. Size Effects on Deformation and Fracture on Nanostructured Metals // Nanostructured Coatings Nanostructure Science and Technology. 2006. Pp. 27–77.
27. Spagnoli A., Vantadori S. et al. Some applications of fractal fracture mechanics to describe the fatigue behaviour of materials // Key Engineering Materials. 2008. Vol. 378–379. Pp. 355–370.
28. Totten G. Fatigue crack propagation // Advanced Materials and Processes. 2008. Pp. 39–41.
29. Wang G., Liaw P. Fatigue and fracture behavior // Bulk Metallic Glasses. 2008. Pp. 169–203.

25. Shen H., Guo W. 3D fracture mechanics investigation on surface fatigue crack propagation. *Fatigue Fract Enging Mater Struct.* 2011. Vol. 34. Pp. 682–688.
26. Moser B., Schwaiger R., Dao M. Size Effects on Deformation and Fracture on Nanostructured Metals. *Nanostructured Coatings Nanostructure Science and Technology*. 2006. Pp. 27–77.
27. Spagnoli A., Vantadori S. et al. Some applications of fractal fracture mechanics to describe the fatigue behaviour of materials. *Key Engineering Materials.* 2008. Vol. 378–379. Pp. 355–370.
28. Totten G. Fatigue crack propagation. *Advanced Materials and Processes.* 2008. Pp. 39–41.
29. Wang G., Liaw P. Fatigue and fracture behavior. *Bulk Metallic Glasses.* 2008. Pp. 169–203.

V.K. Soghomonyan,
+374(10)55-43-62; stakyan.mihran@yandex.ru

G.S. Chibukhchyan,*
+374(93)22-35-04; armenpack@mail.ru

H.S. Chibukhchyan,
+374(55)30-24-02; hovhannesch@gmail.com

Вардан Каренович Согомонян,
+374(10)55-43-62;
эл. почта: stakyan.mihran@yandex.ru

Григор Суренович Чибухчян,*
+374(93)22-35-04;
эл. почта: armenpack@mail.ru

Оганес Суренович Чибухчян,
+374(55)30-24-02;
эл. почта: hovhannesch@gmail.com

Федеральное государственное автономное образовательное учреждение
высшего образования
Санкт-Петербургский политехнический университет Петра Великого

ПОЛИТЕХ
Санкт-Петербургский
политехнический университет
Петра Великого

Инженерно-строительный институт
Центр дополнительных профессиональных программ

195251, г. Санкт-Петербург, Политехническая ул., 29,
тел/факс: 552-94-60, www.stroikursi.spbstu.ru,
stroikursi@mail.ru

Приглашает специалистов проектных и строительных организаций,
не имеющих базового профильного высшего образования
на курсы профессиональной переподготовки (от 500 часов)
по направлению «Строительство» по программам:

П-01 «Промышленное и гражданское строительство»

Программа включает учебные разделы:

- ***Основы строительного дела***
- ***Инженерное оборудование зданий и сооружений***
- ***Технология и контроль качества строительства***
- ***Основы проектирования зданий и сооружений***
- ***Автоматизация проектных работ с использованием AutoCAD***
- ***Автоматизация сметного дела в строительстве***
- ***Управление строительной организацией***
- ***Управление инвестиционно-строительными проектами. Выполнение функций технического заказчика***

П-02 «Экономика и управление в строительстве»

Программа включает учебные разделы:

- ***Основы строительного дела***
- ***Инженерное оборудование зданий и сооружений***
- ***Технология и контроль качества строительства***
- ***Управление инвестиционно-строительными проектами. Выполнение функций технического заказчика и генерального подрядчика***
- ***Управление строительной организацией***
- ***Экономика и ценообразование в строительстве***
- ***Управление строительной организацией***
- ***Организация, управление и планирование в строительстве***
- ***Автоматизация сметного дела в строительстве***

П-03 «Инженерные системы зданий и сооружений»

Программа включает учебные разделы:

- ***Основы механики жидкости и газа***
- ***Инженерное оборудование зданий и сооружений***
- ***Проектирование, монтаж и эксплуатация систем вентиляции и кондиционирования***
- ***Проектирование, монтаж и эксплуатация систем отопления и теплоснабжения***
- ***Проектирование, монтаж и эксплуатация систем водоснабжения и водоотведения***
- ***Автоматизация проектных работ с использованием AutoCAD***
- ***Электроснабжение и электрооборудование объектов***

П-04 «Проектирование и конструирование зданий и сооружений»

Программа включает учебные разделы:

- ***Основы сопротивления материалов и механики стержневых систем***
- ***Проектирование и расчет оснований и фундаментов зданий и сооружений***
- ***Проектирование и расчет железобетонных конструкций***
- ***Проектирование и расчет металлических конструкций***
- ***Проектирование зданий и сооружений с использованием AutoCAD***
- ***Расчет строительных конструкций с использованием SCAD Office***

П-05 «Контроль качества строительства»

Программа включает учебные разделы:

- ***Основы строительного дела***
- ***Инженерное оборудование зданий и сооружений***
- ***Технология и контроль качества строительства***
- ***Проектирование и расчет железобетонных конструкций***
- ***Проектирование и расчет металлических конструкций***
- ***Обследование строительных конструкций зданий и сооружений***
- ***Выполнение функций технического заказчика и генерального подрядчика***

По окончании курса слушателю выдается диплом о профессиональной переподготовке установленного образца, дающий право на ведение профессиональной деятельности